Development of Nano Composite Coatings for Enhanced Performance in Non-Conventional Lubricants under Sliding Contact

Muhammad Usman Bhutta

The thesis is submitted in partial fulfilment of the requirements of Faculty of Science and Technology, Bournemouth University for the degree of Doctor of Philosophy

September 2019

NanoCorr, Energy & Modelling Research Group (NCEM)

Faculty of Science and Technology, Bournemouth University, UK

Copyright Statement

This copy of the thesis has been supplied on condition that anyone who consults it is understood to recognise that its copyright rests with its author and that no quotation from the thesis and no information derived from it may be published without the author's consent.

Reprint Permission

Reprints from published papers can be made subject to permission from the respective publishers.

Abstract

A refrigerant is the most critical ingredient of any air-conditioning, refrigeration or cooling system. Increasing world population and global warming has increased the usage of air-conditioning and refrigeration devices considerably. This has resulted in the development, formulation and use of various refrigerants in the thermodynamic cycle. Most of the refrigerants that are used in domestic appliances, commercial buildings, small scale industrial applications and automobiles are artificially formulated. Although artificially formulated refrigerants have excellent thermodynamic properties, but the use of man-made chemical compounds have damaged the earth's atmosphere either by depleting the ozone layer or by increasing the global warming potential. Some naturally occurring compounds on the other hand have also shown good properties as refrigerants but have various inherent issues associated with them such as toxicity and flammability which limits and restricts their use.

To overcome the issue of ozone depletion and to control the issue of global warming, the refrigeration industry has recently developed and suggested new environment friendly refrigerants. These refrigerants should not only have the thermodynamic properties matching their predecessors but should also have a lower negative impact on the environment. The thermodynamics, physical and chemical properties of the newly developed refrigerants have been the main focus of study by various researcher worldwide. The extensive investigation of material wear and friction properties of the next generation of refrigerants used in mechanical applications is incomplete. The in-use durability performance of these products have to be accessed from the viewpoint of sustainable development. Tribo-performance of refrigerants applied in refrigeration, air-conditioning and energy systems directly influences the durability, reliability and cost effectiveness of the system. The past studies concerning friction, wear and the overall tribological properties of the last generation of refrigerants have shown that the overall life and performance of a mechanical system especially a compressor is highly influenced by the type of refrigerant used.

This research project has evaluated the effects on the mechanical performance of a system utilizing the next generation of refrigerants along with assessing the feasibility and reliability of electrodeposited Nickel based composite coatings for refrigerant-lubricated tribological systems. For this study a micro-friction tribo-meter has been modified to incorporate the testing specimens and refrigerants under various operating conditions. Hydrofluoroethers (HFEs) are within the family of newly developed environmentally friendly refrigerants with a wide range of application areas. HFE-7000 is a replacement solution for the existing harmful refrigerants and thermo-fluids having a broad range of application areas including usage in green energy, low

carbon technologies, in aerospace and automotive industries. This study is divided into two parts. In the first part of the study a detailed investigation has been performed on uncoated steel contacts to assess friction and wear performance of HFE-7000 (HFE-347mcc3). HFE-7000 has been employed as lubricants. In the second part of this study five different types of coatings namely, Ni-Al_2O_3, Ni-ZrO_2, Ni-SiC, Ni-Graphene and Nickel-only have been used to investigate the wear and friction performance of these coatings in systems based on HFE-7000 refrigerant. Extensive experimentation has been performed on these coated contacts using the modified pressurized lubricity tester by changing the refrigerant temperature and the applied normal load in an attempt to enhance the tribological performance of interacting machine parts employing HFE-7000. Experimental results indicate the formation of tribo-films on the topmost surfaces. Energy-Dispersive X-ray Spectroscopic (EDS) and X-ray Photoelectron Spectroscopic (XPS) analyses on the tested samples revealed significant presence of oxygenated and fluorinated anti-wear tribo-films. These oxygen and fluorine containing tribo-layers prevent metal to metal contact and contribute to the reduction of friction and wear. All coatings presented an improvement in the micro-hardness and in hardness to elastic modulus ratio compared to uncoated steel. The results of friction and wear of coated samples were compared to uncoated steel as well. The results show an improvement in wear and friction at most of the operating conditions by applying nickel based coatings on a steel substrate in the presence of HFE-7000. Friction and wear performance of nickel based coatings does drop for some of the coatings at particular testing conditions which leads to conclude that a careful selection of the coatings has to be made depending on the operating refrigerant temperature and applied load.

List of Publications

Journal Publications

1. Muhammad Usman Bhutta, Zulfiqar Ahmad Khan, Nigel Garland and Abdul Ghafoor, 2018. A Historical Review on the Tribological Performance of Refrigerants used in Compressors. Tribology in Industry, 40 (1), pp. 19-51.

2. Muhammad Usman Bhutta, Zulfiqar Ahmad Khan and Nigel Garland, 2019. Novel Experimental Setup to Assess Surfaces in Tribo-contact Lubricated by the Next Generation of Environmentally Friendly Thermo-Fluids. International Journal of Computational Methods and Experimental Measurements, Vol. 7, Issue 3, pp. 226-235.

3. Muhammad Usman Bhutta, Zulfiqar Ahmad Khan and Nigel Garland, 2018. Wear Performance Analysis of Ni-Al$_2$O$_3$ Nanocomposite Coatings under Nonconventional Lubrication. Materials, 12 (36), pp. 1-22.

4. Muhammad Usman Bhutta and Zulfiqar Ahmad Khan, 2019. Friction and Wear Performance Analysis of Hydrofluoroether-7000 Refrigerant. Tribology International, Vol. 139, pp.36-54.

5. Muhammad Usman Bhutta, Zulfiqar Ahmad Khan, 2020. Wear and friction performance evaluation of nickel based nanocomposite coatings under refrigerant lubrication (Accepted: Tribology International).

6. Ashish Kumar Kasar, Muhammad Usman Bhutta, Zulfiqar Ahmad Khan, and Pradeep Menezes, 2020. Corrosion performance of nanocomposite coatings in moist SO$_2$ environment. The International Journal of Advanced Manufacturing Technology.

Conferences

1. M.U. Bhutta, Z.A. Khan, N. Garland, A. Ghafoor, (2017). Development of Nano composite coatings for enhanced performance in non-conventional lubricants under sliding contact. The Faculty of Science and Technology's Third Annual PGR Conference. 24th May 2017. Bournemouth University.

2. M.U. Bhutta, Z.A. Khan, N. Garland, A. Ghafoor, (2018). Friction and wear performance analysis of sliding contacts in non-conventional lubrication. The Faculty of Science and Technology's Fourth Annual PGR Conference. 9th May 2018. Bournemouth University.

3. Arpith Siddaiah, Zulfiqar Ahmad Khan, Muhammad Usman Bhutta and Pradeep L Menezes. Investigation and Fabrication of Multifunctional Nanoparticle Surface Coatings for Wear-Corrosion Synergistic Resistance. At: 73rd STLE Annual Meeting & Exhibition, 20-24 May 2018, Minneapolis, Minnesota (USA).

4. Muhammad Usman Bhutta and Zulfiqar Ahmad Khan. Development of Nano composite Coatings for Enhanced Performance in Non-conventional Lubricants under Sliding Contact. At: UK Tribology 1st National Event, Future cities and mobility: the challenges for tribology, 21st Feb 2019, National Physical Laboratory (NPL), Teddington, UK.

5. Muhammad Usman Bhutta and Zulfiqar Ahmad Khan. Experimental Investigation of Friction and Wear Behavior of 52100 Steel Against Nano-Coated Mild Steel Subject to Refrigerant Lubrication. At: 74th STLE Annual Meeting & Exhibition, 19-23 May 2019, Nashville, Tennessee (USA).

6. Muhammad Usman Bhutta, Zulfiqar Ahmad Khan and Nigel Garland. Novel Experimental Setup to Assess Surfaces in Tribo-Contact Lubricated By the Next Generation of Environmentally Friendly Thermo-Fluids. At: 9th International Conference on Computational Methods and Experiments in Material and Contact Characterisation, 22-24 May 2019, Lisbon, Portugal.

Table of Contents

List of Figures

Fig. 5.33. Coefficient of friction graphs for Nickel-only: Real-time coefficient of friction at refrigerant temperature (a) 20°C (b) 30°C (c) 40°C (d) Average coefficient of friction plot (e) Percentage change in average friction coefficient by applying Nickel-only. 160

List of Tables

Nomenclature

q	Specific Wear Rate $\left(mm^3/Nm\right)$	k	Dimensionless Ellipticity Parameter	
V	Wear Volume (mm^3)	H_{min}	Dimensionless Minimum Lubricant Film Thickness	
A_a	Radius of Contact (m)	V_e	Mean Lubricant Entraining Velocity $\left(m/s\right)$	
ω	Wear Rate $\left(N/m\right)$	η_0	Lubricant Viscosity at Atmospheric Temperature & Pressure $\left(m^2/s\right)$	
K	Probability Factor $(dimensionless)$	R	Equivalent Radius of Curvature (m)	
W	Load (N)	α	Pressure-Viscosity Coefficient $\left(mm^2/N\right)$	
a	Radius of Contact (m)	E'	Equivalent Modulus of Elasticity	
k	Wear Coeffcient $(dimensionless)$	R_x	Effective Radius in X Direction	
N	Normal Force (N)	R_y	Effective Radius in Y Direction	
L	Sliding Distance (m)	E	Elastic Modulus	
H	Hardness $\left(N/m^2\right)$	h_{min}	Lubricant Film Thickness (m)	
F	Friction Force (N)	λ	Stribeck Number	
μ	Coefficient of Friction $(dimensionless)$	T_{ON}	ON-Time (s)	
R	Normal Reaction Force (N)	T_{OFF}	OFF-Time (s)	
A_r	Real Area of Contact (m^2)	I_P	Peak Current Density $\left(A/dm^2\right)$	
Y_s	Yield Strength $\left(N/m^2\right)$	I_A	Average Current Density $\left(A/dm^2\right)$	
τ	Shear Strength $\left(N/m^2\right)$	T_{AA}	Anode Pulse Reverse Time (s)	
μ_p	Coefficient of Friction in Ploughing	T_C	Cathode Pulse Forward Time (s)	
U	Dimensionless Speed Parameter	I_{AA}	Anode Current Density $\left(A/dm^2\right)$	
G	Dimensionless Material Parameter	I_C	Cathode Current Density $\left(A/dm^2\right)$	
W'	Dimensionless Load Parameter	$\bar{I}$	Average Current Density $\left(A/dm^2\right)$	
GWP	Global Warming Potential	ODP	Ozone Depleting Potential	
CFC	Chlorofluorocarbon	HCFC	Hydrochlorofluorocarbons	
HFC	Hydrofluorocarbons	HC	Hydrocarbons	
HFO	Hydrofluoroolefins	HFE	Hydrofluoroethers	
GHG	Greenhouse Gases			

Acknowledgements

Dedication

This thesis is dedicated to my beloved Mother!

Author's Declaration

This report contains the original work of the author except otherwise indicated. This research is match funded by Bournemouth University, UK and National University of Science and Technology, Pakistan. All contents of this report except materials from external referencing are subject to confidentiality under BU-NUST confidentiality and commercialisation contract.

Chapter 1

Research Background

1.1 Introduction

Anthropogenic global climate changes, the increase in global population and the rise in worldwide economic development has considerably increased the use of cooling, refrigeration and air-conditioning systems worldwide. Europe and North America have the highest fridge ownership in the world (BBC 2015). The increase in the domestic air-conditioning requirements in the USA alone which has the highest Gross domestic product (GDP) in the world (IMF 2019) can be seen from figure 1.1. Nowadays almost all new homes have central air-conditioning systems and there are hardly any homes left that are without an air-conditioner in the USA. A refrigerator is a common household item, the ever increasing population means increase in the number of refrigerators/freezers every year.

Fig. 1.1. Increase in central air conditioning in newer homes in USA (Eia, 2009).

A typical home in the USA consumes on average about 27% of the electricity in space cooling and in operating refrigerators/freezers as shown in figure 1.2. Space cooling (air-conditioning) can also be seen as the single largest use of electricity by the USA residential sector in figure 1.2. The data of the commercial USA electricity consumption shown is figure 1.3 is similar to

the residential sector, space cooling and refrigeration takes up 25% of the total electricity consumption. Refrigeration however, is the largest single end use in the USA commercial sector in comparison to air-conditioning in the residential sector. The commercial sector includes, offices, education, retail, public institutes, government facilities, and public and outdoor street lightning.
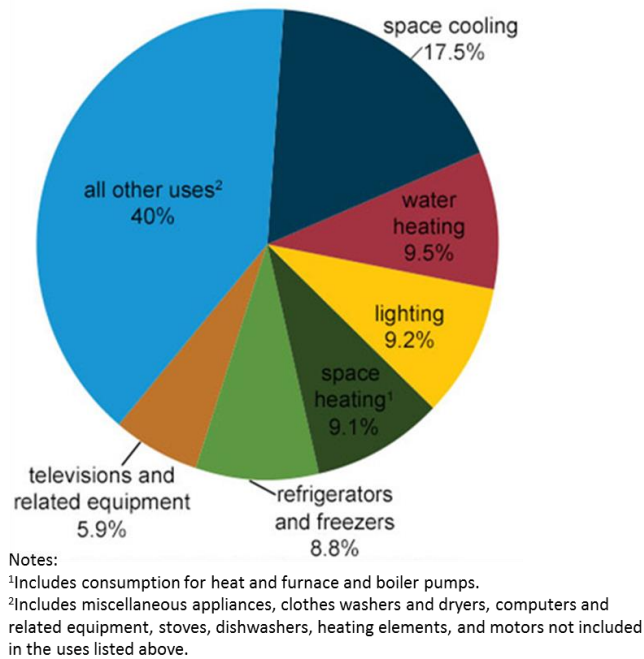
Fig. 1.2. USA Residential sector electricity consumption by major end uses (Eia, 2017a).
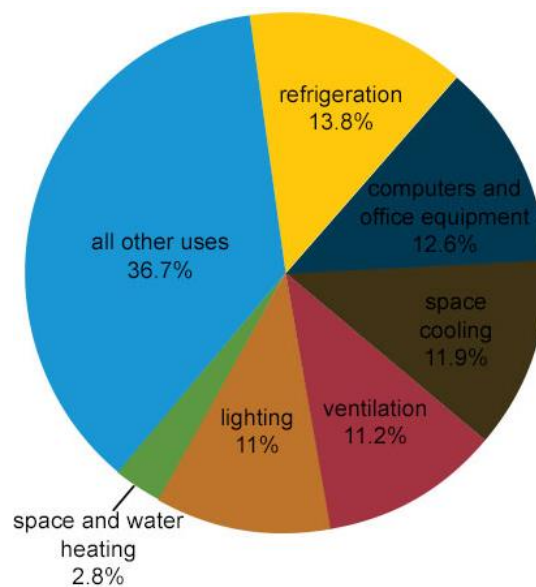
Fig. 1.3. USA commercial sector electricity consumption by major end uses (Eia, 2017b).

This shows that refrigeration and air-conditioning devices are not only growing in usage but are also consuming the major part of the electricity generation in the commercial and domestic sector. Figure 1.4 illustrates the worldwide air-conditioning units and the progressive yearly increase in the number of commercial as well as residential units. All space cooling and refrigeration units require the use of a coolant (refrigerant) in their thermodynamic cycle to operate, which indicates the upward trend in the demand and use of refrigerants.

Chilling times
World, air-conditioning units, bn

- Residential
- Commercial

```
1.6
1.2
0.8
0.4
0

2000 02  04  06  08  10  12  14  16
```

Source: International Energy Agency

Fig. 1.4. Worldwide air-conditioning units (iea 2018).

Figure 1.5 shows the increase in the number of cars sold worldwide, with each passing year the number of cars and other automobiles is increasing globally. Majority of the cars produced nowadays come with a car air-conditioner which requires a refrigerant to function as well,

which indicates that the increase in usage of different refrigerants is not limited to domestic and commercial units but the demand of refrigerates is increasing in the automotive sector as well.

Number of cars sold worldwide from 1990 to 2017 (in million units)
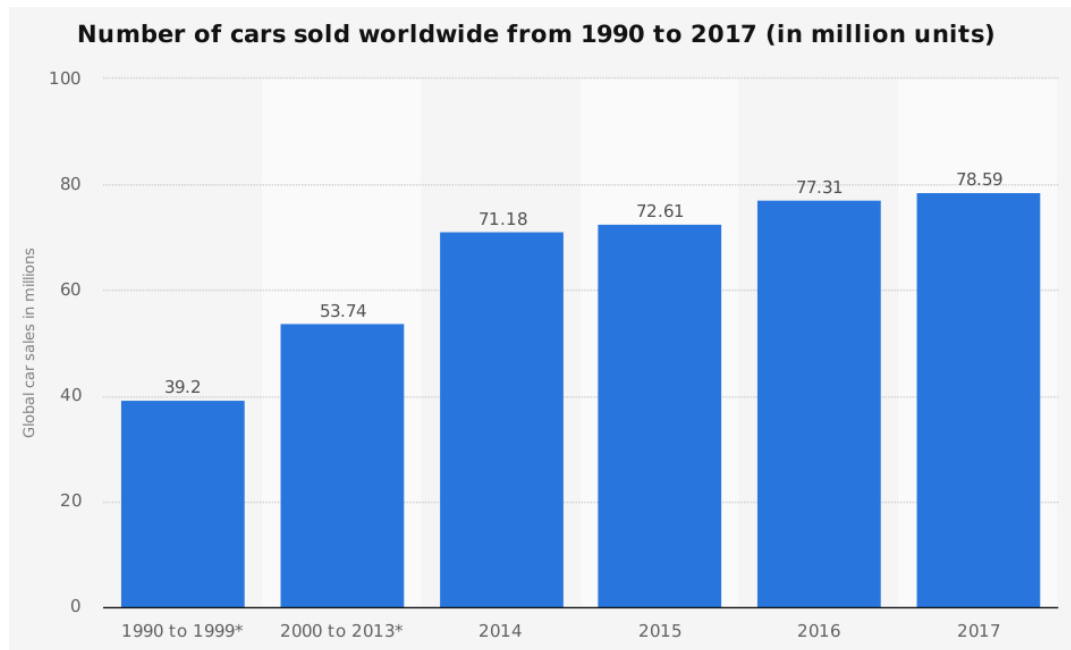
Fig. 1.5. Number of cars sold worldwide from 1990 to 2017 (in million units) (Statista, 2017).

Various refrigerants have been developed and used by different companies over the past years. The selection of a refrigerant depends on its application and place of use. Some of the refrigerants being used today in the domestic and commercial sectors are naturally occurring whereas majority of the refrigerants have been artificially formulated. Before the 1930s some naturally occurring compounds such as Sulfur Dioxide (R-764), Ammonia (R717), Methyl Chloride (R-40) and Methyl Formate (R-611) were being used as refrigerants, but their high toxicity and flammability reduced their potential of being used in domestic refrigeration and cooling systems (Bhutta et al. 2018b).

Several fatal accidents occurred in the 1920s because of methyl chloride leakage from refrigerators (Calm 2008a; Bhutta et al. 2018b). This started a collaborative research in 1928 for a refrigerant replacement that would be nontoxic and non-flammable by Frigidaire, DuPont and General Motors Research Corporation. This collaborative research led to the development of artificially formulated refrigerants namely, Chlorofluorocarbons (CFCs) and Hydrochlorofluorocarbons (HCFCs). CFCs and HCFCs were nontoxic and non-flammable refrigerants that possessed excellent thermodynamic properties. This led to their immediate commercialization. Various studies on the tribological properties of CFCs and HCFCs were

carried out by different researchers in the coming years which showed that these refrigerants formed protective surface films and improved the durability and life of a compressor (Bhutta et al. 2018b). CFCs and HCFCs presented excellent thermodynamic and trribological properties which were ideal to be used in domestic, automotive and commercial applications. However, the adverse effects of CFCs and HCFCs on the stratospheric ozone layer were discovered later which led to the enforcement of the Montreal Protocol in 1989 and the subsequent ban of these refrigerants (Bhutta et al. 2018b).

With a ban on CFCs and HCFCs, the refrigerant manufacturers put forward HFCs which had zero ozone depletion potential, as replacement refrigerants. HFCs matched the thermodynamic properties of CFCs, but showed poorer tribological performance in comparison to their predecessors. In addition, mineral oils that showed good miscibility with CFCs and HCFCs, unfortunately were not compatible with HFCs. Synthetic oils with various additives had to be developed for HFCs. Despite having these drawbacks and limitations, HFCs were adopted as the primary replacement refrigerants for CFCs and HCFCs. HFCs were globally accepted and were charged in automotive air-conditioners and in residential and commercial refrigerators, freezers and cooling units. The damaging implications of HFCs on the earth's atmosphere were realised much later when it was discovered that hydrofluorocarbons are one of the major contributors to global warming (Bhutta et al. 2018b). In 1997, Kyoto protocol to the United Nations Framework Convention on Climate Change established binding limits on emissions of carbon dioxide and other greenhouse gases (GHG), which included HFCs as well. HFCs are now in the process of being phased out (Bhutta et al. 2018b).

This means that new future generation refrigerants have to be introduced. The development of a new generation of artificially formulated refrigerants and the replacement of the previous refrigerants has also sparked a debate to shift towards naturally occurring compounds, because of the argument that the artificially formulated refrigerants have proven to be harmful to the earth's environment one way or another. Most of the naturally occurring compounds have thermodynamic limitations whereas other potential natural refrigerants are either toxic or flammable (Bhutta et al. 2018b). The challenge for the refrigerant manufacturers is even greater this time as they not only have to come up with refrigerants that have zero ozone depletion potential but also have minimum global warming potential. However, the refrigerant industry has introduced replacement refrigerants namely Hydrofluoroolefins (HFOs) and Hydrofluoroethers (HFEs) which have zero ozone depletion potential and have minimum global warming potential, these future generation refrigerants have good heat transfer and

thermodynamic properties, but their investigation from a tribological viewpoint has hardly been carried out.

The life and performance of a compressor or a pump is not only determined by its design and construction material but is also influenced by the type of fluid used and the ambient atmosphere (Bhutta et al. 2018b). Various studies have been conducted in the past to look into the tribological performance of refrigerants, almost all of these past studies are however concerned with the refrigerant in vapour state and most of these studies have been carried out using a refrigerated environment with various oils as lubricants. The true affect on the mechanical performance of refrigerants can only be studied if refrigerants are used in liquid state and the refrigerant itself is used as a lubricant rather than using lubricating oils. Un-lubricated conditions are used to better understand the lubricity of the refrigerants by decoupling refrigerant- lubricant effects. A number of studies have been performed and reported in the past to investigate the tribological performance of numerous refrigerants without using any lubricant (Cannaday and Polycarpou 2005; Khan et al. 2005; Demas and Polycarpou 2006a; Khan et al. 2006; De Mello et al. 2009; Sariibrahimoglu et al. 2010; Akram et al. 2013a; Yeo and Polycarpou 2014; Vergne et al. 2015; Jacobson and Espejel Purdue University, Indiana, USA, 17-20 July, 2006, Paper 1789; Solzak and Polycarpou Purdue University, Indiana, USA, 17-20 July, 2006, Paper 1790; Kawahara et al. Purdue University, Indiana, USA, 23-26 July, 1996, Paper 1141). The tribological evaluation of the future generation refrigerants is incomplete and the extensive investigation of the tribological performance of some of the next generation of refrigerants is yet to be carried out.

Research previously conducted under the PhD project titled 'Electroplated Composite Coatings with Incorporated Nano Particles for the Tribological Systems with the Focus on Water Lubrication' within NanoCorr, Energy & Modelling (NCEM) Research theme in collaboration with Schaeffler Technologies GmbH & Co. KG, Germany has shown the usefulness of surface coatings incorporating nanoparticles with main focus on water lubrication. The current research project will not only test the friction and wear behaviour of future generation refrigerants but will also develop and use nanocomposite coatings incorporating various nanoparticles to improve the overall tribological performance of the next generation of refrigerants.

The research approach adopted for this project is multi-fold; refrigerants, coating development, system setup, experimental testing and analysis as shown in Fig. 1.6. The refrigerant study will include the selection of an appropriate next generation of future refrigerant along with an in-depth literature survey of the previous tribological investigations carried out by past researchers

on the refrigerants used earlier. Coating study will involve the determination of an appropriate substrate material, selection of appropriate nanocomposite coatings and their preparation procedure using electroplating techniques with various Nano particles. The system setup will involve the modification of TE-57/77 tribo-meter to incorporate refrigerants in a sealed environmental chamber. Extensive experimental testing will be carried out in the environmental chamber by varying the applied load, the refrigerant temperature, the surface finish of the testing samples and by applying a number of coatings on the test specimens. The tested samples will be analysed using different analytical equipment.

A detailed literature review of the tribological performance of all the refrigerants that have been used in domestic/residential, small scale commercial and automotive applications in the past has been conducted to understand their behaviour and to gain insight into the various types of investigative methods used. The literature survey has helped in designing the test rig modifications and in understanding the friction and wear pattern of the different families (CFCs, HCFCs. HFCs, HCs, CO_2, HFOs, and HFEs) of refrigerants.

Literature on coatings has also been studied with an emphasis on the coatings prepared by electrodeposition techniques. Nickel based coatings have been selected for this study, with the hardware and facilities available at Bournemouth University, Nickle based coatings are being applied to the substrate. Nickle only coatings and Nickel based coatings incorporating various Nano particles in the Nickel matrix have been prepared. The electrodeposition pulse parameters and the preparation is carefully controlled to ensure uniform and proper deposition.

TE-57/77 tribo-meter was selected for the tribological testing. The TE-57/77 had to be modified and sealed to allow the charging and testing of refrigerants under vacuum and sealed conditions. The initial vacuum is required before the charging of the refrigerant so as to minimize the affect of ambient air and oxygen on the testing. The modification also involved the installation of temperature sensors, a contact potential sensor, a pressure sensor and a pressure gauge. All these sensors were calibrated and integrated with the data acquisition system of the tribo-meter, this allows real time data to be monitored and recorded.

The testing involves the application of a constant normal load, the continuous maintenance of the temperature of the refrigerant during testing and the control of the sealed chamber pressure. All the steps involved in this research project have been summarized in the flow chart presented in figure 1.6.
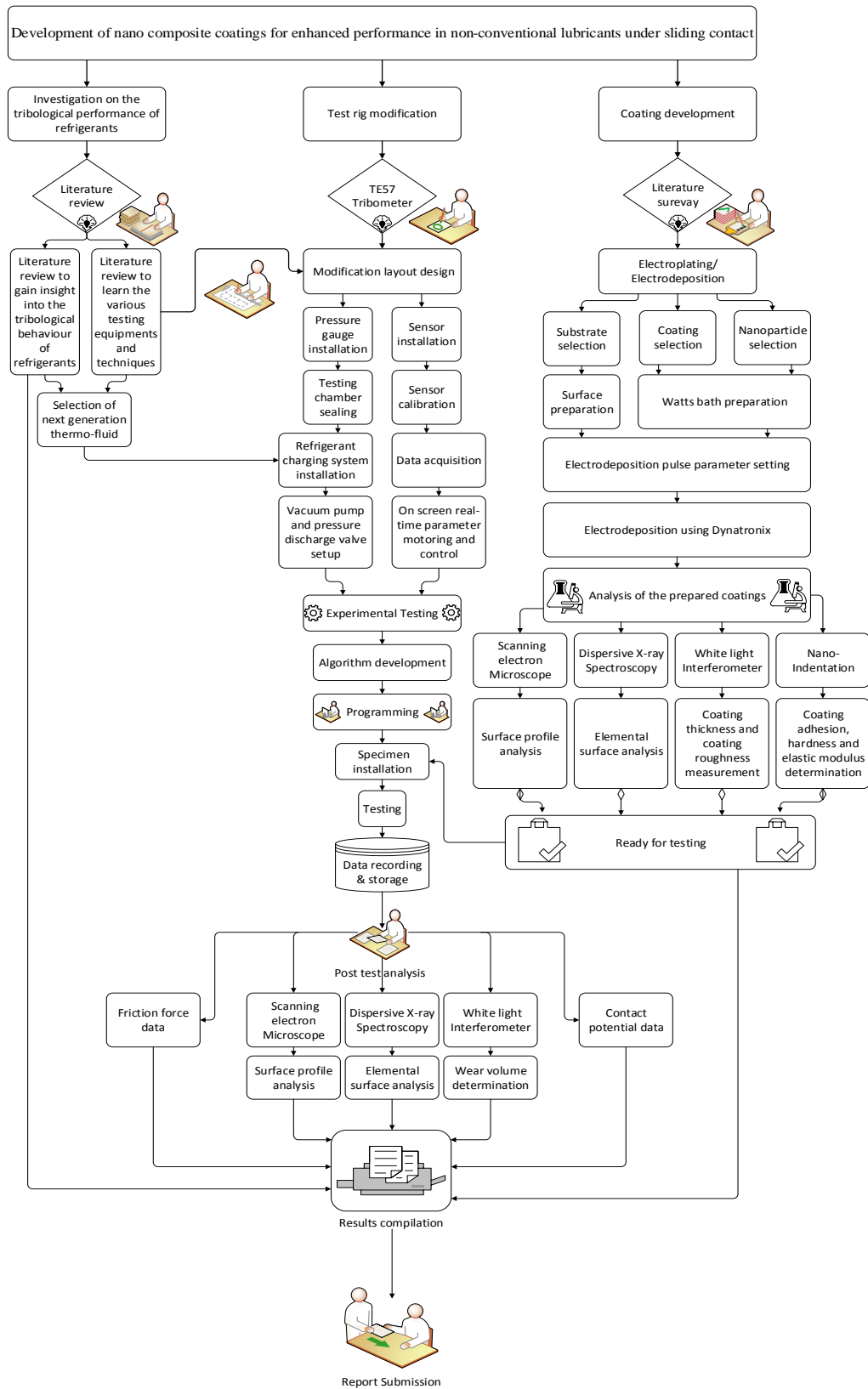
Fig. 1.6. Flow chart identifying various steps involved in this research project.

1.2 Research Question

Can the reliability and durability of complex interacting systems and machines be enhanced by the synergistic tribological and mechanical performance of the next generation of environmentally friendly thermo-fluids and novel nano-composite coatings?

1.3 Novelty

The novelty of this research is the detailed investigation of the tribological performance of Hydrofluoroethers by using uncoated and electrodeposited nanocomposite coatings incorporating various nanoparticles employing a modified micro-friction testing machine. The modified test rig allows for temperature controlled testing in a sealed environmental chamber eliminating the influence of ambient air under varying loads and refrigerant temperatures. The originality of this work lies in the use of Nano-coatings which have not been previously applied under environmentally friendly future generation thermo-fluids. This research will provide novel design solutions for selecting suitable electroplated Nickel composite coatings for the tribological applications in refrigerant-lubricated contacts.

1.4 Aims

The aim of this research is the experimental investigation of environmentally friendly next generation thermo-fluid with electrodeposited Nickel-based composite coatings incorporating various nanoparticles to improve the tribological performance of contacts in a refrigerant environment. This research will provide concrete and substantial experimental results to critically comment on the tribological performance of future generation of refrigerants. Usefulness of Ni-based Nano-coatings under refrigerant lubrication will be determined based on their friction and wear performance.

1.5 Objectives

Research objectives of this research are listed below:

1) To understand various techniques and methods used for the tribological investigation of refrigerants and develop bespoke testing procedure for tribological bench testing focused on the next generation of refrigerants as green thermo-fluids.

2)   Design & commissioning of experimental bench test incorporating refrigerants as sustainable lubricants and nano-coated interacting systems' components in sealed & controlled environmental conditions.

3)   Study and understand the tribo-mechanistic performance of nickel based nanocomposite coatings for sliding contacts.

4)   Critical evaluation of tribological performance of the next generation of refrigerants subject to uncoated and nano-coated tribo-pairs.

5)   Develop best performing nano-composite coating candidates for the new generation of thermo-fluids as environmentally friendly green lubricants; widely used for energy efficiency.

1.6 Research Methodology

The research methodology adopted for this research project is in conjunction to achieve the set objectives, as follows:

1)   Detailed literature survey for the understanding of the methods and techniques used for the evaluation of the tribological performance of refrigerants.

2)   Modification of the pressurized lubricity tester for studying the friction and wear behaviour of Hydrofluoroethers (HFEs).

3)   Evaluation of friction and wear performance of HFEs using the modified tribo-meter of uncoated steel parts.

4)   Deposition of Nickel based coatings using the pulse coating technique on the disc substrate. Testing of the coated samples under identical testing conditions as uncoated samples for a direct comparison between uncoated and coated results in an effort to enhance the tribological performance of rubbing machine parts operating on systems based on Hydrofluoroethers.

5)   A comparative performance evaluation of the coated and uncoated studies to critically comment and recommend the best performing coatings to be used in a range of operating conditions on systems using Hydrofluoroethers.

The main scope of the project is the in-depth experimental analysis of friction and wear of the thermo-fluid (HFE-7000) and the evaluation of the tribological performance of newly developed Nano-coatings under refrigerant lubrication.

Chapter 2

Literature Review

This chapter provides a comprehensive literature survey focusing on the various methods, techniques and equipment used to study the tribological properties of refrigerants. This chapter provides a detailed review of the development of artificially formulated refrigerants and their tribological investigations along with the key findings. Besides focusing on refrigerants, this chapter also describes the various electrodeposition techniques and the tribological improvements made by using electrodeposited nanocomposite coatings examined under various testing conditions. This in depth literature survey will help identify the future generation of environmentally friendly thermo-fluids, will help in designing and planning the project methodology for the tribological testing of refrigerants, and will assist in identifying the types of nanocomposite coatings that should be used.

2. 1   Tribological Considerations

Tribology is the science of interacting surfaces in relative motion. Interacting surfaces subjected to dry or lubricated contacts may result in the loss of material from the bodies in contact. The removal of material from interacting surfaces is known as wear. Wear is conditional upon various parameters that include contact pressure, lubricant properties (viscosity, pressure-viscosity coefficient, and additives), temperature, surface roughness and contact scenarios (rolling, sliding or impact). A force is produced between two bodies in contact in relative motion, this force is known as friction force. The direction of the friction force is always such as to oppose the motion. Friction force is not a physical property, it is a system property and is influenced by a number of parameters that include, applied load, surface roughness, environment (humidity, oxidation, corrosion, dust, particulate, etc.), type of relative motion (sliding, rotating, rolling, etc.), lubrication condition, type of applied lubricant, inherent lubricity of each surface, relative velocity, shape of contacting bodies and surface hardness. A number of theoretical models have been proposed to model the friction and wear experienced in real world contact problems and these are briefly described in this chapter.

Wear and friction, although closely related, are regarded as separate processes for analysis. An increase in wear does not necessarily infer an increase in friction tough a constant friction

coefficient usually indicates a constant value of wear, any variation being indicative of a change in the lubricant regime or surface film.

2. 2   Wear

All machine finished surfaces have a surface roughness, identified by hills and valleys termed as asperities. The approach of modelling friction and wear relies on having knowledge about various surface properties of the interacting materials and the forces between them. Wear can be broadly divided into two categories depending on the operating conditions, dry wear and lubricated wear. Lubricated and dry wear phenomenon are shown figure 2.1. Dry sliding wear exist when there is no lubricant between the contacting surfaces. In case of using a lubricant between the sliding contacts, the amount of wear depends upon the type of lubricant used and the type of lubrication regime.
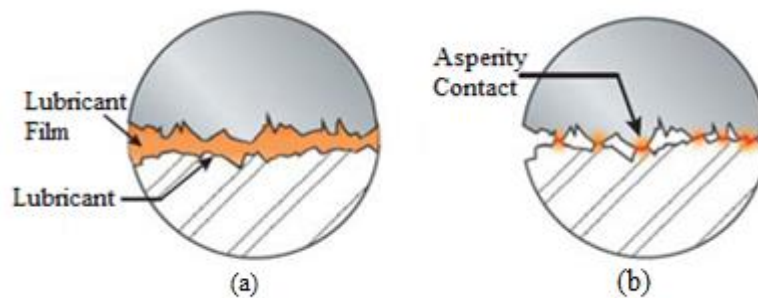
Fig. 2.1. (a) Lubricated Wear (b) Dry Wear (Noria, 2019).

2.2.1 Adhesive Wear

Adhesive wear is the result of localised welding between sliding surfaces. When two surfaces are brought together under load, asperities of the surfaces adhere to each other. The asperities deform elastically and as the asperity contact load is increased they begin to deform plastically. The conditions at the interface of these junctions are similar to those of a cold weld. As the two surfaces separate the welds tend to break away from the junction resulting in material deposition from the softer material to the harder surface (Stolarski, T. A., 1989a). The process of metal transfer due to adhesion is shown in figure 2.2. If adhesive wear is the result of breakdown of lubricating film, the wear can be described as scuffing (Williams, J., 2005).
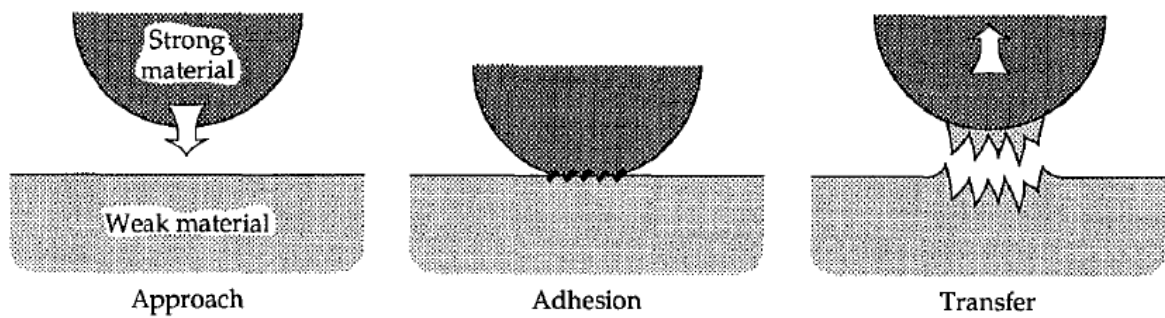
Fig. 2.2. Process of Metal transfer due to Adhesion (Stachowiak, G. W. and Batchelor, A. W., 1993).

2.2.2 Abrasive Wear

Abrasive wear is the process in which a harder material abrades a softer material removing particles from the surface (Bhushan, B., 2013). Abrasive wear can take two forms; two-body abrasive wear and three-body abrasive wear, these abrasive wear types are shown in figure 2.3.
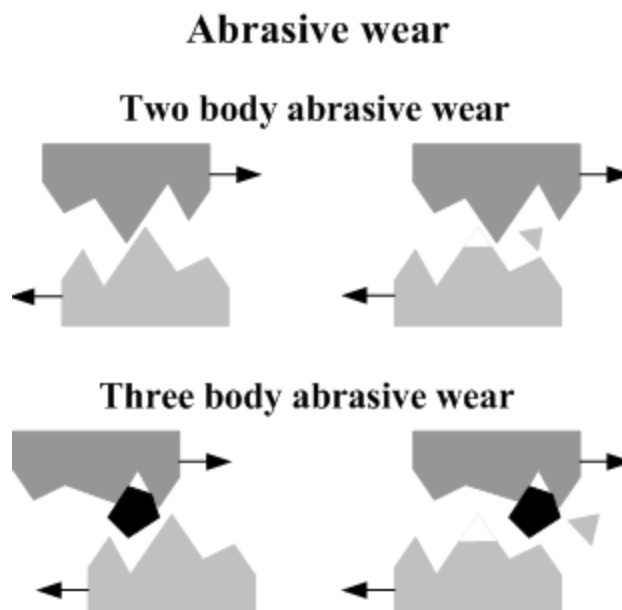
Fig. 2.3. Abrasive Wear types (Stachowiak, G. W. and Batchelor, A. W., 1993).

In two-body abrasive wear the rough surface of the harder material acts to remove the material from the softer surface. Three-body abrasive wear is caused by the hard particles trapped within the interacting parts which act to abrade the surfaces. Three-body wear is much less severe as compared to two-body wear as the particles can break down, be filtered out, or act as surface separation. Abrasive wear can take place as plastic flow, brittle fracture, or as a combination of

both (Hutchings, I. and Shipway, P., 2017). If a trapped particle is significantly harder than the counter-face it will indent the surface causing plastic flow, if the particle is less than 1.2X the hardness of the surface, it will itself be blunted and not indent the counter-face (Hutchings, I. and Shipway, P., 2017). Whilst plastic flow from trapped particles may not be significant, they may cause brittle fracture of both the embedded face and the counter-face (Hutchings, I. and Shipway, P., 2017).

2.2.3   Fatigue Wear

Fatigue wear occurs under cyclic loading when the applied load exceeds the fatigue limit strength of the material. Fatigue cracks start to develop on the surface of the material, a primary crack can originates at the surface at some weak point which propagates downward along weak planes and spreads to the subsurface regions. Delimitation occurs when the cracks get connected to each other resulting in material separation. Fatigue wear mechanism is shown is figure 2.4.
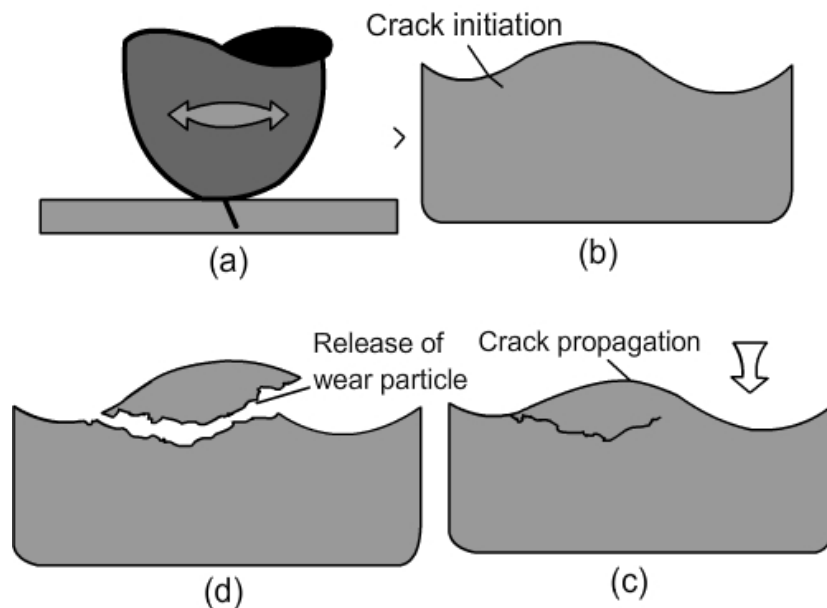
Fig. 2.4. Fatigue Wear (Nptel, 2013).

2.2.4   Corrosive Wear

The degradation of materials as a result of accelerated corrosion between rubbing surfaces is called corrosive wear. Corrosive wear is the combined effect of corrosion and wear and is called tribo-corrosion. It is the chemical wear of materials by a chemical reaction between the contact surfaces and other reactive agents. The reactive agents maybe a lubricant additive or a

compound present in the operational environment. The fundamental cause of corrosive wear is the chemical reaction between the worn surfaces and the corrosive media. Tribo-corrosion is shown in figure 2.5.
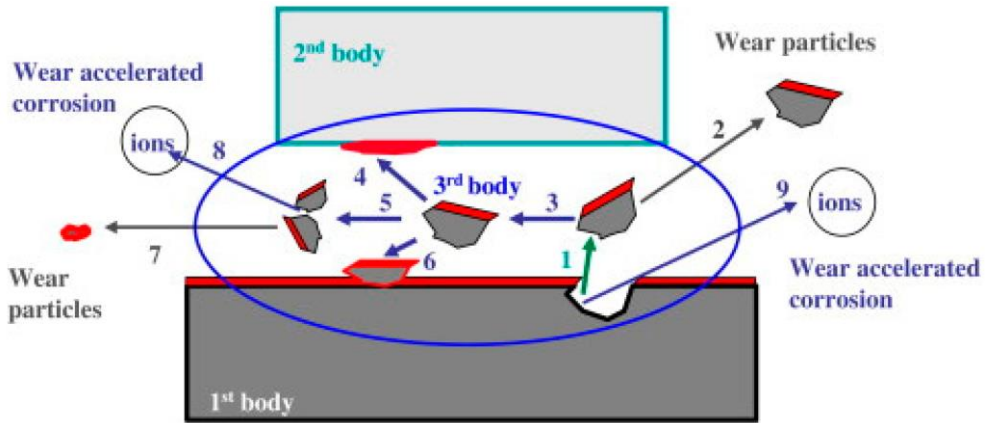
Fig. 2.5. Corrosive Wear (Toh, W. et al., 2018).

2.2.5   Specific Wear Rate

Wear can be expressed as a function of the contact load and sliding distance (equation 1) (Williams, J., 2005).

$$q = \frac{V}{LW}$$

Equation 1

Where q is the specific wear rate (mm^3/Nm), V is the wear volume (mm^3), L is the sliding distance (m) and W is the contact load (N).

2.2.6   Archard Wear Equation

A common starting point to calculate wear is the Archard Wear equation (Archard, J., 1953). Archard proposed a model based on circular contact spots and hemispherical wear particles. The original Archard equation shown below (equation 2).

$$\omega = \frac{KW}{3A_a}$$

Equation 2

Where ω is the wear rate $\left(\frac{N}{m}\right)$, W is the load, K is the probability factor and, A_a is the contact radius.

As mentioned by (Challen, J. et al., 1986), the original Archard equation can be written as equation 3 for sliding contacts.

$$V = \frac{kNL}{3H}$$ Equation 3

Where V is the wear volume, N is the normal force acting between the surfaces in sliding contact, L is the sliding distance and H is the hardness of the wearing surfaces and k is a dimensionless coefficient.

This theory has been confirmed by various experimental results. The Archard wear equation has the following main conclusions:

- The volume of the material removed is proportional to the sliding distance.
- The volume of the material worn is proportional to the applied load.
- The volume of the material removed is inversely proportional to the hardness of the material being worn away.
- The wear rate is independent of the apparent area of contact.

2. 3   Friction

Friction is defined as the force that resists the relative motion of two objects sliding against each other. The understanding of friction has developed gradually over the years with many famous early scientists and engineers contributing to the theory, including Leonardo da Vinci, Guillaume Amontons and Charles-Augustin de Coulomb. These finding can be categorized into three general laws of friction (Dowson, D., 1999) as follows:

1) Friction force is directly proportional to the applied load (Amontons 1st Law).
2) Friction force is independent of the apparent area of contact (Amontons 2nd Law).
3) Kinetic friction is independent of the sliding velocity (Coulomb's Law of Friction).

2.3.1 Coulomb Friction

Coulomb friction model named after Charles-Augustin de Coulomb, is a model used to calculate dry friction force. The model is given by equation 4.

$$F = \mu R$$

<div align="right">Equation 4</div>

Where F is the friction force, R is the normal reaction force at the contact and μ is the coefficient of friction. The coefficient of friction can be divided into two categories; μ_s, coefficient of static friction and μ_k, coefficient of kinetic friction. Static coefficient of friction is used when two bodies are in rest relative to each other and it reflects the force required to cause impending motion. The kinetic coefficient of friction is used when two bodies are in relative motion. Typically the value of the static coefficient of friction is more than the value of the kinetic friction coefficient.

2.3.2 Adhesive Friction

Adhesive component of friction is calculated by first considering the real area of contact (equation 5), this is a function of the material yield strength of the softer surface and the applied load (Ludema, K. C., 1996).

$$A_r = \frac{W}{Y_s}$$

<div align="right">Equation 5</div>

Where A_r is the real are of contact, W is the applied load and Y_s is the yield strength of the softer material.

Adhesive friction is modelled as the load required in breaking asperity adhesions such that the shear strength of the softer material can be used to calculate the friction force (equation 6) (Bowden and Tabor 1950).

$$F = A_r \tau$$

<div align="right">Equation 6</div>

Where F is the friction force, A_r is the real are of contact and τ is the shear strength of the softer material.

In the case of a sliding contact when the reaction is equal to the normal applied load, equation 4, equation 5 and equation 6 can used to drive the expression of the coefficient of friction in terms of the shear strength and yield strength (equation 7).

$$\mu = \frac{\tau}{Y_s}$$
<div align="right">Equation 7</div>

2.3.3 Abrasive Friction

Abrasive wear is modelled similar to adhesive wear, with the hard asperity considered to be ploughing through the softer surface (Hutchings, I. and Shipway, P., 2017). Ploughing of a single asperity is given as (equation 8) (Hutchings and Shipway 1992).

$$\mu_p = \left(\frac{2}{\pi}\right)tan\theta$$
<div align="right">Equation 8</div>

Real life asperities rarely have a slope (θ) more than $5 - 6°$, which means that the friction coefficient would be approximately 0.04. In reality the pileup of the material infront of the asperity would mean that μ_p is significantly higher.

2. 4 Lubricated Wear

The classical Archard wear equations did not take into account the effects of lubricants. To counter this, a number of attempts have been made to incorporate some aspect of lubrication into the equations. Archard and Kirk's (Archard, J. and Kirk, M., 1962) point contact experiments indicated that lubricating films can persist under low speed, lightly loaded conditions, and at higher speeds plastic flow can occur before plastic breakdown. The concept of fractional film defect allowing the wear to be correlated with effectiveness of the lubricant was introduced by Rowe (Rowe, C. N., 1966), however his work did not take into account that the total load was supported by the lubricating film and the contacting asperities, thus it was subjected to some variability compared with the experimental results. The model was further developed by Thompson and Bocchi (Thompson, R. A. and Bocchi, W., 1972), but their approach did not take into account the role of the lubricant in mitigating adhesive wear. In the coming years Stolarski presented a model (Stolarski, T. A., 1979) for the adhesive wear of lubricated contacts, which was further developed to include scuffing (Stolarski, T. A., 1989b) and wear prediction (Stolarski, T., 1996).

2.4.1 Lubrication Regimes

The main purpose of the lubricant is to provide asperity separation by creating a lubricating film, the thickness of which depends upon the contact pressure, on the pressure-viscosity coefficient of the lubricant, lubricants viscosity, the elastic moduli of the interacting materials, the type of contact made by the interacting parts (point contact, line contact, area contact) and the velocities of the rubbing surfaces. A lubricant can form different regimes depending on these parameters and affect wear and friction characteristics accordingly. Under lubricated tribo-test conditions the rubbing surfaces can be presented by a thin lubrication film. The lubricant film separation is used to identify the type of lubrication regime. The minimum film thickness between surfaces in contact can be calculated using the analytical work done by (Chittenden, R. et al., 1985a, 1985b; Dowson, D., 1999; Hamrock, B. and Dowson, D.; Hamrock, B. J. and Dowson, D., 1977, Jan 01, 1981). The elastohydrodynamic film thickness expression for calculating the film thickness for a point contact is given in equation 9.

$$H_{min} = 3.63 U^{0.68} G^{0.49} W'^{-0.073}(1 - e^{-0.68k}) \qquad \text{Equation 9}$$

Where H_{min} is the dimensionless minimum film thickness, U is the dimensionless speed parameter, G is the dimensionless material parameter, W' is the dimensionless load parameter and k is the ellipticity parameter. The dimensionless speed parameter is defined by equation 10.

$$U = \frac{V_e \eta_0}{RE'} \qquad \text{Equation 10}$$

Where V_e is the mean lubricant entraining velocity, η_0 is the lubricant viscosity at atmospheric temperature and pressure, R is equivalent radius of curvature and E' is the equivalent modulus of elasticity. The dimensionless material parameter is defined by equation 11.

$$G = \alpha E' \qquad \text{Equation 11}$$

Where α is the pressure-viscosity coefficient of the lubricant and E' is the equivalent modulus of elasticity. The expression for calculating the dimensionless load parameter is given in equation 12.

$$W' = \frac{W}{E' R_x R_y} \qquad \text{Equation 12}$$

Where W is the load, R_x is effective radius in X direction, R_y is the effective radius in Y direction and E' is the equivalent modulus of elasticity. The ellipticity parameter is defined by equation 13.

$$k = \left(\frac{R_y}{R_x}\right)^{\frac{2}{\pi}}$$

<div align="right">Equation 13</div>

Where R_x is effective radius in X direction and R_y is the effective radius in Y direction. The equivalent modulus of elasticity is defined by equation 14.

$$E' = \frac{2}{\left\{\left[\frac{(1-v_1{}^2)}{E_1}\right] + \left[\frac{(1-v_2{}^2)}{E_2}\right]\right\}}$$

<div align="right">Equation 14</div>

Where v_1 is the Poisson ratio of the first material, v_2 is the Poisson ratio of the second material. E_1 is the elastic modulus of the first material and E_2 is the elastic modulus of the second material.

For a spherical ball on flat contact the ball has equivalent radius in both X and Y direction resulting in the ellipticity parameter equal to 1. The equivalent radius of curvature R can be calculated as given in equation 15.

$$\frac{1}{R} = \frac{1}{R_1} + \frac{1}{R_2}$$

<div align="right">Equation 15</div>

Where R is the equivalent radius of curvature, R_1 is the radius of the first ball and R_2 is the radius of the second ball. For a ball of flat contact geometry the radius of the second ball is taken as infinite resulting in the expression given in equation 16.

$$R = R_1$$

<div align="right">Equation 16</div>

Which means the equivalent radius of curvature for a spherical ball on flat geometry is equal to the radius of the ball. The actual film thickness is the product of the dimensionless minimum film thickness and the equivalent radius of curvature (equation 17).

$$h_{min} = H_{min} R$$

<div align="right">Equation 17</div>

Plotting the coefficient of friction against Hersery Number which is the defined as $\left(\frac{Sliding\ Speed\ \times Lubricant\ Viscosity}{Normal\ Load}\right)$ results in the Stribeck Curve as

shown in figure 2.6. The calculated film thickness can be used in conjunction with equation 18 to calculate the specific film thickness (λ). The value of (λ) can supplement the Stribeck curve providing a more generalized relationship between the film thickness and the coefficient of friction.

$$\lambda = \frac{h_{min}}{\sqrt{R_{qA}^2 + R_{qB}^2}}$$

Equation 18

Where R_{qA} and R_{qB} are the values of the surface roughness of the two interacting bodies.

Specific film thickness can be used to distinguish and define different lubrication regimes in a Stribeck curve. There are three distinguishable lubrication regimes as shown in figure 2.6, these can be distinguished based on the values of λ. When λ is greater than 3, the film thickness is greater than the separation of the surface asperities and the load is fully supported by the lubrication film, this is full elastohydrodynamic lubrication (EHDL). If λ is between 3 and 1, then the surface separation is incomplete and asperity contact is possible resulting in a partial or mixed lubrication regime. λ less than 1 results in boundary lubrication.
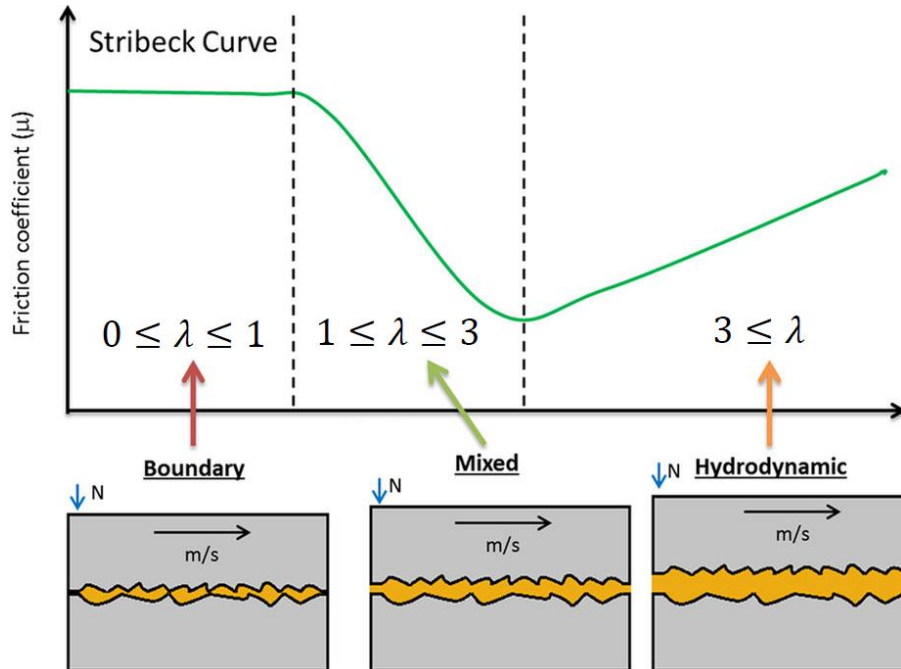
Fig. 2.6. Stribeck Curve (Robinson, J. W. et al., 2016).

Maximum Hertzian Stress for point contact can be calculated by using equation 19 (Hertz 1882; Johnson 1987).

$$P_{max} = \frac{3F}{2\pi a^2}$$

Equation 19

Where a is the radius of contact and is determined using equation 20 (Hertz 1882; Johnson 1987).

Equation 20

$$a = \sqrt[3]{\frac{3F\left[\frac{1-v_1^2}{E_1} + \frac{1-v_2^2}{E_2}\right]}{4\left(\frac{1}{R_1} + \frac{1}{R_2}\right)}}$$

The analytical equations described in sections 2.2, 2.3 and 2.4 were developed for non-lubricated testing conditions or by using lubricating oils. However these equations can be used with confidence for oil/refrigerant mixtures and refrigerants alone (Akei, M. and Mizuhara, K., 1997; Morales-Espejel, G. E. et al., 2015; Muraki, M. et al., 2000; Tanaka, S. et al., 2003; Vergne, P. et al., 2015; Wardle, F. et al., 14-17 July, 1992, Purdue University, Indiana, USA, paper 843).

2. 5 Refrigerants

The use of refrigerants dates back to ancient times when water vaporization and other evaporation processes were used as a means of cooling (Calm 2008b; Bhutta et al. 2018b). The earlier commonly used refrigerants were mostly naturally occurring compounds and were used on the basis of *whatever* worked (Calm 2008a). Almost all of these refrigerants were flammable or toxic, and some also had high reactivity. Some of these included Propane, Ammonia, Sulfur Dioxide, Methyl Formate, Carbon Tetrachloride etc. The refrigerants that were non-reactive, non-hazardous and non-flammable such as water and carbon dioxide had thermodynamic limitations making their use difficult in domestic and commercial applications. A number of investigators in different countries studied phase-change physics in 1600s and 1700s which laid the foundation of artificially formulated refrigerants. A system that used a volatile fluid to produce ice in a closed cycle was first described by Oliver Evans (Evans, O., 1805). The proposed refrigeration system which has no record of being actually built, used Ether as a refrigerant under vacuum. Ether was to be evaporated under vacuum and the vapours were to be pumped to a water cooled heat exchanger to condense for reuse. Perkins probably influenced by

this idea built the first working machine that used mechanical vapour-compression cycle. Perkins 1834 patent describes the use of a volatile fluid for the purpose of cooling/freezing, and at the same time condensing the fluid for reuse without waste (Perkins, J., 1834).

The search for a replacement refrigerant that would be colourless, odourless, tasteless, nontoxic, and non-flammable in the late 1920s by General Motors Research Corporation led to the development of Dichlorodifluoromethane (CFC-12), Trichlorofluoromethane (CFC-11), Chlorodifluoromethane (HCFC-22), Trichlorotrifluoroethane (CFC-113), and Dichlorotetrafluoroethane (CFC-114). Commercial production of CFC-12 started in 1931 followed by CFC-11 in 1932.

Chlorofluorocarbons (CFCs) and Hydrochlorofluorocarbons (HCFCs) possessed excellent thermodynamic properties as refrigerants besides being non-flammable and nontoxic. This made them the ideal refrigerants of their time, especially for use in small commercial, automotive and residential refrigeration applications.

It was discovered that the ozone layer which surrounds the earth's atmosphere and protects us from harmful ultraviolet radiations from the sun was depleting. Man-made chemicals which included halocarbon refrigerants, solvents, propellants, and foam-blowing agents (CFCs, HCFCs, halons) were termed to be the main cause of the ozone depletion. Destructive effects of CFCs on the stratospheric ozone layer were first published in 1974 by (Molina, M. J. and Rowland, F. S., 1974), this work clearly stated that CFCs can remain in the atmosphere from 40 to 150 years and lead to the destruction of the ozone layer by chemically reacting with it. Vienna Convention for the Protection of the Ozone Layer in 1985 was followed by the Montreal Protocol on Substances that Deplete the Ozone Layer in 1987 (Nations, U.), banned the use of CFCs by the end of year 1995 in developed countries. HCFCs which had a lower ozone depletion potential (ODP) as compared to CFCs were suggested as intermediate refrigerants. Different countries adapted different phase out time lines for HCFCs.

The use of refrigerators, freezers and air-conditioners had become common in everyday life and were being widely used on a commercial and domestic level. This meant the development of a replacement refrigerant was imperative. This led to the introduction of HFCs. HFCs which had zero ODP, displayed thermodynamic properties matching CFCs (Eckels, S. J. and Pate, M. B., 1991; Khan, S. H. and Zubair, S. M., 1993). Mineral oils that showed good miscibility with CFCs and HCFCs, unfortunately were not compatible with HFCs. HFCs showed poor compatibility and miscibility in mineral oils. Synthetic oils with various additives were

developed for HFCs. Having good thermodynamic properties and zero ODP, HFCs became the replacement refrigerants for CFCs and HCFCs.

In 1997 Kyoto protocol to the United Nations Framework Convention on Climate Change (Nations, U., 1998) established binding limits on emissions of carbon dioxide and other greenhouse gases (GHG). The main source of the greenhouse emissions is the consumption of fossil fuel which produces carbon dioxide. Nitrous Oxide, Methane, Perfluorocarbons (PFCs) and Hydrofluorocarbons were identified as the other main contributors to global warming (Breidenich, C. et al., 1998). HFCs were recognized as major contributors to global warming and a phase out of HFCs has been planned for the coming years. A ban on non-confined direct evaporation systems using HFCs and PFCs was imposed in 2007. All F gases having 150 or more global warming potential will be banned as refrigerants in any hermetically sealed system from the year 2022.
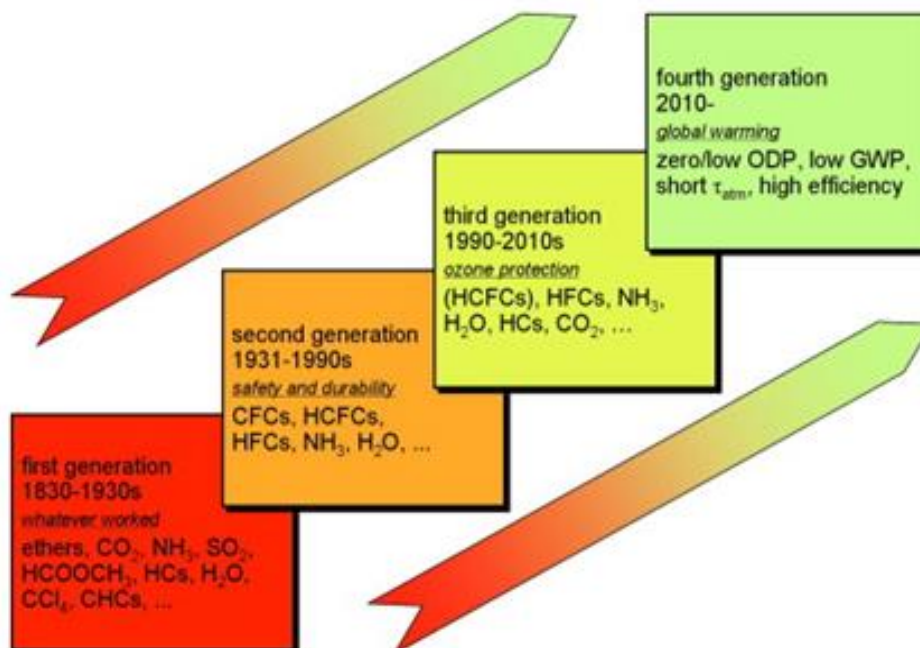
Fig. 2.7. Refrigerant progression (Calm, J. M., 2008).

These international regulations and bans have forced the refrigerant manufacturers and the air conditioning and refrigeration industry to find alternative refrigerants yet again. Figure 2.7 shows the progression of refrigerants over the years along with a highlight of the coming generation of refrigerants. The challenge to come up with refrigerants which not only have the

thermodynamic properties matching their predecessors but also having very low ozone depleting potential (ODP) and low global warming potential (GWP) is even greater.

The refrigerant industry has come up with potential future generation refrigerants having zero OPD, low GWP and low flammability. Some of these refrigerants are already being charged in automotive and domestic air-conditioning and refrigeration systems. There has also been an inclination to shift towards natural refrigerants such as carbon dioxide and avoid the use of chemically formulated coolants which have proven to be harmful to the earth's atmosphere one way or another.

2. 6   Refrigerants and Tribology

Refrigerants directly affect the tribological performance of interacting components. Since the introduction of artificially formulated refrigerants, the types of refrigerants used in compressors have changed over the years. Apart from evaluating the physical, chemical and thermodynamic properties of refrigerants, the refrigerants have also been studied from a view point of tribology by various researchers worldwide. Changing a refrigerant in a compressor not only has an effect on the thermodynamic cycle but also effects the lubricants viscosity, lubricants pressure-viscosity coefficient, oil film thickness, lubricant/refrigerant miscibility, friction, wear, durability, reliability and overall power consumption. Refrigerants have been studied from a view point of tribology by varying the contact geometries, by using different lubricating oils with and without additives, by altering the environmental pressure/temperature, by changing the phase of the refrigerant, by using different interacting materials and by applying numerous surface treatments. This section of the thesis covers the various tribological studies carried out on refrigerants, with focus on refrigerants used in domestic appliances, automobile air-conditioning systems, and small scale industrial and commercial applications.

Ranging from chemically formulated to natural refrigerants, there are a variety of refrigerants available for use. The selection of a refrigerant depends on its application and place of use. Environmental legislations have banned the use of certain refrigerants over the years. Different researchers used different apparatus and varying geometries for the tribological analysis of refrigerants. Most of the studies are concerned with the investigation of an oil/refrigerant mixture, however some researchers have used a refrigerant only for their study. The reason for choosing oil/refrigerant mixture by most of the researchers is that in actual compressors the refrigerant gets mixed with the lubricating oil and the oil/refrigerant mixture then dictates the lubricating properties in a compressor. On the other hand some of the researchers suggest that if

the true friction and wear properties of a refrigerant are to be investigated, then the refrigerant should be tested independently from the lubricating oil.

Almost all of the past studies have used the refrigerant in gaseous phase with the exception of a few investigators who used the refrigerants in liquid state in their study. Most refrigerants are in the gaseous phase under standard room temperature and pressure. The refrigerants are also mostly in gaseous phase when in a compressor is why most of the investigations are concerned with the refrigerant in vapour form. However the refrigerant does undergo a phase change in a refrigeration cycle and turns from gas to liquid and then from liquid back to vapour. According to some researchers the true properties of a refrigerant as a lubricant can only be assessed in liquid phase independent of a lubricating oil. Table 2.1 lists the commonly used refrigerants that have been previously used in domestic, commercial and automotive applications along with potential future generation refrigerants. Table 2.1 also shows the ODP, GWP and flammability of these refrigerants which are extremely important characteristics of any refrigerant.

Table 2.1 Commonly used and potential next generation refrigerants.

Refrigerant	ODP	GWP*	Flammability	Generation	Type
CFC-12	1.00	10,900	Non-flammable	Past	Artificial
CFC-114	1.00	10,000	Non-flammable	Past	Artificial
HCFC-22	0.05	1,810	Non-flammable	Past	Artificial
HCFC-123	0.060	77	Non-flammable	Past	Artificial
HFC-134a	Zero	1,430	Non-flammable	Past	Artificial
HFC-32	Zero	675	Non-flammable	Past	Artificial
HFC-125	Zero	3,500	Non-flammable	Past	Artificial
HFC-407C	Zero	1,774	Non-flammable	Past	Artificial
HFC-404A	Zero	3,922	Non-flammable	Past	Artificial
HFC-245fa	Zero	1,030	Non-flammable	Past	Artificial
HFC-410A	Zero	2,088	Non-flammable	Past	Artificial
HC-600a	Zero	3	High	Future	Natural
HC-290	Zero	3.3	High	Future	Natural

HC-1270	Zero	0.01	High	Future	Natural
R-744	Zero	1.00	Non-flammable	Future	Natural
HFO-1234yf	Zero	4.00	Mild	Future	Artificial
HFO-1233zd	0.0002	1.00	Non-flammable	Future	Artificial
HFE-245mc	Zero	622	Non-flammable	Future	Artificial
HFE-347mcc3	Zero	530	Non-flammable	Future	Artificial

2.6.1 Chlorofluorocarbons (CFCs) and Hydrochlorofluorocarbons (HCFCs)

CFCs are chemicals containing atoms of Chlorine, Carbon and Fluorine. These non-flammable and nontoxic chemicals were used as solvents, blowing agents for packing materials and foam, in the manufacturing of aerosol sprays, and as refrigerants. CFC-12 was the first artificially formulated refrigerant which went into mass production in 1931. It was extensively used in numerous applications since its development because of its excellent thermodynamic properties. Besides being nontoxic and non-flammable the thermodynamics qualities of CFC-12 made it an ideal candidate of its time for automotive, domestic and small scale commercial air-conditioning and refrigeration systems. Production of CFCs was banned by the end of 1995 in developed countries and from the year 2010 in developing countries by the Montreal Protocol.

HCFCs are a group of compounds, whose structure is very close to that of Chlorofluorocarbons (CFCs), but include one or more hydrogen atom. HCFCs were also used as refrigerants in freezers, refrigerators and air-conditioning systems. HCFCs structure resembles closely to CFCs, however HCFCs have lower ODP and lower GWP values compared to CFCs. The use of HCFCs was allowed for a longer period of time due to their lower environmental impact compared to CFCs. HCFCs were also allowed as intermediate refrigerants while switching from CFCs to HFCs. However, the use of HCFCs in new equipment was banned in 2001 in UK. Amongst HCFCs, HCFC-22 was the most popular one. It was commonly used in process cooling, in automobile air conditioning systems, in small scale industrial units and in domestic refrigerators.

Various investigations on the tribological performance of CFCs and HCFCs have been carried out in the past. Table 2.2 summarizes these studies and their findings with consideration of the interacting materials. The testing equipment used for the investigations are also mentioned in this table along with the type of contact geometries used. CFC-12 and HCFC-22 that contain Cl

showed excellent tribological performance. The friction and heat causes the chlorine in HCFC-22 and CFC-12 to form protective tribo-films on the top surfaces, which helps in improving the friction and overall wear. These tribo-films are not only formed under extreme testing conditions but are easily formed under normal compressor operating conditions as well (Fujimoto, S. et al., 1984, Purdue University, Indiana, USA, paper 477). CFCs and HCFCs were used with mineral oils in compressors, the refrigerants have a strong effect on reducing the oil film forming capability and in reducing the lubricants viscosity (Akei, M. et al., 1996; Kruse, H. and Schroeder, M., 1985; Wardle, F. et al., 14-17 July, 1992, Purdue University, Indiana, USA, paper 843). Besides decreasing the lubricants viscosity it was also found that greater amounts of dissolved refrigerant in the oil reduces the pressure-viscosity coefficient as well (Akei, M. and Mizuhara, K., 1997; Wardle, F. et al., 14-17 July, 1992, Purdue University, Indiana, USA, paper 843). The value of the coefficient of friction and frictional coefficient fluctuations have been reported to decrease with increasing load (Kawahara, K. et al., 23-26 July, 1996, Purdue University, Indiana, USA, paper 1141; Mizuhara, K. et al., 1994), indicating that these refrigerants have positive effects on friction. A study (Ciantar, C. and Hadfield, M., 2004) has also shown that the electrical energy consumption of a compressor improves substantially with CFC refrigerants as compared to HFC refrigerants.

Table 2.2 Summary of the tribological testing of CFCs & HCFCs.

Study	Refrigerant	Apparatus	Interacting Materials	Contact Geometries	Surface Treatment	Key findings
(Fujimoto, S. et al., 1984, Purdue University, Indiana, USA, paper 477)	HCFC-22	Modified Piston Compressors	1) Ferrous Bearing against Cast Iron journal 2) Nonferrous Bearing against Cast Iron journal	Bearing against Journal	None	• Increasing refrigerant concentration in oil decreases scuffing load for nonferrous metals • Increasing refrigerant concentration in oil increases scuffing load for ferrous metals
(Davis, B. et al., ACRC Technical Report 19, May 1992)	1) CFC-12 2) HFC-134a	High Pressure Tribometer	1) Hardened Tool Steel Pin against hardened Cast Iron Plate 2) Circular Bronze shoe against rotating Hardened Ductile Cast Iron Plate 3) Hardened Mild Steel Pin against Aluminium Pad	1) Counter-formal 2) Formal 3) Area	None	• Surface films were formed in case of using CFC-12 resulting in lower wear • HFC-134a environment resulted in more wear and produced no surface films
(Mizuhara, K. et al., 1994)	1) CFC-12 2) HFC-134a	Friction and Wear Tester	Leaded Bronze Disk against Cast Iron ring	Ring-on-disk	None	• Protective surface films formed under normal compressor operating conditions only by CFC-12 • Protective surface films formed by both HFC-134a and CFC-12 under sever operating conditions
(Sheiretov, T. et al., 19-22 July, 1994, Purdue University, Indiana, USA, paper 964)	1) CFC-12 2) HFC-134a	High Pressure Tribometer	Ni-Cr-Mo Gray Cast Iron plates against surface treated M2 tool Steel Pins	Cylindrical pin on flat plate	1) Boronizing 2) Gas Nitriding 3) Ion Nitriding 4) Liquid Nitriding 5) TiN Coating	• CFC-12 showed lower wear compared to HFC-134a in all the cases • Boronizing, Ion Nitriding and Liquid Nitriding did not offer any tribological advantage over hardened M2 steel • Gas Nitriding produced a very brittle case and is unsuitable for M2 steel • TiN coating resulted in lower wear but showed higher coefficient of friction
(Muraki, M. et al., 23-26	1) HCFC-22 2) HFC-134a	Tribometer	Nickel Chromium Molybdenum Steel ring against alloy Tool Steel	Block-on-ring	None	• HCFC-22 atmosphere resulted in the least amount of wear compared to all other HFCs

July, 1996, Purdue University, Indiana, USA, paper 336)	3) HFC-407C 4) HFC-404A					• Various anti-wear additives in POE improve the performance of HFC refrigerants • Based on the formation of metal fluorides which depends on the solubility of HFCs in oils, can effectively prevent adhesion and reduce wear
(Kawahara, K. et al., 23-26 July, 1996, Purdue University, Indiana, USA, paper 1141)	1) CFC-12 2) HCFC-22 3) HFC-32 4) HFC-134a 5) HFC-125	Tribometer	Rolling Bearings of Steel	Shell Four Ball Tester	None	• CFC-12 and HCFC-22 that contain Cl showed the maximum seizure load representing effect of Extreme Pressure • The F in HFCs also chemically reacted with steel and showed Extreme Pressure effect

These studies indicate that although these refrigerants decrease the lubricants viscosity, the pressure-viscosity coefficient of the oil and the overall film thickness, however CFCs and HCFCs possess Extreme Pressure properties and have the capability to from protective tribo-films on the rubbing surfaces which have a positive effect on the overall tribological performance.

2.6.2   Hydrofluorocarbons (HFCs)

HFCs are synthetically produced refrigerants containing Hydrogen, Fluorine and Carbon. HFCs were introduced after the Montreal Protocol. The Montreal Protocol which focused primarily on the reasons for the depletion of the ozone layer put restrictions and bans on the production and use of CFCs and HCFCs. HFCs had thermodynamic properties matching their predecessors (Eckels, S. J. and Pate, M. B., 1991; Khan, S. H. and Zubair, S. M., 1993; Shankland, I. R. et al., 1988, Purdue University, Indiana, USA, paper 41; Spauschus, H., 1988; Wilson, D. P. and Basu, R. S., 1988), which resulted in their extensive use as replacement refrigerants. Since the early 1990s, HFCs have been widely used in a number of different fields and applications. The global warming implications of HFCs were not considered at the time of their introduction, however the high global warming impact of HFCs was realized later. Kyoto Protocol addressed the damaged being done to the global atmosphere and the responsible attributes and chemicals causing global warming. A restriction was put on HFCs and HFCs are now in the process of being phased out. The phase out of HFCs started in 2015 in Europe. By the end of 2030 it is expected that HFC availability will be cut by 79% in Europe (Bhutta et al. 2018b).

HFCs remain the most investigated refrigerants from the tribological view point. This is because of their unique position in history. HFCs were initially compared to their predecessors to see how they performed compared to CFCs and HCFCs. A number of studies showed that HCFCs and CFCs have better tribological performance as compared to HFCs especially while being operated in a compressor atmosphere. Various additives and different blends of synthetic oils were developed and investigated to improve the performance of HFCs over the years. CFCs and HCFCs were used as a benchmark to analyse HFCs. After being introduced in the market on a commercial scale, further studies were still conducted on HFCs to look at their behaviour under various different operating conditions. Now a days the potential successors of HFCs are being compared with HFCs to evaluate their performance. Most of the new studies involve the use of future generation refrigerants and their comparison to HFCs. This helps making a comparison between the various refrigerants under identical operating/testing conditions.

Amongst the HFC refrigerants, 1,1,1,2-tetrafluoroethane (HFC-134a) has been the most tested and investigated refrigerant from the view point of tribology. This is because HFC-134a was deployed for systems that previously used CFC-12 and HCFC-22. A number of studies involving HFCs are discussed

below. HFCs are also discussed alongside CFCs, HCFCs, natural and future generation refrigerants. Various tribological studies performed on HFCs have been summarized and are presented in table 2.3.

Table 2.3 Summary of the tribological testing of HFCs.

Study	Refrigerant	Apparatus	Interacting Materials	Contact Geometries	Surface Treatment	Key findings
(Ishida, Y. et al., 1996)	HFC-134a	Tribometer	High Carbon Chromium Bearing Steel Balls	Four Ball Tester	None	• Wear configuration changed from adhesive to corrosive with an increase in refrigeration concentration • A certain fraction of HFC-134a exists that can minimize the wear amount
(Nishiwaki, F. et al., 23-26 July, 1996, Purdue University, Indiana, USA, paper 1117)	HFC-407C	Friction Test Machine	Eutectic Graphite Cast Iron Orbit against Carbon Tool Steel Plate	Orbiting Thrust Bearing in a vessel filled with Refrigeration/Oil mixture	1) Surface roughness of orbiting specimens were between $0.28 - 0.49\ \mu m$ 2) Fixed specimens types: a) Thrust Plate b) Palin Disk c) Single- Grooved d) Double- Grooved	• The friction losses decreased by reducing the surface roughness • The friction losses also reduced by making oil groove • The friction losses increased with increasing load • The friction losses also increased by increasing the orbiting speed
(Sheiretov, T. et al., ACRC Technical Report 92, 1996; Yoon, H. et al., 1998)	1) HCFC-22 2) HFC-134a 3) HFC-407C 4) HFC-410A	High Pressure Tribometer	Carburized Steel Pin against Various Aluminium Alloy Discs	Pin-on-disc	Aluminium discs compositions: 1) HV3 Extruded-T6 2) HV3 Extruded-T4 3) HV4 Squeeze Casted-T61 4) C278 Extruded-T4 5) Die Casted 390-T6 6) 390 Permanent Moulded-T61 7) 356 Die Casted- Untreated 8) 356 Permanent Moulded-T61 9) 356 Coupon Moulded-Untreated 10) 356 Coupon Moulded-T61 11) Coupon Moulded- Anodized 356 12) Die Casted- SiC-AL	• Die Casted discs showed the lowest wear which had the highest hardness • Conventional anodizing did not improve the wear resistance of aluminium alloys • SiC particle reinforcement and hard anodizing provided very good wear resistance • HFCs at high partial pressures increased the brittles of aluminium alloys • Corrosion cracking was viewed as a possible failure mechanism

(Chul Na, B. et al., 1997)	1) CFC-12 2) HFC-134a	Tribometer	Tribo-test: 1) Steel disk against Steel ball 2) Steel disk against Steel pin Compatibility test: 1) Steel with HFC-134a and PAG 2) Copper with HFC-134a and PAG 3) Aluminium with HFC-134a and PAG 4) Stainless Steel with HFC-134a and PAG 5) Silicon with HFC-134a and PAG 6) Turcon with HFC-134a and PAG 7) Viton with HFC-134a and PAG 8) Rubber with HFC-134a and PAG	Tribo-test: 1) Ball-on-disk 2) Pin-on-disk Compatibility test: Immersion of each metals/polymers in HFC-134/PAG mixtures for three months	None	• O-ring made of normal rubber got degraded in HFC-134a/PAG mixture • The other polymers showed no degradation • Metals did not show any corrosion in HFC-134a/PAG environment • Higher viscosity oils are advantageous for improving wear characteristics • HFC-134a/PAG mixtures showed excellent lubricity in extreme contact pressure condition • HFC-134a/lubricant mixtures have the capability of showing similar lubricity to that of CFC-12/lubricant mixtures
(Safari, S. and Hadfield, M., 1998)	HFC-134a	Commercial Compressor	High Silicon Alloy Connecting-Rod against Mild Steel Gudgeon-Pin	Connecting-Rod and Gudgeon-Pin	None	• Lubricant with the least viscosity showed very severe wear • The degree of refrigeration dilution has an effect in supporting the lubricant to be carried up to the connecting-rod/gudgeon-pin interface
(Yamamoto, Y. and Gondo, S., 1998)	HFC-134a	Tribometer	Reciprocating Bearing Steel Ball against stationary Bearing Steel Plate	Ball-on-plate	None	• PAG showed good wear and friction characteristics in HFC-134a environment by forming fluoride on the rubbing surfaces • POE displayed poorer friction and wear characteristics above a transit temperature because an adsorbed POE

Reference	Refrigerant	Equipment	Test Description	Configuration	Materials	Findings
						• film prevented the formation of fluoride • POE however produced very good tribological performance at temperatures below the transient temperature
(Matsuura, H. et al., 14-17 July, 1998, Purdue University, Indiana, USA, paper 1276)	1) HCFC-22 2) HFC-407C	Tribometer	Different types of Aluminium Alloys against Cast Iron	Pin-on-disk	Two different Aluminium alloys with varying Silicon content against Cast Iron	• HCFC-22/mineral oil resulted in noticeable lesser wear as compared to HFC-407C/PVE • Increasing the silicon content in the aluminium alloys showed that it was possible for HFC-407C/PVE to have wear as low as HCFC-22/mineral oil
(Sung, H. C., 1998)	HFC-407C	Tribometer	Ni–Cr–Mo Gray Cast Iron Disk against Vanes comprising of various coatings and materials	Vane-on-disk	Vane compositions: 1) Original-High speed tool Steel (Hv-950) 2) Arc Ion Plated TiN(I) (Hv-1900) 3) RF Magnetron Sputtered TiN(II) (Hv-(1600-1800)) 4) Arc Ion Plated TiAIN (Hv-2700) 5) Magnetron Sputtered WC/C (Hv-100) 6) Dual Ion Beam Sputtered DLC (Hv-2000) 7) Carbon (Hv-458) 8) Pulse Plasma Nitriding Ion Nitriding (Hv-1150)	• TiAlN and DLC are very hard coatings and are not suitable, because they produced high friction and severe wear on the disks • TiN coated vane showed good wear resistance • Ion plating showed lesser wear compared to magnetron sputtering • Ion nitriding proved unsuitable as it was not good enough to sustain the cyclic stress • WC/C coating showed the best tribological performance which was probably due to the formation of a durable tribo-film on the mating surfaces
(Yoon, H. et al., 2000)	HFC-134a	High Pressure Tribometer	Rotating 390-T6 Aluminium-Silicon Disc against Stationary 52100 Steel Shoe of various geometries Types of Shoe Geometries used:	Shoe-on-disk	Tin coatings applied to 390-T6 AI discs	• Crowning helps the shoe/plate contact generate hydrodynamic films • The groove or dimple helps trap lubricant and debris during operation. However the groove or dimple can be detrimental under starved lubrication conditions

			1) Crowned Shoe 2) Crowned Shoe with Dimple 3) Crowned Shoe with a Groove 4) Flat Shoe			• The geometries with a dimple or groove in the crowned shoe resulted in higher peek pressures and temperatures • The effect of tin coatings showed that coated discs offer better scuffing resistance than the uncoated discs • Tin coating acted as a temporary lubricant and also aided initial running-in by covering surface irregularities
(Ciantar, C. et al., 2000)	HFC-134a	Actual Hermetically Sealed Compressors	Hardened Steel Gudgeon Pin against Die-cast Aluminium Alloy Connecting Rod	Conforming Contact between Gudgeon Pin and Connecting Rod of a Compressor	None	• PVE lubricant was more chemically active on the interfaces as compared to POE • Protecting film deposits on the valve plate were less pronounced for PVE as compared to POE • No clear difference was seen in the tribological performance of PVE and POE lubricants
(Tanaka, S. et al., 2003)	HFC-134a	Tribometer	Rotating JIS SUJ-2 Steel Ball against stationary CaF_2 Disk	Ball-on-disk	None	• Decrease in refrigerant concentration at the inlet region increased the elastohydrodynamic lubrication film thickness • The concentration distribution of HFC-134a got affected by the oil temperature, the sliding velocity and the refrigerant concentration in the lubricant
(Ciantar, C. and Hadfield, M., 2004)	1) HFC-134a 2) CFC-12	Rig comprising of a Reciprocating Hermetic Compressor	Aluminium Alloy Connecting Rod against the Gudgeon Steel Pin	Conforming Contact between Gudgeon Pin and Connecting Rod of a Compressor	None	• Electrical energy consumption of the compressor improved substantially with CFC-12 as compared to HFC-134a • The overall analysis concluded that HFC-134a based domestic refrigerators will contribute more towards the environmental damage as compared to CFC-12
(Suh, A. Y. et al., 2003)	HFC-410A	Tribometer	Al390-T6 Discs of different surface roughness against 52100 Steel Pins	Pin-on-disk	None	• Highly negative skewness was observed in the mildly-worn surfaces • Change in kurtosis did not give any significant results • The functional indices remained almost constant on the virgin surfaces

(Lee, Y.-Z. and Oh, S.-D., 2003)	HFC-410A	Tribometer	Ni–Co–Mo Gray Cast Iron Disks against High Speed Tool Steel Vane Coated with TiN	Vane-on-disk	TiN Coating of Different Surface Roughness applied by Physical Vapour Deposition	• The coefficient of friction as well as the wear on TiN coated samples was less as compared to the uncoated samples • The difference in the performance of the coated and the uncoated samples became more apparent with an increase in normal load and an increase in RPM • There is an optimum initial surface roughness value which improves the load carrying capacity and prolongs the wear life of sliding surfaces
(Cannaday, M. L. and Polycarpou, A. A., 2005)	HFC-134a	High Pressure Tribometer	Disks: 1) Aluminium Alloy 2) Gray Cast Iron Pins: 1) PTFE 2)Nylon 6,6 3) Polyimide 4) PEEK 5) WP122 6) WP191 7) Vespel SP-21 8) Vespel SP-211 9) PEEK Bearing Grade, HPV 10) PEEK Carbon Filled	Pin-on-disk	None	• PEEK and Polyimide showed promise as replacements for metallic bearing parts • Unfilled PTFE did not perform as well as PEEK or Polyimide • Unfilled polymers exhibited minimum pin wear and did not wear the metallic disk • Overall all the blended polymers have superior tribological properties compared to unfilled polymers and metals
(Demas, N. G. et al., 2008)	HFC-134a	High Pressure Tribometer	Gray Cast Iron Disks against Pins made of different Polymers Pins: 1) ATSP/PTFE: 75/25 2) ATSP/PTFE: 50/50 3) ATSP/PTFE: 25/75	Pin-on-disk	None	• Synthesized ATSP blends with PTFE were found to have excellent tribological performance under the tested conditions • PTFE improved the wear performance • Greater amounts of ATSP used in the blends lead to lower wear • The coefficient of friction was not significantly altered

			4) Vespel SP-21 5) Vespel SP_211 6) PEEK, Carbon Filled 7) PEEK-Bearing Grade, HPV			by ATSP • Lower friction coefficient values were obtained by increasing PTFE due to material transfer and formation of transfer films on the disk • Overall the newly synthesized composites showed very good tribological properties having very low friction and wear
(Nunez, E. E. et al., 12-15 July, 2010, Purdue University, Indiana, USA, paper 2031; Nunez, E. E. et al., 2011)	HFC-134a	High Pressure Tribometer	Shoe: 52100 Steel Pin: 52100 Steel Disk: Cast Iron coated with different polymeric coatings	1) Pin-on-disk 2) Shoe-on-disk	1) PTFE/MoS_2 2) Fluorocarbon 3) PEEK/PTFE 4) PEEK/PTFE/Ceramic	• Experimental results indicated that in comparison to the other polymeric coatings, PEEK/PTFE coatings performed slightly better in terms of wear and friction • The transfer of films from the disk coating to the 52100 steel shoes enabled the interface to operate without overheating • PEEK/PTFE coating was the only coating that was able to perform well under unlubricated conditions • Fluorocarbon coatings were unable to withstand the aggressive testing conditions
(Yeo, S. M. and Polycarpou, A. A., 2014)	HFC-134a	Tribometer	Gray Cast Iron Pins against Gray Cast Iron Disks coated with different Polymeric Coatings	Pin-on-disk	1) PTFE/Pyrrolidone 2)PEEK/PTFE	• The coatings showed worse performance in the presence of liquid lubricants than under dry conditions because the formation of transfer films was prevented by lubricants • Under fretting conditions, the tribological performance of polymer coatings was highly influenced by the ability of the polymers to form transfer films on the metal counter face
(Tanaka, M. et al., 14-17 July, 2014, Purdue University, Indiana,	1) HFC-410A 2) HFC-32	1)The reliability and durability of the compressor was studied	1) For reliability and durability tests: Gray Cast Iron Shaft against PTFE coated Bronze Bearing 2) For lubricity tests: Gray Cast Iron Ring against	1) Compressor Shaft and Bearing 2) Block-on-ring	PTFE	• HFC-32 had poor miscibility with conventional oils that are normally used with HFC refrigerants • The viscosity dropped more in case of using HFC-32 • HFC-32 decomposed easily and generated organic acids that caused corrosion • Overall HFC-32 was difficult to handle, it showed poor

USA, paper 2299)		by performing drop-in tests using an actual Scroll-Compressor 2) Lubricity was tested using a Hermetic block-on-ring test machine	PTFE Coated Bronze Block			stability and generated acids that caused corrosion and abnormal wear of sliding compressor parts
(Nunez, E. E. and Polycarpou, A. A., 2015a)	HFC-134a	High Pressure Tribometer	Pins made of various Polymers were Tested under Unlubricated Unidirectional conditions against Gray Cast Iron Disks Pins: 1) Vespel SP-21 2) Vespel SP-211 3) PEE/Carbon filled 4) ATSP/PTFE	Pin-on-disk	None	• Higher friction values were obtained when testing smoother pins against smoother disk surfaces, compared to testing of rougher disk surfaces • Transfer layers were uniform and continuous when testing against smooth disks • ATSP performed the best and is promising for use in oil-less compressors
(Tada, A. et al., 2016)	1) HFC-410A 2) HFC-32	Tribometer	SKH51 (HRC63) Block against SNCM (HRC50) Ring	Block-on-ring	None	• Lubricating film formation is affected by both the refrigerants and the base oils • TCP in POE lubricant formed a lubricating film on the sliding surfaces under HFC-410A which enhanced the tribological performance • HFC-32 however, interfered with the formation of phosphate films • High reactivity and polarity of HFC-32 with nascent metal surfaces prevented TCP from adsorbing to the iron on the sliding surfaces

HFCs became the refrigerants of choice in the mid-1990s and they replaced CFCs and HCFCs in automobile, commercial and domestic refrigeration and air-conditioning systems. Various researchers worldwide started investigating HFCs with respect to their oil miscibility, their friction performance, their wear characteristics, etc. Some of the earlier studies which focused on the direct comparison of the tribological performance of HFCs with CFCs and HCFCs concluded that HFCs have inferior friction and wear performance compared to CFCs and HCFCs due to the inability of HFCs to form protective tribo-films under normal compressor operating conditions. Amongst the HFCs, HFC-134a was suggested as the most suitable replacement for CFC-12. Mineral oils that showed good miscibility with CFCs and HCFCs, unfortunately were not compatible with HFCs. HFCs showed poor compatibility and miscibility in mineral oils. Synthetic oils with various additives were developed for HFCs.

2.6.3   Natural Refrigerants

Water, air, carbon dioxide, ammonia and hydrocarbons are considered to be the most environmental friendly and natural occurring refrigerants (Bhutta et al. 2018b). Ammonia has been used for a long period of time in large industrial systems as a refrigerant and is still being used in large industrial applications. Water and air have been used as coolants in engineering and domestic applications since ancient times. Air and water are still being used in various applications for cooling purposes, but are not used as refrigerants due to their thermodynamic limitations. Carbon dioxide is also a good refrigerant which sublimes under normal atmospheric temperature and pressure. It has been used for cooling purposes but its utilization in refrigerator compressors is still under investigation (Bhutta et al. 2018b). Hydrocarbons are found in crude oil and possess good thermodynamic qualities. Hydrocarbons are being used in commercial, domestic and industrial refrigerators, freezers and heat pumps. Their flammability is however a big concern. Hydrocarbons and carbon dioxide are discussed from a tribological view point in sections 2.6.3.1 and 2.6.3.2 respectively.

2.6.3.1 Hydrocarbons (HCs)

Hydrocarbon refrigerants are nontoxic, natural refrigerants that have zero ozone depleting potential and minimal global warming potential. Hydrocarbons which are extracted from crude oil are environmentally safe and efficient refrigerants. Hydrocarbon refrigerants are considered up to 50% more efficient thermal conductors than fluorocarbon refrigerants (Bhutta et al. 2018b). Hydrocarbons also have lower operating pressures than fluorocarbon refrigerants which results in lower power consumption and cost savings (Bhutta et al. 2018b). Many European manufacturers of domestic and commercial refrigeration equipment are using hydrocarbon refrigerants in their compressors. Amongst hydrocarbon refrigerants, Isobutane (HC-600a) is found in most domestic freezers and refrigerators while Propane

(HC-290) is used mostly in commercial refrigeration and heat pump applications. The greatest challenge in handling and designing a cooling system based on hydrocarbons is their extremely high flammability. This is why they have not been used as frequently as HFCs and also have not been deployed in automotive air-conditioning systems. This section covers the tribological investigations done by various researchers on hydrocarbons. Various tribological studies performed on HCs have been summarized and are presented in table 2.4.

Table 2.4 Summary of the tribological testing of HCs.

Study	Refrigerant	Apparatus	Interacting Materials	Contact Geometries	Surface Treatment	Key findings
(Garland, N. and Hadfield, M., 2005)	1) HFC-134a 2) HC-600a	Modified micro-friction pressurized test rig	Aluminium Alloy (LM13AE109) Pin reciprocating against Steel (100/102Cr6) Plate	Pin-on-flat	None	• Additised mineral oils showed very low wear rate and formed a good boundary film • High levels of carbon were found at the pin contact with mineral oil indicating that any boundary layer developed by using mineral oil is more durable than that developed by using POE lubricant • In case of additised POE, deposition was present at the plate but not at the pin
(Solzak, T. A. and Polycarpou, A. A., 17-20 July, 2006, Purdue University, Indiana, USA, paper 1790)	1) HFC-134a 2) HFC-410A 3) HC-600a	High Pressure Tribometer	Rotating Cast Iron Disks against Stationary Coated 52100 Steel Wrist Pins	Pin-on-disk	Disk Coatings: 1) WC/C 2) WC/C+DLC	• HC-600a environment displayed the lowest friction coefficient while HFC-410A environment resulted in the lowest wear • The tests showed that the friction coefficient decreased up to ten times by using coatings • WC/C + DLC Coatings displayed the least wear • WC/C showed slightly higher friction at lower temperatures, this trend was reversed at higher temperatures
(Sariibrahimoglu, K. et al., 2010)	HC-600a	Tribometer	100Cr6 Steel Pin Rubbing against Rotating Sintered Steel	Pin-on-disk	Disk. 1) Sintered Steel Disk Treated with steam 2) Untreated Sintered Steel Disk	• Under dry as well as starved lubrication conditions, HC-600a showed adverse effects • In particular for starved lubrication, the wear life of both steam treated sintered steel and untreated sintered steel was reduced to half in the presence of HC-600a compared to air • The increase in wear under HC-600a was thought to be due to change in viscosity and foaming of the oil. • Oxidation under HC-600a was blocked, which caused an increase in weight loss of untreated sintered steel
(De Mello, J. et al., 2009)	1) HC-600a 2) CO_2	High Pressure Tribometer	Si-rich multifunctional DLC coated Rotating Disks Deposited on 1020 steel against 52100 Stationary Steel Pins	Pin-on-disk	Magnetron Sputtered Diode Multifunctional CrN-Si-rich DLC Coatings were applied to finely ground AISI 1020 Soft Steel Disks	• HC-600a showed the lowest wear rate and coefficient of friction for both the body and the counter-body • The wear rate of the counter bodies increased significantly when tested in CO_2 environment • There was a strong presence of graphitic G-band in the spectra

Reference	Refrigerant	Equipment	Method	Configuration	Materials / Coatings	Findings
						of tribo-layers formed in the presence of HC-600a and coated disks, which induced its superior tribological performance
(Solzak, T. A. and Polycarpou, A. A., 2010)	1) HFC-134a 2) HFC-410A 3) HC-600a	High Pressure Tribometer	1) Piston-type compressor simulation by reciprocating a Disk in contact with a stationary self-aligning Pin 2) Swash-plate compressor simulation by rotating a Disk against a stationary self-aligning Shoe	1) Pin-on-disk 2) Shoe-on-disk	1) Piston-type compressor simulation I) Gray Cast Iron Disk II) 52100 steel wrist pins coated with: a) Single-layer WC/C(B) b) Multi-layered WC/C + DLC c) TiAlN + WC/C 2)Swash-plate compressor simulation: I) 52100 Steel Shoe II)AL390-T6 disks coated with: a) Single-layer WC/C(A) b) Single-layer WC/C(B) c) Multi-layered WC/C + DLC d) TiAlN + WC/C e) Some disks included an additional CrN underlayer	• Friction coefficient was the lowest in HC-600a atmosphere while least amount of wear occurred in the case of HFC-410A • CrN under-layer doubled the load-bearing capacity in some cases and also improved the load-bearing capacity of all coatings by providing a hard supporting layer. • Overall hard protective coatings offered a great advantage in terms of the tribological performance of interacting surfaces
(Silverio, M. et al., 11-14 July, 2016, Purdue University, Indiana, USA, paper 2413)	1) HFC-134a 2) HC-600a	Tribometer	Stationary Si_3N_4 ball against AISI 1020 Low Carbon Steel Coated Flat Surface	Ball-on-flat	Multifunctional CrN-Si rich Diamond-like Carbon Coatings	• HC-600a presented lower coefficient of friction and lower scuffing durability than HFC-134a • Fluorinated compounds were observed on the tribo-layer in the case of HFC-134a. Carbon and silicon were observed in the case of HC-600a • It was recommend by this study to use HC-600a where energy saving is required while HFC-134a was recommend to be used for increased reliability
(Górny, K. et al., 2016)	1) HFC-134a 2) HC-290	Tribometer	Stationary Aluminium Alloy Block loaded against Gray Cast Iron Ring	Block-on-ring	None	• Due to the adverse effects of refrigerants on lubricants, it was concluded that wear in oil-refrigerant mixtures was considerably higher than in oil alone

Hydrocarbon refrigerants also became of interest in 1990s after the limitations on CFCs and HCFCs, but introduction of HFCs did not really allow HCs to be commercialized on a very big scale. This was also due to the high flammability of HCs. Now that more emphasis is towards natural refrigerants and HCs are naturally occurring, a strong focus has shifted towards these refrigerates as well. Their flammability is still a concern which prohibits their use in automotive air-conditioning, but HC refrigerants can be used with confidence in domestic and commercial refrigeration and air-conditioning systems. The use of HC refrigerants in heat pumps, refrigerator and freezer compressors has increased in the recent years. HC-600a has shown better friction and wear properties as compared to HFC-134a as well.

2.6.3.2 Carbon dioxide (CO_2)

Carbon dioxide (R-744) is an environmentally friendly refrigerant, having zero ODP and minimal GWP. CO_2 is abundantly available in the atmosphere and it can be collected/recycled from air. Besides being environmentally friendly, CO_2 is non-flammable and is in fact used in fire extinguishers to put out fires. It also has good thermodynamic properties and is suitable for a range of applications including industrial heat extraction, shipping vessels, commercial refrigeration systems, etc. The major difference between R-744 and the other refrigerants is its temperature/pressure characteristic and having a low critical temperature. CO_2 systems require special design and a high pressure to operate. The operating pressure requirements makes it unsuitable for automobile and domestic applications. An attempt however is being made to design automotive compressors to operate on CO_2 (Hagita et al. Feb 2002). Tribological studies performed on CO_2 have been summarized have been presented in table 2.5.

Table 2.5 Summary of the tribological testing of CO_2.

Study	Refrigerant	Apparatus	Interacting Materials	Contact Geometries	Surface Treatment	Key findings
(Wu, X. et al., 2004)	CO_2	Tribometer	440C Bearing Steel Ball against 52100 Steel Disk	Ball-on-disk	None	• Carbon dioxide reacted with the disk surfaces and formed carbonate and/or bicarbonate on the disk which played a major role in reducing friction • An optimum pressure resulted in effective reduction of friction • Lower CO_2 pressures were insufficient to produce carbonate and/or bicarbonates • Higher CO_2 pressures produced serious chemical wear
(Lee, K. et al., 2005)	1) HFC-134a 2) CO_2	High Pressure Tribometer	Al390-T6 Rotating Disks against Stationary 52100 Steel Pins	Pin-on-disk	None	• It was found that the abundance of oxygen while operating in carbon dioxide atmosphere resulted in the formation of oxides which strengthened the top most layer • PAG showed to be the better lubricant with CO_2
(Demas, N. G. et al., 2005)	1) HFC-134a 2) CO_2	High Pressure Tribometer	Gray Cast Iron Rotating Disks against Stationary Gray Cast Iron Pins	Pin-on-disk	None	• The tribological behaviour of the interacting materials using CO_2 was nearly identical to that of HFC-134a
(Demas, N. G. and Polycarpou, A. A., 2006b)	CO_2	Ultra-High Pressure Tribometer	1) Unlubricated tests: Rotating Gray Cast Iron Disks against Gray Cast Iron Pins 2) Boundary lubricated tests: Rotating 52100 Steel Disks against Al390-T6 Stationary Pins	Pin-on-disk	None	• Under unlubricated conditions the experimental results at different pressures were similar • Higher pressure had slightly positive effect on the friction coefficient • Under boundary lubrication conditions there was no significant wear
(Cannaday, M. and Polycarpou, A., 2006)	1) HFC-410A 2) CO_2	High Pressure Tribometer	Rotating Al390-T6 Disks against Stationary Hardened SAE 52100 Steel Pins	Pin-on-disk	None	• It was concluded in this study that in comparison to the CO_2 environment, HFC-410A environment resulted in increased disk wear • This was because carbon dioxide promoted a strong oxygenated layer which reduced wear
(Demas, N. G. and	1) HFC-134a 2) CO_2	Ultra-High Pressure Tribometer	Rotating Gray Cast Iron Disks against Stationary Gray Cast	Pin-on-disk	None	• CO_2 led to better tribological performance of the interface due to formation of carbonates on the surfaces, which

Polycarpou, A. A., 2006a)			Iron Pins			reduce friction and prevent wear
(Demas, N. G. and Polycarpou, A. A., 2008)	1) HFC-410A 2) CO_2	High Pressure Tribometer	1) Stationary 52100 Steel Pins against Coated Rotating Gray Cast Iron Disks 2) Crowned Stationary 52100 Steel Shoe against Rotating Coated Gray Cast Iron Disks 3) Stationary 52100 Steel Pins against Coated Rotating 4340 Quenched and Tampered Steel Disks 4) Crowned Stationary 52100 Steel Shoe against Coated Rotating 4340 Quenched and Tampered Steel Disks	1) Pin-on-disk 2) Shoe-on-disk	PTFE Coatings: 1) DuPont® 958-303 2) DuPont® 958-414 3)Whitford Xylan® 1052 DLC Coating: 1) Balinit® DLC	• The PTFE-based coatings showed low friction characteristics and high load carrying capacity and it was found that unlike the DLC coating they were not greatly affected by the testing environment • PTFE-based coatings performed better compared to DLC coatings • The generated wear debris acted as third body lubricants and improved the overall wear performance
(Nunez, E. E. et al., 2008)	CO_2	High Pressure Tribometer	Rotating AI390-T6 Disks against Stationary SAE 52100 Pins	Pin-on-disk	None	• The results showed that scuffing and wear resistance with PAG were superior compared to the samples tested with the POE lubricant • Formation of carbonate layers was promoted on the surface in the presence of PAG, leading to improvement in the tribological performance
(Nunez, E. E. et al., 2010a)	CO_2	High Pressure Tribometer	Stationary 52100 Pins against Rotating Disks made of the following materials: 1) Al390-T6 2) Gray Cast Iron 3) Mn-Si Brass	Pin-on-disk	None	• Mn–Si Brass and Gray Cast Iron performed better than Al390-T6 • Unlike Al390-T6 and Gray Cast Iron which failed abruptly in scuffing experiments, Mn–Si Brass melted during scuffing which prevented sudden catastrophic failure of Mn–Si Brass
(Jeon, H.-G. et al., 2009)	CO_2	High Pressure Tribometer	Rotating High Speed Tool Steel Pin against Stationary Disk made of Ni-Cr-Mo Gray Cast Iron	Pin-on-disk	None	• The results showed that PAG oil had better lubricity than POE oil in CO_2 refrigerant environment • An increase in pressure increased the solubility of carbon dioxide in case of POE oil which decreased the oil/refrigerant viscosity, whereas variations in pressure had no noticeable effect on the solubility of CO_2 in PAG
(Nunez, E. E. et	CO_2	Ultra-High Pressure	Rotating Gray Cast Iron Disk	Pin-on-disk	None	• The study reported a substantial drop in friction as carbon

al., 2010b)		Tribometer	against Stationary Gray Cast Iron Disk Pin			dioxide approached the gas-liquid transition region on the P-T phase diagram • This indicated a form of super-lubricity. It was also found that increase in CO_2 pressure caused partial transformation of iron oxides into iron carbonates, which positively affected the tribological performance
(Nunez, E. E. and Polycarpou, A. A., 2015b)	CO_2	High Pressure Tribometer	Stationary 52100 Shoe against Rotating Disks made of the following materials: 1) Al390-T6 2) Mn–Si–Brass 3) Gray Cast Iron	Shoe-on-disk	None	• During the experiments Al390-T6 lost silicon which reduced its structural strength and hardness • Gray Cast Iron showed the least amount of wear and highest fluid and material retention capability compared to the other materials tested

Carbon dioxide is a good natural refrigerant as well. CO_2 has zero OPD and a GWP value of only 1. The physical properties of carbon dioxide unfortunately does not allow it to be used at the operating temperatures and pressures as other refrigerants. The operating pressure has to be much higher for a system based on CO_2 compared to a compressor operating on CFCs or HFCs. Compared to HFC-134a, carbon dioxide has shown good tribological properties by formation of a carbonate layers on the rubbing surfaces. Carbon dioxide which is non-flammable is being investigated for use in automotive air-conditioning applications as well.

2.6.4   Next Generation Refrigerants

The next generation refrigerants are focused on low toxicity, low ODP and low GWP. Focus and attention is also being made on the flammability in the development of the next generation of refrigerants. The focus on HC has increased after the Kyoto Protocol but due to their flammability, HCs cannot be used in commercial automobile air-conditioners. The future generation of refrigerants have to be non-flammable for use and replacement of HFC-134a in the automotive sector. The refrigerant manufacturers have introduced Hydrofluoroolefins and Hydrofluoroethers as potential substitute refrigerants. Hydrofluoroolefins and Hydrofluoroethers are discussed from a tribological point of view in sections 2.6.4.1 and 2.6.4.2 respectively.

2.6.4.1 Hydrofluoroolefins (HFOs)

HFOs are designed to lower the GWP impact that HFCs had while having zero OPD and lower toxicity. One of the most promising future generation refrigerants is 2,3,3,3-Tetrafluoropropene (HFO-1234yf), which is considered a direct replacement of HFC-134a refrigerant (Spatz, M. et al., 14-17 April, 2008, Detroit, Michigan, USA). Although HFO-1234yf has mild flammability, it has been proven to be safe for use as a refrigerant in vehicles (Minor, B. H. et al., 2009). The tribological investigation of HFO-1234yf by various researchers is underway, the work done so far is presented in this section. The tribological studies that have been conducted so far using HFOs have been summarized in table 2.6.

Table 2.6 Summary of the tribological testing of HFOs.

Study	Refrigerant	Apparatus	Interacting Materials	Contact Geometries	Surface Treatment	Key findings
(Tatsuya Sasaki, H. N., Hideaki Maeyama, Kota Mizuno, 12-15 July, 2010, Purdue University, Indiana, USA, paper 1946)	1) HFO-1234yf 2) HFC-134a 3) HC-1270 4) HC-290	Tribometers	1) Stationary Cast Iron Disc against Rotating Cast Iron Disc 2) Stationary Cast Iron Pin against Rotating Cast Iron Disc 3) Stationary High Speed Tool Steel against Rotating Cast Iron Shaft	1) Disc-on-Disc 2) Pin-on-Disc 3) V Block	None	• A fluoride layer was formed with the adsorption effect of HFO-1234yf and the frictional heat, which helped improve the tribological performance • The seizure load of unsaturated HFO-1234yf was larger than saturated HFC-134a and similarly the seizure load of unsaturated HC-1270 was greater than saturated HC-290
(Mishra, S. P. and Polycarpou, A. A., 2011)	1) HFO-1234yf 2) HFC-134a 3) CO_2	Ultra-High Pressure Tribometer	Stationary Gray Cast Iron Surface Textured unpolished Pins against Rotating Gray Cast Iron Disks	Pin-on-disk	Six different surface textures applied to the Pins having varying pattern diameters, depths and area density	• HFO-1234yf showed the least amount of wear • The tribological properties of the textured surfaces were affected by the geometrical parameters; depth, diameter and the area density of the micro-dimples • The textured surfaces had a clear advantage over un-textured surfaces
(Akram, M. W. et al., 2013a)	1) HFO-1234yf 2) HFC-134a	High Pressure Tribometer	1) Stationary Gray Cast Iron Pin against Rotating Gray Cast Iron Disk 2) Stationary 52100 Steel Shoe against Rotating Al390-T6 Shoe	1) Pin-on-disk 2) Shoe-on-disk	None	• Gray Cast Iron pairs performed better in this study compared to 52100 Steel/Aluminium alloy pair for both refrigerants • When used with Gray Cast Iron, HFO-1234yf showed excellent wear performance compared to HFC-134a • The combined effect of the mechanical forces and frictional heating resulted in a tribo-chemical reaction. • This fluorine containing layer acted as a protective tribo-layer on the top most surface.
(Akram, M. W. et al., 2013b)	1) HFO-1234yf 2) HFC-134a	High Pressure Tribometer	Stationary Gray Cast Iron Pins against Rotating Gray Cast Iron Disks	Pin-on-disk	None	• HFO-1234yf sustained twice the load before failing compared to HFC-134a • Fluorine was detected upon surface analysis in the case of using HFO-1234yf

						• The fluorine containing tribo-layers prevented mental to metal contact and helped sustain extended interface functionality
(Akram, M. W. et al., 2014)	HFO-1234yf	High Pressure Tribometer	Stationary Gray Cast Iron Pins against Rotating Gray Cast Iron Disks	Pin-on-disk	None	• PAG showed the best performance with HFO-1234yf compared to POE/HFO-1234yf and mineral oil/HFO-1234yf combinations • PAG has the lowest solubility in HFO-1234yf compared to POE and mineral oil, this allows the lubricant and the refrigerant to preserve their unique properties giving PAG/HFO-1234yf combination the maximum tribological advantage
(Akram, M. W. et al., 2016)	HFO-1234yf	High Pressure Tribometer	Stationary 52100 Shoe against Rotating Gray Cast Iron Coated Disks	Shoe-on-disk	Coatings: 1) PTFE/ATSP 2) PTFE/pyrrolidone 3) PTFE/MoS$_2$ 4) PTFE/PEEK 5) Fluorocarbon	• ATSP/PTFE coatings performed better compared to PTFE-based and Fluorocarbon-based coatings under boundary and dry lubrication conditions • Tribo-chemical benefits were offered by the segregation associated with material enrichment which resulted in continuous lubricant supply, which was the case for ATSP/PTFE

Hydrofluoroolefins are newly formulated refrigerants which have zero OPD and lower GWP as compared to HFC refrigerants. HFO-1234yf is considered a direct replacement of HFC-134a, especially in automotive air conditioning applications. The physical and thermodynamic properties of HFO-1234yf are very similar to those of HFC-134a. HFO-1234yf is also compatible with the synthetic oils that were developed for HFC-134a. Unlike HFC-134a, the fluorine in HFO-1234yf has been reported to form protective films on the rubbing surfaces with and without lubricants, which improves the friction and wear performance of the system. HFO-1234yf has an unsaturated bond which makes it easier for it to chemically react with the metallic surfaces to improve the tribological performance. The only drawback of HFO-1234yf compared to HFC-134a is that HFO-1234yf has higher flammability than HFC-134a.

2.6.4.2 Hydrofluoroethers (HFEs)

Hydrofluoroethers are man-made refrigerants that have been developed to replace CFCs, HCFCs and HFCs. HFEs are non-flammable, odourless, colourless, low toxic and low viscous refrigerants having zero OPD and low GWP. Different variants of HFEs have been developed in the recent past. HFEs have higher boiling points compared to CFCs, HFCs, and HCFCs. HFEs are normally liquid at room temperature and look identical to water. HFO-1234yf has a boiling point comparable to HFC-134a and HFO-1234yf has shown compatibility with synthetic lubricants which were developed for HFC-134a, this makes HFO-1234yf an excellent replacement of HFC-134a. Due to the higher boiling points of HFEs, HFEs are not considered as a direct drop-in solution for HFCs and HFEs cannot be introduced into the same thermodynamics cycle and system that was previously used by HFC-134a. Besides having a very low environmental impact, HFEs are non-flammable and possess good thermodynamics properties as coolants (Akasaka, R. and Kayukawa, Y., 2012; Helvaci, H. and Khan, Z., 2017; Helvaci, H. and Khan, Z. A., 2016). The only known reported tribological analysis has been performed on HFE-245mc, this study has been summarized in table 2.8.

HFEs have a number of applications and places of use; they can be used in auto cascade refrigeration systems, in freeze dryers, in fuels cells, in chemical reactors, in high voltage transformers, as cleaning and rinsing agents, as lubricant carriers, in vapour degreasing applications, etc (3M 3M™ Novec™ 7000 Engineered Fluid). HFEs are also considered potential replacements for PFCs, HCFCs and HFCs (Sekiya and Misaki 2000). HFE-7000 is a promising new thermo-fluid and is considered a direct replacement of HCFC-123. There are however no known reported studies on the tribological testing of HFE-7000. HFE-7000 has already been investigated for use in Solar Organic Rankine Cycle (Helvaci and Khan 2017a), in renewable energy systems (Helvaci and Khan 2016; Helvaci and Khan 2017b), as jet impinging dielectric coolant (Shin et al. 2019), in Electrohydrodynamics applications (Blaineau et

al. 2019), etc. Table 2.7 lists various different properties of HFE-7000 along with HFC-134a which is now in the process of being phased out and with HFO-1234yf which is a new refrigerant replacing HFC-134a.

Table 2.7 Different properties of HFE-7000, HFC-134a and HFO-1234yf (Bhutta and Khan 2019).

Refrigerant	HFE-7000	HFC-134a	HFO-1234yf
Structure	$C_3F_7OCH_3$	Ch_2FCF_3	$CF_3CF=CH_2$
Molecular Weight (g/mol)	200	102	114
Freeze Point (°C)	-122.5	-103.3	-150
Boiling Point @ 1 atmosphere (°C)	34	-26	-29
Critical Temperature (°C)	165	101	95
Liquid Density (kg/m^3)	1400	1206	1094
Critical Pressure (MPa)	2.48	4.06	3.38
Flash Point (°C)	None	250	Not applicable
Appearance	Clear, colourless	Colourless gas	Colourless gas
Flammability	Non-flammable	Non-flammable	Mildly-Flammable
Ozone Depletion Potential (ODP)	Zero	Zero	Zero
Global Warming Potential (GWP)	530*	1430*	4*

*GWP 100-year integrated time horizon (ITH), IPCC 2013 (ipcc The Intergovernmental Panel on Climate Change).

It can be observed from the table that both the future generation of refrigerants i.e. HFE-7000 and HFO-1234yf having a lower GWP in comparison to HFC-134a. HFO-1234yf has a much lower GWP value in contrast to HFE-7000, but HFO-1234yf is flammable which restricts its application range and places of use. On the other hand HFE-7000 is a non-flammable refrigerant with GWP of about 1/3 to that of HFC-134a.

Table 2.8 Summary of the tribological testing of HFEs.

Study	Refrigerant	Apparatus	Interacting Materials	Contact Geometries	Surface Treatment	Key findings
(Muraki, M. et al., 2002)	1) HFE-245mc 2) HFC-134a	Tribometers	1) Optical Interferometry (Steel Ball Coated with a Chromium Semi-Reflective Layer) 2) SAE4320 Ring against ASE01 Block	1) Ball-on-disc 2) Block-on-ring	None	• HFE-245mc/lubricant mixture displayed the lowest film thickness formation capability compared to HFC-134a/lubricant and air/lubricant mixtures • HFE-245mc however displayed the lowest coefficient of friction after running-in of the components was achieved • HFC-245mc was believed to have reacted with the rubbing surfaces, resulting in the formation of FeF_2 and thick iron oxide films resulting in good anti-wear performance which resulted in the lowest wear in HFE-245mc atmosphere

2. 7 Electrodeposition

Nanostructured design obtained by the dispersion of nano particles into a matrix has been demonstrated in enhancing optical, electrical, thermal and mechanical properties in comparison to conventionally used metallic materials (Kumar et al. 2003; Zong and Zuo 2003; Meyers et al. 2006). A number of studies (Chen et al. 2006a; Chen et al. 2006b; Zhou et al. 2009; Saha and Khan 2010; Borkar and Harimkar 2011; Bajwa et al. 2016c, 2016b; Nazir et al. 2017; Nazir et al. 2018a; Nazir et al. 2018b) have been performed by various different researchers to investigate the mechanical, wear, friction and corrosion performance of electrodeposited Nickel based coatings under a number of different environmental and testing conditions. These studies have shown that electrodeposited Nickel coatings can significantly improve the wear, friction and corrosion performance of rubbing parts.

Electrodeposition also commonly known as electroplating is an electro-chemical process in which a metal is deposited (coated) on a metallic surface by electrolysis in an electrolytic cell. When a current is applied to the conductor to be coated, metal ions in the solution are reduced onto the electrode to form a thin layer. Italian chemist Luigi Valentino Brugnatelli is credited as the inventor of modern electrochemistry. In 1805 Brugnatelli used the voltaic pile invented by Alessandro Volta to perform the first electrodeposition. However, Brugnatelli's work was suppressed. Russian and British scientists independently invented deposition methods that came into use by 1839 to copper plate printing press plates. In 1840, George and Henry Elklington were awarded patents for electroplating. Englishman John Wright discovered that potassium cyanide could be used as an electrolyte to electroplate gold and silver. By the 1850s, commercial processes for electroplating brass, nickel, zinc, and tin were developed. The first modern electroplating plant to start production was the Norddeutsche Affinerie in Hamburg in 1867.

The electrolytic solution contains metal salts dissolved in an aqueous solution, some additive chemicals such as acids, bases or buffers which help promote conduction and are used in optimizing the coating properties. Figure 2.8 illustrates the basic principle of electroplating for depositing (coating) Nickel on a metallic substrate.
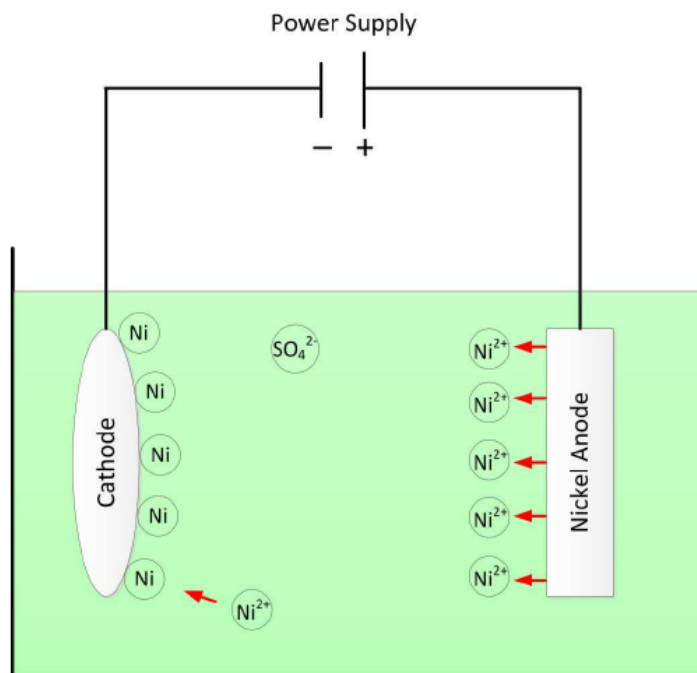
Fig. 2.8. Nickel Electroplating (Bajwa 2016).

In figure 2.8 a metal salt such as Nickel Sulphate ($NiSO_4$) is dissolved in water, which creates Ni^{2+} and $SO_4{}^{2-}$ ions. In the presence of an external power supply, Nickel is oxidized at the anode to Ni^{2+} by losing two electrons. Ni^{2+} associates with the $SO_4{}^{2-}$ ions in the solution to form Nickel Sulphate. At the cathode, the Ni^{2+} is reduced to metallic Nickel by gaining two electrons. This result is the effective transfer of Nickel from the anode source to a plate covering the cathode.

Besides electroplating, two other commonly used chemical coating techniques are Electroless Chemical Deposition and Laser-Enhanced Deposition. Electroless plating, also known as chemical or auto-catalytic plating is a plating method that involves several simultaneous reactions in an aqueous solution which occurs without the use of external electrical power. It is mainly different from electroplating by not using external electrical power. Laser-Induced or Laser-Enhanced Deposition is based on laser technology and an external light source is applied to either electroless or electroplating process to accelerate metal deposition.

2. 8   Electrodeposition Techniques

There are three different types of electrodeposition techniques which have been developed over the years. These techniques are shown in the flowchart in figure 2.9.
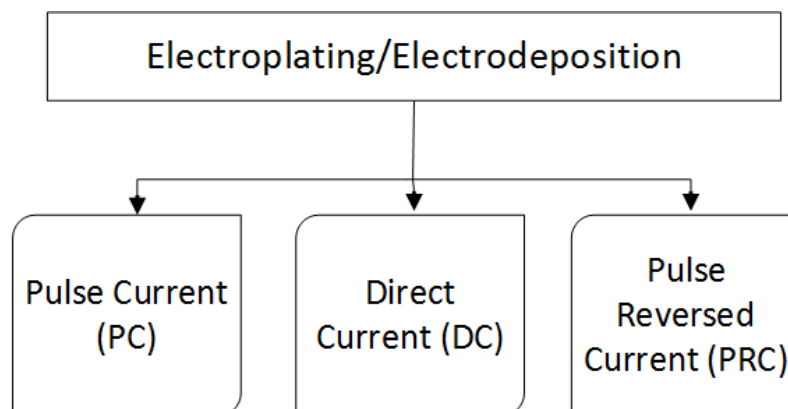
Fig. 2.9. Flowchart of Electroplating Techniques.

2.8.1   Direct Current Electrodeposition

The direct current electrodeposition technique is the oldest and the simplest electroplating technique. The conventional direct current electrodeposition method is an economical approach which does not include the additional cost of sophisticated controlled pulse/power supply equipment. Simple batteries/direct current supply is used to start the deposition process. The current density is controlled and adjusted in order to optimise the morphological and physical properties of direct current electrodeposition coating (Lee, S., 2006).

Although the direct current electrodeposition technique is the simplest, it has several disadvantages which include non-uniform current distribution (higher at sharp edges and lower at recessed areas of the cathode) which results in non-symmetrical thickness of the depositing materials (Allahkaram, S. R. et al., 2011). Due to the direct current supply in DC electroplating there is a non-homogenous distribution ions in the bath, this uneven distributions of ions affects the morphological properties of the coating (Kelly, J. et al., 2000). The current flow is a continuous phenomenon in DC electrodeposition having a duty cycle of 100%.

2.8.2   Pulse Current (PC)

In pulse electrodeposition (PED) the potential or current is alternated swiftly between two different values. This results in a series of pulses of equal amplitude, duration and polarity, separated by zero current (Chandrasekar, M. S. and Pushpavanam, M., 2008). Each pulse consists of an ON-time (T_{ON}) during which potential and/current is applied, and an OFF-time (T_{OFF}) during which zero current is applied as shown in figure 2.10.
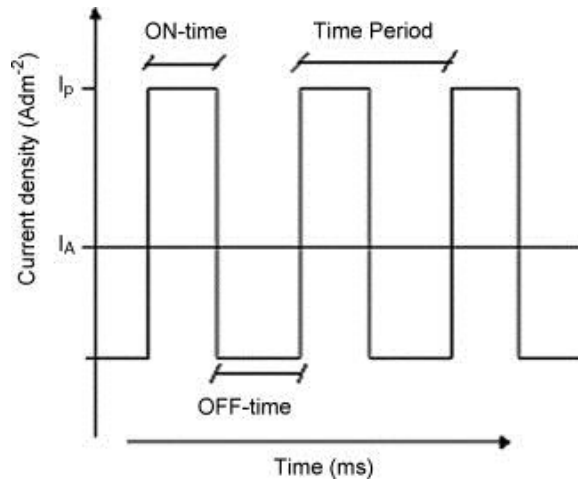
Fig. 2.10. Typical Pulse-Current Waveform (Chandrasekar, M. S. and Pushpavanam, M., 2008).

It is possible to control the deposited film composition and thickness in an atomic order by regulating the pulse amplitude and width (Alper, M. et al., 1993; Ueda, Y. et al., 1996). This results in finer grained deposit with better properties than conventionally direct current plated coatings (Chandrasekar, M. S. and Pushpavanam, M., 2008).

To characterise the pulse current the following parameters are considered:

- ON-Time (T_{ON})
- OFF-Time (T_{OFF})
- Peak Current Density (I_P)

Using these parameters the duty cycle (γ) and frequency can be defined by equation 21 and equation 22 respectively (Chandrasekar, M. S. and Pushpavanam, M., 2008). The peak current density can be calculated by using equation 23.

$$Duty\ Cycle = \frac{T_{ON}}{T_{ON} + T_{OFF}}$$ Equation 21

Duty cycle is defined as the portion of each cycle during which current is ON.

$$Frequency = \frac{1}{T_{ON} + T_{OFF}}$$ Equation 22

Frequency is defined as the reciprocal of the total time i.e. $(T_{ON} + T_{OFF})$.

$$I_P = \frac{Peak\ Current}{Coating\ Surface\ Area} \qquad \text{Equation 23}$$

The peak current density is defined as the ratio of the peak current flowing through the circuit during electroplating to the coating surface area and has the units $\left(A/_{dm^2} \right)$. The peak current is in amperes (A) and the coating surface are is taken in units (dm^2), where $1\ dm^2 = 0.01\ m^2$. The average current density (I_A) is defined by equation 24 (Chandrasekar, M. S. and Pushpavanam, M., 2008).

$$I_A = Peak\ Current\ Density\ (I_P) \times Duty\ Cycle\ (\gamma) \qquad \text{Equation 24}$$

2.8.3 Pulse Reverse Current (PRC) Electrodeposition

PRC plating is the bipolar electrodeposition process where DC current is continuously changing its direction (polarity). A typical waveform of the pulse reverse current is shown in figure 2.11.
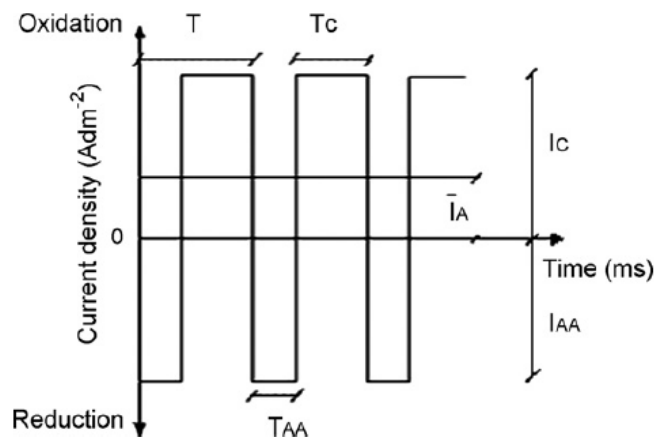
Fig. 2.11. Typical Pulse Reverse Current Waveform (Chandrasekar, M. S. and Pushpavanam, M., 2008).

In Pulse Reverse Current the plating current is interrupted and a reverse time is introduced into the plating cycle. The introduction of high frequency PRC reduces the use of additives, which limits the deposit ductility and electrical conductivity (Chandrasekar, M. S. and Pushpavanam, M., 2008). PRC avoids the drawbacks of additives while the superimposed pulsation keeps control of the crystal structure (Chandrasekar, M. S. and Pushpavanam, M., 2008). The following parameters are considered in order to characterize the pulse reverse current:

- Anode Pulse Reverse Time T_{AA}
- Cathode Pulse Forward Time T_C

- Anode Current Density I_{AA}
- Cathode Current Density I_C
- Average Current Density $\bar{I}$

In case of PRC technique, the average current density ($\bar{I}$) and the duty cycle (γ') are given by equation 25 and equation 26 respectively (Chandrasekar, M. S. and Pushpavanam, M., 2008).

$$\bar{I}_A = \frac{I_C T_C - I_{AA} T_{AA}}{T_{AA} + T_C}$$

<div align="right">Equation 25</div>

$$\gamma' = \frac{T_C}{T_{AA} + T_C}$$

<div align="right">Equation 26</div>

PC and PCR offer several advantages in enhancing the deposition rate and the quality of deposited coatings. The independent control of various pulse coating parameters in PC/PCR techniques can significantly improve the micro/nano structures and morphological properties of the deposited coatings of metals, alloys and nano-particle composites which is not possible with DC techniques (Kelly, R. G. et al., 2002; Marlot, A. et al., 2002; Nakanishi, T. et al., 2001). Unlike the DC technique which creates an uneven distribution of ions which effects the quality of the coating, the PC/PCR technique enhances the quality of the coatings by increasing the ion distribution in the electroplating solution (Chandrasekar, M. S. and Pushpavanam, M., 2008). Researchers have also conducted comparative studies to compare the porosity of PC/PRC coating in comparison to DC electrodeposition and have stated that PC/PCR coated surfaces had a lower porosity (Balasubramanian, A. et al., 2009; Barcena, J. et al., 2008; Liu, Z. et al., 2011; Ramanauskas, R. et al., 2008). Porosity is linked to the quality of the deposition which effects the mechanical, tribological and corrosion properties directly. Increase in porosity leads to penetration of unwanted ions trough the pores which can increase the pitting and corrosion behaviour of the underlying substrate (Notter, I. M. and Gabe, D. R., 1992; Zhou, Q. et al., 2009). The porosity is effected by the formation of hydrogen bubbles during the electroplating process (Nakahara, S. and Okinaka, Y., 1974) which can be improved by using PCR/PC techniques (Liu, Z. et al., 2010). The disadvantage of PC/PCR is that the cost of a pulse rectifier is much greater than a DC unit.

The recent work done on the electrodeposited nanocomposite coatings to examine the friction, wear and corrosion properties of the coatings has been summarized in table 2.9.

Table 2.9 Summary of tribological properties of electrodeposited nanoparticles-filled nanocomposites.

Study	Coating	Nanoparticle Size (µm)	Method	Wear Resistance	Micro Hardness	Corrosion Resistance
(Hou, K. H. et al., 2002)	Ni-SiC	0.3	DC	Improved	Increased	-
(Surender, M. et al., 2004)	Ni-WC	5	DC	Improved	Increased	-
(Wang, L. et al., 2005)	Ni-Diamond	0.01	DC	Improved	Increased	-
(Shi, L. et al., 2005)	Ni-Co-Si$_3$N$_4$	0.02	DC	Improved	Increased	-
(Aal, A. A. et al., 2006)	Ni-AlN	0.040-0.150	DC	Improved	Increased	Improved
(Hou, K.-H. et al., 2006)	Ni-P-SiC	0.3	DC, PC	Improved	Increased	-
(Aruna, S. T. et al., 2006)	Ni-CeO$_2$	2-20	DC	Improved	Increased	Improved
(Xue, Y.-J. et al., 2006)	Ni-CeO$_2$	40	DC	Improved	Increased	-
(Lampke, T. et al., 2006)	Ni-SiC Ni-TiO$_2$	0.5-5 0.021-5	DC	-	Increased	Improved
(Chen, L. et al., 2006)	Ni-Al$_2$O$_3$	0.8	DC	Improved	Increased	-
(Sun, X. J. and Li, J. G., 2007)	Ni-TiO$_2$	0.012	DC	Improved	Increased	-
(Hou, K.-H. et al., 2007)	Ni-P	Different weight %	DC, PC	Improved	Increased	-
(Vaezi, M. R. et al., 2008)	Ni-SiC	0.05	DC	Improved	Increased	Improved
(Thiemig, D. and Bund, A., 2008)	Ni-TiO$_2$	0.021	DC	Improved	Increased	-
(Zhou, Q. et al., 2009)	Ni-Al$_2$O$_3$	0.382	DC	Improved	Increased	Improved
(Saha, R. K. and Khan, T. I., 2010)	Ni-Al$_2$O$_3$	0.05	DC	Improved	Increased	-
(Srivastava, M. et al., 2010)	Ni-Co	0.02-0.03	DC	Improved	Increased	Unaffected
(Argañaraz, M. P. Q. et al., 2011)	Ni-W	0.065-.0140	PC	-	Increased	Improved
(Liu, Y. et al., 2011)	Ni-SiO$_2$	<100	DC	Improved	Increased	-
(Hou, K.-H. and Chen, Y.-C., 2011)	Ni-W-Al$_2$O$_3$	0.08	PC	Improved	Increased	-
(Borkar, T. and Harimkar, S. P.,	Ni-Al$_2$O$_3$	0.15	DC, PC, PRC	Improved	Increased	-

2011)	Ni-SiC	0.03-0.06				
	Ni-ZrO$_2$	0.2				
(Haq, I. U. and Khan, T. I., 2011)	Ni-SnO$_2$	<100	DC	Improved	Increased	-
(Haq, I. U. et al., 2013)	Ni-Fe$_2$O$_3$	<100	DC	Improved	Increased	Improved
(Algul, H. et al., 2015)	Ni-Al$_2$O$_3$	0.08	DC	Improved	Increased	-
(Algul, H. et al., 2015)	Ni-Graphene	0.032-0.036	PC	Improved	Increased	-
(Bajwa, R. S. et al., 2016a)	Ni-Al$_2$O$_3$	0.05	PC	Improved	Increased	Improved
(Bajwa, R. S. et al., 2016b)	Ni-Al$_2$O$_3$ Ni-SiC Ni-ZrO$_2$	0.05	PC	Improved	Increased	Improved
(Chen, J. et al., 2016)	Ni-Graphene	0.030-0.039	PRC	Improved	Increased	-
(Szeptycka, B. et al., 2016)	Ni-Graphene	5	DC	Improved	-	Improved
(Bajwa, R. et al., 2016)	Ni-Al$_2$O$_3$	0.04-0.05	PC	Improved	-	-
(Nazir et al. 2017)	Ni-Al$_2$O$_3$ Ni-SiC Ni-ZrO$_2$ Ni-Graphene	0.05-0.06 0.04-0.05 0.03-0.04 0.005-0.007	PC	-	-	Improved
(Nazir et al. 2018b)	Ni-Graphene	0.004-0.006	PC	Improved	Improved	Improved
(Nazir et al. 2018a)	Ni-Al$_2$O$_3$ Ni-SiC Ni-ZrO$_2$ Ni-Graphene	0.03-0.04 0.04-0.05 0.1 0.006-0.008	PC	Improved	Improved	-

It is a common practice to use ceramic oxides and compounds as nanoparticles in the Nickel matrix. As shown in the studies listed in table 2.9, the addition of nanoparticles in the Nickel matrix have a positive impact on the overall tribological properties as compared to the base metal and as compared to purely Nickel based coatings. Graphene which was successfully isolated in 2004 is also being used at Nano level and is being integrated in the Nickel matrix using electrodeposition process to develop Graphene based nanocomposite coatings.

The in-depth literature survey focused on the tribological testing of refrigerants. They key findings of these studies have been comprehensively summarized besides describing the types of equipment and materials used by different researchers. The literature also describes different electrodeposition techniques and lists a number of tribological studies carried out on electrodeposited metals incorporating different Nano-particles. The tribological studies performed by using coated contacts have shown a clear advantages and usefulness of nanocomposite coatings. The literature review and survey has helped identify the literature gaps and has assisted in selecting; the appropriate testing procedure, the thermo-fluids and the types of coatings.

An appropriate test method has been developed and the existing tribo-testing machine has been modified to experimentally investigate and enhance the tribological performance of next generation of thermo-fluids using nanocomposite coatings under sliding contact.

Chapter 3

The purpose of this study is multifold: (a) to investigate the friction and wear behaviour of HFE-7000 by using steel contacts; and (b) to evaluate the friction and wear performance along with the compatibility of Nickel based nanocomposite coatings to look into the possibility to reduce wear and improve the friction performance of interacting parts of a system using HFE-7000 by utilizing nanocomposite coatings. This chapter provides a detailed description of the test rig design and setup which will be used to study the tribological performance of rubbing uncoated and coated steel parts under HFE-7000 lubrication.

Test Rig Design

For the tribological evaluation of the next generation of refrigerants, a micro-friction machine has been modified. The machine is Phoenix TE-57/77 tribo-meter. The TE-57/77 tribo-meter has been modified to allow for the tribological testing of the next generation of thermo-fluids keeping in view the following key parameters:

- The testing chamber should remain sealed under all testing conditions at all times and the modifications should allow for the assembly to sustain pressures in the range of $-1 \, to + 3 \, bar$.
- The modifications should allow the direct measurement of; the fluid temperature, the gauge pressure inside the chamber, the contact potential, the friction force, sliding/reciprocating frequency and the heater block temperature.
- Machine feedback should not be effected by the modifications.
- The thermo-fluid should be charged directly at the interface allowing fully lubricated conditions between the interacting parts at all times.
- The testing assembly should be easy to install with minimum time and effort.
- All components within the pressurised chamber should be easy to disassemble and clean to prevent contamination of subsequent test samples.

3.1 TE-57/77 Tribo-Meter

The TE-57/77 tribo-meter in its original form is shown in figure 3.1. The TE-57/77 micro-friction bench-top machine operates by sliding a sample plate in a reciprocating motion against a fixed ball or a pin (cylinder) sample. The machine comprises of a variable speed controlled

electric motor and a reciprocating drive mechanism. The load is applied normally from the top to the static specimen through a spring balance, load arm and linkage. The specimen block is mounted on an electrically heated block. The flat plate specimen reciprocates in a horizontal plane by a motor through a scotch yoke mechanism against a fixed pin/ball that is connected to a transducer to provide friction force feedback. The reciprocating amplitude can be set by adjusting the driver cam to give strokes in the range of 0-5 mm. The moving components within the test chamber are sealed to the test chamber by means of steel bellows and Viton O-ring seals. The arrangement is such that all relative movement is accommodated by the bellows with the O-ring contacts all effectively static. Two bellows transmit the power from the motor to the slider which holds the flat specimen. Two spate bellows are connected with a shaft that is used to mount the ball/pin and also help transmit the normal load.
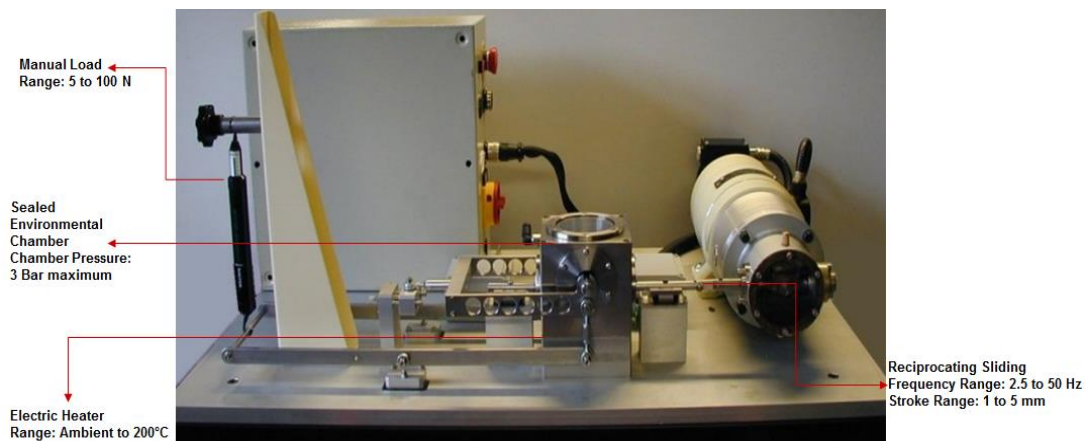
Fig. 3.1. TE-57 Tribo-meter original form.

The positioning of the bellows is shown in detail in figure 3.3. The pin or ball can be electrically isolated from the flat plate to install a contact potential sensor to observe the lubrication film formation and metal to metal interactions. Wear at the contact is evaluated by post-test analysis.

Data from SLIM 2000 is transmitted serially on a host PC. The serial link interface is a micro-controller based multichannel and multifunctional interface. COMPEND 2000 software is used for sequence control, data monitoring and data recording. The software requires a PC with the minimum specifications; Pentium II 233 MHz, 32 Mbytes RAM. The software provides a graphical user interface and provides a platform for open system architecture and connectivity. The graphical user interface provides real-time data acquisition, monitoring and control. A separate test sequence file is written for each test. A data file has to be specified before the start of a test to record the data.

3.2 Design Outline

The modified micro-friction testing machine should be able to envelop the whole apparatus under sealed conditions. The design should allow the connection of a vacuum pump to the chamber. The chamber has to be vacuumed before the start of each test to minimize the effects of ambient air and oxygen. The modifications should allow the continuous monitoring and control of the testing parameters, namely; friction force, motor speed, chamber temperature, chamber pressure and contact potential.

The small chamber of the micro-friction machine provides several advantages, which include:

- Low volume of thermo-fluid is required to achieve fully lubricated conditions.
- Less time to heat the thermo-fluid.
- Small size of the testing specimens reduces the overall martial requirement for testing.
- Easy to visually observe the testing through the glass chamber lid.
- Less time required to vacuum.

3.3 Design Modification Layout and Schematic

All modifications have to be made in a way that will not disturb any original settings of the machine and to allow complete disassembly of the modifications for future use without any damage to the original components. The modifications have to ensure that the testing chamber remains sealed throughout a test and any pipes, fittings and valves sustain the pressure limits. The design modification layout schematic diagram of the tribo-meter is shown in figure 3.2. The schematic diagram shows all the modifications required for experimentation. The complete working of the modified tribo-meter is explained in the flowing sections in this chapter.
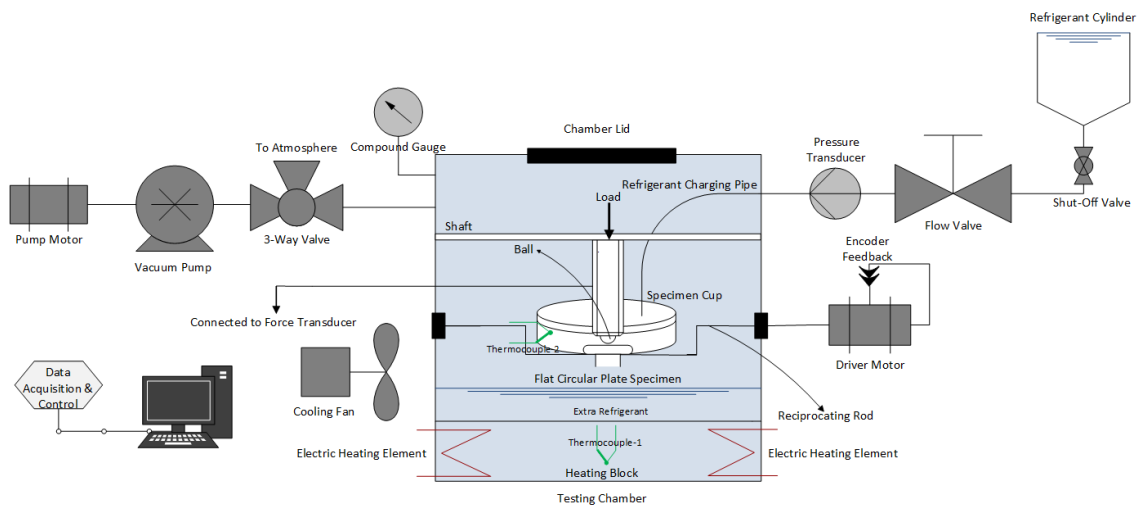
Fig. 3.2. Modification Schematic Layout (Bhutta and Khan 2019).

3.4 Contact Geometry

A Ball-on-Flat contact geometry has been chosen for experimentation. The balls are made of 52100 steel of 10 mm diameter which are commercially easily available and do not have to be specially manufactured. AISI 52100 steel is a common metal used in compressors and is tested by researchers when experimentally assessing the friction and wear performance of refrigerants (Yoon et al. 2000; Suh et al. 2003; Wu et al. 2004; Lee et al. 2005; Cannaday and Polycarpou 2006; Demas and Polycarpou 2006b; Nunez et al. 2008; De Mello et al. 2009; Solzak and Polycarpou 2010; Akram et al. 2013a; Akram et al. 2016; Nunez et al. Purdue University, Indiana, USA, 12-15 July, 2010, Paper 2031). The ball specimens are oil hardened, having excellent deformation and wear resistance. The 52100 steel ball specimens used in this study are vacuum degassed and evenly through hardened in electric furnaces. The flat disc specimen chosen for testing is mild steel (EN1A). EN1A is cheap, commercially easily available and easy to machine. EN1A has been proven to be a suitable substrate for the application of Nickel based coatings with good stability and good adhesion properties for electrodeposition of Nickel coatings (Bajwa et al. 2016a; Bajwa et al. 2016c, 2016b; Nazir et al. 2017; Nazir et al. 2018a). The arrangement and positioning of the specimens in shown in the drawing in figure 3.3. The flat specimen is circular in shape having diameter of 30 mm and thickness of 2.75 mm. Each flat specimen has two holes on its sides for securing it inside the specimen cup on the reciprocating rod of the machine. The flat mild steel specimens are cut from a circular rod and machined to the specifications.
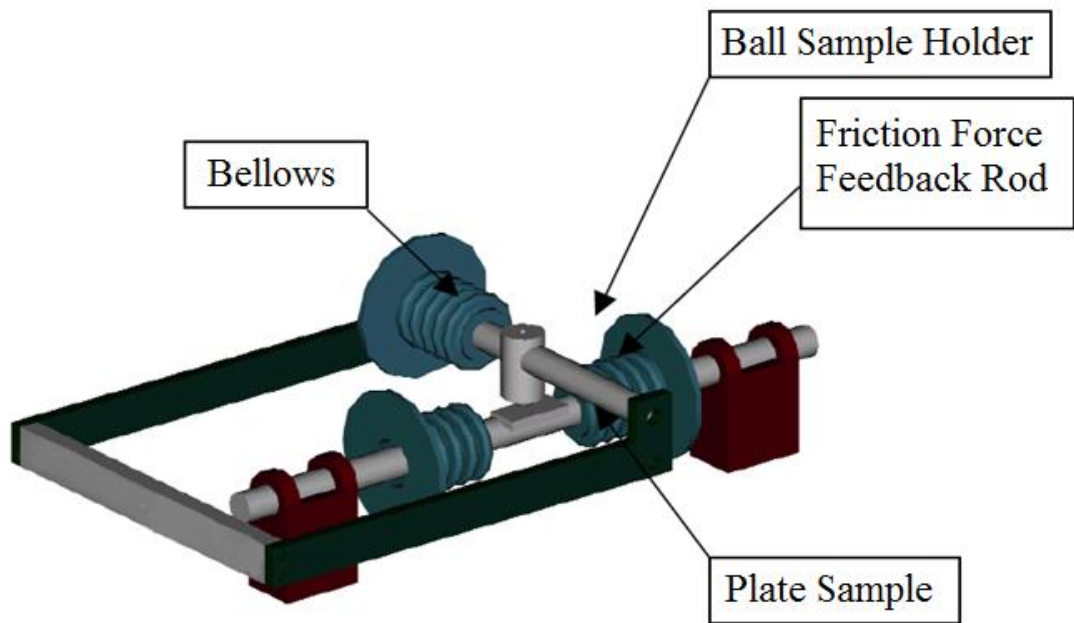
Fig. 3.3. Positioning of the specimens inside the pressure chamber (Garland, N. P., 2004).

The testing specimens are shown in figure 3.4. Various different refrigerants have been known to form tribological films on the surface of the rubbing parts which enhance friction and wear performance especially in the case of using ferrous metals. The testing materials will allow us to see if HFEs have the capability to form surface films and whether these are protective tribo-films which help reduce friction and/or wear or whether HFEs adversely react with the interacting materials resulting in increased wear and/or friction.
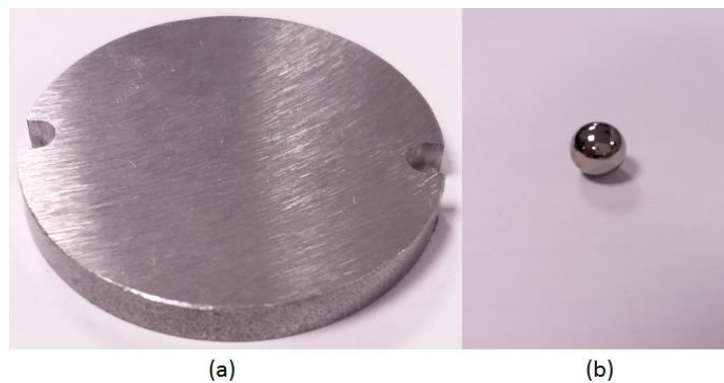
Fig. 3.4. Testing Specimens (a) EN1A Mild Steel flat circular disk (b) 52100 Steel ball.

The next phase of the experiments will be to study the tribological behaviour of HFE-7000 on Nickel-coated contacts and to suggest feasible electrodeposited Nickel based coatings which

will help improve the overall mechanical and tribological performance of interacting components in the presence of the future generation of refrigerants.

3.5 Instrumentation and Data Acquisition

The design modification of the test rig has been done in such a way to allow the control, monitoring, and recording of various test parameters. The various sensors, gauges and transducers installed in the system along with the data acquisition technique have been explained in the sections 3.5.1-3.5.6. Refrigerant charging system and the testing procedure has been explained in sections 3.5.7 and 3.5.9 respectively. The modified tribo-meter has been presented in section 3.5.8.

3.5.1   Chamber Pressure Measurement

The test chamber has the capability to be pressurized up to +3 bar and to be vacuumed to -1 bar. To monitor both the positive and negative pressure in the range of $-1\ to + 3\ bar$, a compound manual gauge and a pressure transducer have been installed. The pressure transducer allows on screen monitoring of the pressure and recording of the pressure values inside the testing chamber during the course of an experiment. A Telemecanique pressure transducer made of stainless steel having a transmitter range of $-1\ to + 9\ bar$ has been selected and installed, it can measure the pressure of refrigerants in the temperature range of $-20\ to\ 120°C$, the connections type is $G\ 1/4$ male, the output signal is linear in the range of $4\ to\ 20\ mA$, it has a response time of less than $5\ ms$, it is shock and vibration resistant having good repeatability and accuracy (Sensors, T., 2016). The pressure transducer has been connected to one of the analogue input channels of SLIM 2000. The additional compound gauge has been added in the system to allow for visual indication of the pressure variations. If the data acquisition system or the computer freezes for some reason the manual gauge will always allow an operator to observe the pressure readings and make sure that the pressure reading is within the safe operating limits.

3.5.2   Temperature Monitoring and Control

TE-57/77 allows the installations of multiple K-type thermocouples. To allow the control of temperature, two separate thermocouples have been installed. The first thermocouple is a probe type thermocouple which has been installed directly in the heater block to allow the monitoring of the temperature of the heating block. The heater block has the capability to be heated up to 200°C. The second thermocouple is a wire type thermocouple that is used to monitor the real

time temperature of the refrigerant in the specimen holding cup. The wire type thermocouple is secured by the means of a screw in the specimen cup before the start of each experiment. The wires of the thermocouple are run through the manual gauge which has been sealed on the other end with the help of a sealant. During the course of an experiment the temperature of the testing fluid is controlled by using the temperature readings from the wire type thermocouple, which are used in a PID algorithm for temperature control feedback for the heating elements. The heating elements are connected to a digital input/out port to allow the switching ON/OFF of the heaters. The two K-type thermocouples are connected to two separate analogue input ports that enables temperature monitoring, temperature control and recording of the temperature values. The output of the wire type thermocouple that monitors and controls the temperature of the refrigerant is connected to an analogue output port as well as being used in feedback control to maintain the fluid temperature. The feedback control loop to maintain the temperature of the refrigerant is shown in figure 3.5.
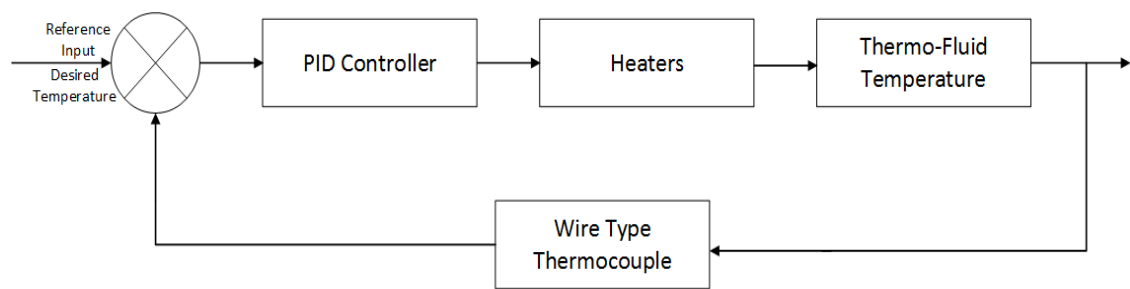
Fig. 3.5. Temperature control feedback loop.

The heating block is located at the very bottom of the pressure chamber as shown in figure 3.2. After the test specimens have been installed and the chamber has been vacuumed, the fluid is charged in the specimen cup. Additional fluid is charged in the system to make it over flow, the extra thermo-fluid drops at the bottom of the pressure chamber where the heater block is located. This extra fluid helps the transfer of heat and also ensures that not only the contacts are fully lubricated but also the chamber atmosphere contains sufficient vapours of the refrigerant. This further minimizes the effect of ambient air.

3.5.3 Lubricant Film Formation Measurement

TE-57/77 has an input port dedicated to contact potential measurement. The contact potential measurement enables; to observe the metal-to-metal interactions between the reciprocating parts, to judge if a suitable lubrication film was formed during various testing conditions and to

comment on the separation between the test specimens. The contact potential sensing is based on the principle of contact resistance measurement. The internal electrical circuit for the contact potential sensor is shown in figure 3.6.
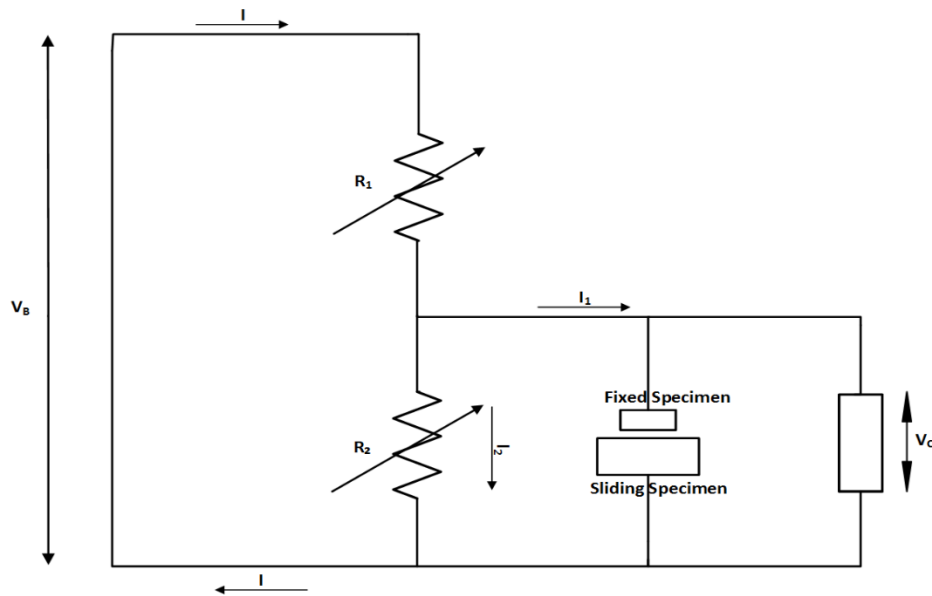
Fig. 3.6. Contact potential measurement circuit (Phoenix Tribology, 2002).

The internal electrical circuit allows the sensor to be calibrated in the range of 0-50 mV, with 0 volts referring to short circuit (metal-to-metal contact) and 50mV meaning open circuit (fully lubricated conditions). The sensor has been fine-tuned with the help of the two variable resistors R_1 and R_2 to give values in the full range of 0-50 mV, this increases the output resolution. V_B is the excitation voltage applied to the circuit and V_C is the output voltage that is sensed. The sensed voltage signal is fed to the contact potential input of the SLIM board using BNC connector.

For the sensor to be installed, the two contact geometries have to be electrically isolated. If the specimens are not isolated before the start of an experiment then the sensor will always read the state of a short circuit. The sensor should read a state of short circuit only when there is a metal-to-metal contact and should show values in the range of 0-50 mV during testing. To achieve this the two test specimens namely, the flat circular plate and the steel ball have to be electrically isolated. The specimen holding cup has been isolated from the body of the machine using insulation tape and nylon screws. The specimen holding cup is used to hold the flat circular specimen, isolating the cup isolates the flat circular specimen from the steel ball.

3.5.4   Reciprocating Frequency Measurement and Control

A tachometer is coupled directly at the back end of the driver motor shaft which provides the rotational speed of the motor. The signals from the tachometer are fed to the speed input unit on the SLIM board which are then used to determine the offset between the set point and the current speed to help maintain the motor speed. The feedback control loop for the motor speed is shown in figure 3.7.
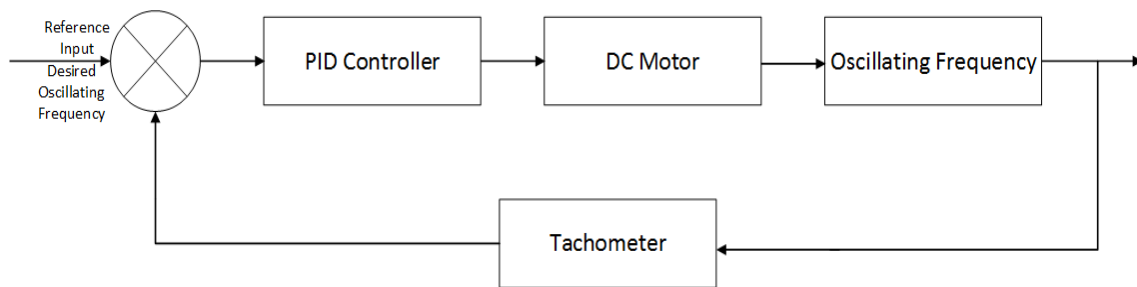
Fig. 3.7. Oscillating frequency feedback control loop.

The motor shaft is linked to the scotch yoke mechanism. The mechanism is secured with the reciprocating rod which holds the flat plate specimen with the help of a screw. The power is transmitted through the reciprocating rod which is supported by bearings on a linear guide rail. The amplitudes can be adjusted to give stroke lengths in the range of 0-5 mm.

3.5.5   Friction Force Measurement

A Kistler Piezo-electric friction force transducer comes fitted with the TE-57/77 tribometer. Normal load is applied by means of a spring balance attached to a cantilever arrangement. The cantilever exerts a force upon the force feedback transfer mechanism, hence on the contact. The position of the friction force transducer has been shown in figure 3.8. The sensor is attached to a yoke, the yoke is connected to a force feedback rod upon which a ball housing is mounted that holds the ball sample.
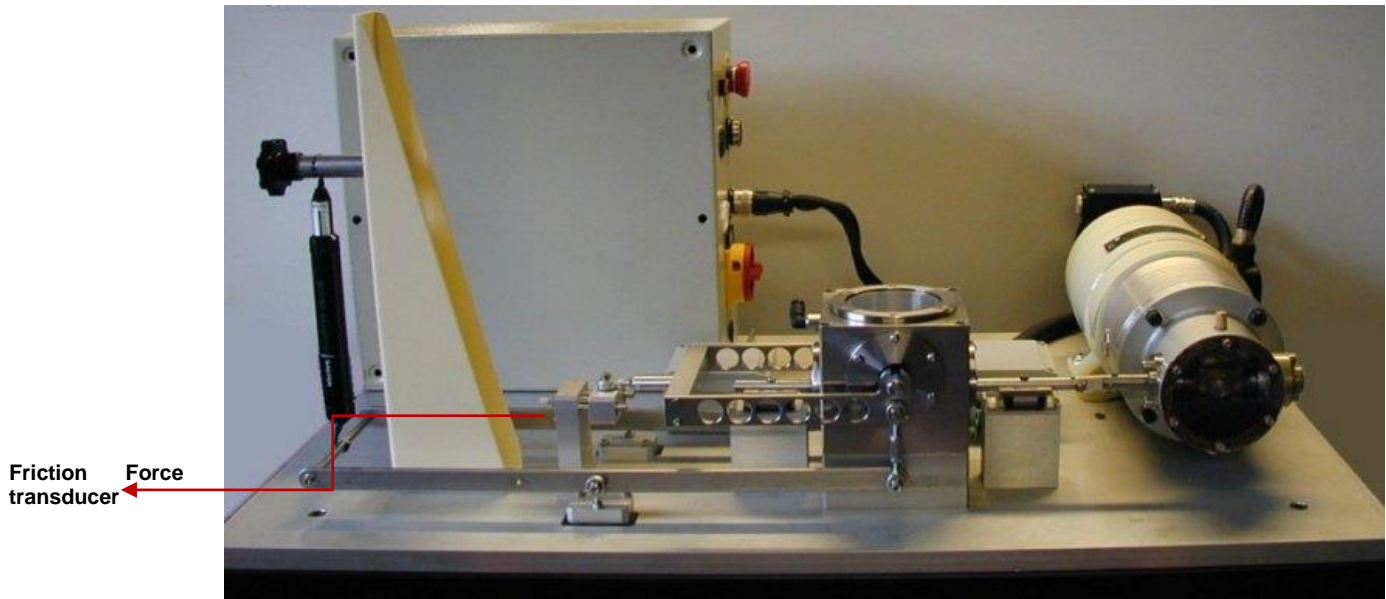
Fig. 3.8. Friction Force Transducer position.

Data from the friction force transducer is read through the friction force input port located at back of the SLIM data acquisition board. The applied manual normal load and the values of the friction force are used to calculate the real-time coefficient of friction in the software by means of equation 4.

3.5.6   Sample Installation

To start a test the ball and the flat disc samples have to be properly installed inside the testing chamber. Sample installation begins by placing the prepared flat disc sample in the specimen cup after which the holes in the disc sample are aligned with the pin holes in the specimen cup. Once the holes have been aligned the specimen cup containing the disc sample is fastened on the reciprocating rod of the tribo-meter with the help of nylon screws. This is followed by positioning and securing the wire-type thermocouple i.e. thermocouple-2 in the specimen holding cup. The ball sample is then fixed inside the ball holder with grub a screw after which the ball holder is screwed on the ball holder shaft. The ball holder shaft not only functions as a means to hold the ball sample in position but also provides the means to apply the normal load. Once both the samples have been secured in position the chamber lid is closed and sealed. The sealed chamber is then vacuumed with the help of the vacuum pump in order to minimize the effects of atmospheric oxygen and ambient air on the tests.

3.5.7 Refrigerant Charging System

After the samples have been secured into their respective positions and once the test chamber has been vacuumed the system is ready to be charged with the refrigerant. The fluid charging system has been designed in a way to always allow fully lubricated conditions while using minimum thermo-fluid. The fluid is contained in a fluid charging cylinder that has a flexible hose which connects the charging cylinder to a shut-off vale. The other side of the shut-off valve is connected to the copper pipes which runs through a flow control valve and contains a pressure transducer. The diameter of the copper pipe is reduced after it enters the pressure chamber to allow the pipe to go directly into the specimen cup as shown in the schematic diagram in figure 3.2. The shut-off valve and the flow control valve are used to control the volume of the fluid being charged in the system. The operator can manually observe the filling of the cup and charging of the thermo-fluid through the glass in the chamber's lid. The vacuum in the chamber and gravity helps the fluid to flow in the chamber. If required, a syringe can also be used to inject the fluid through the charging line. The syringe can be directly connected to the flexible hose at the shut-off valve. Sufficient quantity of the refrigerant is introduced so that the specimen holding cup overflows; this ensures fully-lubricated conditions at all times. The overflown/extra refrigerant gets collected at the bottom of the testing chamber where the heating block is located. The extra overflown refrigerant assists in heat transfer from the heater block to the refrigerant in the specimen holding cup.

3.5.8 Modified TE-57/77 Tribo-meter

Once modification of the tribo-meter was complete; all the sensors, transducers and the complete data acquisition was calibrated by the service engineer from Phoenix Tribology Ltd to ensure reliability of the readings from the modified test rig. The modified tribo-meter is shown in figure 3.9. A syringe is being used to charge the refrigerant, the pipe fittings are supported by screw-jacks and the environmental chamber of the modified tribo-meter can be completely sealed. Various program algorithms have been developed for use on the modified machine.

Experimental methodology followed to test the friction and wear behaviour of HFE-7000 was divided into two main parts. In the first part, un-coated flat steel discs samples of three different surface finish were used against 52100 steel ball in a ball-on-flat configuration. Different operating conditions were simulated by altering the applied normal load and by changing the refrigerant temperature. Uncoated study is discussed in detail in chapter 4. In the second part of the study five different types of Nickel coatings were deposited on the flat disc samples to test

them under identical operating conditions as the uncoated samples. Coated study is described in chapter 5.
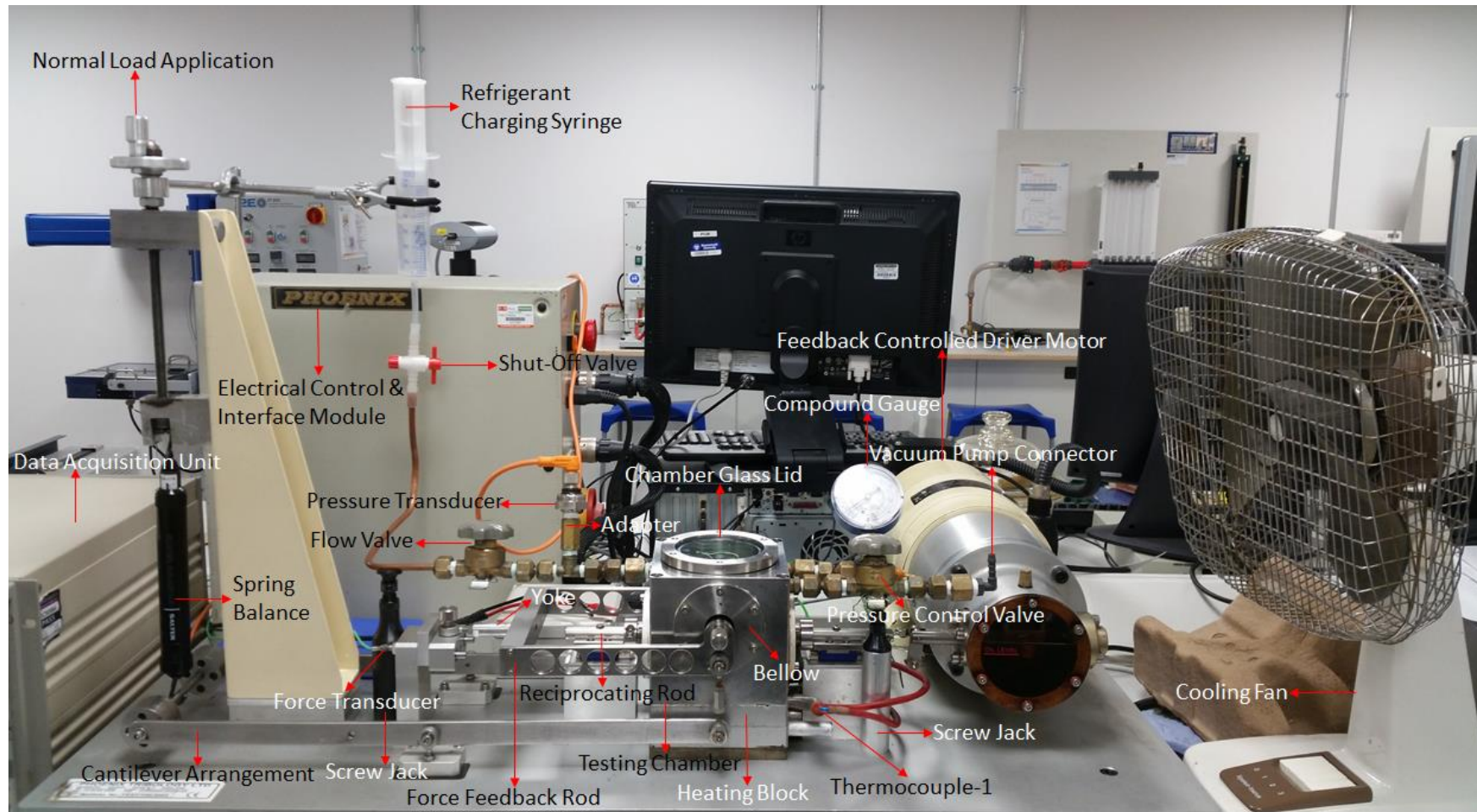
Fig. 3.9. The Modified tribo-meter.

3.5.9   Testing Procedure

The steel flat circular specimen is placed in the cup which is then secured on the oscillating rod with the help of screws. Then the wire type thermocouple is fastened into position. Steel ball is fixed on the ball-holder with the help of grub screws and ball holder is connected to the ball holder shaft. The shaft provides a means to secure the ball-holder in position and also functions as a means to apply the vertical normal load. After this the chamber is closed and sealed. The chamber is then vacuumed so as to minimise the effects of oxygen and ambient air during testing.

After the chamber has been vacuumed, HFE-7000 is introduced in the system by using the shut-off and flow valves. Sufficient amount of refrigerant is charged so that the cup overflows and the bottom flat specimen is fully immersed in the fluid which ensures fully lubricated conditions at all times. The extra overflown refrigerant gets collected at the bottom of the chamber where the heating block is located. This overflown refrigerant assists heat transfer from the heater block and helps maintain the refrigerant temperature in the specimen cup. The vacuum inside the test chamber and gravitational force helps the refrigerant to flow from the cylinder into the cup. The chamber lid has a transparent glass top which allows the operator to physically observe chamber conditions at all times. Next the desired load is manually applied. After this the control algorithm is run and the refrigerant inside the cup in the testing chamber is heated to the required temperature. The refrigerant temperature is controlled by using values from the wire type thermocouple and feedback PID control. Once the temperature reaches its specific value, the temperature of the refrigerant is stabilised and maintained for one hour before starting a test. After the temperature has been stabilised and has been maintained to the desired value for one hour, a test is run for two hours.

The oscillating frequency is controlled by using feedback controlled driver motor. The motor, the heater and all the transducers are connected to a microprocessor based central data acquisition and control system. The values of the friction force, the chamber pressure values, the temperature readings from the heater block, temperature of the refrigerant and the motor speed are continuously recorded in a spreadsheet. Each experiment will be repeated at least twice to ensure repeatability.

Coated and uncoated samples will be investigated under identical operating conditions. The testing procedures for uncoated and coated specimens are given in tables 4.1 and 5.2 respectively. The uncoated specimens have been tested by varying their average surface

roughness, the applied normal load and the bulk refrigerant temperature. The results obtained by this study will give a clear understanding about the tribological behaviour of HFE-7000 under varying operating conditions. The uncoated study will be followed by Nickel based electrodeposited coatings, the coated samples will be investigated under the same conditions as uncoated test specimens. Testing of coated and uncoated samples under identical operating conditions will provide a direct comparison of the effect of coatings on the tribological performance to uncoated specimens. The results of these studies will be used to identify the most suitable coatings for enhancing the tribological performance of interacting parts operating in HFE-7000 refrigerant environment.

Chapter 4

Uncoated Study

Testing methodology followed for testing the wear and friction performance of HFE-7000 using uncoated specimens has been summarized in table 4.1. Flat plate circular specimens of three different surface roughness; 0.05 μm, 0.1 μm and 1.0 μm of EN1A steel were used against 52100 steel ball. These surface roughness values indicate fine surface finish (0.05 μm), average surface finish (0.1 μm) and rough surface finish (1.0 μm). Surface finish is normally achieved by a mechanical grinding and polishing process. Mechanically grinding and polishing requires material, energy and man-hours. Having parts of a range of surface finish will show the influence of friction and wear by change in surface roughness of rubbing parts subject to HFE-7000 lubrication. Interacting parts of various surface roughness operating under different conditions with different refrigerants show different results. A study conducted by using parts of *three* different surface finish to evaluate the effect of surface roughness on scuffing using HFC-134a as refrigerant concluded that parts with a lower surface roughness result in lower friction force and friction coefficient values (Yoon et al. 2000). However another study conducted to access the influence of surface roughness under sliding condition of rubbing parts in HFC-410A environment concluded that an optimum initial surface roughness value prolongs the wear life and enhances the load carrying ability of interacting parts (Lee and Oh 2003); parts of *three* different surface values were also used in this investigation. In another study conducted to investigate effects of change in surface roughness on polymer films with HFC-134a showed discontinuous transfer layers on rougher surfaces while smooth continuous transfer layers were formed on surfaces with lower roughness (Nunez and Polycarpou 2015). HFE-7000 has never been investigated from a tribological point of view which makes it imperative to study its behaviour at changing load and temperature conditions in addition to analysing the role of surface finish of mating parts.

4.1   Sample Preparation of Uncoated Samples

Each flat circular sample was machined to a thickness of 2.75 mm from a circular steel rod using conventional machining methods. The diameter of each flat disc sample was 30 mm. Every sample was then mechanically grinded and polished to achieve the average roughness values of 0.05 μm, 0.1 μm and 1.0 μm. Average surface values of each sample was ensured by using a white light interferometer (ZYGO). After the desired surface finish had been achieved,

each sample was conditioned in an ultrasonic bath for 5 minutes. After 5 minutes the sample was removed from the ultrasonic bath and was dried with warm air using a specimen drier. The grinding and polishing process followed by conditioning of each sample with acetone ensured the removal of any oxides and/or unwanted surface films present on the disc surface. The ball samples were also conditioned with acetone for 5 minutes in the ultrasonic bath and dried with warm air before each experiment. Once the samples are ready they are installed in the testing chamber following the steps described in section 3.5.6. After sample installation the refrigerant is introduced in the testing chamber using the procedure described in section 3.5.7. At this point the system is ready for testing and a test algorithm is run following the procedure mentioned in section 3.5.9. Results of the uncoated study have been presented in terms of friction and wear in sections 4.2 and 4.3 respectively.

Table 4.1 Testing methodology for uncoated specimens.

Sr No	Surface Roughness, R_a (μm)	Refrigerant Temperature (°C)	Load (N)
1	0.05	20	10
2	0.05	20	20
3	0.05	20	30
4	0.05	30	10
5	0.05	30	20
6	0.05	30	30
7	0.05	40	10
8	0.05	40	20
9	0.05	40	30
10	0.1	20	10
11	0.1	20	20
12	0.1	20	30
13	0.1	30	10
14	0.1	30	20
15	0.1	30	30
16	0.1	40	10
17	0.1	40	20
18	0.1	40	30
19	1.0	20	10
20	1.0	20	20
21	1.0	20	30
22	1.0	30	10
23	1.0	30	20
24	1.0	30	30
25	1.0	40	10
26	1.0	40	20
27	1.0	40	30

Mechanical properties of the samples used in the uncoated study have been listed in table 4.2. Poisson's ratio of 52100 was set at 0.30 while 0.25 was used as the Poisson's ratio for EN1A in equations 19 and 20 along with the measured mechanical properties listed in table 4.2 to

determine the Maximum Hertzian Pressure. A load range of 10-30 N translates into a Hertzian Contact Stress range of 983.5-1418.4 Mpa.

Table 4.2 Measured mechanical properties of uncoated specimens.

Specimen	Hardness (HV)	Elastic Modulus (Gpa)	R_a (μm)
Steel Ball	810	210	0.010
Uncoated Steel Specimens	180	200	0.05, 0.1, 1.0

4.2 Friction Behaviour of Uncoated Steel

Results of friction have been presented and discussed in terms of real-time coefficient of friction, average friction coefficient and average frictional force.

4.2.1 Real-time Coefficient of Friction of Uncoated Steel

Real-time coefficient of friction graphs of flat disc sample having 0.05 μm average surface roughness values have been presented in figure 4.1. The coefficient of friction was calculated in real time by using the values of the friction force from the friction force transducer and the applied normal load using equation 4.

Figure 4.1 (a) shows that at refrigerant temperature of 20°C, the values of the coefficient of friction decrease with increase in load from 10 N to 30 N. It is also observed from the real-time coefficient of friction data that increase in applied normal load results in fewer variations in the friction coefficient and more stable values. At the least applied load of 10 N the friction coefficient increased sharply and reached a maximum value after which the coefficient of friction decreased. After a dip in the values, the friction coefficient increases again and reaches a stable value at the end of the experiment.

Increasing the normal load to 20 N at 20°C refrigerant temperature decreased the values of friction coefficient compared to 10 N/20°C. The maximum values of the coefficient of friction at 20 N/20°C were also less than the maximum friction coefficient values observed at 10 N/20°C.

For 30 N/20°C, the coefficient of friction was observed to be much more stable and resulted in much lower values for the first half of the experiment, the friction coefficient however increased just before the end of the experiment.
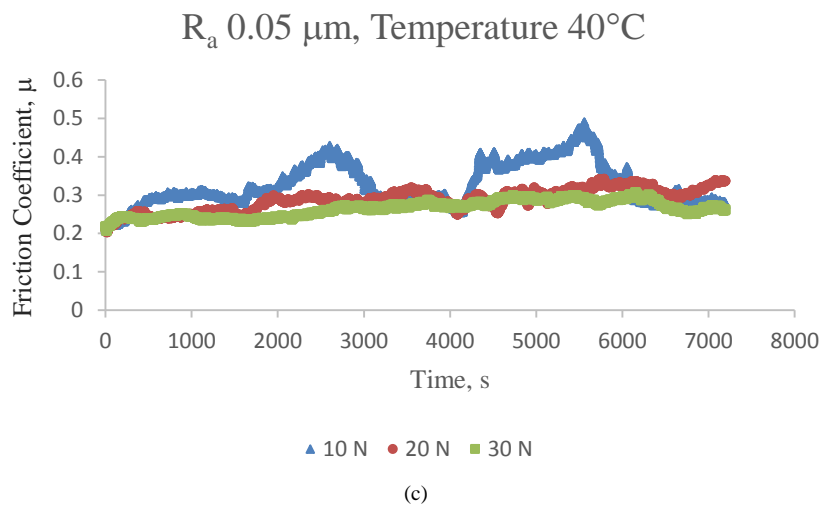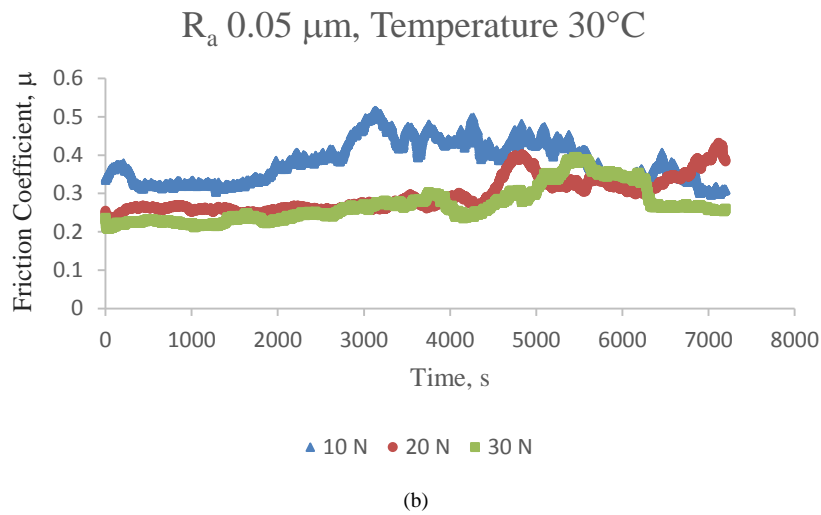
Fig. 4.1. Coefficient of friction graphs for R_a 0.05 µm, Refrigerant temperature: (a) 20°C (b) 30°C (c) 40°C (Bhutta and Khan 2019).

An increase in refrigerant temperature by 10°C lowered the coefficient of friction at 10 N load as seen in figure 4.1 (b). The values of the friction coefficient were higher at 10 N/20°C in comparison to 10 N/30°C. Steep gradient and rise in values as seen at 10 N/20°C was also not observed at 10 N/30°C. 10 N/30°C testing conditions also showed fluctuations in the coefficient of friction values and the friction coefficient decreased at the end of the experiment displaying similar values to those that were produced at the start of the test.

Increasing the applied load to 20 N at 30°C refrigerant temperature produced similar overall results to 20 N/20°C. Friction coefficient was fairly stable during the first half of the test after which the values of the coefficient of friction were seen to increase.

Real-time friction coefficient results generated at 30 N/30°C followed almost the same pattern and produced similar values to 30 N/20°C for the first half of the test. During the second hour of the test a raise and fall in the coefficient of friction was observed. At the end of the experiment the friction coefficient obtained low, steady and stable values.

A rise in the refrigerant temperature to 40°C resulted in a further drop in the values of the coefficient of friction. Compared to 10 N/20°C and 10 N/30°C, the values were seen to fluctuate as the experiment progressed but a sharp increase in the friction coefficient was not observed at 10 N/40°C during the first 30 minutes of testing. After an initial increase the values, the coefficient of friction stabilised. The friction coefficient increased and decreased twice resulting the in the formation of two separate peaks with the second peak being higher than the first one.

20 N/40°C conditions produced a similar overall behaviour to 20 N/20°C and 20 N/30°C. Some fluctuations can be seen, but 20 N/40°C conditions did not result in the generation of any steep gradients and major peaks.

The overall results of the coefficient of friction of 30 N/40°C were also similar to 30 N/20°C and 30 N/30°C. Very minor fluctuations were noted at 30 N/40°C. 30 N/40°C also produced the most stable coefficient of friction values from all the experiments conducted at R_a 0.05 μm.

Once all the tests had been performed on the discs with fine surface finish (R_a 0.05 μm), experiments were conducted on the discs of average surface finish having R_a 0.1μm at the same testing conditions. Results of the tests performed at R_a 0.1 μm have been presented in figure 4.2. The friction coefficient data obtained by using discs with R_a of 0.1 μm displayed similar results to those generated by using discs with R_a of 0.05 μm.
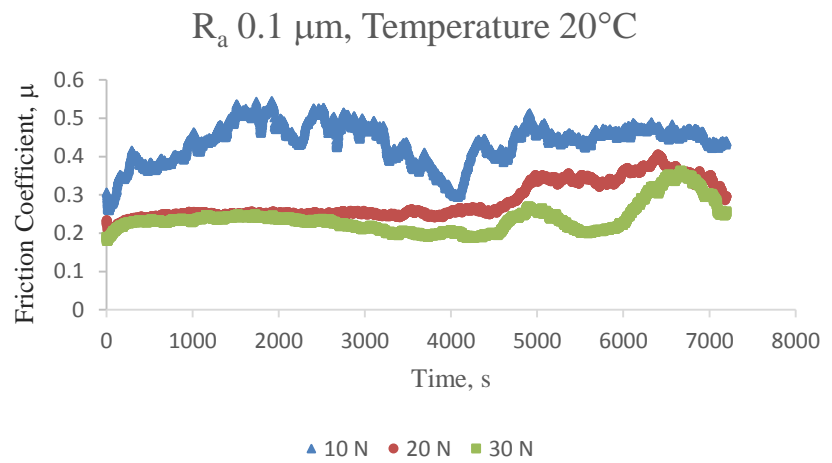
(a)
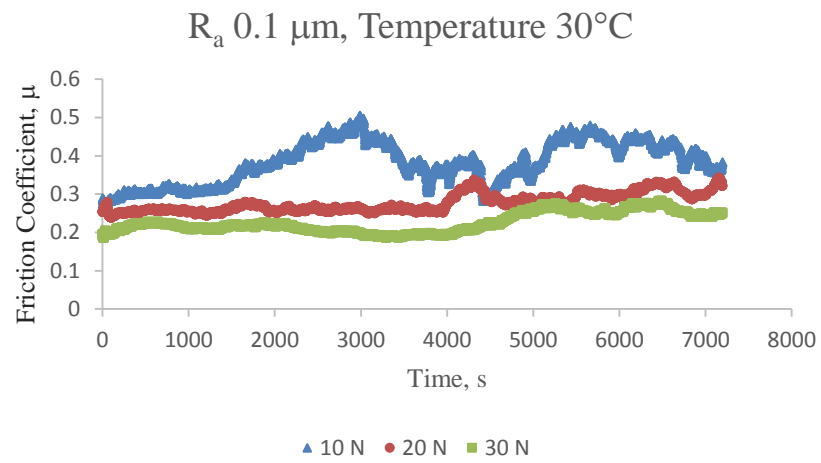
(b)
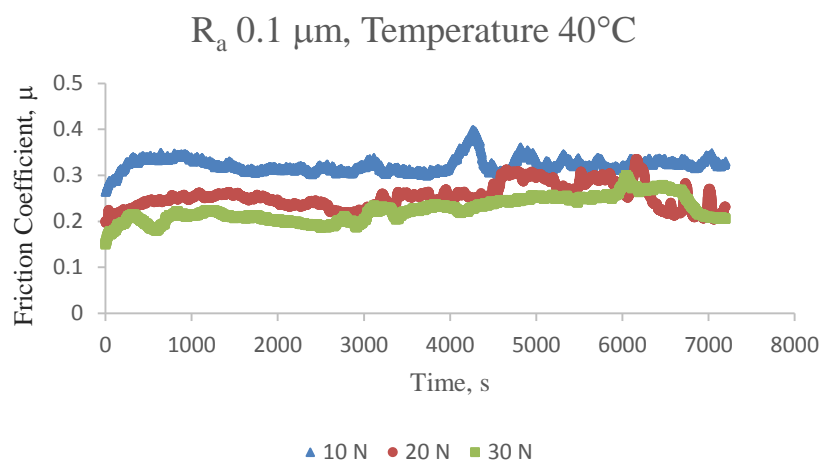
(c)

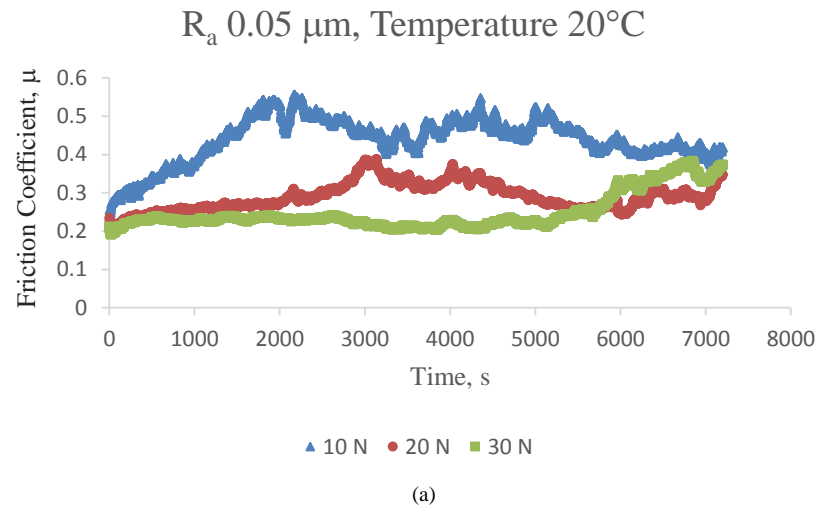**Fig. 4.2.** Coefficient of friction graphs for R_a 0.1 μm, refrigerant temperature: (a) 20°C (b) 30°C (c) 40°C (Bhutta and Khan 2019).

At 10 N/20°C with R_a 0.1 µm the overall values and variations in the friction coefficient were very similar to the values obtained at 10 N/20°C with R_a 0.05 µm. The coefficient of friction displayed a similar initial increase and fluctuations followed by stabilisation towards the end of the experiment.

Increasing the normal applied load to 20 N at 20°C refrigerant temperature for R_a 0.1 µm produced initial results of friction coefficient that were very similar to those produced at R_a 0.05 µm, 20 N load and 20°C. Values at 20°C/20 N for R_a 0.1 µm show stable values for the coefficient of friction for a longer time period. The values of the friction coefficient did increase but only in the second half of the test, friction coefficient values are also seen to decrease at the end of the test after increasing.

At refrigerant temperature 20°C, normal load 30 N for R_a 0.1 µm, the range of values of the friction coefficient are very similar to the values generated at 20°C/30 N with R_a of 0.05 µm.

For R_a 0.1 µm, refrigerant temperature 30°C and applied loads of 10 N and 20 N produced similar results to R_a 0.05 µm, refrigerant temperature 30°C and normal applied loads of 10 N and 20 N respectively. At testing conditions of 30°C/30 N for discs with R_a 0.1 µm the overall friction coefficient was lower in comparison to R_a of 0.05 µm tested at 30°C/30 N.

The coefficient of friction becomes more stable and the values of the friction coefficient decrease by increasing the refrigerant temperature to 40°C at 10 N load in comparison to 20°C/10 N and 30°C/10 N for R_a of 0.1 µm. The coefficient of friction was also more stable with lower overall values for R_a 0.1 µm tested at 40°C/10 N in comparison to R_a 0.05 µm tested at 40°C/10 N.

For HFE-7000 temperature of 40°C at 20 N load for R_a 0.1 µm the values of the coefficient of friction were lower than the values obtained at 20 N load, R_a 0.1 µm and refrigerant temperatures of 20°C and 30°C. The values in this case are also lower than the values obtained at HFE-7000 temperature of 40°C at 20 N load with R_a 0.05 µm.

The data obtained for the coefficient of friction for R_a 0.1 µm tested at 30 N load 40°C refrigerant temperature shows a decrease in the values of the friction coefficient in comparison to the friction coefficient values produced at 40°C/30N with R_a of 0.05 µm. However when

comparing the results of 40°C/30N to 20°C/30N and 30°C/30N, with R_a 0.1 μm mostly similar results can be seen.

Results of the real-time coefficient of friction by using flat disc sample with the rough surface finish having average surface roughness of 1.0 μm are shown in figure 4.3. Increasing the average surface roughness by 10 times from 0.1 μm to 1.0 μm showed a very similar trend, overall behaviour and coefficient of friction values for all testing conditions.

R_a 1 μm, Temperature 20°C

(a)

R_a 1 μm, Temperature 30°C

(b)

R$_a$ 1 µm, Temperature 40°C

(c)
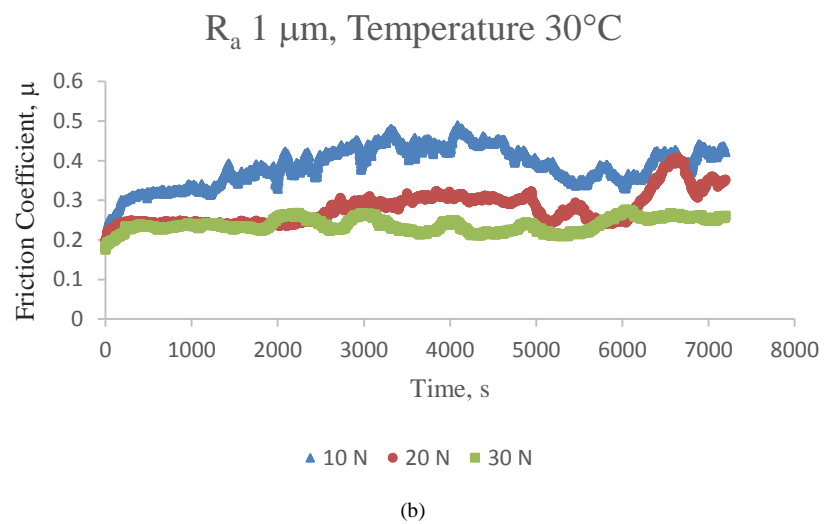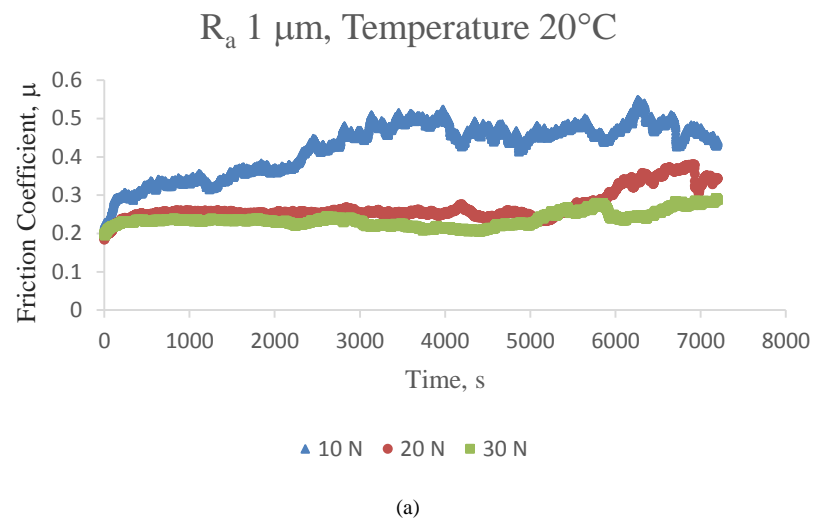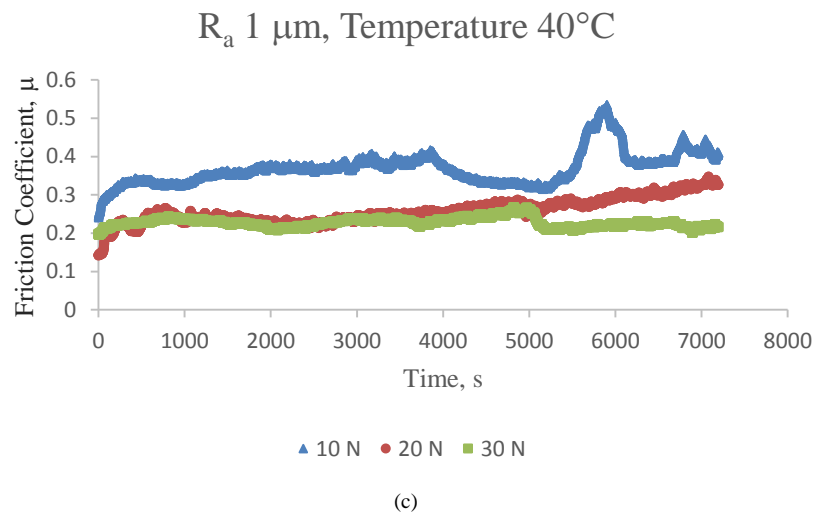
Fig. 4.3. Coefficient of friction graphs for R$_a$ 1.0 µm, refrigerant temperature: (a) 20°C (b) 30°C (c) 40°C (Bhutta and Khan 2019).

52100 steel ball starts to wear during the course of an experiment leading to an increase in the area of contact. The wear scar produced in a ball-on flat contact configuration on the stationary steel ball loaded against a disc has been known to change shape resulting in an increase in the apparent contact area. Increase in the area of contact leads to a decrease in the average contact pressure (Jean-Fulcrand et al. 2017). Increase in wear in an oscillating ball-on-flat test geometry has also been reported to cause an increase in the Hertzian diameter of 52100 steel balls (Deshpande et al. 2018). The coefficient of friction is seen to decrease with an increase in load and a rise in the refrigerant temperature, this decrease in the friction coefficient is due to the development of protective surface tribological films on the freshly exposed metallic surfaces. The coefficient of friction reaches a stable value with the progression of an experiment as the contact geometries become more favourable and once the tribo-films have been uniformly formed. Multiple peaks can be seen in some of the results of the real-time coefficient of friction graphs. The first peak denotes the initiation of the flattening of the steel ball and the second peak indicates a further change in the contact area of the ball. Shape of the wear scar on the ball changes with a change in testing conditions. Wear scar generated on a steel ball has bene known to shift from a circular shape at lower applied loads towards an elliptical shape at higher loads (Jean-Fulcrand et al. 2017). Increasing the average surface roughness at the same testing conditions leads to higher asperity interactions which accelerates the change in ball contact area, however at the same time harsher testing environments assist in the formation protective tribo-films.

The variations and fluctuations in the coefficient of friction especially at low loads at lower refrigerant temperature are believed to be caused by multiple reasons. The generated wear debris are trapped inside the specimen holding cup, these debris are believed to cause wear by three body abrasive wear mechanism. Initial fluctuations at the start of a test which are more evident at lower surface roughness can also be a result of the uneven development of surface films, these tribo-films are believed to be uniformly adhered to the metallic surfaces after a certain amount of time which is also apparent from the real-time friction coefficient graphs which can be seen to stabilise with time. Fluctuations in the coefficient of friction are also linked to adhesive wear. Soft EN1A steel is adhered to the top surface of the hard 52100 steel ball and the continuous reciprocating motion of the disc against the stationary ball with adhered particles gives rise to fluctuations and variations in the friction coefficient.

4.2.2   Average Coefficient of Friction of Uncoated Samples

The results of the average coefficient of friction for all the tests conducted on uncoated steel samples have been presented in figure 4.4. The graphs show a similar trend and pattern for all the surface roughness values investigated in the uncoated study. Increase in load at a constant temperature results in the reduction in the values of the coefficient of friction. Increase in load implies harsher testing conditions which assist in chemical reactions between the refrigerant (HFE-7000) and the rubbing metals.

R_a 0.05 µm
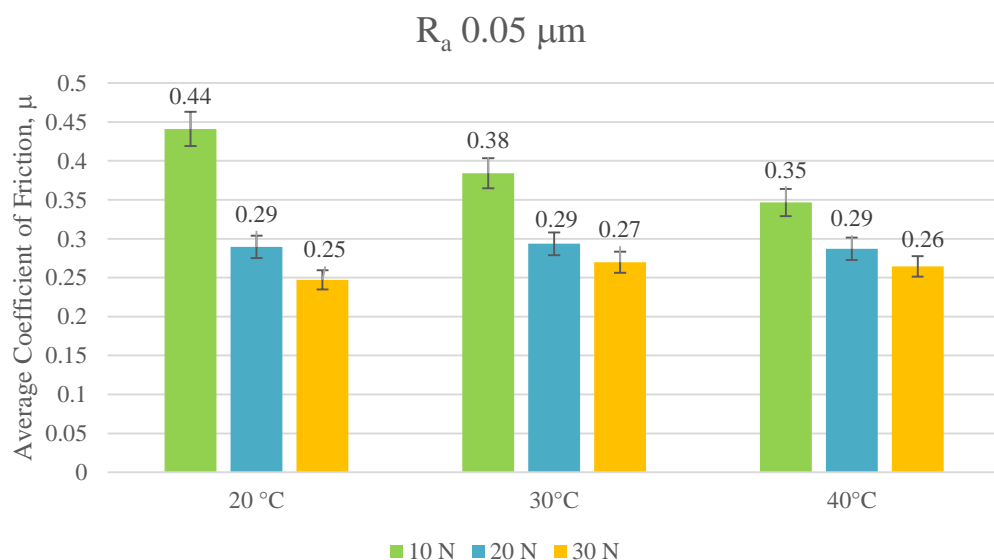
(a)
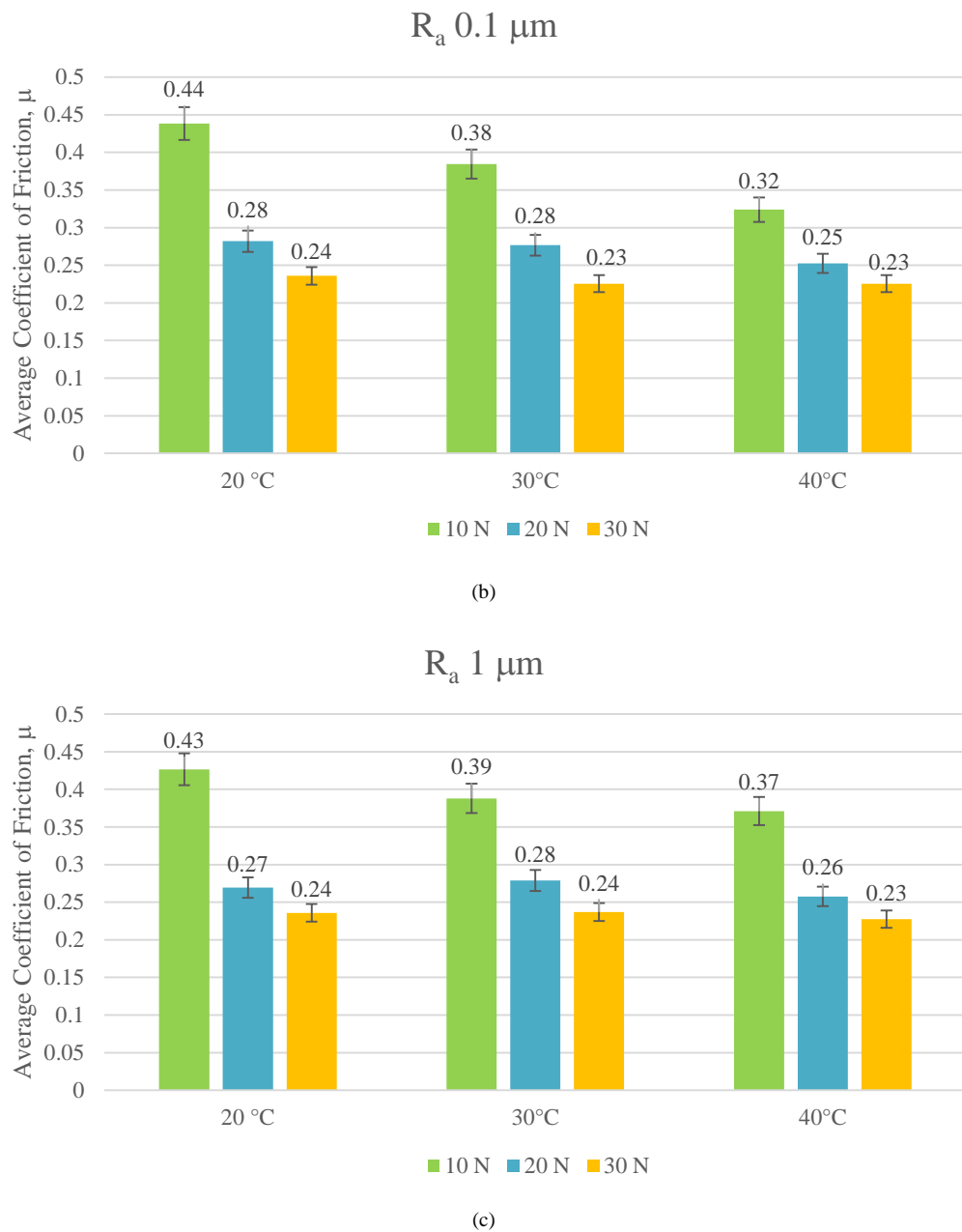
Fig. 4.4. Average coefficient of friction plots: (a) R_a 0.05 µm (b) R_a 0.1 µm (c) R_a 1.0 µm (Bhutta and Khan 2019).

The chemical reaction between the refrigerant and the mating metallic bodies results in the production of protective tribo-films on the top surface of the metallic parts which results in a decrease in the coefficient of friction. Increase in refrigerant temperature at 10 N load also showed a decrease in the average coefficient of friction. At higher loads a significant change in the average friction coefficient was not observed by increasing the temperature of the refrigerant at the same applied load. Increasing the refrigerant temperature at any load reduces its viscosity.

Reduction in viscosity means a decrease in separation between the ball and the disc which should result in higher asperity interactions and lead to an increase in the coefficient of friction. The coefficient of friction however decreased at lower loads and stayed almost constant at higher applied loads with increase in refrigerant temperature. The results of the average coefficient of friction indicate that the reactivity of HFE-7000 increases with increase in temperature which accelerates the process of development of protective surface films. Formation and development of these protective tribological films has been explained in the Tribochemistry Discussion Section in section 4.4.

4.2.3   Average Friction Force of Uncoated Samples

The results of the average friction force for all the uncoated samples are presented in figure 4.5. For all the surface roughness values tested in the uncoated study the average frictional force can be seen to increase with an increase in applied normal load at a constant refrigerant temperature. Increase in the refrigerant temperature at 10 N load resulted in a decrease in the coefficient of friction for all surface roughness values. 20 N and 30 N loads tested at Ra 0.05 μm and Ra 1.0 μm produced a minor increase in the average frictional force values with an increase in refrigerant temperature from 20°C to 30°C, the average friction force decreased for both these loads by increasing the refrigerant temperature from 30°C to 40°C.

(a)

R$_a$ 0.1 μm

(b)

R$_a$ 1 μm

(c)
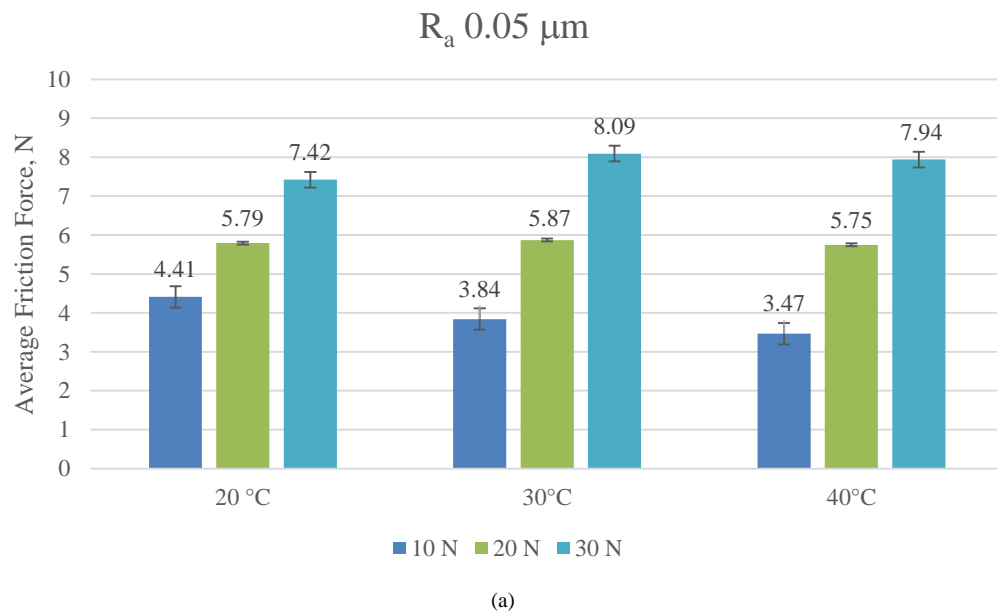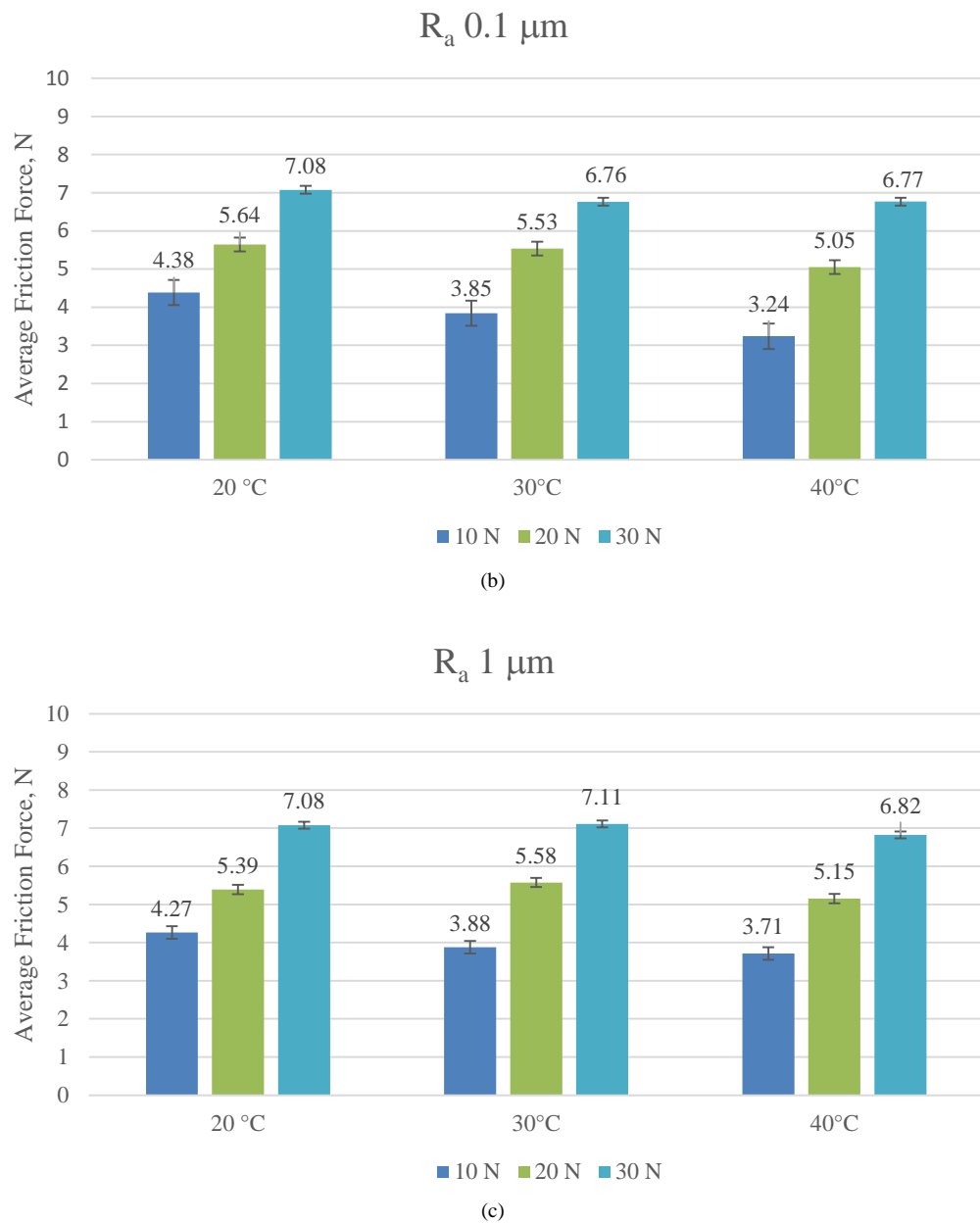
Fig. 4.5. Average friction force plots: (a) R$_a$ 0.05 μm (b) R$_a$ 0.1 μm (c) R$_a$ 1.0 μm (Bhutta and Khan 2019).

The average frictional force values reduced with a rise in refrigerant temperature at 20 N load for R$_a$ 0.1 μm. Increasing the refrigerant temperature from 20°C to 30°C decreased the average coefficient of friction at 30 N load for R$_a$ of 0.1 μm, however average friction force values remained almost constant by further increasing the temperature from 30°C to 40°C for steel disc with average surface roughness value of 0.1 μm.

Minimum frictional force values were recorded at 40°C with R_a of 0.1 μm for all the applied loads in comparison to R_a 0.05 μm and R_a 1.0 μm. These results indicate that there is an optimum value of surface roughness when operating at higher refrigerant temperatures at which the best values of frictional force are achieved.

4.3 Wear Performance of Uncoated Steel Samples

Post-test analysis of the flat disc and ball samples presented a combination of abrasive and adhesive wear. Adhesive wear was witnessed mostly at the far ends of the wear scar while abrasive wear was more dominant in the middle section of the wear scar. Soft EN1A steel discs were ploughed by the hard 52100 steel balls. Material pileup was observed at the extreme ends of the wear track.

Fig. 4.6. Micrographs of wear track on disc samples with R_a 0.05 μm: (a) 10 N, 20°C (b) 20 N, 20°C (c) 30 N, 20°C (d) 10 N, 30°C (e) 20 N, 30°C (f) 30 N, 30°C (g) 10 N, 40°C (h) 20 N, 40°C (i) 30 N, 40°C (Bhutta and Khan 2019).

Micrographs generated through Scanning Electron Microscope (SEM) of the disc samples with average surface roughness of 0.05 μm have been displayed in figure 4.6. The high magnification SEM images interestingly revealed more abrasive wear and less adhesive wear for applied load of 20 N for all the refrigerant temperatures. Magnified SEM images of a 52100 steel ball tested against EN1A steel disc of R_a 0.05 μm at 10 N applied normal load with 20°C refrigerant temperature are shown in figure 4.7. The magnified images show adhered soft EN1A steel to the hard surface of the 52100 steel ball. Adhesive wear is presumably more dominant at the start of a test. Once the normal load has been applied and the reciprocating motion has not yet started the entire contact load is supported only through very small area of asperity contacts which generates very high real contact pressure values. Fragments from the surface of the soft EN1A steel disc detach under relative motion and get attached to the hard 52100 steel ball. With the normally loaded EN1A steel disc sliding against the hard stationary steel ball, an adhesive junction breaks. With continuous sliding motion fresh junctions form and rupture. As the experiment progresses running-in of the components is achieved with the contact geometries become more favourable with time and after the formation of tribo-films has been initiated the wear phenomenon shifts more towards abrasive wear. Wear debris produced during the course of an experiment are trapped in the specimen holding cup with leads to three body abrasive wear. The continuous reciprocating motion causes ploughing of soft steel discs by the hard steel balls and causes material pileup on the sides of the wear track.

Fig. 4.7. Magnified images of the ball sample tested at 10 N, 20°C (Bhutta and Khan 2019).

All other sample pairs with different surface roughness were also thoroughly examined under SEM and similar results were observed by examining the other surface values as well.

4.3.1   Wear Volume of Uncoated Steel Samples

Each flat disc sample also analysed under ZYGO, the white light interferometer as shown in figure 4.8 to generate 3D plots of the wear track. The 3D plot of each wear track was used to calculate the wear volume of each sample post-experimentation. Figure 4.9 shows the 3D oblique plots of all the tests conducted on the disc samples with R_a 0.05 μm.
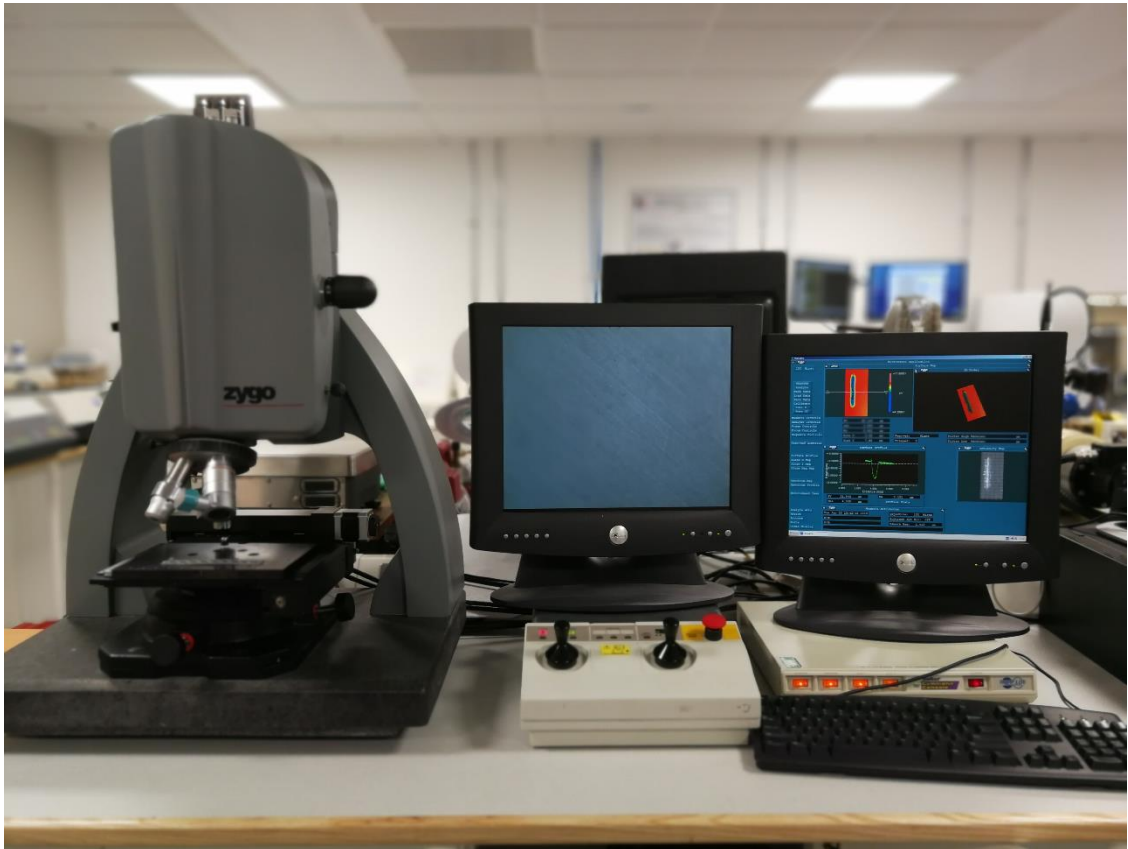
Fig. 4.8. White Light Interferometer (ZYGO NewView 5000).

Increasing the applied load at 20°C refrigerant temperature produced a deeper and wider wear track indicating an increase in wear volume. A similar pattern was also noted at 30°C refrigerant temperature, increase in normal applied load generated more wear. The 3D oblique plots also show that by increasing the temperature of HFE-7000 from 20°C to 30°C at any given load reduces the width and depth of the wear scar indicating reduction in wear volume. The shallowest wear track was produced at 40°C/20 N testing conditions. Wear tracks generated at 40°C at any given load resulted in the generation of shallower wear tracks in comparison to test conducted at 20°C and 30°C.

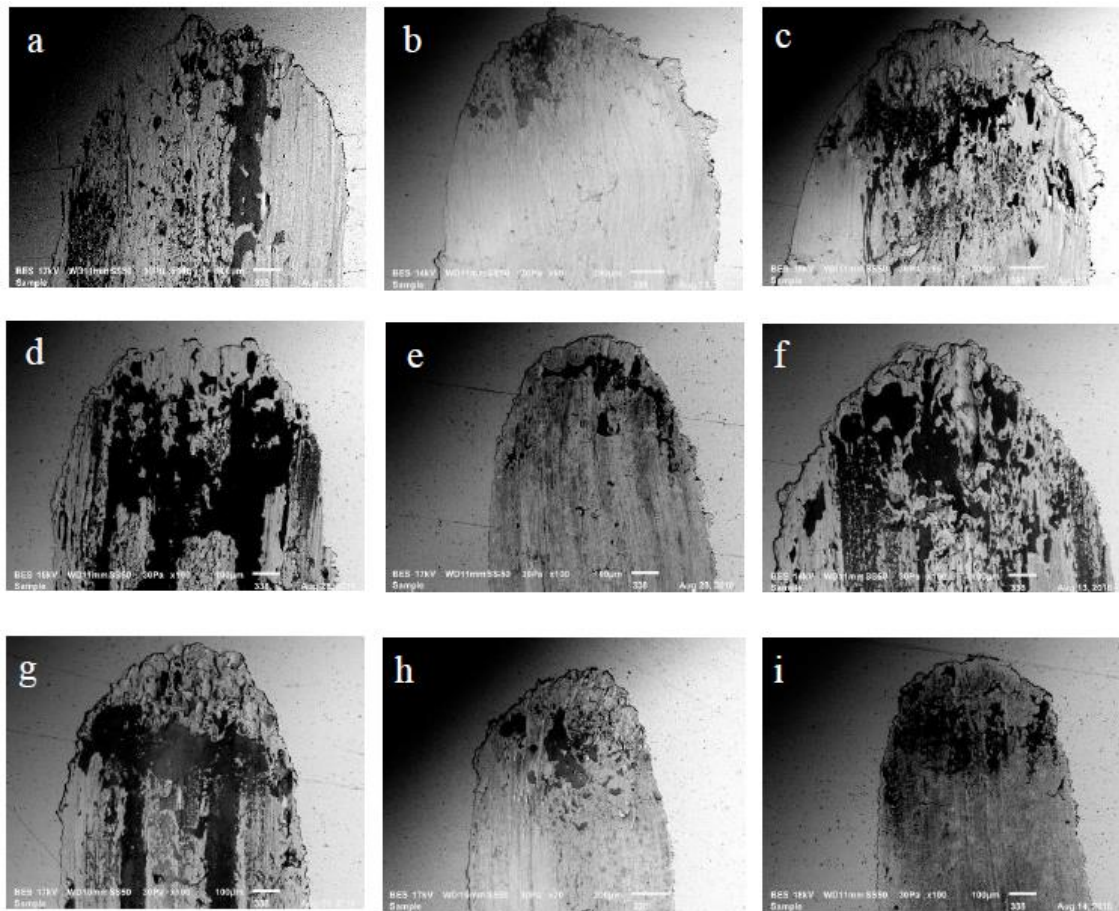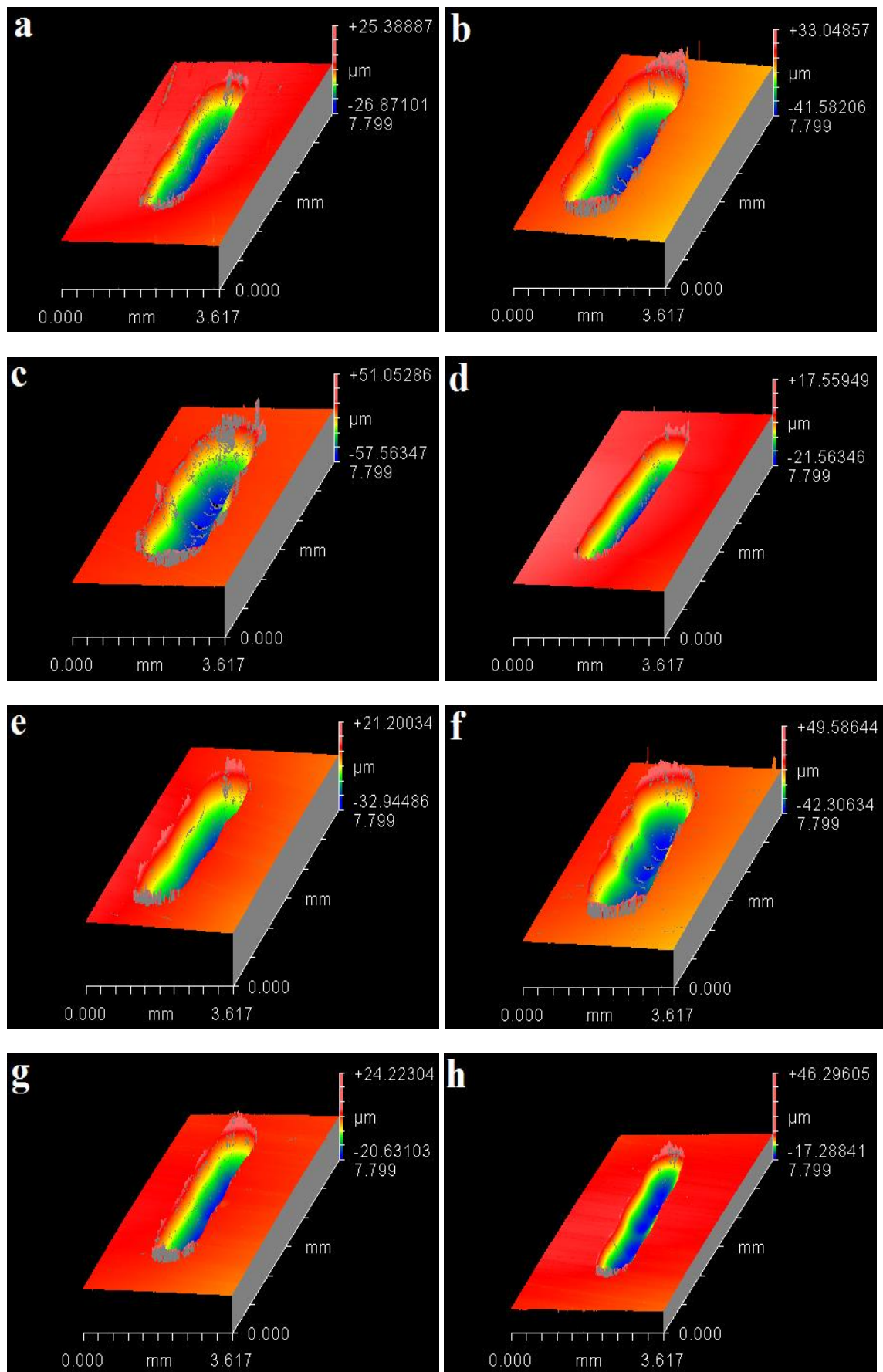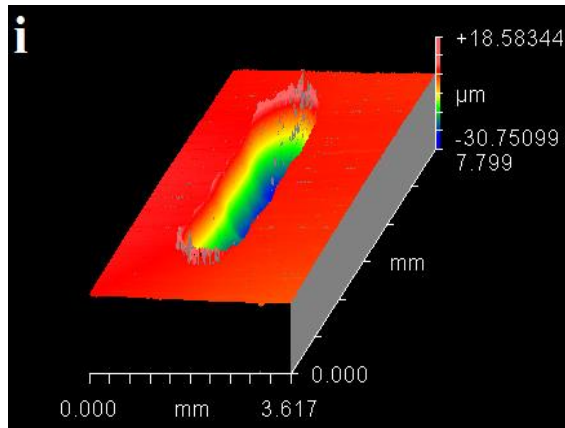**Fig. 4.9.** 3D oblique plots of wear track on disc samples with R$_a$ 0.05 μm: (a) 10 N, 20°C (b) 20 N, 20°C (c) 30 N, 20°C (d) 10 N, 30°C (e) 20 N, 30°C (f) 30 N, 30°C (g) 10 N, 40°C (h) 20 N, 40°C (i) 30 N, 40°C (Bhutta and Khan 2019).

3D oblique plots were used to measure the wear volume of the wear track produced on each flat sample. The results of the wear volume for all the samples have been presented in figure 4.10.
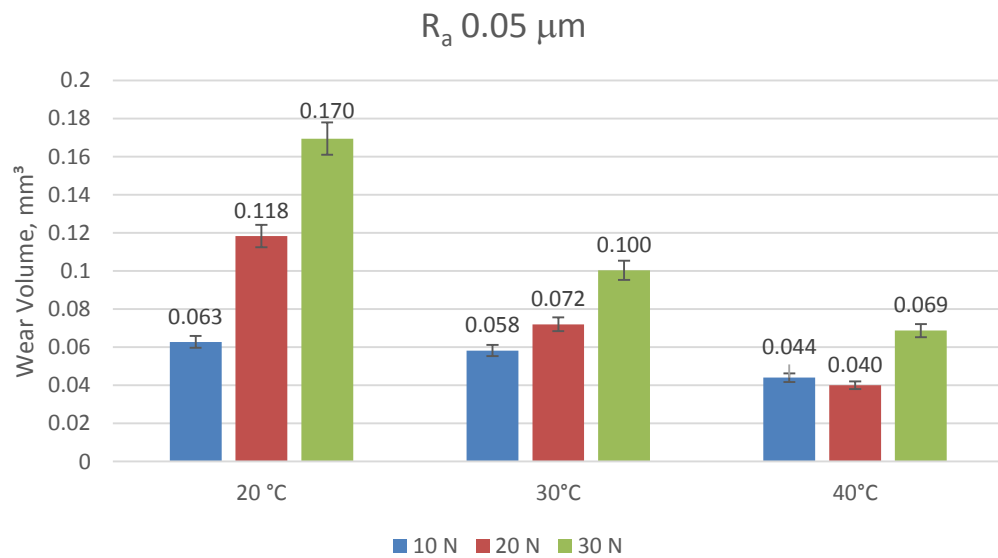
(a)
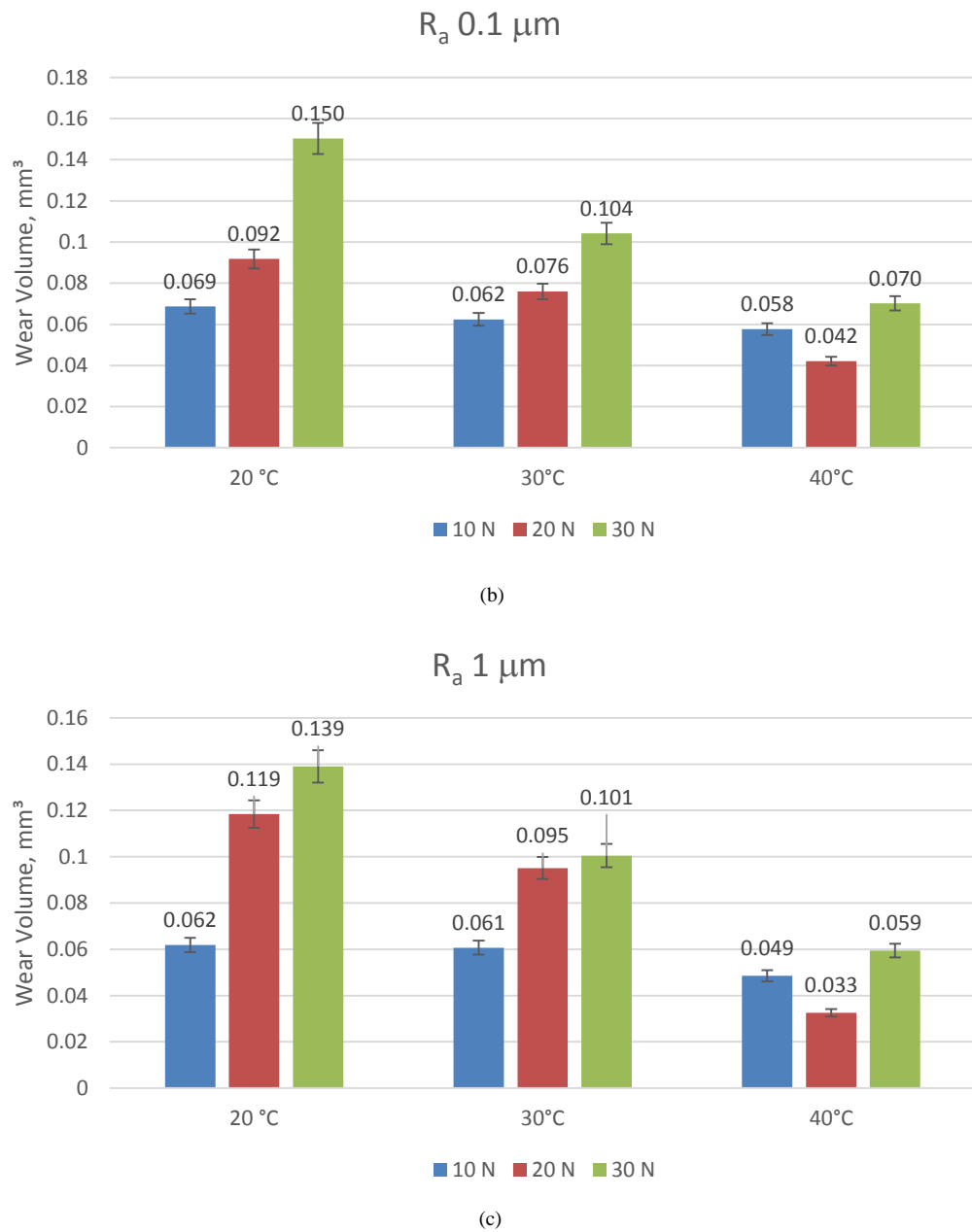
Fig. 4.10. Wear volume plots: (a) R_a 0.05 μm (b) R_a 0.1 μm (c) R_a 1.0 μm (Bhutta and Khan 2019).

At a particular surface roughness an increase in the refrigerant temperature reduces wear volume for the same applied normal load. This trend in a drop in wear volume with increase in temperature shows that the reactivity of HFE-7000 increases with the metallic rubbing surfaces with an increase in temperature. The increased reactivity of the refrigerant means acceleration in the formation of protective surface films on the mating top surfaces which results in a decrease in wear volume. Wear volume is observed to increase with increase in load for all surface roughness values at refrigerant temperatures of 20°C and 30°C. However at 40°C for all the

tested surface roughness values the wear volume generated at 20 N load was less than the wear volume produced at 10 N. At a particular testing temperature the wear volume for all the surface roughness values investigated had the highest values at 30 N load. These results indicate that there exists an optimum combination of refrigerant temperature and applied normal load which generates minimal wear.

At all the refrigerant temperatures investigated in the uncoated study an increase in average surface roughness from 0.05 μm to 0.1 μm generated more wear at 10 N load. A further increase in the average surface of the flat discs from 0.1 μm to 1.0 μm showed a decrease in wear volume at each refrigerant temperature for 10 N load. The least rough surface produced the minimum wear for normal load of 10 N. This shows that an increase in surface roughness at lower applied loads increases wear due to increase in asperity interactions. A further increase in average surface roughness produces harsher operating conditions causing more asperity interactions, however these harsher conditions proved to be more beneficial in the chemical breakdown and reaction of HFE-7000 with the metallic surfaces resulting in the generation of protective surface films which leads to wear reduction.

Increasing the load at 20°C refrigerant temperature from 10 N to 20 N generated almost the same amount of wear volume for R_a of 0.05 μm and R_a of 1.0 μm, however for R_a 0.1 μm least values of wear volume were observed at 20°C/20 N. This result shows that for operating conditions of 20°C/20 N an optimum average surface values exists that produces lower wear. At 20°C/30 N testing conditions an increase in surface roughness resulted in an increase in wear volume. For 40°C/20 N conditions an increase in surface roughness from 0.05 μm to 0.1 μm resulted in an increase in wear volume, however least amount of wear volume was observed at Ra 1.0 μm. This shows that although the production of surface tribo-films is promoted by harsher loading conditions, the temperature of the refrigerant (HFE-7000) has to increase as well in order to accelerate the formation of these protective surface films. Least amount of wear was noticed at 20 N/40°C for each surface roughness. This indicates that an optimum combination of temperature and load exists which produces the least amount of wear irrespective of the average surface roughness. Best operating conditions in terms of wear were identified as; normal applied load 20 N, HFE-7000 temperature 40°C and R_a 1.0 μm as least amount of wear was generated at these testing conditions.

At 30 N/20°C increasing the average surface roughness of the flat disc samples resulted in a drop in wear volume. Any noticeable effect on wear volume was not observed by increasing the

surface values at 30 N/30°C. For 30 N/40°C, increasing surface roughness values from 0.05 μm to 0.1 μm increased wear, however a further increase in the average surface values of the flat disc to 1.0 μm reduced wear and produced the least amount of wear for these testing conditions.

4.4 Tribochemistry Discussion on Uncoated Steel Samples

Energy-Dispersive X-ray Spectroscopic (EDS) analysis were performed in a vacuumed chamber on *all* the tested specimens post experimentation. The results of the EDS analysis showed a strong presence of O and F on *all* of the flat EN1A discs as well as on *all* of the 52100 steel balls. EDS analysis was also carried out on a number of ball and disc specimens before experimentation.

(a)

(b)

(c)
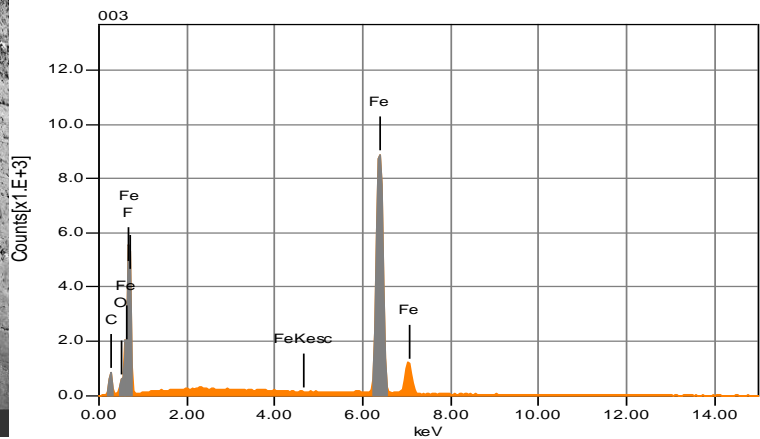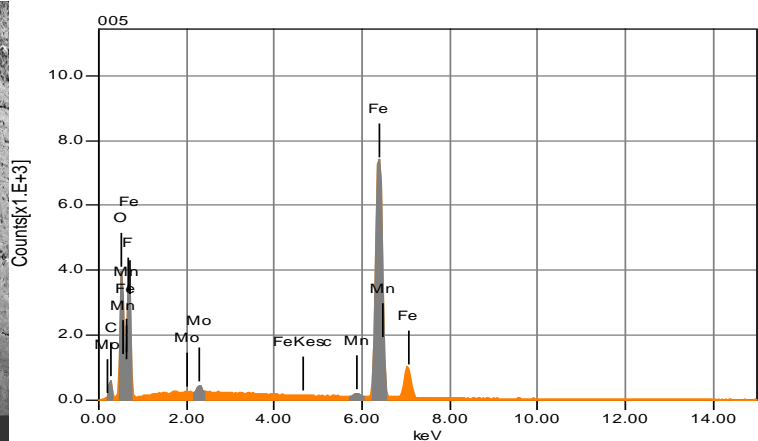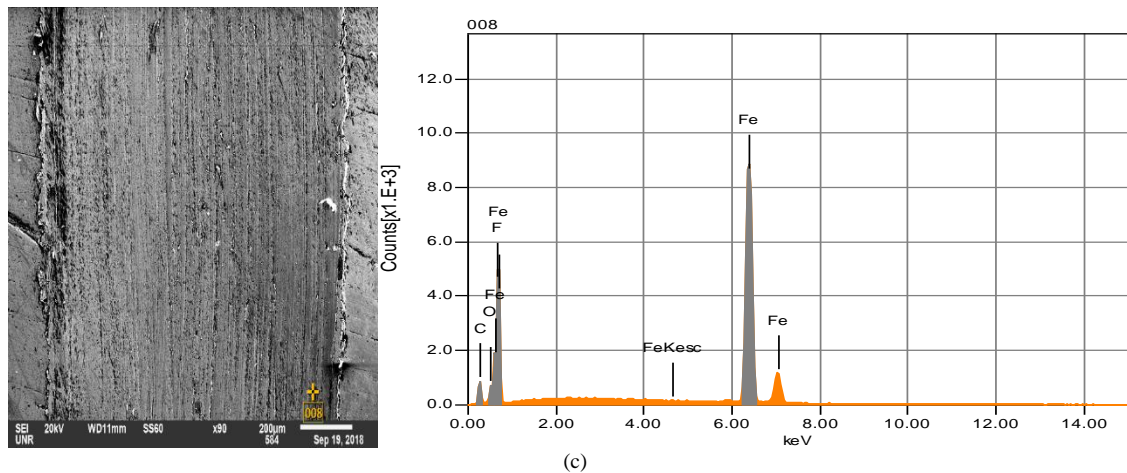
Fig. 4.11. Magnified images of the wear scar indicating the analysis region along with the EDS analysis (Bhutta and Khan 2019).

No fluorine or oxygen was detected pre-experimentation; the grinding, polishing and the ultrasonic treatment with acetone of each disc sample pre-experimentation ensured the removal of unwanted/oxide surface films. Post experimentation EDS results of one of the sample pairs have been presented in figure 4.11 and 4.12 respectively.

Chemical characterization results obtained by analysing various different regions on the wear scar generated on the EN1A flat steel disc have been presented in figure 4.11 alongside the SEM images. Similar analysis were also performed on the wear tracks produced on the other disc samples as well which also revealed similar results. EDS results show a presence of both oxygen and fluorine on the wear scar indicating the formation of tribological films on the wear track.

(a)

(b)

(c)
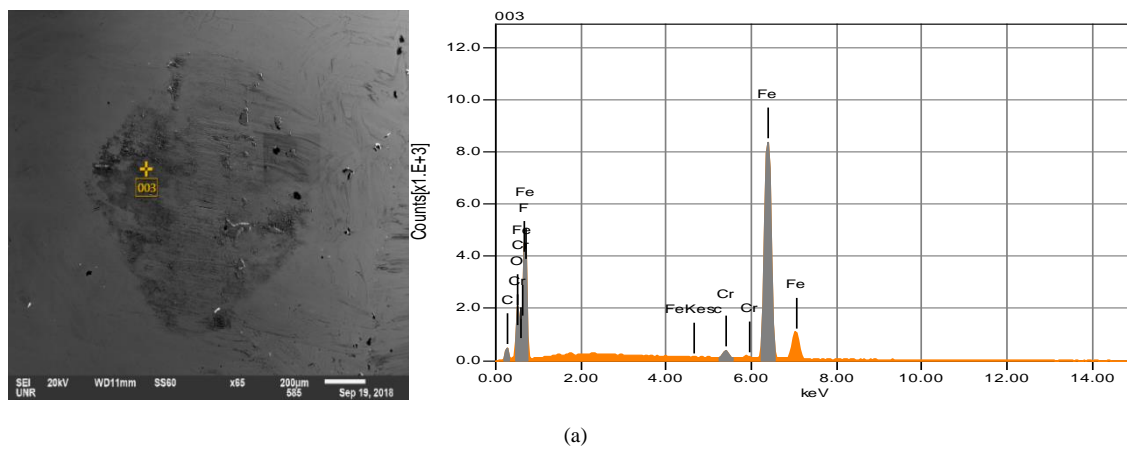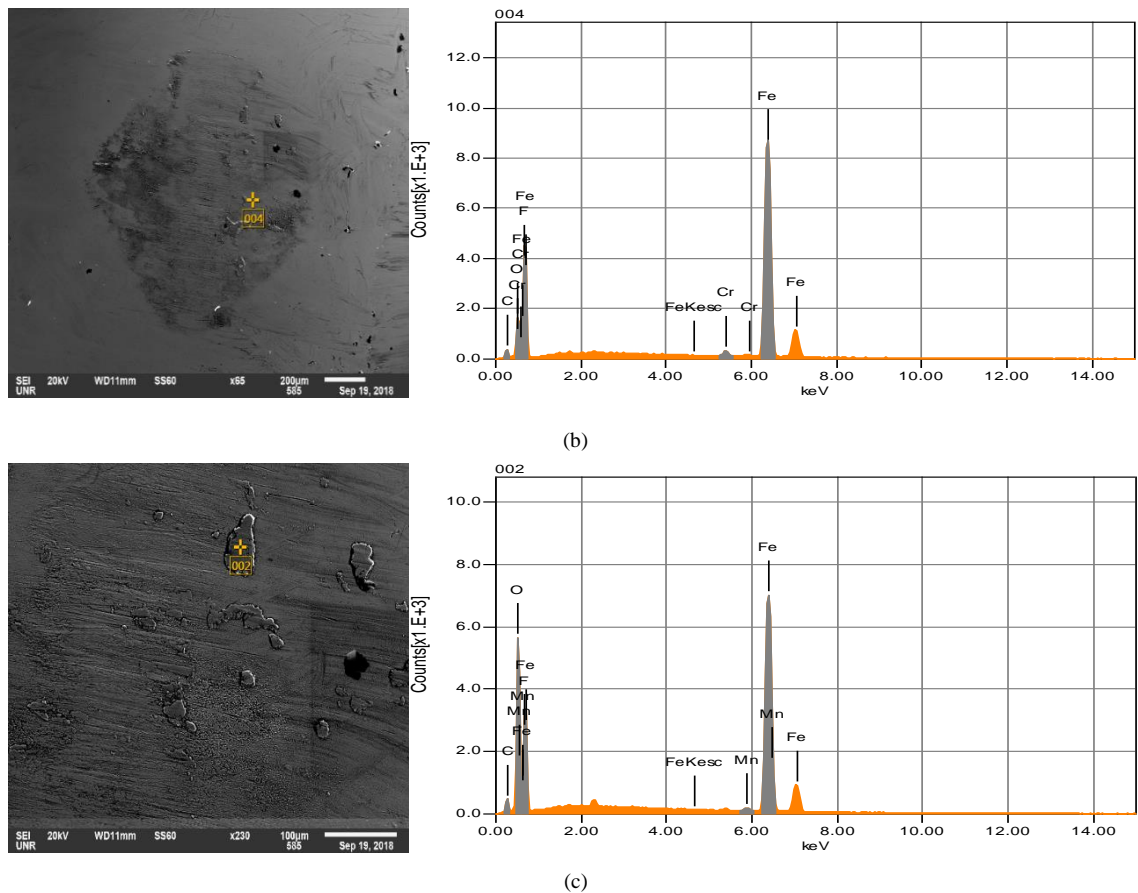
Fig. 4.12. Magnified images of a ball specimen indicating the analysis region along with the EDS results (Bhutta and Khan 2019).

Elemental analysis on the 52100 steel ball sample have been presented in figure 4.12. EDS analysis on the ball was also performed on a number of different regions within the contact zone. EDS results of the ball also revealed the presence of both oxygen and fluorine demonstrating that oxygenated and fluorinated tribological films did not form only on the flat disc samples were also formed on the ball specimen as well.

In order to minimize the influence of ambient air and atmospheric oxygen on a test, the testing chamber was vacuumed before introducing the refrigerant HFE-7000 into the system and establishing fully lubricated conditions after which the testing chamber was fully sealed. Which leads to the conclusion that the origin of the fluorine and oxygen detected post experimentation is the refrigerant (HFE-7000). After an experiment had been completed the tested samples were securely stored in a desiccator. Even if aerial oxidation is taken into consideration while transporting and handling of the tested specimens post experimentation will still not explain high percentage of fluorine and oxygen detected on the surface of the tested specimens.

X-ray Photoelectron Spectroscopic (XPS) analysis was performed on a selected number of sample pairs using Kartos Axis Ultra in ultra-high vacuum. A 10 mA emission, monochromated aluminium X-ray source was operated at 15 KV. Each performed analysis had an approximate area of $300\ \mu m\ X\ 700\ \mu m$. Analysis conditions used were 1 eV steps, 160 eV pass energy and 0.2 s dwell per step. Survey spectra in the range of 1350 to -10 eV binding energy were taken at 0° emission angle to the surface normal. The XPS survey spectra results of one of the tested samples pairs is shown in figure 4.13.
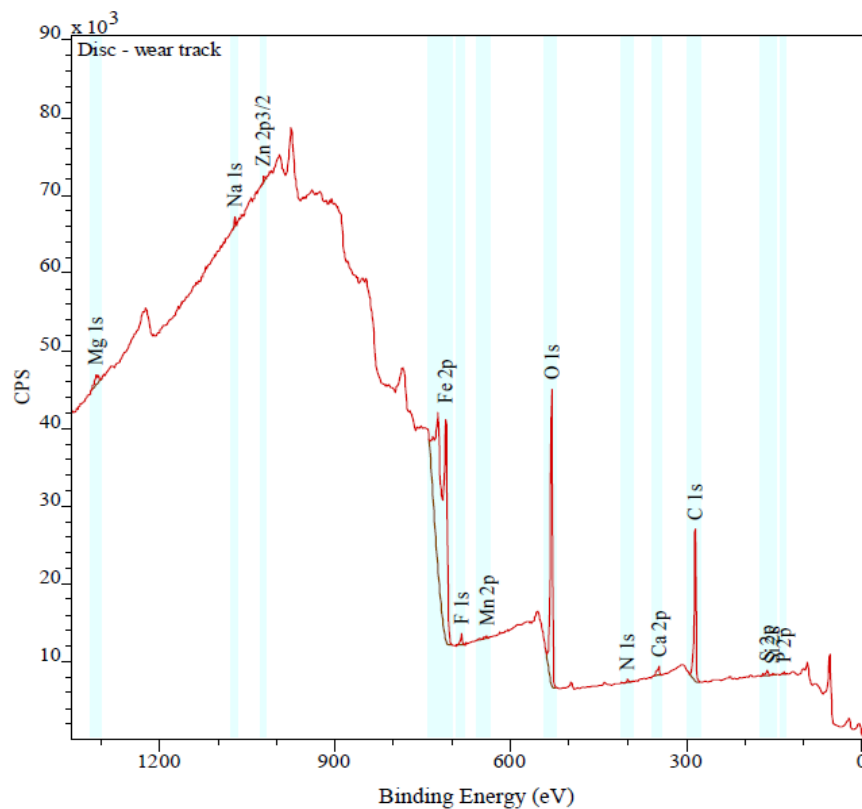
(a)
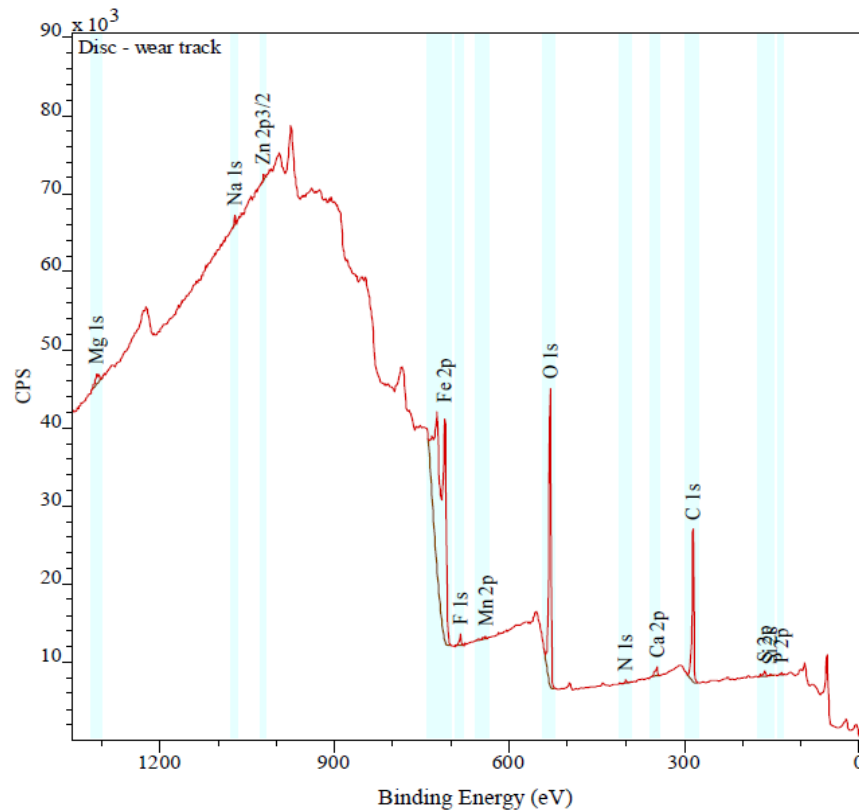
Fig. 4.13. XPS survey spectra: (a) Disc (b) Ball (Bhutta and Khan 2019).

Besides Carbon, Iron, Manganese, Silicon, Phosphorous, Sulfur and Chromium which are typically present in 52100 steel and EN1A steel, elements such as Zinc, Nitrogen, Calcium and Sodium have also been detected by XPS. The source of Calcium, Zinc and Sodium is believed to be the latex and nitrile laboratory rubber gloves. Calcium, Zinc and Sodium presence on the ball and flat specimens is most likely due to the transfer of particles from the disposable laboratory gloves onto the surfaces of the disc and ball specimens. A number of constituents within the material of a glove and manufacturing residues left on the surface of a glove have been known to get easily transferred to the specimens being handled using these gloves with Calcium, Zinc and Sodium being a common contamination being caused by laboratory gloves (XPS 2019). The source of Nitrogen in the XPS analysis is often linked with carbon contamination from the atmosphere (Bhutta and Khan 2019). The elements of interest i.e. the constituents and elements present in the steel samples and the refrigerant were further investigated and have been presented in figure 4.14.

(a)

(b)

(c)

(d)

(e)

(f)

(g)
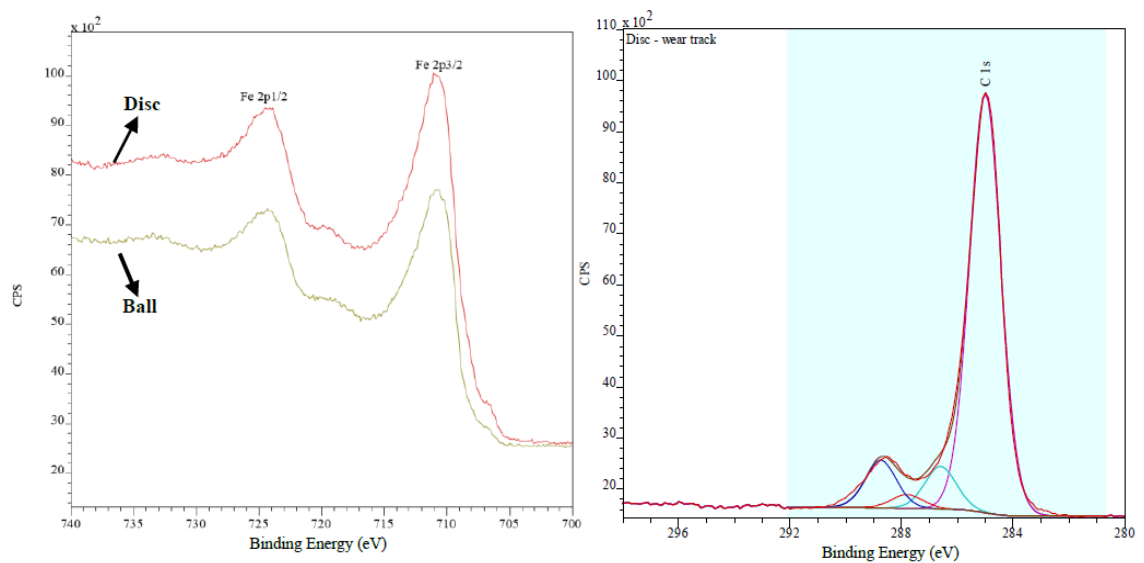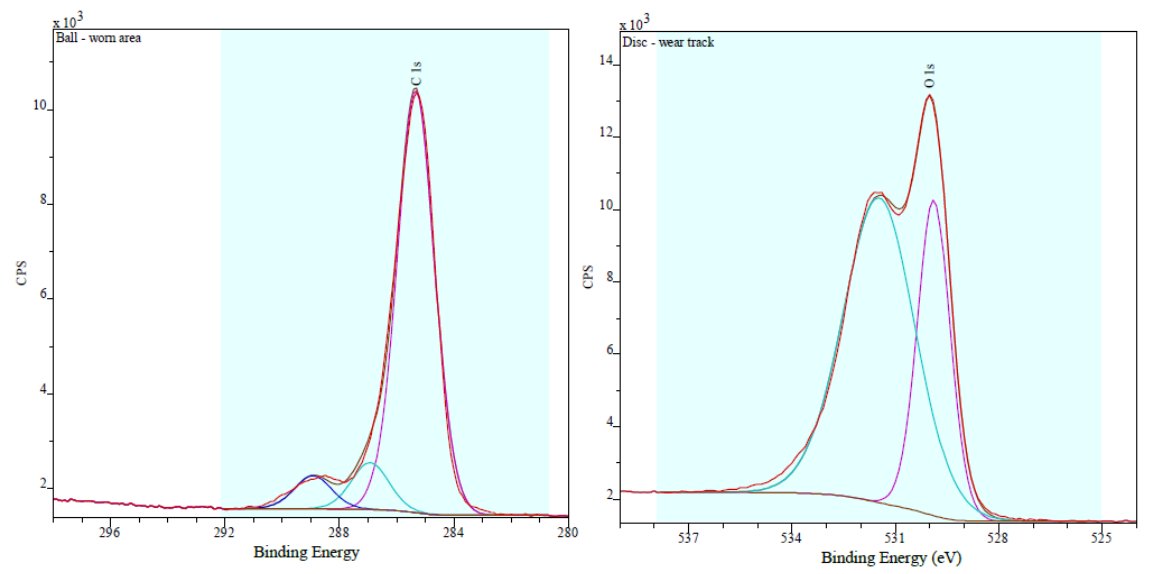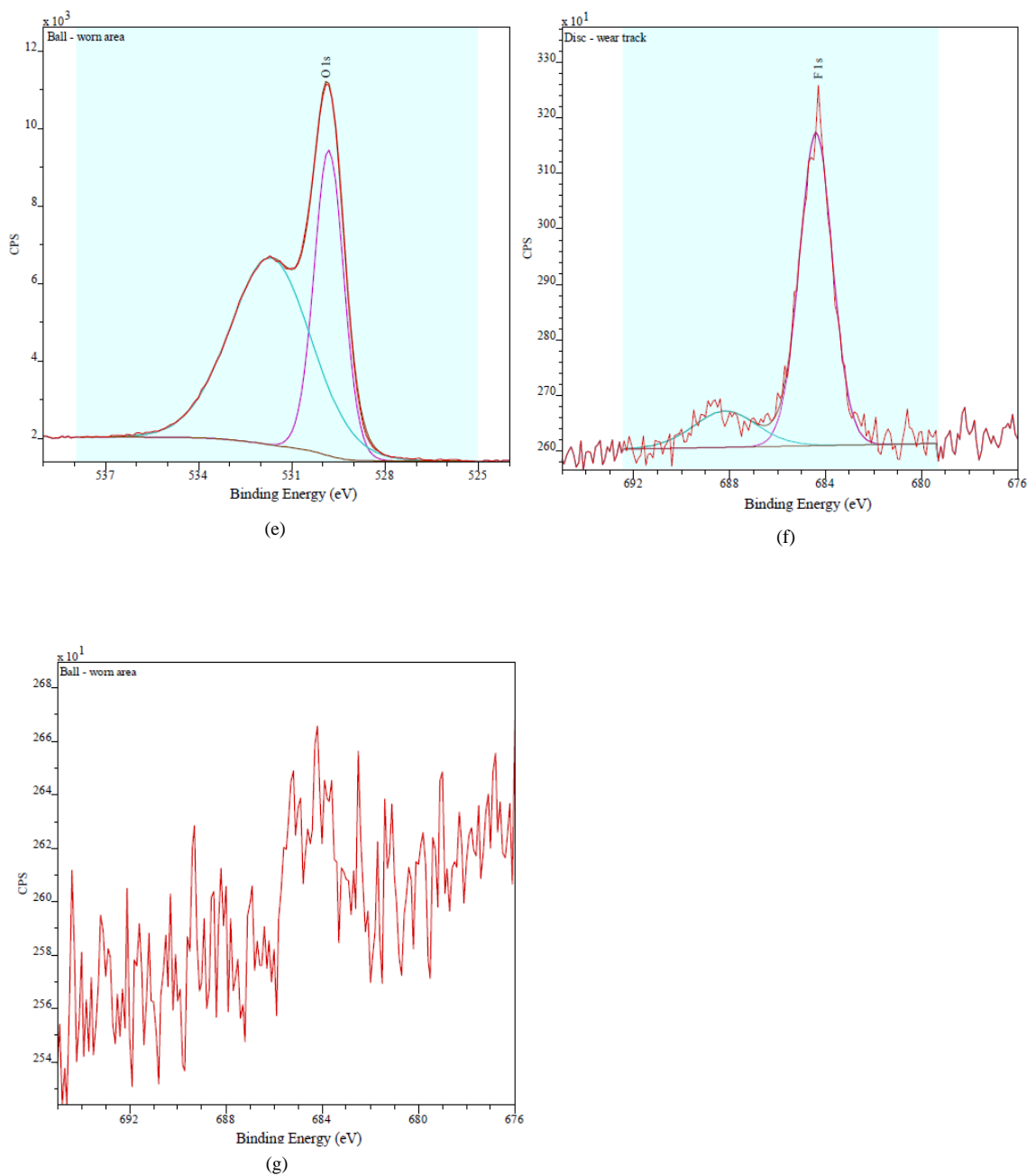
Fig. 4.14. XPS high resolution core level spectrums: (a) Fe2p disc and ball (b) C1s disc (c) C1s ball (d) O1s disc (e) O1s ball (f) F1s disc (g) F1s ball (Bhutta and Khan 2019).

High resolution XPS core level spectrum results for Carbon, Iron, Fluorine and Oxygen have been presented in figure 4.14. High resolution Fe2P core level spectra for the flat circular disc and the ball are shown in figure 4.14 (a). Binding energy peaks of Fe $2p_{3/2}$ for the disc as well as the ball sample equal to 710.7 eV can be seen in the results which refer to the formation of Fe_2O_3 (Scientific 2019). A small $2p_{3/2}$ peak is also present in the spectra at ~706.7 eV which

represents Fe metal (Scientific 2019). In comparison to metal, peaks of iron oxide are shifted significantly towards higher binding energy (Scientific 2019).

High resolution C1s core level spectra of the ball sample and the flat disc are shown in figures 4.14 (b) and 4.14 (c). The C1s spectra for the disc sample shown in figure 4.14 (b) can be fitted four different peaks. The C1s spectrum results for the ball sample shown in figure 4. 14 (c) present very similar results to the disc sample except for the fact that the disc specimen can be fitted for four different peaks while the ball spectrum can be fitted for just three different peaks instead of four. This indicates that similar constituents of carbon are present on the ball as well as disc specimens, with one additional carbon compound being present on the disc. Binding energy peaks of 285.00 and 285.3 eV are extant on both the samples. Of the total carbon percentage present on the analysed disc area, 80.1% of carbon lies within these binding energy limits. For the ball specimen, 84.5% of the carbon sensed on the analysed area is present within these binding energy limits. C-C carbon contamination for adventitious carbon typically has binding energy of 284.8 eV (Scientific 2019). The XPS analysis process has an associated inherited error of at least $\pm$ 0.1 eV to $\pm$ 0.2 eV (XPS 2019). For organic systems it is convenient to charge correct to the C-H, C-C signal and readjust it to 285.0 eV (XPS 2019). Higher binding energy constituents can be examined above this main peak. The second peak present at (285.0-285.3 eV) +1.6 eV refer to C-O-C and C-OH (Scientific 2019; XPS 2019). The third peak generated at (285.0-285.3 eV) +2.8 eV which is present only at the disc sample refers to C=O (XPS 2019). The fourth peaks which are detected in the range of 288.7-288.9 eV represent O-C=O (Scientific 2019; XPS 2019). Binding energies between 288-290 eV for Metal Carbonates also indicates the presence of metal carbonates (XPS 2019). This leads to a deduction that the C1s spectra peaks within binding energies of (288-290 eV) could possibly also refer to the generation of iron carbonates. The disc and ball C1s spectra shows the presence of various carbon based compounds which indicates that not only the bonds of the refrigerant (HFE-7000) have been broken but also new bonds have been formed on both the mating metallic surfaces.

Figures 4.14 (d) and 4.14 (e) represent the O1s spectrum attained by analysing the disc and ball specimens respectively. Similar to the results obtained for C1s spectra, O1s spectrum of the disc and ball samples generated through XPS displayed similar peaks. Multiple peaks were obtained at 529.8 eV-529.9 eV and 531.5 eV-531.8 eV binding energies for both the ball as well as the flat disc samples. This implies that similar oxygen components are existent on both the tested specimens. The analysed area on the disc showed that 68% of the detected oxygen is present in

the range of 531.5-531.8 eV and 32% of oxygen is present between 529.8-529.9 eV. 64.2% of the oxygen on the ball specimen is present between 531.5-531.8 eV and 35.8% is in the range of 529.8 and 529.9 eV. Besides oxides of metals, O1s binding energy of different compounds and species lies within a very narrow range (Scientific 2019). O1s spectra is not straightforward to interpret because O1s peaks are broader having multiple overlapping components (Scientific 2019) 529-530 eV binding energies imply the possible development of metal oxides, most possibly Fe_2O_3 (Nunez et al. 2010; Scientific 2019). Fe_2O_3 is the most probable metal oxide to have been formed on the metallic surfaces as Iron (III) Oxide was directly sensed in the Fe2p spectrum. 531.5-532 eV range of binding energies imply C-O presence on the surfaces (Scientific 2019), C1s spectra also showed the presence of C-O. 531.5-531.9 eV binding energies also refers to the formation of carbonates and/or bicarbonates for O1s spectrum (Wu et al. 2004; Nunez et al. 2010). C1s spectrum also indicated the possibility of the formation of metal carbonates. Organic compounds bonded to oxygen can lie in the binding energies from as low as 530.9 eV to as high as 533.8 eV and 531.3 eV binding energy for metal hydroxides with 0.3 eV standard deviation (XPS 2019). $Fe(OH)_2$ and $Fe(OH)_3$ could be the most likely metal hydroxides, if present. The XPS results indicate a larger percentage, more than 60% of the detected oxygen bonded to either organic components or probably in the form of metal hydroxides. The remainder of the detected oxygen is attached to metal with Fe_2O_3 being the most likely metal oxide formed on the surface.

F1s spectra for the disc and ball samples have been displayed in figures 4.14 (f) and 4.14 (g) respectively. F1s spectrum of the disc and ball are different which makes the results of F1s unlike the other XPS results. 81.7% of the detected fluorine on the disc specimen was identified at 684.4 eV binding energy while 18.3% of fluorine was recognised at 688.2 eV binding energy. Only a peak at ~684.5 eV was detected for the ball sample. F1s spectra for fluorine in the binding energies from 684 eV to 685.5 eV refers to the presence of metal fluorides (Scientific 2019) and the binding energy range of 688 eV to 689 eV indicates organic fluorine (Bhutta and Khan 2019). For the ball specimen no peak was sensed in the range of 688-689 eV while a peak was detected in the range of 684-685.5 eV, which leads to the conclusion that fluorine is not present in organic state and is only present in the form of metal fluorides on the analysed area. For the flat disc specimen 81.7%, a very high percentage of fluorine is present as metal fluorides, while 18.3%, a smaller percentage is detected as organic fluorine. The detection of organic fluorine and metal fluorides also indicates the breaking up of bonds of HFE-7000 and the formation of new bonds and compounds on the surfaces of the rubbing metals. The XPS results of fluorine are in contrast to the results of oxygen. As discussed in the O1s spectrum

results a lower percentage of oxygen is present as metal oxides while a higher percentage of oxygen is present in organic form. In addition metal fluorides have been detected on both the metallic samples while the presence of organic fluorine was detected only on the disc specimen. These results indicate the oxygen in HFE-7000 has a higher tendency to form metal oxides in comparison to fluorine in HFE-7000 which showed a greater tendency to form metal fluorides. The metal fluorides formed on the rubbing surfaces of both the samples are most probably FeF_2 and/or FeF_3 (Muraki et al. 2002; Akram et al. 2013a; Akram et al. 2013b).

The detection of inorganic compounds such as metal fluorides and Iron (III) Oxide originate as a result of the tribochemical reaction between steel disc/ball and the fragmented species originating from the breakdown of the refrigerant, HFE-7000 (Bhutta and Khan 2019). The organic species have been known to act as third body which ensure interface sustainability in terms of friction and wear, whereas on the other hand better adhesion on the surfaces of the interacting metals is provided by the metallic components (fragmented refrigerant reacted with steel) (Akram et al. 2013b).

The formation of oxygen containing tribo-layer in the presence of carbon dioxide as refrigerant (Cannaday and Polycarpou 2006; Jeon et al. 2009; Nunez et al. 2010) and the formation of fluorinated layer by various different refrigerants (Mizuhara et al. 1994; Akram et al. 2013a; Akram et al. 2013b; Akram et al. 2014; Bhutta et al. 2018a; Tatsuya Sasaki Purdue University, Indiana, USA, 12-15 July, 2010, Paper 1946; Kawahara et al. Purdue University, Indiana, USA, 23-26 July, 1996, Paper 1141) developed on the rubbing surfaces have been reported to be advantageous in improving the tribological performance. The refrigerant, HFE-7000 ($C_3F_7OCH_3$) chemically breaks down under the application of applied normal load, heat, mechanical motion and frictional force. Single Carbon-Fluorine bonds are highly polar bonds ($C^{\delta+} - F^{\delta-}$) and C-F bond is shorter than C-H bond which makes C-H bond easier to break in contrast to C-F bond (Gu et al. 2009; Akram et al. 2013a). Carbon-Carbon, C-C bond has also been reported to be stronger than C-O, Carbon-Oxygen bond (Lide 73rd edition, 1992-1993, pp. 9-145; Muraki et al. 2002). It is highly probable that C-O bond is the first bond to break in HFE-7000 which frees OCH_3 from the rest of the molecule. Removal of material from the surface of EN1A steel disc exposes fresh surface containing dangling bonds or immobilised free radicals. Unlike free radicals, the limited mobility of immobilised free radicals in a solid medium makes them kinetically more stable. However, similar to free radicals, immobilised free radicals i.e. dangling bonds are also extremely reactive. The exposure of highly reactive fresh bonds on the surface of the EN1A steel disc accompanied by the chemical breakdown of the refrigerant leads

to a chemical reaction between the EN1A steel disc and the refrigerant. This chemical reaction leads to HFE-7000 adsorption on to the disc surface forming fluorinated and oxygenated tribological films which result in friction and wear reduction. Besides the adhered EN1A steel on the surface of the ball, scratch marks and abrasive wear is also clearly visible on the ball surface in the contact region, which produces a similar chemical reaction between HFE-7000 and the ball. These protective tribo-layers are well adhered to the rubbing surfaces of the disc and ball as the presence of oxygen and fluorine was not only detected throughout the wear track on the flat disc sample but, the presence of oxygen and fluorine was also detected at different regions within the contact zone of the ball sample (Bhutta and Khan 2019).

4.5 Conclusions of the Uncoated Study

A series of tests have been successfully conducted within tribological context to evaluate the friction and wear performance of the environmentally friendly refrigerant HFE-7000 simulating a range of different operating conditions. Tests were performed by using flat disc samples of EN1A steel of various surface finish against 52100 steel balls, by changing the applied normal load and by heating the refrigerant (HFE-7000) to several different temperatures. The friction and wear performance of HFE-7000 was analysed at low loads and low temperatures starting from room temperature.

An increase in load at low refrigerant temperature of even 20°C resulted in a substantial reduction of the coefficient of friction and increasing the refrigerant temperature at a low load of even 10 N reduced wear.

Overall the results show that an increase in the operating temperature at a constant applied load reduces both wear and friction coefficient. Increasing the applied normal load at a constant refrigerant temperature increased wear but resulted in a reduction in the coefficient of friction. The drop in the coefficient of friction with increase in applied load and the decrease in the friction coefficient along with a decrease in wear volume with increase in refrigerant temperature is believed to be associated with the formation of protective tribo-films on the interacting surfaces. The production and development of these protective tribological films accelerates at elevated refrigerant temperatures and with increase in applied normal load. Increasing the applied load and the temperature of the refrigerant results in an increase in reactivity of HFE-7000 with the rubbing metals.

EDS analysis results performed on the disc and ball samples within the contact region reveal a significant presence of fluorine, oxygen and carbon. The detailed high resolution XPS analysis showed the formation of new compounds/bonds on the surfaces of the mating metallic samples. Post-experiment EDS and XPS analysis performed at different samples at various regions on the wear track and at different areas with the contact zone of the ball samples demonstrate that fluorinated and oxygenated layers are well adhered on the surfaces of the ball and disc specimens. The results also show that surface roughness i.e. surface finish does not have a very significant effect on wear volume and friction coefficient. This implies that metallic parts of a range of surface finish and even metallic parts with rough surfaces can be used in interacting systems based on HFE-7000 refrigerant.

Overall it can be stated with confidence evidenced by the presented results that HFE-7000 refrigerant which is a very promising next generation refrigerant having a broad range of applications areas also has good friction and wear behaviour which improves at higher operating temperatures will lead to good tribological performance of mechanical systems run on HFE-7000.

Chapter 5

Coated Study

The results of the coated study have been presented in this chapter. Five different types of coatings namely Ni-Al$_2$O$_3$, Ni-SiC, Ni-ZrO$_2$, Ni-Graphene and Nickel-only were prepared using the pulse coating technique in an attempt on enhance and improve the wear and friction of interacting metallic parts in HFE-7000 based systems.

5.1 Sample Preparation

All the coatings will be Nickel based, Nickel based electrodeposition has been selected because Nickle based coatings provide several benefits which includes better wearability than softer metals such as copper or zinc which can be used when wear resistance is needed (Snyder, D., 2011). Nickel plating is typically used to provide greater wear and corrosion resistance and to add thickness to undersized parts (SPC, 2018). Nickel plating is also frequently used as a method of friction reduction in certain materials (SPC, 2018). Nanostructured design achieved by the electrodeposition of nano particles into the Nickel matrix has been proven to enhance friction, wear, corrosion and overall mechanical performance of interacting parts under a range of testing conditions as summarized in table 2.8. The electroplating process consists of several steps. These steps are explained in sections 5.1.1-5.1.3.

5.1.1   Substrate preparation

Prior to starting the actual electroplating the surface of the mild steel circular samples have to be prepared for the deposition process. Nickel based coatings having surface roughness of less than $1\,\mu m$ have shown good adhesion properties on mild steel (Bajwa, R. et al., 2016; Bajwa, R. S. et al., 2016a, 2016b). One side of the samples is mechanically grinded and polished using grinding and polishing wheels to bring the average surface roughness (R_a) of the samples to $0.05\,\mu m$. After the gridding and polishing process has been completed, the sample is cleaned by first using water and then by dipping the sample in acetone and placing it in an ultrasonic bath for five minutes. Afterwards the sample is removed from acetone and dried using hot air from a specimen drier. The mechanical grinding and surface polishing process followed by ultrasonic surface conditioning of each flat sample with acetone ensured the removal of any oxides or undesired surface films that might be present. After the sample has dried the unpolished side of the sample is sealed and attached to a metal hanger using polyvinyl chloride tape.

5.1.2   Electrolytic solution preparation

The solution used for the electrodeposition process is called the electrolytic solution and it is chemically prepared using various combination of chemicals. The chemicals typically used in the preparation for the Nickel based coatings along with their quantity are (Hou, K.-H. and Chen, Y.-C., 2011; Xia, Y. et al., 2007)(Bajwa, R. et al., 2016; Bajwa, R. S. et al., 2016a, 2016b)(Algul, H. et al., 2015; Borkar, T. and Harimkar, S. P., 2011; Chen, J. et al., 2016; Chen, L. et al., 2006; Shi, L. et al., 2006):

- $NiSO_4\ 6H_2O\ (200 - 300\ ^g/_L)$
- $NiCl_2 6H_2O\ (40 - 50\ ^g/_L)$
- $H_3BO_3\ (30 - 40\ ^g/_L)$
- $Deionised\ Water\ (1\ L)$

Experimental studies involving steel substrates and Nickel based electrodeposition coatings involving Nano-particles (Bajwa, R. et al., 2016; Bajwa, R. S. et al., 2016a, 2016b; Borkar, T. and Harimkar, S. P., 2011; Khan, Z. A. et al., 2015; Rizwan Bajwa, Z. a. K., Vasilios Bakolas, Wolfgang Braun, 2014, 2015) have shown the following composition of chemicals to be the most optimum:

- $NiSO_4\ 6H_2O\ (265\ ^g/_L)$
- $NiCl_2 6H_2O\ (48\ ^g/_L)$
- $H_3BO_3\ (31\ ^g/_L)$
- $Deionised\ Water\ (1\ L)$

The optimum composition described above will be used to prepare the electrolytic solution. These chemicals will be precisely weighed and will be put in a beaker. Five different electrolytic solutions were prepared using the optimum chemical compositions described above to develop the five different types of coatings. The procedure for preparing the coatings is described in section 5.1.3.

5.1.3   Coating procedure

Pulse electrodeposition was used to develop coatings of ~ 10 μm thickness on the flat circular steel specimens. 20 g/L Al_2O_3 nanoparticles having average particle size of less than 50 nm

were added in the first solution for the preparation of Ni-Al$_2$O$_3$ nanocomposite coatings. To prepare Ni-ZrO$_2$ nanocomposite coatings, 20 g/L ZrO$_2$ nanoparticles with an average particle size between 20-30 nm were added to the second solution. 20 g/L SiC nanoparticles with an average particle size between 50-60 nm were added in the third solution for the development of Ni-SiC nano coatings. 0.1 g/L Graphene nanoparticles with average particle size of 6-8 nm were added in the fourth solution for the deposition of Ni-Graphene (Ni-GPL) nanocomposite coatings. Nano particles were not added in the fifth solution because this solution was used in the preparation of pure Nickel-only coatings. Each solution was stirred magnetically for a period of 24 hours. After stirring each solution for 24 hours the solutions containing the nanoparticles were ultrasonically agitated for 4 additional hours. This process confirmed proper dispersion and suspension of particles inside the solution. This stirring and agitation process established proper suspension and dispersion of particles inside each solution. To start the coating process each solution was heated to 40°C after which a solution is ready for the deposition process.

The prepared solution is continuously stirred while being maintained at 40 ℃, the temperature of the solution is maintained for one hour in order to ensure that the solution is homogeneously mixed. For Nano-composite coatings an additional ultra-sonic horn is placed in the solution and is set at a frequency of 10 Hz. For pure nickel based coatings the ultra-sonic horn is not required. Afterwards 99.99 % pure Nickel plates are used as anode and the EN1A steel substrates are used as cathode. The Nickel plate and the EN1A steel specimen are hanged in the prepared electrolytic solution. The anode and cathode leads are connected to the pulse plating equipment MiCroStar DPR: 20-15-30 Dynatronix. This equipment is a PC controlled pulse coating equipment that allows the control of pulse parameters and can be used in DC, PC and PRC mode. After hanging the Nickel plate and the steel specimen the complete setup is given a 30 minutes pause before starting the plating process. During this time the nickel plate and the substrate reach the temperature of the solution and the pH is also measured and controlled between $4.0 - 4.5$. The complete experimental setup is shown in figure 5.1.
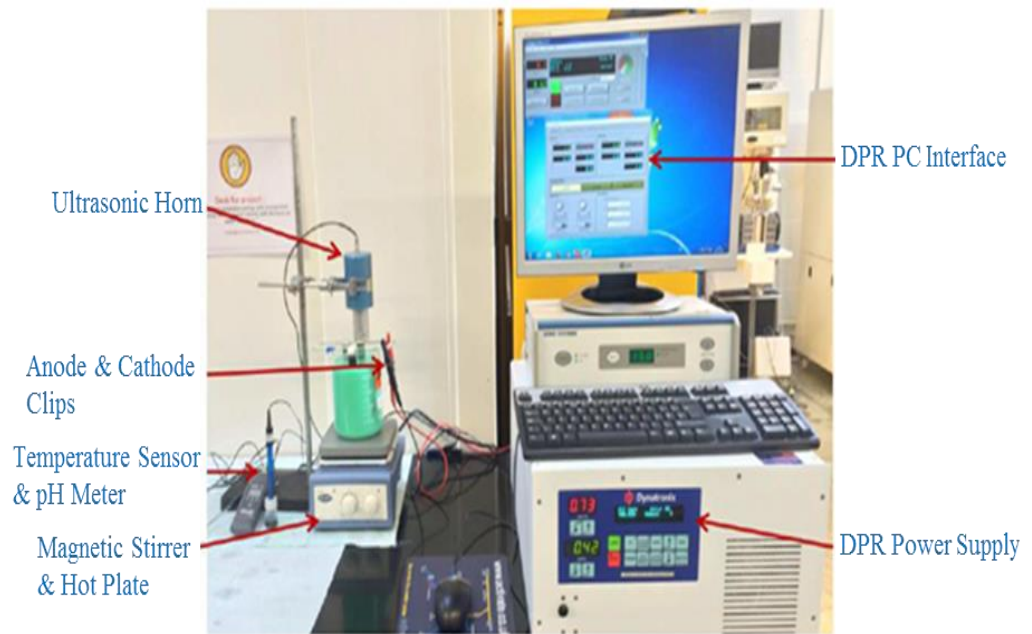
Fig. 5.1. Electrodeposition setup.

The deposition pulse parameters are controlled through the MiCroStar DPR interface. The current density is kept constant throughout the coating process. A current density of 3 $A/_{dm^2}$, frequency of 10 Hz and a duty cycle of 20% with pulse ON-OFF time of (20 ms-80 ms) have shown good results (Bajwa, R. et al., 2016; Bajwa, R. S. et al., 2016a, 2016b; Borkar, T. and Harimkar, S. P., 2011; Hou, K.-H. and Chen, Y.-C., 2011; Hou, K.-H. et al., 2006; Marlot, A. et al., 2002; Rizwan Bajwa, Z. a. K., Vasilios Bakolas, Wolfgang Braun, 2014, 2015). The same parameters were used to develop the coatings in this study. All the pulse parameters are kept constant throughout the coating process and the deposition procedure is stopped after 1 hour (T_{ON} + T_{OFF} = 3600 s).

5.2 Electrodeposited Coatings

The microstructure of each coating developed was examined using a Scanning Electron Microscope (SEM). Energy Dispersive X-ray Spectroscopic (EDS) Analysis was performed at various different regions on the surface of each coating. The SEM and EDS system used in this study is shown in figure 5.2.

Fig. 5.2. Scanning Electron Microscope and Energy Dispersive X-ray Spectroscopic Analyser (JEOL JSM-6010PLUS/LV).

EDS results and high magnification micrographs of all the coatings prepared in this study are presented in figure 5.3. EDS results presented in figure 5.3 show a clear presence of nickel on the surface of each of the electrodeposited coatings. Besides nickel the presence of the respective Nano particles embedded in the Nickel matrix can also be observed. EDS results and the microstructure of the prepared coatings is in agreement with the results reported by various different researchers (Bajwa et al. 2016c, 2016b; Jabbar et al. 2017; Nazir et al. 2017; Nazir et al. 2018a) which shows that the coating have been deposited successfully. Micrographs reveal the presence of pores on the surface of all the prepared coatings and the coatings exhibit a compact and fine grain structure. These pores are distributed randomly on the surface of the electrodeposited coatings and are highlighted better by applying false colour to the micrographs generated by SEM. These false coloured image of each coating is also shown in figure 5.3. These randomly distributed pores are an inherent property of Nickel based nanocomposite coatings (Bajwa et al. 2016c; Nazir et al. 2017; Nazir et al. 2018a).
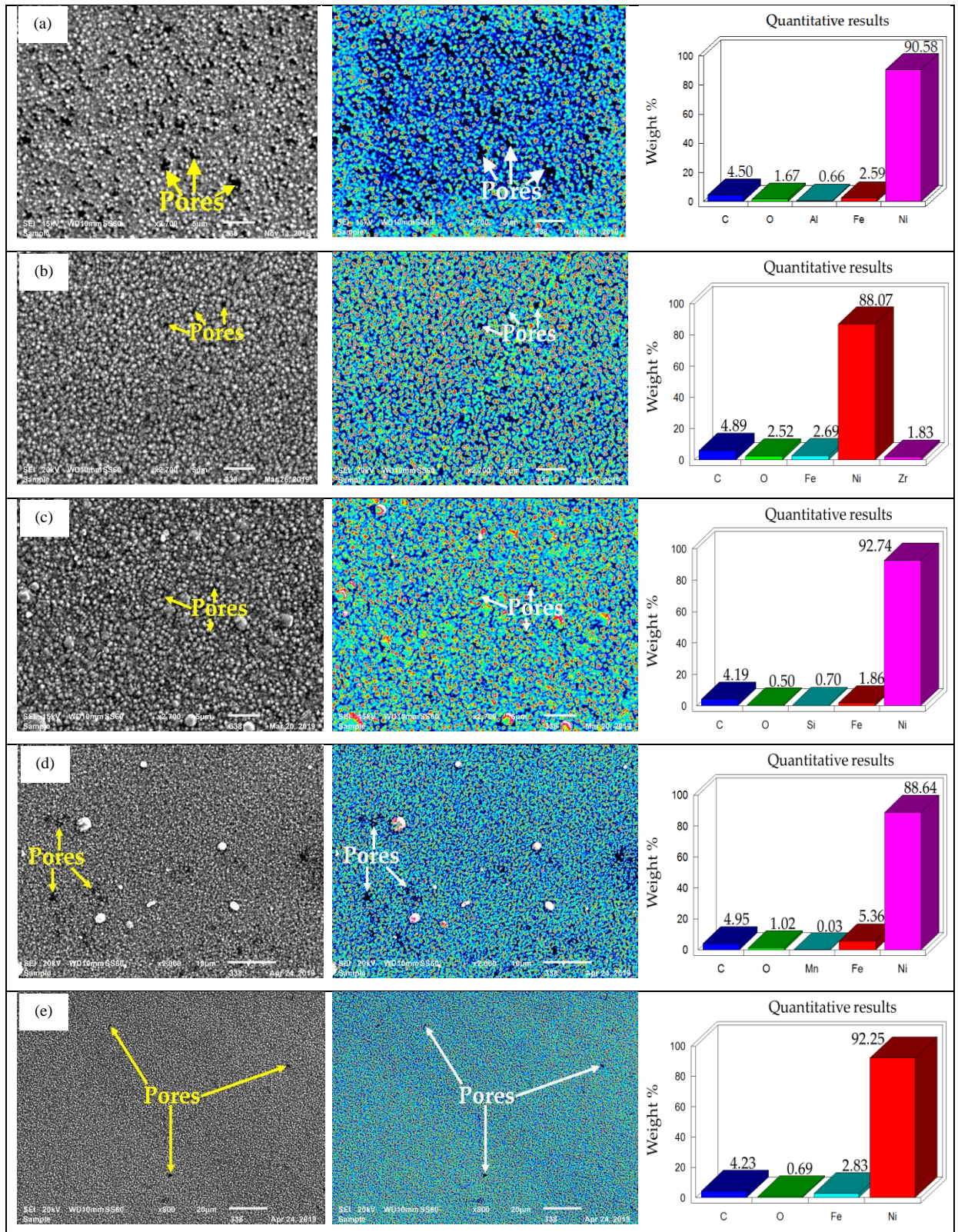
Fig. 5.3. SEM images and EDS analysis of coated samples: (a) Ni-Al$_2$O$_3$ (b) Ni-ZrO$_2$ (c) Ni-SiC (d) Ni-GPL (e) Pure Nickel.

Coating thickness was ensured by measuring the thickness of each prepared coatings using ZYGO. The thickness of all the deposited coating was measured with reference to the steel substrate, the height of the coatings was measured with respect to the substrate and was in the range of 8-10 μm for all the prepared coatings. Grain size measurement on all the prepared coatings was performed using Keyence microscope VHX5000 shown in figure 5.4.
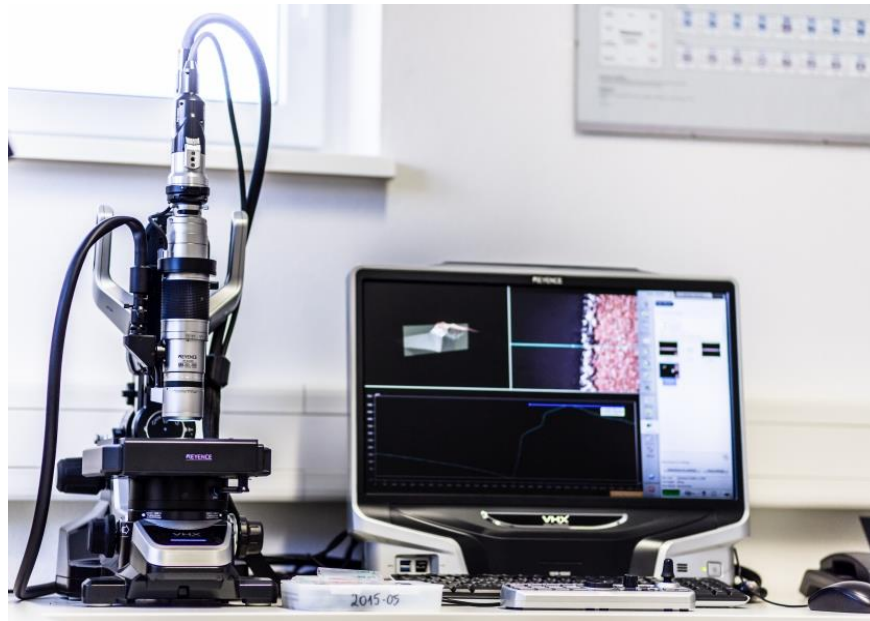
Fig. 5.4. Keyence microscope VHX5000.

The results of the grain size measurement have been presented in figure 5.5. The grain size measurement results show Ni-ZrO$_2$ and Ni-SiC to have the highest results of maximum average grain size values flowed by Ni-Al$_2$O$_3$ and Ni-Only coatings, Ni-Graphene presented the least values of the maximum average grain size.
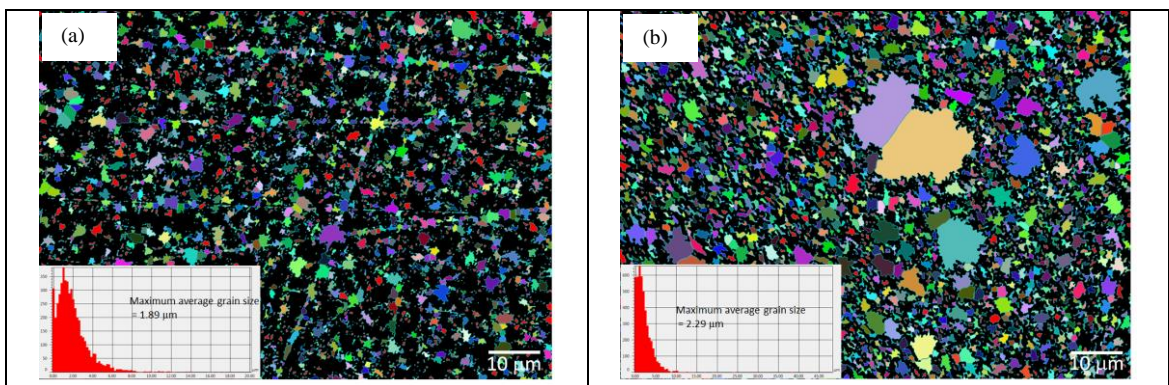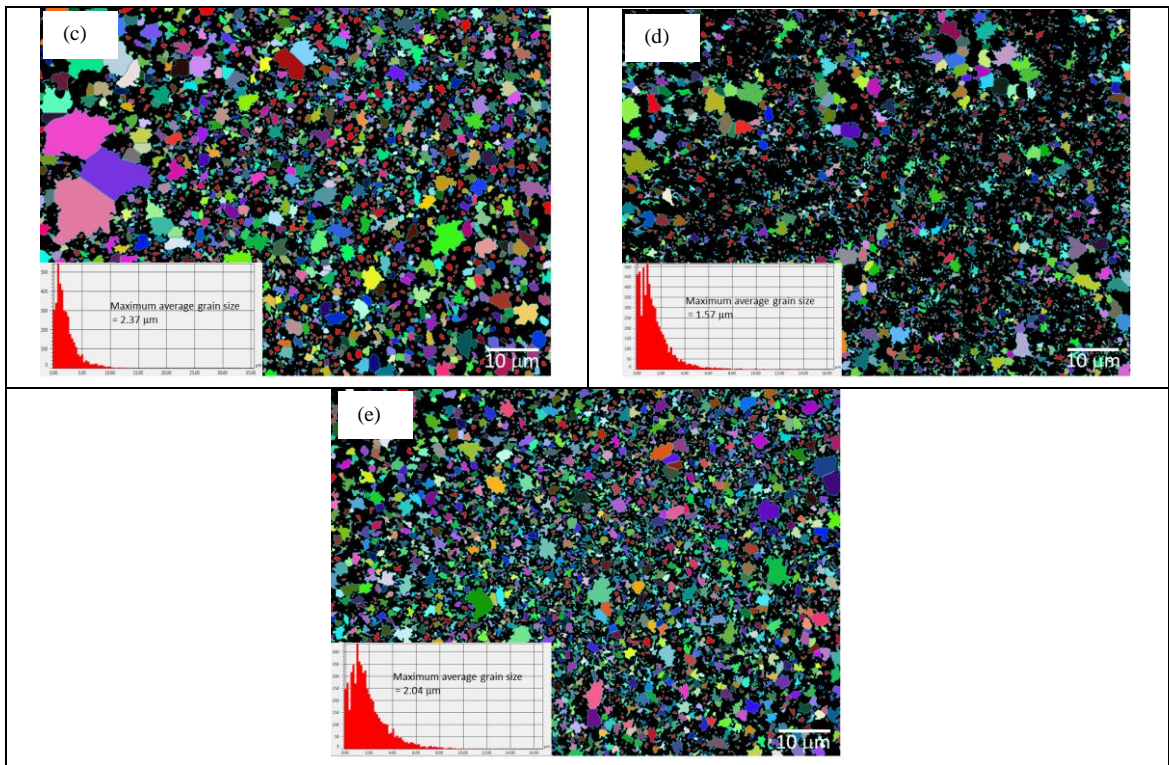
Fig. 5.5. Pre-test grain size maps: (a) Ni-Al$_2$O$_3$ (b) Ni-ZrO$_2$ (c) Ni-SiC (d) Ni-GPL (e) Nickel-only.

Ni-Graphene coatings have been reported to have refined grains, Ni-ZrO$_2$ and Ni-SiC have been known to have larger grains while Ni-Al$_2$O$_3$ have been observed to have larger grain size than Ni-Graphene but smaller grain size than Ni-ZrO$_2$ and Ni-SiC (Nazir et al. 2018a). A cause of higher grain size of Ni-SiC and Ni-ZrO$_2$ is due to particle agglomeration (Bajwa et al. 2016c), Ni-GPL electrodeposited coatings produced on a steel substrate have been known to develop bulges morphology and agglomerated particles which gives rise to higher surface roughness values (Jabbar et al. 2017), surface roughness of Ni-GPL increases with increase in Watts bath temperature while the best hardness and grain size values of Ni-GPL coatings are achieved at a Watts bath temperature of about 45°C (Jabbar et al. 2017).

A Nano indentation setup as shown in figure 5.6 was used to measure the micro-hardness and elastic modulus of each of the prepared coating. Depth controlled nano-indentations were performed and the penetration depth of the indentation was kept at 1/10 of the coating thickness to eliminate the substrate effects on the measured data. ZYGO was used to measure the average surface roughness of all the coatings. The results of the measured average surface roughness elastic modulus and micro hardness have been presented in table 5.1. Ni-GPL, Ni-Al$_2$O$_3$ and Ni-SiC nanocomposite coatings demonstrated the maximum nano-hardness values followed by Ni-ZO$_2$. In Comparison to the uncoated steel sample, Nickel-only coatings also showed an

improvement in surface hardness. *All* the coatings displayed an improvement in the micro-hardness. Ni-Al$_2$O$_3$ displayed the least values for average surface roughness because of the finer surface morphology of Ni-Al$_2$O$_3$ nanocomposite coatings followed by pure Nickel, particle agglomeration and higher grain size caused higher surface roughness values for Ni-ZrO$_2$ and Ni-SiC (Bajwa et al. 2016c; Nazir et al. 2018a).
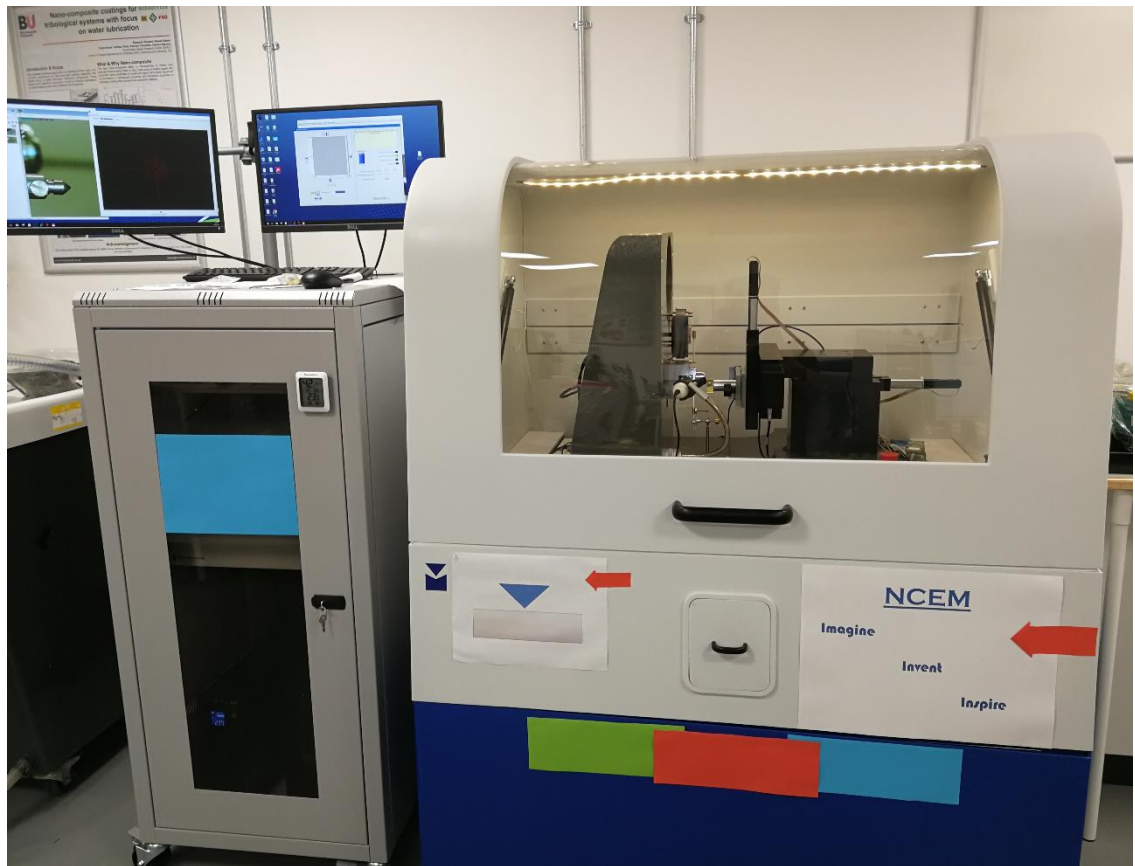
Fig. 5.6. Nano Indentation System (Nano Test Vantage Alpha).

Table 5.1 Measured mechanical properties of uncoated specimens.

Specimen	Ni-Al$_2$O$_3$	Ni-ZrO$_2$	Ni-SiC	Ni-GPL	Nickel	Uncoated
R$_a$ (μm)	0.045	0.20	0.18	1.17	0.12	0.10
Hardness (GPa)	3.85±0.28	3.54±0.36	3.84±0.24	3.87±0.38	3.22±0.22	3.00±0.09
Elastic Modulus (GPa)	203.48±11.67	207.17±12.88	247.76±27.24	212.86±15.73	215.94±14.87	212.28±9.32
Mean (H/E) Ratio	0.0189	0.0171	0.0154	0.0182	0.0149	0.0141

Compared to all the other coatings the pulse electrodeposition of Ni-GPL produced coatings with maximum surface roughness values. The presence of embedded nano graphene particles on the top most surface of the coatings result in a rough surface finish and a greyish black appearance which gives Ni-Graphene coatings higher average surface roughness values. Ni-GPL are also known to have higher surface roughness values and coarser surface at higher deposition temperatures (Jabbar et al. 2017). All the other coatings exhibited a shiny grey appearance.

Scratch tests were performed on all the prepared coatings. The results of the scratch test have been shown in figure 5.7. The loading conditions were kept constant for all the scratch tests. Multi-pass Wear Tests with 4 passes and 2 scratches per topography were conducted with a scanning velocity of 20 um/s. 150 mN of scratch load was applied by using a spherical indenter of 5 μm following the loading profile in figure 5.5 (f). The multi-pass wear test results of the scratch test indicate Ni-GPL to have very good wear resistance, the spikes in the data are due to the high surface roughness value of Ni-GPL coating and due to the removal of the loosely embedded graphene nano particles from the top surface of the coating by applying the load during scratch test. Nickel only, Ni-Al$_2$O$_3$ and Ni-ZO$_2$ exhibited an increase in wear scratch depth on the second pass; maximum wear depth was noted for Nickel-only coatings. Ni-SiC coatings also showed good resistance to wear. The thickness of all the coatings was in the range of 8-10 μm and none of the scratches was able to penetrate the entire depth of a coating. In fact the penetration depth was less the 50% of the thickness of any given coating.

Fig. 5.7. Scratch Test Results: (a) Ni-Al$_2$O$_3$ (b) Ni-ZrO$_2$ (c) Ni-SiC (d) Ni-GPL (e) Nickel-only (f) Loading profile.

The testing procedure used for the testing of the uncoated samples was followed for the testing of the coated samples as well to ensure identical operating conditions. Each coating was tested at three different loads and three different temperatures with a constant reciprocating frequency of 5 Hz and a stroke length of 5 mm. Testing methodology for coated specimens is summarized in table 5.2. Each coatings was tested at least twice as well to ensure repeatability.

Table 5.2 Testing methodology for coated specimens.

Sr No	Coating Type	Refrigerant Temperature (°C)	Load (N)
1	Pure Nickel	20	10
2	Pure Nickel	20	20
3	Pure Nickel	20	30
4	Pure Nickel	30	10
5	Pure Nickel	30	20
6	Pure Nickel	30	30
7	Pure Nickel	40	10
8	Pure Nickel	40	20
9	Pure Nickel	40	30
10	Ni-Al$_2$O$_3$	20	10

11	Ni-Al$_2$O$_3$	20	20
12	Ni-Al$_2$O$_3$	20	30
13	Ni-Al$_2$O$_3$	30	10
14	Ni-Al$_2$O$_3$	30	20
15	Ni-Al$_2$O$_3$	30	30
16	Ni-Al$_2$O$_3$	40	10
17	Ni-Al$_2$O$_3$	40	20
18	Ni-Al$_2$O$_3$	40	30
19	Ni-SiC	20	10
20	Ni-SiC	20	20
21	Ni-SiC	20	30
22	Ni-SiC	30	10
23	Ni-SiC	30	20
24	Ni-SiC	30	30
25	Ni-SiC	40	10
26	Ni-SiC	40	20
27	Ni-SiC	40	30
28	Ni-Graphene	20	10
29	Ni-Graphene	20	20
30	Ni-Graphene	20	30
31	Ni-Graphene	30	10
32	Ni-Graphene	30	20
33	Ni-Graphene	30	30
34	Ni-Graphene	40	10
35	Ni-Graphene	40	20
36	Ni-Graphene	40	30
37	Ni-ZrO$_2$	20	10
38	Ni-ZrO$_2$	20	20
39	Ni-ZrO$_2$	20	30
40	Ni-ZrO$_2$	30	10
41	Ni-ZrO$_2$	30	20
42	Ni-ZrO$_2$	30	30
43	Ni-ZrO$_2$	40	10
44	Ni-ZrO$_2$	40	20
45	Ni-ZrO$_2$	40	30

All the sample pairs were examined using SEM to understand and observe the type and extent of wear. EDS analysis was done within the contact regions of each flat and ball samples to examine the formation of tribo-films on the top mating surfaces and to determine the extent of damage on the flat disc samples. After performing SEM, ZYGO was used to measure the wear volume of the wear track on each disc specimen. The results of wear volume of all the coatings were compared to one another and also to an uncoated flat disc sample. Flat disc samples with a mid-ranged surface finish i.e. uncoated disc samples with Ra 0.1 μm were chosen as a reference for comparison. The results of coefficient of friction have been presented in terms of real-time coefficient of friction and average friction coefficient plots after the results of wear. The results of coefficient of friction were also compared to one another and also to the uncoated steel disc sample with R_a 0.1 μm. These results indicate and highlight whether or not Nickel based Nanocomposite coatings are helpful in improving the tribological performance of rubbing parts with HFE-7000 as refrigerant.

5.3 Wear of Coated Samples

SEM was used to investigate the wear mechanism and surface morphologies of all the sample pairs post-experimentation. EDS was performed on all the samples within the contact region of each sample pair as well. High magnification images revealed adhesive and abrasive wear mechanisms by examining the ball and disc specimens. A combination of micro-ploughing, micro-cutting and micro-delamination was observed on the wear scars. Plastic deformation was apparent for all the coatings due to higher hardness value of the counter steel ball in comparison to all the coatings. Elemental analysis results of EDS and micrographs of Ni-ZrO$_2$ are presented in figure 5.8, figure 5.9 and figure 5.10.

(a)

(b)

(c)
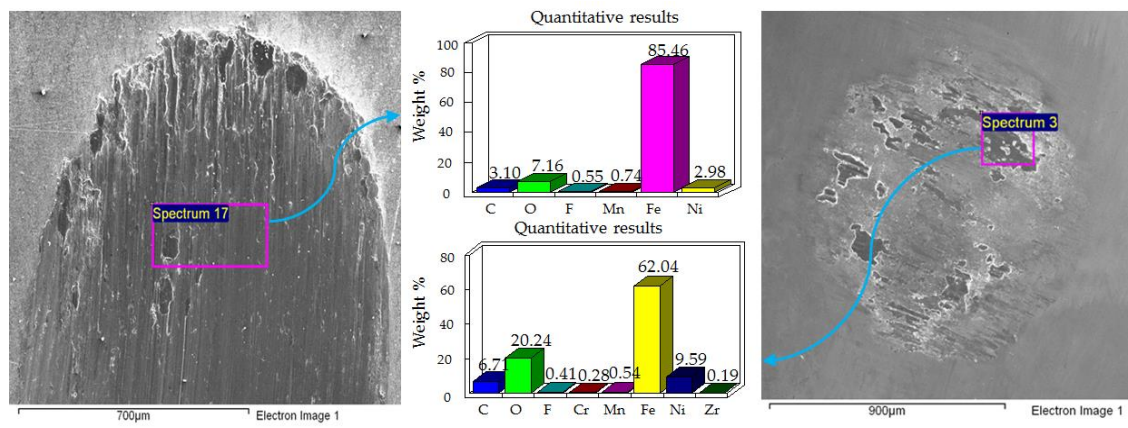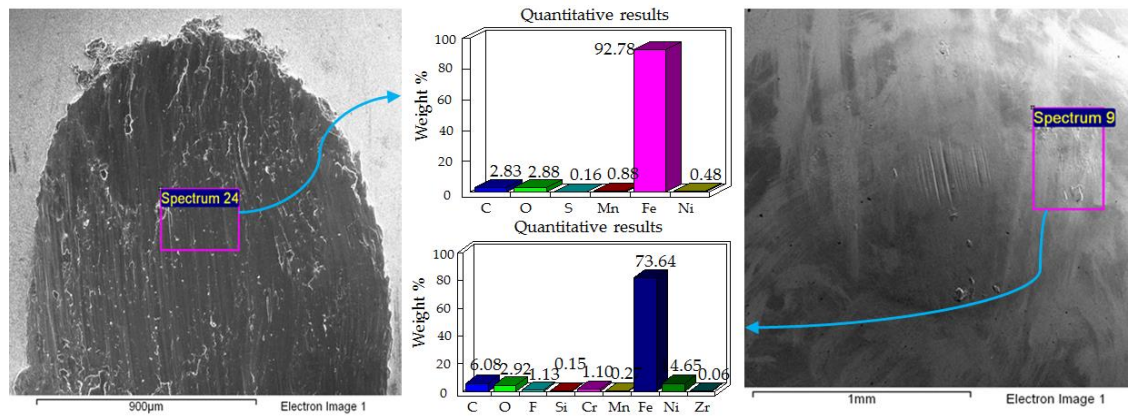
Fig. 5.8. EDS elemental results and SEM Micrographs of Ni-ZrO$_2$ coated flat samples and counter steel ball: (a) 20°C, 10 N (b) 20°C, 20 N (c) 20°C, 30 N.

Maximum wear occurred at low refrigerant temperature of 20°C as shown in figure 5.8. A high presence of iron only and only a slight presence of nickel is revealed by the EDS analysis of the wear scar at 20°C which indicates that the coatings have completely worn out. The presence of fluorine and/or oxygen is also revealed by the elemental EDS analysis performed on the wear track. Adhesion of the disc surface on the surface of the counter steel ball can be seen from the SEM images of the 52100 steel ball. Adhesion of the delaminated coatings on the surface of the steel ball is also confirmed by the EDS elemental analysis results in the contact region of the ball sample, with more adhesion present at 10 N in comparison to higher loads. The EDS results also show the presence of fluorine and oxygen. Increasing the applied load at 20°C refrigerant temperature increases wear; EDS analysis results of the wear scar also demonstrates a reduced presence of fluorine and oxygen with increase in load as shown in figure 5.8.

(a)
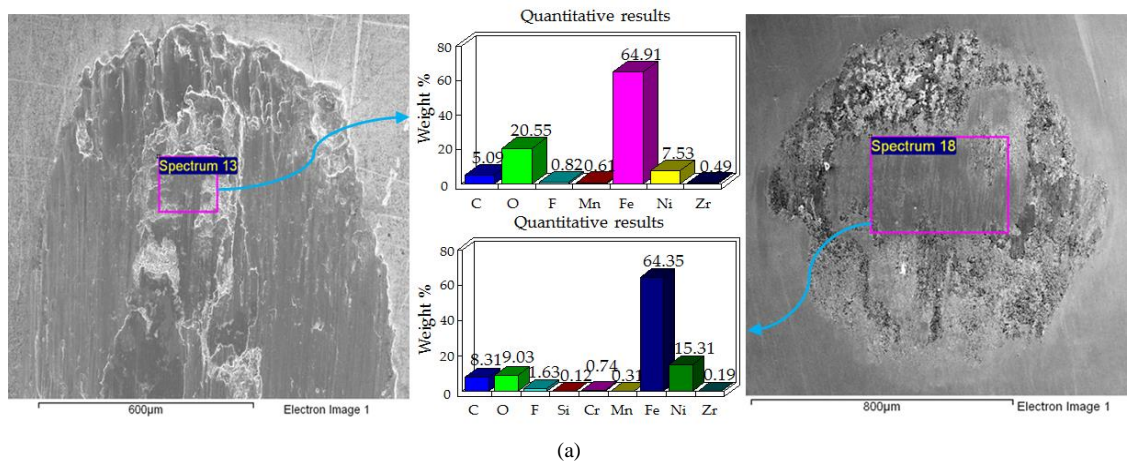
Fig. 5.9. EDS elemental results and SEM Micrographs of Ni-ZrO$_2$ coated flat samples and counter steel ball: (a) 30°C, 10 N (b) 30°C, 20 N (c) 30°C, 30 N.

An increase in the temperature of the refrigerant from 20°C to 30°C results in a higher percentage of fluorine and oxygen on the wear scar as shown in figure 5.9. A higher presence of zirconium and nickel is also detected through EDS on the wear track indicating a decrease in wear. Micrographs of the wear scar show micro-delamination and micro-cutting of the coated surfaces. EDS results and SEM micrographs of the 52100 counter steel ball show more adhesion of the coatings on the ball surface in contrast to the tests conducted at 20°C.

SEM images of the wear scar generated by increasing the temperature of the refrigerant from 30°C to 40°C show a decrease in the wear track width and overall wear as shown in figure 5.10. This is also evident from the EDS results; which reveal a significant percentage of zirconium and nickel in comparison to the tests conducted at 20°C and 30°C. For the tests conducted at 40°C EDS results also present a higher percentage of oxygen and fluorine on the ball and disc samples in comparison to the tests conducted at lower refrigerant temperatures.

Fig. 5.10. EDS elemental results and SEM Micrographs of Ni-ZrO$_2$ coated flat samples and counter steel ball: (a) 40°C, 10 N (b) 40°C, 20 N (c) 40°C, 30 N.

Micrographs of the flat disc and the ball sample show that wear occurred mainly because of micro-cutting at 20°C, wear due to micro-delamination dominated at 30°C and a mix of micro-delamination and micro-cutting occurred at 40°C.

EDS elemental analysis results and SEM micrographs of tests conducted on Ni-SiC nanocomposite coatings have been presented in figures 5.11, 5.12 and 5.13.

(a)

(b)

(c)

Fig. 5.11. EDS elemental results and SEM Micrographs of Ni-SiC coated flat samples and counter steel ball: (a) 20°C, 10 N (b) 20°C, 20 N (c) 20°C, 30 N.

Results of the tests conducted at 20°C refrigerant temperature shown in figure 5.11 display wear due to micro-delamination and micro-cutting of Ni-SiC coatings. Micro-delamination and micro-cutting occurred at 20°/10 N and 20°/20 N, increasing the applied normal load to 30 N shifted the wear mechanism more towards micro-cutting as shown in figure 5.11.

Increasing the temperature of the refrigerant to 30°C resulted in a shift in wear mechanism more towards micro-cutting and a decrease in wear as shown in figure 5.12. Increasing the refrigerant temperature also resulted in increased adhesion of the coatings onto the counter steel ball.
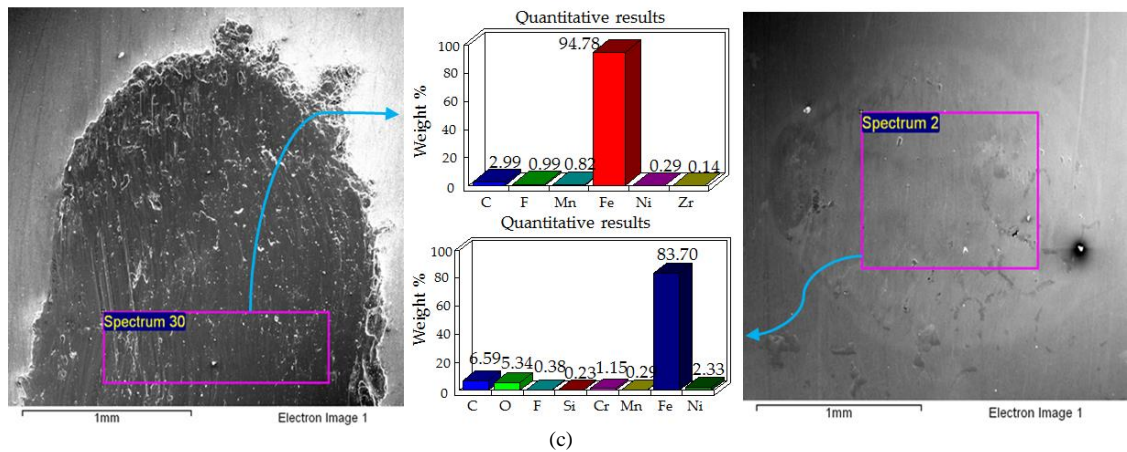

(a)

(b)

(c)
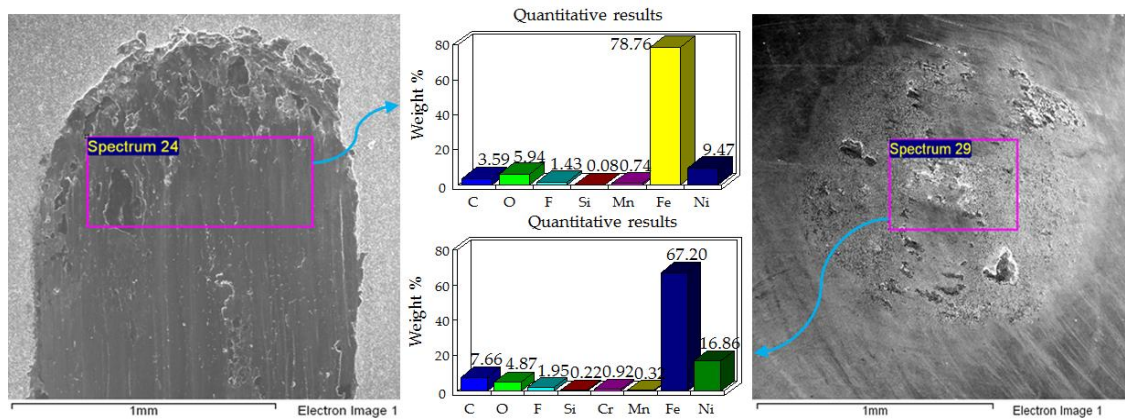
Fig. 5.12. EDS elemental results and SEM Micrographs of Ni-SiC coated flat samples and counter steel ball: (a) 30°C, 10 N (b) 30°C, 20 N (c) 30°C, 30 N.

(a)


(b)

Fig. 5.13. EDS elemental results and SEM Micrographs of Ni-SiC coated flat samples and counter steel ball: (a) 40°C, 10 N (b) 40°C, 20 N (c) 40°C, 30 N.

The severity of wear is reduced by increasing the temperature of the refrigerant from 30°C to 40°C. As presented in figure 5.13, micro-cutting and micro-delamination is visible on the wear scar at 40°C/10 N; while micro-delamination and micro-ploughing is visible at 40°C/20 N and 40°C/30 N. Adhesion of the coatings is also observed on the steel ball for tests conducted at 40°C.

SEM images and EDS results of Ni-Al$_2$O$_3$ have been presented in figures 5.14, 5.15 and 5.16. At low refrigerant temperature of 20°C, an increase in applied load increased wear. SEM images and EDS resulted shown in figure 5.14 show delamination of Ni-Al$_2$O$_3$ coating at 20°C/20 N and 20°C/30N. Micro-cutting and micro-delamination resulted in wear at 20°C/10 N and 20°C/30 N. At 20°C/20 N testing conditions micro-cutting was observed as the main cause of wear.
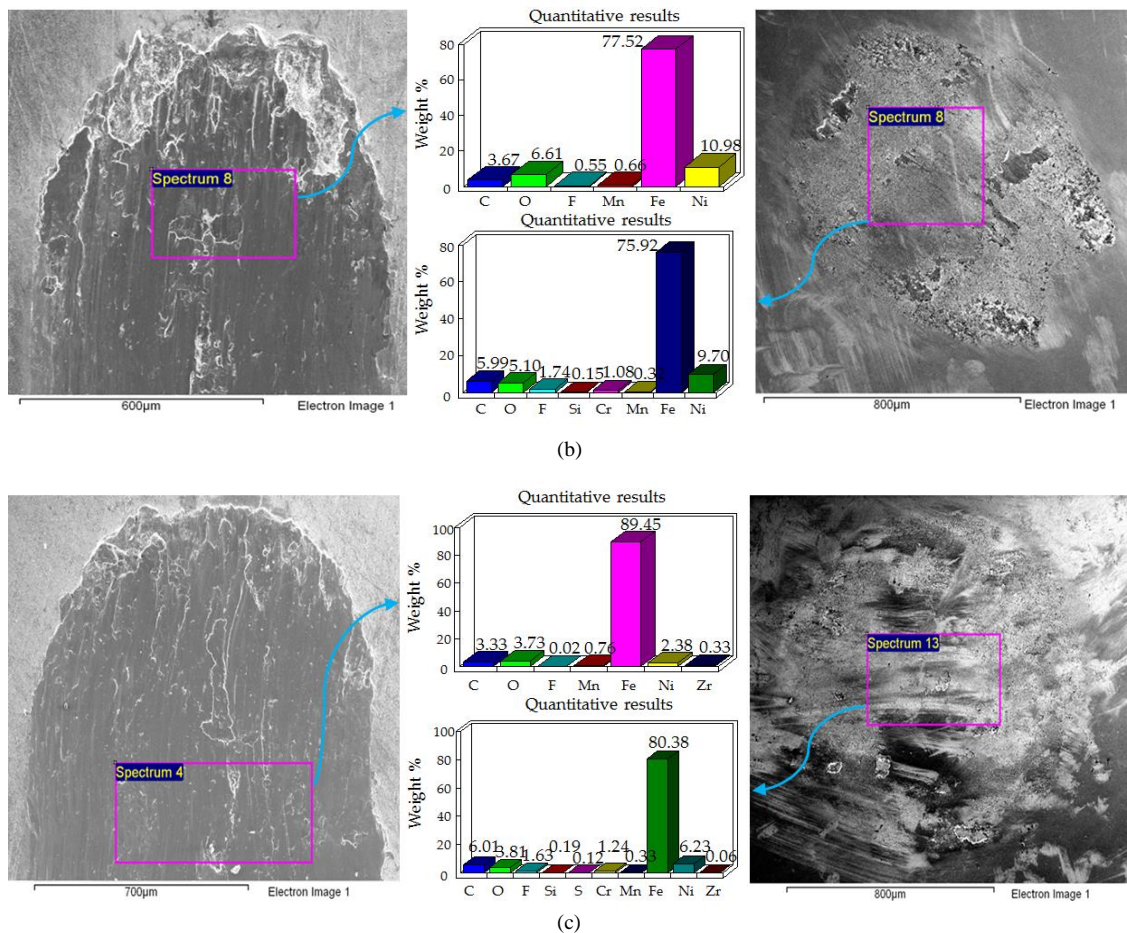

(a)

(b)

(c)

Fig. 5.14. EDS elemental results and SEM Micrographs of Ni-Al$_2$O$_3$ coated flat samples and counter steel ball: (a) 20°C, 10 N (b) 20°C, 20 N (c) 20°C, 30 N (Bhutta et al. 2018a).

Increasing the refrigerant temperature to 30°C produced a significant positive effect on wear reduction at applied load of 20 N as shown in figure 5.15. A complete delamination of the coating was not observed at 30°C/20 N. 30°C/30 N showed similar results to 20°C/30 N, a total coating delamination was also observed at 30°C/30 N. 30°C/10 N results were different in terms of wear mechanism; micro-delamination governed the wear phenomenon at 20°C/10 N whereas wear mainly due to micro-cutting was witnessed at 30°C/10 N.

(a)

Fig. 5.15. EDS elemental results and SEM Micrographs of Ni-Al$_2$O$_3$ coated flat samples and counter steel ball: (a) 30°C, 10 N (b) 30°C, 20 N (c) 30°C, 30 N.

Figure 5.16 shows the results by increasing the temperature of the refrigerant from 30°C to 40°C. A combination of micro-cutting and micro-delamination was observed at 40°C/10N. All the tests conducted at load of 10 N show a substantial amount of aluminium along with nickel representing that Ni-Al$_2$O$_3$ coatings did not totally wear out at low loads. At 40°C micro-cutting was witnessed on the wear track with an increase in applied normal load to 20 N. Further increasing the load at 40°C to 30 N produced micro-delamination and micro-cutting. EDS elemental analysis results of the wear track at 40°C on all the disc samples displayed a significance percentage of nickel which implies that at higher refrigerant temperatures wear has been reduced.
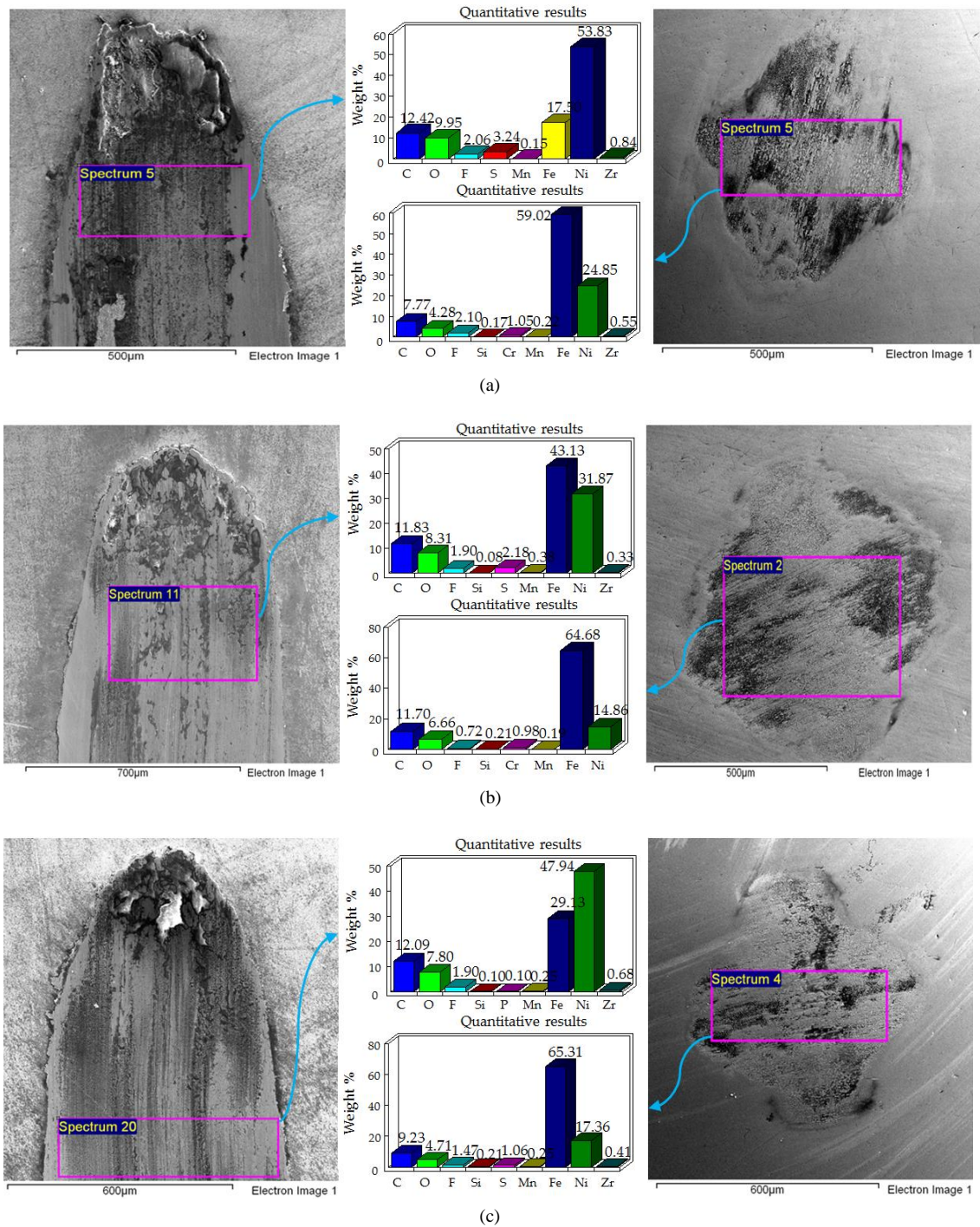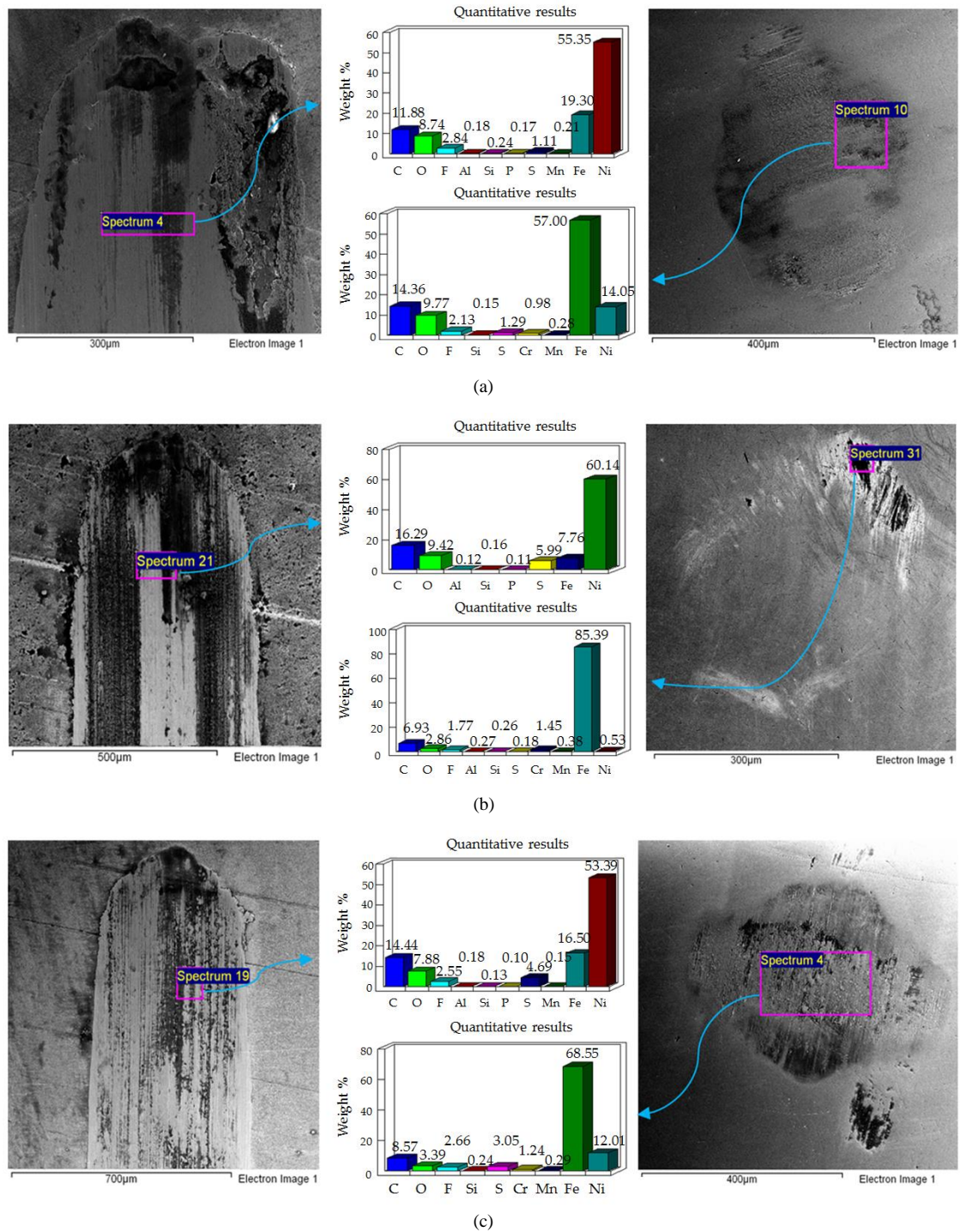
Fig. 5.16. EDS elemental results and SEM Micrographs of Ni-Al$_2$O$_3$ coated flat samples and counter steel ball: (a) 40°C, 10 N (b) 40°C, 20 N (c) 40°C, 30 N (Bhutta et al. 2018a).

SEM images and EDS results of the tests conducted on Nickel-Graphene (Ni-GPL) coatings have been presented 5.17, 5.18 and 5.19. SEM micrographs at 20°C refrigerant temperature at any given load displayed high wear and the results expose Ni-GPL coatings to be completely worn out mainly due to micro-cutting as shown in figure 5.17.
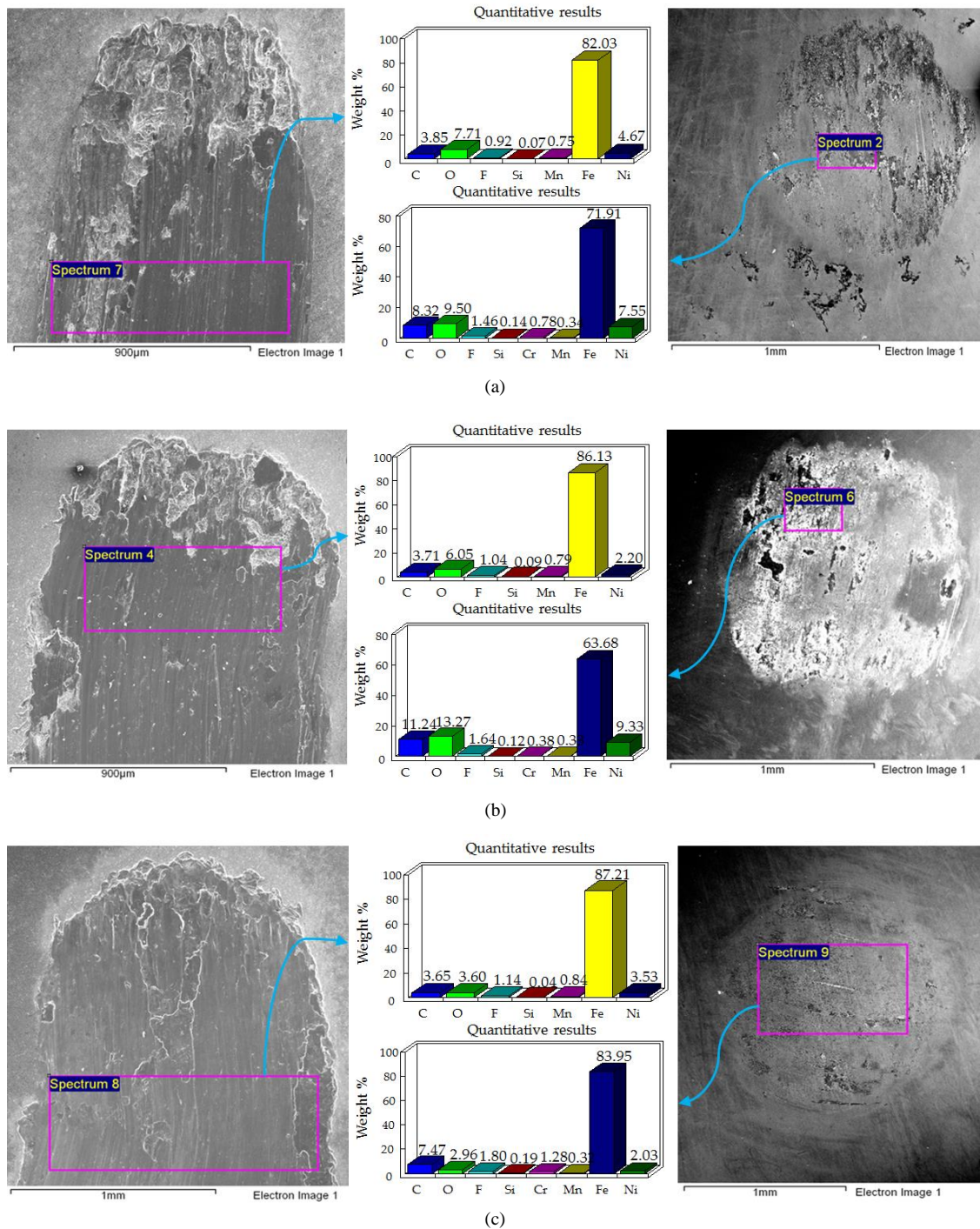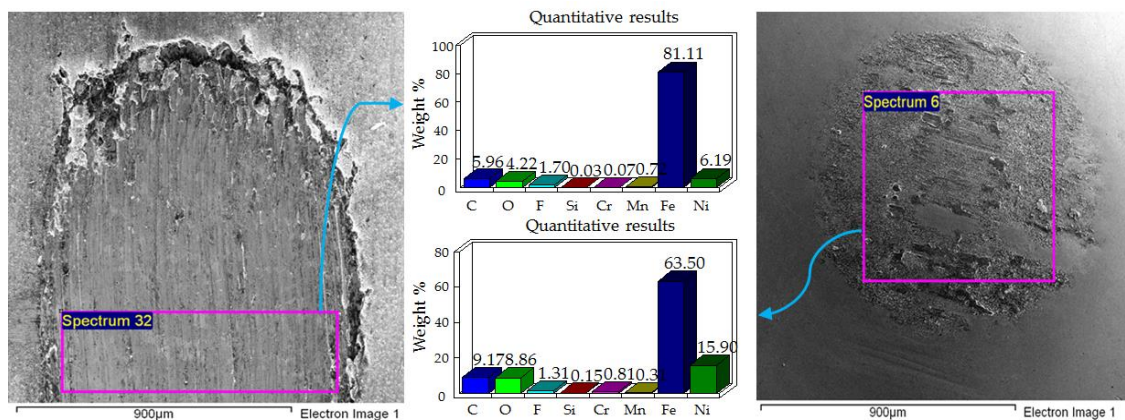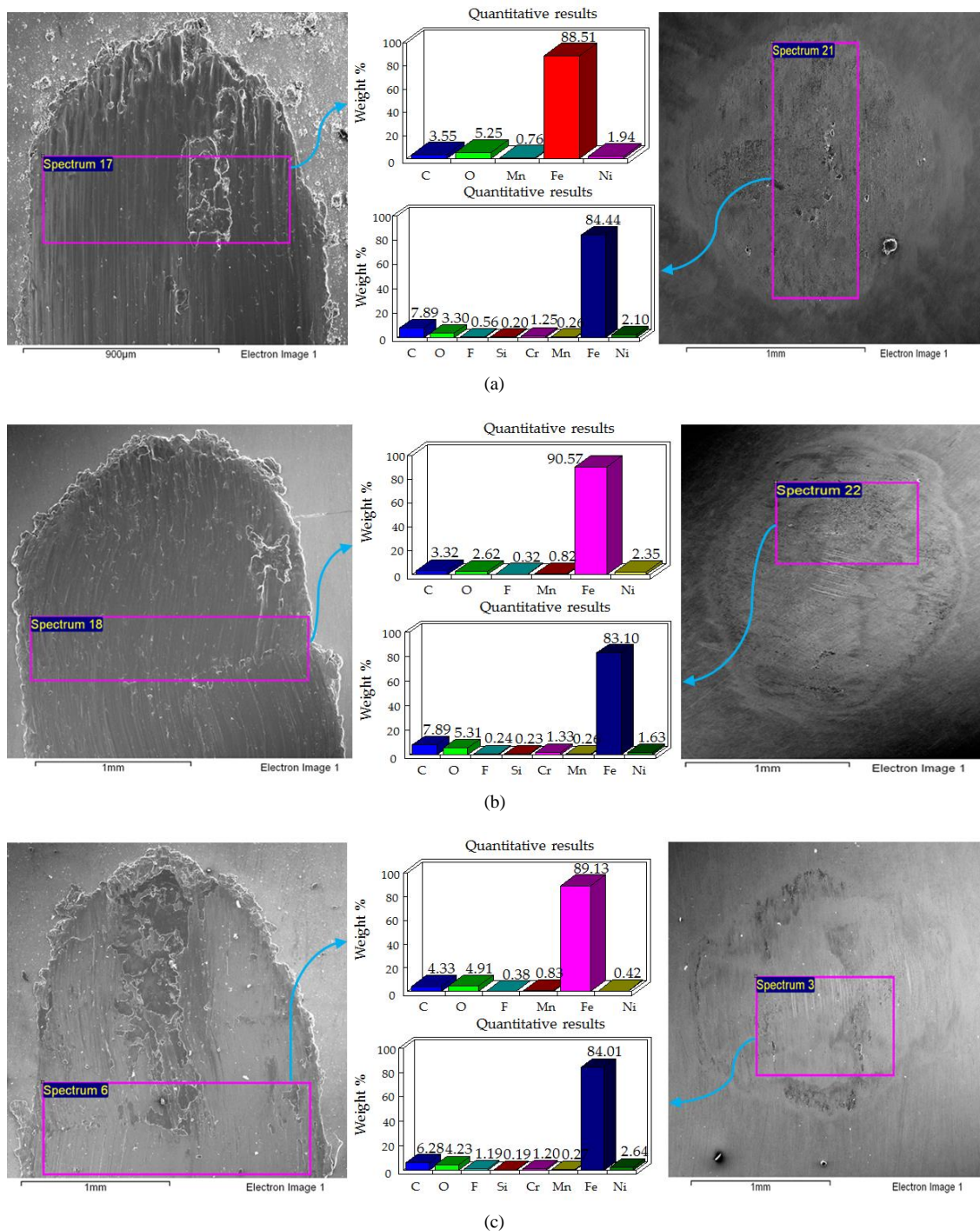
Fig. 5.17. EDS elemental results and SEM Micrographs of Ni-GPL coated flat samples and counter steel ball: (a) 20°C, 10 N (b) 20°C, 20 N (c) 20°C, 30 N.

Increasing the temperature of the refrigerant from 20°C to 30°C at 10 N load produced lesser damage and micro-ploughing was observed on the wear scar at 30°C/10 N as shown in figure 5.18. Micro-delamination and micro-ploughing was observed at 30°/20 N and 30°/30 N as

shown in figure 5.18. At 30°for all the loads the EDS results show a higher percentage of nickel in comparison to the tests conducted at 20°C, this specifies a decrease in wear with a rise in refrigerant temperature.
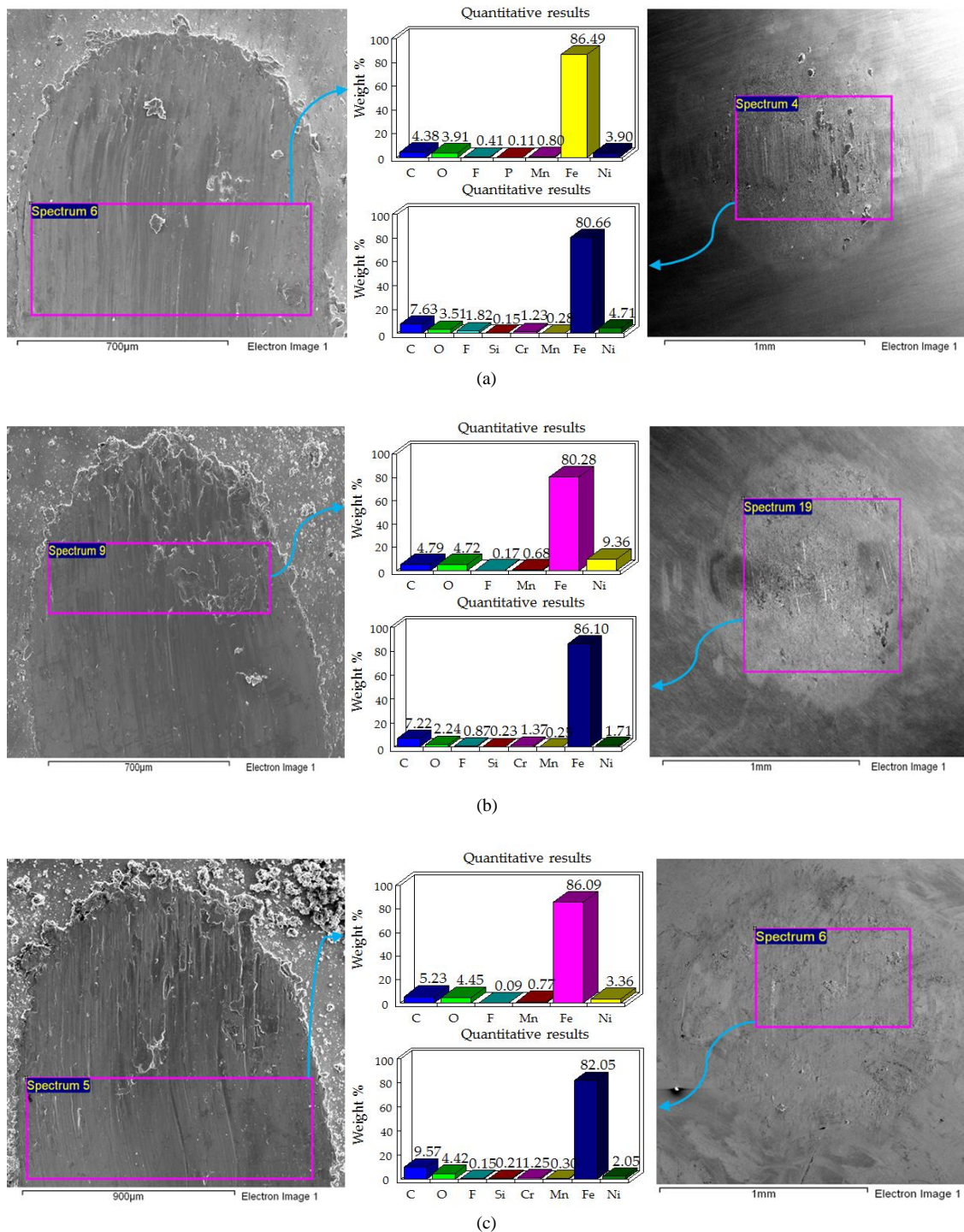
Fig. 5.18. EDS elemental results and SEM Micrographs of Ni-GPL coated flat samples and counter steel ball: (a) 30°C, 10 N (b) 30°C, 20 N (c) 30°C, 30 N.

Results of Ni-GPL at 40°C refrigerant temperature presented in figure 5.19 show micro-cutting and micro-delamination at 40°C/10 N. EDS results at 40°C/10 N presented the highest percentage of nickel amongst all the tests that were conducted on Ni-GPL. Micro-delamination and micro-ploughing were the main causes of wear at 40°C/20 N. Test at 40°C/30 N show wear due to micro-delamination and micro-cutting. Elemental EDS results of the wear scar of all the flat disc samples display a higher percentage of nickel at 40°C at any given load in comparison to tests conducted at lower refrigerant temperatures.

This indicates a decrease in wear when using Nickel-Graphene coatings by increasing the temperature of the refrigerant from 20°C to 40°C. Adhesion of the coatings on the steel ball also increases with an increase in the temperature of the refrigerant from 20°C to 40°C.
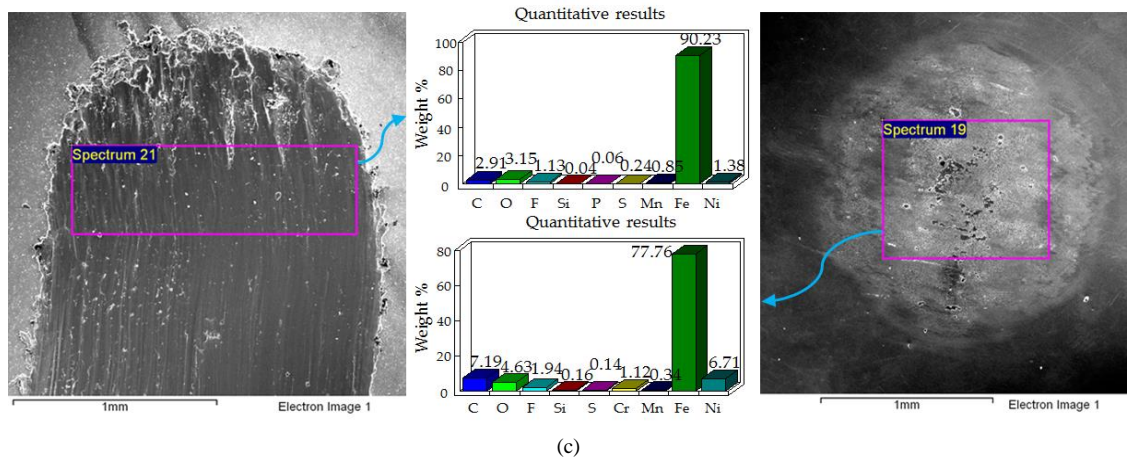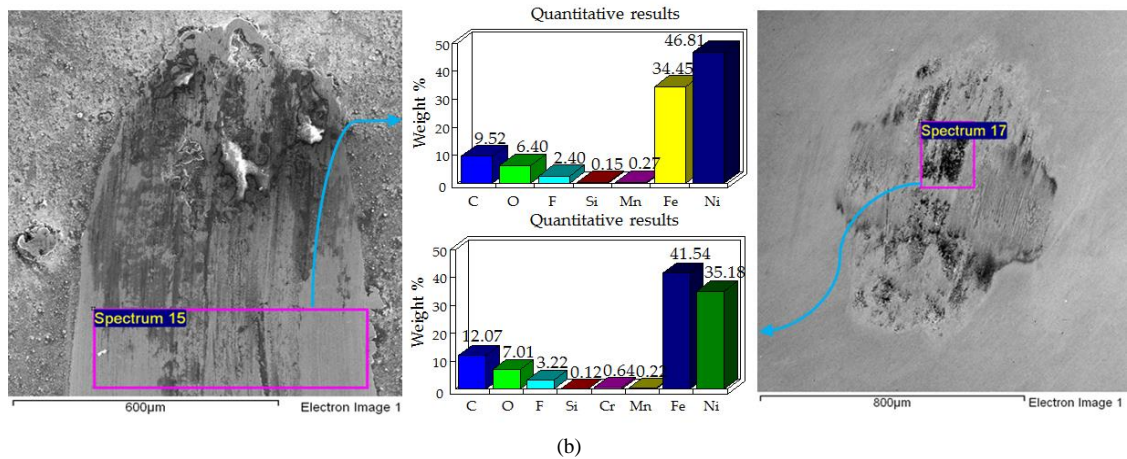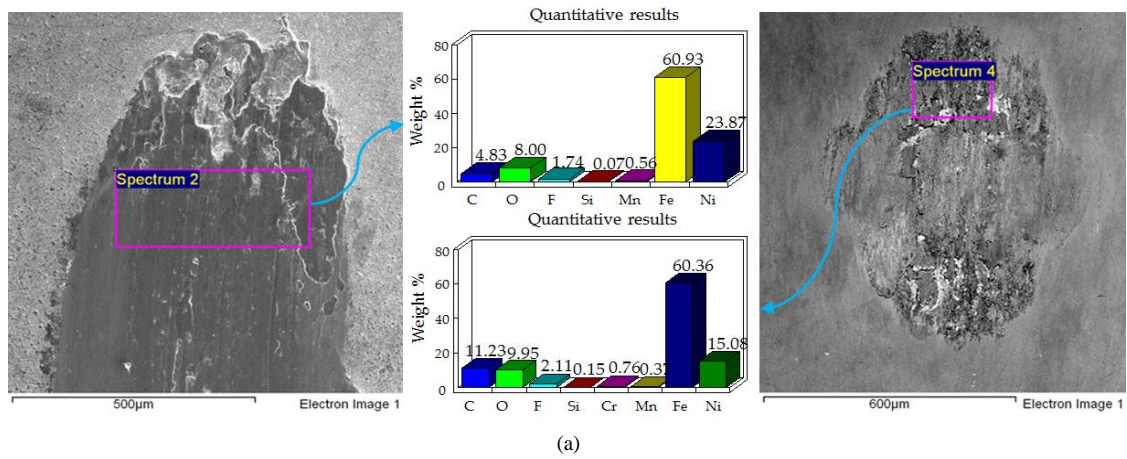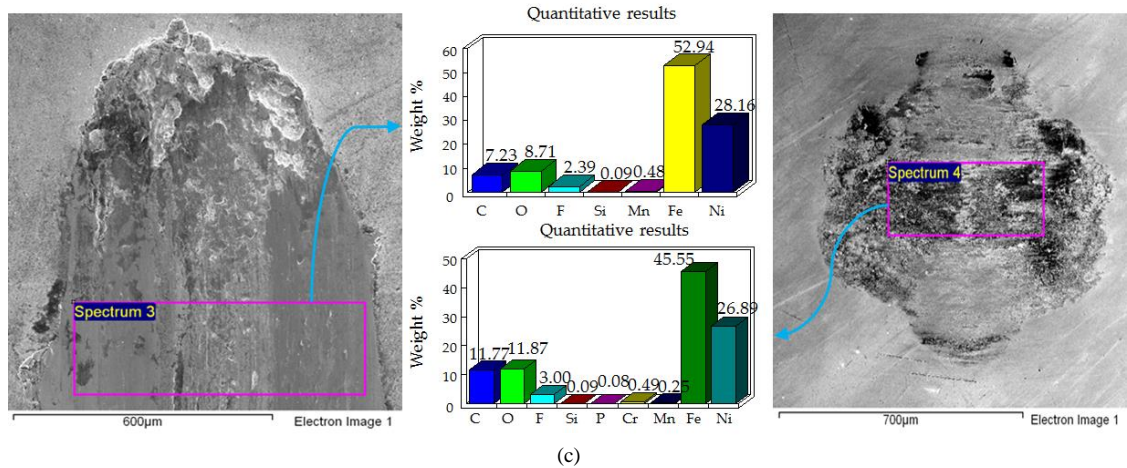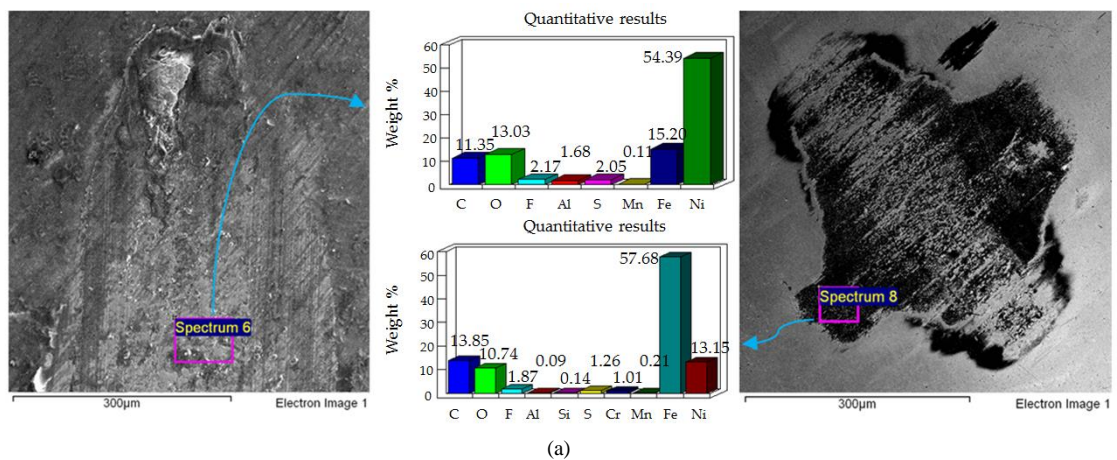

(a)

(b)

(c)
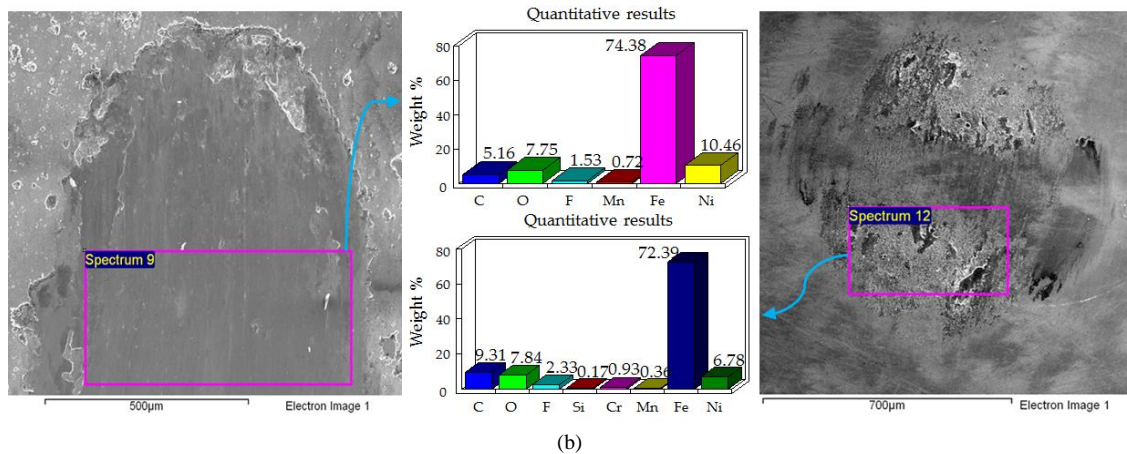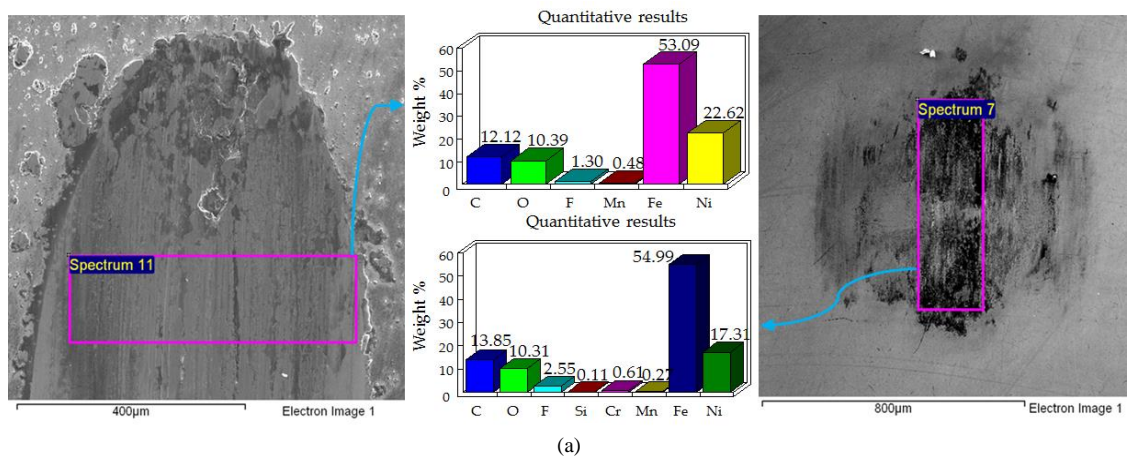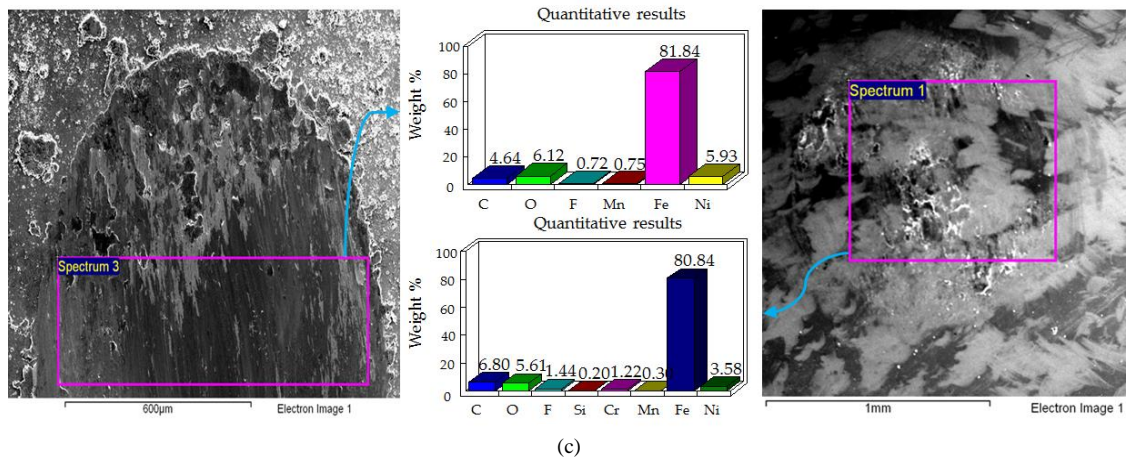
Fig. 5.19. EDS elemental results and SEM Micrographs of Ni-GPL coated flat samples and counter steel ball: (a) 40°C, 10 N (b) 40°C, 20 N (c) 40°C, 30 N.

EDS results and SEM micrographs of Nickel-only coatings have been presented in figure 5.20, 5.21 and 5.22. Figure 5.20 shows the results of Nickel-only coatings at 20°C refrigerant temperature, the results show micro-delamination and micro-cutting to be the primary cause of wear. EDS results at 20°C display only a small percentage of nickel on the wear scar implying high wear at low refrigerant temperature. At 20°C/10 N micro-delamination is seen to be the more dominant wear mechanism whereas micro-cutting is the more prominent wear mechanism at 20°C/30 N, while 20°C/20 N presents a mix of micro-cutting and micro-delamination.

(a)

(b)

(c)
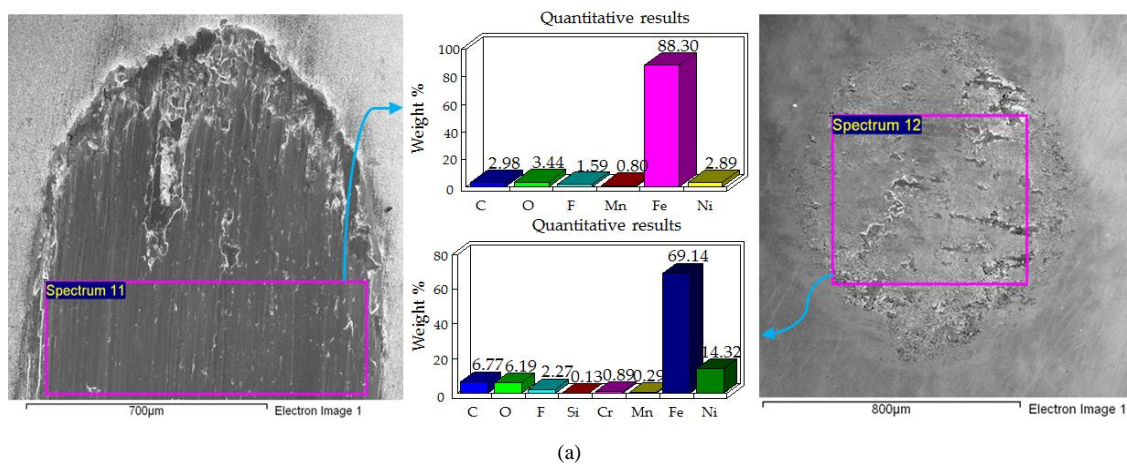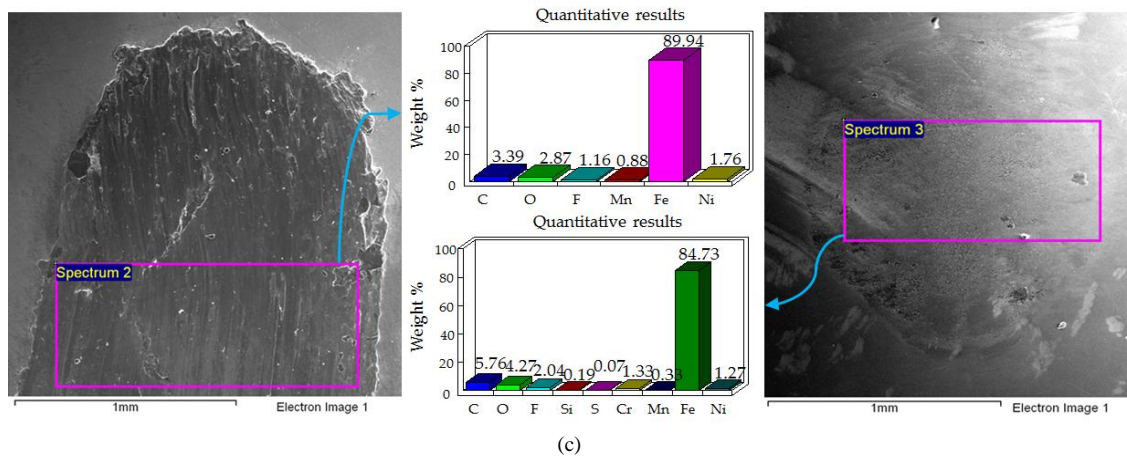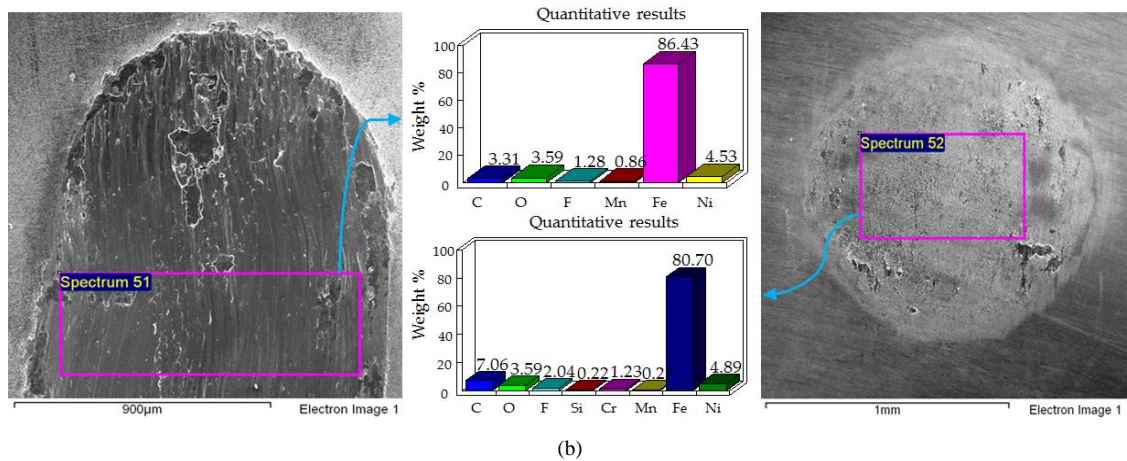
Fig. 5.20. EDS elemental results and SEM Micrographs of Nickel-only coated flat samples and counter steel ball: (a) 20°C, 10 N (b) 20°C, 20 N (c) 20°C, 30 N.

EDS results obtained by increasing the temperature of the refrigerant to 30°C presented in figure 5.21 show a higher presence of nickel in contrast to the experiments conducted at 20°C which indicates a decline in wear by a rise in the temperature of the refrigerant. At 30°C wear is seen to be mainly due to micro-delamination and micro-cutting.
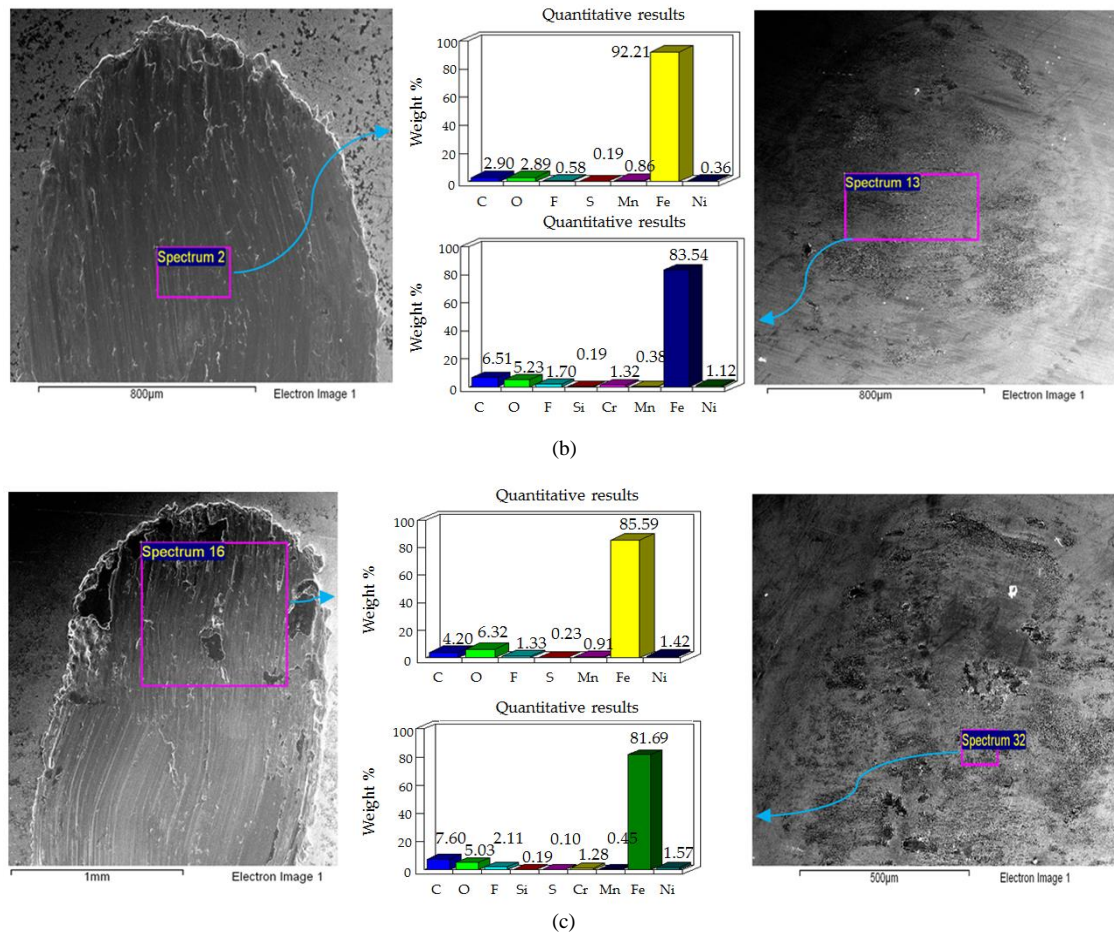

(a)

(b)

(c)
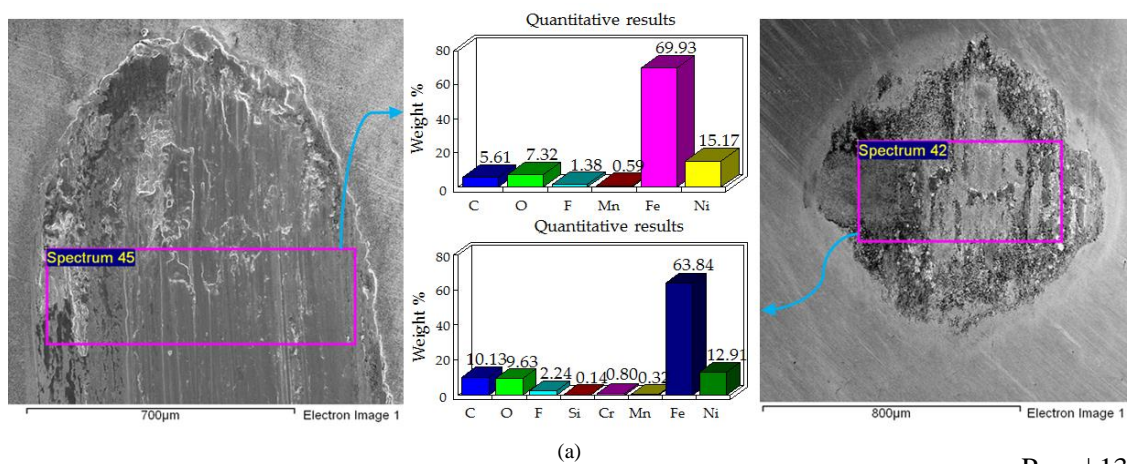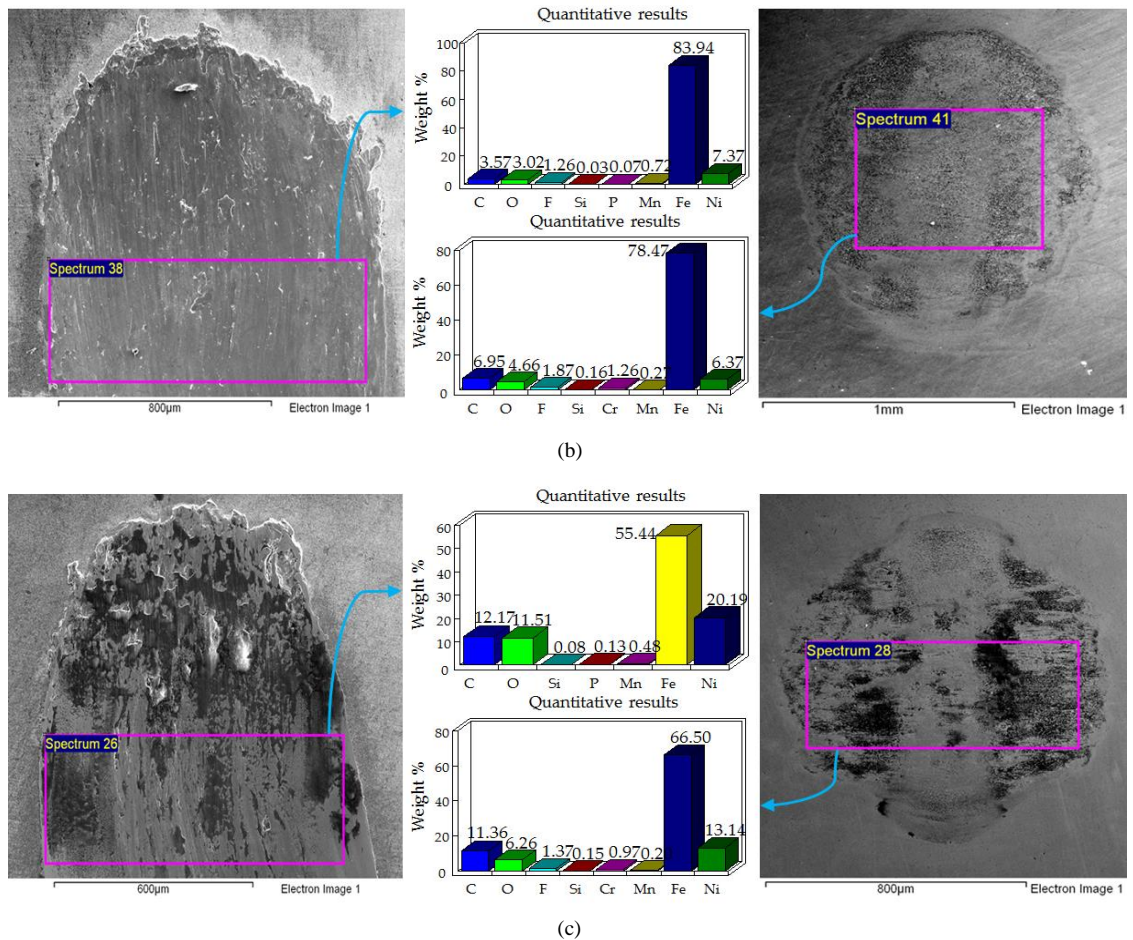
Fig. 5.21. EDS elemental results and SEM Micrographs of Nickel-only coated flat samples and counter steel ball: (a) 30°C, 10 N (b) 30°C, 20 N (c) 30°C, 30 N.

At 30°C/20 N, wear occurred primarily due to micro-cutting whereas wear due to a mix of micro-cutting and micro-delamination was observed at 30°C/10 N and 30°C/30 N.
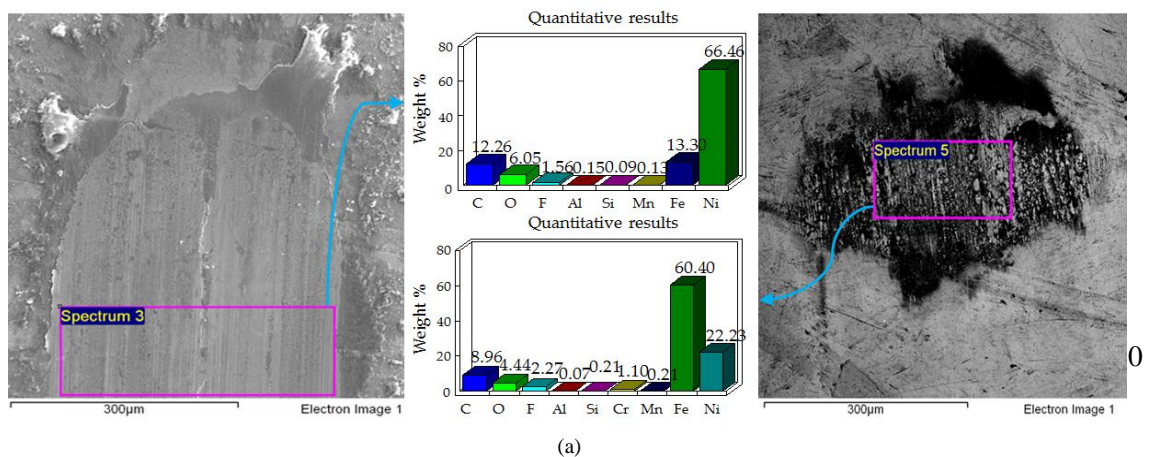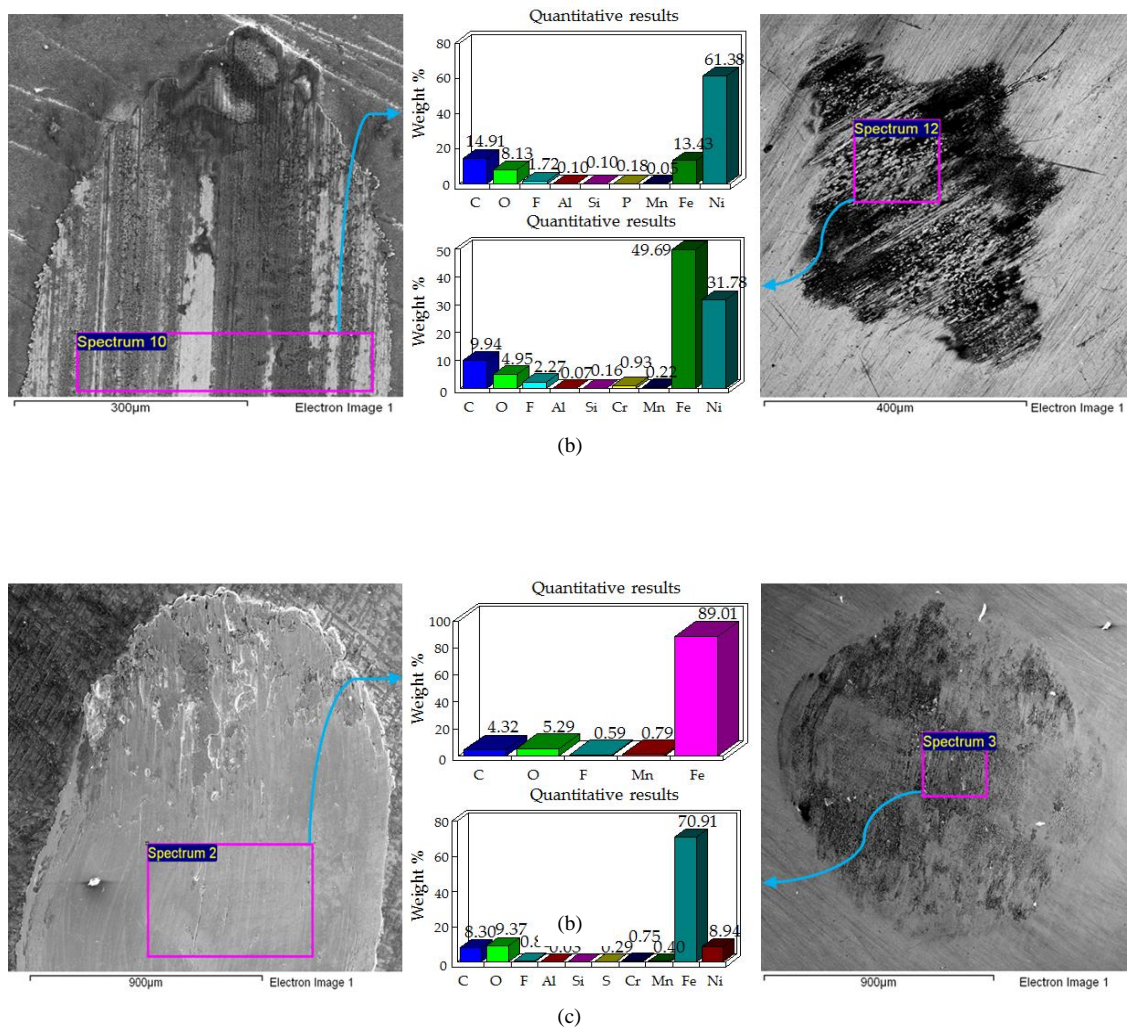

(a)
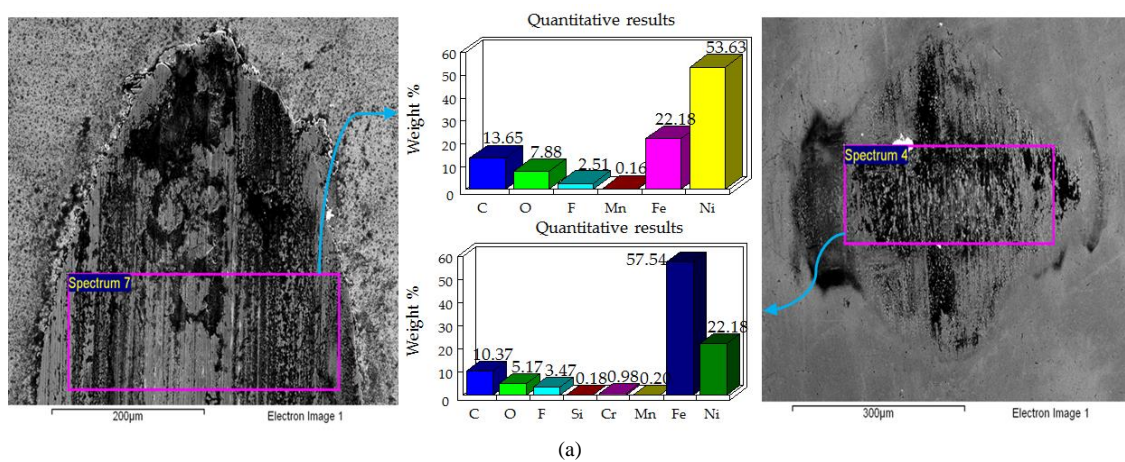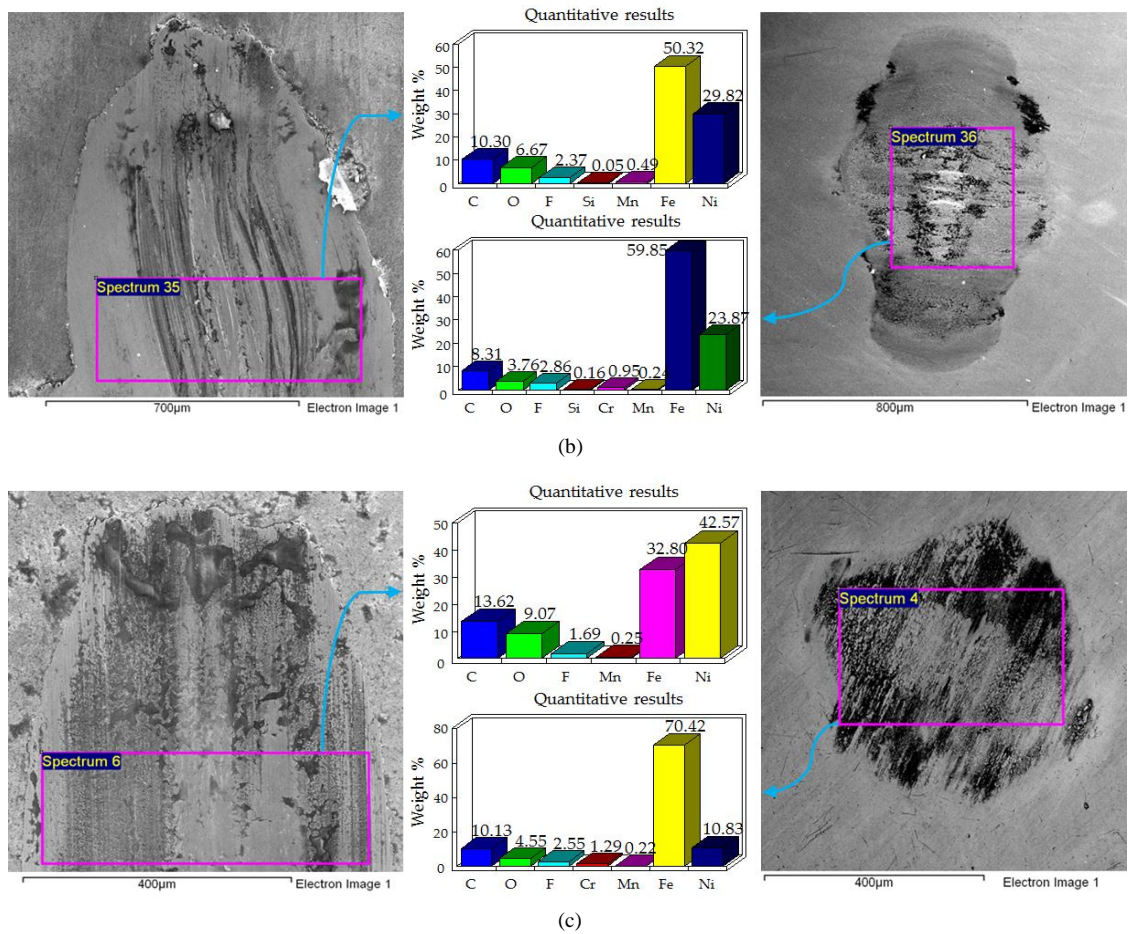
Fig. 5.22. EDS elemental results and SEM Micrographs of Nickel-only coated flat samples and counter steel ball: (a) 40°C, 10 N (b) 40°C, 20 N (c) 40°C, 30 N.

The results of the tests conducted at 40°C for Nickel-only coatings shown in figure 5.22 reveal an even higher presence of nickel at any applied load on the wear scar indicating a further decrease in wear by increasing the temperature of the refrigerant. Micro-cutting and micro-delamination were the main cause of wear at 40°C/10 N and 40°C/30 N; whereas micro-ploughing was the main cause of wear at 40°C/20 N.

5.3.1 Wear Volume of Coated Samples

The same method that was used for measuring the wear volume of uncoated samples was used for measuring the wear volume of coated samples using ZYGO.
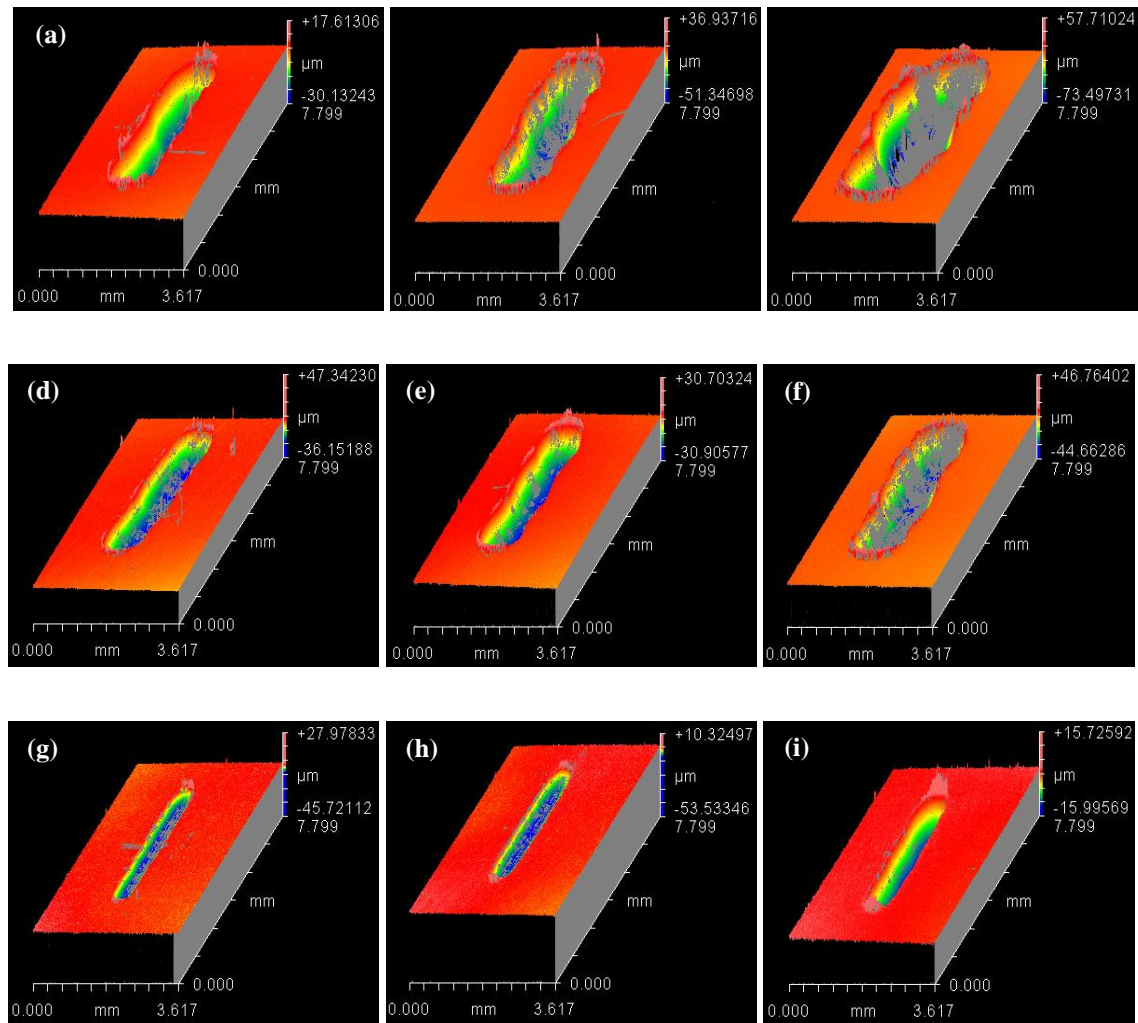
Fig. 5.23. 3D plots of the wear tracks of Ni-ZrO2 coated specimens: (a) 10 N, 20°C (b) 20 N, 20°C (c) 30 N, 20°C (d) 10 N, 30°C (e) 20 N, 30°C (f) 30 N, 30°C (g) 10 N, 40°C (h) 20 N, 40°C (i) 30 N, 40°C.

Each wear track was stitched in a similar pattern to generate 3D plots of the complete wear track. Figure 5.23 shows the results of Ni-ZrO$_2$ obtained from the interferometer. Similar wear profiles were generated for other coatings as well. The 3D plots were used to measure the wear volume through ZYGO.

Results of the wear volume of the coated samples were compared with the uncoated samples to gauge and evaluate the effect of using nickel based coatings in comparison to non-coated specimens. Uncoated samples having average surface finish of 0.1 µm were used as a reference from which all the coated samples were compared to. Figure 5.24 presents the plot of wear volume of Ni-ZrO$_2$ nanocomposite coatings and the percentage change in wear volume by the deposition of Ni-ZrO$_2$ on EN1A steel substrate. Wear volume increased with increase in applied

normal load at low refrigerant temperature of 20°C. Increasing the temperature of the refrigerant to 30°C produced almost the same amount of wear volume at applied load of 10 N, however at higher applied loads of 20 N and 30 N; a very substantial decrease in wear volume is observed in comparison to wear produced at 20°C. Interestingly least amount of wear was produced at 20 N load and 10 N load caused maximum wear for 30°C refrigerant temperature. A further increase in the temperature of the refrigerant by 10°C dropped wear even further and it can be observed from the plots that least amount of wear happened at 40°C at any given load for Ni-ZrO_2 coatings. A clear presence of oxygen and fluorine on the wear track as well as on the counter steel ball can be seen through the EDS analysis results. This decline in wear volume with rise in refrigerant temperature is due to the formation fluorinated and oxygenated anti-wear tribo-films on the top most surfaces of the mating parts. EDS results also display an increase in the percentage of oxygen and fluorine on the wear track as well as on the counter steel ball with rise in refrigerant temperature from 20°C to 40°C. Overall least amount of wear for ZrO_2 coatings was observed at 40°C/20 N.

A comparison of the wear volume produced by using Ni-ZrO_2 nanocomposite coatings to uncoated steel with R_a 0.1 μm at each testing conditions is shown in figure 5.24 (b), the percentage change in wear volume by using Ni-ZrO_2 show clear reduction in wear volume at all the testing conditions. Improvement in wear is less at lower refrigerant temperature of 20°C and maximum reduction in wear occurs at higher refrigerant temperature of 40°C. 20°C/20 N testing conditions resulted in minimum wear improvement, EDS results and SEM images at these conditions showed high wear due to micro-cutting and almost complete wear out of the coatings. A combination of micro-delamination and micro-cutting at 30°C/10 N also produced high wear which caused minimum improvement in wear at 30°C.

A decreases in wear volume by over 70% at 40°C was observed for loads of 10 N and 30 N; an improvement of just below 65% was seen at 40°C/20 N. Both the Ni-ZrO_2 coated samples and uncoated steel presented best wear results at 40°C/20 N, this indicates that there is an optimum temperature and load combination that generates best wear performance results when using HFE-7000. Micro-hardness and H/E ratio improved by applying Ni-ZrO_2 coatings when compared to uncoated steel, which helped improve the wear performance of rubbing parts.

Wear produced by using Ni-ZrO$_2$ Nanocomposite Coating

(a)

Percentage change in wear volume by applying Ni-ZrO$_2$ Nanocomposite Coating
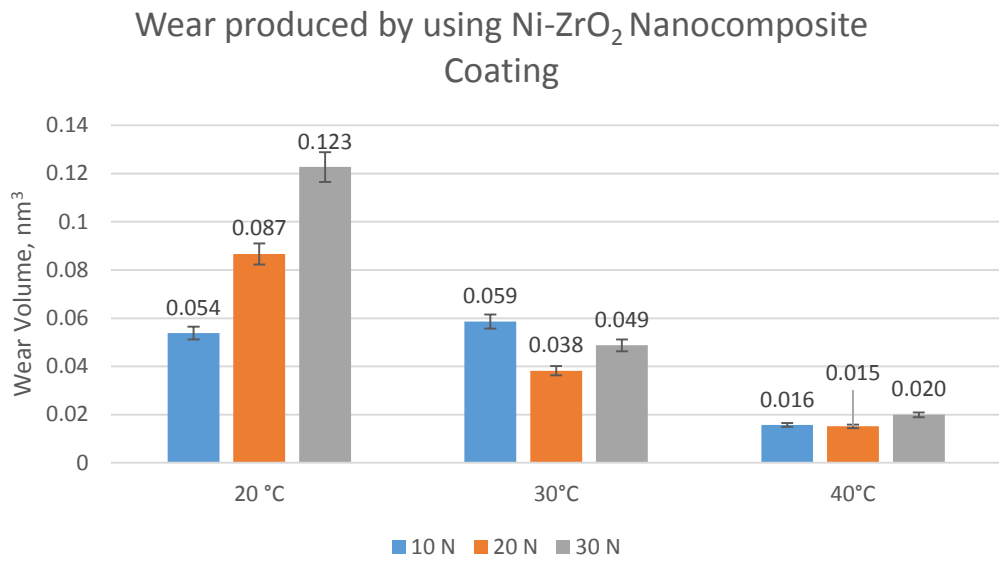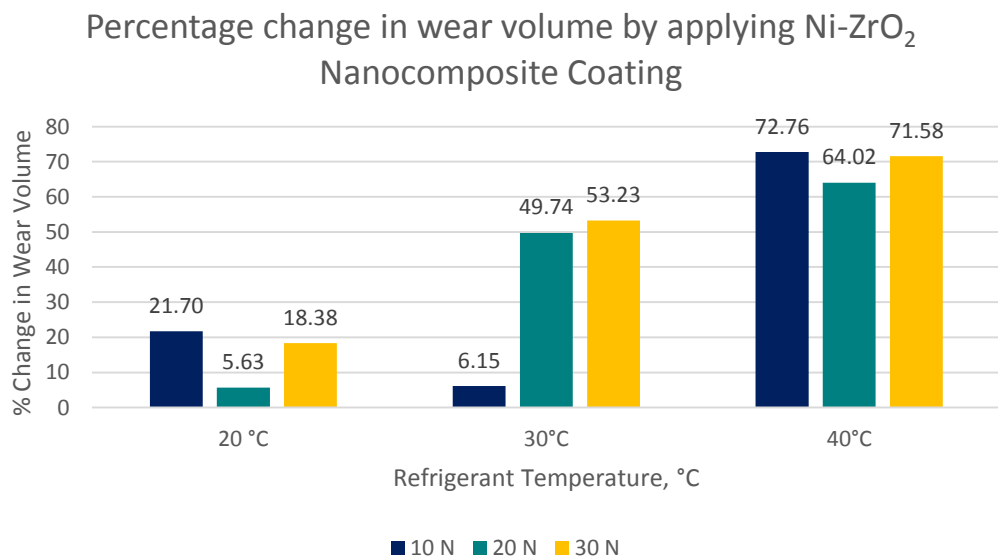
(b)

Fig. 5.24. (a) Wear volume plot of Ni-ZrO$_2$ nanocomposite coatings disc. (b) Percentage change in wear volume by applying Ni-ZrO$_2$.

Wear volume results produced by the deposition of Ni-SiC nanocomposite coatings on the EN1A steel substrate have been presented in figure 5.25. An increase in applied normal load increased wear volume at refrigerant temperatures of 20°C and 30°C. A drop in wear volume

was observed at all the applied loads by increasing the temperature of the refrigerant to 30°C from 20°C.
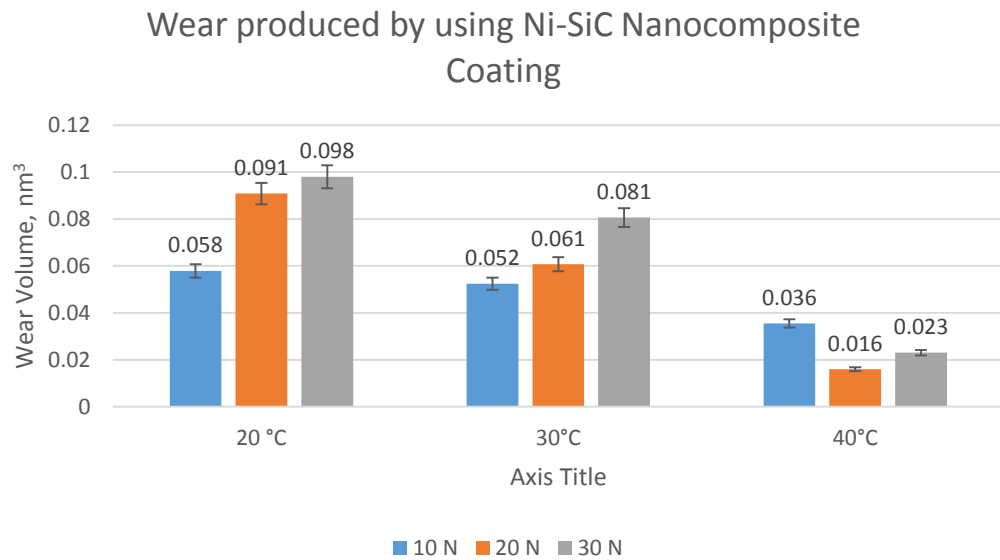
(a)
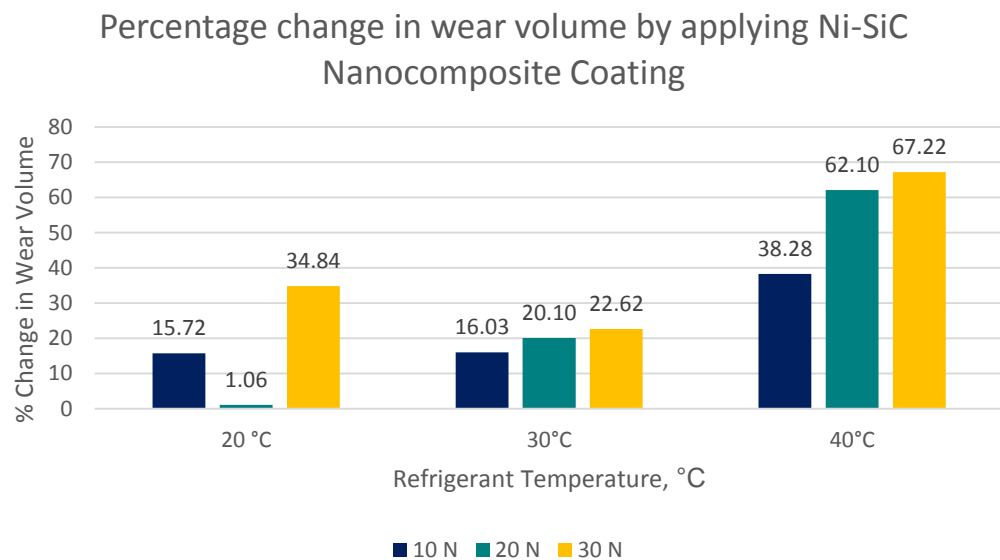
(b)

Fig. 5.25. (a) Wear volume plot of Ni-SiC nanocomposite coatings disc. (b) Percentage change in wear volume by applying Ni-SiC.

Increasing the temperature of the refrigerant to 40°C further reduced wear. This decrease in wear with rise in refrigerant temperature is associated with the development of fluorine and oxygen containing tribological films on the top surfaces of the rubbing parts.

Similar to Ni-ZrO$_2$ coated steel and uncoated steel samples, Ni-SiC coated samples also showed minimum wear occurred at 40°C/20 N. EDS results indicate an acceleration in the formation of protective surface films as the results display an increase in the content of oxygen and fluorine on the wear track. A clear reduction in wear volume is observed by using Ni-SiC nanocomposite coatings in comparison to uncoated steel. Similar to Ni-ZrO$_2$, Ni-SiC coatings also caused the least positive effect at 20°C/ 20 N. Micro-cutting and micro-delamination were the cause of high wear at 20°C/ 20 N. In contrast to Ni-ZrO$_2$ coatings at which 10 N load caused the highest drop in wear, 30 N load showed to be more favourable for Ni-SiC at 20°C. Increase in load at 30°C and 40°C resulted in a higher percentage drop in the wear volume by the deposition of Ni-SiC coatings in comparison to uncoated steel. Ni-SiC nanocomposite coatings enhanced the micro-hardness of the surface and had the third best hardness amongst the coatings produced. (H/E) ratio also improved by applying Ni-SiC coatings in comparison to the steel substrate. An enhancement in the mechanical properties improved the wear resistance of the coatings and resulted in a decrease in wear.

Wear volume results by the application of Ni-Al$_2$O$_3$ nanocomposite coatings have been displayed in figure 5.26. A very significant drop in wear volume at 20°C/10 N was observed when using Ni-Al$_2$O$_3$ coatings in comparison to only uncoated steel but also when compared to Ni-SiC and Ni-ZrO$_2$. Percentage wear volume drop by the deposition of Ni-Al$_2$O$_3$ coatings in comparison to uncoated steel demonstrate a remarkable improvement in wear loss and a drop in wear by over 92%. Ni-Al$_2$O$_3$ nanocomposite coatings presented the best (H/E) ratio and the second best hardness when compared to all the other samples. This improvement in the surface mechanical properties provides superior wear resistance which decreases wear significantly. Increasing the applied normal load to 20 N at 20°C created substantial wear. At 20°C/20 N wear increased by applying Ni-Al$_2$O$_3$ coatings. Ni-Al$_2$O$_3$ coatings have been known to delaminate under constant reciprocating/oscillating motion (Bhutta et al. 2018a; Nazir et al. 2018a) which causes delamination of these coatings from the steel substrate by increasing load which leads to high wear.

Wear produced by using Ni-Al$_2$O$_3$ Nanocomposite Coating

(a)

Percentage change in wear volume by applying Ni-Al$_2$O$_3$ Nanocomposite Coating
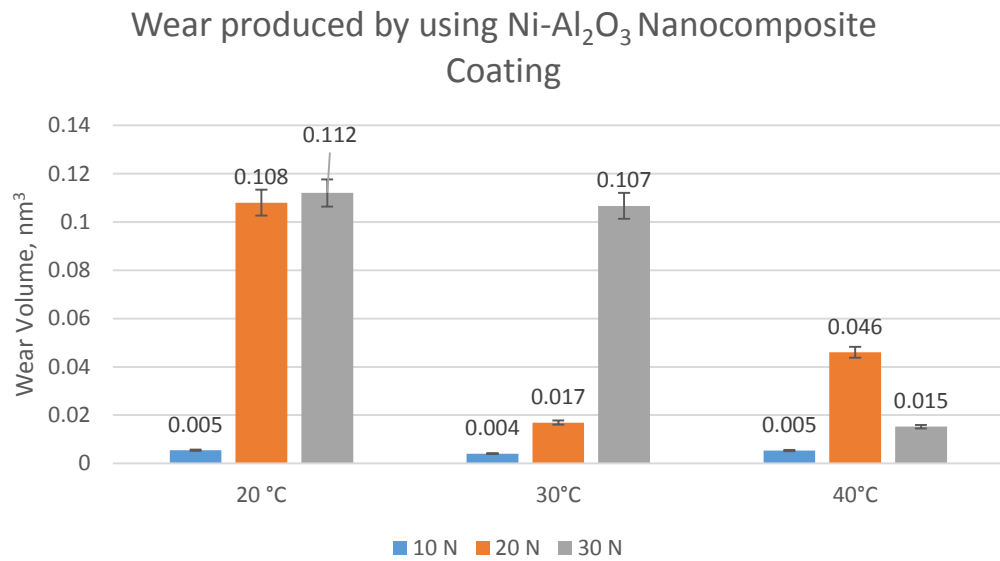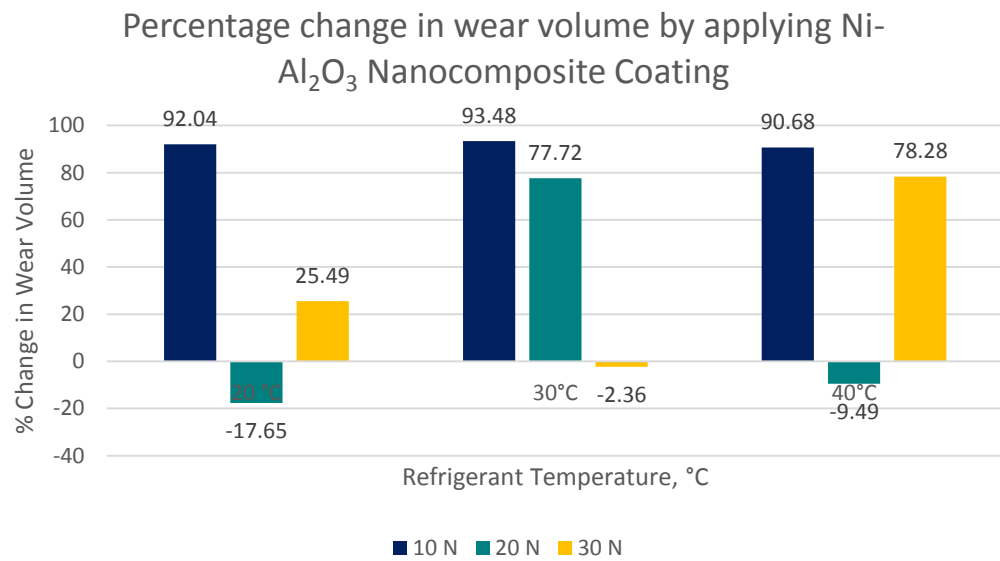
(b)

Fig. 5.26. (a) Wear volume plot of Ni-Al$_2$O$_3$ nanocomposite coatings disc. (b) Percentage change in wear volume by applying Ni-Al$_2$O$_3$.

Delamination of Ni-Al$_2$O$_3$ coatings from the steel substrate is also evident from the micrographs presented in figure 5.14. As noticed with the other coatings, increasing the applied normal load at 20°C to 30 N further increased wear. Ni-Al$_2$O$_3$ coatings showed an improvement in wear loss when compared to uncoated steel. Although a complete delamination of the coatings is also observed at 20°C/30 N similar to 20°C/20 N, however higher percentage of oxygen and fluorine

is present on the wear scar at 30°C/30 N in contrast to 20°C/20 N; which signifies a higher presence of tribo-films which play a vital role in reducing wear.

Wear reduced at any given load by a rise in the temperature of the refrigerant from 20°C to 30°C by using Ni-Al$_2$O$_3$ nanocomposite coatings. 30°C/10 N testing conditions also resulted in a very substantial decline in wear volume, in comparison to uncoated steel wear decreased by over 93% by using Ni-Al$_2$O$_3$ coatings at these testing conditions. Unlike 20°C/20 N testing conditions at which wear volume increased by using Ni-Al$_2$O$_3$, the tests conducted at 30°C/20 N reduced wear and in comparison to uncoated steel wear volume was observed to decrease by over 77% at 30°C/20 N. Test conducted at 30°C/30 N also produced a different result than 20°C/30 N, wear volume increased slightly at 30°C/30 N whereas wear decreased at 20°C/30 N in comparison to uncoated steel. Complete delamination of these coatings was observed at 30°C/30 N as shown in figure 5.15 which resulted in higher wear. Results at 40°C were similar to the results attained at 20°C, wear reduction was noticed at 10 N and 30 N whereas increase in wear occurred at 20 N. At 40°C/10 N, wear volume reduced by more than 90% and at 40°C/30 N more than 78%. EDS analysis results and the micrographs presented in figure 5.16 display a significant presence of nickel at 40°C/20 N indicating that the coating has not been worn out, still at 40°C/20 N the amount of wear generated is higher by using Ni-Al$_2$O$_3$ coatings when compared to uncoated steel. This is due to the fact that 40°C/20 N produced least amount of wear when using uncoated steel and 40°C/20 N presented the most optimum testing conditions when using uncoated steel. In contrast to Ni-Al$_2$O$_3$ coated samples, a higher percentage of oxygen and fluorine was also present on uncoated steel samples at 40°C/20 N (Bhutta et al. 2018a) which highlights the importance of oxygenated and fluorinated films in decreasing wear. Compared to the other coatings and the uncoated sample, at 40°C/20 N Ni-Al$_2$O$_3$ coated samples did not result in minimum wear. Minimum wear for Ni-Al$_2$O$_3$ coated samples was observed at 30°C/10 N.

Figure 5.27 presents the wear volume results of Ni-GPL coatings. Ni-GPL coatings had the second best (H/E) ration and the best hardness values amongst all the coatings. The results however present an entirely different behaviour at 20°C refrigerant temperature by using Ni-GPL compared to the rest of the coatings.

Wear produced by using Ni-GPL Nanocomposite coating

(a)

Percentage change in wear volume by applying Ni-GPL Nanocomposite Coating
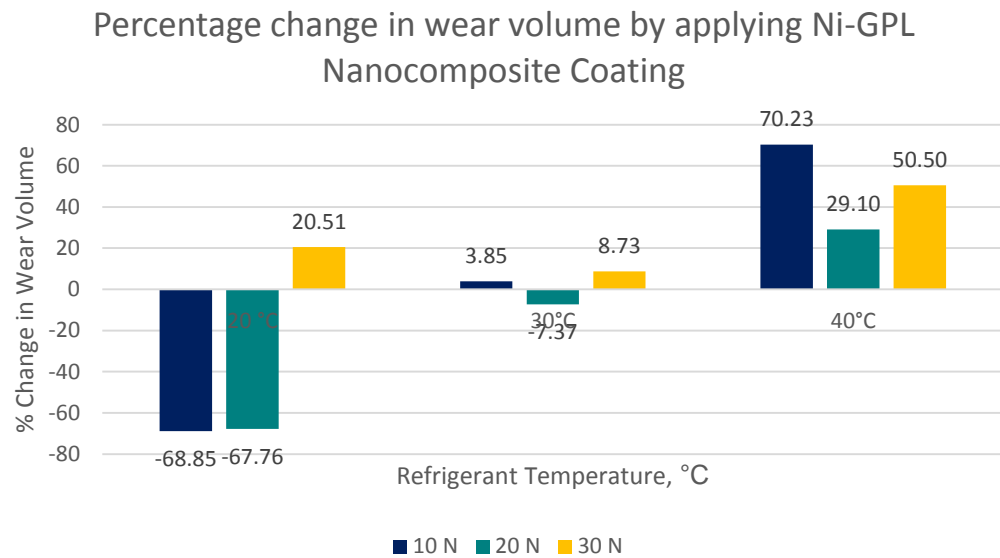
(b)

Fig. 5.27. (a) Wear volume plot of Ni-GPL nanocomposite coatings disc. (b) Percentage change in wear volume by applying Ni-GPL

20 N load produced maximum wear at 20°C instead of 30 N. 20°C/10 N and 20°C/20 N had a very adverse effect on wear and wear volume increased drastically at both of these testing conditions. EDS results on the wear track at 20°C/10 N show no fluorine and at 20°C/20 N only a very small percentage of oxygen and fluorine was detected showing that Ni-GPL coatings have completely worn out at these testing conditions as shown in figure 5.17. This indicates

extremely high wear and a very minor presence of anti-wear tribo-films under these conditions. Comparing Ni-GPL with uncoated steel shows an increase in wear by over 67% at these two conditions. Such high wear when using Ni-Graphene is believed to be because of two reasons.

The first reason for this high wear is probably due to the incompatibility of Graphene based Nano coatings with HFE-7000. $C_3F_7OCH_3$ is the chemical formula of HFE-7000 which contains highly polar single bonds of Carbon-Fluorine (C-F) and HFE-7000 has been reported to break and from new bonds leading the production of tribo-films (Bhutta and Khan 2019). Also, C-H bond is weaker than C-F (Gu et al. 2009; Akram et al. 2013a; Bhutta and Khan 2019) bonds and C-O bond is weaker than the C-C bond (Lide 73rd edition, 1992-1993, pp. 9-145; Muraki et al. 2002). Break down of the molecular structure of the refrigerant (HFE-7000) means it can result in the generation of carbonyl products e.g. esters which are also polar in nature (Tsai 2005). On the other hand graphene crystallites demonstrate that graphene have the fastest electron mobility in comparison to all other materials (Brownson and Banks 2010). Graphene also displays remarkable electrocatalytic behaviour that is attributed to its unique chemical and physical properties, for example subtle electronic characteristics ($\pi - \pi$ interactions and its strong absorptive capability) (Brownson and Banks 2010; Kang et al. 2010). Graphene has ballistic electron mobility, large surface area and excellent conductivity (Liu et al. 2010). In addition the existence of the extended C=C conjugation in graphene also probably shuttles electrons (Liu et al. 2010). These physical/chemical properties of Graphene clearly indicate that Graphene not only has the fastest electron mobility and is also rich in electrons but also possesses electrocatalytic behaviour which causes the pulling out of Graphene nanoparticles from the nanocoatings due to the polar nature of the refrigerant. Larger sized Nano particles having average size ($\geq$ 20 nm) were used in preparation all the other coatings used in this study except for Graphene for which nanoparticles of 6-8 nm were used. The presence of polar molecules at fully lubricated refrigerant conditions with small sized electron rich Graphene nanoparticles under the influence of constant reciprocating motion ejects the nanoparticles from the surface of the coatings.

In addition the wear tracks of these tests showed very low oxygen and fluorine showing that Graphene is not favourable for the generation of tribo-films at low operation temperatures and low applied loads. Increasing load at 20°C to 30 N facilitates the chemical breakdown of HFE-7000 and establishment of tribo-films on the wear scar which reduces wear at 20°C/30 N. Increase in load also assists in retaining Graphene in the Nickel matrix which helps in wear reduction. Increasing the temperature of the refrigerant to 30°C resulted in a slight positive

effect on wear at 10 N load and 30 N load. Higher percentage of nickel was observed on the wear tracks as shown in figure 5.18 confirming a drop in wear. A greater presence of oxygen and fluorine is also shown by the EDS results which signifies a higher presence of surface tribo-films as compared to the tests conducted at 20°C. In comparison to the uncoated steel sample, increasing the temperature of the refrigerant to 30°C at 20 N load however did not have a positive effect on wear and wear volume in fact increased at these conditions, this is probably due to the accelerated development of tribo-films on the uncoated surface as compared to Ni-GPL coated surface under these testing conditions. Increasing the temperature of the refrigerant further to 40°C resulted in a drop in wear at all loads, highest decrease in wear was viewed at 10 N load and the least positive effect on wear was seen at 20 N load. EDS results presented in figure 5.19 reveal the highest percentage of nickel at 40°C/10 N for Ni-GPL amongst all the tests and a good proportion of oxygen/fluorine presence which aid in reducing wear. Unlike Ni-ZrO_2, Ni-SiC, and the uncoated steel, minimum wear for Ni-GPL coatings was observed at 40°C/10 N.

Figure 5.28 displays the results of wear on Nickel-only coatings. The wear volume results show a different pattern at 20°C refrigerant temperature as compared to uncoated steel, Ni-SiC, Ni-ZrO_2 and Ni-Al_2O_3 coated contacts; at 20°C all these samples displayed an increase in wear volume whereas Nickel-only coatings display a decline in wear volume by increasing the applied load at 20°C. A combination of micro-cutting and micro-delamination was observed for Nickel-only coatings at 20°C/ 10 N; the wear phenomenon however shifted primarily towards micro-cutting and less micro-delamination took place with increase in applied normal load as presented in figure 5.20, this shift in wear mechanism supports wear reduction with increase in load at 20°C refrigerant temperature for Nickel-only coatings. Comparing the wear volume of Nickel-only coated to uncoated samples, a drop in wear volume was observed by the deposition of Nickel-only coatings. An increase in the applied load at 20°C results in a greater percentage in wear reduction, this is due to the fact that wear volume decreases at 20°C with increase in load for Nickel-only coatings. Increasing the temperature of the refrigerant to 30°C results in a reduction in wear.

20 N load generated maximum wear at 30°C refrigerant temperature which is due to the accelerated micro-cutting of the coating at 30°C/20 N in comparison to 30°C/10 N and 30°C/30 N as shown in figure 5.21. Results of EDS analysis also confirm a reduced percentage of Nickel at 30°C/20 N in contrast to 30°C/10 N and 30°C/30 N.

Wear produced by using Ni-only Coating

(a)

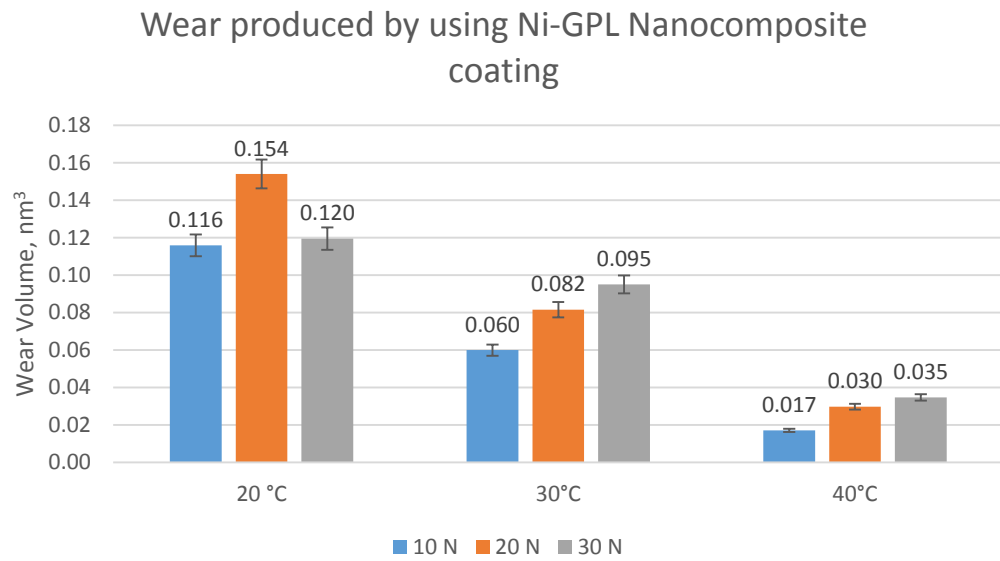## Percentage change in wear volume by applying Ni-only Coating
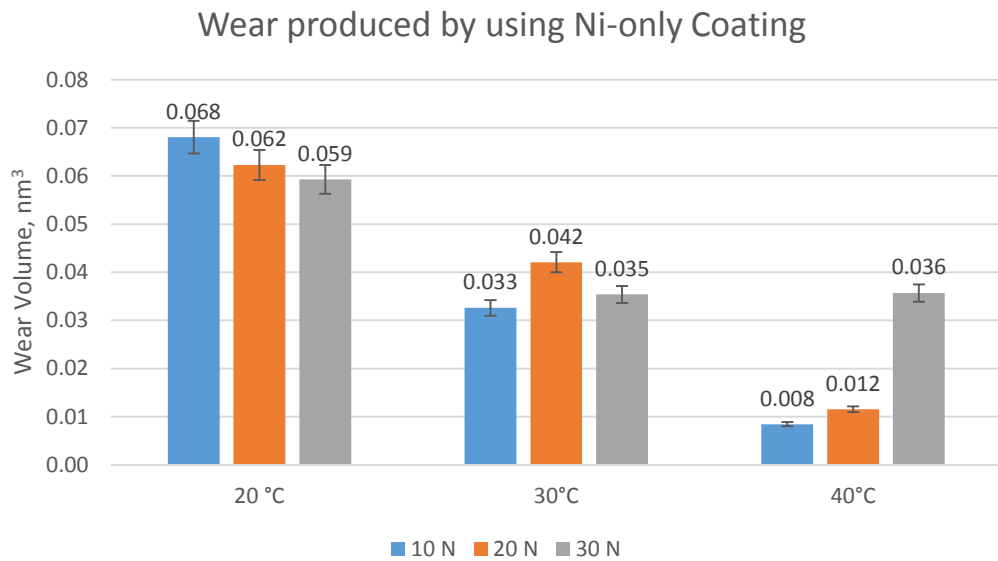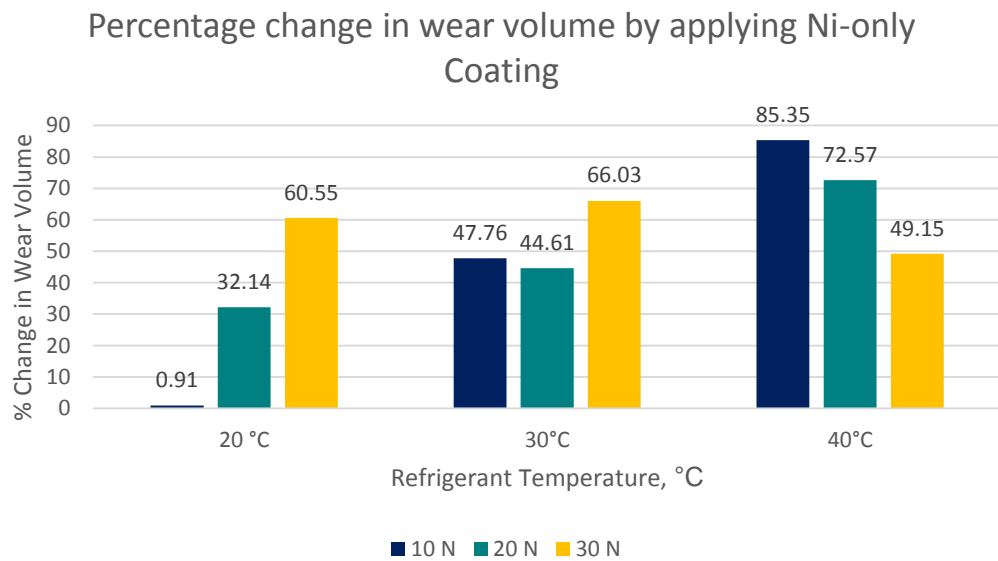
(b)

Fig. 5.28. (a) Wear volume plot of Nickel-only nanocomposite coatings disc. (b) Percentage change in wear volume by applying Nickel

Change in wear volume by the deposition of Nickel-only coatings at 30°C show a reduction in wear at all applied loads in comparison to uncoated steel sample. A further rise in the temperature of the refrigerant to 40°C decreases wear volume further. Similar to Ni-GPL nanocomposite coating; an increase in wear is seen with increase in load at 40°C and also the minimum amount of wear was generated at 40°C/10 N. Wear volume reduced by the deposition

of Nickel-only coatings compared to the uncoated steel. Maximum positive effect on wear volume occurred at 40°C/10 N. By increasing the applied normal load at 40°C the positive effect on wear drops from about 85% to about 49% due to an increase in wear volume with increase in load at 40°C.

To summarize the results of wear volume, similar to the behaviour noted by using uncoated steel samples; for *all* of the coatings used in this study the wear volume also decreased with increase in the temperature of the refrigerant. Wear predominantly occurred due to micro-delamination, micro-cutting and micro-ploughing. Wear mechanism depends on the type of coating (Bajwa et al. 2016c; Nazir et al. 2018a), wear mechanism also shifted from one form to another at different testing conditions for the same coatings. The amount of wear volume generated is also dependent on the creation of protective surface tribo-films on the rubbing metals. Hardness to elastic modulus ratio (H/E) and micro-hardness improved by applying Nickel based coatings on the steel substrate. Ni-GPL presented the highest hardness values followed by Ni-Al$_2$O$_3$. The highest hardness to elastic modulus (H/E) ratio was displayed by Ni-Al$_2$O$_3$, the second best (H/E) ratio was displayed by Ni-GPL. Ni-ZrO$_2$ presented an improvement in wear at all operating conditions in comparison to the uncoated steel and the highest drop in wear was observed at higher refrigerant temperature of 40°C at which wear dropped by more than 72% at 40°C/10 N. Ni-SiC coatings also produced a positive effect on reducing wear, similar to Ni-ZrO$_2$, Ni-SiC coatings also exhibited good wear performance for all testing conditions and maximum positive effect on wear reduction was also observed at 40°C refrigerant temperature. The maximum effect on wear loss for Ni-ZrO$_2$ was observed at 40°C/10 N, however the maximum effect on wear loss occurred at 40°C/30 N by using Ni-SiC coatings. Ni-Al$_2$O$_3$ coatings produced some interesting results in terms wear volume. In comparison to uncoated steel, three of the testing conditions by using Ni-Al$_2$O$_3$ coatings (20°C/20 N, 30°C/30 N and 40°C/20 N) resulted in an increase in wear volume. Under the influence of reciprocating motion Ni-Al$_2$O$_3$ coatings have been known to delaminate (Bhutta et al. 2018a; Nazir et al. 2018a) which increases wear. However, the best (H/E) ratio and the second best hardness values were presented by Ni-Al$_2$O$_3$ coatings amongst all the coatings, which results in a significant drop in wear loss especially at low loads; a drop in wear by more than 90% was seen at all the test conducted at low loads (20°C/10 N, 30°C/10 N and 40°C/10 N). None of the other coatings tested in this study showed such a substantial drop in wear volume at low loads. Testing conditions of 20°C/30 N, 30°C/20 N and 40°C/30 N also demonstrated to be beneficial in wear reduction. Although Ni-GPL coatings had the lowest values of the maximum grain size and also displayed the best micro-hardness value amongst all the prepared coatings, but a drastic increase

in wear volume was seen by applying Ni-GPL coatings at low testing temperature of 20°C and at low loads. This is believed to be due the slow formation of tribo-films and due to the incompatibility of HFE-7000 with Graphene nanoparticles. Increasing the temperature of the refrigerant and the applied normal load however proved to be advantageous in reducing wear for Ni-GPL, wear dropped at higher refrigerant temperature and at higher applied loads due to the acceleration in the formation of protective tribo-films which assist in reducing wear. Ni-GPL showed a reduction in wear volume for all the tests conducted at 40°C. Good results in terms of wear reduction were also provided by Nickel-only coatings. At higher refrigerant temperatures higher wear reduction was noted. The maximum drop in wear volume was also noted at 20°C/20 N and 20°C/30 N for Nickel-only coatings. Refrigerant temperatures of 30°C and 40°C also showed good wear results for Nickel-only coatings. Good performance of Nickel-only coatings in comparison to other coatings is believed to be related with reduced damage caused by three body abrasive wear. The wear debris produced during testing are trapped inside the disc and refrigerant holding cup; hard nanoparticles are present in all of the nanocomposite coatings, debris of the worn out coating and hard nanoparticles trapped inside the cup caused three body wear and resulted in increase in wear. Wear debris generated by Nickel-only coatings do not contain hard nanoparticles and three body abrasive wear phenomenon which is also believed to take place when using Nickel-only coatings did not produce the same amount of damage. In contrast to the coatings containing different nano-particles in the Nickel matrix, Nickel-only coatings are believed to be more beneficial in the production and development surface tribo-films.

5.4 Friction of Coated Samples

Results of the coefficient of friction have been presented in terms of real-time friction coefficient graphs and also as average coefficient of friction plots. Results obtained from each of the coatings have also been compared to the uncoated samples with R_a of 0.1 μm.

Results of Ni-ZrO$_2$ coated steel have presented in figure 5.29. Figures 5.29 (a), 5.29 (b) and 5.29 (c) show the real-time coefficient of friction plots. All the plots show a decline in the coefficient of friction values with increase in applied normal load. An increase in the temperature of the refrigerant from 20°C to 30°C does not produce a noticeable effect on the values of friction coefficient. Increasing the refrigerant temperature to 40°C however produced a positive effect on the coefficient of friction. The coefficient of friction drops at each of the applied normal

loads by increasing the temperature of the refrigerant from 20°C to 40°C, this is also apparent from the plots of average coefficient of friction shown in figure 5.29 (d).

Fig. 5.29. Coefficient of friction graphs for Ni-ZrO₂: Real-time coefficient of friction at refrigerant temperature (a) 20°C (b) 30°C (c) 40°C (d) Average coefficient of friction plot (e) Percentage change in average friction coefficient by applying Ni-ZrO₂.

There are more fluctuations in the coefficient of friction at lower applied loads, increase in load at any given temperature reduced not only the fluctuations in the coefficient of friction but also the values of the friction coefficient. This drop in friction coefficient values with increasing

refrigerant temperatures and the decline in average friction coefficient values with increase in normal load at any given temperature is linked with the development of protective tribological films on the surfaces of the mating parts.

A comparison of the average friction coefficient by using Ni-ZrO$_2$ nanocomposite coatings to uncoated steel is shown in figure 5.29 (e). The plot shows that all of the operating conditions are not beneficial in reducing friction by using Ni-ZrO$_2$ coatings, a small increase in the average friction coefficient is observed at 20°C/20 N and 30°C/10 N. These two testing conditions also proved to be least beneficial in improving wear. Maximum improvement in friction coefficient was observed at 20°C/10 N. In comparison to the uncoated steel samples, refrigerant temperature of 40°C improved friction at all loads.

Results of the coefficient of friction obtained by the deposition of Ni-SiC coatings have been presented figure 5.30. An increase in applied normal load at any given temperature for Ni-SiC coatings also show a drop in the friction coefficient values similar to Ni-ZrO$_2$ nanocomposite coatings. In addition a constant decline in the coefficient of friction is observed with an increase in refrigerant temperature. The average friction coefficient decreases with increase in load at all testing temperatures and a decline in the average coefficient of friction can be observed with an increase in refrigerant temperature from 20°C to 40°C as shown in figure 5.30 (d). Similar to the real time coefficient of friction results of Ni-ZrO$_2$, higher fluctuations in the coefficient of friction are visible at lower loads and an increase in load reduces the variations in the coefficient of friction for Ni-SiC coatings as well.

A comparison of the results of the average coefficient of friction of uncoated steel to Ni-SiC shows an improvement in the friction coefficient at almost all of the testing conditions, only 20°C/30 N and 40°C/10 N presented a slight increase (less than 1%) in the average coefficient of friction by the deposition Ni-SiC coatings. Besides these two testing conditions, an improvement in the average friction coefficient is clearly visible in the plot displayed in figure 5.30 (e). Testing conditions of 30°C/20 N exhibited the maximum improvement in the friction coefficient by depositing Ni-SiC coatings.

Fig. 5.30. Coefficient of friction graphs for Ni-SiC: Real-time coefficient of friction at refrigerant temperature (a) 20°C (b) 30°C (c) 40°C (d) Average coefficient of friction plot (e) Percentage change in average friction coefficient by applying Ni-SiC.

Results of the friction coefficient of Ni-Al$_2$O$_3$ have been shown in figure 5.31. These coatings produced a different behaviour in comparison to Ni-SiC and Ni-ZrO$_2$. Spikes and fluctuations in the real-time friction coefficient graphs at applied load of 10 N as seen for the previous two coatings were not observed in the case of Ni-Al$_2$O$_3$. Ni-Al$_2$O$_3$ also presented the best wear performance at low loads compared to all the other coatings investigated in this study. A decrease in wear at low loads produces less wear debris and a substantial reduction in three

body abrasive wear which decreases the fluctuations and variations in the friction coefficient. Ni-Al$_2$O$_3$ nanocomposite coatings had the best surface finish amongst all the electrodeposited coatings prepared in this study and had R$_a$ of only 0.045 μm. A smoother surface implies lesser asperity interactions which decreases friction as well as wear. Average coefficient of friction plots for Ni-Al$_2$O$_3$ are also different from the Ni-ZrO$_2$, Ni-SiC and the uncoated steel samples.

Fig. 5.31. Coefficient of friction graphs for Ni-Al$_2$O$_3$: Real-time coefficient of friction at refrigerant temperature (a) 20°C (b) 30°C (c) 40°C (d) Average coefficient of friction plot (e) Percentage change in average friction coefficient by applying Ni-Al$_2$O$_3$.

An increase in normal load at 20°C from 10 N to 20 N decreases friction coefficient, but a further increase in load to 30 N did not affect the average friction coefficient. Compared to 20°C, increasing of the temperature of the refrigerant to 30°C did result in a drop in the coefficient of friction, however an increase in applied load at 30°C did not produce any effect on the coefficient of friction. Increasing the temperature of the refrigerant to 40°C shows a slight increase in the friction coefficient at 40°C/10 N in comparison to 30°C/10 N. 40°C/20 N and 40°C/30 N show a decrease in the average friction coefficient compared to 30°C/20 N and 30°C/30 N. A comparison of the average coefficient of friction of the uncoated steel to Ni-Al$_2$O$_3$ show an improvement in the values of the coefficient of friction at all the testing conditions. The highest enhancement was observed at 30°C/10 N at which the friction coefficient improved by over 40%, 30°C/10 N also produced the best enhancement in wear for Ni-Al$_2$O$_3$. In comparison to uncoated steel, Ni-Al$_2$O$_3$ did not show an increase in the average coefficient of friction values at any of the testing conditions.

Analogous to the results of wear, at low refrigerant temperature Ni-GPL also displayed poor coefficient of friction. An increase in applied load from 10 N to 20 N at 20°C decreased the coefficient of friction but a further increase in the applied load at 20°C from 20 N to 30 N did not affect the average friction coefficient as shown in figure 5.32. Compared to all the other coatings and also in comparison to the uncoated steel disc samples Ni-GPL coatings had the highest average surface roughness value (1.17 μm). This high surface value of Ni-GPL was due to the existence of nano graphene particles at the very top of the coated surface and also due to particle agglomeration. When compared to the uncoated steel, 20°C/10 N produced an improvement in the friction coefficient, however an increase in normal load at 20°C produced higher coefficient of friction values in comparison to uncoated steel and the coefficient of friction increased at 20°C/30 N by almost 45%. Increase in the temperature of the refrigerant from 20°C to 30°C however proved to be extremely advantageous in reducing the coefficient of friction and when compared to the uncoated steel, the friction coefficient at 30°C/10 N decreased by more than 33%. Although the viscosity of the refrigerant reduces with an increase in the temperature of the refrigerant which leads to more asperity interaction which should increase friction, but the coefficient of friction decreases which is because of the increase in reactivity of the refrigerant with the mating surfaces and development of protective tribo-films. For 30°C tests, however wear did not display a very significant improvement and in fact at 30°C/20 N wear volume increased. Increasing the temperature of the refrigerant to 40°C decreases the friction coefficient at 40°C/20 N and 40°C/30 N in comparison to the tests conducted at lower temperatures, however the average friction coefficient is seen to increase

slightly at 40°C/10 N in contrast to 30°C/10 N. Comparing the results of uncoated steel to Ni-GPL also show that these coatings improve friction at 40°C at all the loads. At 40°C wear was also observed to improve for Ni-GPL.
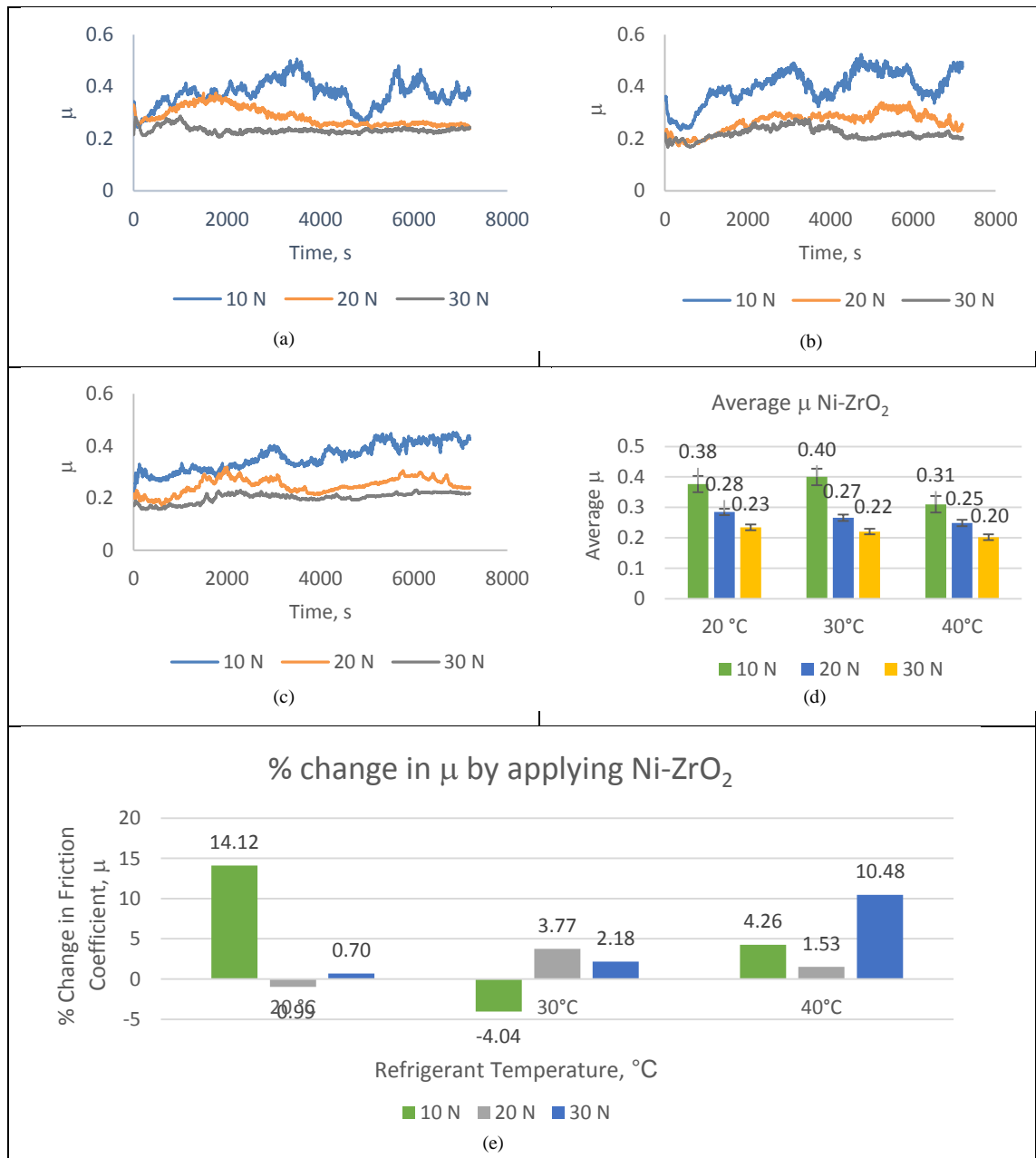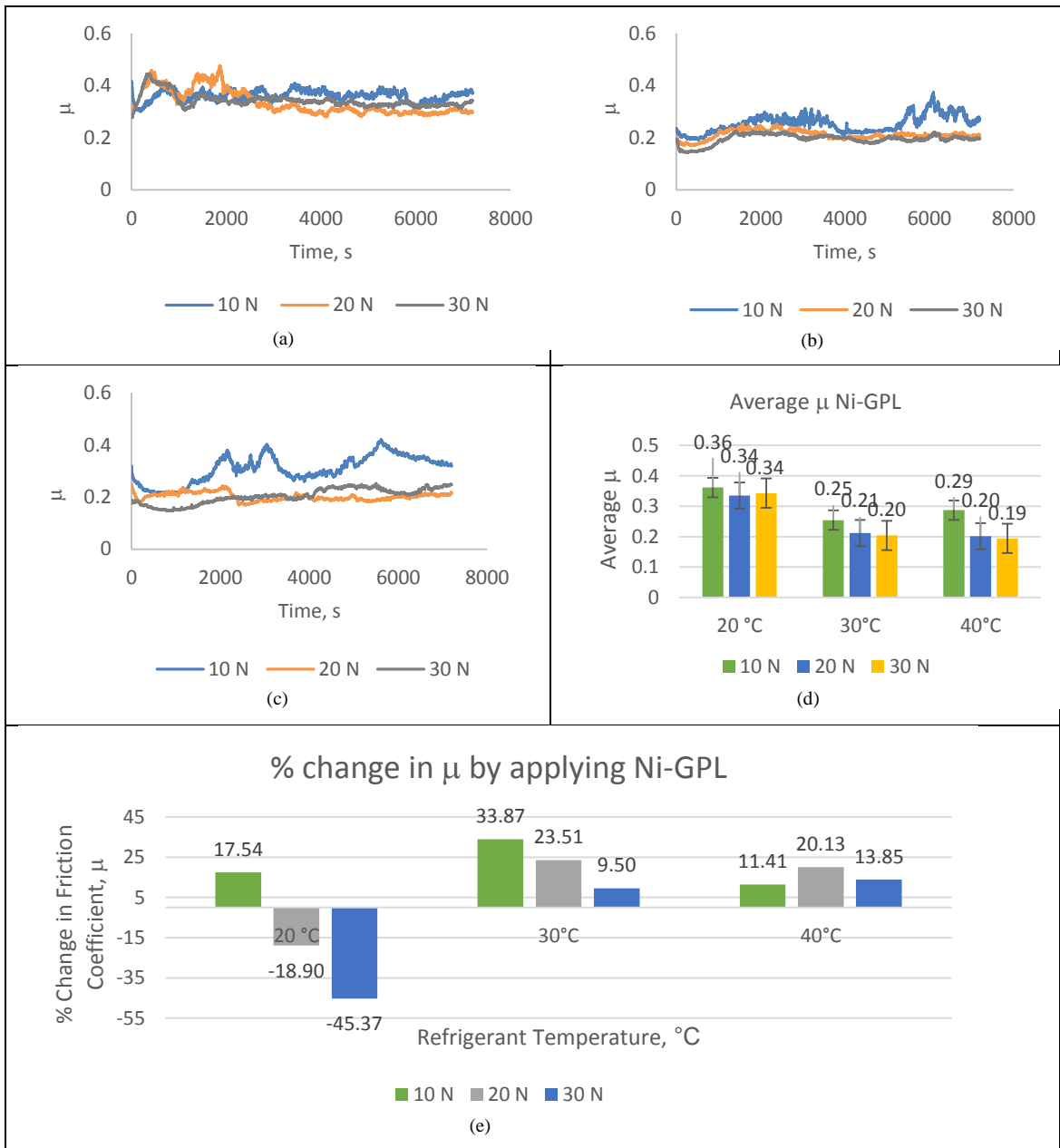

Fig. 5.32. Coefficient of friction graphs for Ni-GPL: Real-time coefficient of friction at refrigerant temperature (a) 20°C (b) 30°C (c) 40°C (d) Average coefficient of friction plot (e) Percentage change in average friction coefficient by applying Ni-GPL.

Results obtained by the application of Nickel-only coatings have been presented in figure 5.33. Variations in the coefficient of friction can also be seen in the results of the real-time friction

coefficient especially at low loads. Increasing the applied normal load at any particular temperature also decreases the values of the real-time coefficient of friction as well as the average friction coefficient. An effect on the average friction coefficient was not seen by increasing the temperature of the refrigerant from 20°C to 30°C. However an additional increase in the temperature of the refrigerant to 40°C resulted in a drop in the coefficient of friction values. The least values of the average friction coefficient were presented at 40°C/30 N for not only Nickel-only coatings but also in comparison to all the other coatings. Nickel-only coatings also presented the second best surface finish amongst all the prepared coatings. Comparing the results of the average coefficient of friction of uncoated steel to Nickel-only coatings show a very slight increase in the coefficient of friction values at 20°C/30 N and an increase in friction was also observed at 30°C/30 N. Other than these two conditions the coefficient of friction was enhanced by applying Nickel-only coatings.

Friction coefficient and wear for Nickel-only coatings did not follow the same pattern. At 20°C and 40°C wear volume increased with increase in load whereas coefficient of friction reduced with increase in applied normal load at 20°C and 40°C for Nickel-only coatings. For 20°C, parentage change in friction coefficient decreased with an increase in load whereas for 20°C, percentage change in wear increased with increase in applied load. Also, percentage effect in wear volume decreased with increase in load whereas percentage effect in the friction coefficient increased with increase in applied load at 40°C. Besides two of the testing conditions which increased the coefficient of friction values for Nickel-only coatings, the results of wear volume improved at all the testing conditions by the application of Nickel-only coatings.
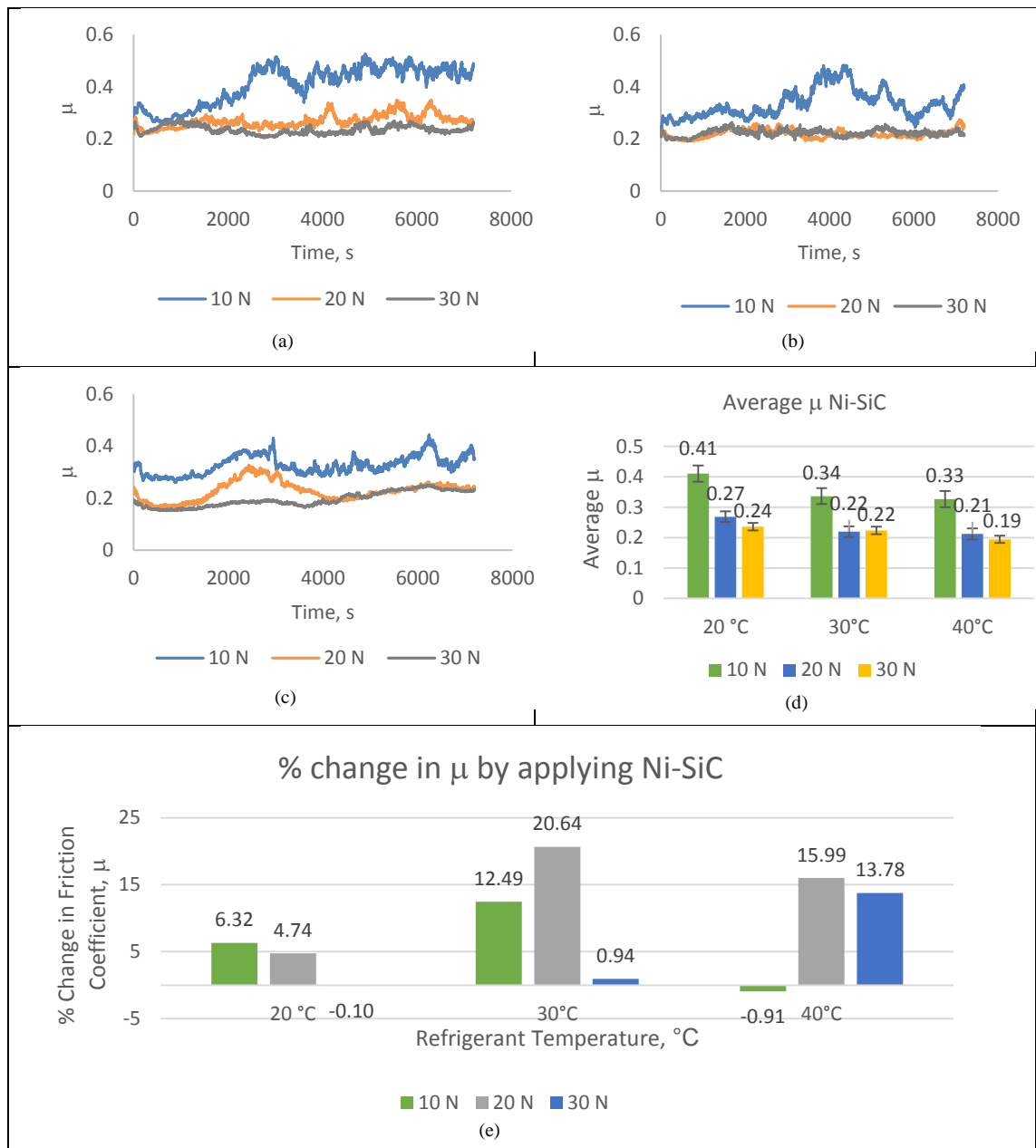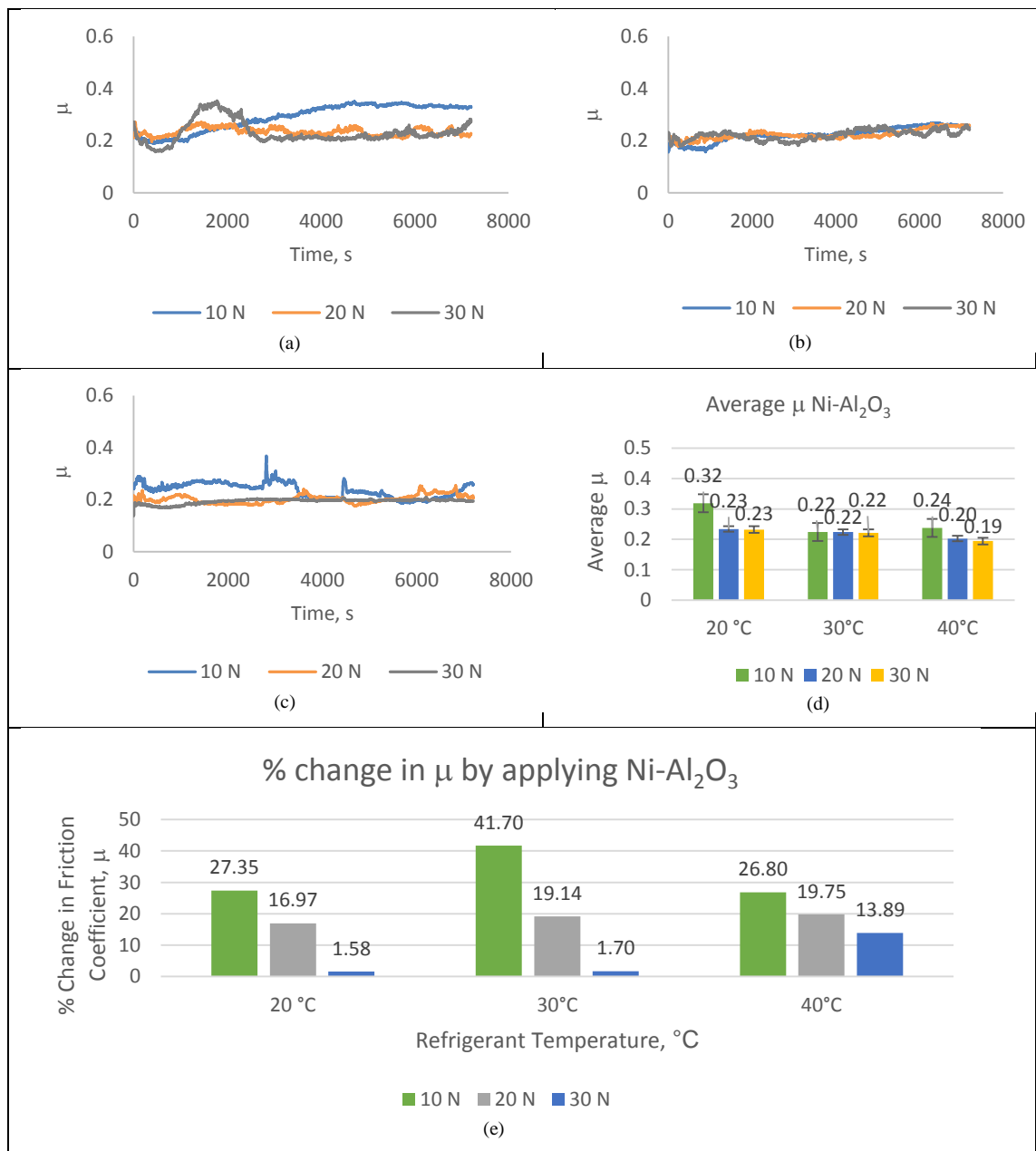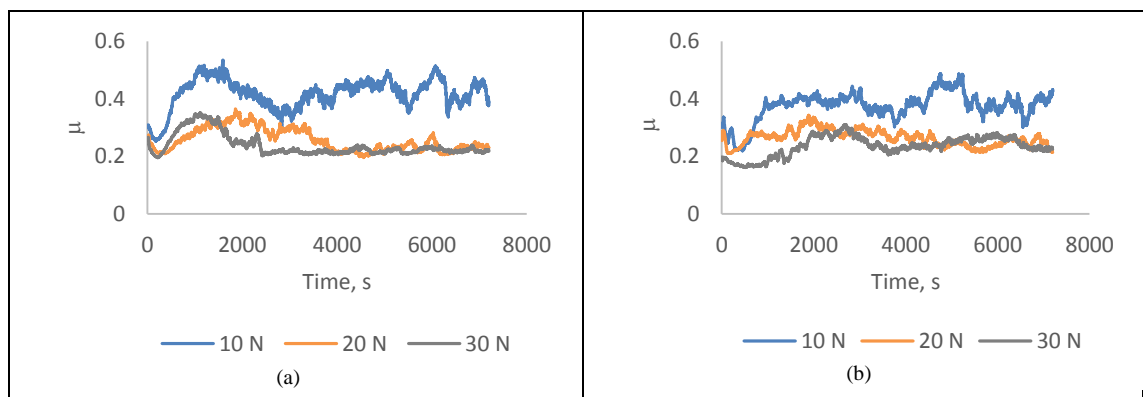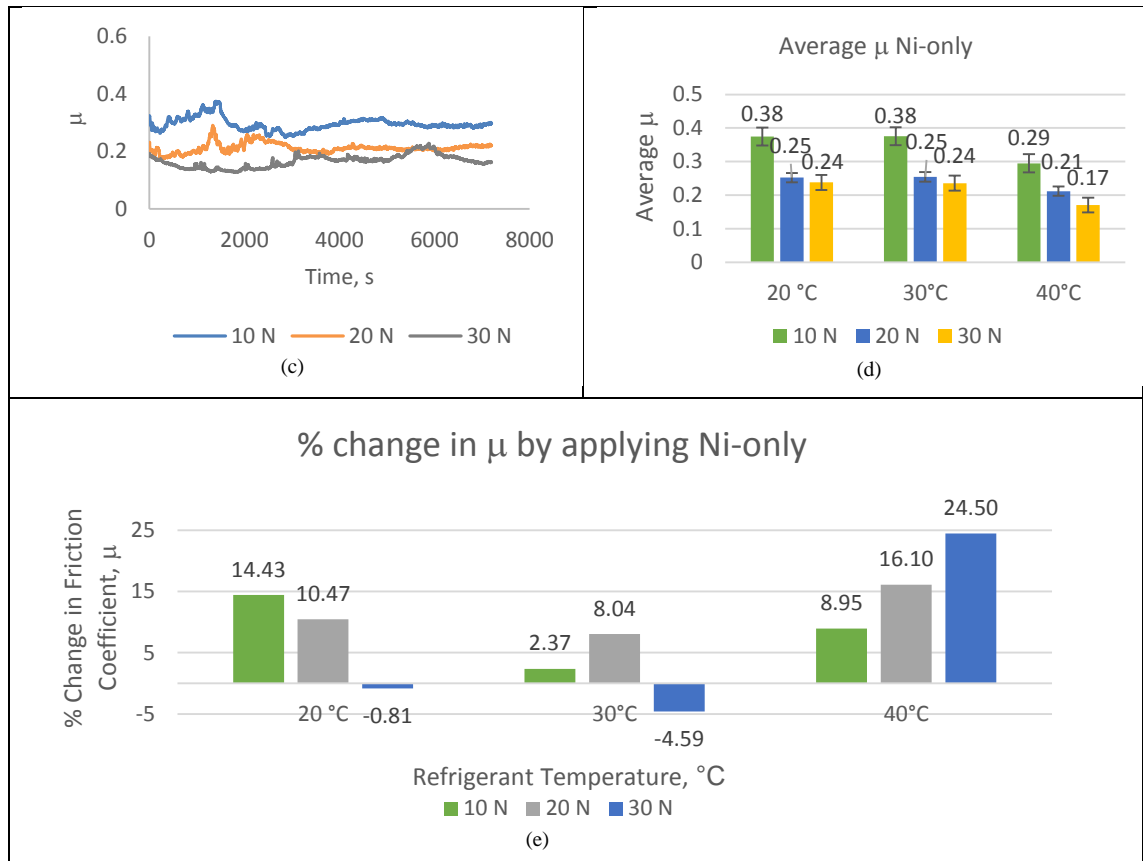
Fig. 5.33. Coefficient of friction graphs for Nickel-only: Real-time coefficient of friction at refrigerant temperature (a) 20°C (b) 30°C (c) 40°C (d) Average coefficient of friction plot (e) Percentage change in average friction coefficient by applying Nickel-only.

An improvement for most of the conditions in the coefficient of friction was witnessed by the deposition of nanocomposite coatings. Cavities and micro-dimpled groves have been known to enhance the tribological performance of mating parts (Bai et al. 2017; Abdullah et al. 2018) and pores in Ni-Al$_2$O$_3$ nanocomposite coatings have been reported to retain liquid refrigerant and to improve the lubricity of rubbing parts which assists in improving wear (Bhutta et al. 2018a). As displayed in figure 5.3, all the prepared coatings have micro-pores, these micro-pores also assisted in lubricant retention which reduced friction. The variation in the contact area of the counter steel ball causes the generation of peaks in the real-time coefficient of friction graphs. Wear on the steel ball increases the apparent area of contact during the course of a test. The increase in the ball contact area increases the coefficient of friction. The Hertzian contact diameter of 52100 steel ball is known to increase with increase in wear for a oscillating /reciprocating ball-on-flat contact geometry (Deshpande et al. 2018). The wear scar generated on a 52100 steel ball with a fixed steel ball against a reciprocating disc in a ball-on-flat contact geometry has also been reported to alter shape which leads to an increase in the apparent area

Page | 160

of contact which also reduces contact pressure (Jean-Fulcrand et al. 2017). High magnification SEM micrographs of the wear scar generated on the steel ball reveal that the shape and size of the wear scar changed with a change in loading conditions and by changing the type of applied coatings. Reciprocating flat sample loaded against a stationary 52100 steel ball results in a shift in wear scar from circular contact at lower loads to elliptical contact at higher applied loads (Jean-Fulcrand et al. 2017; Bhutta and Khan 2019). As observed at some of the real-time friction coefficient graphs, multiple peaks and sharp gradients were generated at a few of the testing conditions. The first peak in the real-time coefficient of friction graphs is due to the initiation of the change in the apparent area of contact of the steel ball and the production of a second peak indicates a further alteration in the contact area of the ball (Bhutta and Khan 2019). Variations and fluctuations in the coefficient of friction are believed to be due to the change in contact area of the steel ball, due to three body abrasive wear caused by the wear debris trapped inside the refrigerant holding cup, due to the uneven formation of surface tribo-films especially at lower loads and due to the adhesion of the worn coatings on the surface of the steel ball; continuous reciprocating motion of the steel ball with adhered particles leads to rise in fluctuations in the friction coefficient.

5.5 Conclusions of the Coated Study

The results of the coefficient of friction and wear by using nanocomposite coatings were examined and compared to uncoated contacts in an effort to improve the tribological performance of rubbing parts utilizing HFE-7000. Following conclusions can be drawn from the coated study:

1. The nanocomposite coatings have been successfully prepared using the pulse coating technique. All the coatings show a fine and compact grain structure. The coatings prepared using pure Nickel, Ni-Al$_2$O$_3$, Ni-SiC, Ni-ZrO$_2$ and Ni-Graphene show different surface roughness and different grain size which shows that a type of coating not only effects mechanical parameters such as hardness but also dictates the complete surface morphology. The surface morphology has a direct effect on tribology.
2. Friction and wear behaviour of nickel based coatings applied on a mild steel (EN1A) substrate with HFE-7000 refrigerant is not straightforward. A mix of micro-cutting, micro-delamination and micro-ploughing was witnessed on the worn disc surfaces. Wear mechanism was seen to change with a change in testing conditions and also with a change in coating.
3. In contrast to the uncoated steel the surface mechanical properties of the all coatings improved. The hardness to elastic modulus ratio and the surface hardness was improved for all coatings. Ni-GPL nanocomposite coatings showed the highest hardness value which was followed by Ni-Al$_2$O$_3$, Ni-SiC, Ni-ZrO$_2$ and Nickel. As Nickel-only coatings

did not contain the hard nanoparticles imbedded in its matrix, this led to its least micro-hardness values. Ni-Al$_2$O$_3$ nanocomposite coatings showed the best surface roughness values and the best (H/E) ratio while Ni-GPL coatings presented the worst values of surface roughness.

4. Different coatings performed differently under identical testing conditions:

   a) Ni-Al$_2$O$_3$ nanocomposite coatings performed the best in terms of coefficient of friction in comparison to all the other coatings. In comparison to uncoated steel the testing conditions of 30°C/10 N exhibited an improvement of over 40% in the coefficient of friction. Wear results revealed an improvement of over 90% in wear loss at low loads by applying Ni-Al$_2$O$_3$ coatings, such an improvement at any of the testing condition was not shown by any of the other coatings. Delamination of these coatings at some of the conditions did result in an increase in wear. However it can be stated with confidence that Ni-Al$_2$O$_3$ nanocomposite coatings are most suitable for improving both friction and wear at a range of operating temperatures at low loads.

   b) In comparison to uncoated steel, Ni-SiC coatings proved to be beneficial in improving wear at all testing conditions. Only a minor improvement of about 1% was seen at 20°C/20 N, other than that all other testing conditions improved wear by at least 15%. Refrigerant temperature 40°C proved to be more beneficial in improving wear performance and highest improvement was observed at 40°C/30 N. In comparison to uncoated steel, coefficient of friction also decreased by using Ni-SiC at all the testing conditions except for 20°C/30 N and 40°C/10 N, these two conditions increased the friction coefficient but only by less than 1%. Maximum friction coefficient reduction was observed at 30°C/20 N. This leads to the conclusion that in comparison to uncoated steel, Ni-SiC nanocomposite coatings are favourable in enhancing the tribological performance of mating parts.

   c) Ni-ZrO$_2$ coatings displayed the best results of wear at 40°C refrigerant temperature. None of the other coatings showed such an improvement i.e. an improvement of over 64% at all loads at 40°C. Maximum improvement in wear was observed at 40°C/10 N and the results also show an improvement in wear at all testing conditions. The results of friction coefficient however show an increase in friction coefficient by almost 1% at 20°C/20 N and by about 4% at 30°C/10 N. All other testing conditions show an improvement in friction coefficient by using Ni-ZrO$_2$ coatings and maximum improvement in friction coefficient was observed at 20°C/10 N. It can be inferred from these results that Ni-ZrO$_2$ coatings are extremely beneficial in reducing wear in comparison to uncoated steel. These coatings can be used with assurance at higher operating temperatures at which not only a substantial reduction in wear was observed but also higher refrigerant temperature resulted in a drop in friction coefficient as well.

   d) Ni-GPL nanocomposite coatings presented the worst results at lower refrigerant temperature of 20°C in terms of wear and friction. The incompatibility of these coatings with HEF-7000 is believed to be the reason of the poor performance of Nickel-Graphene coatings. HEF-7000 is polar in nature and Graphene has large

surface area which is rich in fast moving mobile electrons. The ejection of graphene from the surface of the coating by the polar refrigerant at low loads is believed to be the cause of higher wear. Increase in load helps retain Graphene in the Nickel matrix. An increase in the temperature of the refrigerant proves to be tremendously helpful in reducing the friction coefficient. A reduction in the coefficient of friction by almost 34% can be observed at 30°C/10 N. 30°C refrigerant temperature however does not show a significant improvement in wear and in comparison to the uncoated steel, 30°C/20 N conditions results in an increase in wear. 40°C refrigerant temperature however proved to be extremely helpful in not only reducing wear but also in reducing friction. At 40°C/10 N, wear volume dropped by about 70% and by almost 50% at 40°C/30 N. From these results it can be deduced that one has to be very careful in using Ni-GPL nanocomposite coatings in systems utilizing HFE-7000. These coatings can be used at higher operating temperatures but if a system is operating at changing refrigerant temperatures and at varying load then Ni-GPL coatings would not be recommended for use in HFE-7000 based systems.

e) In comparison to uncoated steel, Nickel-only coatings resulted in an improvement in; (H/E) ratio, the micro-hardness, and in the average surface roughness. This improvement in the surface mechanical properties helped improve wear at all the operating conditions. Maximum improvement in wear was noticed at 40°C/10 N while minimum enhancement in wear was observed at 20°C/10 N. Hard nanoparticles were not present in the in the nickel matrix of Nickel-only coatings, when using nanocomposites the hard nanoparticles are believed to increase wear by three body abrasive wear phenomenon. At 40°C the friction coefficient results showed a reduction in the coefficient of friction values for all loads. In comparison to uncoated steel, a slight increase in friction coefficient was however observed at 20°C/30 N and 30°C/30 N. Nickel-only coatings also showed very good results especially for wear improvement and Nickel-only coatings can be recommended with confidence for use at elevated refrigerant temperatures.

5. Wear and friction behaviour of Nickel based coatings under HFE-7000 lubrication is a complex mix of different mechanisms which is not only determined by the type of coating but is also highly dependent on the reaction of the refrigerant with the metallic surfaces. Application of normal load, friction, heat and mechanical motion results in the breaks down of HFE-7000. HFE-7000 breaks down and forms new bonds/compounds with the freshly exposed worn surfaces. This results in the development of fluorinated and oxygenated surface films on the top surfaces. These tribological films results in a drop in wear and friction.

6. The nano-particles embedded in the Nickel matrix are believed to hinder the development of anti-wear tribo-films whereas pure Nickel and Steel metal surfaces are more favourable in the tribo-chemical reaction between the mating surfaces and the refrigerant HFE-7000.

7. A general pattern in the drop in wear with increase in refrigerant temperature and a reduction in friction coefficient with increase in applied normal load and temperature

was witnessed from the results. This is due to the increase in reactivity of HFE-7000 with the mating metallic surfaces with increase in temperature and load.

8. Nickel based coatings show a clear improvement in wear and friction at most of the testing conditions. Selection of a particular coating depends on load and operating temperature.

Chapter 6

Conclusions and Future Work

This chapter provides the conclusion derived from the complete study. An existing tribo-meter has been successfully modified and commissioned for bench testing of the future generation of refrigerants within tribological context. A series of tests have been conducted to access the tribological performance of the environmentally friendly refrigerant HFE-7000 by varying the tribo-operating conditions. Experiments were divided into two main parts. The first part of the study was based on the evaluation of the tribological performance of uncoated steel contacts under variable operating environments; tests were carried out by changing the applied normal load, by using samples of different surface finish and by heating the refrigerant to various different temperatures. The results of the uncoated study indicate that increasing the operating temperature at a constant load reduces both friction coefficient and wear. Increasing the load at a constant temperature increased wear but resulted in a reduction in friction coefficient. EDS analyses on the samples in the contact region and wear track have shown a significant presence of oxygen, fluorine and carbon on the rubbing surfaces. The detailed high resolution XPS analysis reveal the formation of new bonds/compounds on the surfaces of the interacting metals and indicate breaking up of the bonds of the refrigerant. Analysis on different regions within the contact zone of the rubbing metals post-experimentation has demonstrated that oxygenated and fluorinated layers are well adhered on the disc wear track and ball. The reduction in the friction coefficient with increasing load and decrease in wear along with a decrease in coefficient of friction with increasing temperature is believed to be associated with the development of protective tribo-films on the interacting surfaces. The formation of these films is accelerated by an elevation in the refrigerant temperature and increase in the applied load. Increasing the applied load and operating temperature increases the reactivity of the refrigerant HFE-7000 with the rubbing metals. It is also observed from the results obtained that the surface roughness does not have a very significant effect on the coefficient of friction and on wear. This shows that metallic parts of a range of surface finish and even parts with rough surface finish can be used in HFE-7000 run interacting systems. Five different types of Nickel based coatings were applied to the uncoated EN1A steel substrate to enhance the friction and wear performance of HFE-7000 based systems. Results of the coated study also showed the presence of oxygenated and fluorinated films on the top surface on all the coatings. All the coatings displayed an improvement in the nano-hardness and (H/E) ratio. Friction and wear behaviour of Nickel based coatings under HFE-7000 lubrication is a complex mix of different mechanisms which is not only determined by the type of coating but is also highly dependent on the reaction of the

refrigerant with the metallic surfaces. A similar pattern in the drop in wear with increase in refrigerant temperature and a reduction in friction coefficient with increase in applied normal load and temperature was also witnessed for the coated contacts. Nickel based coatings show a clear improvement in wear and friction at most of the testing conditions. Selection of a particular coating depends on load and operating temperature.

The future work to be conducted on the modified test rig which requires no further alterations and modifications should be:

1) The investigation of refrigerant/oil mixtures. HFE-7000 should be studied by using it with various oils commonly used in compressors. Refrigerator oils are diluted by refrigerants, therefore, understanding the tribological performance of refrigerant/oil mixture is crucial to optimize the tribological behaviour when focusing on compressors. The first part of this study should be to investigate a number of compressor oils with HFE-7000 using uncoated contacts and the second part of this investigation should be to enhance the tribological performance of HFE-7000/oil mixtures using Nickel based coatings.

2) Evaluation of performance enhancement of machine parts by using the coatings in actual pumps/compressors with HFE-7000.

3) Investigation of other coatings for the enhancement and improvement of the tribological performance of rubbing parts based on HFE-7000.

4) Mechanical wear behaviour of electrodeposited nanocomposite coatings using PRC technique in comparison to PC technique.

5) Comparative tribological evaluation of Hydrofluoroethers using uncoated and coated specimens. A comparison of the tribological performance of different HFEs using the modified test rig. Testing of HFE-7100 and HFE-7200, etc. all of which are environmentally friendly future generation commercially available refrigerants.

6) Nano-refrigerants i.e. HFE-7000 composing of various nano-particles and varying percentage composition by weight should also be investigated to see if the tribological performance of reciprocating parts in enhanced by using various nanoparticles with HFE-7000.

References

Aal, A. A., Bahgat, M., and Radwan, M., 2006. Nanostructured ni–aln composite coatings. *Surface and Coatings Technology,* 201 (6), 2910-2918.

Akasaka, R., and Kayukawa, Y., 2012. A fundamental equation of state for trifluoromethyl methyl ether (hfe-143m) and its application to refrigeration cycle analysis. *International Journal of Refrigeration,* 35 (4), 1003-1013.

Akei, M., and Mizuhara, K., 1997. The elastohydrodynamic properties of lubricants in refrigerant environments©. *Tribology Transactions,* 40 (1), 1-10.

Akei, M., Mizuhara, K., Taki, T., and Yamamoto, T., 1996. Evaluation of film-forming capability of refrigeration lubricants in pressurized refrigerant atmosphere. *Wear,* 196 (1-2), 180-187.

Akram, M. W., Meyer, J. L., and Polycarpou, A. A., 2016. Tribological interactions of advanced polymeric coatings with polyalkylene glycol lubricant and r1234yf refrigerant. *Tribology International,* 97, 200-211.

Akram, M. W., Polychronopoulou, K., and Polycarpou, A. A., 2013a. Lubricity of environmentally friendly hfo-1234yf refrigerant. *Tribology International,* 57, 92-100.

Akram, M. W., Polychronopoulou, K., and Polycarpou, A. A., 2014. Tribological performance comparing different refrigerant–lubricant systems: The case of environmentally friendly hfo-1234yf refrigerant. *Tribology International,* 78, 176-186.

Akram, M. W., Polychronopoulou, K., Seeton, C., and Polycarpou, A. A., 2013b. Tribological performance of environmentally friendly refrigerant hfo-1234yf under starved lubricated conditions. *Wear,* 304 (1), 191-201.

Algul, H., Tokur, M., Ozcan, S., Uysal, M., Cetinkaya, T., Akbulut, H., and Alp, A., 2015. The effect of graphene content and sliding speed on the wear mechanism of nickel–graphene nanocomposites. *Applied Surface Science,* 359, 340-348.

Allahkaram, S. R., Towhid, N., and Cheraghi, M. S., 2011. Effects of direct current and pulse electrodeposition parameters on the properties of nano cobalt coatings. *Paper presented at the Key Engineering Materials.*

Alper, M., Attenborough, K., Hart, R., Lane, S., Lashmore, D., Younes, C., and Schwarzacher, W., 1993. Giant magnetoresistance in electrodeposited superlattices. *Applied physics letters,* 63 (15), 2144-2146.

Stachowiak, G. W., and Batchelor, A. W. eds., 1993. 12 Adhesion and Adhesive wear. *In Tribology series* Vol. 24. Amsterdam: Elsevier, 613-635.

Archard, J., 1953. Contact and rubbing of flat surfaces. *Journal of applied physics,* 24 (8), 981-988.

References

Archard, J., and Kirk, M., 1962. *Lubrication at point contacts.* Paper presented at the Proc. R. Soc. Lond. A.

Argañaraz, M. P. Q., Ribotta, S. B., Folquer, M. E., Gassa, L. M., Benítez, G., Vela, M. E., and Salvarezza, R. C., 2011. Ni–w coatings electrodeposited on carbon steel: Chemical composition, mechanical properties and corrosion resistance. *Electrochimica Acta,* 56 (17), 5898-5903.

Aruna, S. T., Bindu, C. N., Ezhil Selvi, V., William Grips, V. K., and Rajam, K. S., 2006. Synthesis and properties of electrodeposited ni/ceria nanocomposite coatings. *Surface and Coatings Technology,* 200 (24), 6871-6880.

Bajwa, R., Khan, Z., Nazir, H., Chacko, V., and Saeed, A., 2016. Wear and friction properties of electrodeposited ni-based coatings subject to nano-enhanced lubricant and composite coating. *Acta Metallurgica Sinica (English Letters),* 29 (10), 902-910.

Bajwa, R. S., Khan, Z., Bakolas, V., and Braun, W., 2016a. Effect of bath ionic strength on adhesion and tribological properties of pure nickel and ni-based nanocomposite coatings. *Journal of Adhesion Science and Technology,* 30 (6), 653-665.

Bajwa, R. S., Khan, Z., Bakolas, V., and Braun, W., 2016b. Water-lubricated ni-based composite (ni–al2o3, ni–sic and ni–zro2) thin film coatings for industrial applications. *Acta Metallurgica Sinica (English Letters),* 29 (1), 8-16.

Balasubramanian, A., Srikumar, D. S., Raja, G., Saravanan, G., and Mohan, S., 2009. Effect of pulse parameter on pulsed electrodeposition of copper on stainless steel. *Surface Engineering,* 25 (5), 389-392.

Barcena, J., Maudes, J., Coleto, J., Baldonedo, J. L., and Gomez De Salazar, J. M., 2008. Microstructural study of vapour grown carbon nanofibre/copper composites. *Composites Science and Technology,* 68 (6), 1384-1391.

Bhushan, B., 2013. *Introduction to tribology.* John Wiley & Sons.

Birol, Y., and Birol, F., 2008. Sliding wear behaviour of thixoformed alsicufe alloys. *Wear,* 265 (11), 1902-1908.

Borkar, T., and Harimkar, S. P., 2011. Effect of electrodeposition conditions and reinforcement content on microstructure and tribological properties of nickel composite coatings. *Surface and Coatings Technology,* 205 (17), 4124-4134.

Breidenich, C., Magraw, D., Rowley, A., and Rubin, J. W., 1998. The kyoto protocol to the united nations framework convention on climate change. *American Journal of International Law,* 92 (2), 315-331.

Calm, J. M., 2008. The next generation of refrigerants–historical review, considerations, and outlook. *international Journal of Refrigeration,* 31 (7), 1123-1133.

Cannaday, M., and Polycarpou, A., 2006. Advantages of co2 compared to r410a refrigerant of tribologically tested aluminum 390-t6 surfaces. *Tribology Letters,* 21 (3), 185-192.

References

Cannaday, M. L., and Polycarpou, A. A., 2005. Tribology of unfilled and filled polymeric surfaces in refrigerant environment for compressor applications. *Tribology Letters,* 19 (4), 249-262.

Challen, J., Oxley, P., and Hockenhull, B., 1986. Prediction of archard's wear coefficient for metallic sliding friction assuming a low cycle fatigue wear mechanism. *Wear,* 111 (3), 275-288.

Chandrasekar, M. S., and Pushpavanam, M., 2008. Pulse and pulse reverse plating—conceptual, advantages and applications. *Electrochimica Acta,* 53 (8), 3313-3322.

Chen, J., Li, J., Xiong, D., He, Y., Ji, Y., and Qin, Y., 2016. Preparation and tribological behavior of ni-graphene composite coating under room temperature. *Applied Surface Science,* 361, 49-56.

Chen, L., Wang, L., Zeng, Z., and Zhang, J., 2006. Effect of surfactant on the electrodeposition and wear resistance of ni–al2o3 composite coatings. *Materials Science and Engineering: A,* 434 (1), 319-325.

Chittenden, R., Dowson, D., Dunn, J., and Taylor, C., 1985a. A theoretical analysis of the isothermal elastohydrodynamic lubrication of concentrated contacts. I. Direction of lubricant entrainment coincident with the major axis of the hertzian contact ellipse. *Proceedings of the Royal Society of London A: Mathematical, Physical and Engineering Sciences,* 397 (1813), 245-269.

Chittenden, R., Dowson, D., Dunn, J., and Taylor, C., 1985b. A theoretical analysis of the isothermal elastohydrodynamic lubrication of concentrated contacts. Ii. General case, with lubricant entrainment along either principal axis of the hertzian contact ellipse or at some intermediate angle. *Proceedings of the Royal Society of London A: Mathematical, Physical and Engineering Sciences,* 397 (1813), 271-294.

Chul Na, B., Jin Chun, K., and Han, D.-C., 1997. A tribological study of refrigeration oils under hfc-134a environment. *Tribology International,* 30 (9), 707-716.

Ciantar, C., and Hadfield, M., 2004. A study of tribological durability with associated environmental impacts of a domestic refrigerator. *Materials & Design,* 25 (4), 331-341.

Ciantar, C., Hadfield, M., Swallow, A., and Smith, A., 2000. The influence of poe and pve lubricant blends within hermetic refrigerating compressors operating with hfc-134a refrigerant. *Wear,* 241 (1), 53-64.

Davis, B., Sheiretov, T. K., and Cusano, C., ACRC Technical Report 19, May 1992. Tribological evaluation of contacts lubricated by oil-refrigerant mixtures. *Air Conditioning and Refrigeration Center, College of Engineering, University of Illinois at Urbana-Champaign.*

De Mello, J., Binder, R., Demas, N., and Polycarpou, A., 2009. Effect of the actual environment present in hermetic compressors on the tribological behaviour of a si-rich multifunctional dlc coating. *Wear,* 267 (5), 907-915.

References

Demas, N. G., and Polycarpou, A. A., 2006a. Tribological investigation of cast iron air-conditioning compressor surfaces in CO_2 refrigerant. *Tribology Letters,* 22 (3), 271-278.

Demas, N. G., and Polycarpou, A. A., 2006b. Ultra high pressure tribometer for testing CO_2 refrigerant at chamber pressures up to 2000 psi to simulate compressor conditions. *Tribology transactions,* 49 (3), 291-296.

Demas, N. G., and Polycarpou, A. A., 2008. Tribological performance of ptfe-based coatings for air-conditioning compressors. *Surface and Coatings Technology,* 203 (3), 307-316.

Demas, N. G., Polycarpou, A. A., and Conry, T. F., 2005. Tribological studies on scuffing due to the influence of carbon dioxide used as a refrigerant in compressors. *Tribology Transactions,* 48 (3), 336-342.

Demas, N. G., Zhang, J., Polycarpou, A. A., and Economy, J., 2008. Tribological characterization of aromatic thermosetting copolyester–ptfe blends in air conditioning compressor environment. *Tribology Letters,* 29 (3), 253-258.

Dowson, D., 1999. *History of tribology.* Second ed. Bury St Edmunds, United Kingdom: John Wiley and Sons Ltd.

Eckels, S. J., and Pate, M. B., 1991. An experimental comparison of evaporation and condensation heat transfer coefficients for hfc-134a and cfc-12. *International Journal of Refrigeration,* 14 (2), 70-77.

Eia. 2009. Residential energy consumption and survey (recs). *Independent Statistics & Analysis. U.S. Energy Information Administration.*

Eia. 2017a. Annual energy outlook 2017, table 4, january 2017. *U.S. Energy Information Administration.*

Eia. 2017b. Annual energy outlook 2017, table 5, january 2017. *U.S. Energy Information Administration.*

Evans, O., 1805. *The abortion of the young steam engineer's guide.* Philadelphia: Printed for the author by Fry and Kammerer.

Fujimoto, S., Sakitani, K., and Watada, M., 1984. Tribology analysis in rolling piston type compressor. *Paper presented at the International Compressor Engineering Conference.* Paper 477, 1984, Purdue University, Indiana, USA,.

Garland, N., and Hadfield, M., 2005. Environmental implications of hydrocarbon refrigerants applied to the hermetic compressor. *Materials & Design,* 26 (7), 578-586.

Garland, N. P., 2004. *Sustainable design of hydrocarbon refrigerants applied to the hermetic compressor.* Thesis (PhD). Bournemouth University, UK.

Górny, K., Stachowiak, A., Tyczewski, P., and Zwierzycki, W., 2016. Lubricity evaluation of oil–refrigerant mixtures with r134a and r290. *International Journal of Refrigeration,* 69, 261-271.

References

Hamrock, B., and Dowson, D., 1981. *Ball Bearing Lubrication*. New York: John wiley & sons.

Hamrock, B. J., and Dowson, D., 1977. Isothermal elastohydrodynamic lubrication of point contacts: Part iii—fully flooded results. *Journal of Lubrication Technology,* 99 (2), 264-275.

Hamrock, B. J., and Dowson, D., Jan 01, 1981. *Ball bearing lubrication: The elastohydrodynamics of elliptical contacts.* NASA Technical Reports, NASA.

Haq, I. U., Akhtar, K., Khan, T. I., and Ali Shah, A., 2013. Electrodeposition of ni–fe2o3 nanocomposite coating on steel. *Surface and Coatings Technology,* 235, 691-698.

Haq, I. U., and Khan, T. I., 2011. Tribological behavior of electrodeposited ni–sno2 nanocomposite coatings on steel. *Surface and Coatings Technology,* 205 (8), 2871-2875.

Helvaci, H., and Khan, Z., 2017. Thermodynamic modelling and analysis of a solar organic rankine cycle employing thermofluids. *Energy Conversion and Management,* 138, 493-510.

Helvaci, H., and Khan, Z. A., 2016. Experimental study of thermodynamic assessment of a small scale solar thermal system. *Energy Conversion and Management,* 117, 567-576.

Hou, K.-H., and Chen, Y.-C., 2011. Preparation and wear resistance of pulse electrodeposited ni–w/al2o3 composite coatings. *Applied Surface Science,* 257 (15), 6340-6346.

Hou, K.-H., Hwu, W.-H., Ke, S.-T., and Ger, M.-D., 2006. Ni–p–sic composite produced by pulse and direct current plating. *Materials Chemistry and Physics,* 100 (1), 54-59.

Hou, K.-H., Jeng, M.-C., and Ger, M.-D., 2007. A study on the wear resistance characteristics of pulse electroforming ni–p alloy coatings as plated. *Wear,* 262 (7), 833-844.

Hou, K. H., Ger, M. D., Wang, L. M., and Ke, S. T., 2002. The wear behaviour of electro-codeposited ni–sic composites. *Wear,* 253 (9), 994-1003.

Hutchings, I., and Shipway, P., 2017. *Tribology: Friction and wear of engineering materials.* Oxford: Butterworth-Heinemann.

Ishida, Y., Nishiwaki, F., and Ikoma, M., 1996. A study on lubricity of polyolester for alternative refrigerant hfc-134a. *Paper presented at the International Compressor Engineering Conference.* Paper 1140, 1996, Purdue University, Indiana, USA,

Jeon, H.-G., Oh, S.-D., and Lee, Y.-Z., 2009. Friction and wear of the lubricated vane and roller materials in a carbon dioxide refrigerant. *Wear,* 267 (5), 1252-1256.

Kawahara, K., Mishina, S., Kamino, A., Ochiai, K., Okawa, T., and Fujimoto, S., 1996. Tribological evaluation of rotary compressor with hfc refrigerants. *Paper presented at the International Compressor Engineering Conference.* Paper 1141, 23-26 July 1996, Purdue University, Indiana, USA.

References

Kelly, J., Bradley, P., and Landolt, D., 2000. Additive effects during pulsed deposition of cu-co nanostructures. *Journal of The Electrochemical Society,* 147 (8), 2975-2980.

Kelly, R. G., Scully, J. R., Shoesmith, D., and Buchheit, R. G., 2002. *Electrochemical techniques in corrosion science and engineering.* CRC Press.

Khan, S. H., and Zubair, S. M., 1993. Thermodynamic analyses of the cfc-12 and hfc-134a refrigeration cycles. *Energy,* 18 (7), 717-726.

Khan, Z. A., Pashaei, P., Bajwa, R., Nazir, H., and Cakmak, M., 2015. Fabrication and characterisation of electrodeposited and magnertron-sputtered thin films. *International Journal of Computational Methods & Experimental Measurements,* 3 (2), 165-174.

Kruse, H., and Schroeder, M., 1985. Fundamentals of lubrication in refrigerating systems and heat pumps. *International journal of refrigeration,* 8 (6), 347-355.

Lampke, T., Leopold, A., Dietrich, D., Alisch, G., and Wielage, B., 2006. Correlation between structure and corrosion behaviour of nickel dispersion coatings containing ceramic particles of different sizes. *Surface and Coatings Technology,* 201 (6), 3510-3517.

Lee, K., Suh, A., Demas, N., and Polycarpou, A., 2005. Surface and sub-micron sub-surface evolution of al390-t6 undergoing tribological testing under submerged lubrication conditions in the presence of co_2 refrigerant. *Tribology Letters,* 18 (1), 1-12.

Lee, S., 2006. *Encyclopedia of chemical processing.* Vol. 1: Taylor & Francis US.

Lee, Y.-Z., and Oh, S.-D., 2003. Friction and wear of the rotary compressor vane–roller surfaces for several sliding conditions. *Wear,* 255 (7–12), 1168-1173.

Limited, P. T., 2002. Operating instructions *TE 57 Pressurized Lubricity Tester.*

Liu, Y., Yu, S.-R., Liu, J.-D., Han, Z.-W., and Yuan, D.-S., 2011. Microstructure and wear resistance of electrodeposited ni-sio2 nano-composite coatings on az91hp magnesium alloy substrate. *Transactions of Nonferrous Metals Society of China,* 21, s483-s488.

Liu, Z., Zheng, M., Hilty, R. D., and West, A. C., 2010. Effect of morphology and hydrogen evolution on porosity of electroplated cobalt hard gold. *Journal of the Electrochemical Society,* 157 (7), D411-D416.

Liu, Z., Zheng, M., Hilty, R. D., and West, A. C., 2011. The effect of pulse reversal on morphology of cobalt hard gold. *Electrochimica Acta,* 56 (5), 2546-2551.

Ludema, K. C., 1996. *Friction, wear, lubrication: A textbook in tribology.* Florida: CRC Press.

Marlot, A., Kern, P., and Landolt, D., 2002. Pulse plating of ni–mo alloys from ni-rich electrolytes. *Electrochimica Acta,* 48 (1), 29-36.

Matsuura, H., Minowa, M., Fudemato, Y., Hiodoshi, S., and Nomura, M., Evaluation of refrigerant oil for hfc refrigerants and selection of sliding materials. *Paper presented at*

the International Compressor Engineering Conference. Paper 1276, 14-17 July 1998, Purdue University, Indiana, USA,

Minor, B. H., Herrmann, D., and Gravell, R., 2009. Flammability characteristics of hfo-1234yf. *Process Safety Progress,* 29 (2), 150-154.

Mishra, S. P., and Polycarpou, A. A., 2011. Tribological studies of unpolished laser surface textures under starved lubrication conditions for use in air-conditioning and refrigeration compressors. *Tribology International,* 44 (12), 1890-1901.

Mizuhara, K., Akei, M., and Matsuzaki, T., 1994. The friction and wear behavior in controlled alternative refrigerant atmosphere. *Tribology transactions,* 37 (1), 120-128.

Molina, M. J., and Rowland, F. S., 1974. Stratospheric sink for chlorofluoromethanes: Chlorine atom-catalysed destruction of ozone. *Nature,* 249 (5460), 810-812.

Morales-Espejel, G. E., Meeuwenoord, R., Quiñonez, A. F., and Hauleitner, R., 2015. Film thickness and traction measurements of refrigerant r1233zd used as lubricant in elastohydrodynamic conditions. *Proceedings of the Institution of Mechanical Engineers, Part C: Journal of Mechanical Engineering Science,* 229 (2), 244-253.

Muraki, M., Sano, T., and Dong, D., 2000. Rheological properties of polyolester under an ehd contact in some refrigerant environments. *Journal of Tribology,* 123 (1), 54-60.

Muraki, M., Sano, T., and Dong, D., 2002. Elastohydrodynamic properties and boundary lubrication performance of polyolester in a hydrofluoroether refrigerant environment. *Proceedings of the Institution of Mechanical Engineers, Part J: Journal of Engineering Tribology,* 216 (1), 19-26.

Muraki, M., Tagawa, K., and Dong, D., 1996. Refrigeration lubricant based on polyolester for use with hfcs and prospect of its application with r-22 (part 1) tribological characteristics. *Paper presented at the International Refrigeration and Air Conditioning Conference.* Paper 336, 23-26 July 1996, Purdue University, Indiana, USA.

Nakahara, S., and Okinaka, Y., 1974. Properties of electrodeposits-their measurement and significance. *R. Sard, H. Leidheiser, F. Ogburn 編, 第 3 章 (The Electrochemical Society, 1975).*

Nakanishi, T., Ozaki, M., Nam, H.-S., Yokoshima, T., and Osaka, T., 2001. Pulsed electrodeposition of nanocrystalline conife soft magnetic thin films. *Journal of the Electrochemical Society,* 148 (9), C627-C631.

Nations, U., 1998. Kyoto Protocol to the United Nations Framework Convention on Climate Change

Nations, U., . Montreal Protocol on Substances that Deplete the Ozone Layer. Montreal. *United Nations Environment Programme,* 2, FINAL ACT.

Nishiwaki, F., Hasegawa, H., Matsuzaki, R., and Muramatsu, S., 1996. Mechanical loss reduction at thrust bearings of scroll compressors using r407c. *Paper presented at the*

References

International Compressor Engineering Conference. Paper 1117, 23-26 July 1996, Purdue University, Indiana, USA,

Noria. Machinery lubrication. *Industrial lubricants*. Available from: http://www.machinerylubrication.com/Read/30027/lubricant-starvation-signs [Accessed 1 July 2019].

Notter, I. M., and Gabe, D. R. 1992. Porosity of electrodeposited coatings: Its cause, nature, effect and management, *Corrosion Reviews* (Vol. 10, pp. 217).

Nptel. Tribology (web). Available from: http://nptel.ac.in/courses/112102015/14 [Accessed 15 January 2018].

Nunez, E. E., Demas, N. G., Polychronopoulou, K., and Polycarpou, A. A., 2008. Tribological study comparing pag and poe lubricants used in air-conditioning compressors under the presence of co_2. *Tribology Transactions,* 51 (6), 790-797.

Nunez, E. E., Demas, N. G., Polychronopoulou, K., and Polycarpou, A. A., 2010a. Comparative scuffing performance and chemical analysis of metallic surfaces for air-conditioning compressors in the presence of environmentally friendly co_2 refrigerant. *Wear,* 268 (5), 668-676.

Nunez, E. E., and Polycarpou, A. A., 2015a. The effect of surface roughness on the transfer of polymer films under unlubricated testing conditions. *Wear,* 326-327, 74-83.

Nunez, E. E., and Polycarpou, A. A., 2015b. Wear study of metallic interfaces for air-conditioning compressors under submerged lubrication in the presence of carbon dioxide. *Wear,* 326-327, 28-35.

Nunez, E. E., Polychronopoulou, K., and Polycarpou, A. A., 2010b. Lubricity effect of carbon dioxide used as an environmentally friendly refrigerant in air-conditioning and refrigeration compressors. *Wear,* 270 (1), 46-56.

Nunez, E. E., Yeo, S. M., and Polycarpou, A. A., 2010. Tribological behavior of ptfe, peek, and fluorocarbon-based polymeric coatings used in air-conditioning and refrigeration compressors. *Paper presented at the International Compressor Engineering Conference.* Paper 2031, 12-15 July 2010, Purdue University, Indiana, USA.

Nunez, E. E., Yeo, S. M., Polychronopoulou, K., and Polycarpou, A. A., 2011. Tribological study of high bearing blended polymer-based coatings for air-conditioning and refrigeration compressors. *Surface and Coatings Technology,* 205 (8), 2994-3005.

Perkins, J., 1834. *Apparatus for producing ice and cooling fluids*. UK Patent 6662.

Ramanauskas, R., Gudavičiūtė, L., Ščit, O., Bučinskienė, D., and Juškėnas, R., 2008. Pulse plating effect on composition and corrosion properties of zinc alloy coatings. *Transactions of the IMF,* 86 (2), 103-108.

Rizwan Bajwa, Z. a. K., Vasilios Bakolas, Wolfgang Braun., 2014. Tribological performance of water lubricated electrodeposited nanocoatings in rolling contacts. *23rd Mission of*

References

Tribology Research. Institution of Mechanical Engineers (IMechE)., One Birdcage Walk, London, London, UK.

Rizwan Bajwa, Z. a. K., Vasilios Bakolas, Wolfgang Braun., 2015. An experimental investigation of water lubricated electroplated nanocomposite coatings. *STLE 70th Annual Meeting & Exhibition,* Dallas, Texas, USA.

Robinson, J. W., Zhou, Y., Bhattacharya, P., Erck, R., Qu, J., Bays, J. T., and Cosimbescu, L., 2016. Probing the molecular design of hyper-branched aryl polyesters towards lubricant applications. *Scientific Reports,* 6, 18624.

Rowe, C. N., 1966. Some aspects of the heat of adsorption in the function of a boundary lubricant. *A S L E Transactions,* 9 (1), 101-111.

Safari, S., and Hadfield, M., 1998. Wear behaviour of the piston/gudgeon pin in a hermetic compressor with replacement cfc refrigerants. *Wear,* 219 (1), 8-15.

Saha, R. K., and Khan, T. I., 2010. Effect of applied current on the electrodeposited ni–al2o3 composite coatings. *Surface and Coatings Technology,* 205 (3), 890-895.

Sariibrahimoglu, K., Kizil, H., Aksit, M. F., Efeoglu, I., and Kerpicci, H., 2010. Effect of r600a on tribological behavior of sintered steel under starved lubrication. *Tribology International,* 43 (5), 1054-1058.

Sensors, T., 2016. Telemecanique Sensors, Xmlpm09bd21vq. *Product data sheet*.

Shankland, I. R., Basu, R. S., and Wilson, D. P., 1998. Thermal conductivity and viscosity of a new stratospherically safe refrigerant-1, 1, 1, 2-tetrafluoroethane (r-134a). *Paper presented at the International Refrigeration and Air Conditioning Conference.* Paper 41, 1988, Purdue University, Indiana, USA.

Sheiretov, T., Glabbeek, W. V., and Cusano, C., 1994. Tribological evaluation of various surface treatments for m2 tool steel in a refrigerant environment. *Paper presented at the International Compressor Engineering Conference.* Paper 964, 19-22 July 1994, Purdue University, Indiana, USA.

Sheiretov, T., Yoon, H., and Cusano, C., ACRC Technical Report 92, 1996. Tribological evaluation of various aluminum alloys in lubricant/refrigerant mixtures. *Air Conditioning and Refrigeration Center, College of Engineering, University of Illinois at Urbana-Champaign*.

Shi, L., Sun, C., Gao, P., Zhou, F., and Liu, W., 2006. Mechanical properties and wear and corrosion resistance of electrodeposited ni–co/sic nanocomposite coating. *Applied Surface Science,* 252 (10), 3591-3599.

Shi, L., Sun, C. F., Zhou, F., and Liu, W. M., 2005. Electrodeposited nickel–cobalt composite coating containing nano-sized si3n4. *Materials Science and Engineering: A,* 397 (1), 190-194.

References

Silverio, M., Binder, R., Hulse, E. R., and De Mello, J. D. B., 2016. Effect of refrigerant gases (hfc134a and r600a) on the tribological behaviour of a multifunctional dlc coating. *Paper presented at the International Compressor Engineering Conference*. Paper 2413, 11-14 July 2016, Purdue University, Indiana, USA,.

Snyder, D. Nickel electroplating. *Applications, plating solutions, brighteners, good operating practices and troubleshooting*. Available from: https://www.pfonline.com/articles/nickel-electroplating [Accessed 15 March 2019].

Solzak, T. A., and Polycarpou, A. A., 2006. Tribology of protective hard coatings for use in oil-less, piston-type compressors. *Paper presented at the International Compressor Engineering Conference.* Paper 1790, 17-20 July 2006, Purdue University, Indiana, USA.

Solzak, T. A., and Polycarpou, A. A., 2010. Tribology of hard protective coatings under realistic operating conditions for use in oilless piston-type and swash-plate compressors. *Tribology Transactions,* 53 (3), 319-328.

Spatz, M., Minor, B., and Dupont, H., 2008. Hfo-1234yf a low gwp refrigerant for mac. Honeywell/dupont joint collaboration. *Paper presented at the SAE World Congress*. 14-17 April 2008, Detroit, Michigan, USA.

Spauschus, H., 1988. Hfc 134a as a substitute refrigerant for cfc 12. *International Journal of Refrigeration,* 11 (6), 389-392.

Srivastava, M., William Grips, V. K., and Rajam, K. S., 2010. Electrodeposition of ni–co composites containing nano-ceo2 and their structure, properties. *Applied Surface Science,* 257 (3), 717-722.

Statista. 2017. Number of cars sold worldwide from 1990 to 2017 (in million units). *The Statistics Portal*.

Stolarski, T., 1996. A system for wear prediction in lubricated sliding contacts. *Lubrication Science,* 8 (4), 315-351.

Stolarski, T. A., 1979. Adhesive wear of lubricated contacts. *Tribology International,* 12 (4), 169-179.

Stolarski, T. A., 1989a. Fracture mechanics and the contact between a pair of surface asperities during rolling. *International Journal of Engineering Science,* 27 (2), 169-179.

Stolarski, T. A., 1989b. Probability of scuffing in lubricated contacts. *Proceedings of the Institution of Mechanical Engineers, Part C: Mechanical Engineering Science,* 203 (6), 361-369.

Suh, A. Y., Polycarpou, A. A., and Conry, T. F., 2003. Detailed surface roughness characterization of engineering surfaces undergoing tribological testing leading to scuffing. *Wear,* 255 (1), 556-568.

References

Sun, X. J., and Li, J. G., 2007. Friction and wear properties of electrodeposited nickel–titania nanocomposite coatings. *Tribology Letters,* 28 (3), 223-228.

Sung, H. C., 1998. Tribological characteristics of various surface coatings for rotary compressor vane. *Wear,* 221 (2), 77-85.

Surender, M., Basu, B., and Balasubramaniam, R., 2004. Wear characterization of electrodeposited ni–wc composite coatings. *Tribology International,* 37 (9), 743-749.

Szeptycka, B., Gajewska-Midzialek, A., and Babul, T., 2016. Electrodeposition and corrosion resistance of ni-graphene composite coatings. *Journal of Materials Engineering and Performance,* 25 (8), 3134-3138.

Tada, A., Okido, T., Shono, Y., Takahashi, H., Shitara, Y., and Tanaka, S., 2016. Tribological characteristics of polyol ester type refrigeration oils under refrigerants atmosphere. *Tribology Online,* 11 (2), 348-353.

Tanaka, M., Matsuura, H., Taira, S., and Nakai, A., 2014. Selection of a refrigeration oil for the r32 refrigerant and evaluation of the compressor reliability. *Paper presented at the International Compressor Engineering Conference.* Paper 2299, 14-17 July 2014, Purdue University, Indiana, USA.

Tanaka, S., Nakahara, T., and Kyogoku, K., 2003. Measurements of two-dimensional distribution of refrigerant concentration in ehl film using micro ft-ir and effect of variation of concentration on oil film thickness. *Tribology Letters,* 14 (1), 9-15.

Tatsuya Sasaki, H. N., Hideaki Maeyama, Kota Mizuno., 2010. Tribology characteristics of hfo and hc refrigerants with immiscible oils - effect of refrigerant with unsaturated bond. *Paper presented at the International Compressor Engineering Conference.* Paper 1946, 12-15 July 2010, Purdue University, Indiana, USA.

Thiemig, D., and Bund, A., 2008. Characterization of electrodeposited ni–tio2 nanocomposite coatings. *Surface and Coatings Technology,* 202 (13), 2976-2984.

Thompson, R. A., and Bocchi, W., 1972. A model for asperity load sharing in lubricated contacts. *A S L E Transactions,* 15 (1), 67-79.

Toh, W., Tan, X., Bhowmik, A., Liu, E., and Tor, S., 2018. Tribochemical characterization and tribocorrosive behavior of cocrmo alloys: A review. *Materials,* 11 (1), 30.

Ueda, Y., Hataya, N., and Zaman, H., 1996. Magnetoresistance effect of co/cu multilayer film produced by electrodeposition method. *Journal of Magnetism and Magnetic Materials,* 156 (1), 350-352.

Vaezi, M. R., Sadrnezhaad, S. K., and Nikzad, L., 2008. Electrodeposition of ni–sic nano-composite coatings and evaluation of wear and corrosion resistance and electroplating characteristics. *Colloids and Surfaces A: Physicochemical and Engineering Aspects,* 315 (1), 176-182.

References

Vergne, P., Fillot, N., Bouscharain, N., Devaux, N., and Morales-Espejel, G. E., 2015. An experimental and modeling assessment of the hcfc-r123 refrigerant capabilities for lubricating rolling ehd circular contacts. *Proceedings of the Institution of Mechanical Engineers, Part J: Journal of Engineering Tribology,* 229 (8), 950-961.

Wang, L., Gao, Y., Xue, Q., Liu, H., and Xu, T., 2005. Effects of nano-diamond particles on the structure and tribological property of ni-matrix nanocomposite coatings. *Materials Science and Engineering: A,* 390 (1), 313-318.

Wardle, F., Jacobson, B., Dolfsma, H., Hoglund, E., and Jonsson, U., 1992. The effect of refrigerants on the lubrication of rolling element bearings used in screw compressors. *Paper presented at the International Compressor Engineering Conference.* Paper 843, 14-17 July 1992, Purdue University, Indiana, USA.

Williams, J., 2005. *Engineering tribology.* Cambridge University Press.

Wilson, D. P., and Basu, R. S., 1988. Thermodynamic properties of a new stratospherically safe working fluid-refrigerant 134a. *Paper presented at the ASHRAE Transactions.* Paper 94, Pages 2095-2118.

Wu, X., Cong, P., Nanao, H., Minami, I., and Mori, S., 2004. Tribological behaviors of 52100 steel in carbon dioxide atmosphere. *Tribology Letters,* 17 (4), 925-930.

Xia, Y., Sasaki, S., Murakami, T., Nakano, M., Shi, L., and Wang, H., 2007. Ionic liquid lubrication of electrodeposited nickel–si3n4 composite coatings. *Wear,* 262 (7), 765-771.

Xue, Y.-J., Jia, X.-Z., Zhou, Y.-W., Ma, W., and Li, J.-S., 2006. Tribological performance of ni–ceo2 composite coatings by electrodeposition. *Surface and Coatings Technology,* 200 (20), 5677-5681.

Yamamoto, Y., and Gondo, S., 1998. Friction and wear characteristics of lubricants for alternative refrigerant hfc 134a. *JSME International Journal Series C Mechanical Systems, Machine Elements and Manufacturing,* 41 (2), 278-284.

Yeo, S. M., and Polycarpou, A. A., 2014. Fretting experiments of advanced polymeric coatings and the effect of transfer films on their tribological behavior. *Tribology International,* 79, 16-25.

Yoon, H., Sheiretov, T., and Cusano, C., 1998. Tribological evaluation of some aluminum-based materials in lubricant/refrigerant mixtures. *Wear,* 218 (1), 54-65.

Yoon, H., Sheiretov, T., and Cusano, C., 2000. Scuffing behavior of 390 aluminum against steel under starved lubrication conditions. *Wear,* 237 (2), 163-175.

Zhou, Q., He, C. L., and Cai, Q. K., 2009. Effect of al2o3 powders on properties of electrodeposited ni matrix. *Advanced Materials Research,* 79-82, 631-634.

References

3M, 3M™ Novec™ 7000 Engineered Fluid. *Data sheet* [online]. Available from: https://multimedia.3m.com/mws/media/121372O/3m-novec-7000-engineered-fluid-tds.pdf [Accessed 1 September 2019].

Abdullah, M. U., Shah, S. R., Bhutta, M. U., Mufti, R. A., Khurram, M., Najeeb, M. H., Arshad, W. and Ogawa, K., 2018. Benefits of wonder process craft on engine valve train performance. *Proceedings of the Institution of Mechanical Engineers, Part D: Journal of Automobile Engineering*.

Akram, M. W., Meyer, J. L. and Polycarpou, A. A., 2016. Tribological interactions of advanced polymeric coatings with polyalkylene glycol lubricant and r1234yf refrigerant. *Tribology International*, 97, 200-211.

Akram, M. W., Polychronopoulou, K. and Polycarpou, A. A., 2013a. Lubricity of environmentally friendly HFO-1234yf refrigerant. *Tribology International*, 57, 92-100.

Akram, M. W., Polychronopoulou, K. and Polycarpou, A. A., 2014. Tribological performance comparing different refrigerant–lubricant systems: The case of environmentally friendly HFO-1234yf refrigerant. *Tribology International*, 78, 176-186.

Akram, M. W., Polychronopoulou, K., Seeton, C. and Polycarpou, A. A., 2013b. Tribological performance of environmentally friendly refrigerant HFO-1234yf under starved lubricated conditions. *Wear*, 304 (1), 191-201.

Bai, L., Meng, Y., Khan, Z. A. and Zhang, V., 2017. The Synergetic Effects of Surface Texturing and MoDDP Additive Applied to Ball-on-Disk Friction Subject to Both Flooded and Starved Lubrication Conditions. *Tribology Letters*, 65 (4), 163.

Bajwa, R., Khan, Z., Nazir, H., Chacko, V. and Saeed, A., 2016a. Wear and Friction Properties of Electrodeposited Ni-Based Coatings Subject to Nano-enhanced Lubricant and Composite Coating. *Acta Metallurgica Sinica (English Letters)*, 29 (10), 902-910.

Bajwa, R. S., 2016. *Electroplated Composite Coatings with Incorporated Nano Particles for Tribological Systems with the Focus on Water Lubrication.* Thesis (PhD). Bournemouth University, UK.

Bajwa, R. S., Khan, Z., Bakolas, V. and Braun, W., 2016b. Effect of bath ionic strength on adhesion and tribological properties of pure nickel and Ni-based nanocomposite coatings. *Journal of Adhesion Science and Technology*, 30 (6), 653-665.

Bajwa, R. S., Khan, Z., Bakolas, V. and Braun, W., 2016c. Water-Lubricated Ni-Based Composite (Ni–Al2O3, Ni–SiC and Ni–ZrO2) Thin Film Coatings for Industrial Applications. *Acta Metallurgica Sinica (English Letters)*, 29 (1), 8-16.

BBC, 2015, 28 January 2015. FRIDGEONOMICS. *Fridge ownership around the world*. Available from: https://www.bbc.co.uk/news/magazine-30925252 [Accessed 5 August 2019].

Bhutta, M., Khan, Z. and Garland, N., 2018a. Wear Performance Analysis of Ni–Al$_2$O$_3$ Nanocomposite Coatings under Nonconventional Lubrication. *Materials*, 12 (1), 36.

References

Bhutta, M. U. and Khan, Z. A., 2019. Friction and wear performance analysis of hydrofluoroether-7000 refrigerant. *Tribology International*, 139, 36-54.

Bhutta, M. U., Khan, Z. A., Garland, N. P. and Ghafoor, A., 2018b. A Historical Review on the Tribological Performance of Refrigerants used in Compressors. *Tribology in Industry*, 40 (1), 19-51.

Blaineau, B., Dutour, S., Callegari, T., Lavieille, P., Miscevic, M., Blanco, S., Schlegel, B., Bertin, Y. and Benselama, A. M., 2019. Experimental investigation of a dielectric liquid-vapor interface between two vertical planar electrodes: Influence of the DC electric field and temperature. *Experimental Thermal and Fluid Science*, 105, 144-152.

Borkar, T. and Harimkar, S. P., 2011. Effect of electrodeposition conditions and reinforcement content on microstructure and tribological properties of nickel composite coatings. *Surface and Coatings Technology*, 205 (17), 4124-4134.

Bowden, F. P. and Tabor, D., 1950. *The Friction and Lubrication of Solids*. Vol. 1. Oxford University Press.

Brownson, D. A. C. and Banks, C. E., 2010. Graphene electrochemistry: an overview of potential applications. *Analyst*, 135 (11), 2768-2778.

Calm, J. M., 2008a. The next generation of refrigerants–Historical review, considerations, and outlook. *international Journal of Refrigeration*, 31 (7), 1123-1133.

Calm, J. M., 2008b. The next generation of refrigerants – Historical review, considerations, and outlook. *La prochaine génération de frigorigènes – historique, analyse et perspectives*, 31 (7), 1123-1133.

Cannaday, M. and Polycarpou, A., 2006. Advantages of CO_2 compared to R410a refrigerant of tribologically tested Aluminum 390-T6 surfaces. *Tribology Letters*, 21 (3), 185-192.

Cannaday, M. L. and Polycarpou, A. A., 2005. Tribology of unfilled and filled polymeric surfaces in refrigerant environment for compressor applications. *Tribology Letters*, 19 (4), 249-262.

Chen, L., Wang, L., Zeng, Z. and Xu, T., 2006a. Influence of pulse frequency on the microstructure and wear resistance of electrodeposited Ni–Al_2O_3 composite coatings. *Surface and Coatings Technology*, 201 (3), 599-605.

Chen, L., Wang, L., Zeng, Z. and Zhang, J., 2006b. Effect of surfactant on the electrodeposition and wear resistance of Ni–Al_2O_3 composite coatings. *Materials Science and Engineering: A*, 434 (1), 319-325.

De Mello, J., Binder, R., Demas, N. and Polycarpou, A., 2009. Effect of the actual environment present in hermetic compressors on the tribological behaviour of a Si-rich multifunctional DLC coating. *Wear*, 267 (5), 907-915.

Demas, N. G. and Polycarpou, A. A., 2006a. Tribological investigation of cast iron air-conditioning compressor surfaces in CO_2 refrigerant. *Tribology Letters*, 22 (3), 271-278.

References

Demas, N. G. and Polycarpou, A. A., 2006b. Ultra high pressure tribometer for testing CO_2 refrigerant at chamber pressures up to 2000 psi to simulate compressor conditions. *Tribology transactions*, 49 (3), 291-296.

Deshpande, P., Minfray, C., Dassenoy, F., Thiebaut, B., Le Mogne, T., Vacher, B. and Jarnias, F., 2018. Tribological behaviour of TiO2 Atmospheric Plasma Spray (APS) coating under mixed and boundary lubrication conditions in presence of oil containing MoDTC. *Tribology International*, 118, 273-286.

Gu, G., Wu, Z., Zhang, Z. and Qing, F., 2009. Tribological properties of fluorine-containing additives of silicone oil. *Tribology International*, 42 (3), 397-402.

Hagita, T., Makino, T., Horaguchi, N. and Ukai, T., Feb 2002. Tribology in CO_2 Scroll Compressors, *Mitsubishi Heavy Industries, Ltd., Technical Review* (Vol. 39, no. 1).

Helvaci, H. and Khan, Z., 2017a. Thermodynamic modelling and analysis of a solar organic Rankine cycle employing thermofluids. *Energy Conversion and Management*, 138, 493-510.

Helvaci, H. and Khan, Z. A., 2016. Experimental study of thermodynamic assessment of a small scale solar thermal system. *Energy Conversion and Management*, 117, 567-576.

Helvaci, H. U. and Khan, Z. A., 2017b. Heat transfer and entropy generation analysis of HFE 7000 based nanorefrigerants. *International Journal of Heat and Mass Transfer*, 104, 318-327.

Hertz, H. R. J. V. d. V. z. B. d. G., Berlin, 1882. Uber die Beruhrung fester elastischer Korper und Uber die Harte. 449.

Hutchings, I. and Shipway, P., 1992. *Tribology: Friction and Wear of Engineering Materials*. Butterworth-Heinemann.

iea, 2018. World Air-Conditioning Units. *International Energy Agency.*

IMF, 2019. *International Monetary Fund*.

ipcc, The Intergovernmental Panel on Climate Change *Global Warming Potential Values,* [online]. Available from: https://www.ghgprotocol.org/sites/default/files/ghgp/Global-Warming-Potential-Values%20%28Feb%2016%202016%29_1.pdf [Accessed 18 April 2019]

Jabbar, A., Yasin, G., Khan, W. Q., Anwar, M. Y., Korai, R. M., Nizam, M. N. and Muhyodin, G. J. R. A., 2017. Electrochemical deposition of nickel graphene composite coatings: effect of deposition temperature on its surface morphology and corrosion resistance. 7 (49), 31100-31109.

Jacobson, B. O. and Espejel, G. E. M., 2006. High pressure investigation of refrigerants HFC245fa, R134a and R123. *International Compressor Engineering Conference*. Paper 1789, 17-20 July, 2006, Purdue University, Indiana, USA.

References

Jean-Fulcrand, A., Masen, M. A., Bremner, T. and Wong, J. S. S., 2017. High temperature tribological properties of polybenzimidazole (PBI). *Polymer*, 128, 159-168.

Jeon, H.-G., Oh, S.-D. and Lee, Y.-Z., 2009. Friction and wear of the lubricated vane and roller materials in a carbon dioxide refrigerant. *Wear*, 267 (5), 1252-1256.

Johnson, K. L., 1987. *Contact mechanics*. Cambridge University Press.

Kang, X., Wang, J., Wu, H., Liu, J., Aksay, I. A. and Lin, Y., 2010. A graphene-based electrochemical sensor for sensitive detection of paracetamol. *Talanta*, 81 (3), 754-759.

Kawahara, K., Mishina, S., Kamino, A., Ochiai, K., Okawa, T. and Fujimoto, S., 1996. Tribological Evaluation of Rotary Compressor with HFC Refrigerants, *International Compressor Engineering Conference*. Paper 1141, 23-26 July, 1996, Purdue University, Indiana, USA.

Khan, Z. A., Hadfield, M., Tobe, S. and Wang, Y., 2006. Residual stress variations during rolling contact fatigue of refrigerant lubricated silicon nitride bearing elements. *Ceramics International*, 32 (7), 751-754.

Khan, Z. A., Hadfield, M. and Wang, Y., 2005. Pressurised chamber design for conducting rolling contact experiments with liquid refrigerant lubrication. *Materials & Design*, 26 (8), 680-689.

Kumar, K. S., Van Swygenhoven, H. and Suresh, S., 2003. Mechanical behavior of nanocrystalline metals and alloys. *Acta Materialia*, 51 (19), 5743-5774.

Lee, K., Suh, A., Demas, N. and Polycarpou, A., 2005. Surface and sub-micron sub-surface evolution of Al390-T6 undergoing tribological testing under submerged lubrication conditions in the presence of CO_2 refrigerant. *Tribology Letters*, 18 (1), 1-12.

Lee, Y.-Z. and Oh, S.-D., 2003. Friction and wear of the rotary compressor vane–roller surfaces for several sliding conditions. *Wear*, 255 (7–12), 1168-1173.

Lide, D. R., 73rd edition, 1992-1993, pp. 9-145. *CRC handbook of chemistry and physics*. Florida: CRC Press.

Liu, C., Alwarappan, S., Chen, Z., Kong, X. and Li, C.-Z., 2010. Membraneless enzymatic biofuel cells based on graphene nanosheets. *Biosensors and Bioelectronics*, 25 (7), 1829-1833.

Meyers, M. A., Mishra, A. and Benson, D. J., 2006. Mechanical properties of nanocrystalline materials. *Progress in Materials Science*, 51 (4), 427-556.

Mizuhara, K., Akei, M. and Matsuzaki, T., 1994. The friction and wear behavior in controlled alternative refrigerant atmosphere. *Tribology transactions*, 37 (1), 120-128.

Muraki, M., Sano, T. and Dong, D., 2002. Elastohydrodynamic properties and boundary lubrication performance of polyolester in a hydrofluoroether refrigerant environment.

References

Proceedings of the Institution of Mechanical Engineers, Part J: Journal of Engineering Tribology, 216 (1), 19-26.

Nazir, M. H., Khan, Z. A., Saeed, A., Bakolas, V., Braun, W. and Bajwa, R., 2018a. Experimental analysis and modelling for reciprocating wear behaviour of nanocomposite coatings. *Wear*, 416-417, 89-102.

Nazir, M. H., Khan, Z. A., Saeed, A., Bakolas, V., Braun, W., Bajwa, R. and Rafique, S., 2017. Analyzing and Modelling the Corrosion Behavior of Ni/Al_2O_3, Ni/SiC, Ni/ZrO_2 and $Ni/Graphene$ Nanocomposite Coatings. *Materials*, 10 (11), 1225.

Nazir, M. H., Khan, Z. A., Saeed, A., Siddaiah, A. and Menezes, P. L., 2018b. Synergistic wear-corrosion analysis and modelling of nanocomposite coatings. *Tribology International*, 121, 30-44.

Nunez, E. E., Demas, N. G., Polychronopoulou, K. and Polycarpou, A. A., 2008. Tribological study comparing PAG and POE lubricants used in air-conditioning compressors under the presence of CO_2. *Tribology Transactions*, 51 (6), 790-797.

Nunez, E. E. and Polycarpou, A. A., 2015. The effect of surface roughness on the transfer of polymer films under unlubricated testing conditions. *Wear*, 326-327, 74-83.

Nunez, E. E., Polychronopoulou, K. and Polycarpou, A. A., 2010. Lubricity effect of carbon dioxide used as an environmentally friendly refrigerant in air-conditioning and refrigeration compressors. *Wear*, 270 (1), 46-56.

Nunez, E. E., Yeo, S. M. and Polycarpou, A. A., 2010. Tribological Behavior of PTFE, PEEK, and Fluorocarbon-based Polymeric Coatings used in Air-Conditioning and Refrigeration Compressors, *International Compressor Engineering Conference*. Paper 2031, 12-15 July, 2010, Purdue University, Indiana, USA.

Saha, R. K. and Khan, T. I., 2010. Effect of applied current on the electrodeposited $Ni−Al_2O_3$ composite coatings. *Surface and Coatings Technology*, 205 (3), 890-895.

Sariibrahimoglu, K., Kizil, H., Aksit, M. F., Efeoglu, I. and Kerpicci, H., 2010. Effect of R600a on tribological behavior of sintered steel under starved lubrication. *Tribology International*, 43 (5), 1054-1058.

Scientific, T., 2019. Thermo Scientific. *Thermo Scientific XPS* [online]. Available at: *https://xpssimplified.com/periodictable.php* [Accessed 5 September 2019].

Sekiya, A. and Misaki, S., 2000. The potential of hydrofluoroethers to replace CFCs, HCFCs and PFCs. *Journal of Fluorine Chemistry*, 101 (2), 215-221.

Shin, J.-H., Rozenfeld, T., Shockner, T., Kumar Vutha, A., Wang, Y., Ziskind, G. and Peles, Y., 2019. Local heat transfer under an array of micro jet impingement using HFE-7000. *Applied Thermal Engineering*, 113716.

References

Solzak, T. A. and Polycarpou, A. A., 2010. Tribology of hard protective coatings under realistic operating conditions for use in oilless piston-type and swash-plate compressors. *Tribology Transactions*, 53 (3), 319-328.

Solzak, T. A. and Polycarpou, A. A., 2006. Tribology of protective hard coatings for use in oil-less, piston-type compressors, *International Compressor Engineering Conference*. Paper 1790, 17-20 July, 2006, Purdue University, Indiana, USA.

Suh, A. Y., Polycarpou, A. A. and Conry, T. F., 2003. Detailed surface roughness characterization of engineering surfaces undergoing tribological testing leading to scuffing. *Wear*, 255 (1), 556-568.

Tatsuya Sasaki, H. N., Hideaki Maeyama, Kota Mizuno., 2010. Tribology Characteristics of HFO and HC Refrigerants with Immiscible Oils - Effect of Refrigerant with Unsaturated Bond. *International Compressor Engineering Conference*. Paper 1946, 12-15 July, 2010, Purdue University, Indiana, USA.

Tsai, W.-T., 2005. Environmental risk assessment of hydrofluoroethers (HFEs). *Journal of Hazardous Materials*, 119 (1), 69-78.

Vergne, P., Fillot, N., Bouscharain, N., Devaux, N. and Morales-Espejel, G. E., 2015. An experimental and modeling assessment of the HCFC-R123 refrigerant capabilities for lubricating rolling EHD circular contacts. *Proceedings of the Institution of Mechanical Engineers, Part J: Journal of Engineering Tribology*, 229 (8), 950-961.

Wu, X., Cong, P., Nanao, H., Minami, I. and Mori, S., 2004. Tribological behaviors of 52100 steel in carbon dioxide atmosphere. *Tribology Letters*, 17 (4), 925-930.

XPS, 2019. *X-ray Photoelectron Spectroscopy (XPS) Reference Pages*. Available at: *http://www.xpsfitting.com/* [Accessed 5 September 2019].

Yeo, S. M. and Polycarpou, A. A., 2014. Fretting experiments of advanced polymeric coatings and the effect of transfer films on their tribological behavior. *Tribology International*, 79, 16-25.

Yoon, H., Sheiretov, T. and Cusano, C., 2000. Scuffing behavior of 390 aluminum against steel under starved lubrication conditions. *Wear*, 237 (2), 163-175.

Zhou, Q., He, C. L. and Cai, Q. K., 2009. Effect of Al_2O_3 Powders on Properties of Electrodeposited Ni Matrix. *Advanced Materials Research*, 79-82, 631-634.

Zong, Y. and Zuo, L., 2003. Materials design of microstructure in grain boundary and second phase particles. *JOURNAL OF MATERIALS SCIENCE & TECHNOLOGY*, 19 (2), 97-101.
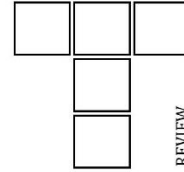
Appendices

Appendix A: Publications

Paper I

A Historical Review on the Tribological Performance of Refrigerants used in Compressors

M.U. Bhutta [a,b], Z.A. Khan [a], N. Garland [a] A. Ghafoor [b]

[a] *Bournemouth University, Department of Design & Engineering, NanoCorr, Energy & Modelling (NCEM) Research Group, Poole, Dorset, United Kingdom,*
[b] *School of Mechanical & Mechanical Engineering (SMME), National University of Sciences and Technology (NUST), Campus H-12, Islamabad, Pakistan.*

Keywords:

Corresponding author:

Muhammad Usman Bhutta
Faculty of Science & Technology,
Department of Design & Engineering,
NanoCorr, Energy & Modelling (NCEM)
Research Group, Bournemouth
University, P520, Poole House, Talbot
Campus, Fern Barrow, Poole, BH12 5BB.
Email: mbhutta@bournemouth.ac.uk

A B S T R A C T

Refrigerants directly affect the tribological performance of interacting components in a compressor. Since the introduction of artificially formulated refrigerants, the types of refrigerants used in compressors have changed over the years. Apart from evaluating the physical, chemical and thermodynamic properties of refrigerants, the refrigerants have also been studied from a view point of tribology by various researchers worldwide. Changing a refrigerant in a compressor not only has an effect on the thermodynamic cycle but also effects the lubricants viscosity, lubricants pressure-viscosity coefficient, oil film thickness, lubricant/refrigerant miscibility, friction, wear, durability, reliability and overall power consumption. Refrigerants have been studied from a view point of tribology by varying the contact geometries, by using different lubricating oils with and without additives, by altering the environmental pressure/temperature, by changing the phase of the refrigerant, by using different interacting materials and by applying numerous surface treatments. The tribological behavior of refrigerants can be better understood by consolidating the findings in a comprehensive manner. An in-depth review on the tribological behavior of refrigerants is missing from the literature. This article reviews the tribological studies carried out on refrigerants, with focus on refrigerants used in domestic appliances, automobile air-conditioning systems and small scale industrial and commercial applications.

1. INTRODUCTION

Use of refrigerants dates back to ancient times where water vaporization and other evaporation processes were used as a means of cooling. A system that used a volatile fluid to produce ice in a closed cycle was first described by Oliver Evans. The proposed system which has no record of being actually built, used ether as a refrigerant under vacuum. Ether was to be evaporated under vacuum and the vapors were to be pumped to a water cooled heat exchanger

to condense for reuse. Perkins probably influenced by this idea built the first working machine that used mechanical vapor-compression cycle. Perkins patent describes the use of a volatile fluid for the purpose of cooling/freezing, and at the same time condensing the fluid for reuse without waste.

Compounds such as Sulfur Dioxide (R-764), Ammonia (R-717), Methyl Chloride (R-40) and Methyl Formate (R-611) were being used as refrigerants before the 1930s but, their high toxicity and flammability reduced their potential of being used on a global scale in domestic cooling and refrigeration systems. Several fatal accidents occurred in the 1920s because of methyl chloride leakage from refrigerators. This started a collaborative research in 1928 for a refrigerant replacement that would be nontoxic and nonflammable by Frigidaire, DuPont and General Motors Research Corporation. This collaborative research led to the development of Dichlorodifluoromethane (CFC-12), Trichlorofluoromethane (CFC-11), Chlorodifluoromethane (HCFC-22), Trichlorotrifluoroethane (CFC-113), and Dichlorotetrafluoroethane (CFC-114). Commercial production of CFC-12 started in 1931. Chlorofluorocarbons (CFCs) and Hydrochlorofluorocarbons (HCFCs) possessed excellent thermodynamic properties as refrigerants besides being nonflammable and nontoxic. This made them the ideal refrigerants of their time, especially for use in small commercial, automotive and residential refrigeration applications.

Tribological studies of CFCs and HCFCs have also been carried out by various researchers to evaluate their mechanical, friction and wear properties. The lubrication conditions in a rolling piston type rotary compressor using HCFC-22 were investigated by [1]. The study focused on the friction and wear behavior of journal bearings and the vane-tip using ferrous and nonferrous metals. Focusing on CFCs; the viscosity, density and miscibility of various refrigerants in oils for use in refrigerator compressors was discussed by [2]. These factors affect the lubrication regime in a compressor which influences the friction coefficient and the amount of wear. Lubrication film thickness is a function of physical parameters including the lubricants viscosity and pressure-viscosity

coefficient. The lubrication film dictates the wear in interacting parts and components. Viscosity and the pressure-viscosity coefficient for roller bearings element used in screw compressors were experimentally investigated by using oil-rich solution of naphthenic oil and HCFC-22 as refrigerant [3]. The results showed that viscosity of the oil dropped sharply after charging the refrigerant and then slowly increased until the solution reached an equilibrium value. Tribological assessment of contacts lubricated by oil-refrigerant mixtures using CFC-12 and various oils was studied by [4]. The researchers used counterformal contacts, area contacts and conformal contacts in their study. They concluded that the chlorine atom in CFC-12 serves to form protective surface films which effectively reduces friction and wear. Lubricant-refrigerant mixture using mineral oil and HCFC-22 was analyzed by [5]. Their results showed that the rate of change of pressure as seen by the lubricant-refrigerant mixture while circulation in the system was too fast to allow the mixture to reach equilibrium. The mixture concentration lagged behind the pressure-temperature changes in the system. Friction and wear characteristics in refrigerant atmosphere using CFC-12, mineral oil and synthetic oil were experimentally investigated by [6]. Their results showed that CFC-12 has Extreme Pressure properties. Chloride layer and fluorine were detected on the sliding surfaces in the post test analysis which contributed to the anti-wear properties. Their results also showed that the wear rates were reduced with increasing speeds or loads. An apparatus working on the principle of optical interferometry was developed [7] to study the film-forming capability in pressurized refrigerant atmosphere. One of their tests with CFC-12 and mineral oils showed that the refrigerant has a strong effect on reducing the oil film forming capability. This effect however decreased with a rise in oil temperature. Dry friction tests of a number of refrigerants including CFC-12 and HCFC-22 were performed by [8]. CFC-12 and HCFC-22 showed the highest seizure load amongst the tested refrigerants indicating the effect of Extreme Pressure. Although the tribological studies of refrigerants were not very large in number till the 1990s, but their results clearly showed that CFCs and HCFCs had good tribological properties especially for use in domestic, commercial and automobile applications. The viscosity of the

20

lubricating oils decreased in refrigerant environment, which was unavoidable. However the formation of protective surface films made it possible for the compressor to run at very low lubricant viscosities and show good wear and friction characteristics.

Destructive effects of CFCs on the stratospheric ozone layer were published by [9] in 1974. This work clearly stated that chlorofluoromethanes can remain in the atmosphere from 40 to 150 years and lead to the destruction of the ozone layer by chemically reacting with it. Vienna Convention for the Protection of the Ozone Layer in 1985 was followed by the Montreal Protocol on Substances that Deplete the Ozone Layer in 1987 [10]. Montreal Protocol was enforced in 1989 which banned the use of CFCs by the end of year 1995 in developed countries. HCFCs were suggested as transitional refrigerants. Their consumption was also limited by Montreal Protocol. Different countries adapted different phase out strategies of HCFCs. Having zero ozone depleting potential the focus shifted to hydrofluorocarbons (HFCs).

HFCs became the refrigerants of choice in the mid-1990s and they replaced CFCs and HCFCs in automobile, commercial and domestic refrigeration and air-conditioning systems. Various researchers worldwide started investigating HFCs with respect to their oil miscibility, their friction performance, their wear characteristics, etc. Some of the earlier studies focused on their direct comparison with CFCs and HCFCs. Amongst the HFCs, HFC-134a was suggested as the most suitable replacement for CFC-12. Studies on HFC-134a involving specific gravity, vapor pressure, vapor thermal conductivity, liquid viscosity and its overall physical and thermodynamic properties [11-13] made a direct comparison with CFC-12 and recommend it as the best replacement.

Mineral oils that showed good miscibility with CFCs and HCFCs, unfortunately were not compatible with HFCs. HFCs showed poor compatibility and miscibility in mineral oils. Synthetic oils with various additives were developed for HFCs. Using nine different polyalkylene glycols (PAG) with HFC-134a, wear tests were performed and compared to the performance of CFC-12/mineral oil by [14]. Their results indicated that the CFC-12/mineral oil

showed no wear in a compressor connecting rod; however, all PAG/HFC-134a showed distress at the wrist pin. This study also concluded the oil/refrigerant miscibility to be the most dominant factor. Lubricant properties including solubility, thermal stability, viscosity, water adsorption, lubricant compatibility and lubricity of HFC-134a and synthetic oils were studied by [15]. Using 10 different synthetic oils with HFC-134a, the study [15] suggested esters, amides and polyalkylene glycols to be the most suitable oils for HFC-134a. The study [4] compared the friction and wear properties of HFC-134a with CFC-12 using different contact geometries. This study showed that CFC-12/oil mixture had much better wear results as compared to HFC-134a/oil mixtures. HFC-134a does not have any chlorine atom whereas the chlorine in CFC-12 forms protective surface films and decreases wear. The conclusion of the study [16] indicated that various kinds of additives were required for oils to be used with HFC-134a, whereas CFC-12 and HCFC-22 need no or very few additives. The experimental investigation [6] compared the tribological performance of HFC-134a and CFC-12 stated that the coefficient of friction and the fluctuations increase in HFC-134a environment, whereas the fluctuations and the friction coefficient decreases in the case of CFC-12. Friction experiments conducted under dry conditions [8] showed that the fluorine in HFC-134a had somewhat of a lubricating effect; however in comparison, CFC-12 and HCFC-22 showed better results. Similar studies [3, 17-20] compared HFCs with HCFCs. Almost all of the studies carried out to compare HFCs which CFCs and HCFCs concluded that that HFCs had poorer tribological properties in contrast to their predecessors. Due to the zero ozone depleting potential of HFCs, they are being used till date in a number of air-conditioning and refrigeration applications.

In 1997 Kyoto protocol to the United Nations Framework Convention on Climate Change [21] established binding limits on emissions of carbon dioxide and other greenhouse gases (GHG). The main source of the greenhouse emissions is the consumption of fossil fuel which produces carbon dioxide. Nitrous oxide, methane, perfluorocarbons (PFCs) and hydrofluorocarbons were identified as the other main contributors to global warming [22]. HFCs were recognized as major contributors to global

21

warming and a phase out of HFCs has been planned for the coming years. A ban on non-confined direct evaporation systems using HFCs and PFCs was imposed in 2007. All F gases having 150 or more global warming potential will be banned as refrigerants in any hermetically sealed system from the year 2022. This directly affects HFC-134a, which has a global warming potential of 1430 for integrated time of 100 years [23].

These international regulations and bans have forced the refrigerant manufacturers and the air conditioning and refrigeration industry to find alternative refrigerants yet again. The challenge to come up with refrigerants which not only have the thermodynamic properties matching their predecessors but also having very low ozone depleting potential (ODP) and low global warming potential (GWP) is even greater.

The refrigerant industry has come up with potential future generation refrigerants having low OPD, low GWP and low flammability. Some of these refrigerants are already being charged in automotive and domestic air-conditioning and refrigeration systems. There has also been advice to shift towards natural refrigerants such as carbon dioxide and avoid the use of chemically formulated coolants which have proven to be harmful to the earth's atmosphere one way or another. The friction, wear and the overall tribological properties of these next generation refrigerants like Hydrofluoroolefins, Hydrofluoroether, and natural refrigerants like carbon dioxide are being studied by various researcher around the globe. This review paper focuses on the investigations carried out on the tribological performance of domestic, small scale commercial and automotive refrigerants.

2. REFRIGERANTS CONSIDERED

Ranging from chemically formulated to natural refrigerants, there are a variety of refrigerants available for use. The selection of a refrigerant depends on its application and place of use. Environmental legislations have banned the use of certain refrigerants over the years. This has forced the development of new refrigerants. Initially this paper presents the work done on CFCs and HCFCs in the 1980s and 1990s, which is followed by HFCs. After HFCs, natural refrigerants

i.e. carbon dioxide and hydrocarbons are presented. At the end, recently developed refrigerants, Hydrofluoroolefins (HFOs) and Hydrofluoroethers (HFEs) are discussed.

Different researchers used different apparatus and varying geometries for the tribological analysis of refrigerants. This paper classifies the findings in terms of the refrigerant used in a study. Most of the studies are concerned with the investigation of an oil/refrigerant mixture, however some researchers have used a refrigerant only for their study. The reason for choosing oil/refrigerant mixture by most of the researchers is that in actual compressors the refrigerant gets mixed with the lubricating oil and the oil/refrigerant mixture then dictates the lubricating properties in a compressor. On the other hand some of the researchers say that if the true friction and wear properties of a refrigerant are to be investigated, then it should be tested independently from the lubricating oil.

Almost all of the studies have used the refrigerant in gaseous phase with the exception of a few investigators who used the refrigerants in liquid state in their study. Most refrigerants are in the gaseous phase under standard room temperature and pressure. The refrigerants are also mostly in gaseous phase when in a compressor is why most of the investigations are concerned with the refrigerant in vapor form. However the refrigerant does go under a phase change in a refrigeration cycle and turns from gas to liquid and then from liquid back to vapor. According to some researchers the true properties of a refrigerant as a lubricant can only be seen in liquid phase independent of a lubricating oil.

The published/reported studies are mainly concerned with simulating conditions present in a compressor. Some researchers have developed their own customized rigs for investigating the tribological behavior of refrigerants, some investigators have used actual compressors in their study, whereas standard tribo-testing machines have been utilized in the other studies. Many studies also include the influence of the materials under contact. Various different metals, metal alloys and hybrid contacts have been used in the earlier investigations. Recently the focus has shifted towards the investigation of surface coated contacts. The effect of surface texturing

22

has also been investigated in the recent past. Table 1 summarizes all the refrigerants that have been discussed in this article along with their OPD, GWP and flammability.

Table 1. Refrigerants considered.

Refrigerant	ODP	GWP*	Flammability
CFC-12	1.00	10,900	Nonflammable
CFC-114	1.00	10,000	Nonflammable
HCFC-22	0.05	1,810	Nonflammable
HCFC-123	0.060	77	Nonflammable
HFC-134a	Zero	1,430	Nonflammable
HFC-32	Zero	675	Nonflammable
HFC-125	Zero	3,500	Nonflammable
HFC-407C	Zero	1,774	Nonflammable
HFC-404A	Zero	3,922	Nonflammable
HFC-245fa	Zero	1,030	Nonflammable
HFC-410A	Zero	2,088	Nonflammable
HC-600a	Zero	3	High
HC-290	Zero	3.3	High
HC-1270	Zero	0.01	High
R-744	Zero	1.00	Nonflammable
HFO-1234yf	Zero	4.00	Mild
HFO-1233zd	0.0002	1.00	Nonflammable
HFE-245mc	Zero	622	Nonflammable

*GWP values for 100 year based on the Fourth Assessment Report [24].

3. CHLOROFLUOROCARBONS (CFCs)

The search for a nonflammable, colorless, tasteless, odorless and nontoxic refrigerant in the late 1920s led to the development of CFCs and HCFCs in 1928. CFCs are chemicals containing atoms of chlorine, carbon and fluorine. These nonflammable and nontoxic chemicals were used as solvents, blowing agents for packing materials and foam, in the manufacturing of aerosol sprays, and as refrigerants. Production of CFCs was banned by the end of 1995 in developed countries and from the year 2010 in developing countries by the Montreal Protocol.

Besides being nontoxic and nonflammable the thermodynamics qualities of CFC-12 made it an ideal candidate for automotive, domestic and small scale commercial air-conditioning and refrigeration systems.

A study based on the mixture of CFC-114 and CFC-12 with synthetic oil for screw compressors for heat pump applications was conducted by [2]. Small heat pumps are designed normally without oil separators, this is to allow relatively large amounts of oil to be entrained in the refrigerant circuit [2]. Figure 1 shows oil in a refrigeration system.
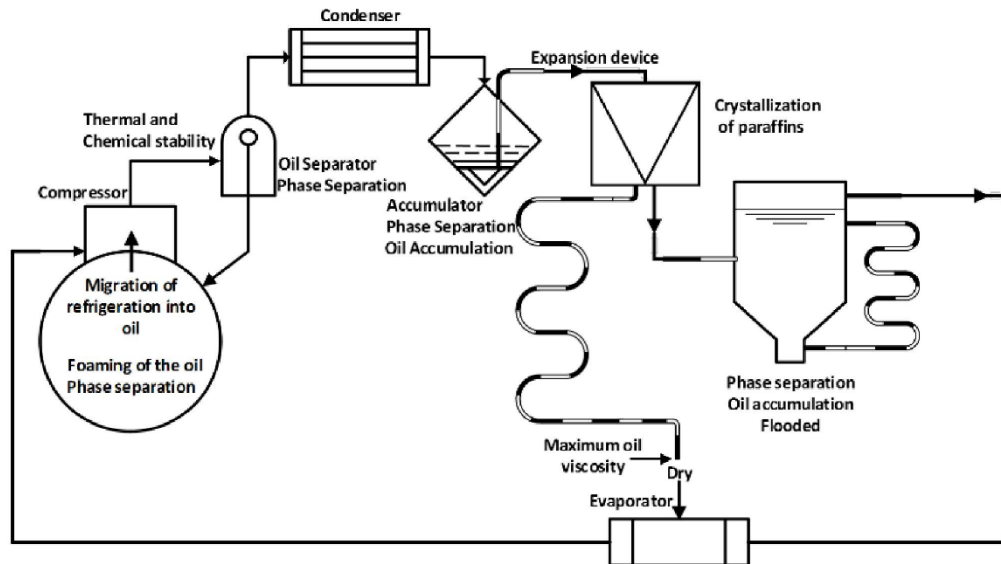

Fig. 1. Oil in a refrigerating system [2].

23

This [2] project was based on the study of the effects of the refrigerant on the oil density and oil viscosity. An oil having kinematic viscosity at $40\,°C$, $405\ mm^2\ s^{-1}$; density at $15\,°C$, $0.853\ g\ cm^{-3}$; flash point, $285\,°C$; pour point, $-43\,°C$ was used. The viscosities of pure CFC-12 with oil and pure CFC-114 with oil using pressure-proofed rolling ball viscometer were measured. The results showed a straight line relationship between the kinematic viscosity and temperature. CFC-114/oil mixture showed a lower viscosity compared to CFC-12/oil mixture. The viscosity of the oil/refrigerant mixtures decreases in both cases with increase in temperature, and also with increase in refrigerant concentration in oil. The viscosity of the lubricant has a direct impact on the lubricant film thickness which effects friction and wear. This study also compared their measured values with previously developed analytical equations and empirical relationships for calculating the viscosity and density.

A reciprocating semi-hermetic compressor, die cast aluminum connecting rod, cast iron piston, gray cast iron crank shaft, hardened steel wrist pin and steel-backed bronze main bearing was chosen for investigation by [14]. This study was done at five different conditions representing start/stop, high-compression ratio, normal load, high load and flooded start conditions. The purpose of the study was to evaluate the performance of CFC-12/mineral oil and its comparison to HFC-134a/synthetic oil. Nine different synthetic oils were used in this study with HFC-134a. All the synthetic oil combinations with HFC-134a showed wrist pin distress. CFC-12/mineral oil testing resulted in no connecting rod wear at the wrist pin probably due to the fact that CFCs form protective surface coatings on the interacting surfaces.

The tribological characteristics of the critical contacts in a rolling piston, in a swash plate and a reciprocating compressor have been studied by using a high pressure tribometer [4]. The critical contacts investigated in this study were the vane-piston contact in the rolling piston type compressor, the wrist pin bearing contact in the reciprocating piston type compressor and the shoe-plate contact in the swash plate type compressor. These three geometries represent counterformal, conformal and area contacts respectively. The vane-piston contact was

simulated by a stationary hardened tool steel pin rubbing against an oscillating hardened cast iron plate. The wrist pin-bearing contact was simulated by a stationary case-hardened mild steel pin rubbing against an oscillating aluminum pad. Finally, the shoe-plate contact was simulated by a stationary circular bronze shoe rubbing against a rotating hardened ductile cast iron plate. This study used CFC-12/mineral oil and HFC-134a/synthetic oil mixtures. Their results of area contact showing the wear are presented in Fig. 2. CFC-12 chemically reacted with the bronze shoe producing $CuCl_2$ and very small amount of ZnF_2 as surface films. These films help lowering the wear by protecting the surface. Such phenomenon was not observed in the case of HFC-134a and it showed higher wear and friction. Similar wear results were observed for the counterformal and conformal contacts as CFC-12 produced $FeCl_2$ with iron. Friction is a complex phenomenon and occurs at the interface of two components in relative motion [25]. The results for the coefficient of friction for counterformal and conformal contacts of HFC-134a were found to be comparable to CFC-12.
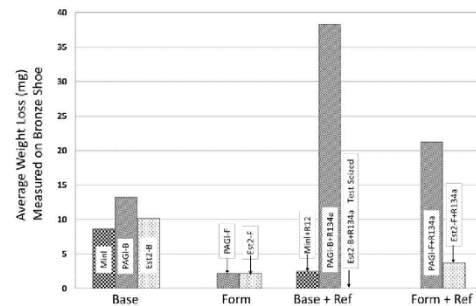
Fig. 2. Area contact wear results [4].

The miscibility of various synthetic oils was studied with HFC-134a and the lubricity of CFC-12 was compared to HFC-134a by [16]. It was concluded that oils used with CFC-12 require very few or no additives. Due to the fact that HFCs lack the ability to form protective surface films under normal compressor operating conditions, oils to be used with HFC-134a require various combinations of additives to improve performance.

A high pressure tribometer was used by [26] to experimentally investigate the wear and friction characteristics of the vane-piston contact of a

24

rolling piston compressor. Cast iron piston running against M2 tool steel was the material pair studied. Different surface treatments for M2 steel were evaluated. Hardened steel samples were tested against gas, ion, and liquid nitrided, as well as boronized and TiN coated specimens. Using polyolester and alkylbenzene oils as lubricants, friction and wear were evaluated in HFC-134a, CFC-l2, argon, and air environments. The results of the study indicated that the diffusion processes, namely; liquid nitriding, ion nitriding, and boronizing did not offer any tribological benefits over hardened M2 steel under the conditions studied. Chemical vapor deposition (CVD) used to deposit TiN coatings lowered the wear magnitude than the other surface treatments because CVD process produces a smoother surface with more rounded asperities. The coefficient of friction and wear depth on the surface was higher with the TiN coated samples as compared with the other surface treatments. This was due to the sharp and very hard asperities formed by the CVD process. Figure 3 shows the results of the pin wear with respect to the testing environment. The results in Fig. 3 also show that the least amount of wear occurred in the case of refrigerant CFC-12 irrespective of the surface treatment.
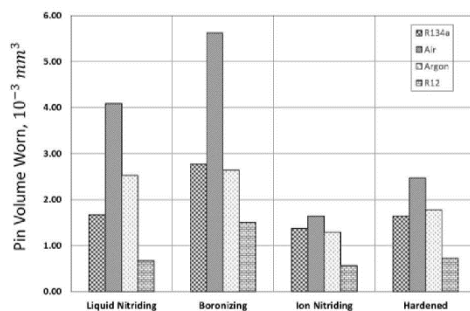

Fig. 3. Effect of test environment on pin wear [26].

Wear and friction characteristics in refrigerant environment with and without lubricants were investigated by [6]. A ring-on-disk apparatus was used in their experiments. The ring used was made of cast iron while the disk was made of leaded bronze. CFC-12 and HFC-134a along with nitrogen gas were investigated with and without synthetic lubricants. Figure 4 shows the comparison of wear rates and the friction coefficient obtained in this study.
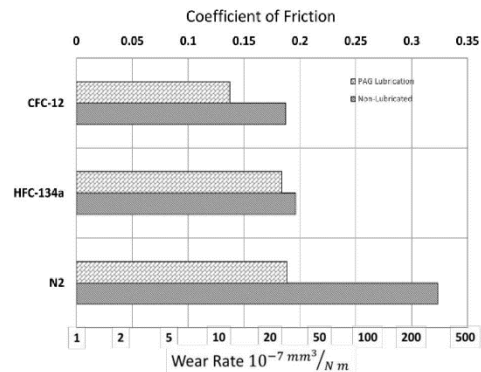

Fig. 4. Comparison of friction coefficients and wear rates in different gases with and without lubricant [6].

CFC-12 showed the lowest wear and the lowest coefficient of friction with and without the lubricant. In this study chlorine was detected on the bronze surface but not on the iron surface. Bronze also experienced more wear than the iron surface which suggested that exposure of an active fresh surface was necessary for the formation of a chloride layer. Another explanation could be that under the given conditions chlorine reacted more readily with the lead in bronze as compared to iron. The formation of a surface film gives CFC-12 Extreme Pressure properties. The difference between the wear of HFC-134a when tested with and without the lubricant is not as significant as compared to CFC-12 and nitrogen. Surface analysis of the samples tested under HFC-134a atmosphere without the lubricant revealed the presence of metal fluorides on the surface. This showed that HFC-134a also decomposed to form fluoride layers when used under more severe conditions, such as when running it without any lubricant.

A specialized optical interferometry equipment to investigate the film-forming capability of refrigeration lubricants was developed by [7]. Their results showed that CFC-12 had a better ability to form a film as compared to HFC-134a at elevated temperatures.

Roller steel bearings were used in a Shell Four Ball Test to study dry friction [8]. CFC-12, HCFC-22, HFC-32, HFC-125, HFC-134a, and nitrogen gas were used in this study without any lubricant. Seizure loads were studied, CFC-12 and HCFC-22 that contained chlorine molecules showed the highest seizure load, representing

25

the effect of Extreme Pressure. The HFCs that did not contain chlorine showed the next heaviest seizure load. Surface analysis of the samples tested under HFCs revealed fluorine on the surface. This showed that the fluorine in HFC acted as an Extreme Pressure agent as well.

4. HYDROCHLOROFLUOROCARBONS (HCFCs)

HCFCs were used as refrigerants in freezers, refrigerators and air-conditioning systems. HCFCs structure resembles closely to CFCs, however HCFCs have lower ODP and lower GWP compared to CFCs. The use of HCFCs was allowed for a longer period of time due to their lower environmental impact compared to CFCs. HCFCs were also allowed as intermediate refrigerants while switching from CFCs to HFCs. However, the use of HCFCs in new equipment was banned in 2001 in UK. Amongst HCFCs, HCFC-22 was the most popular one. It was commonly used in process cooling, in automobile air conditioning systems, in small scale industrial units and in domestic refrigerators.

Tribological analysis in rolling piston type compressor using ferrous and nonferrous metals was conducted by [1]. Using HCFC-22, this study analyzed the lubrication conditions of journal bearings and the vane-tip using modified compressors. The results indicated that the scuffing behavior is sensitive to the refrigerant atmosphere. Scuffing is a complex phenomenon in which adhesive wear occurs under particular combinations of lubrication, contact pressure, friction and speed [27]. The scuffing load of the nonferrous metal bearings decreased with increase in refrigerant concentration. The contrary was observed for ferrous metals; with increase in refrigerant concentration the scuffing load increased for ferrous metal bearings. This may be due to the chemical reaction of chlorine with ferrous metals which results in the formation of chloride films on ferrous metals under these operating conditions. The increase in refrigerant concentration increased the chlorine in the system and resulted in the faster and thicker development of chloride films.

Optical interferometry was used [3] to study the effects of refrigerants on the lubrication of rolling bearing element used in screw

compressors. Lubricant film thickness was evaluated with and without refrigerants. Mineral oil was used with HCFC-22 and synthetic oil was used with HFC-134a. The study concluded that the mechanism of lubrication of rolling element bearings operating in the presence of oil-refrigerant solutions is similar to that for oil only. The refrigerants reduced the lubricants viscosity as well as the lubricants pressure-viscosity coefficient. This study also used the equations presented by Hamrock and Dowson [28] to theoretically calculate the values of the central film thickness and compared them to their experimental results.

Lubrication of screw compressor bearings in the presence of HCFC-22 and HCF-134a was studied by [5]. Experiments were performed to determine the properties of some alternative compressor lubricants in bearing test machines. Tests included a ball bearing test, a taper roller bearing flange contact test and a test with sets of angular contact ball bearings. Different loads were used to study how the behavior of the refrigerant-lubricant mixture changes during the flow through a set of three bearings in each direction. The results showed that the compressors can be treated by elastohydrodynamic lubrication theory only when the refrigerant-lubricant is in equilibrium with the temperature and pressure at the bearing surfaces with fully-flooded conditions.

Tribological behavior using block-on-ring apparatus for polyolester base oil and formulated oils in HFCs and HCFCs refrigerant environment was evaluated by [17]. The ring was made of nickel chromium molybdenum steel and the block was made of tool steel. HFC-134a, HFC-407C, HFC-404A and HCFC-22 were used in this study. HCFC-22 gave the best performance due to the ability of HCFCs to form protective surface films on the interacting surfaces. Different additives were used in the lubricants with HFCs to match their performance to HCFC-22. Sulfur-phosphorus type additive together with aryl phosphate in HFC environment showed performance comparable to that of formulated alkylbenzene in HCFC-22.

Various HFCs and HCFC-22 were used by [18] to study; the hydrolytic stability, thermal stability, moisture removal effect, endurance of compressors and the endurance of refrigeration

26

systems. This study concluded that alpha-branched acid rich polyester is most suitable for HCFC-22 and HFCs.

In the research done by [20] it was stated that because HFCs produce no Extreme Pressure effect in comparison to HCFCs, HFC-134a/oil mixtures require typically 50 % higher viscosity compared to HCFC-22/oil mixtures for the same wear rate. The conducted experiments investigated the possibility to increase oil concentration in the bearings for better lubrication. The conclusion of this study was to decrease flow rate of the oil-refrigerant mixture to get good bearing lubrication.

An interferometric Elastohydrodynamic (EHD) tester equipped with a pressurized vessel was used [29] to investigate the EHD film-forming characteristics of several oils with a number of refrigerants. The refrigerants used in this study were CFC-12, HCFC-22 and HFC-134a respectively. A ball-on-disk apparatus comprising of optical interferometry equipment to monitor and measure the oil film thickness was used in this study. Hamrock-Dawson's equations [28] were also used in this study to compare the experimental results with theoretical calculations. It was concluded that the EHD film thickness formed by oil/refrigerant mixture is the same as that of oil itself and increasing the amount of dissolved refrigerant in oil reduces not only the viscosity, but also the viscosity-pressure coefficient of oil.

A high pressure chamber capable of liquefying refrigerants was used by [30] to investigate the high pressure effects on HFC-245fa, HFC-134a and HCFC-123. The purpose of this study was to see the performance of these refrigerants as lubricants without using any oil. This was to look into the possibility of making compressors oil free. The refrigerants were liquefied and their share stresses were measured. Compared to HFC-134a and HCFC-123, HFC-245fa showed a smaller decrease in share strength with share rate. This study concluded that HFC-245fa has better mechanical properties and can be considered for bearing lubrication without any oil.

To study the compressibility of oil/refrigerant lubricants in elastohydrodynamic contacts a high pressure tribometer was used [31]. This study included mineral oils, synthetic oils, HCFC-

22 and HFC-134a. The study concluded that stiffness of the lubricating oils increases more with HFC-134a as compared to HCFC-22.

A bearing test rig was designed and equipped with a capacitance measuring device to study the bearing on-line lubrication status [32]. HCFC-22 and HFC-134a were used as refrigerants along with lubricating oils. The metal to metal contacts were counted and the microscope analysis of the samples was done post testing. The study showed that there were more metal to metal contacts in the case of HFC-134a as compared to HCFC-22. The chlorine in HCFC-22 showed Extreme Pressure effects in comparison to HFC-134a which did not produce any Extreme Pressure effects and does not have chlorine in its molecular structure. Resultantly HFC-134a showed more wear in contrast to HCFC-22.

A modeling and experimental assessment of HCFC-123 for lubricating rolling elastohydrodynamic (EHD) circular contacts was performed by [33]. Their results revealed that refrigerants indeed can build up a satisfactory film thickness for lubricating EHD rolling point contacts. Their study used full numerical models developed by [34-36], analytical elastohydrodynamic film-thickness expressions developed by [37, 38] and experimental work. Their experiments were performed using a ball-on-disk tribometer equipped with an interferometry facility to measure the film thickness under pure rolling conditions.

5. HYDROFLUOROCARBONS (HFCs)

HFCs are synthetically produced refrigerants containing hydrogen, fluorine and carbon. HFCs were introduced after the Montreal Protocol. The Montreal Protocol which focused primarily on the reasons for the depletion of the ozone layer put restrictions and bans on the production and use of CFCs and HCFCs. HFCs had thermodynamic properties matching their predecessors [11-13, 39, 40], which resulted in their extensive use as replacement refrigerants. HFCs started being widely used as coolants instead. Since the early 1990s, HFCs have been widely used in a number of different fields and applications. The global warming implications of HFCs were not considered at the time of their introduction, however the high global warming

27

impact of HFCs was realized later. Kyoto Protocol addressed the damaged being done to the global atmosphere and the responsible attributes and chemicals causing global warming. A restriction was put on HFCs and HFCs are now in the process of being phased out. The phase out of HFCs started in 2015 in Europe. By the end of 2030 it is expected that HFC availability will be cut by 79 % in Europe.

HFCs remain the most investigated refrigerants from the tribological view point. This is because of their unique position in history. HFCs were initially compared to their predecessors to see how they performed compared to CFCs and HCFCs. A number of studies showed that HCFCs and CFCs have better tribological performance as compared to HFCs especially while being operated in a compressor atmosphere. Various additives and different blends of synthetic oils were developed and investigated to improve the performance of HFCs over the years. CFCs and HCFCs were used as a benchmark to analyze HFCs. After being introduced in the market on a commercial scale, further studies were still conducted on HFCs to look at their behavior under various different operating conditions. Now a days the potential successors of HFCs are being compared with HFCs to evaluate their performance. Most of the new studies involve the use of future generation refrigerants and HFCs. This helps making a comparison between the various refrigerants under identical operating/testing conditions.

Amongst the HFC refrigerants, 1,1, 1,2-tetrafluoroethane (HFC-134a) has been the most tested and investigated refrigerant from the view point of tribology. This is because HFC-134a was deployed for systems that previously used CFCs and HCFCs. A number of studies involving HFCs are discussed below. HFCs are also discussed alongside CFCs, HCFCs, natural and future generation refrigerants.

A pin-on-disk and a ball-on-disk configuration was used [41] in a test rig designed to simulate the conditions of a compressor. The purpose of this investigation was to study various refrigerant oils under HFC-134a environment and compare them to CFC-12. Mineral oils, alkylbenzenes, and polyalpha olefins tested immiscible with HFC-134a. However ester oils and PAG were miscible with HFC-134a. This study suggested that ester oils are preferable at

start and stop conditions. PAG demonstrated good lubricity in extreme pressure conditions and HFC-134a/PAG mixture showed friction coefficient similar to CFC-12/mineral oil. PAG increased friction considerably under boundary lubrication, however CFC-12/mineral oil and HFC-134a/ester oil indicated good lubricity in that condition. Easter oil/HFC-134a showed highly unstable friction behavior due to the lack of extreme pressure durability. PAG on the other hand has extreme pressure enhancement and produced a stable lubricating film by the chemical reaction of metal surfaces in the presence of HFC-134a environment.

Bearing steel ball and bearing steel plate were used by [42] in a reciprocating test rig to investigate the friction and wear characteristics of polyalkylene glycol (PAG) and a polyol ester (POE) oils. The behaviors of these oils along with the effect of additives were examined in HFC-134a environment. Additives improved the friction and wear performance in both the lubricants. PAG showed good wear and friction characteristics in HFC-134a environment by forming fluoride on the rubbing surfaces. POE displayed poorer friction and wear characteristics above a transit temperature because an adsorbed POE film prevented the formation of fluoride. However POE produced very good tribological performance at temperatures below the transient temperature. TCP significantly improved the tribological performance of PAG due to the adsorption film of TCP in low temperature range and formation of phosphate in high temperature range. TCP did not improve the friction and wear characteristics of POE because POE prevented the adsorption of TCP on the rubbing surfaces. MoDTC with POE in HFC-134a environment lowered the friction coefficient by forming MoS_2 in spite of no oxygen in the environment below the transient temperature. Friction characteristics of PAG were not improved with the addition of MoDTC as no MoS_2 was formed with PAG in HFC-134a environment.

A sealed block-on-ring wear tester was used [43] to experimentally investigate the tribological characteristics of various lubricating oils under HFC-134a environment. The lubricants used were linear polyolesters (L-POE), branched polyolesters (HS-POE), polyvinylethers (PVE) and polyalkylene glycols (PAG). PAG and PVE displayed better anti-

28

wear performance compared to linear and branched POE under boundary lubrication conditions. POE produced carboxylic compounds under boundary lubrication. These compounds were produced by POE's reaction with iron. These reactions occur due to the $C = O$ bond present in POE. These compounds are easily removed by rubbing from the friction surface. PVE and PAG have no $C = O$ bonds which explains why POE showed significant wear in comparison to PVE and PAG. PVE has higher resistance to breakdown under shear stress and has the ability to form a thick oil film in elastohydrodynamic lubrication region, this protects the rubbing surfaces from scuffing and wear.

A domestic compressor test-rig was manufactured by [44] to study the wear behavior of piston/gudgeon pin by using HFC-134a in hermetic compressors. Different synthetic lubricants were used with HFC-134a in this study. The results showed that higher viscosity lubricants produced minimum plastic deformation. Higher the viscosity higher is the film thickness resulting in lesser asperity interactions resulting in lower wear.

Refrigerant/lubricant mixtures were tested against: aluminum alloys, surface treated 356 aluminum alloy and an aluminum composite [45, 46]. Pin-on-disk line contact geometry was used in this study in which the pin was composed of carburized steel and the disk was of aluminum based materials. The study was divided in two parts. The first part consisted of aluminum/steel contacts lubricated by HFC-134a/polyester oil and HFC-134a/polyalkylene glycol oil mixtures. Amongst the aluminum alloys tested, 390-T6 die cast alloy showed the best wear resistance because it had the highest hardness. Due to the fact that SiC particle reinforcement provide very good wear resistance, the amount of wear decreased with increasing silicon content in aluminum alloys [47]. The wear resistance was not improved by conventional anodizing techniques of the 356 aluminum alloy because the hard layers cracked under high contact stress causing an increase in wear. Good wear resistance was observed in hard anodizing of 356, however it increased the wear on the counter face. In comparison to the PAG/HFC-134a mixtures, Ester/HFC-134a mixtures provided better protection of the aluminum alloys due to the ability of the esters to form

bidentate bonds with aluminum. Increased amount of HFC-134a showed extensive surface fatigue on 356 aluminum. In the second part of the study, 390-T61 and 356-T61 aluminum alloys were tested in various refrigerant/lubricant mixtures. HFC-134a, HFC-407C, HFC-410A and HCFC-22 refrigerants were used with different lubricants. No significant difference in lubricity of alkylbenzene and mineral lubricants when used with HCFC-22, HFC-407C and HFC-410A was observed. This study also showed that at sufficiently high partial pressures, HFCs chemically react with the freshly exposed aluminum and increase the brittleness of aluminum alloys.

A pin-on-disk setup was used [48] to study the lubricity of HFC refrigerant oils in a scroll compressor. This study involved the use of HCFC-22, HFC-407C, mineral oil and polyvinylether (PVE) oil. Two types of aluminum alloys against cast iron were used in this study. The results showed that there was a noticeable difference in the wear amounts of HCFC-22/mineral oil and HFC-407C/PVE. The effect on wear of increasing the silicon content in the aluminum alloys showed that it was possible for HFC-407C/PVE to have wear as low as HCFC-22/mineral oil. Silicon content largely influences the anti-wear performance by suppressing wear in aluminum alloys.

Table 2. Properties of various coatings and vane material [49].

Vane	Hardness (Hv)	Deposition method
Original	950	-
TiN(I)	1900	Arc ion plating
TiN(II)	1600–1800	RF magnetron sputtering
TiAlN	2700	Arc ion plating
WC/C	1000	Magnetron sputtering
DLC	2000	Dual ion beam sputtering
Carbon vane	458	-
Ion nitriding	1150	Pulse plasma nitriding

A vane-on-disk setup comprising of Ni–Cr–Mo gray cast iron disks and vanes comprising of various coatings and materials was used [49] to study the tribological characteristics of HFC refrigerants in rotary compressors. Table 2 shows the various coatings and vane materials used in this study. The surface roughness and

29

the coating thickness values have not been mentioned in this table, these values can be seen in the original table given in [49]. Tests were conducted using HFC-407C refrigerant with and without POE oil. One the results for wear obtained without using lubricant and by using the refrigerant only is shown in Fig. 5.
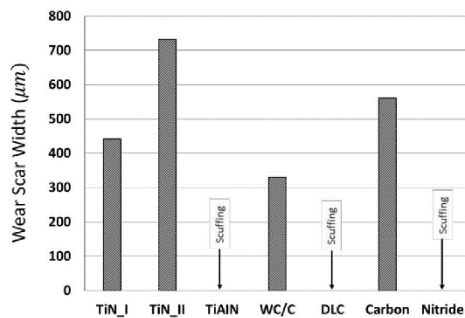

Fig.5. Wear scar width in HFC-407C only, tested in normal load of 440 N, speed of 70 rpm, 20 °C and test duration of 1 h [49].

Based on the results obtained in this study, the conclusions were that TiAlN (titanium aluminium nitride) and DLC (diamond-like carbon) are very hard coatings and are not suitable, because they produced high friction and severe wear on the roller. Good wear resistance was shown by TiN coated vane. Ion plating showed lesser wear compared to magnetron sputtering. Ion nitriding proved unsuitable as it was not good enough to sustain the cyclic stress. WC/C (tungsten carbon carbide) coating showed the best tribological performance which was probably due to the formation of a durable tribo-film on the mating surfaces.

Three different types of ester oils were used by [50] with HFC-134a to study the impact of lubricant viscosity on the wear of hermetic compressor components. Tribological behavior of the conforming contact between hardened steel gudgeon pin and die-cast aluminum alloy connecting rod of a reciprocating compressor were investigated. The conclusion was that the lubricant viscosity plays a major role in governing the tribological properties of the system. Low viscosity lubricants resulted in boundary lubrication regime which produced high friction, severe wear and material transfer. Increase in the lubricants viscosity shifted the

system towards the mixed lubrication regime which improved the wear and friction of the system.

A shoe-on-disc geometry to simulate the plate/shoe contacts in a swashplate automotive air conditioning compressor was used in an experimental study conducted by [51]. Starved lubrication conditions were used to study the scuffing characteristics of 52100 steel against 390-T6 aluminum–silicon alloy. All tests were conducted with HFC-134a and PAG lubricant in a high-pressure tribometer. Four different shoe geometries were used to study the effects of sliding velocity, degree of lubrication starvation, contact geometry, skewness, surface roughness and the effect of a tin coating on scuffing. Crowning is used to help the shoe/plate contact generate hydrodynamic films, a perfectly flat and smooth shoe supported at its geometrical center theoretically is unable to generate these films. The groove or dimple helps trap lubricant and debris during operation. However the groove or dimple can be detrimental under starved lubrication conditions. In starved lubrication conditions the lubricant supplied is not sufficient for a groove or dimple to act as an effective reservoir. Scuffing results of 390-T6 Al on the crowned shoe, crowned shoe with dimple and crowned shoe with groove are shown is Fig. 6. The geometries with a dimple or groove in the crowned shoe resulted in higher peek pressures and temperatures.
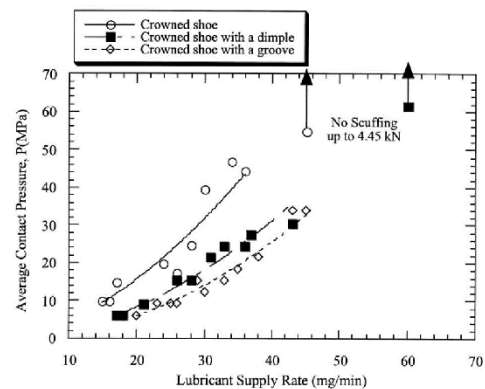

Fig. 6. Scuffing results for 390-T6 Al obtained with various crowned shoes. Sliding velocity: 1.86 $^m/_s$ [51].

The influence of surface roughness on scuffing was studied using 390-T6 aluminum discs with

three different values of surface roughness against crowned shoes. The results of the effects of change in surface roughness on the coefficient of friction and friction force are shown in figures 7 (a) and 7 (b) respectively.
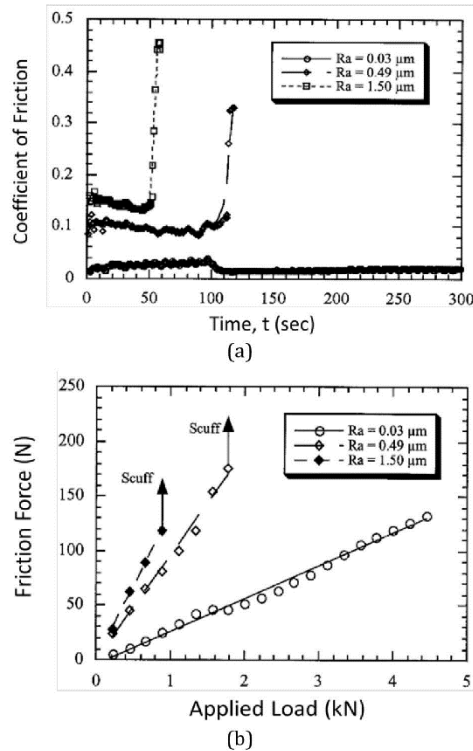

Fig. 7. Variation of coefficient of friction and friction force for different surface roughness. Lubricant supply rate: 40 mg/min; sliding velocity: 1.86 m/s. (a) Coefficient of friction, (b) Friction force [51].

Improved surface finish having lower surface roughness gave a lower value of the coefficient of friction and the friction force. The results of the scuffing resistance with change in the lubricant supply rate at various sliding velocities showed that for a given lubricant supply rate, the scuffing pressure decreases with increase in the sliding velocity, higher sliding velocities result in higher lubricant entrainment and an increase in the lubricant film thickness. No apparent effect was observed by changing the skewness in this study. The effect of tin coatings showed that coated discs offer better scuffing resistance than the uncoated discs. This is due to the low shear strength characteristics of tin. The conformity of

the sliding surfaces is increased by tin, because tin deforms quickly and results in lower local temperatures and pressures. Tin coating acted as a temporary lubricant and also aided initial running-in by covering surface irregularities.

Using a ball-on-disk apparatus the lubrication of rolling element bearing with HFC was studied by [52]. Viscosity, pressure–viscosity, and the film thickness data for three polyolester oils was studied and it was concluded that branched lubricants give the benefit of a higher pressure–viscosity coefficient under normal conditions. However a branched lubricant is more susceptible to dilution by the refrigerant compared to a linear lubricant. To obtain maximum effectiveness, the lubricant should be formulated with as little branched acids as possible.

The solubility, viscosity and oil film thickness of HFC-134a, HFC-125 and HCFC-22 were studied with POE by using a ball-on-disk apparatus [53]. Increase in gas pressure increased the solubility of the refrigerant in the lubricant. HCFC-22 showed the highest solubility and HFC-125 revealed to be the least soluble refrigerant in POE. This resulted in HFC-125 having the highest film thickness and HCFC-22 having the least film thickness. The results of the influence of the gas pressure on the film thickness showed that the oil film thickness decreases with increasing gas pressure. The solubility of the refrigerants in the lubricating oil increases with increasing gas pressure, the increased solubility of refrigerants decreases the lubricants viscosity which results in lowering of the film thickness. HCFC-22 displayed the highest decrease in the oil film thickness and HFC-125 displayed the least decrease in the oil film thickness by increasing the gas pressure. The film thickness increased with increasing rolling speed due to higher lubricant entrainment.

Experimental investigation using hermetically sealed refrigerating compressors to compare the tribological performance of PVE lubricants to POE lubricants using HFC-134a was done by [54]. Their investigation included the study of the conformal contacts between the small end of the connecting rod and the gudgeon pin as well as observing the compressor vane plates and the large end of the connecting rod. No clear difference was seen in the tribological performance of PVE and POE lubricants under the tested conditions.

31

A number of fluorinated alkyl aryl ethers were evaluated by [55] as refrigerant lubricants with HFC-134a. The fluorinated alkyl aryl ethers showed high miscibility with HFC-134a along with high stability, very good lubricity, and low moisture absorption.

A case study to evaluate the overall influence of HFCs compared to CFCs on the environment was done by [56]. Factors like the contribution of the individual compressor components to human toxicity, the contribution of the individual compressor components to acidification, the electricity consumption to make the individual components of a compressor, etc. were discussed in this study. A comparison on the overall effects of CFC compressors was made to the overall environmental effects of HFC compressors. Although CFCs are labelled as being more harmful to the atmosphere [57], it was indicated by this study that CFC systems would have a lower impact on the environment as compared to HFC systems keeping in view the complete life cycle of each individual component of a compressor from material extraction, to fabrication to disposal.

A reciprocating ball-on-disk apparatus was used [58] to investigate the effects of HFC-134a on the solubility, viscosity and lubricant film thickness with PAG, POE and PVE oils. The study concluded that the dissolving of HFC-134a in the lubricants is an exothermic reaction. The dissolution of HFC-134a in the lubricants worsened the wear characteristics of lubricants by reducing their viscosity. The mean molecular weights of the lubricants also effected the viscosity. There was a decrease in viscosity reduction with an increase in the ratio of the HFC-134a solubility to the mean molecular weight of the lubricant.

HFC-125, HFC-134a and HCFC-22 were used with POE lubricant by [59] to study the rheological properties of polyolester oil under elastohydrodynamic (EHD) contact conditions in refrigerant environments. Analytical work as well as experimentation involving a ball-on-disk EHD tester were used in this study. The results of the coefficient of traction of the refrigerants at two different gas pressures with respect to the slide roll ratio are shown in Figs. 8(a) and 8(b) respectively. HFC-125 showed the highest coefficient of traction and HCFC-22 showed the lowest coefficient of traction. The values of the coefficient of traction decreased with an increase in the gas pressure. The effect on the effective viscosity-pressure coefficient and the effect on the representative stress with change in the gas pressure of all three refrigerants showed that, the values of the effective viscosity-pressure coefficient decreases while the value of the representative stress increases with increasing gas pressure. The results of the viscous volume with the molecular volume of the mixture are shown in Fig. 9. The results shown in Fig. 9 indicated that the relation of the viscous volume with the molecular volume can be represented by a single line irrespective of the refrigerants.
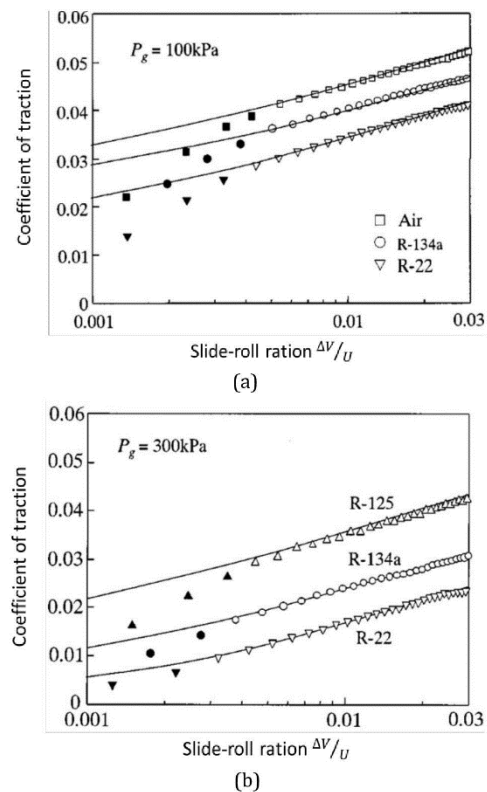

Fig. 8. Traction curves in some refrigeration environment. Solid lines are the calculated results based on the work described in [60] and the symbols are the measure data (a) at gas pressure of 100 kPa, (b) at gas pressure of 300 kPa [59].

It was also concluded by [59] that the POE characteristics in refrigerant gases are governed primarily by the pressure-viscosity coefficient.
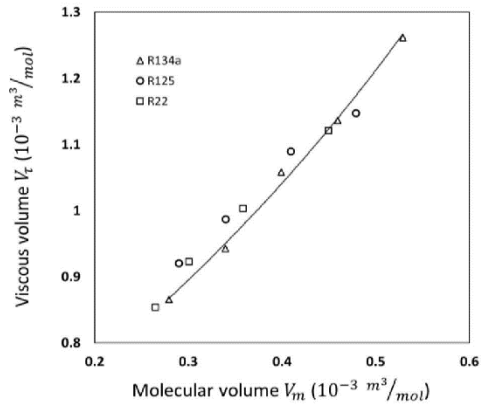
32

Fig. 9 Viscous volume versus molecular volume of refrigerant/POE mixture [59].

The elastohydrodynamic lubrication film in the presence of HFC-134a and POE lubricant was studied by [61]. This work involved the use of a ball-on-disk apparatus along with the use of analytical equations developed by [62] and [63]. The results of this study showed that a decrease in refrigerant concentration at the inlet region increased the elastohydrodynamic lubrication film thickness, decrease in refrigerant concentration increases the oil's viscosity increasing the film thickness. The concentration distribution of HFC-134a got affected by the oil temperature, the sliding velocity and the refrigerant concentration in the lubricant.

A pin-on-disk high pressure tribometer consisting of Al390-T6 discs and 52100 steel pins was used to investigate the effects of surface roughness of engineering surfaces by using HFC-410A and POE oil [64]. Factors like core fluid retention index, bearing area ratio, bearing ratio, surface roughness, skewness and kurtosis were studied. Highly negative skewness was observed in the mildly-worn surfaces supporting the theory that mildly worn asperities result in a more negatively skewed surface by revealing lesser peaks than valleys and pits. Change in kurtosis did not give any significant results. This study also concluded that the functional parameters or indices derived from bearing area curve, namely the fluid retention index and the surface bearing index can be used to draw sound conclusions of the tribological progression of roughness. The functional indices remained almost constant on the virgin surfaces, but with the surface approaching scuffing, the effects of progressive

wear related to increased bearing index and a decreased fluid retention capability were observed.

In continuation of their [56] previous case study, an experimental test rig was built to monitor slight variations in the electrical power consumption by a reciprocating hermetic compressor [65]. The purpose of this investigation was to study the environmental impacts of a domestic refrigerator. The tribological characteristics of the aluminum alloy connecting rod and the steel gudgeon pin were also studied using CFC-12/mineral oil and HFC-134a/different synthetic lubricants. Furthermore, a comprehensive life cycle assessment on a domestic refrigerator was done to help quantify the environmental burdens. The experimental results showed that overall there was more damage to the parts in HFC-134a environment than that obtained from the CFC-12 tests. The electrical energy consumption when using CFC-12 was thus found to be substantially less as compared to HFC-134a. A four-ball test was done on oil samples before and after being tested in the compressor, the Extreme Pressure performance of a synthetic lubricant was observed to deteriorate more than that of mineral oil. Based on these results, this study concluded that HFC-134a based domestic refrigerators will contribute more towards the environmental damage as compared to CFC-12 based domestic refrigerators.

HFC-410A was used with POE lubricant to study the friction and wear of rotary compressor vane-roller surfaces using a vane-on-disk setup [66]. The disk was made of Ni–Co–Mo gray cast iron and a TiN coating using physical vapor deposition technique was applied to the vane made of high speed tool steel. Tests were conducted at different normal loads and speeds. A few of the results obtained in this study are shown in Fig. 10. TiN coatings improve the tribological characteristics of sliding surfaces which resulted in the better performance of the TiN coated samples as compared to the uncoated ones. The coefficient of friction as well as the wear on TiN coated samples was less as compared to the uncoated samples. The difference in the performance of the coated and the uncoated samples became more apparent with an increase in normal load and an increase in RPM. Effect of surface roughness was also

33

studied by including TiN coatings of three different surface roughness in this investigation. The results of the effect of the surface roughness are shown in Fig. 11. Based on these results it was concluded that there exists an optimum initial surface roughness value which improves the load carrying ability and prolongs the wear life of interacting surfaces.
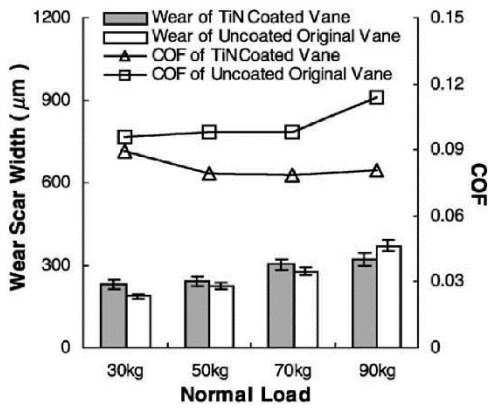
(a) 100 rpm
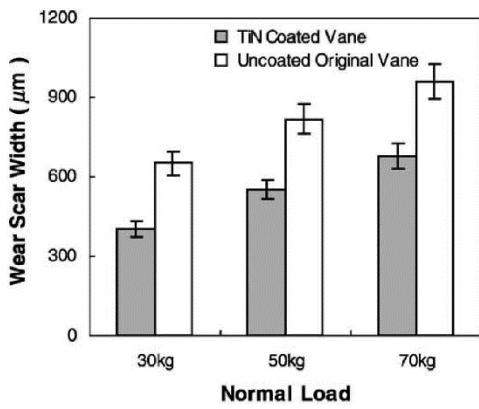
(b) 500 rpm

Fig. 10. Wear scar width of the vane tip under various normal loads and sliding speeds [66].

Employing ten different polymers as potential bearing materials, six blended polymers and four unfilled polymers; a high pressure pin-on-disk tribometer was used to examine the tribological performance of polymer/metal contacts under HFC-134a environment [67]. The disks were made of cast iron and aluminum alloys and pins were made of the various polymers. It was concluded that overall all the blended polymers have superior tribological properties compared to unfilled polymers and metals.
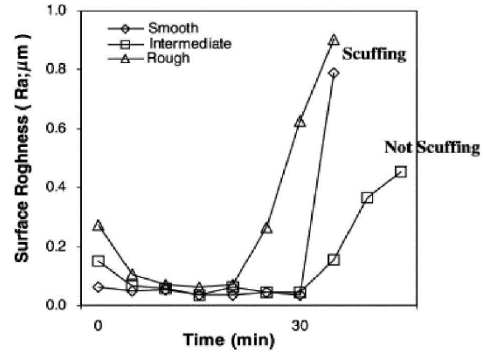

Fig. 11. Changes of surface roughness depending on the initial surface roughness [66].

A pin-on-disk apparatus comprising of gray cast iron disks and pins made of composites of different blends of polytetrafluoroethylene (PTFE) with aromatic thermosetting polyester (ATSP) under HFC-134a refrigerant were investigated by [68]. Controlled tribological experiments simulating an air conditioning compressor environment using ATSP/PTFE compositions, as well as four dissimilar commercially available composites containing graphite, carbon fibers, and PTFE were used. It was found that the newly synthesized composites showed very good tribological properties having very low friction and wear. ATSP did not significantly change the friction coefficient while it was shown that greater amounts of ATSP used in the blend lead to lower wear. However, lower friction coefficient values were obtained with increasing amounts of PTFE due to material transfer and development of a transfer film on the disk surface.

A shoe-on-disk setup in a high pressure tribometer was used [69] to investigate the tribological behavior of PEEK, PTFE and Fluorocarbon based polymeric coatings in HFC-134a environment for use in air-conditioning and refrigeration compressors. The shoe and pin were made of 52100 steel while the disk was made of cast iron and coated with different polymeric coatings. The experimental results indicated that in comparison to the other polymeric coatings, PEEK/PTFE coating performed slightly better in terms of wear and

34

friction. In spite of the aggressive tribological conditions, the transfer of films from the disk coating to the 52100 steel shoes enabled the interface to operate without overheating.

Another study involving the tribological investigation of four different polymer based coatings for air-conditioning and refrigeration compressors was done [70]. A high pressure pin-on-disk tribometer with HFC-134a was used. It was found that compared to other coatings, in terms of the tribological performance, PEEK/PTFE coating performed better. This enhanced performance is associated with the arrangement of polymers in PEEK/PTFE coatings. PEEK is positioned below which provides wear resistance and strength and is responsible for the good adhesion with cast iron. PTFE particles migrate to the top (surface) and are responsible for supplying C_iF_j species to the wear track which contributes to lowering the friction.

Compressor performance in HFC-32 atmosphere was studied by [71]. HFC-32 has zero ozone depleting potential and has a GWP value of only about $^1/_3$ of HFC-410A. A comparison of HFC-32 with HFC-410A using PVE and POE lubricants was done to evaluate the reliability, durability and lubricity of a compressor in these refrigerant atmospheres. The reliability and durability of the compressor was studied by performing drop-in tests using an actual composer and the lubricity was tested using a hermetic block-on-ring test machine. The study revealed that HFC-32 has poor miscibility with conventional oils that are normally used with HFC refrigerants, the viscosity dropped more in case of using HFC-32, HFC-32 decomposed easily and generated organic acids that caused corrosion. New-PVE and New-POE have to be used with HFC-32 instead. Overall HFC-32 refrigerant was difficult to handle, it showed poor stability and generated acids that caused corrosion and abnormal wear of sliding compressor parts.

The tribological performance of PEEK and PTFE-based polymeric coatings with HFC-134a was also done by using a pin-on-disk setup [72]. Both the pin and the disk were made of gray cast iron with the disks being coated with various polymeric coatings. Scuffing experiments and the effect of transfer films was studied. The coatings showed worse performance in the

presence of liquid lubricants than under dry conditions. This was because the formation of transfer films was prevented by lubricants. Under fretting conditions, the tribological performance of polymer coatings was highly influenced by the ability of the polymers to form transfer films on the metal counter face.

A study to investigate the effects of surface roughness on polymer films under unlubricated conditions using a pin-on-disk setup and HFC-134a as refrigerant was done by [73]. Pins made of various polymers were tested under unlubricated unidirectional conditions against gray cast iron disks. Polymer pins having high surface roughness produced discontinuous transfer layers while pins with low surface roughness produced a continuous transfer layer of polymer on the surface of the cast iron.

A new high pressure viscometer that can operate with oil/refrigerant mixtures at elastohydrodynamic lubrication was designed and fabricated by [74]. Various concentrations of HFC-134a were measured with POE oils using this high pressure viscometer.

A block-on-ring tribometer was used [75] to study the tribological characteristics of POE refrigeration oils under HFC-410A and HFC-32 refrigerants. The study concluded that lubricating film formation is affected by both the refrigerants and the base oils. It was found that the TCP in POE lubricant formed a lubricating film on the sliding surfaces under HFC-410A which enhanced the tribological performance. HFC-32 however, interfered with the formation of phosphate films. The high reactivity and polarity of HFC-32 with nascent metal surfaces prevented TCP from adsorbing to the iron on the sliding surfaces.

6. NATURAL REFRIGERANTS

Water, air, carbon dioxide, ammonia and hydrocarbons are considered to be the most environmental friendly and natural occurring refrigerants. Ammonia has been used for a long period of time in large industrial systems as a refrigerant and is still being used in large industrial applications. Water and air have been used as coolants in engineering and domestic applications since ancient times. Air and water

35

are still being used in various applications for cooling purposes, but are not used as refrigerants due to their thermodynamic limitations. Carbon dioxide is also a good refrigerant which sublimes under normal atmospheric temperature and pressure. It has been used for cooling purposes but its utilization in refrigerator compressors is still under investigation. Hydrocarbons are found in crude oil and possess good thermodynamic qualities. Hydrocarbons are being used in commercial, domestic and industrial refrigerators, fridges and heat pumps. Their flammability is however a big concern. Hydrocarbons and carbon dioxide are discussed from a tribological view point in sections 6.1 and 6.2 respectively.

6.1 Hydrocarbons (HCs)

Hydrocarbon refrigerants are nontoxic, natural refrigerants that have zero ozone depleting potential and minimal global warming potential. Hydrocarbons which are extracted from crude oil are environmentally safe and efficient refrigerants. Hydrocarbon refrigerants are considered up to 50 % more efficient thermal conductors than fluorocarbon refrigerants. Hydrocarbons also have lower operating pressures than fluorocarbon refrigerants which results in lower power consumption and cost savings. Many European manufacturers of domestic and commercial refrigeration equipment are using hydrocarbon refrigerants in their compressors. Amongst hydrocarbon refrigerants Isobutane (HC-600a) is found in most domestic freezers and fridges while Propane (HC-290) is used mostly in commercial refrigeration and heat pump applications. The greatest challenge in handling and designing a cooling system based on hydrocarbons is their extremely high flammability. This is why they have not been used as frequently as HFCs and also have not been deployed in automotive air-conditioning systems. This section covers the tribological investigations done by various researchers on hydrocarbons.

A study involving the use of a modified micro-friction pressurized test rig with a pin-on-flat configuration was conducted by [76]. HC-600a and HFC-134a were used as refrigerants with synthetic and minerals oils. Friction and wear tests were performed on aluminum and steel samples. Mineral and synthetic oils with and without various additives were tested using HFC-134a/POE as benchmark. The results showed that the additised mineral oils had very low wear rate and formed a good boundary film. High levels of carbon were found at the pin contact with mineral oil indicating that any boundary layer developed by using mineral oil is more durable than that developed by using POE lubricant. In case of additised POE, deposition was present at the plate but not at the pin. The wear rate was higher in the beginning, which reduced as the contact geometries became more favorable. Initially the contact stresses are high resulting in the removal of any films by abrasive wear causing higher wear rate, the increase in wear scar size with time reduces the contact stresses which gradually enhances the friction and wear performance. This study also looked at the life cycle of HC-600a compressors and compared it to HFC-134a compressors. Extended life economic valuations of annual emissions are given in Table 3. The vales of only 25 years have been presented in Table 3. The values of 15 and 20 years can also be found in the original article [76]. This data implies that the environmental burden is more by using HFC-134a systems than using HC-600a systems.

Table 3. Economic valuation of annual emissions, extended life [76].

Key indicator	HFC-134a	HC-600a
	Year 25	Year 25
GWP	32	16
SO_2	35	13
NO_x	7	3.1
PM10	30	13
Total	105	45

A novel pressurized chamber was designed and manufactured [77, 78] to achieve liquid state of refrigerants. The liquid state of refrigerants was required to perform rolling contact fatigue experiments of silicon nitride/steel bearing materials under the influence of HFC-134a and HC-600a refrigerants. The chamber ensured that the refrigerants achieved saturated liquid state which was important to simulate practical conditions and lubrication film. This was to satisfy the boundary conditions as no lubricants were used. A four ball machine consisting of three steel balls and one ceramic ball was modified to incorporate the chamber and to charge the refrigerants. The system was also vacuumed before charging the refrigerant to minimize the

36

effects of atmosphere and air on the tests. It was concluded that the state of the refrigerant affects the wear and the positioning of the pre-induced crack influences the fatigue life.

Rolling contact fatigue testing with refrigerant as lubricant using liquid state HC-600a refrigerant in the modified four ball machine [77, 78] was done by [79]. The rolling direction influenced the fatigue life. The crack initiation and propagation is a function of the microstructure of materials [80]. With an induced ring crack, the residual stresses were relieved at the crack tip in the element.

The setup [77, 78] was also used by [81] to study the relationship between residual stresses and rolling contact fatigue cycles under liquefied HC-600a at different pressures. Interfacial stress distribution of contact spots is independent of the squeezing pressure [82, 83]. It was observed that there is an inverse relationship between rolling contact fatigue and residual stresses as shown in Fig. 12.
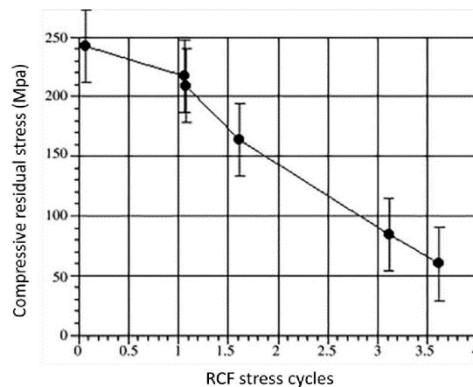

Fig. 12. Compressive residual stress relation to Rolling Contact Fatigue (RCF) stress cycles [83].

The same equipment [77, 78] was used to study; the residual stress relation to the distance from the ring induced crack, the number of stress cycles, the residual stress relation to contact path and the measuring direction [84]. HC-600a was used in liquid state and it was concluded that the compressive residual stresses relieve faster in rolling contact fatigue at elevated contact stress levels. A sub-surface damage in the spall region was observed with reduction in compressive residual stress values.

Controlled pin-on-disk experiments under unlubricated (oil-less) conditions to imitate the wrist pin-connecting rod interface were performed using a High Pressure Tribometer by [85]. Cast iron disks were tested against 52100 steel wrist pins coated with either WC/C or multi-layer WC/C + DLC. HFC-410A, HFC-134a and HC-600a refrigerants were used in this study. HC-600a environment displayed the lowest friction coefficient while HFC-410A environment resulted in the lowest wear. Tests in nitrogen environment were also conducted but the tests resulted in scuffing and the tests had to be stopped. The tribological tests showed that the friction coefficient decreased up to ten times by using coatings. Wear of the pin increases with temperature resulting in the formation of transfer films on the disk from the coating, this caused the steady-state friction coefficient to decrease. The multi-layer coatings have higher hardness which gives these coatings resistance to abrasive wear, this resulted in WC/C + DLC coatings having the least wear. WC/C showed slightly higher friction at lower temperatures, this trend was reversed at higher temperatures.

A pin-on-disk setup comprising of sintered iron disk and 100Cr6 steel pin was used under starved and dry lubrication by [86]. The study involved the investigation of friction and wear performance of 100Cr6/sintered iron pair in HC-600a environment. Sintered iron was treated with and without steam. This study showed that under dry as well as starved lubrication conditions, HC-600a showed adverse effects. In particular for starved lubrication, the wear life of both steam treated sintered steel and untreated sintered steel was reduced to half in the presence of HC-600a compared to air. The increase in wear under HC-600a was thought to be due to change in viscosity and foaming of the oil. Surface analysis also revealed that oxidation under HC-600a was blocked, which caused an increase in weight loss of untreated sintered steel.

Si-rich multifunctional DLC coatings were deposited on 1020 steel and tested against 52100 steel pins using a high pressure pin-on-disk tribometer [87]. Unlubricated friction and wear tests were performed using air, carbon dioxide and HC-600a. HC-600a showed the lowest wear rate and coefficient of friction for both the body and the counter-body. There was a strong presence of graphitic G-band in the

37

spectra of tribolayers formed in the presence of HC-600a which induced its superior tribological performance. The results of the coefficient of friction are shown in Fig. 13.
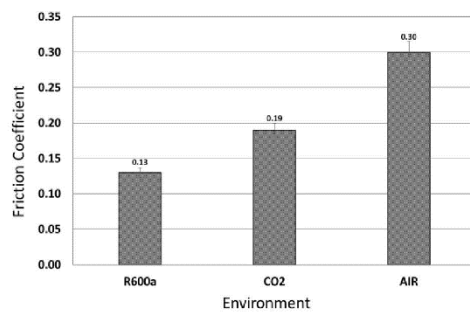

Fig. 13. Average friction coefficient as function of environment [87].

Single-layer WC/C, multilayered WC/C + DLC and TiAlN + WC/C coatings were applied to 52100 steel and Al390-T6 using various contact geometries [88]. The investigation under HC-600a, HFC-134a and HFC-410A atmosphere showed that friction coefficient was the lowest in HC-600a atmosphere while least amount of wear occurred in the case of HFC-410A. HC-600a has the highest percentage of hydrogen atoms per unit volume and hydrogen has a healing effect on hydrogenated DLC coatings in tribological testing, which resulted in lowest friction in HC-600a atmosphere. It was concluded that hard protective coatings offer a great advantage in terms of the tribological performance on interacting surfaces.

A reciprocating ball-on-flat tribometer was used [89] to study the influence of HC-600a and HFC-134a on the friction and wear behavior of multifunctional CrN-Si rich Diamond-like Carbon coatings. The purpose of the study was to investigate the tribo-chemical reactions and the self-lubricating properties of coatings simulating oil-less compressor conditions by using silicon nitride balls against coated flat surfaces. HC-600a presented lower coefficient of friction and lower scuffing durability than HFC-134a. Traces of oxygen were observed in both the cases. Fluorinated compounds were observed on the tribo-layer in the case of HFC-134a. Carbon and silicon were observed in the case of HC-600a. The differences were caused due to the variations in the tribo-chemical reactions caused

between the refrigerant gases, the counter body and the multifunctional coatings. It was recommend by this study to use HC-600a where energy saving is required as HC-600a resulted in lower coefficient of friction while HFC-134a was recommend to be used for increased reliability as it resulted in lower wear.

A block-on-ring tribometer comprising of an aluminum alloy block and gray cast iron ring was used [90] to evaluate the lubricity of oil-refrigerant mixtures. Various mineral and POE lubricants were used with HC-290 and HFC-134a. Due to the adverse effects of refrigerants on lubricants, it was concluded that wear in oil-refrigerant mixtures was considerably higher than in oil alone.

6.2 Carbon dioxide (CO_2)

Carbon dioxide (R-744) is an environmentally friendly refrigerant, having zero ODP and minimal GWP. CO_2 is abundantly available in the atmosphere and it can be collected/recycled from air. Besides being environmentally friendly, CO_2 is nonflammable and is in fact used in fire extinguishers to put out fires. It also has good thermodynamic properties and is suitable for a range of applications including industrial heat extraction, shipping vessels, commercial refrigeration systems, etc. The major difference between R-744 and the other refrigerants is its temperature/pressure characteristic and having a low critical temperature. CO_2 systems require special design and a high pressure to operate. The operating pressure requirements make it unsuitable for automobile and domestic applications. An attempt however is being made to design automotive compressors to operate on CO_2.

A scroll compressor to operate on CO_2 was developed [91] for automotive air-conditioning systems. The operating pressure of CO_2 was much higher as compared to HFC-134a, which resulted in low CO_2 scroll compressor thrust bearing reliability and low efficiency due to the large gas thrust. The study concluded to make the compressor lighter and reliable to contribute to its commercialization.

A study [92] was performed to experimentally investigate the physical and chemical properties of CO_2 with various lubricants. The miscibility, viscosity, solubility, lubricity and stability of CO_2

38

with a number of refrigerant lubricants was studied. The aim of this investigation was to check the compatibility and performance of carbon dioxide with various existing commercial refrigerant lubricants. The lubricants used were Polyalkylene glycol (PAG), Polyol ester (POE), Polyvinylether (PVE) and Polycarbonate (PC). Based on the chemical stability, miscibility and better lubricity under high pressure, PAG was found to be the best lubricant for CO_2 refrigeration systems.

A tribological investigation of 52100 steel disk on 440C bearing steel ball using a reciprocating ball-on-disk tribometer under CO_2 atmosphere was done by [93]. Experiments were conducted in vacuum, air and carbon dioxide atmosphere. The results of the friction coefficient of these experiments are shown in Fig. 14. CO_2 atmosphere resulted in the lowest coefficient of friction.
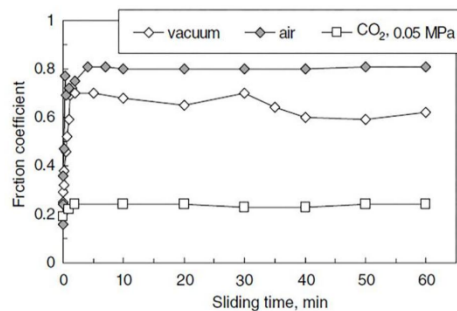

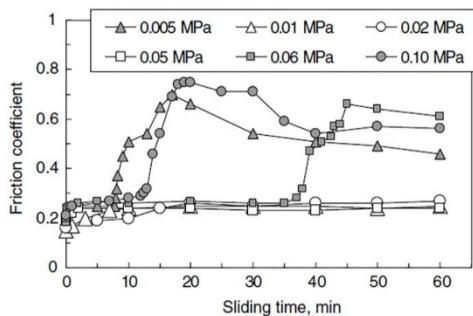**Fig. 14.** Lubricant effect of CO_2 on steel couple [93].

Fig. 15. Effect of CO_2 pressure on lubricating behavior [93].

The effect of the change in pressure of carbon dioxide on the friction coefficient was also studied. The results of this investigation are presented in Fig. 15. It was concluded that carbon dioxide reacted with the disk surfaces and formed carbonate and/or bicarbonate on the disk which played a major role in reducing friction. An optimum pressure in the range of 0.02-0.05 MPa resulted in effective reduction of friction. Lower CO_2 pressures were insufficient to produce carbonate and/or bicarbonates while higher CO_2 pressures produced serious chemical wear.

The tribological performance of carbon dioxide was compared to HFC-134a using 52100 steel pins and Al390-T6 disks under submerged lubricated conditions [94]. PAG and POE were used as lubricants in various combinations with the refrigerants. It was found that the abundance of oxygen while operating in carbon dioxide atmosphere resulted in the formation of oxides which strengthened the top most layer. PAG showed to be the better lubricant with CO_2.

Gray cast iron pins and disks were used in a study [95] to evaluate the tribological performance of CO_2 refrigerant in comparison to HFC-134a under identical operating conditions. PAG lubricants were used in this study. The study concluded by stating that the tribological behavior of the interacting materials using CO_2 was nearly identical to that of HFC-134a.

An ultra-high pressure tribometer was designed and manufactured to study the tribological behavior of carbon dioxide up to 13.8 MPa [96]. Experiments were conducted in the range of 1.4 MPa-6.9 MPa. Boundary lubrication tests were performed using PAG oil with 52100 steel disks against Al390-T6 pins, and unlubricated tests were conducted using gray cast iron pins and disks. Under unlubricated conditions the results at different pressures were similar and under boundary lubrication conditions there was no significant wear. It was also found that increasing the pressure had a positive effect on the coefficient of friction.

A pin-on-disk geometry comprising of Al390-T6 disks and SAE 52100 steel pins was used to study the tribological performance of CO_2 in comparison to HFC-410A [97]. POE and PAG lubricants were used. It was concluded in this study that in comparison to the CO_2 environment, HFC-410A environment resulted in increased disk wear. This was because carbon dioxide promoted a strong oxygenated layer which reduced wear.

39

A pin-on-disk geometry was used in a high pressure chamber to investigate the friction and wear performance of CO_2 with PAG and POE oils [98]. The pin was made of high speed tool steel and the disk was made of Ni–Cr–Mo gray cast iron. The purpose of the study was to compare the performance of carbon dioxide under PAG and POE oils and examine the influence of pressure variations on friction and wear. The results showed that PAG oil had better lubricity than POE oil in CO_2 refrigerant environment. An increase in pressure increased the solubility of carbon dioxide in case of POE oil which decreased the oil/refrigerant viscosity, whereas variations in pressure had no noticeable effect on the solubility of CO_2 in PAG. As a result the viscosity of PAG was less reduced as compared to POE. The reduction in POE/ CO_2 viscosity was linked to the formation of thin lubricating films on the rubbing surfaces, the thinner film resulted in higher friction and higher wear. In comparison a thick tribo layer was formed when carbon dioxide was used with PAG, the variation in operating pressure did not effect this layer because the solubility of PAG in CO_2 was not effected by pressure which resulted in less friction and wear.

A study involving the use of a pin-on-disk configuration using gray cast iron pins and gray cast iron disks was performed by [99]. The purpose of this study was to investigate the tribological properties of carbon dioxide under a range of pressures and compare its results to air, nitrogen and HFC-134a. Oxide layers were formed under carbon dioxide and oxygen atmospheres, but carbon dioxide showed the best friction and wear results.

Different PTFE-based coatings and DLC coatings were tested using pin-on-disk and shoe-on-disk configurations under air, carbon dioxide and HFC-410A atmospheres [100]. 52100 steel was used as a pin and shoe material, against coated gray cast iron disks. The change of environment showed no significant effect on the tribological behavior of the tested coatings. Overall the use of coatings resulted in a significant improvement in the tribological characteristics. PTFE-based coatings performed better compared to DLC coatings. It was also concluded that the generated wear debris acted as third body lubricants and improved the overall wear performance.

The study [101] compared the tribological performance of POE and PAG lubricants in the presence of carbon dioxide. AI390-T6 disks were used against SAE 52100 pins in a pin-on-disk configuration. It was concluded in this study that formation of carbonate layers are promoted on the surface in the presence of PAG, leading to improvement in the tribological performance.

Al390-T6, gray cast iron and Mn-Si brass disks were used against 52100 steel pins in a pin-on-disk configuration [102]. CO_2 was used as refrigerant with PAG oil. The purpose of the study was to perform a comparative scuffing analysis of metallic surfaces under carbon dioxide environment. Mn–Si brass and gray cast iron performed better than Al390-T6. Unlike Al390-T6 and gray cast iron which failed abruptly in scuffing experiments, Mn–Si brass melted during scuffing which prevented sudden catastrophic failure of Mn–Si brass.

Three different PTFE-based coatings were applied to sintered iron, gray cast iron and Al390-T6 disks to study the significance of tribochemistry on PTFE-based coatings against 52100 steel pins in a pin-on-disk setup in the presence of CO_2 [103]. It was found that the substrate played a major role on the friction and wear properties. *PTFE/MoS*$_2$ coatings considerably improved the scuffing performance of Al390-T6 substrate. Increase in CO_2 pressure resulted in a thicker PTFE transfer layer which improved the tribological performance.

A pin-on-disk geometry made of gray cast iron was used to study the lubricity effects of carbon dioxide in an ultra-high pressure tribometer [104]. To understand the role of temperature, pressure, carbon dioxide mass and the chemical interaction of CO_2 with gray cast iron on the tribological behavior of CO_2; various regions of CO_2 pressure-temperature (P-T) phase diagrams were studied. The study reported a substantial drop in friction as carbon dioxide approached the gas-liquid transition region on the P-T phase diagram. This indicated a form of super-lubricity. It was also found that increase in CO_2 pressure caused partial transformation of iron oxides into iron carbonates, which positively affected the tribological performance.

A study on the tribological behavior of Mn–Si–brass, Al390-T6 and gray cast iron disks against

40

52100 steel shoes was performed by [105]. A shoe-on-disk tribometer was used under submerged lubrication condition using PAG oil and CO_2. During the experiments Al390-T6 lost silicon which reduced its structural strength and hardness. Silicon particles have been known to drop out of the aluminum matrix leaving cavities on the surface [106]. Gray cast iron showed the least amount of wear and highest fluid and material retention capability compared to the other materials tested.

7. NEXT GENERATION REFRIGERANTS

The next generation refrigerants are focused on low toxicity, low ODP and low GWP. Focus and attention is also being made on the flammability in the development of next generation refrigerants. The focus on HC has increased after the Kyoto Protocol but due to their flammability, HCs cannot be used in commercial automobile air-conditioners. The future generation refrigerants have to be non-flammable for use and replacement of HFC-134a in the automotive sector. The refrigerant manufacturers have introduced Hydrofluoroolefins and Hydrofluoroethers as potential substitute refrigerants.

7.1 Hydrofluoroolefins (HFOs)

HFOs are designed to lower the GWP impact that HFCs had while having zero OPD and lower toxicity. One of the most promising future generation refrigerants is 2,3,3,3-Tetrafluoropropene (HFO-1234yf), which is considered a direct replacement of HFC-134a [107]. Although HFO-1234yf has mild

flammability, it has been proven to be safe for use as a refrigerant in vehicles [108]. The tribological investigation of HFO-1234yf by various researchers is underway, the work done so far is presented in this section.

A study involving the investigation of ant-seizure characteristics, anti-wear characteristics and chemical stability analysis of saturated and unsaturated refrigerants was done by [109] using disc-on-disc, pin-on-disk and V-block apparatus. Unsaturated refrigerants are those refrigerants that have a double bond in their chemical structure, while saturated refrigerants have only single bonds in their molecular structure. HFO-1234yf is an unsaturated refrigerant having a double bond in its chemical structure. This can cause additional reactions and is expected to influence the tribological performance of the sliding surfaces. This study also used another saturated refrigerant namely, HC-1270 and two unsaturated refrigerants, namely, HFC-134a and HC-290 for comparison. Table 4 shows the molecular structure of these refrigerants. The GWP values, saturation vapor pressures and the refrigeration oils used are also mentioned in Table 4.

The results of the seizure load are shown in Figs. 16(a) and 16(b) respectively. The seizure load of unsaturated HFO-1234yf was larger than saturated HFC-134a and similarly the seizure load of unsaturated HC-1270 was greater than saturated HC-290. The wear results confirmed the superiority of unsaturated refrigerants as compared to saturated refrigerants. The surface analysis revealed substantial amount of fluorine ions on surfaces tested in HFO-1234yf.

Table 4. Refrigerant characteristics and combinations of oil [109].

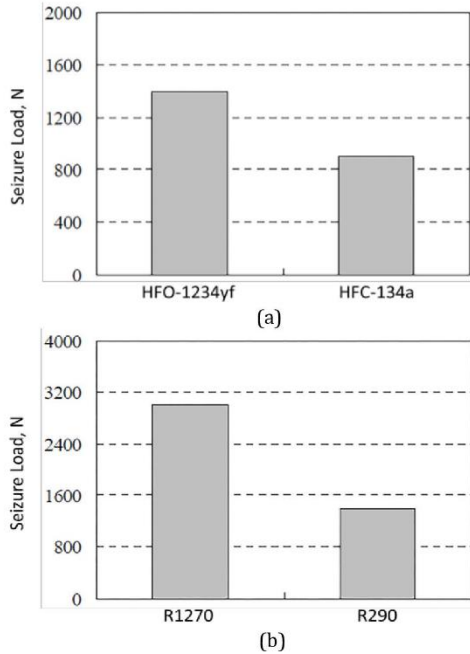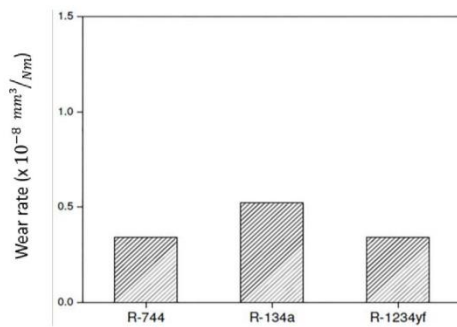| Series	Hydrofluorocarbon (HFCs)		Hydrocarbon (HCs)	
Refrigerant	HFO-1234yf	HFC-134a	R1270	R290
Molecular structure	F—C—C=C—H (with F, F above and F, H below)	H—C—C—F (with F, F above and H, F below)	H—C—C=C—H (with H above and H, H below)	H—C—C—C—H (with H, H, H above and H, H, H below)
GWP	4	1410	3	3
Saturated vapor pressure at 298 K (MPa)	0.7	0.7	1.2	1.0
Refrigeration oil	Alkyl benzene (AB)		Polyalkylene glycol (PAG)	

41

Fig. 16. Seizure load [109].

Fig. 17. Calculated average wear rates of a textured pattern in the presence of different refrigerants with PAG lubricant directly applied at interface [110].

A fluoride layer was formed with the adsorption effect of HFO-1234yf and the frictional heat, which helped improve the tribological performance. These results indicate that unsaturated refrigerants perform better than saturated refrigerants from the view point of tribology. The results also show that HFO-1234yf refrigerant has a lot better tribological performance compared to HFC-134a.

A pin-on-disk setup made of grey cast iron pins and disks was used by [110, 111] to

experimentally investigate the tribological performance of various unpolished surface textured patters with R-744, HFC-134a and HFO-1234yf under starved lubrication conditions. PAG, POE and mineral oils were used as lubricants and the tests were also conducted on un-textured surfaces under identical conditions. The results of the wear rates by using one of the laser textured geometries with PAG are shown in Fig. 17. HFO-1234yf showed the least amount of wear. The tribological properties of the textured surfaces were affected by the geometrical parameters; depth, diameter and the area density of the micro-dimples. The study concluded that the textured surfaces have a clear advantage over un-textured surfaces.
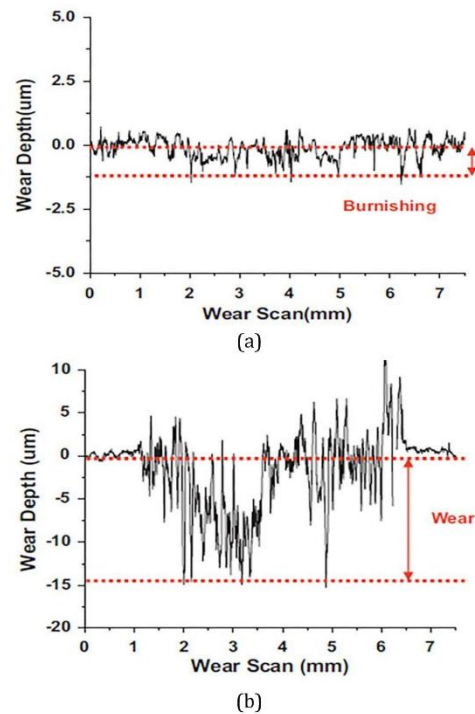

Fig. 18 Profilometric scans of the cast iron wear tracks after experiments in the presence of (a) HFO-1234yf and (b) HFC-134a [112].

A pin-on-disk setup was used [112, 113] to study the tribological effects of HFO-1234yf in comparison to HFC-134a under identical conditions. Two different material pairs were used in this study, namely gray cast iron disk against gray cast iron pin and Al390-T6 disk against 52100 crowned steel pin. No lubricant was used in

42

this study to emphasize the effects of the refrigerants. Wear results of one of the tests are shown in Fig. 18. It can be seen from Fig. 18 that there was less wear in the case of HFO-1234yf. Gray cast iron pairs performed better in this study compared to 52100 steel/aluminum alloy pair for both refrigerants. When used with gray cast iron, HFO-1234yf showed excellent wear performance compared to HFC-134a. The combined effect of the mechanical forces and frictional heating resulted in a tribochemical reaction between the fluorine coming from the unsaturated refrigerant breakdown and the gray cast iron surface. This fluorine containing layer acted as a protective tribo-layer on the top most surface.

Another study to investigate the tribological performance of HFO-1234yf in comparison to HFC-134a was performed by [114]. Gray cast iron pins and disks were used on a pin-on-disk setup. Unlubricated and starved lubrication conditions using PAG oil were simulated in this study. It was seen that HFO-1234yf could sustain twice the load before failing compared to HFC-134a. Fluorine was detected upon surface analysis in the case of using HFO-1234yf. The fluorine containing tribo-layers prevented mental to metal contact and helped sustain extended interface functionality.

The performance of HFO-1234yf was studied with different lubricants, namely, PAG, POE and mineral oils using a gray cast iron pin-on-disk apparatus [115]. Surface analysis of the tested surfaces revealed that fluorine enriched protective surface layers were present by using HFO-1234yf with PAG. PAG showed the best performance with HFO-1234yf compared to POE/HFO-1234yf and mineral oil/HFO-1234yf combinations. PAG has the lowest solubility in HFO-1234yf compared to POE and mineral oil, this allows the lubricant and the refrigerant to preserve their unique properties giving PAG/HFO-1234yf combination the maximum tribological advantage.

52100 steel shoes were tested against different polymeric coated gray cast iron disks in HFO-1234yf atmosphere using a shoe-on-disk tribometer [116]. PAG was used as a lubricant and it was concluded that ATSP/PTFE coatings performed better compared to PTFE-based and Fluorocarbon-based coatings under boundary and dry lubrication conditions. Tribo-chemical benefits were offered by the segregation associated with material enrichment. Oil

retention capabilities can improve by the valleys of segregated components that can act as micro-reservoirs under starved lubrication conditions. This results in continuous lubricant supply, which was the case for ATSP/PTFE.

HFO-1233zd which has a boiling point of about 18 °C [117] under normal atmospheric pressure, was used as a lubricant to study film thickness and traction in elastohydrodynamic conditions [118]. This study involved the use of a 52100 steel ball loaded against a glass disk for film thickness measurements using optical interferometry. A ceramic ball was used against steel disk for traction measurements. Numerical and analytical work is also presented in this study for film thickness calculation. The results of the theoretical calculations are compared to the measured film thickness values as well.

7.2 Hydrofluoroethers (HFEs)

Hydrofluoroethers are man-made refrigerants that have been developed to replace CFCs, HCFCs and HFCs. HFEs are nonflammable, odorless, colorless, low toxic and low viscous refrigerants having zero OPD and low GWP. Different variants of HFEs have been developed in the recent past. HFEs have higher boiling points compared to CFCs, HFCs, and HCFCs. HFEs are normally liquid at room temperature and look identical to water. HFO-1234yf has a boiling point comparable to HFC-134a and HFO-1234yf has shown compatibility with synthetic lubricants which were developed for HFC-134a, this makes HFO-1234yf an excellent replacement of HFC-134a. HFEs however have higher boiling points so it is difficult to introduce HFEs into the same thermodynamics cycle and system that was previously used by HFC-134a. Besides having a very low environmental impact, HFEs are nonflammable and possess good thermodynamics properties as coolants [119, 120]. This makes them good candidates for use in various applications.

A study based on the tribological properties of HFE-245mc using a ball-on-sapphire disk-type elastohydrodynamic tester was done by [121]. POE oil having branched chains designed for use with HFC refrigerants was used as a lubricant. HFC-134a and air environment were used as a yardstick to evaluate the performance of this HFE. The chemical formula and various properties of the refrigerants are given in Table 5.

43

Table 5. Some properties of refrigerants [121].

Refrigerant	HFE-245mc	HFC-134a
Structure	$CF_3CF_2OCH_3$	CH_2FCF_3
Boiling Point (°C)	5	-26
GWP	622	1300
ODP	0	0

The elastohydrodynamic central film thickness was measured using the optical interferometry technique. HFE-245mc/lubricant mixture displayed the lowest film thickness formation capability compared to HFC-134a/lubricant and air/lubricant mixtures.
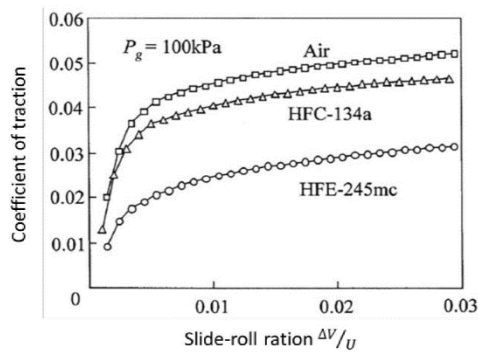

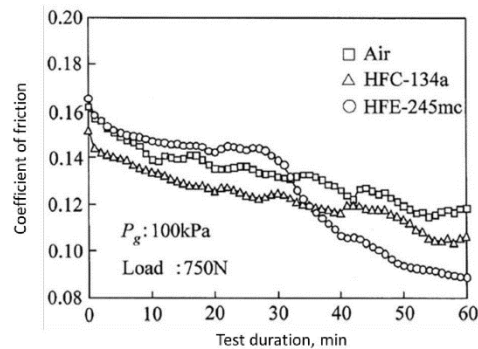**Fig. 19.** Traction curves in refrigerants at identical gas pressure [121].

Fig. 20. Boundary friction characteristics in some environments [121].

This was due to the fact that HFC-245mc was more miscible in the lubricant than HFC-134a and air. The high miscibility of HFE-245mc in POE lubricant decreased the viscosity of POE more as compared to HFC-134a and air, this resulted in HFC-245mc having the lowest coefficient of traction as well as shown in Fig. 19.

HFE-245mc however displayed the lowest coefficient of friction after running-in of the components was achieved on a block-on-ring tribometer as displayed in Fig .20. HFC-245mc was believed to have reacted with the rubbing surfaces, resulting in the formation of FeF_2 and thick iron oxide films which resulted in good anti-wear performance which resulted in the lowest wear in HFE-245mc atmosphere.

8. CONCLUSION

This review article presents the reported work on the testing of refrigerants from the view point of tribology. An attempt has been made to discuss the major findings while showing selected results from the studies in order not to repeat or present similar results. The similar findings however have been listed in a few cases to highlight the fact that same results were obtained by different studies. The tribological testing of refrigerants from the 1980s to the present day has been discussed.

CFCs and HCFCs refrigerants were chemically formulated in the 1920s to overcome the toxicity and flammability problem of some of the naturally occurring refrigerants. CFCs and HCFCs were used extensively as refrigerants owing to their excellent thermodynamic properties. CFCs and HCFCs showed excellent tribological performance as well. In the presence of CFCs and HCFCs, protective chloride surface films were formed on the interacting surfaces which gave good friction and wear performance. The discovery of the ozone depletion by these refrigerants and the enforcement of Montreal Protocol in 1989 banned the use of CFCs and HCFCs. CFCs have a higher ozone depleting potential than HCFCs, which allowed the use of HCFCs for a longer period of time in comparison to CFCs.

HFCs having zero ozone depleting potential were introduced in the market as replacement refrigerants. They matched the thermodynamic properties of their predecessors but did not show good tribological properties in comparison to CFCs and HCFCs. CFCs and HCFCs were used in compressors with mineral oils as lubricants but HFCs were immiscible and incompatible with mineral oils. New synthetic oils having numerous additives had to be developed for HFCs. In comparison to CFCs and HCFCs, HFCs

44

did not show good friction and wear properties. The fluorine in HFCs did not decompose and form protective surface layers under normal compressor operating conditions. The fluorine in HFCs did decompose at elevated pressures and temperatures and at extreme testing and unlubricated conditions, but was still not as effective as chlorine in CFCs and HCFCs. HFC-134a was adopted as the primary refrigerant for many domestic and commercial applications including uses in fridges, freezers and air-conditioners. Being nonflammable, HFC-134a was also the main candidate for use in automotive air-conditioning systems after CFC-12. The harmful global warming effects of HFCs were realized later after they had been accepted and deployed all over the world. After Kyoto Protocol in 1997, which focused on the causes contributing to global warming, the phase out of HFCs was planned for the coming years.

Natural refrigerants such as hydrocarbon refrigerants also became of interest in 1990s after the limitations on CFCs and HCFCs, but introduction of HFCs did not really allow HCs to be commercialized on a very big scale. This was also due to their high flammability. Now that more emphasis is towards natural refrigerants and HCs are naturally occurring, a strong focus has shifted towards these refrigerates as well. Their flammability is still a concern which prohibits their use in automotive air-conditioning, but HC refrigerants can be used with confidence in domestic and commercial refrigeration and air-conditioning systems. The use of HC refrigerants in heat pumps and fridge and freezer compressors has increased in the recent years. HC-600a has shown better friction and wear properties as compared to HFC-134a as well.

Other than hydrocarbons which inherently have high flammability, carbon dioxide is a good natural refrigerant as well. CO_2 has zero OPD and a GWP value of 1, and it can be collected/recycled from the atmosphere. The physical properties of carbon dioxide unfortunately does not allow it to be used at the operating temperatures and pressures as other refrigerants. The operating pressure has to be much higher for a system based on CO_2 compared to a compressor operating on CFCs or HFCs. Compared to HFC-134a, carbon dioxide has shown good tribological properties by formation of a carbonate layers on the rubbing surfaces. Carbon dioxide which is nonflammable is being investigated for use in automotive air-conditioning applications as well.

Hydrofluoroolefins are newly formulated refrigerants which have zero OPD and lower GWP as compared to HFC refrigerants. HFO-1234yf is considered a direct replacement of HFC-134a, especially in automotive air conditioning applications. The physical and thermodynamic properties of HFO-1234yf are very similar to those of HFC-134a. HFO-1234yf is also compatible with the synthetic oils that were developed for HFC-134a. Unlike HFC-134a, the fluorine in HFO-1234yf has been reported to form protective films on the interacting surfaces with and without lubricants, which improves the friction and wear performance of the system. HFO-1234yf has an unsaturated bond which makes it easier for it to chemically interact with the metallic surfaces and the lubricating oils to improve the tribological performance. The only drawback of HFO-1234yf compared to HFC-134a is that HFO-1234yf has higher flammability than HFC-134a.

Hydrofluoroethers are nontoxic, nonflammable refrigerants which have zero OPD and very low GWP. Their boiling point is much higher than the other commercial refrigerants, this makes them unsuitable for use in the existing fridge, freezer and air-conditioning compressors. However their tribological performance has been reported to be better than HFCs. HFEs have also been reported to form protective tribo-films.

REFERENCES

[1] S. Fujimoto, K. Sakitani, M. Watada, *Tribology Analysis in Rolling Piston Type Compressor*, in International Compressor Engineering Conference, 11-13 July, 1984, Purdue University, Indiana, USA, pp. 377–382.

45

[2] H. Kruse, M. Schroeder, *Fundamentals of lubrication in refrigerating systems and heat pumps*, International Journal of Refrigeration, vol. 8, iss. 6, pp. 347-355, 1985, doi: 10.1016/0140-7007(85)90030-1

[3] F. Wardle, B. Jacobson, H. Dolfsma, E. Hoglund, U. Jonsson, *The effect of refrigerants on the lubrication of rolling element bearings used in screw compressors*, in International Compressor Engineering Conference, 14-17 July, 1992, Purdue University, Indiana, USA, pp 523-534.

[4] B. Davis, T.K. Sheiretov, C. Cusano, *Tribological Evaluation of Contacts Lubricated by Oil-Refrigerant Mixtures*, Air Conditioning and Refrigeration Center, College of Engineering, University of Illinois at Urbana-Champaign, ACRC Technical Report 19, May 1992.

[5] B. Jacobson, *Lubrication of Screw Compressor Bearings in the Presence of Refrigerants*, in International Compressor Engineering Conference, 19-22 July, 1994, Purdue University, Indiana, USA, pp 115-120.

[6] K. Mizuhara, M. Akei, T. Matsuzaki, *The friction and wear behavior in controlled alternative refrigerant atmosphere*, Tribology Transactions, vol. 37, iss. 1, pp. 120-128, 1994, doi: 10.1080/10402009408983274

[7] M. Akei, K. Mizuhara, T. Taki, T. Yamamoto, *Evaluation of film-forming capability of refrigeration lubricants in pressurized refrigerant atmosphere*, Wear, vol. 196, iss. 1-2, pp. 180-187, 1996, doi: 10.1016/0043-1648(95)06917-8

[8] K. Kawahara, S. Mishina, A. Kamino, K. Ochiai, T. Okawa, S. Fujimoto, *Tribological Evaluation of Rotary Compressor with HFC Refrigerants*, in International Compressor Engineering Conference, 23-26 July, 1996, Purdue University, Indiana, USA, pp. 413-418.

[9] M.J. Molina, F.S. Rowland, *Stratospheric sink for chlorofluoromethanes: chlorine atom-catalysed destruction of ozone*, Nature, vol. 249, no. 5460, pp. 810-812, 1974, doi: 10.1038/249810a0

[10] U. Nations, *Montreal Protocol on Substances that Deplete the Ozone Layer. Montreal*, United Nations Environment Programme, vol. 2, FINAL ACT, 16 September 1987

[11] D.P. Wilson, R.S. Basu, *Thermodynamic properties of a new stratospherically safe working fluid-refrigerant 134a*, in ASHRAE transactions, 1988, pp. 2095-2118.

[12] I.R. Shankland, R.S. Basu, D.P. Wilson, *Thermal conductivity and viscosity of a new stratospherically safe refrigerant-1, 1, 1, 2-tetrafluoroethane (R-134a)*, in International Refrigeration and Air Conditioning Conference, 1988, Purdue University, Indiana, USA, pp. 56-64.

[13] H. Spauschus, *HFC 134a as a substitute refrigerant for CFC 12*, International Journal of Refrigeration, vol. 11, iss. 6, pp. 389-392, 1988, doi: 10.1016/0140-7007(88)90063-1

[14] S. Jollev, *New and Unique Lubricants for Use in Compressors Utilizing R-134a Refrigerant*, in International Refrigeration and Air Conditioning Conference, 17-20 July, 1990, Purdue University, Indiana, USA, pp. 145-152.

[15] S. Kitaichi, S. Sato, R. Ishidoya, T. Machida, *Tribological Analysis of Metal Interface Reactions in Lubricant Oils/CFC12 and HFC 134a System*, in International Refrigeration and Air Conditioning Conference, 17-20 July, 1990, Purdue University, Indiana, USA, paper 97.

[16] S. KOMATSUZAKI, Y. HOMMA, *Lubricants for HFC Refrigerant Compressors*, Journal of The Japan Petroleum Institute, vol. 37, iss. 3, pp. 226-235, 1994, doi: 10.1627/jpi1958.37.226

[17] M. Muraki, K. Tagawa, D. Dong, *Refrigeration Lubricant Based on Polyolester for Use With HFCs and Prospect of Its Application With R-22 (Part 1) Tribological Characteristics*, in International Refrigeration and Air Conditioning Conference, 23-26 July, 1996, Purdue University, Indiana, USA, paper 336.

[18] T. Hamada, N. Nishiura, *Refrigeration lubricant based on polyolester for use with HFCs and prospect of its application with R-22 (Part 2) Hydrolytic stability and compressor endurance test results*, in International Refrigeration and Air Conditioning Conference, 23-26 July, 1996, Purdue University, Indiana, USA, paper 337.

[19] F. Nishiwaki, H. Hasegawa, R. Matsuzaki, S. Muramatsu, *Mechanical loss reduction at thrust bearings of scroll compressors using R407C*, in International Compressor Engineering Conference, 23-26 July, 1996, Purdue University, Indiana, USA, paper 1117.

[20] B. Jacobson, *Ball Bearing Lubrication in Refrigetation Compressors*, in International Compressor Engineering Conference, 23-26 July, 1996, Purdue University, Indiana, USA, paper 1090.

[21] U. Nations, *Kyoto protocol to the united nations framework convention on climate change*, 1998.

[22] C. Breidenich, D. Magraw, A. Rowley, J.W. Rubin, *The Kyoto protocol to the United Nations framework convention on climate change*, American Journal of International Law, vol. 92, no. 2, pp. 315-331, 1998, doi: 10.2307/2998044

[23] DAIKIN, *HFC-134a*, Data Sheet _ HCF- 134a, vol. 01, May 2009.

46

[24]   S. Solomon, D. Qin, M. Manning, Z. Chen, M. Marquis, K.B. Averyt, M. Tignor, H.L. Miller, *Contribution of working group I to the fourth assessment report of the intergovernmental panel on climate change*. Cambridge: Cambridge University Press, 2007.

[25]   Z.A. Khan, V. Chacko, H. Nazir, *A review of friction models in interacting joints for durability design*, Friction, vol. 5, iss. 1, pp. 1-22, 2017, doi: 10.1007/s40544-017-0143-0

[26]   T. Sheiretov, W.V. Glabbeek, C. Cusano, *Tribological evaluation of various surface treatments for M2 tool steel in a refrigerant environment*, in International Compressor Engineering Conference, 19-22 July, 1994, Purdue University, Indiana, USA, paper 964.

[27]   C. Bujoreanu, S. Cretu, D. NELIAS, *An Investigation of Scuffing Failure in Angular Contact Ball-Bearings*, Tribology in Industry, vol. 25, no. 1&2, pp. 20-26, 2003.

[28]   B.J. Hamrock, D. Dowson, *Ball bearing lubrication: The elastohydrodynamics of elliptical contacts*, NASA Technical Reports, NASA, Jan 01, 1981.

[29]   M. Akei, K. Mizuhara, *The Elastohydrodynamic Properties of Lubricants in Refrigerant Environments©*, Tribology Transactions, vol. 40, iss. 1, pp. 1-10, 1997, doi: 10.1080/10402009708983622

[30]   B.O. Jacobson, G.E.M. Espejel, *High pressure investigation of refrigerants HFC245fa, R134a and R123*, in International Compressor Engineering Conference, 17-20 July, 2006, Purdue University, Indiana, USA, paper 1789.

[31]   R. Tuomas, O. Isaksson, *Compressibility of Oil/Refrigerant Lubricants in Elasto-Hydrodynamic Contacts*, Journal of Tribology, vol. 128, iss. 1, pp. 218-220, 2005, doi: 10.1115/1.2125967

[32]   R. Tuomas, O. Isaksson, *Measurement of lubrication conditions in a rolling element bearing in a refrigerant environment*, Industrial Lubrication and Tribology, vol. 61, iss. 2, pp. 91-99, 2009, doi: 10.1108/00368790910940419

[33]   P. Vergne, N. Fillot, N. Bouscharain, N. Devaux, G.E. Morales-Espejel, *An experimental and modeling assessment of the HCFC-R123 refrigerant capabilities for lubricating rolling EHD circular contacts*, Proceedings of the Institution of Mechanical Engineers, Part J: Journal of Engineering Tribology, vol. 229, iss. 8, pp. 950-961, 2015, doi: 10.1177/1350650115574537

[34]   G. Nijenbanning, C. Venner, H. Moes, *Film thickness in elastohydrodynamically lubricated elliptic contacts*, Wear, vol. 176, iss. 2, pp. 217-229, 1994, doi: 10.1016/0043-1648(94)90150-3

[35]   W. Habchi, I. Demirci, D. Eyheramendy, G. Morales-Espejel, P. Vergne, *A finite element approach of thin film lubrication in circular EHD contacts*, Tribology International, vol. 40, iss. 10, pp. 1466-1473, 2007, doi: 10.1016/j.triboint.2007.01.017

[36]   T. Doki-Thonon, N. Fillot, P. Vergne, G.E. Morales Espejel, *Numerical insight into heat transfer and power losses in spinning EHD non-Newtonian point contacts*, Proceedings of the Institution of Mechanical Engineers, Part J: Journal of Engineering Tribology, vol. 226, iss. 1, pp. 23-35, 2012, doi: 10.1177/1350650111419567

[37]   B.J. Hamrock, D. Dowson, *Isothermal elastohydrodynamic lubrication of point contacts: part III—fully flooded results*, Journal of Lubrication Technology, vol. 99, iss. 2, pp. 264-275, 1977, doi: 10.1115/1.3453074

[38]   D. Dowson, G.R. Higginson, *Elasto-hydrodynamic lubrication: the fundamentals of roller and gear lubrication* vol. 23. Oxford: Pergamon Press, 1966.

[39]   S.J. Eckels, M.B. Pate, *An experimental comparison of evaporation and condensation heat transfer coefficients for HFC-134a and CFC-12*, International Journal of Refrigeration, vol. 14, iss. 2, pp. 70-77, 1991, doi: 10.1016/0140-7007(91)90078-U

[40]   S.H. Khan, S.M. Zubair, *Thermodynamic analyses of the CFC-12 and HFC-134a refrigeration cycles*, Energy, vol. 18, iss. 7, pp. 717-726, 1993, doi: 10.1016/0360-5442(93)90031-8

[41]   B. Chul Na, K. Jin Chun, D.-C. Han, *A tribological study of refrigeration oils under HFC-134a environment*, Tribology International, vol. 30, iss. 9, pp. 707-716, 1997, doi: 10.1016/S0301-679X(97)00072-8

[42]   Y. Yamamoto, S. Gondo, *Friction and wear characteristics of lubricants for alternative refrigerant HFC 134a*, JSME International Journal Series C Mechanical Systems, Machine Elements and Manufacturing, vol. 41, iss. 2, pp. 278-284, 1998, doi: 10.1299/jsmec.41.278

[43]   M. Takesue, S. Tominaga, *Wear and Scuffing Characteristics of Polyvinylether (PVE) in an HFC Atmosphere*, in International Refrigeration and Air Conditioning Conference, 14-17 July, 1998, Purdue University, Indiana, USA, paper 440.

[44]   S. Safari, M. Hadfield, *Wear behaviour of the piston/gudgeon pin in a hermetic compressor with replacement CFC refrigerants*, Wear, vol. 219, iss. 1, pp. 8-15, 1998, doi: 10.1016/S0043-1648(98)00197-5

47

[45] H. Yoon, T. Sheiretov, C. Cusano, *Tribological evaluation of some aluminum-based materials in lubricant/refrigerant mixtures*, Wear, vol. 218, iss. 1, pp. 54-65, 1998, doi: 10.1016/S0043-1648(98)00195-1

[46] T. Sheiretov, H. Yoon, C. Cusano, *Tribological Evaluation of Various Aluminum Alloys in Lubricant/Refrigerant Mixtures*, Air Conditioning and Refrigeration Center, College of Engineering, University of Illinois at Urbana-Champaign, ACRC Technical Report 92, 1996.

[47] Y. Birol, F. Birol, *Sliding wear behaviour of thixoformed AlSiCuFe alloys*, Wear, vol. 265, iss. 11-12, pp. 1902-1908, 2008, doi: 10.1016/j.wear.2008.05.001

[48] H. Matsuura, M. Minowa, Y. Fudemato, S. Hiodoshi, M. Nomura, *Evaluation of Refrigerant Oil for HFC Refrigerants and Selection of Sliding Materials*, in International Compressor Engineering Conference, 14-17 July, 1998, Purdue University, Indiana, USA, paper 1276.

[49] H.C. Sung, *Tribological characteristics of various surface coatings for rotary compressor vane*, Wear, vol. 221, iss. 2, pp. 77-85, 1998, doi: 10.1016/S0043-1648(98)00244-0

[50] C. Ciantar, M. Hadfield, A. Smith, A. Swallow, *The influence of lubricant viscosity on the wear of hermetic compressor components in HFC-134a environments*, Wear, vol. 236, iss. 1-2, pp. 1-8, 1999, doi: 10.1016/S0043-1648(99)00267-7

[51] H. Yoon, T. Sheiretov, C. Cusano, *Scuffing behavior of 390 aluminum against steel under starved lubrication conditions*, Wear, vol. 237, iss. 2, pp. 163-175, 2000, doi: 10.1016/S0043-1648(99)00321-X

[52] U.J. Jonsson, *Lubrication of rolling element bearings with HFC–polyolester mixtures*, Wear, vol. 232, iss. 2, pp. 185-191, 1999, doi: 10.1016/S0043-1648(99)00144-1

[53] M. Muraki, T. Sano, *Determination of film thickness and traction of polyol ester under an EHD contact in some refrigerant environments*, Tribology Transactions, vol. 43, iss. 1, pp. 15-20, 2000, doi: 10.1080/10402000008982306

[54] C. Ciantar, M. Hadfield, A. Swallow, A. Smith, *The influence of POE and PVE lubricant blends within hermetic refrigerating compressors operating with HFC-134a refrigerant*, Wear, vol. 241, iss. 1, pp. 53-64, 2000, doi: 10.1016/S0043-1648(00)00361-6

[55] H. Fukui, K.-i. Sanechika, M. Ikeda, *Novel refrigeration lubricants for use with HFC refrigerants*, Tribology International, vol. 33, iss. 10, pp. 707-713, 2000, doi: 10.1016/S0301-679X(00)00107-9

[56] C. Ciantar, M. Hadfield, *An environmental evaluation of mechanical systems using environmentally acceptable refrigerants*, The International Journal of Life Cycle Assessment, vol. 5, iss. 4, pp. 209-220, 2000, doi: 10.1007/BF02979362

[57] S. Milojević, R. Pešić, D. Taranović, *Tribological Principles of Constructing the Reciprocating Machines*, Tribology in Industry, vol. 37, no. 1, pp. 13-19, 2015.

[58] Y. Yamamoto, S. Gondo, J. Kim, *Solubility of HFC134a in Lubricants and Its Influence on Tribological Performance*, Tribology Transactions, vol. 44, iss. 2, pp. 209-214, 2001, doi: 10.1080/10402000108982450

[59] M. Muraki, T. Sano, D. Dong, *Rheological Properties of Polyolester Under an EHD Contact in Some Refrigerant Environments*, Journal of Tribology, vol. 123, iss. 1, pp. 54-60, 2000, doi: 10.1115/1.1326443

[60] M. Muraki, D. Dong, *Derivation of basic rheological parameters from experimental elastohydrodynamic lubrication traction curves of low-viscosity lubricants*, Proceedings of the Institution of Mechanical Engineers, Part J: Journal of Engineering Tribology, vol. 213, iss. 1, pp. 53-61, 1999, doi: 10.1243/1350650991542613

[61] S. Tanaka, T. Nakahara, K. Kyogoku, *Measurements of two-dimensional distribution of refrigerant concentration in EHL film using micro FT-IR and effect of variation of concentration on oil film thickness*, Tribology Letters, vol. 14, iss. 1, pp. 9-15, 2003, doi: 10.1023/A:1021706014202

[62] R. Chittenden, D. Dowson, J. Dunn, C. Taylor, *A theoretical analysis of the isothermal elastohydrodynamic lubrication of concentrated contacts. I. Direction of lubricant entrainment coincident with the major axis of the Hertzian contact ellipse*, Proceedings of the Royal Society of London A: Mathematical, Physical and Engineering Sciences, vol. 397, iss. 1813, pp. 245-269, 1985, doi: 10.1098/rspa.1985.0014

[63] R. Chittenden, D. Dowson, J. Dunn, C. Taylor, *A theoretical analysis of the isothermal elastohydrodynamic lubrication of concentrated contacts. II. General Case, with lubricant entrainment along either principal axis of the Hertzian contact ellipse or at some intermediate angle*, Proceedings of the Royal Society of London A: Mathematical, Physical and Engineering Sciences, vol. 397, iss. 1813, pp. 271-294, 1985, doi: 10.1098/rspa.1985.0015

[64] A.Y. Suh, A.A. Polycarpou, T.F. Conry, *Detailed surface roughness characterization of*

48

engineering surfaces undergoing tribological testing leading to scuffing, Wear, vol. 255, iss. 1-6, pp. 556-568, 2003, doi: 10.1016/S0043-1648(03)00224-2

[65] C. Ciantar, M. Hadfield, *A study of tribological durability with associated environmental impacts of a domestic refrigerator*, Materials & Design, vol. 25, iss. 4, pp. 331-341, 2004, doi: 10.1016/j.matdes.2003.10.016

[66] Y.-Z. Lee, S.-D. Oh, *Friction and wear of the rotary compressor vane–roller surfaces for several sliding conditions*, Wear, vol. 255, iss. 7–12, pp. 1168-1173, 2003, doi: 10.1016/S0043-1648(03)00278-3

[67] M.L. Cannaday, A.A. Polycarpou, *Tribology of unfilled and filled polymeric surfaces in refrigerant environment for compressor applications*, Tribology Letters, vol. 19, iss. 4, pp. 249-262, 2005, doi: 10.1007/s11249-005-7441-9

[68] N.G. Demas, J. Zhang, A.A. Polycarpou, J. Economy, *Tribological characterization of aromatic thermosetting copolyester–PTFE blends in air conditioning compressor environment*, Tribology Letters, vol. 29, iss. 3, pp. 253-258, 2008, doi: 10.1007/s11249-008-9303-8

[69] E.E. Nunez, S.M. Yeo, A.A. Polycarpou, *Tribological Behavior of PTFE, PEEK, and Fluorocarbon-based Polymeric Coatings used in Air-Conditioning and Refrigeration Compressors*, in International Compressor Engineering Conference, 12-15 July, 2010, Purdue University, Indiana, USA, paper 2031.

[70] E.E. Nunez, S.M. Yeo, K. Polychronopoulou, A.A. Polycarpou, *Tribological study of high bearing blended polymer-based coatings for air-conditioning and refrigeration compressors*, Surface and Coatings Technology, vol. 205, iss. 8-9, pp. 2994-3005, 2011, doi: 10.1016/j.surfcoat.2010.11.008

[71] M. Tanaka, H. Matsuura, S. Taira, A. Nakai, *Selection of a refrigeration oil for the R32 refrigerant and evaluation of the compressor reliability*, in International Compressor Engineering Conference, 14-17 July, 2014, Purdue University, Indiana, USA, paper 2299.

[72] S.M. Yeo, A.A. Polycarpou, *Fretting experiments of advanced polymeric coatings and the effect of transfer films on their tribological behavior*, Tribology International, vol. 79, pp. 16-25, 2014, doi: 10.1016/j.triboint.2014.05.012

[73] E.E. Nunez, A.A. Polycarpou, *The effect of surface roughness on the transfer of polymer films under unlubricated testing conditions*, Wear, vol. 326-327, pp. 74-83, 2015, doi: 10.1016/j.wear.2014.12.049

[74] S. Bair, *A New High-Pressure Viscometer for Oil/Refrigerant Solutions and Preliminary Results*, Tribology Transactions, vol. 60, iss. 3, pp. 392-398 2017, doi: 10.1080/10402004.2016.1168902

[75] A. Tada, T. Okido, Y. Shono, H. Takahashi, Y. Shitara, S. Tanaka, *Tribological Characteristics of Polyol Ester Type Refrigeration Oils under Refrigerants Atmosphere*, Tribology Online, vol. 11, iss. 2, pp. 348-353, 2016, doi: 10.2474/trol.11.348

[76] N. Garland, M. Hadfield, *Environmental implications of hydrocarbon refrigerants applied to the hermetic compressor*, Materials & Design, vol. 26, iss. 7, pp. 578-586, 2005, doi: 10.1016/j.matdes.2004.08.009

[77] Z.A. Khan, M. Hadfield, Y. Wang, *Design of a novel pressurized chamber to assess in-use durability performance of rolling contact elements using refrigerant lubrication*, in 4th International Conference of Advanced Engineering Design, 5-8 September, 2004, Glasgow, Scotland, UK.

[78] Z.A. Khan, M. Hadfield, Y. Wang, *Pressurised chamber design for conducting rolling contact experiments with liquid refrigerant lubrication*, Materials & Design, vol. 26, iss. 8, pp. 680-689, 2005, doi: 10.1016/j.matdes.2004.08.006

[79] Z.A. Khan, M. Hadfield, S. Tobe, Y. Wang, *Ceramic rolling elements with ring crack defects—A residual stress approach*, Materials Science and Engineering: A, vol. 404, iss. 1-2, pp. 221-226, 2005, doi: 10.1016/j.msea.2005.05.087

[80] A. Saifullah, B. Thomas, R. Cripps, K. Tabeshfar, L. Wang, C. Muryn, *Fracture toughness of rotationally molded polyethylene and polypropylene*, Polymer Engineering & Science, vol. 58, iss. 1, pp. 63–73, 2017, doi: 10.1002/pen.24531

[81] Z.A. Khan, M. Hadfield, S. Tobe, Y. Wang, *Residual stress variations during rolling contact fatigue of refrigerant lubricated silicon nitride bearing elements*, Ceramics international, vol. 32, iss. 7, pp. 751-754, 2006, doi: 10.1016/j.ceramint.2005.05.012

[82] Z.A. Khan, A. Saeed, O. Gregory, A. Ghafoor, *Biodiesel Performance within Internal Combustion Engine Fuel System: A Review*, Tribology in Industry, vol. 38, no. 2, pp. 197-213, 2016.

[83] Z.A. Khan, *Rolling contact wear of hybrid ceramic bearings with refrigerant lubrication*, PhD thesis, Faculty of Science & Technology, Bournemouth University, Bournemouth, 2006.

49

[84] Z.A. Khan, M. Hadfield, *Manufacturing induced residual stress influence on the rolling contact fatigue life performance of lubricated silicon nitride bearing materials*, Materials & Design, vol. 28, iss. 10, pp. 2688-2693, 2007, doi: 10.1016/j.matdes.2006.10.003

[85] T.A. Solzak, A.A. Polycarpou, *Tribology of protective hard coatings for use in oil-less, piston-type compressors*, in International Compressor Engineering Conference, 17-20 July, 2006, Purdue University, Indiana, USA, paper 1790.

[86] K. Sariibrahimoglu, H. Kizil, M.F. Aksit, I. Efeoglu, H. Kerpicci, *Effect of R600a on tribological behavior of sintered steel under starved lubrication*, Tribology International, vol. 43, iss. 5-6, pp. 1054-1058, 2010, doi: 10.1016/j.triboint.2009.12.035

[87] J. De Mello, R. Binder, N. Demas, A. Polycarpou, *Effect of the actual environment present in hermetic compressors on the tribological behaviour of a Si-rich multifunctional DLC coating*, Wear, vol. 267, iss. 5-8, pp. 907-915, 2009, doi: 10.1016/j.wear.2008.12.070

[88] T.A. Solzak, A.A. Polycarpou, *Tribology of hard protective coatings under realistic operating conditions for use in oilless piston-type and swash-plate compressors*, Tribology Transactions, vol. 53, iss. 3, pp. 319-328, 2010, doi: 10.1080/10402000903283300

[89] M. Silverio, R. Binder, E.R. Hulse, J.D.B. De Mello, *Effect of Refrigerant Gases (HFC134a and R600a) on the Tribological Behaviour of a Multifunctional DLC Coating*, in International Compressor Engineering Conference, 11-14 July, 2016, Purdue University, Indiana, USA, paper 2413.

[90] K. Górny, A. Stachowiak, P. Tyczewski, W. Zwierzycki, *Lubricity evaluation of oil–refrigerant mixtures with R134a and R290*, international Journal of Refrigeration, vol. 69, pp. 261-271, 2016, doi: 10.1016/j.ijrefrig.2016.06.011

[91] T. Hagita, T. Makino, N. Horaguchi, T. Ukai, *Tribology in CO_2 Scroll Compressors*, Mitsubishi Heavy Industries, Ltd., Technical Review, vol. 39, no. 1, Feb 2002.

[92] H. Ikeda, J.I. Yagi, Y. Kawaguchi, *The development of PAG refrigeration lubricants for hermetic compressors with CO_2*, in International Refrigeration and Air Conditioning Conference, 12-15 July, 2004, Purdue University, Indiana, USA, paper 680.

[93] X. Wu, P. Cong, H. Nanao, I. Minami, S. Mori, *Tribological behaviors of 52100 steel in carbon dioxide atmosphere*, Tribology Letters, vol. 17, iss. 4, pp. 925-930, 2004, doi: 10.1007/s11249-004-8101-1

[94] K. Lee, A. Suh, N. Demas, A. Polycarpou, *Surface and sub-micron sub-surface evolution of Al390-T6 undergoing tribological testing under submerged lubrication conditions in the presence of CO_2 refrigerant*, Tribology Letters, vol. 18, iss. 1, pp. 1-12, 2005, doi: 10.1007/s11249-004-1698-2

[95] N.G. Demas, A.A. Polycarpou, T.F. Conry, *Tribological Studies on Scuffing Due to the Influence of Carbon Dioxide Used as a Refrigerant in Compressors*, Tribology Transactions, vol. 48, iss. 3, pp. 336-342, 2005, doi: 10.1080/05698190590970525

[96] N.G. Demas, A.A. Polycarpou, *Ultra high pressure tribometer for testing CO_2 refrigerant at chamber pressures up to 2000 psi to simulate compressor conditions*, Tribology Transactions, vol. 49, iss. 3, pp. 291-296, 2006, doi: 10.1080/05698190600550003

[97] M. Cannaday, A. Polycarpou, *Advantages of CO_2 compared to R410a refrigerant of tribologically tested Aluminum 390-T6 surfaces*, Tribology Letters, vol. 21, iss. 3, pp. 185-192, 2006, doi: 10.1007/s11249-005-9013-4

[98] H.-G. Jeon, S.-D. Oh, Y.-Z. Lee, *Friction and wear of the lubricated vane and roller materials in a carbon dioxide refrigerant*, Wear, vol. 267, iss. 5-8, pp. 1252-1256, 2009, doi: 10.1016/j.wear.2008.12.097

[99] N.G. Demas, A.A. Polycarpou, *Tribological investigation of cast iron air-conditioning compressor surfaces in CO_2 refrigerant*, Tribology Letters, vol. 22, iss. 3, pp. 271-278, 2006, doi: 10.1007/s11249-006-9094-8

[100] N.G. Demas, A.A. Polycarpou, *Tribological performance of PTFE-based coatings for air-conditioning compressors*, Surface and Coatings Technology, vol. 203, iss. 3-4, pp. 307-316, 2008, doi: 10.1016/j.surfcoat.2008.09.001

[101] E.E. Nunez, N.G. Demas, K. Polychronopoulou, A.A. Polycarpou, *Tribological study comparing PAG and POE lubricants used in air-conditioning compressors under the presence of CO_2*, Tribology Transactions, vol. 51, iss. 6, pp. 790-797, 2008, doi: 10.1080/10402000801911861

[102] E.E. Nunez, N.G. Demas, K. Polychronopoulou, A.A. Polycarpou, *Comparative scuffing performance and chemical analysis of metallic surfaces for air-conditioning compressors in the presence of environmentally friendly CO_2 refrigerant*, Wear, vol. 268, iss. 5-6, pp. 668-676, 2010, doi: 10.1016/j.wear.2009.11.002

50

[103] D. Dascalescu, K. Polychronopoulou, A. Polycarpou, *The significance of tribochemistry on the performance of PTFE-based coatings in CO₂ refrigerant environment*, Surface and Coatings Technology, vol. 204, iss. 3, pp. 319-329, 2009, doi: 10.1016/j.surfcoat.2009.07.042

[104] E.E. Nunez, K. Polychronopoulou, A.A. Polycarpou, *Lubricity effect of carbon dioxide used as an environmentally friendly refrigerant in air-conditioning and refrigeration compressors*, Wear, vol. 270, iss. 1-2, pp. 46-56, 2010, doi: 10.1016/j.wear.2010.09.005

[105] E.E. Nunez, A.A. Polycarpou, *Wear study of metallic interfaces for air-conditioning compressors under submerged lubrication in the presence of carbon dioxide*, Wear, vol. 326-327, pp. 28-35, 2015, doi: 10.1016/j.wear.2014.12.031

[106] Y. Birol, F. Birol, *Wear properties of thixoformed AlSiCuFe alloys*, International Journal of Material Forming, vol. 1, no. 1, pp. 981-984, 2008/04/01 2008, doi: 10.1007/s12289-008-0222-x

[107] M. Spatz, B. Minor, H. DuPont, *HFO-1234yf A low GWP refrigerant for MAC. Honeywell/DuPont joint collaboration*, in SAE World Congress 14-17 April, 2008, Detroit, Michigan, USA.

[108] B.H. Minor, D. Herrmann, R. Gravell, *Flammability characteristics of HFO-1234yf*, Process Safety Progress, vol. 29, iss. 2, pp. 150-154, 2009, doi: 10.1002/prs.10347

[109] H.N. Tatsuya Sasaki, Hideaki Maeyama, Kota Mizuno, *Tribology Characteristics of HFO and HC Refrigerants with Immiscible Oils - Effect of Refrigerant with Unsaturated Bond*, in International Compressor Engineering Conference, 12-15 July, 2010, Purdue University, Indiana, USA, pp. 1-8.

[110] S.P. Mishra, *Tribological Studies Of Surface Texturing For Application In Air-Conditioning And Refrigeration Compressors*, M.Sc. thesis, Graduate College of the University of Illinois at Urbana-Champaign, Urbana, Illinois, 2011.

[111] S.P. Mishra, A.A. Polycarpou, *Tribological studies of unpolished laser surface textures under starved lubrication conditions for use in air-conditioning and refrigeration compressors*, Tribology International, vol. 44, iss. 12, pp. 1890-1901, 2011, doi: 10.1016/j.triboint.2011.08.005

[112] M.W. Akram, *Tribology Of Engineering And Coated Materials In The Presence Of Environmentally Friendly Refrigerant*, PhD thesis, Graduate College of the University of Illinois at Urbana-Champaign, Urbana, Illinois, 2015.

[113] M.W. Akram, K. Polychronopoulou, A.A. Polycarpou, *Lubricity of environmentally friendly HFO-1234yf refrigerant*, Tribology International, vol. 57, pp. 92-100, 2013, doi: 10.1016/j.triboint.2012.07.013

[114] M.W. Akram, K. Polychronopoulou, C. Seeton, A.A. Polycarpou, *Tribological performance of environmentally friendly refrigerant HFO-1234yf under starved lubricated conditions*, Wear, vol. 304, iss. 1-2, pp. 191-201, 2013, doi: 10.1016/j.wear.2013.04.035

[115] M.W. Akram, K. Polychronopoulou, A.A. Polycarpou, *Tribological performance comparing different refrigerant–lubricant systems: The case of environmentally friendly HFO-1234yf refrigerant*, Tribology International, vol. 78, pp. 176-186, 2014, doi: 10.1016/j.triboint.2014.05.015

[116] M.W. Akram, J.L. Meyer, A.A. Polycarpou, *Tribological interactions of advanced polymeric coatings with polyalkylene glycol lubricant and r1234yf refrigerant*, Tribology International, vol. 97, pp. 200-211, 2016, doi: 10.1016/j.triboint.2016.01.026

[117] R.J. Hulse, R.S. Basu, R.R. Singh, R.H. Thomas, *Physical properties of HCFO-1233zd (E)*, Journal of Chemical & Engineering Data, vol. 57, iss. 12, pp. 3581-3586, 2012, doi: 10.1021/je300776s

[118] G.E. Morales-Espejel, R. Meeuwenoord, A.F. Quiñonez, R. Hauleitner, *Film thickness and traction measurements of refrigerant R1233zd used as lubricant in elastohydrodynamic conditions*, Proceedings of the Institution of Mechanical Engineers, Part C: Journal of Mechanical Engineering Science, vol. 229, iss. 2, pp. 244-253, 2015, doi: 10.1177/0954406214533530

[119] H. Helvaci, Z.A. Khan, *Experimental study of thermodynamic assessment of a small scale solar thermal system*, Energy Conversion and Management, vol. 117, pp. 567-576, 2016, doi: 10.1016/j.enconman.2016.03.050

[120] H. Helvaci, Z. Khan, *Thermodynamic modelling and analysis of a solar organic Rankine cycle employing thermofluids*, Energy Conversion and Management, vol. 138, pp. 493-510, 2017, doi: 10.1016/j.enconman.2017.02.011

[121] M. Muraki, T. Sano, D. Dong, *Elastohydrodynamic properties and boundary lubrication performance of polyolester in a hydrofluoroether refrigerant environment*, Proceedings of the Institution of Mechanical Engineers, Part J: Journal of Engineering Tribology, vol. 216, iss. 1, pp. 19-26, 2002, doi: 10.1243/1350650021543852

51

Paper II

NOVEL EXPERIMENTAL SETUP TO ASSESS SURFACES IN TRIBO-CONTACT LUBRICATED BY THE NEXT GENERATION OF ENVIRONMENTALLY FRIENDLY THERMOFLUIDS

MUHAMMAD USMAN BHUTTA[1,2], ZULFIQAR AHMAD KHAN[1] & NIGEL GARLAND[1]
[1] Faculty of Science & Technology, Department of Design & Engineering, NanoCorr, Energy & Modelling
(NCEM) Research Group, Bournemouth University, Talbot Campus, Fern Barrow, Poole, BH12 5BB.
[2] School of Mechanical & Manufacturing Engineering (SMME), National University of Sciences & Technology
(NUST), Campus H-12, Islamabad, Pakistan.

ABSTRACT

Environmental concerns related to global warming and ozone depletion triggered the introduction of the fourth generation of thermofluids. Amongst the recently introduced thermofluids, one of the most promising fourth generation of thermofluids are hydrofluoroethers (HFEs). HFEs have zero ozone depletion potential and have a lower global warming potential as compared to widely used thermofluids. The type of thermofluid used in a thermodynamic cycle directly affects the tribological performance of the system. HFEs have been reported to have good thermodynamic properties. The overall tribological performance of HFEs however have to be investigated in detail in order to fully assess the mechanical behaviour of interacting components utilizing these thermofluids. This study is concerned with the experimental test rig design modifications and commissioning to conduct tribological testing with HFEs as lubricants. This article covers the experimental test rig design and setup. Experiments to analyse the frictional force, the coefficient of friction and wear by using Hydrofluororther-7000 (HFE-347mcc3) as lubrication medium have been conducted. Industrial applications were simulated by varying test conditions and the results are presented in this paper.

Keywords: bench testing, environment-friendly thermofluids, friction, refrigerants, tribology, wear.

1 INTRODUCTION

Increase in global population, rise in worldwide economic development and the anthropogenic global climate change have considerably increased the use of cooling, refrigeration and air-conditioning systems worldwide. The selection of a refrigerant depends on the place of use and its application. Some of the refrigerants being used today in the domestic and commercial sector such as ammonia, carbon dioxide and various hydrocarbons are naturally occurring whereas majority of the thermofluids have been artificially formulated.

The first artificially formulated commercial refrigerants were chlorofluorocarbons (CFCs) and hydrochlorofluorocarbons (HCFCs) which were introduced in the 1930s [1]. CFCs and HCFCs proved to possess excellent thermodynamic, heat transfer and tribological properties especially when used in domestic, commercial and small-scale industrial applications [1]. CFCs and HCFCs showed extreme pressure effect and resulted in the formation of protective surface films on the operating machine parts which helped in reducing friction and wear [2–4]. However, the destructive effects of CFCs and HCFCs on the ozone layer were discovered and Montreal Protocol on the substances that deplete the ozone layer was enforced in 1989 which banned the use of CFCs by the end of year 1995 in developed countries. This made way to the introduction of hydrofluorocarbons (HFCs) which have zero ozone depletion potential. HFCs matched the thermodynamic properties of CFCs [5–8], but showed poorer tribological performance in comparison to their predecessors [1]. The inability of HFCs to form surface films under normal compressor operating conditions

contributed to their inferior tribological performance [2–4]. In addition mineral oils that showed good miscibility with CFCs and HCFCs, unfortunately, were not compatible with HFCs and synthetic oils with various additives had to be developed for HFCs [1]. Despite having these drawbacks, HFCs were globally accepted. The damaging implications of HFCs on the earth's atmosphere were realized much later when it was found that HFCs are one of the major contributors to global warming [9]. Kyoto Protocol to the United Nations Framework Convention on Climate Change in 1997 established binding limits on CO_2 and other greenhouse gases, which included HFCs as well. HFCs are now in the process of being phased out and it is expected that by the end of year 2030 HFC availability will drop by 79% in Europe.

Most of the naturally occurring compounds have either thermodynamic limitations or have high toxicity or high flammability. This means that new future generation of artificially formulated thermofluids have to be introduced. The challenge for the refrigerant manufacturers is even greater this time as they not only have to come up with refrigerants that have zero ozone depletion potential but also should have minimum global warming potential. The refrigerant manufacturers have introduced new thermofluids which have a lower environmental impact. Hydrofluoroolefins (HFOs) and hydrofluoroethers (HFEs) are the newly introduced replacement refrigerants which have been reported to have good heat transfer and thermodynamic properties [10–14]. However, no significant investigations have been published on the tribological performance of HFEs.

This work is being carried out to investigate the interfacial properties of HFEs, for this purpose an experimental setup has been designed and commissioned. The setup allows a platform to conduct detailed tribological testing under varying operating conditions.

2 TEST RIG

The test rig is based upon an existing reciprocating microfriction machine which has been modified to test the future generation of thermofluids. Bespoke design of the test rig is shown in Fig. 1. The most integral part of the rig is the testing chamber which houses the testing parts. The chamber is designed in a way to be fully sealed and hold pressure in a range of −1 to +3 bar. The moving components within the test chamber are sealed to the test chamber by means of steel bellows and Viton O-rings seals. The arrangement is such that all relative movement is accommodated by the bellows. O-ring contacts are all static, meaning that there are no sliding seals. The apparatus can be used to test separate contact configurations which include, point contact, line contact and area contact. For this study point contact configuration was chosen which allows maximum Hertzian contact pressure for the same applied load.

2.1 Temperature monitoring and control

A heater block is located at the bottom of the chamber. The heater block comprises electric heating elements possesing a heating power of 800 W. The apparatus has been fitted with two K-type thermocouples. Thermocouple-1 is directly embedded in the heater block that contains the electric heating elements. The heater block can be heated up to 200°C. Thermocouple-2 is a wire-type thermocouple that is positioned in the specimen cup, and it is fixed with the help of screws. The specimen cup contains the flat specimen and is filled with the thermofluid. Thermocouple-2 directly measures the exact temperature of the thermofluid being tested and helps maintain the temperature of the tested thermofluid by utilizing feedback PID control during the course of a test.

228   *M. U. Bhutta, et al., Int. J. Comp. Meth. and Exp. Meas., Vol. 7, No. 3 (2019)*
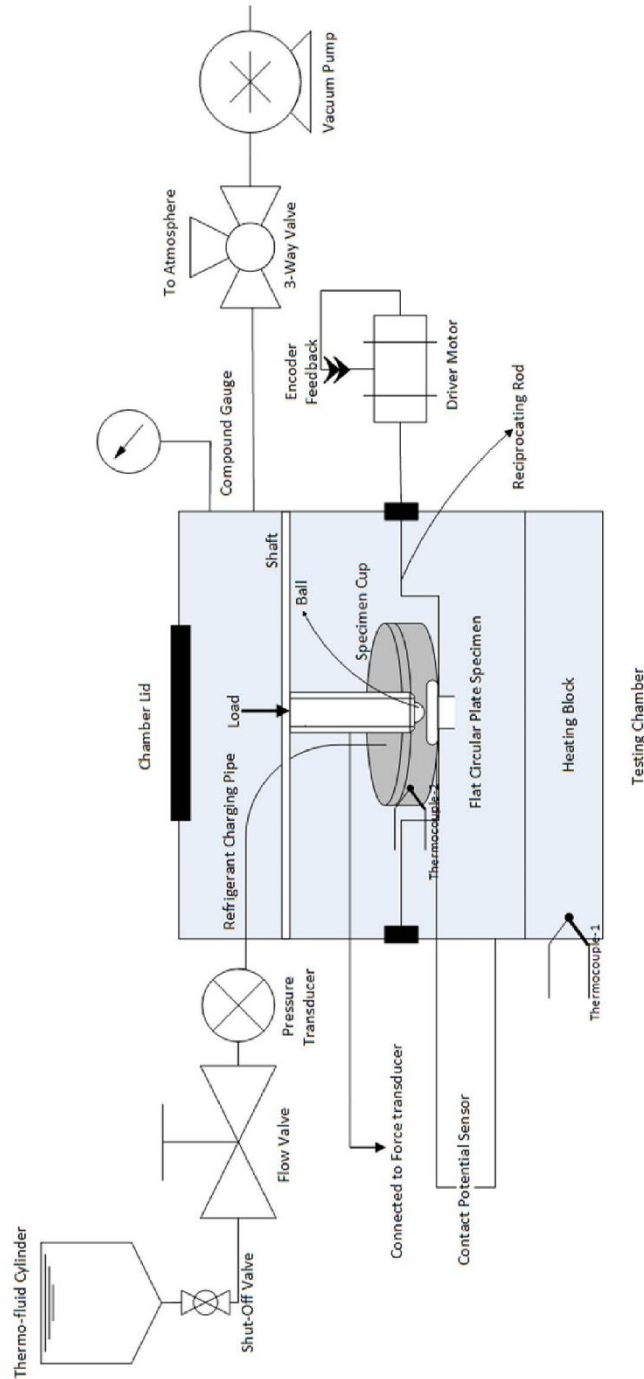
Figure 1: Test rig schematic.

2.2 Chamber pressure measurement

The testing chamber can be pressurized up to +3 bar and can be vacuumed to −1 bar. A compound manual gauge and a pressure transducer have been installed to monitor both the positive and negative pressure in this range. The pressure transducer allows on screen motoring and recording of the chamber pressure during the course of an experiment. The pressure transducer is made of stainless steel having a transmitter range of −1 to +9 bar, it can measure the pressure of refrigerants in the range of −20 to +120°C. The output signal is linear in the range of 4 to 20 mA, having a response time of less than 5 ms. The pressure transducer is also shock and vibration resistant having good accuracy and repeatability. The compound gauge has been added for additional safety to always allow for visual pressure variations in the pressure chamber. If the data acquisition system or the computer freezes for some reason the manual gauge will always allow observations of the pressure readings to make sure that the pressure is within the safe operating limit.

2.3 Lubricant film formation measurement

Lubricant film formation between the contacts is sensed via a contact potential sensor. The contact potential measurement enables the observation of metal-to-metal interactions between the reciprocating parts. The data can be used to judge if a suitable lubrication film was formed during various testing conditions. The contact potential sensing is based on the principle of contact resistance measurement. The internal circuit for the contact potential sensor is shown in Fig. 2.

Figure 2: Contact potential measurement circuit.

The internal electrical circuit allows the sensor to be calibrated in the range of 0–50 mV, with 0 V referring to short circuit (metal-to-metal co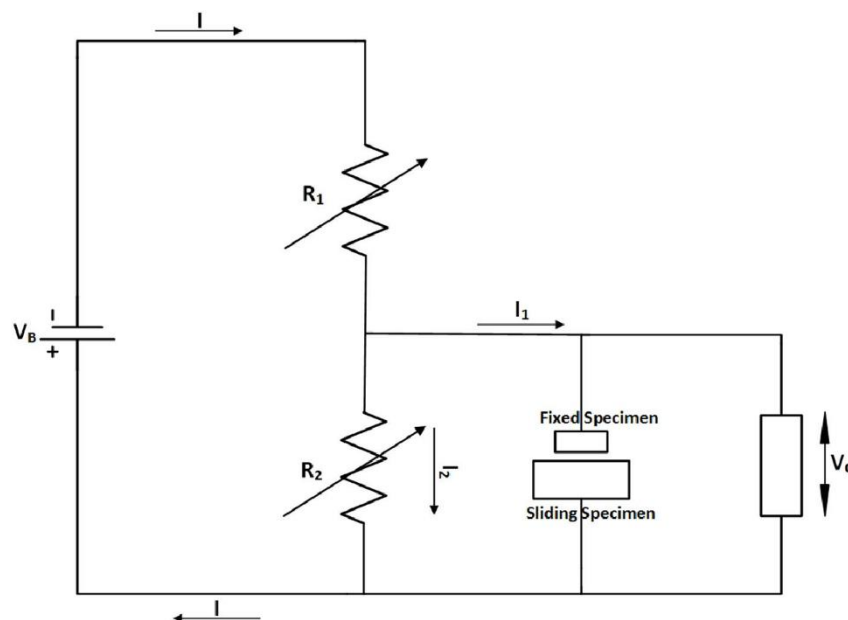ntact) and 50 mV means open circuit. The sensor has been fine-tuned with the help of the two variable resistors R_1 and R_2 to give values in the full range of 0–50 mV, and this increases the output resolution. V_B is the excitation voltage applied to the circuit and V_C is the output voltage that is sensed.

For the sensor to be installed, the two contact geometries have to be electrically isolated. If the specimens are not isolated before the start of an experiment then the sensor will always read the state of short circuit. The sensor should read a state of short circuit only when there is a metal-to-metal contact and should show values in the range of 0–50 mV during testing. For this the two test specimens namely the flat circular plate and the steel ball have to be electrically isolated. The specimen holding cup has been isolated from the body of the machine using insulation tape and nylon screws. The specimen holding cup is used to hold the flat circular specimen, isolating the cup isolates the flat circular specimen from the steel ball.

2.4 Friction force measurement

The rig has been fitted with a Kistler Piezo-electric friction force transducer having a range of −100 to 100 N. Normal load is applied by means of a spring balance attached to a cantilever arrangement. The cantilever exerts a normal force on the contact. The friction force sensor is attached to a yoke, and the yoke is connected to a force feedback rod upon which a housing is mounted that holds the fixed sample. The applied normal load and the values of the friction force are used to calculate the coefficient of friction in the software.

2.5 Oscillating frequency measurement and control

A 0.37 kW PID controlled DC motor drives the machine by sliding a lower flat plate sample in a reciprocating motion against a fixed upper sample using a scotch yoke mechanism. The mechanism is secured with the reciprocating rod which holds the flat plate specimen. The power is transmitted through the reciprocating rod which is supported by bearings on a linear guide rail. The setup allows the application of normal load in the range 5–50 N. The stroke length can be continuously varied between 1–5 mm. The frequency of oscillation can be varied between 2.5–50 Hz. A tachometer is coupled directly at the back end of the driver motor shaft which provides the rotational speed. The data from the tachometer is used as feedback to maintain a constant oscillating frequency with the help of PID control.

All the inputs and outputs are fed into a purpose built data acquisition system which serially transmits the data to a microprocessor. The computer has a specialized software that is used to monitor, control and record the operating parameters in real time.

3 TESTING PROCEDURE

Testing procedure consists of a number of different steps. 52100 steel ball bearings have been chosen as the ball specimen. Mild steel has been machined into flat circular disks and disks have been grinded and polished to an average surface roughness of 0.1 μm, which are used as the flat plate specimen. This arrangement allows ball-on-flat, that is, point contact configuration. The thermofluid being used in these tests is HFE-7000. HFE-7000 is a non-flammable, non-corrosive, low toxic chemical with a chemical formula $C_3F_7OCH_3$. It has a wide range of application areas which include use in high voltage transformer, in medical laboratory devices

such as Histobath, in freeze-drying units, in ion implanters and in auto-cascade refrigeration systems. It has an ozone depletion potential of zero and a global warming potential value of 530 for 100-year integrated time horizon.

3.1 Sample installation

The flat circular specimen is secured in the cup on the oscillating rod with the help of screws. Then the wire type thermocouple-2 is secured into position which is used to measure the thermofluid temperature. The ball is secured on the ball-holder with the help of grub screws and the ball holder is connected to a ball holder shaft. The shaft provides a means to fasten the ball-holder in position and also serves as a means to apply the vertical load. After this the chamber is closed and sealed.

3.2 Thermofluid charging

After closing the chamber it is vacuumed so as to minimize the effects of ambient air and oxygen during testing. After the chamber has been vacuumed the thermofluid is introduced in the system using the shut-off and flow valves. Sufficient amount of thermofluid is introduced in the cup so that the cup is full and the bottom flat specimen is fully immersed in the fluid to ensure fully lubricated conditions at all times. The vacuum inside the testing chamber and gravity helps the fluid to flow from the cylinder into the cup. The pressure inside the chamber is controlled in a way to keep the thermofluid in liquid state during testing to always maintain fully lubricated conditions. The chamber lid has a transparent glass top that allows a person to physically observe the chamber conditions at all times.

3.3 Testing

The desired load is manually applied. After this the control algorithm is run and the chamber thermofluid is heated to the desired temperature. The temperature of the fluid is precisely controlled using temperature values from thermocouple-2 and feedback PID control. After the temperature has reached to its specific value, the temperature of the fluid is stabilized and maintained for 1 h before starting a test. After the temperature has been stabilized and has been maintained, a test is run for 2 h. The oscillating frequency is precisely controlled using feedback controlled driver motor. The motor, the heater and all the transducers are connected to a microprocessor based central data acquisition and control system. The real-time values of the friction force, of the heater block temperature, temperature of the thermofluid, the chamber pressure and the motor speed are continuously recorded in a spreadsheet.

4 RESULTS AND DISCUSSION

The only published works on the tribological assessment of HFEs are [15, 16]. The study [15] was performed in 2002 which investigated the elastohydrodynamic and boundary lubrication performance of polyester (POE) in HFE-245mc and HFC-134a environment. A recent study [16] concerning the tribological performance of HFE-347mcc3 has been published in 2018. The study [16] however looks only into wear and there is no discussion about friction.

    Tests in this study have been performed by varying the applied normal load and the thermofluid temperature. Each test was performed for 2 h and each test was repeated two times

to ensure repeatability. The applied normal load was gradually increased from 10 to 30 N and the thermofluid temperature was increased from 20°C to 40°C.

4.1 Coefficient of friction

The results for the average coefficient of friction are presented in Fig. 3. The average coefficient of friction at 10 N and 20°C thermofluid temperature is 0.44, this value reduces to 0.32 at 10 N, 40°C. At 20 N, 20°C the average coefficient of friction is 0.28 which is reduced to 0.25 at 20 N, 40°C. At 30 N, 20°C the friction coefficient is 0.25 which decreases to 0.23 at 30 N, 40°C.

For a given load increase in temperature decreases the coefficient of friction and the frictional force. The difference in reduction in the coefficient of friction is higher at lower loads. Increase in load at the same temperature also gives a lower coefficient of friction. With increasing load the coefficient of friction is reduced for the same thermofluid temperature but the difference in reduction is not as significant as at lower loads.

The coefficient of friction dropped due to the formation of FeF_2 and iron oxide films after running-in of the components was achieved in the study [15] when POE was used in HFE-245mc environment, however no such tribo-films were detected when POE was tested with HFC-134a under identical testing conditions. The chemical composition of HFE-245mc is $CH_3OCF_2CF_3$ which is similar to that of HFE-7000 with HFE-7000 having a larger molecular structure as compared to HFE-245mc. It is believed that similar to [15], the HFE in our case reacted with the rubbing surfaces as well and formed iron oxide and FeF_2 films which reduced the coefficient of friction. The results show that increasing temperatures and operating loads will result in the reduction of the coefficient of friction. The decrease in coefficient of friction with increasing temperatures is due to the increase in reactivity of HFE-7000 with the interacting metals. Similarly increasing load at the same temperature decreased the coefficient of friction because increasing the load helped in the chemical breakdown and reaction of HFE-7000 with the interacting metals.
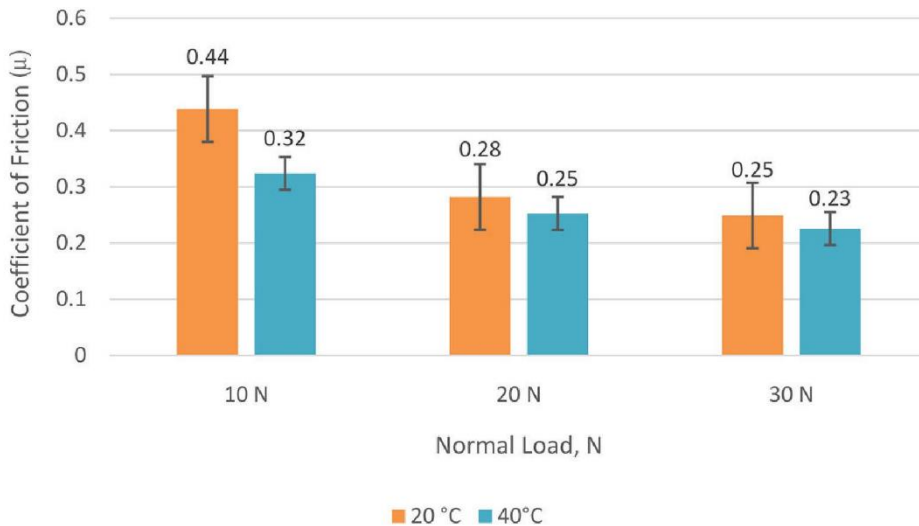

Figure 3: Effect of load and temperature on the average coefficient of friction.

4.2 Wear

The wear track formed on the flat circular mild steel specimens was examined under a white light interferometer. The interferometer was used to 3D stitch the wear track which was then used to calculate the wear volume. 3D oblique plots for 20°C and 40°C testing conditions are shown in Figs. 4 and 5, respectively.

For the tests conducted at 20°C, increasing the load results in a deeper and wider wear track. The widening of the wear track is associated with the change in sliding contact area of the point contact with time. As the testing progresses the point contact becomes flatter with wear which produces a wider wear track for each load. Increasing load produces a wider wear track due to the increased flattening on the ball. Increasing load also generates a deeper wear track. This shows that increasing load at the same temperature will produce more wear.

For the tests conducted at 40°C, increasing load from 10 to 20 N generated a shallower and narrower wear track. Increasing the load further to 30 N, produced the deepest and widest wear track for HFE-7000 temperature of 40°C. This indicates that there exist an optimum load and temperature combination which produces the least amount of wear.

Wear volume was measured using the white light interferometer after obtaining the 3D profiles. The results of the wear volume have been summarized in Fig. 6. It is evident from Fig. 6 that increasing the load at 20°C thermofluid temperature generates more wear. It can also be clearly seen from Fig. 6 that increasing the testing temperature at the same load helps in reducing wear. The results of wear at 40°C however are different from the results of wear at 20°C. Least amount of wear was obtained at 20 N, 40°C form all the samples tested.

(a)   (b)   (c)
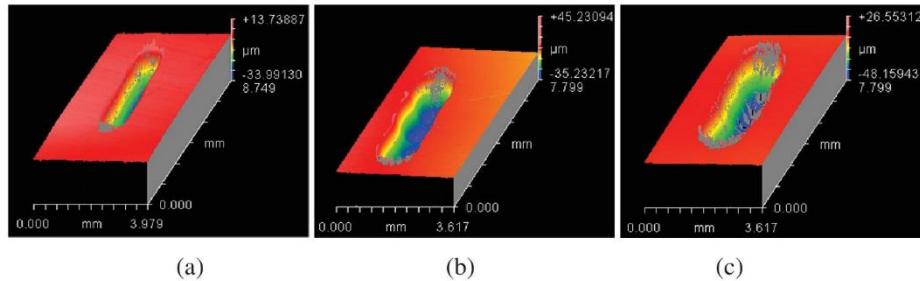
Figure 4: Wear track for HFE-7000 temperature 20°C. At normal loads of:
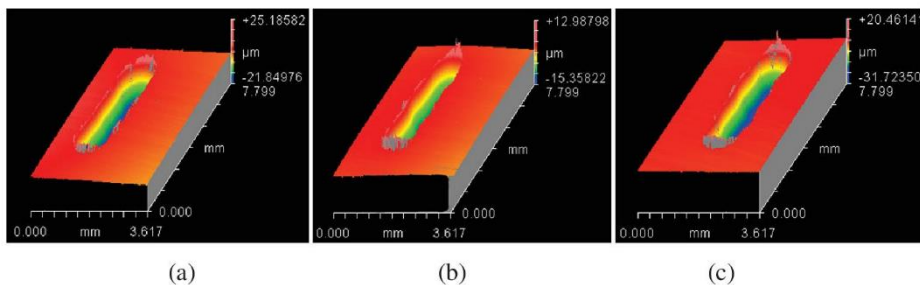(a) 10 N, (b) 20N and (c) 30N.

(a)   (b)   (c)

Figure 5: Wear track for HFE-7000 temperature 40°C. At normal loads of:
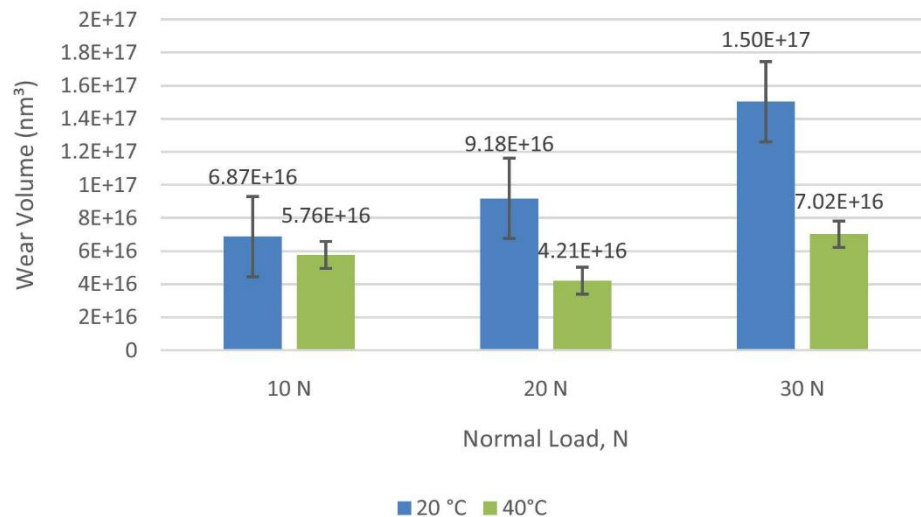(a) 10 N, (b) 20 N and (c) 30 N.

Figure 6: Effect of load and temperature on wear [16].

5 CONCLUSION

A micro friction testing machine has been successfully modified and commissioned that is capable of testing the next generation of thermofluids from a tribological view point. Various tests have been carried out by altering the testing conditions and the results for varying the applied normal load and by changing the operating temperature of HFE-7000 have been presented.

The results show that increasing the operating temperature and load reduces the coefficient of friction which is believed to be associated with the formation of protective tribo-films on the rubbing surfaces. The formation of these films is accelerated by increasing the temperature and applied load.

Wear volume increases with increasing load for 20°C thermofluid temperature. However wear volume decreases as the load is increased from 10 N to 20 N at thermofluid temperature of 40°C. Upon increasing the applied normal load further from 20 N to 30 N at 40°C increases wear. This shows that there exists an optimum combination of load and temperature which generates the least amount of wear.

This study shows that HFE-7000 which is a promising new generation environmentally friendly thermofluid from a thermodynamics point of view also has good tribological properties. This study indicates that HFE-7000 is capable of generating protective tribo-films on the materials tested, which help reduce friction and wear. With these results it can be inferred that HFE-7000 based systems will offer better tribological performance in comparison to systems using HFCs.

REFERENCES

[1] Bhutta, M.U., Khan, Z.A., Garland, N.P. & Ghafoor, A., A Historical Review on the Tribological Performance of Refrigerants used in Compressors. *Tribology in Industry*, **40(1)**, pp. 19–51, 2018, https://doi.org/10.24874/ti.2018.40.01.03

[2] Davis, B., Sheiretov, T. & Cusano, C., Tribological Evaluation of Contacts Lubricated by Oil-Refrigerant Mixtures. *Air Conditioning and Refrigeration Center*, College of Engineering, University of Illinois at Urbana-Champaign, ACRC Technical Report, 19 May 1992.

[3] Mizuhara, K., Akei, M. & Matsuzaki, T., The friction and wear behavior in controlled alternative refrigerant atmosphere. *Tribology Transactions*, **37(1)**, pp. 120–128, 1994, https://doi.org/10.1080/10402009408983274

[4] Kawahara, K., Mishina, S., Kamino, A., Ochiai, K., Okawa, T. & Fujimoto, S., *Tribological Evaluation of Rotary Compressor with HFC Refrigerants*, In International Compressor Engineering Conference, Purdue University, Indiana, USA, paper 1141, 23-26 July 1996.

[5] Spauschus, H.O., HFC 134a as a substitute refrigerant for CFC 12. *International Journal of Refrigeration*, **11(6)**, pp. 389–392, 1988, https://doi.org/10.1016/0140-7007(88)90063-1

[6] Shankland, I.R., Basu, R.S. & Wilson, D.P., Thermal conductivity and viscosity of a new stratospherically safe refrigerant-1, 1, 1, 2-tetrafluoroethane (R-134a). In *International Refrigeration and Air Conditioning Conference*, Purdue University, Indiana, USA, paper 41, 1988.

[7] Eckels, S.J. & Pate, M.B., An experimental comparison of evaporation and condensation heat transfer coefficients for HFC-134a and CFC-12. *International Journal of Refrigeration*, **14(2)**, pp. 70–77, 1991, https://doi.org/10.1016/0140-7007(91)90078-u

[8] Khan, S.H. & Zubair, S.M., Thermodynamic analyses of the CFC-12 and HFC-134a refrigeration cycles. *Energy*, **18(7)**, pp. 717–726, 1993, https://doi.org/10.1016/0360-5442(93)90031-8

[9] Breidenich, C., Magraw, D., Rowley, A. & Rubin, J.W., The Kyoto protocol to the United Nations framework convention on climate change. *American Journal of International Law*, **92(2)**, pp. 315–331, 1998, https://doi.org/10.2307/2998044

[10] Spatz, M., Minor, B. & DuPont, H., *HFO-1234yf A low GWP refrigerant for MAC. Honeywell/DuPont joint collaboration*, In SAE World Congress, Detroit, Michigan, USA, 14-17 April 2008.

[11] Akasaka, R., An application of the extended corresponding states model to thermodynamic property calculations for trans-1,3,3,3-tetrafluoropropene (HFO-1234ze(E)). *International Journal of Refrigeration*, **33(5)**, pp. 907–914, 2010, https://doi.org/10.1016/j.ijrefrig.2010.03.003

[12] Richter, M., McLinden, M.O. & Lemmon, E.W., Thermodynamic Properties of 2,3,3,3-Tetrafluoroprop-1-ene (R1234yf): Vapor Pressure and p–ρ–T Measurements and an Equation of State. *Journal of Chemical & Engineering Data*, **56(7)**, pp. 3254–3264, 2011, https://doi.org/10.1021/je200369m

[13] Helvaci, H. & Khan, Z.A., Experimental study of thermodynamic assessment of a small scale solar thermal system. *Energy Conversion and Management*, **117**, pp. 567–576, 2016, https://doi.org/10.1016/j.enconman.2016.03.050

[14] Helvaci, H.U. & Khan, Z., Thermodynamic modelling and analysis of a solar organic Rankine cycle employing thermofluids. *Energy Conversion and Management*, **138**, pp. 493–510, 2017, https://doi.org/10.1016/j.enconman.2017.02.011

[15] Muraki, M., Sano, T. & Dong, D., Elastohydrodynamic properties and boundary lubrication performance of polyolester in a hydrofluoroether refrigerant environment, *Proceedings of the Institution of Mechanical Engineers, Part J: Journal of Engineering Tribology*, **216(1)**, pp. 19–26, 2002, https://doi.org/10.1243/1350650021543852

[16] Bhutta, M., Khan, Z. & Garland, N., Wear performance analysis of Ni–Al2O3 nanocomposite coatings under nonconventional lubrication. *Materials*, 12(1), p. 36, 2018. doi: 10.3390/ma12010036

10   *M. U. Bhutta, et al., Int. J. Comp. Meth. and Exp. Meas., Vol. 0, No. 0 (2019)*

[3] Mizuhara, K., Akei, M. & Matsuzaki, T., The friction and wear behavior in controlled alternative refrigerant atmosphere. *Tribology Transactions*, **37(1)**, pp. 120–128, 1994, https://doi.org/10.1080/10402009408983274

[4] Kawahara, K., Mishina, S., Kamino, A., Ochiai, K., Okawa, T. & Fujimoto, S., *Tribological Evaluation of Rotary Compressor with HFC Refrigerants*, In International Compressor Engineering Conference, Purdue University, Indiana, USA, paper 1141, 23-26 July 1996.

[5] Spauschus, H.O., HFC 134a as a substitute refrigerant for CFC 12. *International Journal of Refrigeration*, **11(6)**, pp. 389–392, 1988, https://doi.org/10.1016/0140-7007(88)90063-1

[6] Shankland, I.R., Basu, R.S. & Wilson, D.P., Thermal conductivity and viscosity of a new stratospherically safe refrigerant-1, 1, 1, 2-tetrafluoroethane (R-134a). In *International Refrigeration and Air Conditioning Conference*, Purdue University, Indiana, USA, paper 41, 1988.

[7] Eckels, S.J. & Pate, M.B., An experimental comparison of evaporation and condensation heat transfer coefficients for HFC-134a and CFC-12. *International Journal of Refrigeration*, **14(2)**, pp. 70–77, 1991, https://doi.org/10.1016/0140-7007(91)90078-u

[8] Khan, S.H. & Zubair, S.M., Thermodynamic analyses of the CFC-12 and HFC-134a refrigeration cycles. *Energy*, **18(7)**, pp. 717–726, 1993, https://doi.org/10.1016/0360-5442(93)90031-8

[9] Breidenich, C., Magraw, D., Rowley, A. & Rubin, J.W., The Kyoto protocol to the United Nations framework convention on climate change. *American Journal of International Law*, **92(2)**, pp. 315–331, 1998, https://doi.org/10.2307/2998044

[10] Spatz, M., Minor, B. & DuPont, H., *HFO-1234yf A low GWP refrigerant for MAC. Honeywell/DuPont joint collaboration*, In SAE World Congress, Detroit, Michigan, USA, 14-17 April 2008.

[11] Akasaka, R., An application of the extended corresponding states model to thermodynamic property calculations for trans-1,3,3,3-tetrafluoropropene (HFO-1234ze(E)). *International Journal of Refrigeration*, **33(5)**, pp. 907–914, 2010, https://doi.org/10.1016/j.ijrefrig.2010.03.003

[12] Richter, M., McLinden, M.O. & Lemmon, E.W., Thermodynamic Properties of 2,3,3,3-Tetrafluoroprop-1-ene (R1234yf): Vapor Pressure and p– –T Measurements and an Equation of State. *Journal of Chemical & Engineering Data*, **56(7)**, pp. 3254–3264, 2011, https://doi.org/10.1021/je200369m

[13] Helvaci, H. & Khan, Z.A., Experimental study of thermodynamic assessment of a small scale solar thermal system. *Energy Conversion and Management*, **117**, pp. 567–576, 2016, https://doi.org/10.1016/j.enconman.2016.03.050

[14] Helvaci, H.U. & Khan, Z., Thermodynamic modelling and analysis of a solar organic Rankine cycle employing thermofluids. *Energy Conversion and Management*, **138**, pp. 493–510, 2017, https://doi.org/10.1016/j.enconman.2017.02.011

[15] Muraki, M., Sano, T. & Dong, D., Elastohydrodynamic properties and boundary lubrication performance of polyolester in a hydrofluoroether refrigerant environment, *Proceedings of the Institution of Mechanical Engineers, Part J: Journal of Engineering Tribology*, **216(1)**, pp. 19–26, 2002, https://doi.org/10.1243/1350650021543852

[16] Bhutta, M., Khan, Z. & Garland, N., Wear performance analysis of Ni–Al2O3 nanocomposite coatings under nonconventional lubrication. *Materials*, 12(1), p. 36, 2018. doi: 10.3390/ma12010036

Paper III

materials

MDPI

Article

Wear Performance Analysis of Ni–Al$_2$O$_3$ Nanocomposite Coatings under Nonconventional Lubrication

Muhammad Usman Bhutta [1,2,*], **Zulfiqar Ahmad Khan** [1] and **Nigel Garland** [1]

[1] Department of Design & Engineering, NanoCorr, Energy & Modelling (NCEM) Research Group, Talbot Campus, Bournemouth University, Fern Barrow, Poole BH12 5BB, UK; zkhan@bournemouth.ac.uk (Z.A.K.); ngarland@bournemouth.ac.uk (N.G.)
[2] School of Mechanical & Manufacturing Engineering (SMME), Campus H-12, National University of Sciences & Technology (NUST), Islamabad 44000, Pakistan
*   Correspondence: mbhutta@bournemouth.ac.uk; Tel.: +44-746-202-6669

check for updates

Abstract: This article presents a wear study of Ni–Al$_2$O$_3$ nanocomposite coatings in comparison to uncoated steel contacts under reciprocating motion. A ball-on-flat type contact configuration has been used in this study in which a reciprocating flat steel sample has been used in a coated and uncoated state against a stationary steel ball under refrigerant lubrication. The next generation of environmentally friendly refrigerant HFE-7000 has been used itself as lubricant in this study without the influence of any external lubricant. The thermodynamic applications and performance of HFE-7000 is being studied worldwide, as it is replacing the previous generation of refrigerants. No work however has been previously performed to evaluate the wear performance of HFE-7000 using nanocomposite coatings. The wear scar developed on each of the flat and ball samples was studied using a Scanning Electron Microscope (SEM). The micrographs show that a combination of adhesive and abrasive wear occurs when using uncoated steel samples. Micro-delamination is observed in the case of Ni–Al$_2$O$_3$ nanocomposite coatings accompanied by adhesive and abrasive wear. Wear volume of the wear track was calculated using a White Light Interferometer. Energy-Dispersive X-ray Spectroscopic (EDS) analysis of the samples reveals fluorine and oxygen on the rubbing parts when tested using coated as well as uncoated samples. The formation of these fluorinated and oxygenated tribo-films helps to reduce wear and their formation is accelerated by increasing the refrigerant temperature. Ni–Al$_2$O$_3$ nanocomposite coatings show good wear performance at low and high loads in comparison to uncoated contacts. At intermediate loads the coated contacts resulted in increased wear, especially at low loads. This increase in wear is associated with the delamination of the coating and the slow formation of protective surface films under these testing conditions.

Keywords: Ni–Al$_2$O$_3$ nanocomposite coatings; wear; reciprocating motion; environmental friendly refrigerant; low carbon technology

1. Introduction

The use of refrigeration and air-conditioning systems has increased considerably with an increase in the global population. The ever increasing demand and usage of air-conditioning and cooling systems is also linked to global anthropogenic climate change. With increasing global warming, the demand on air-conditioning and refrigeration systems remains high. According to the International Energy Agency, air conditioning demands are set to grow rapidly over the coming decades [1]. An increasing number of air-conditioning and refrigeration units means increase in anthropogenic global warming, which is an inherited issue with the operation of an air-conditioning/refrigeration system.

Besides rejecting heat to the atmosphere, an air-conditioning/refrigeration system also contributes towards global climate change through the type of refrigerant it employs in its thermodynamic cycle.

Artificially formulated refrigerants have been forced to change over the years, due to their damaging environmental implications [2]. Chlorofluorocarbons (CFCs) and Hydrochlorofluorocarbons (HCFCs) were the first artificially formulated refrigerants that went into production in 1930s [2]. In addition to having excellent heat transfer and thermodynamic properties CFCs and HCFCs also have phenomenal trigological properties [3–12]. The phenomenal trigological properties of CFCs and HCFCs are associated with the capability of these refrigerants to form protective surface films on the rubbing machine parts, which reduces wear and friction. However, the discovery of the catastrophic effects of CFCs and HCFCs on the Ozone layer surrounding the earth's atmosphere in 1974 [13] led to a ban on these refrigerants by the Montreal Protocol on Substances that Deplete the Ozone Layer [14]. CFCs have higher Ozone Depletion Potential (ODP) in comparison to HCFCs. Use of CFCs was banned by the end of year 1995 in developed countries and HCFCs can no longer be used after 2020 [2].

Restrictions and bans on CFCs and HCFCs forced the introduction of another family of artificially formulated refrigerants called Hydrofluorocarbons (HFCs). HFCs had zero ODP and the thermodynamic properties of HFCs were reported to be similar to CFCs [15–19], making HFCs suitable substitute refrigerants. A number of studies were also conducted to evaluate the tribological behavior of HFCs in comparison to CFCs and HCFCs [3–9,11,12,20–27]. Almost all of the studies that compared the performance of HFCs to CFCs and HCFCs from a tribological viewpoint concluded that HFCs have inferior tribological performance in comparison to CFCs and HCFCs. The inferior tribological performance of HFCs is linked to the fact that, unlike CFCs and HCFCs, HFCs lack the capability to form protective surface films on the rubbing surfaces under normal compressor operating conditions. HFC refrigerants started getting used worldwide due to their zero ODP value and the fact that HFCs possessed good thermodynamic properties. The harmful global warming impact of HFCs were realized much later when HFCs were recognized as one of the major contributors towards global warming [28]. Kyoto Protocol to the United Nations Framework Convention of Climate Change in 1997 put restrictions on carbon dioxide and other greenhouse gases, banning HFCs from 2022 in any hermetically sealed system.

Naturally occurring refrigerants such as hydrocarbons gained interest due to the enforcement of Environmental Impact Legislation. A number of studies were performed to evaluate the tribological behavior of hydrocarbons under various operating conditions [29–40]. Hydrocarbons are considered to be more efficient thermal conductors than HFCs [2], however hydrocarbons are highly flammable, which seriously restricts their commercialization. Carbon dioxide is another naturally occurring compound that has good thermodynamic properties and has a global warming potential (GWP) value of only one. This makes carbon dioxide a good candidate to be used as a refrigerant. A number of experimental investigations have been performed to study the behavior and performance of CO_2 [41–54]. The studies concerned with the tribological analysis of CO_2 are mainly conducted at high pressures because of its low critical temperature. A scroll compressor was also developed for automotive air-conditioning system based on CO_2 [55], but the operating pressure for carbon dioxide was very high which resulted in its low efficiency due to the large gas thrust. These studies show that carbon dioxide which is non-flammable and a good thermal conductor with a GWP value of only one is not a suitable replacement for HFCs, because of the requirement of very high operating pressures and special system design constraints.

Environmental Impact Legislation, the inherited safety and operational requirements concerning issues with the naturally occurring compounds, has yet again forced the introduction of the future generation of refrigerants. The future generation of refrigerants that have been introduced in the market not only have zero ODP but also have lower GWP values. HFOs (Hydrofluoroolefins) and HFEs (Hydrofluoroethers) are amongst these future generation of refrigerants. These refrigerants not only have zero ODP but also have lower GWP values compared to the previous generation of refrigerants. A number of studies have been performed by various researchers to assess the tribological

behavior of HFOs [56–61] under various conditions and the studies have revealed that, unlike HFCs, Hydrofluoroolefins form protective tribo-films on the rubbing surfaces, which gives them very good tribological properties in comparison to HFCs. HFOs are, however, flammable and are termed as "mildly-flammable" which limits and restricts their application areas.

HFEs (Hydrofluoroethers) are non-flammable thermos-fluids having zero ODP and a low GWP value. HFEs are low toxic, colorless, odorless refrigerants having a number of application areas. The application areas include usage in fuel cells, in renewable solar thermal systems, in auto-cascade refrigeration systems, in high voltage transformers, in vapor degreasing applications, in chemical reactors, as lubricant carriers, as cleaning and rinsing agents, and so on [62]. Recent studies [63–65] have shown HFEs to have good thermal properties, particularly in renewable and green energy applications. HFE-7000 has significant industrial applications, including clean energy, low carbon technologies, aerospace and automotive applications. No work has also been performed to access the wear performance of HFE-7000 by using nanocomposite coatings. HFE-7000 has a GWP value of 530 and ODP value of zero [62], whereas HFC-134a, which is commonly used in domestic and automotive units, has zero ODP and a GWP value of 1430 [58]. Various other properties of HFE-7000 have been listed in Table 1. The purpose of this study is multifold: (a) to study the wear behavior of HFE-7000 by using steel contacts; and (b) to evaluate the wear performance and compatibility of Ni–Al$_2$O$_3$ nanocomposite coatings and look into the possibility to reduce wear of interacting parts of a system using HFE-7000 by using nanocomposite coatings.

Table 1. Various properties of hydrofluoroether (HFE)-7000 [62].

HFE-7000	
Structure	C$_3$F$_7$OCH$_3$
Molecular Weight (g/mol)	200
Freeze Point (°C)	−122.5
Boiling Point @ 1 atmosphere (°C)	34
Critical Temperature (°C)	165
Critical Pressure (MPa)	2.48
Flash Point (°C)	None
Kinematic Viscosity @−120°C (cSt)	17
Kinematic Viscosity @20°C (cSt)	0.32
Kinematic Viscosity @40°C (cSt)	0.27
Flammability	Non-flammable
Ozone Depletion Potential (ODP)	Zero
Global Warming Potential (GWP)	530 *

* GWP 100-year integrated time horizon [62].

Nanostructured design obtained by the dispersion of nano particles into a matrix has been demonstrated in enhancing optical, electrical, thermal and mechanical properties in comparison to conventionally used metallic materials [66–68]. A number of studies [69–77] have been performed by various different researchers to investigate the mechanical, wear, friction and corrosion performance of electrodeposited Nano Ni–Al$_2$O$_3$ coatings under a number of different environments and testing conditions. These studies have shown that electrodeposited Nano Ni–Al$_2$O$_3$ coatings can significantly improve the wear, friction and corrosion performance of rubbing parts.

In this study the wear behavior of HFE-7000 has been studied using a modified reciprocating tribo-meter. The initial part of the study is concerned with evaluating the wear performance of HFE-7000 using two different types of steel in a ball-on-flat contact configuration. In the second part of this study the flat steel specimen was coated using the electrodeposition process, in which Nano Al$_2$O$_3$ particles were embedded in the nickel matrix and deposited on the flat steel substrate.

2. Materials and Methods

A reciprocating ball-on-flat contact configuration has been chosen for this study. The ball specimen is 10 mm in diameter made of AISI 52100 steel. The ball specimens are oil hardened, having excellent wear and deformation resistance. The balls are vacuum degassed and evenly through hardened in electric furnaces. The flat specimen is made of 230M07 (EN1A) steel and is circular in shape, having a diameter of 30 mm and thickness of 2.75 mm. AISI 52100 steel is a common material tested by researchers [35,37,42,43,45,46,50,58,61,78–80] when experimentally assessing the friction and wear performance of refrigerants, as it a common metal used in compressors. EN1A steel has shown good adhesion properties as a substrate for depositing Nano Ni–Al$_2$O$_3$ coatings using pulse current [74–77,81] and is also cheaper and easily available, in contrast to other specialized metals.

Phoenix Tribology reciprocating tribo-meter, TE 57 Pressurized Lubricity Tester (Phoenix Tribology, Kingsclere, UK) was modified to test the next generation of refrigerant, HFE-7000. The modified tribo-meter is schematically represented in Figure 1.
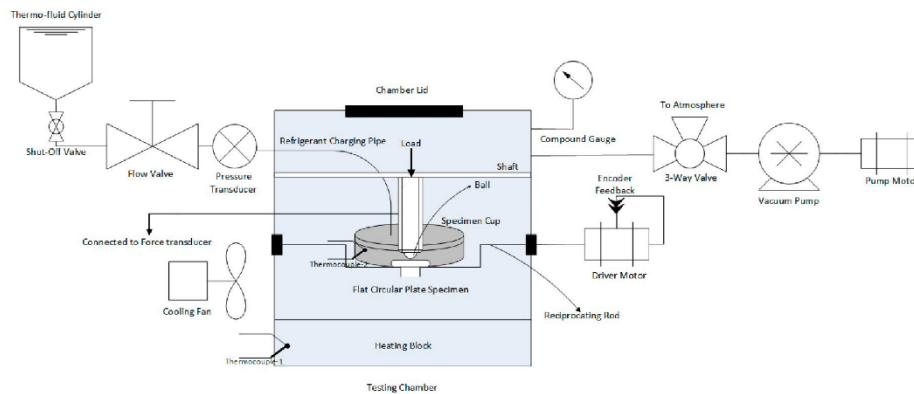

Figure 1. Experimental setup schematic diagram.

The parts that are to be evaluated are fixed in position in the testing chamber. The flat circular sample is positioned on the oscillating rod inside the cup. A wire-type thermocouple is positioned to directly read the temperature of the refrigerant in the specimen cup. Grub screws are used to fix the steel ball in the ball holder. The ball holder is then fastened to the horizontal shaft. The shaft not only holds the ball holder in position but is also used to apply the vertical normal load. Once the samples have been positioned the chamber lid is closed and a vacuum pump is used to vacuum the chamber in order to reduce the effects of ambient atmosphere and air on the testing. Once the chamber has been vacuumed, the refrigerant is introduced in the chamber. HFE-7000 has a boiling point of 34 °C and is liquid under normal atmospheric pressure and temperature. Gravity and the vacuum helps HFE-7000 to flow from the storage cylinder into the specimen cup. A sufficient amount of HFE-7000 is introduced in the chamber so that it not only fills the cups completely but also overflows and is gathered at the bottom of the testing chamber where the heating block is located. The additional overflown refrigerant helps maintain the temperature inside the chamber. The temperature of the fluid and the oscillating frequency are controlled by feedback PID (Proportional–Integral–Derivative) control. The pressure of the chamber is recorded and monitored by a pressure transducer and a pressure gauge. All the data is monitored, recorded and controlled using specialized software, COMPEND. The behavior of the refrigerant was studied under relatively low loads and temperatures because of its wide application areas and due to the fact that it is not only used in compressors.

3. Experimentation

The experimentation section is divided into two main parts. The first part of the experimentation is concerned with the wear study of rubbing steel parts in the presence of HFE-7000 under fully lubricated conditions. The second part of the study explains the development of Nano Ni–Al$_2$O$_3$ coatings using the pulse current technique, which is followed by the wear study of the coated samples under identical testing conditions as the uncoated samples.

3.1. Sample Preparation

Sample preparation involves preparing the surfaces of the flat circular steel specimens to the desired conditions for testing. Sample preparation for uncoated samples is discussed in Section 3.1.1 and the sample preparation of coated samples is discussed in Section 3.1.2 respectively.

3.1.1. Sample Preparation of Uncoated Samples

The flat circular specimens were machined into a thickness of 2.75 mm and a diameter of 30 mm using conventional machining methods. Each sample was then grinded and polished to reach an average surface roughness value of 0.1 μm. Each sample was then conditioned with acetone (Fisher Scientific, Pittsburgh, PA, USA) for 5 min in an ultrasonic bath (Grant Instruments, Shepreth, UK) after which it was dried using a specimen drier and warm air. The grinding, polishing and surface conditioning of the samples with acetone also insured the removal of any oxide or unwanted surface films from the metal surface.

3.1.2. Sample Preparation of Coated Samples

Nano Ni–Al$_2$O$_3$ coatings were prepared using the pulse electrodeposition process with a coating thickness of ~10 μm on the EN1A steel substrate. The electrolyte was prepared using NiCl$_2$·6H$_2$O (48 g/L), NiSO$_4$·6H$_2$O (265 g/L), H$_3$BO$_3$ (31 g/L), Nano Al$_2$O$_3$ (20 g/L). The size of the Nano Al$_2$O$_3$ particles was less than 50 nm, as given by the manufacturer (Sigma-Aldrich, Gillingham, UK). The solution was magnetically stirred for 24 h, after which it was ultrasonically agitated for an additional 4 h. This ensured the proper suspension and dispersion of the particles inside the solution. The next step involved heating the solution to 40 °C. After being heated to 40 °C, the solution is ready to be used. Each machined flat circular steel specimen was grinded and polished to achieve an average surface roughness of 0.05 μm, after which it was conditioned with acetone in an ultrasonic bath for 5 min. Once the EN1A steel sample had been prepared it was suspended in the prepared solution and was used as cathode. A pure nickel sheet was also suspended in the solution and was used as the anode. The electrodeposition was started once everything was ready and in place. The pulse parameters were kept constant during the deposition process. The current density was set at (3 A/dm^2), the duty cycle was kept at 20% and the pulse on-off time was maintained at (20 ms–80 ms). During ON-time current is applied and during OFF-time current is kept at zero. The solution was constantly magnetically stirred, ultrasonically agitated and kept at a temperature of 40 °C during the complete coating process. The coating process was stopped after 1 h i.e. (T$_{ON}$ + T$_{OFF}$ = 3600 s).

The microstructure of the prepared coating was studied using a Scanning Electron Microscope (JEOL, Tokyo, Japan). High magnification images of the prepared nanocomposite coating are presented in Figure 2. The microstructure of the prepared Ni–Al$_2$O$_3$ nanocomposite coating is similar to the microstructure reported by various other researchers [74–76,81]. The high magnification image shown in Figure 2a shows that there are pores on the surface of the electrodeposited nanocomposite coating. These pores are a characteristic of Ni–Al$_2$O$_3$ nanocomposite coatings [76]. Figure 2b shows the nanocomposite coating after the application of false color to the Scanning Electron Microscope (SEM) image. The colored image better reveals the pores on the coating, which are randomly distributed and are visible as dark colored spots in the colored image.
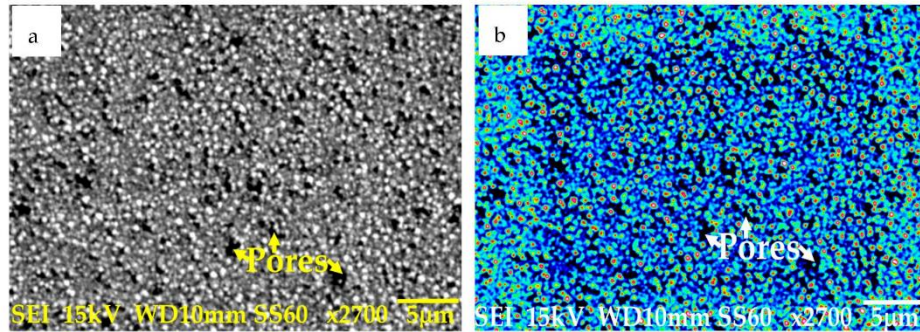
Figure 2. Micrograph of Ni–Al$_2$O$_3$ nanocomposite coating (**a**) High magnification image (**b**) False color applied to the high magnification image.

Energy-Dispersive X-ray Spectroscopic (EDS, JEOL, Tokyo, Japan) Analysis was performed at various regions on the surface of the nanocomposite coating. One of the results obtained by performing EDS analysis is shown in Figure 3b, which clearly shows the presence of Nickel, Aluminum and Oxygen confirming the deposition of Nickel on the steel substrate with Nano Al$_2$O$_3$ particles embedded in the Nickel matrix.
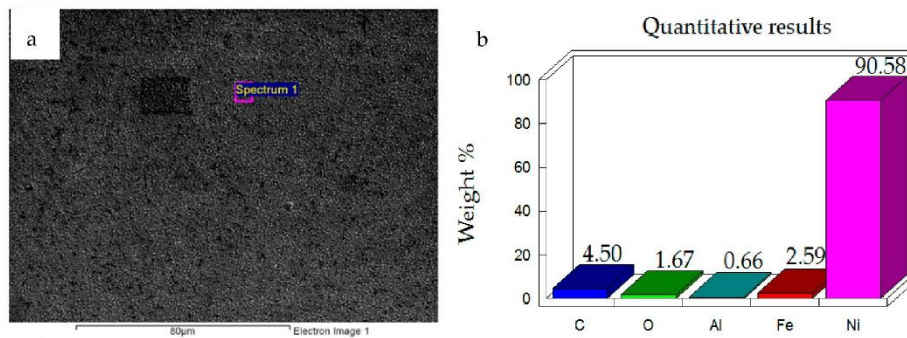

Figure 3. (**a**) Micrograph of Ni–Al$_2$O$_3$ nanocomposite coating (**b**) Energy-Dispersive X-ray Spectroscope (EDS) analysis results.

The pre-test elemental analysis and surface examination of the prepared coatings show that the Ni–Al$_2$O$_3$ nanocomposite coatings have been successfully prepared.

3.2. Testing

Both the uncoated and coated sample were tested against 52100 steel balls. Testing was performed using two different temperatures, 20 °C and 40 °C with three different loads 10 N, 20 N and 30 N. The stroke length was kept constant at 5 mm for all the tests. All the experiments were conducted at a constant frequency of 5 Hz. Each experiment was performed at least twice to ensure repeatability. A PID-controlled feedback algorithm was used to maintain the temperature during the course of a test. Before starting a test, the refrigerant was heated to the desired temperature and the temperature was maintained for 1 h. After maintaining the temperature of the refrigerant for 1 h, a test was started. Each test lasted for 2 h. The mechanical properties of all the samples were measured and are summarized in Table 2. It can be seen from the values in Table 2 that the mechanical surface properties of steel are significantly improved with the application of Ni–Al$_2$O$_3$ nanocomposite coating. The hardness improves from 180 HV to 450 HV and Elastic Modulus improves from 200 GPa to 280 GPa. The

elastic modulus and hardness of the coated samples were measured using a Nano-indentation tester (Micro Materials, Wrexham, UK). The hardness of the steel ball and the uncoated steel specimen were measured using a Vickers hardness tester (BUEHLER, Lake Bluff, IL, USA). The average surface roughness of all the samples was measured using the white light interferometer (ZYGO, Zygo Corporation, Middlefield, CT, USA).

Table 2. Measured mechanical properties of all the samples used.

Specimen	Hardness (HV)	Elastic Modulus (GPa)	Average Surface Roughness (μm)
Steel ball	810	210	0.010
Uncoated steel specimen	180	200	0.1
Coated steel specimen	450 ± 25	280	0.045

4. Results and Discussion

This section has been divided into further subsections to clearly state the findings of all the coated and uncoated tests. Section 4.1 covers the study of the uncoated flat circular specimens while the results of the Nano Ni–Al$_2$O$_3$ coated specimens are presented in Section 4.2. A brief explanation of the observations of each test is given as it is presented. Full explanation of all the observations is given at the end of Section 4.

Each sample pair, that is, the flat circular EN1A steel sample and the 52100 steel ball, were analyzed. Post-test analyses was performed on each sample pair initially under a Scanning Electron Microscope (SEM) to observe the wear mechanism at the micron level. Energy-Dispersive X-ray Spectroscopic (EDS) Analysis was done on each sample at various regions of the wear scar for the elemental analysis and chemical characterization. The wear scar on each of the flat circular specimens was stitched using a white light interferometer (ZYGO). The stitched wear scar presented the wear profile, which was used to calculate the wear volume.

4.1. Wear of Uncoated Specimens

The hard 52100 steel ball ploughed through the EN1A steel, and material pileup was observed at the extreme ends of the wear tracks of the uncoated specimens. A combination of adhesive and abrasive wear was observed. Abrasive wear dominated at the mid-portions of the circular specimens. Adhesive wear was more prominent at the extreme ends and boundaries of the wear track. Under the application of normal load and reciprocating motion, the soft EN1A steel asperity junctions with the steel ball break and become adhered to the hard steel ball. The micrographs and EDS analysis results of all the tests are presented in Figures 4–9.
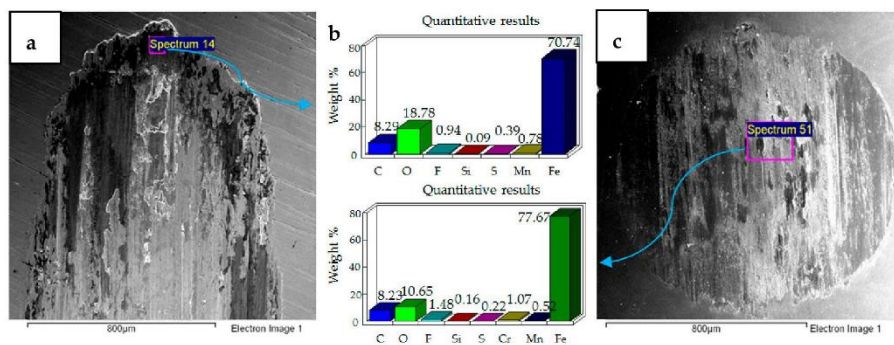

Figure 4. Uncoated samples. Operating conditions 10 N, 20 °C: (**a**) Scanning Electron Microscope (SEM) image of flat specimen (**b**) EDS analysis results (**c**) SEM image of ball.

Figure 5. Uncoated samples. Operating conditions 20 N, 20 °C: (**a**) SEM image of flat specimen (**b**) EDS analysis results (**c**) SEM image of ball.

Figure 6. Uncoated samples. Operating conditions 30 N, 20 °C: (**a**) SEM image of flat specimen (**b**) EDS analysis results (**c**) SEM image of ball.

Figure 7. Uncoated samples. Operating conditions 10 N, 40 °C: (**a**) SEM image of flat specimen (**b**) EDS analysis results (**c**) SEM image of ball.

Figure 8. Uncoated samples. Operating conditions 20 N, 40 °C: (**a**) SEM image of flat specimen (**b**) EDS analysis results (**c**) SEM image of ball.
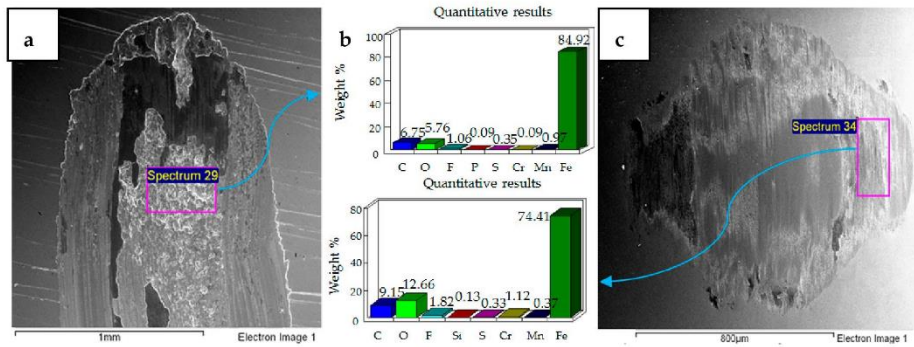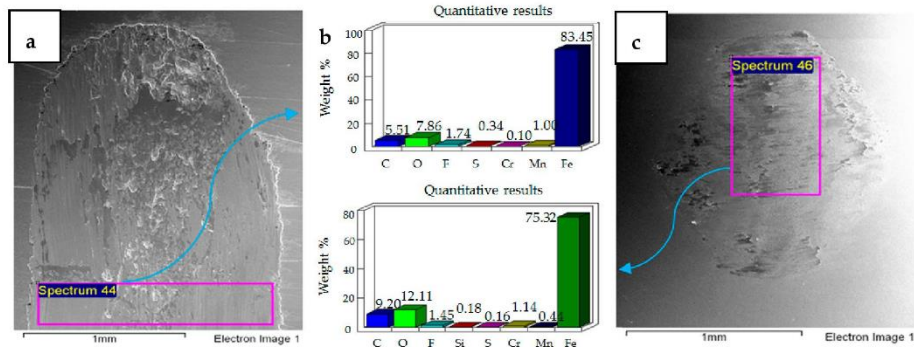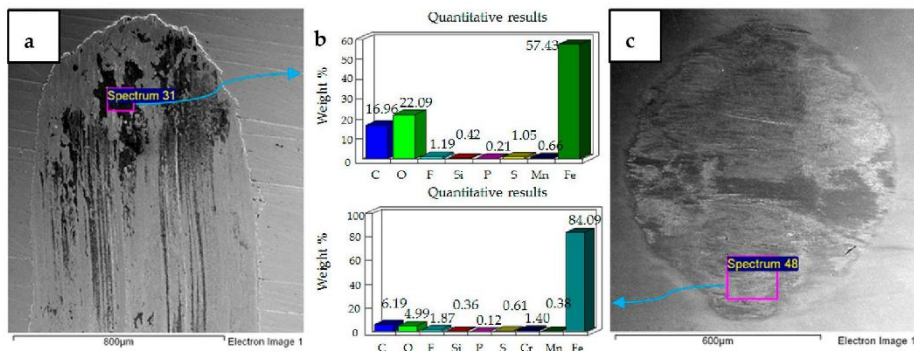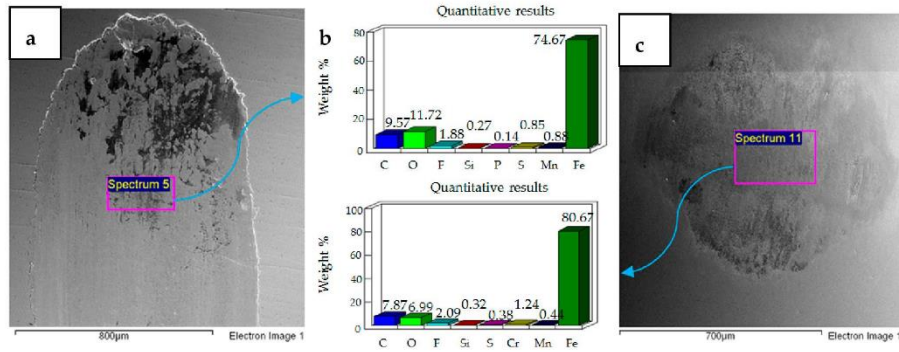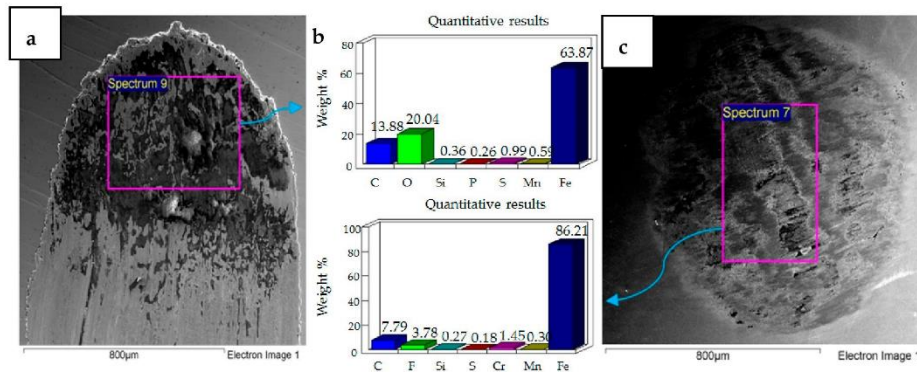

Figure 9. Uncoated samples. Operating conditions 30 N, 40 °C: (**a**) SEM image of flat specimen (**b**) EDS analysis results (**c**) SEM image of ball.

The results of the test performed at 10 N, 20 °C are presented in Figure 4. SEM micrographs of the flat specimen reveal wear as a combination of adhesive and abrasive wear. The SEM image of the steel ball indicates scratch marks, along with a strong presence of adhered particles from the flat EN1A steel specimen, which implies that adhesive wear is more dominant under these operating conditions. The EDS analysis on the flat circular specimen, as well as on the steel ball, reveal a presence of fluorine and oxygen, which indicates the formation of tribo-films. EDS analysis revealed similar results at the mid-section of the wear track, as well as at the other extreme end of the wear scar.

SEM micrographs of 20 N, 20 °C are presented in Figure 5. Compared to 10 N/20 °C, 20 N/20 °C operating conditions produced more abrasive wear of both the flat and ball samples. EDS analysis also revealed the transfer of particles from the ball onto the flat circular specimen, along with the presence of oxygen and fluorine on the rubbing surfaces.

SEM micrographs of 30 N, 20 °C are shown in Figure 6. Under these operating conditions the wear mechanism has shifted towards a combination of adhesive and abrasive wear, indicating a considerable increase in wear compared to the previous two conditions. Compared to 20 N/20 °C, which produced more abrasive wear, adhesion of EN1A steel on the hard steel ball along with scratch marks can be clearly observed at 30 N/20 °C. EDS analysis reveal the presence of oxygen and fluorine on both the specimens. Transfer of steel ball particles onto the flat specimen is also evident from the EDS results.

Results of increasing the refrigerant temperature from 20 °C to 40 °C are presented in Figures 7–9. Figure 7 shows the results of 10 N/40 °C. Severe wear as observed at 10 N/20 °C is not visible at

10 N/40 °C. Unlike the wear scar at 10 N/20 °C the flat specimen at 10 N/40 °C also showed less adhesive wear, which is also evident by observing the ball specimen. EDS analysis of the ball and flat sample reveal the presence of fluorine and oxygen under these operating conditions as well.

Figure 8 shows the micrographs and the results of EDS analysis of operating conditions of 20 N, 40 °C. Similar to 20 N/20 °C, wear at operating conditions of 20 N/40 °C is also mainly due to abrasion. However, unlike 20 N/20 °C, SEM images show that less wear is generated at 20 N/40 °C. Fluorine and oxygen were also detected on the ball and flat sample at these operating conditions.

Figure 9 shows the micrographs and EDS results of 30 N, 40 °C testing conditions. The micrographs show a combination of adhesive and abrasive wear similar to the test performed at 30 N, 20 °C. EDS analysis of the wear scar on the flat sample shows a strong presence of oxygen but no fluorine. EDS results of the ball sample, on the other hand, show fluorine on the top surface but no oxygen. These EDS results are different from all the other tests of the uncoated samples, as fluorine and oxygen were both detected under each of the other testing conditions on the ball, as well as the flat specimen.

The wear scar on each of the flat circular specimens was stitched using the white light interferometer (ZYGO). The stitched image provided a complete 3D profile of the wear scar and was used to calculate the wear volume. The type of 3D images obtained from ZYGO are shown in Figures 17 and 18 for the coated samples; similar images were obtained for the uncoated samples, as well from ZYGO. The wear volume generated at each of the operating temperatures and load for the flat uncoated samples is shown in Figure 10. Comparing the effect of the increase in temperature from 20 °C to 40 °C at any given load shows a decrease in wear volume. The effect of increasing the refrigerant temperature on wear becomes more prominent with increasing load. Increasing the refrigerant temperature from 20 °C to 40 °C reduces wear by more than 50% at 20 N and 30 N. This reduction in wear is due to the formation of protective tribo-films on the top surface of the rubbing parts.
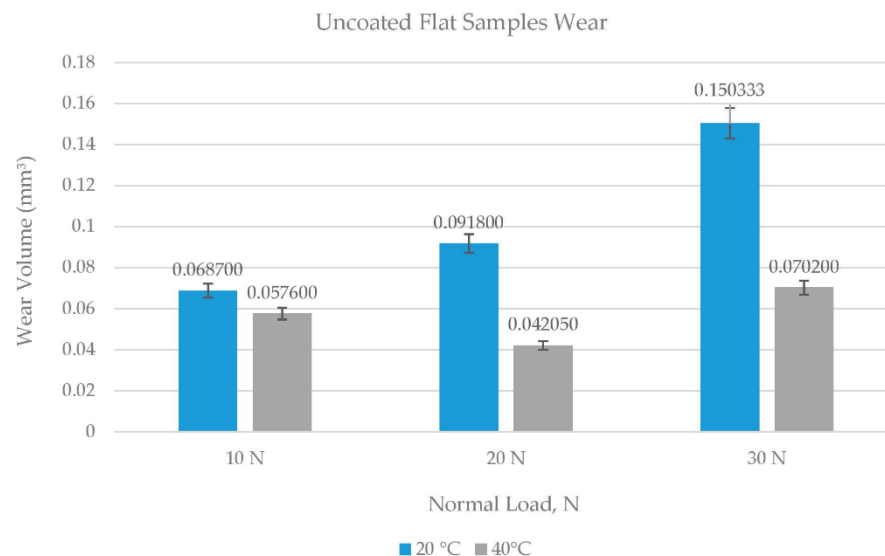

Figure 10. Wear volume of uncoated flat specimens.

HFE-7000 disassociates with the application of load and constant reciprocating mechanical motion, which leads to the formation of new compounds on the freshly exposed surfaces. These fluorinated and oxygenated compounds protect the top surface. Increase in temperature from 20 °C to 40 °C at

any given load decreases the viscosity of the refrigerant, reducing the separation between the rubbing parts, which should result in increased wear due to more asperity interactions. However, increase in temperature has shown a decrease in wear volume at any given load. This indicates that an increase in temperature at the same applied load increases the reactivity of HFE-7000 with the rubbing metals, resulting in a faster formation of protective tribo-films.

4.2. Wear of Coated Specimens

Ni–Al$_2$O$_3$ nanocomposite coatings were tested under identical operating conditions as the uncoated samples. EDS analysis was performed on each of the samples tested and the wear on all the samples was examined using SEM. Micrographs and EDS results of the coated samples have been presented in Figures 11–16.

Figure 11. Ni–Al$_2$O$_3$ coated flat specimen. Operating conditions 10 N, 20 °C: (**a**) SEM image of flat specimen (**b**) EDS analysis results (**c**) SEM image of ball.

Figure 12. Ni–Al$_2$O$_3$ coated flat specimen. Operating conditions 20 N, 20 °C: (**a**) SEM image of flat specimen (**b**) EDS analysis results (**c**) SEM image of ball.
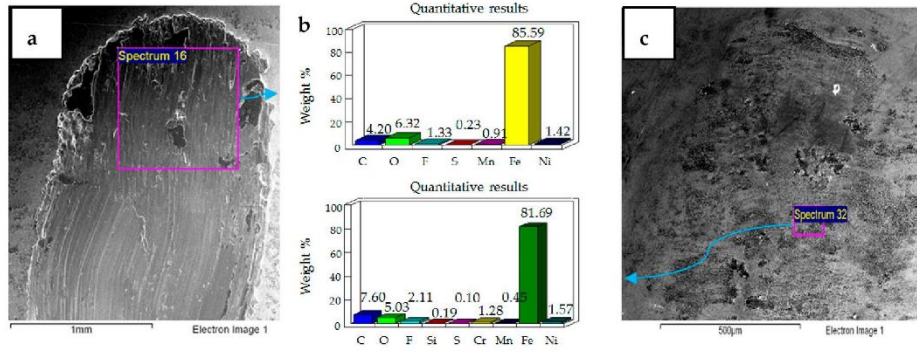
Figure 13. Ni–Al$_2$O$_3$ coated flat specimen. Operating conditions 30 N, 20 °C: (**a**) SEM image of flat specimen (**b**) EDS analysis results (**c**) SEM image of ball.

Figure 14. Ni–Al$_2$O$_3$ coated flat specimen. Operating conditions 10 N, 40 °C: (**a**) SEM image of flat specimen (**b**) EDS analysis results (**c**) SEM image of ball.

Figure 15. Ni–Al$_2$O$_3$ coated flat specimen. Operating conditions 20 N, 40 °C: (**a**) SEM image of flat specimen (**b**) EDS analysis results (**c**) SEM image of ball.
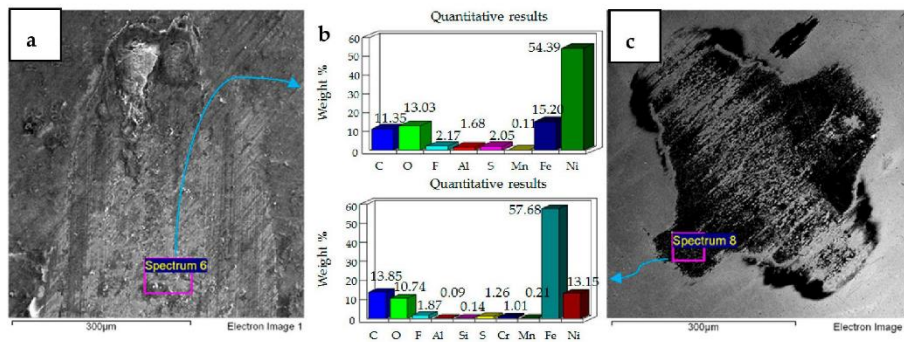
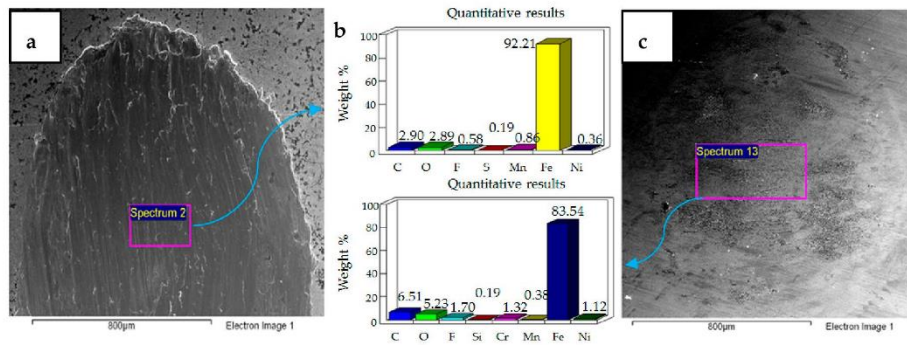**Figure 16.** Ni–Al$_2$O$_3$ coated flat specimen. Operating conditions 30 N, 40 °C: (**a**) SEM image of flat specimen (**b**) EDS analysis results (**c**) SEM image of ball.

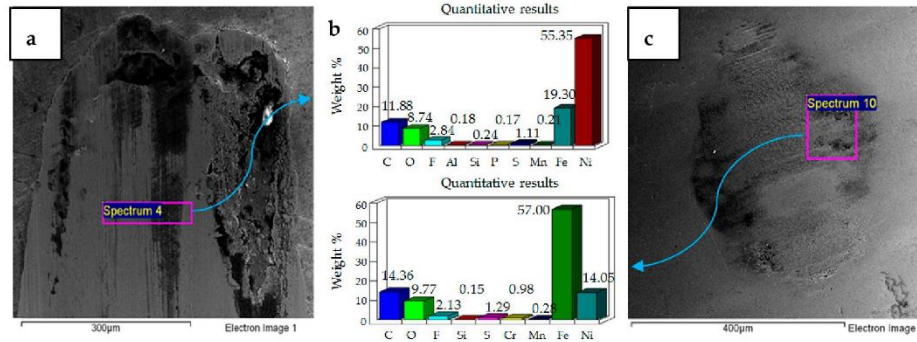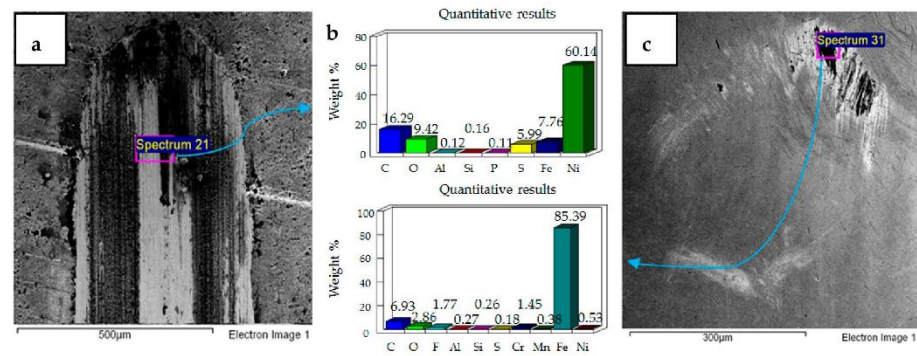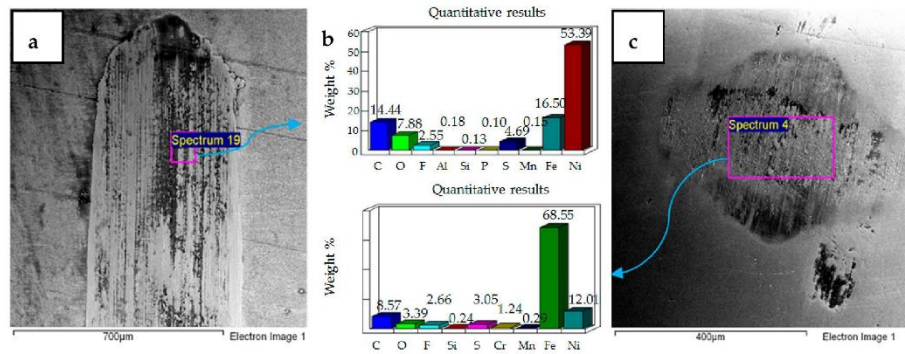Micrographs and EDS results of flat Ni–Al$_2$O$_3$ nanocoated samples against 52100 steel ball at 10 N, 20 °C are shown in Figure 11. Figure 11a shows the micrograph of wear on the flat specimen. The image shows micro-delamination of the coating and exposure of the steel substrate. Ni–Al$_2$O$_3$ nanocomposite coatings have been reported to delaminate under reciprocating motion [76]. Micro-delamination of the coating was observed throughout the wear scar. The coating under these operating conditions is, however, still very much intact, and comparing the coated steel sample to the uncoated steel sample at 10 N/20 °C shows a reduction in wear. Micrographs of the steel ball show a combination of adhesive and abrasive wear, along with the adhesion of the delimited particles on the steel ball. Post-test EDS analysis of the steel ball shows a presence of nickel and aluminum, indicating adhesion of the delaminated coating from the flat sample on the steel ball along with fluorine and oxygen. EDS analysis on the flat sample shows iron, indicating the exposure of the steel substrate. Fluorine and oxygen were also detected on the flat sample, implying the formation of tribo-films.

The effect of increasing the load from 10 N to 20 N for the coated sample at a refrigerant temperature of 20 °C is shown in Figure 12. Figure 12a shows the micrographs of the flat specimen. This image is very different from the image obtained at 10 N/20 °C. EDS analysis of the flat specimen reveals a very strong percentage of iron, indicating that the applied coating has not only been delaminated but has also been completely worn out throughout the wear track. EDS results of the wear scar show only traces of nickel and a slight presence of oxygen and fluorine. Comparing the EDS results of the flat coated sample to the flat uncoated sample under the same testing conditions shows a lesser presence of oxygen and fluorine, which implies that protective tribo-films are not well-formed in the case of the coated sample under these testing conditions. The micrograph of the ball sample shows a combination of abrasive and adhesive wear, with abrasive wear being the more dominant wear mechanism. In comparison to the flat steel sample, the EDS results of the ball sample show a stronger presence of oxygen and fluorine, indicating that under these testing conditions the tribo-films are being more easily formed on the ball sample.

The results of increasing the normal load further from 20 N to 30 N at 20 °C refrigerant temperature are shown in Figure 13. The micrograph and EDS analysis of the flat sample show that the coating has been completely delaminated and worn out under these operating conditions as well. Elemental analysis shows the presence of fluorine and oxygen on the flat as well as ball samples. Increasing load from 20 N to 30 N at 20 °C shows an increase in adhesive wear, which is evident from the flat and ball samples indicating an increase in wear volume. The wear mechanism of the uncoated sample at 30 N/20 °C is similar to the coated sample at 30 N/20 °C, in both of these cases wear is a combination of adhesive and abrasive wear. However there is more adhesive wear for the coated sample because of the adhesion of the delaminated coating on the ball.

The effect of increasing the refrigerant from 20 °C to 40 °C at 10 N load is shown in Figure 14. The micrograph of the flat sample shows more delamination of the coating at the sides and top of the wear scar. This micrograph is different from 20 °C/10 N, in which delamination of the coating was observed throughout the wear track. EDS analysis of the wear scar shows the presence of iron, along with oxygen and fluorine, indicating formation of surface films and micro-delamination of the coating along the wear track. The micrograph of the ball specimen at these operating conditions shows less adhesive wear in comparison to the micrograph of the ball sample at 20 °C/10 N. EDS analysis of the ball sample also shows the presence of oxygen and fluorine. Wear of the coated sample at 40 °C/10 N presents a combination of adhesive and abrasive wear whereas the uncoated sample at 40 °C/10 N shows more abrasive wear.

Increasing load from 10 N to 20 N at refrigerant temperature 40 °C increases abrasive wear as shown in Figure 15. The micrograph and EDS results show micro-delamination of the coating along the sides of the wear track due to abrasion. Unlike 10 N/40 °C, which displayed strong delamination at the top and extreme corners of the wear track, at 20 N/40 °C the wear track shows a more uniform micro-delamination of the coating along the wear scar. Similar to 20 N/ 20 °C, abrasive wear is the more dominant wear phenomenon at 20 N/ 40 °C as well. However, unlike 20 N/ 20 °C, at which a total delamination of the coating was observed, the coating at 20 N/ 40 °C is still very much intact, indicating a reduction in wear. Coated and uncoated samples at 20 N/ 40 °C present similar results in terms of wear mechanism, as abrasive wear was dominant in the case of coated as well as uncoated samples under these testing conditions.

Similar to 30 N/20 °C testing conditions, increasing the load from 20 N to 30 N at 40 °C results in a combination of adhesive and abrasive wear, also shown in Figure 16. However, unlike 30 N/20 °C, at which a complete delamination of the coating was observed, the coating at 30 N/40 °C is still intact. The EDS analysis of both the flat and ball samples reveal the presence of fluorine and oxygen. EDS results and micrograph of the flat sample show more micro-delamination of the coating along the center of the wear scar as compared to the sides. The micrograph of the coated flat steel sample also demonstrates a combination of adhesive and abrasive wear similar to the uncoated sample tested at 30 N/40 °C, but differs in regards to the extent of wear. The coated flat sample shows less wear damage in comparison to the uncoated sample. The steel ball tested with the coated sample also shows less wear than the ball used in the uncoated test.

The white light interferometer (ZYGO) was also used to stitch the wear track of the flat coated samples to provide the complete 3D plot of the wear scar. The 3D images of the wear track for both the testing temperatures have been presented in Figures 17 and 18. The stitched 3D profiles of the wear tracks were used to calculate the wear volume for each of the testing conditions.
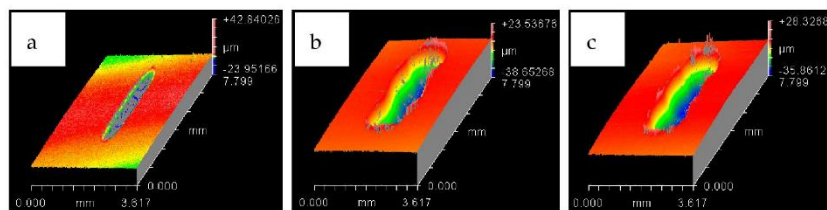

Figure 17. Wear track for HFE–7000 temperature 20 °C with Ni–Al$_2$O$_3$ coated specimens. At normal loads of: (**a**) 10 N (**b**) 20 N (**c**) 30 N.
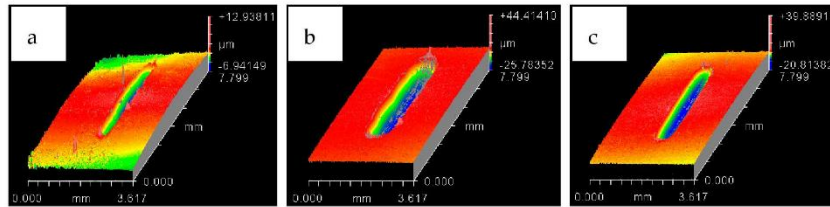
Figure 18. Wear track for HFE–7000 temperature 40 °C with Ni–Al$_2$O$_3$ coated specimens. At normal loads of: (**a**) 10 N (**b**) 20 N (**c**) 30 N.

Wear volume of each of the coated flat samples was determined using the 3D images shown in Figures 17 and 18 generated by ZYGO. The results of the wear volume of the coated flat samples have been presented in Figure 19. Similar to the uncoated samples, increase in load at the same temperature increases wear. Less wear is generated at 10 N/20 °C by using a coated flat specimen in comparison to uncoated flat sample at the sample testing conditions. This indicates that at low loads and lower HFE-7000 temperature, Ni–Al$_2$O$_3$ nanocomposite coatings help reduce wear. Wear is influenced by the surface mechanical properties which improve considerably by the application of Ni–Al$_2$O$_3$ nanocomposite coatings which results in wear reduction. The hardness, elastic modulus and the surface roughness are all improved by the application of Ni–Al$_2$O$_3$ nanocomposite coatings in comparison to the uncoated samples. The smoother surface of the coated samples have an average surface roughness value of only 0.045 μm, whereas the uncoated flat specimens have a higher average surface roughness value of 0.1 μm. Smoother surface of the coated samples means lesser asperity interactions, resulting in reduction in wear. Another reason for reduction in wear volume when using coated specimens is due to the micro-pores that exist in Ni–Al$_2$O$_3$ nanocomposite coatings, as shown in Figure 2; these pores help retain the liquid refrigerant, increasing the lubricity of the rubbing parts. Micro dimpled grooves and cavities in the surface have been reported to improve the tribological performance of interacting parts [82,83]. The presence of micro-pores in this case similarly helped improve the wear performance.
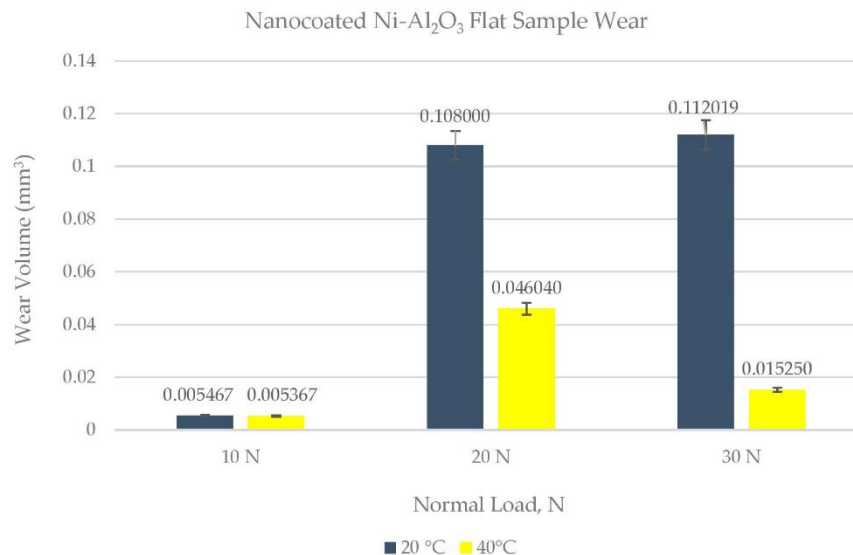

Figure 19. Wear volume of Ni–Al$_2$O$_3$ coated flat specimens.

For 20 °C refrigerant temperature, wear volume increases rapidly by increasing the load from 10 N to 20 N for coated flat specimens. In the case of uncoated specimens, an increase in load from 10 N to 20 N does result in slightly higher wear, but the rate of increase in wear volume is not as sharp in the case of an uncoated specimen. Also comparing the wear volume of the uncoated specimen to the coated specimen at 20 N/20 °C shows that more wear has occurred when using the coated specimen. This shows that increasing the load at a low refrigerant temperature of 20 °C has an adverse effect on wear. The micrographs of the wear scar as presented in Figure 12 show a total delamination of the coating. The EDS results of the wear scar show scarce presence of oxygen and fluorine. This shows that not only has the coating completely worn out under these conditions, the protective surface films have also not fully formed on the surface of the flat specimen. This result shows that using this coating at low temperatures and slightly higher loads results in an increase in wear. EDS results of the ball show the presence of oxygen and fluorine, indicating that protective surface films are being formed on the counter-face under these operating conditions.

A further increase in load at 20 °C from 20 N to 30 N further increases wear. The wear volume generated using coatings is less compared to the uncoated sample under these conditions. The coating has also been completely worn out at 30 N/20 °C, similar to at 20 N/20 °C. Similar to the uncoated test at 30 N/20 °C the coated test at 30 N/20 °C also produced a combination of adhesive and abrasive wear. Adhesive wear is more prominent in the coating study because of the delamination and wear of the coating, which becomes adhered to the steel ball under constant reciprocating motion. The normal applied load has been further increased by 10 N, but the wear volume reduces by using coating unlike the previous testing conditions, that is, 20 N/20 °C. EDS results of the ball and flat sample show a higher percentage of fluorine and oxygen in comparison to the 20 N/20 °C testing conditions. This shows that increasing the load at a constant temperature helps the faster chemical breakdown of HFE-7000, which results in the accelerated formation of protective surface films which help reduce wear.

Doubling the refrigerant temperature from 20 °C to 40 °C at 10 N load results in the reduction of wear compared to the uncoated test at 10 N/40 °C. Doubling the temperature also shows a decrease in wear volume compared to the 10 N/20 °C coated test. The delamination process of the coating is slow under these testing conditions, which is mainly due to the low load and healthy formation of oxygenated/fluorinated tribo-films on the top surfaces of the rubbing parts at elevated temperatures.

Increasing the load to 20 N at 40 °C increases wear of the coated flat sample, which is different from the results obtained when using uncoated parts. The uncoated flat specimen showed the least amount of wear at 20 N/40 °C amongst all the uncoated tests, showing an optimum load and temperature combination. The micrographs and EDS analysis of the wear track of the coated flat sample show that there is micro-delamination of the coating and the presence of oxygen and fluorine. Comparing the wear volumes of the coated and uncoated wear tracks shows that the difference in the wear volumes is not as high as it was at 20 °C at the same load. A reason for this increased wear when using the coating is the micro-delamination of the coating, which increases the wear volume. Comparing the results of the coated contacts at 20 °C and 40 °C at 20 N load shows that increasing the refrigerant temperature has a high positive impact on reducing wear.

Increasing the load further to 30 N at 40 °C reduces wear. This wear volume is less than the wear generated by using uncoated samples. This wear is also less in comparison to the wear at 30 N/20 °C. The EDS results and micrographs show that, although there is micro-delamination of the coating, the coating is still well adhered to the steel substrate. This micro-delamination is also less than the micro-delamination at 20 N/40 °C. These results show that increasing the temperature increases the reactivity of the refrigerant with the rubbing parts, resulting in the accelerated formation of protective tribo-films which reduce wear.

The least amount of wear for coated specimens was observed at a low load of 10 N and at a high refrigerant temperature of 40 °C. The percentage change in wear volume by using Ni–Al$_2$O$_3$ nanocomposite coatings in comparison uncoated samples is shown in Figure 20.
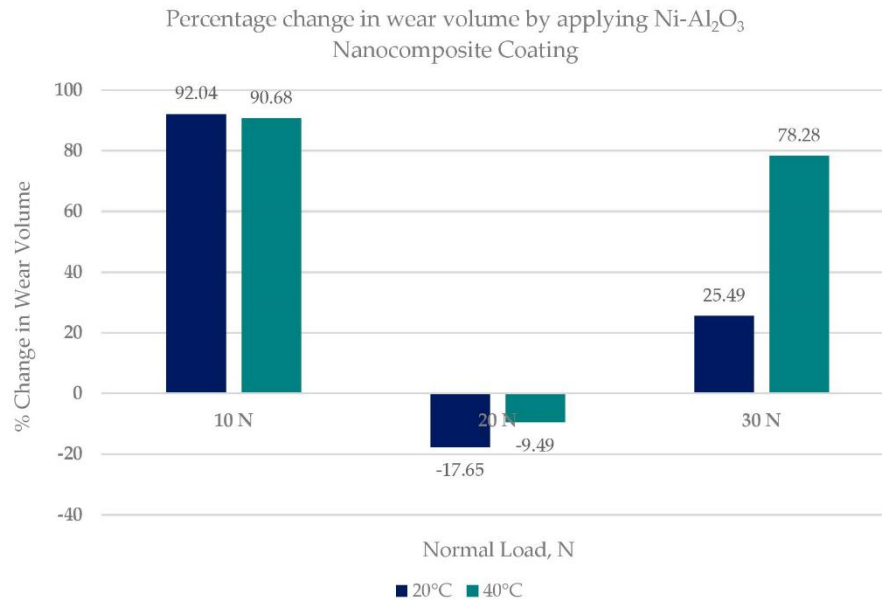
Figure 20. Percentage change in the wear volume of flat specimens by using Ni–Al$_2$O$_3$ nanocomposite coatings.

Figure 20 shows that applying Ni–Al$_2$O$_3$ nanocomposite coatings has a positive effect on wear and these coatings can reduce wear by more than 90% at low loads. Increasing the load to 20 N has an adverse effect on wear of coated flat samples especially at low refrigerant temperature. However increasing the applied load further to 30 N reduces wear as well in comparison to the uncoated tests. This shows that Ni–Al$_2$O$_3$ nanocomposite coatings can significantly reduce wear in systems employing HFE-7000 at low and high operating loads.

5. Conclusions

In this work, wear performance analysis of Ni–Al$_2$O$_3$ nanocomposite coating was performed under nonconventional, that is, refrigerant lubrication and the results were compared to uncoated steel samples. The study concludes the following points:

- A modified tribo-meter was used to study the wear performance of Ni–Al$_2$O$_3$ nanocomposite coating under HFE-7000 refrigerant lubrication under varying operating conditions.
- Ni–Al$_2$O$_3$ nanocomposite coatings were successfully developed using the pulse coating technique. The wear mechanism of the coatings developed has been studied and has been compared to uncoated contacts under the same operating conditions.
- Ni–Al$_2$O$_3$ nanocomposite coating shows good wear performance at low loads and can reduce wear by more than 90% compared to uncoated parts. At intermediate loads, the wear performance of these coatings showed adverse effects and increased the wear by 18% at low operating temperatures of 20 °C. Further increase in load to 30 N reduced wear by 25% at the low refrigerant temperature of 20 °C and by 78% at the higher refrigerant temperature of 40 °C.
- Post-test elemental analysis of the surfaces revealed oxygen and fluorine on the interacting parts by using coated as well as uncoated steel samples. This indicates that HFE-7000 formed new compounds on the metallic surfaces, resulting in the formation of protective tribo-films which help reduce wear.

- Increase in temperature has a very positive impact on reducing wear of both the coated and uncoated samples. The ability of HFE-7000 to from protective tribo-films on the rubbing surfaces increases with increase in temperature, resulting in the accelerated formation of protective surface films on the rubbing metals.
- HFE-7000, which is an environmentally friendly future generation thermo-fluid, having good thermodynamic properties, has shown good wear performance as well.
- Wear can be reduced by using Ni–Al$_2$O$_3$ nanocomposite coating on EN1A-steel substrate instead of using specialized expensive metal alloys.

6. Future Work

Ni–Al$_2$O$_3$ nanocomposite coating has been examined in this study, and the results were compared to the uncoated parts of a specific surface finish. The future work should investigate other nanocomposite coatings as well to evaluate their performance and compatibility with HFE-7000. Application of Ni–Al$_2$O$_3$ nanocomposite coatings indicated that a considerable reduction in wear can be achieved at low and high operating loads; however, these nanocomposite coatings showed poor wear performance at intermediate loads. It would be extremely beneficial to study other nanocomposite coatings under the same operating conditions to determine which coatings perform better at intermediate loads as well. For the uncoated sample, only a single value of surface roughness has been used; it will be very useful to experimentally evaluate how uncoated EN1A steel parts of various surface finish perform under HFE-7000 refrigerant lubrication.

References

1. International Energy Agency (iea). Available online: https://www.iea.org/newsroom/news/2016/august/air-conditioning-demand-set-to-grow-rapidly-over-the-coming-decades.html (accessed on 19 December 2018).
2. Bhutta, M.U.; Khan, Z.A.; Garland, N.P.; Ghafoor, A. A historical review on the tribological performance of refrigerants used in compressors. *Tribol. Ind.* **2018**, *40*, 19–51. [CrossRef]
3. Jollev, S. New and unique lubricants for use in compressors utilizing R-134a refrigerant. In Proceedings of the International Refrigeration and Air Conditioning Conference, Purdue University, West Lafayette, IN, USA, 17–20 July 1990; p. 96.
4. Davis, B.; Sheiretov, T.K.; Cusano, C. Tribological evaluation of contacts lubricated by oil-refrigerant mixtures. *Am. J. Hematol.* **1992**, *71*, 66.
5. Komatsuzaki, S.; Homma, Y. Lubricants for HFC refrigerant compressors. *J. Japn. Petrol. Inst.* **1994**, *37*, 226–235. [CrossRef]
6. Mizuhara, K.; Akei, M.; Matsuzaki, T. The friction and wear behavior in controlled alternative refrigerant atmosphere. *Tribol. Trans.* **1994**, *37*, 120–128. [CrossRef]
7. Sheiretov, T.; Glabbeek, W.V.; Cusano, C. Tribological evaluation of various surface treatments for M2 tool steel in a refrigerant environment. In Proceedings of the International Compressor Engineering Conference, Purdue University, West Lafayette, IN, USA, 19–22 July 1994; p. 964.
8. Akei, M.; Mizuhara, K.; Taki, T.; Yamamoto, T. Evaluation of film-forming capability of refrigeration lubricants in pressurized refrigerant atmosphere. *Wear* **1996**, *196*, 180–187. [CrossRef]

9.   Kawahara, K.; Mishina, S.; Kamino, A.; Ochiai, K.; Okawa, T.; Fujimoto, S. Tribological evaluation of rotary compressor with HFC refrigerants. In Proceedings of the International Compressor Engineering Conference, Purdue University, West Lafayette, IN, USA, 23–26 July 1996; p. 1141.

10. Fujimoto, S.; Sakitani, K.; Watada, M. Tribology analysis in rolling piston type compressor. In Proceedings of the International Compressor Engineering Conference, Purdue University, West Lafayette, IN, USA; 1984; p. 477.

11. Muraki, M.; Tagawa, K.; Dong, D. Refrigeration lubricant based on polyolester for use with HFCs and prospect of its application with R-22 (Part 1) tribological characteristics. In Proceedings of the International Refrigeration and Air Conditioning Conference, Purdue University, West Lafayette, IN, USA, 23–26 July 1996; p. 336.

12. Tuomas, R.; Isaksson, O. Measurement of lubrication conditions in a rolling element bearing in a refrigerant environment. *Ind. Lubr. Tribol.* **2009**, *61*, 91–99. [CrossRef]

13. Molina, M.J.; Rowland, F.S. Stratospheric sink for chlorofluoromethanes: Chlorine atom-catalysed destruction of ozone. *Nature* **1974**, *249*, 810–812. [CrossRef]

14. Nations, U. Montreal Protocol on Substances that Deplete the Ozone Layer Final Act 1987. *J. Environ. Law* **1989**, *1*, 128–136.

15. Wilson, D.P.; Basu, R.S. Thermodynamic properties of a new stratospherically safe working fluid-refrigerant 134a. *ASHRAE Trans.* **1988**, *94*, 2095–2118.

16. Shankland, I.R.; Basu, R.S.; Wilson, D.P. Thermal conductivity and viscosity of a new stratospherically safe refrigerant-1,1,1,2-tetrafluoroethane (R-134a). In Proceedings of the International Refrigeration and Air Conditioning Conference, Purdue University, West Lafayette, IN, USA; 1988; p. 41.

17. Spauschus, H. HFC 134a as a substitute refrigerant for CFC 12. *Int. J. Refrig.* **1988**, *11*, 389–392. [CrossRef]

18. Eckels, S.J.; Pate, M.B. An experimental comparison of evaporation and condensation heat transfer coefficients for HFC-134a and CFC-12. *Int. J. Refrig.* **1991**, *14*, 70–77. [CrossRef]

19. Khan, S.H.; Zubair, S.M. Thermodynamic analyses of the CFC-12 and HFC-134a refrigeration cycles. *Energy* **1993**, *18*, 717–726. [CrossRef]

20. Na, B.C.; Chun, K.J.; Han, D.-C. A tribological study of refrigeration oils under HFC-134a environment. *Tribol. Int.* **1997**, *30*, 707–716. [CrossRef]

21. Wardle, F.; Jacobson, B.; Dolfsma, H.; Hoglund, E.; Jonsson, U. The effect of refrigerants on the lubrication of rolling element bearings used in screw compressors. In Proceedings of the International Compressor Engineering Conference, Purdue University, West Lafayette, IN, USA, 14–17 July 1992; p. 843.

22. Jacobson, B. Lubrication of Screw Compressor Bearings in the Presence of Refrigerants. In Proceedings of the International Compressor Engineering Conference, Purdue University, West Lafayette, IN, USA, 19–22 July 1994; p. 966.

23. Hamada, T.; Nishiura, N. Refrigeration lubricant based on polyolester for use with HFCs and prospect of its application with R-22 (Part 2) Hydrolytic stability and compressor endurance test results. In Proceedings of the International Refrigeration and Air Conditioning Conference, Purdue University, West Lafayette, IN, USA, 23–26 July 1996; p. 337.

24. Jacobson, B. Ball Bearing Lubrication in Refrigetation Compressors. In Proceedings of the International Compressor Engineering Conference, Purdue University, West Lafayette, IN, USA, 23–26 July 1996; p. 1090.

25. Akei, M.; Mizuhara, K. The Elastohydrodynamic Properties of Lubricants in Refrigerant Environments©. *Tribol. Trans.* **1997**, *40*, 1–10. [CrossRef]

26. Jacobson, B.O.; Espejel, G.E.M. High pressure investigation of refrigerants HFC245fa, R134a and R123. In Proceedings of the International Compressor Engineering Conference, Purdue University, West Lafayette, IN, USA, 17–20 July 2006; p. 1789.

27. Tuomas, R.; Isaksson, O. Compressibility of Oil/Refrigerant Lubricants in Elasto-Hydrodynamic Contacts. *J. Tribol.* **2005**, *128*, 218–220. [CrossRef]

28. Breidenich, C.; Magraw, D.; Rowley, A.; Rubin, J.W. The Kyoto protocol to the United Nations framework convention on climate change. *Am. J. Int. Law* **1998**, *92*, 315–331. [CrossRef]

29. Garland, N.; Hadfield, M. Environmental implications of hydrocarbon refrigerants applied to the hermetic compressor. *Mater. Des.* **2005**, *26*, 578–586. [CrossRef]

30. Khan, Z.A.; Hadfield, M.; Wang, Y. Design of a novel pressurized chamber to assess in-use durability performance of rolling contact elements using refrigerant lubrication. In Proceedings of the 4th International Conference of Advanced Engineering Design, Glasgow, Scotland, UK, 5–8 September 2004.

31. Khan, Z.A.; Hadfield, M.; Wang, Y. Pressurised chamber design for conducting rolling contact experiments with liquid refrigerant lubrication. *Mater. Des.* **2005**, *26*, 680–689. [CrossRef]

32. Khan, Z.A.; Hadfield, M.; Tobe, S.; Wang, Y. Ceramic rolling elements with ring crack defects—A residual stress approach. *Mater. Sci. Eng A* **2005**, *404*, 221–226. [CrossRef]

33. Khan, Z.A.; Hadfield, M.; Tobe, S.; Wang, Y. Residual stress variations during rolling contact fatigue of refrigerant lubricated silicon nitride bearing elements. *Ceram. Int.* **2006**, *32*, 751–754. [CrossRef]

34. Khan, Z.A.; Hadfield, M. Manufacturing induced residual stress influence on the rolling contact fatigue life performance of lubricated silicon nitride bearing materials. *Mater. Des.* **2007**, *28*, 2688–2693. [CrossRef]

35. Solzak, T.A.; Polycarpou, A.A. Tribology of protective hard coatings for use in oil-less, piston-type compressors. In Proceedings of the International Compressor Engineering Conference, Purdue University, West Lafayette, IN, USA, 17–20 July 2006; p. 1790.

36. Sariibrahimoglu, K.; Kizil, H.; Aksit, M.F.; Efeoglu, I.; Kerpicci, H. Effect of R600a on tribological behavior of sintered steel under starved lubrication. *Tribol. Int.* **2010**, *43*, 1054–1058. [CrossRef]

37. De Mello, J.; Binder, R.; Demas, N.; Polycarpou, A. Effect of the actual environment present in hermetic compressors on the tribological behaviour of a Si-rich multifunctional DLC coating. *Wear* **2009**, *267*, 907–915. [CrossRef]

38. Solzak, T.A.; Polycarpou, A.A. Tribology of hard protective coatings under realistic operating conditions for use in oilless piston-type and swash-plate compressors. *Tribol. Trans.* **2010**, *53*, 319–328. [CrossRef]

39. Silverio, M.; Binder, R.; Hulse, E.R.; De Mello, J.D.B. Effect of refrigerant gases (HFC134a and R600a) on the tribological behaviour of a multifunctional DLC coating. In Proceedings of the International Compressor Engineering Conference, Purdue University, West Lafayette, IN, USA, 11–14 July 2016; p. 2413.

40. Górny, K.; Stachowiak, A.; Tyczewski, P.; Zwierzycki, W. Lubricity evaluation of oil–refrigerant mixtures with R134a and R290. *Int. J. Refrig.* **2016**, *69*, 261–271. [CrossRef]

41. Ikeda, H.; Yagi, J.I.; Kawaguchi, Y. The development of PAG refrigeration lubricants for hermetic compressors with CO_2. In Proceedings of the International Refrigeration and Air Conditioning Conference, Purdue University, West Lafayette, IN, USA, 12–15 July 2004; p. 680.

42. Wu, X.; Cong, P.; Nanao, H.; Minami, I.; Mori, S. Tribological behaviors of 52100 steel in carbon dioxide atmosphere. *Tribol. Lett.* **2004**, *17*, 925–930. [CrossRef]

43. Lee, K.; Suh, A.; Demas, N.; Polycarpou, A. Surface and sub-micron sub-surface evolution of Al390-T6 undergoing tribological testing under submerged lubrication conditions in the presence of CO_2 refrigerant. *Tribol. Lett.* **2005**, *18*, 1–12. [CrossRef]

44. Demas, N.G.; Polycarpou, A.A.; Conry, T.F. Tribological Studies on Scuffing Due to the Influence of Carbon Dioxide Used as a Refrigerant in Compressors. *Tribol. Trans.* **2005**, *48*, 336–342. [CrossRef]

45. Demas, N.G.; Polycarpou, A.A. Ultra high pressure tribometer for testing CO_2 refrigerant at chamber pressures up to 2000 psi to simulate compressor conditions. *Tribol. Trans.* **2006**, *49*, 291–296. [CrossRef]

46. Cannaday, M.; Polycarpou, A. Advantages of CO_2 compared to R410a refrigerant of tribologically tested Aluminum 390-T6 surfaces. *Tribol. Lett.* **2006**, *21*, 185–192. [CrossRef]

47. Jeon, H.-G.; Oh, S.-D.; Lee, Y.-Z. Friction and wear of the lubricated vane and roller materials in a carbon dioxide refrigerant. *Wear* **2009**, *267*, 1252–1256. [CrossRef]

48. Demas, N.G.; Polycarpou, A.A. Tribological investigation of cast iron air-conditioning compressor surfaces in CO_2 refrigerant. *Tribol. Lett.* **2006**, *22*, 271–278. [CrossRef]

49. Demas, N.G.; Polycarpou, A.A. Tribological performance of PTFE-based coatings for air-conditioning compressors. *Surf. Coat. Tech.* **2008**, *203*, 307–316. [CrossRef]

50. Nunez, E.E.; Demas, N.G.; Polychronopoulou, K.; Polycarpou, A.A. Tribological study comparing PAG and POE lubricants used in air-conditioning compressors under the presence of CO_2. *Tribol. Trans.* **2008**, *51*, 790–797. [CrossRef]

51. Nunez, E.E.; Demas, N.G.; Polychronopoulou, K.; Polycarpou, A.A. Comparative scuffing performance and chemical analysis of metallic surfaces for air-conditioning compressors in the presence of environmentally friendly CO_2 refrigerant. *Wear* **2010**, *268*, 668–676. [CrossRef]

52. Dascalescu, D.; Polychronopoulou, K.; Polycarpou, A. The significance of tribochemistry on the performance of PTFE-based coatings in CO₂ refrigerant environment. *Surf. Coat. Tech.* **2009**, *204*, 319–329. [CrossRef]
53. Nunez, E.E.; Polychronopoulou, K.; Polycarpou, A.A. Lubricity effect of carbon dioxide used as an environmentally friendly refrigerant in air-conditioning and refrigeration compressors. *Wear* **2010**, *270*, 46–56. [CrossRef]
54. Nunez, E.E.; Polycarpou, A.A. Wear study of metallic interfaces for air-conditioning compressors under submerged lubrication in the presence of carbon dioxide. *Wear* **2015**, *326*, 28–35. [CrossRef]
55. Hagita, T.; Makino, T.; Horaguchi, N.; Ukai, T. Tribology in CO₂ Scroll Compressors. Available online: https://www.mhi.co.jp/technology/review/pdf/e391/e391031.pdf (accessed on 19 December 2018).
56. Sasaki, T.; Nakao, H.; Maeyama, H.; Mizuno, K. Tribology characteristics of HFO and HC refrigerants with immiscible oils—Effect of refrigerant with unsaturated bond. In Proceedings of the International Compressor Engineering Conference, Purdue University, West Lafayette, IN, USA, 12–15 July 2010; p. 1946.
57. Mishra, S.P.; Polycarpou, A.A. Tribological studies of unpolished laser surface textures under starved lubrication conditions for use in air-conditioning and refrigeration compressors. *Tribol. Int.* **2011**, *44*, 1890–1901. [CrossRef]
58. Akram, M.W.; Polychronopoulou, K.; Polycarpou, A.A. Lubricity of environmentally friendly HFO-1234yf refrigerant. *Tribol. Int.* **2013**, *57*, 92–100. [CrossRef]
59. Akram, M.W.; Polychronopoulou, K.; Seeton, C.; Polycarpou, A.A. Tribological performance of environmentally friendly refrigerant HFO-1234yf under starved lubricated conditions. *Wear* **2013**, *304*, 191–201. [CrossRef]
60. Akram, M.W.; Polychronopoulou, K.; Polycarpou, A.A. Tribological performance comparing different refrigerant–lubricant systems: The case of environmentally friendly HFO-1234yf refrigerant. *Tribol. Int.* **2014**, *78*, 176–186. [CrossRef]
61. Akram, M.W.; Meyer, J.L.; Polycarpou, A.A. Tribological interactions of advanced polymeric coatings with polyalkylene glycol lubricant and r1234yf refrigerant. *Tribol. Int.* **2016**, *97*, 200–211. [CrossRef]
62. 3M™ Novec™ 7000 Engineered Fluid. Available online: https://multimedia.3m.com/mws/media/121372O/3m-novec-7000-engineered-fluid-tds.pdf (accessed on 19 December 2018).
63. Helvaci, H.; Khan, Z.A. Experimental study of thermodynamic assessment of a small scale solar thermal system. *Energy Convers. Manag.* **2016**, *117*, 567–576. [CrossRef]
64. Helvaci, H.; Khan, Z. Thermodynamic modelling and analysis of a solar organic Rankine cycle employing thermofluids. *Energy. Convers. Manag.* **2017**, *138*, 493–510. [CrossRef]
65. Helvaci, H.U.; Khan, Z.A. Heat transfer and entropy generation analysis of HFE 7000 based nanorefrigerants. *Int. J. Heat. Mass. Trans.* **2017**, *104*, 318–327. [CrossRef]
66. Meyers, M.A.; Mishra, A.; Benson, D.J. Mechanical properties of nanocrystalline materials. *Prog. Mater. Sci.* **2006**, *51*, 427–556. [CrossRef]
67. Kumar, K.S.; Van Swygenhoven, H.; Suresh, S. Mechanical behavior of nanocrystalline metals and alloys. *Acta Mater.* **2003**, *51*, 5743–5774. [CrossRef]
68. Zong, Y.; Zuo, L. Materials design of microstructure in grain boundary and second phase particles. *J. Mater. Sci. Tech.* **2003**, *19*, 97–101.
69. Chen, L.; Wang, L.; Zeng, Z.; Xu, T. Influence of pulse frequency on the microstructure and wear resistance of electrodeposited Ni–Al₂O₃ composite coatings. *Surf. Coat. Tech.* **2006**, *201*, 599–605. [CrossRef]
70. Chen, L.; Wang, L.; Zeng, Z.; Zhang, J. Effect of surfactant on the electrodeposition and wear resistance of Ni–Al₂O₃ composite coatings. *Mater. Sci. Eng. A* **2006**, *434*, 319–325. [CrossRef]
71. Zhou, Q.; He, C.L.; Cai, Q.K. Effect of Al₂O₃ Powders on Properties of Electrodeposited Ni Matrix. *Adv. Mater. Res.* **2009**, *79*, 631–634. [CrossRef]
72. Saha, R.K.; Khan, T.I. Effect of applied current on the electrodeposited Ni–Al₂O₃ composite coatings. *Surf. Coat. Tech.* **2010**, *205*, 890–895. [CrossRef]
73. Borkar, T.; Harimkar, S.P. Effect of electrodeposition conditions and reinforcement content on microstructure and tribological properties of nickel composite coatings. *Surf. Coat. Tech.* **2011**, *205*, 4124–4134. [CrossRef]
74. Bajwa, R.S.; Khan, Z.; Bakolas, V.; Braun, W. Water-lubricated Ni-based composite (Ni–Al₂O₃, Ni–SiC and Ni–ZrO₂) thin film coatings for industrial applications. *Acta Metall. Sin. (Eng. Lett.)* **2016**, *29*, 8–16. [CrossRef]

75. Bajwa, R.S.; Khan, Z.; Bakolas, V.; Braun, W. Effect of bath ionic strength on adhesion and tribological properties of pure nickel and Ni-based nanocomposite coatings. *J. Adhes. Sci. Tech.* **2016**, *30*, 653–665. [CrossRef]

76. Nazir, M.H.; Khan, Z.A.; Saeed, A.; Bakolas, V.; Braun, W.; Bajwa, R. Experimental analysis and modelling for reciprocating wear behaviour of nanocomposite coatings. *Wear* **2018**, *416–417*, 89–102. [CrossRef]

77. Nazir, M.H.; Khan, Z.A.; Saeed, A.; Bakolas, V.; Braun, W.; Bajwa, R.; Rafique, S. Analyzing and Modelling the Corrosion Behavior of Ni/Al$_2$O$_3$, Ni/SiC, Ni/ZrO$_2$ and Ni/Graphene Nanocomposite Coatings. *Materials* **2017**, *10*, 1225. [CrossRef]

78. Yoon, H.; Sheiretov, T.; Cusano, C. Scuffing behavior of 390 aluminum against steel under starved lubrication conditions. *Wear* **2000**, *237*, 163–175. [CrossRef]

79. Suh, A.Y.; Polycarpou, A.A.; Conry, T.F. Detailed surface roughness characterization of engineering surfaces undergoing tribological testing leading to scuffing. *Wear* **2003**, *255*, 556–568. [CrossRef]

80. Nunez, E.E.; Yeo, S.M.; Polycarpou, A.A. Tribological behavior of PTFE, PEEK, and fluorocarbon-based polymeric coatings used in air-conditioning and refrigeration compressors. In Proceedings of the International Compressor Engineering Conference, Purdue University, West Lafayette, IN, USA, 12–15 July 2010; p. 2031.

81. Bajwa, R.; Khan, Z.; Nazir, H.; Chacko, V.; Saeed, A. Wear and Friction Properties of Electrodeposited Ni-Based Coatings Subject to Nano-enhanced Lubricant and Composite Coating. *Acta Metall. Sin. (Eng. Lett.)* **2016**, *29*, 902–910. [CrossRef]

82. Bai, L.; Meng, Y.; Khan, Z.A.; Zhang, V. The Synergetic Effects of Surface Texturing and MoDDP Additive Applied to Ball-on-Disk Friction Subject to Both Flooded and Starved Lubrication Conditions. *Tribol. Lett.* **2017**, *65*, 163. [CrossRef]

83. Abdullah, M.U.; Shah, S.R.; Bhutta, M.U.; Mufti, R.A.; Khurram, M.; Najeeb, M.H.; Arshad, W.; Ogawa, K. Benefits of wonder process craft on engine valve train performance. *Proc. Inst. Mech. Engs. Part D J. Automb. Eng.* **2018**. [CrossRef]

Paper IV

Friction and wear performance analysis of hydrofluoroether-7000 refrigerant

Muhammad Usman Bhutta [a,b], Zulfiqar Ahmad Khan* [a]

[a] NanoCorr, Energy & Modelling (NCEM) Research Group, Department of Design & Engineering, Bournemouth University, Talbot Campus, Fern Barrow, Poole, BH12 5BB
[b] School of Mechanical & Manufacturing Engineering (SMME), National University of Sciences & Technology (NUST), Campus H-12, Islamabad, Pakistan
*Corresponding author: zkhan@bournemouth.ac.uk

Abstract

The disquiet about global warming has triggered the formulation and introduction of new generation of refrigerants. Hydrofluoroethers (HFEs) are within the family of newly developed environmentally friendly refrigerants with a wide range of application areas. Hydrofluoroethers reportedly have better heat transfer and thermodynamic properties. In addition to an understanding and knowledge of the thermodynamic properties of refrigerants, it is essential to understand the tribological properties of refrigerants within the context of sustainable development. Tribo-performance of refrigerants applied in refrigeration, air-conditioning and energy systems directly influences the durability, reliability and cost effectiveness of the system. HFE-7000 has considerable potential for engineering applications in green energy and low carbon technologies. In this research, a detailed investigation has been performed to assess the friction and wear performance of HFE-7000 (HFE-347mcc3). HFE-7000 has been employed itself as lubricant. Experimental results indicate the formation of tribo-films on the topmost surfaces. Energy-Dispersive X-ray Spectroscopic (EDS) and X-ray Photoelectron Spectroscopic (XPS) analyses on the tested samples revealed significant presence of oxygenated and fluorinated anti-wear tribo-films. These oxygen and fluorine containing tribo-layers prevent metal to metal contact and contribute to the reduction of friction and wear.

Keywords: Environment-friendly refrigerants, tribo-films, sliding contact, low carbon technology, EDS, XPS.

1. Introduction

Anthropogenic global climate change, rise in worldwide economic development and the increase in global population has substantially increased the use of air-conditioning and refrigeration systems worldwide. Previous generation of artificially formulated refrigerants have high environmental implications and these refrigerants contribute towards global warming and/or ozone depletion [1, 2]. Although the ozone depleting refrigerants have almost been phased out, the artificially formulated refrigerants which are one of the main contributors towards global warming are still largely in use [3]. The types of refrigerants employed in cooling, refrigeration and air-conditioning systems have evolved over the years.

Naturally occurring compounds which have good heat transfer and thermodynamic properties such as Ammonia, Hydrocarbons, Sulfur Dioxide, Methyl Formate and Methyl Chloride were being used in refrigeration systems before 1930s. Almost all of these compounds are toxic, flammable or both. As a result of their use accidents were common [4]. Sulfur Dioxide, Methyl Formate and Methyl Chloride were being commonly used in domestic refrigerators which are highly toxic and highly flammable.

1

Several fatal accidents occurred due to methyl chloride leakage from refrigerators in 1920s [3]. This led to a collaborative research in 1928 to find alternative replacement refrigerants that would be nontoxic and non-flammable which resulted in the development of Chlorofluorocarbons and Hydrochlorofluorocarbons.

Chlorofluorocarbons (CFCs) and Hydrochlorofluorocarbons (HCFCs) were extensively used as refrigerants till the mid-1990s. CFCs are chemicals containing atoms of chlorine, carbon and fluorine. HCFCs have an additional hydrogen atom and their molecular structure resembles closely to CFCs. CFCs and HCFCs are non-toxic and non-flammable refrigerants possessing excellent thermodynamic properties. This led to the extensive use of CFCs and HCFCs in various applications including usage in residential refrigerators, domestic air-conditioning systems, commercial applications, small scale industrial and in automotive air-conditioning units. Besides having excellent thermodynamic qualities, CFCs and HCFCs also possess exceptional tribological properties [5-14]. CFCs and HCFCs were reported to form protective surface films under normal compressor operating conditions which enhanced the friction and wear of interacting parts. The discovery of the depletion of the ozone layer and publication of the destructive effects of CFCs on the stratospheric ozone layer in 1974 [15] led to the realisation that CFCs have an extremely high ozone depletion potential and are leading to the destruction of the ozone. Vienna Convention for the Protection of the Ozone layer which was followed by the Montreal Protocol on Substances that Deplete the Ozone Layer in 1987 put a ban on CFCs [16]. Montreal Protocol was enforced in 1989 worldwide which banned the use of CFCs by the start of year 1996 in developed countries. HCFCs have lower ODP (Ozone Depletion Potential) values as compared to CFCs, which has allowed their use for a longer period of time. HCFCs are planned to be phased out by the end of year 2020.

Refrigerators and air-conditioners had become common household items, bans and restrictions on CFCs and HCFCs meant that alternative refrigerants had to be introduced, however this led to the need for assessing tribo-implications of these refrigerants in turn their implications on the durability. This paved the way to the development and introduction of Hydrofluorocarbons (HFCs). HFCs are synthetically produced refrigerants which contains hydrogen atoms, fluorine and carbon with zero ODP. HFCs had thermodynamic properties matching CFCs [17-21], which resulted in their extensive use as substitute refrigerants. CFCs and HCFCs were compatible with mineral oils, HFCs however were incompatible and immiscible with mineral oils. This meant that new lubricants with various additives had to be developed for the use of HFC refrigerants in compressors. After the introduction and acceptance of HFC refrigerants various researchers around the world started investigating the tribological performance of these refrigerants. A number of tribological studies including [5, 6, 22-33] were conducted to evaluate the performance of HFC refrigerants by using a range of lubricants and additives. Numerous studies [5-11, 13, 14, 23, 34-40] were also conducted which compared the friction, wear and lubricity performance of HFCs to HCFCs and CFCs. Most of the investigations that directly compared the tribological properties of HFCs to HCFCs and CFCs concluded that CFCs and HCFCs have superior tribological performance as compared to HFCs. Fluorine in HFCs did not decompose under normal compressor operating conditions and did not form protective surface films. Having zero ODP, HFCs were deployed worldwide and their harmful global warming implications were not considered at the time of their commercialisation, however high global warming implications of HFCs were realised later. The Kyoto Protocol in 1997 to the United Nations Framework Convention of Climate Change placed limits on CO_2 and other greenhouse gases. HFCs were identified to be amongst the main contributors to global warming [41] and they will be banned in any hermetically sealed system from the year 2022.

As a response to Environmental Impact Legislations naturally occurring hydrocarbons became of interest after Kyoto Protocol. Amongst hydrocarbons, HC-600a gained particular attention as it can replace HFC-134a. Various different investigations were conducted to examine the tribological performance of HC-R600a under different testing conditions [42-49]. The study [42] showed that environmental burden is greater by using HFC-134a based systems in comparison to systems based on HC-600a. Hydrocarbon refrigerants are also considered to be up to 50% more efficient thermal conductors than fluorocarbon refrigerants [3]. However due to the inherited high flammability concerns associated with hydrocarbons their applications are limited and thus new refrigerants have to be introduced.

This has now forced the introduction of new artificially formulated alternative refrigerants. The refrigerant industry has introduced new refrigerants namely Hydrofluoroolefins (HFOs) and Hydrofluoroethers (HFEs). HFOs and HFEs have zero ODP and lower global warming potential (GWP). HFO-1234yf has thermodynamic properties matching HFC-134a and is considered a direct replacement of HFC-134a [50]. This means that HFO-1234yf can be easily introduced into HFC-134a based refrigeration cycles. Tribological evaluation of HFOs is underway and various studies [51-57] have shown that HFOs possess very good tribological properties because the fluorine in HFOs chemically reacts with the interacting metals to form protective tribological films on the rubbing surfaces. Some of these studies have also compared HFO-1234yf directly with HFC-134a under identical operating conditions and have concluded that HFO-1234yf has superior tribological properties compared to HFC-134a [51-54]. HFOs however are mildly flammable and their flammability restricts their application areas and places of use.

In recent years focus has also shifted towards refrigerants that are naturally occurring such as hydrocarbons and carbon dioxide, however the high flammability of hydrocarbons restricts their application range. CO_2 based refrigeration systems require extremely high pressures to operate which results in higher design, material and operation costs.

HFEs are non-flammable refrigerants having low GWP and zero ODP. HFEs are odourless, colourless, low toxic, low viscous refrigerants which are normally liquid at room temperature and look identical to water. HFEs have a number of applications for example they can be used in cascaded refrigeration systems, in freeze drying units, in fuels cells, in chemical reactors, in high voltage transformers, as cleaning and rinsing agents, as lubricant carriers, in vapour degreasing applications and in renewable solar thermal systems [58]. Various studies like [59, 60] have demonstrated that hydrofluoroethers possess good thermodynamics properties especially in low carbon technology and energy applications [61]. HFEs are also potential replacements of HFCs, HCFCs and PFCs [62]. There is however very limited work that has been reported on the tribological performance of newly developed HFEs. The only reported works are [63, 64]. The study [63] examined the properties of polyester in HFE-245mc atmosphere which was published back in 2002 while only wear performance analysis of HFE-347mcc3 was performed with no comment on friction in [64].

At the time of writing this paper, no work has been published that looks into the wear as well as friction performance of 1-methoxyheptafluoropropane (HFE-7000). The study of tribo performance of this refrigerant is the novelty in this research. This promising new refrigerant has significant potential for industrial applications including low carbon technologies, clean energy, automotive and aerospace industries.

This study has been undertaken to experimentally evaluate the friction, wear and lubricity performance of HFE-7000 in a modified micro-friction machine. The chamber pressure and

3

temperature were continuously monitored and controlled to keep the refrigerant in liquid state during the testing to sustain saturated contacts. The tribological effects of load, temperature and surface roughness were studied by using Hydrofluororther-7000 as lubrication medium without using any external lubricant. A number of studies have been performed and reported in the past to investigate the tribological performance of numerous refrigerants without using any lubricants [11, 39, 43, 45, 47, 48, 53, 65-70]. Un-lubricated conditions are used to better understand the lubricity of the refrigerants by decoupling refrigerant- lubricant effects. Some of the characteristics of HFE-7000 are listed in the table 1 along with HFC-134a and HFO-1234yf. HFC-134a has a GWP value of about three times to that of HFE-7000. HFO-1234yf has a much lower GWP but is "flammable".

Table 1. Various different properties of HFE-7000, HFC-134a and HFO-1234yf [50, 53, 58, 64, 71].

Refrigerant	HFE-7000	HFC-134a	HFO-1234yf
Structure	$C_3F_7OCH_3$	Ch_2FCF_3	$CF_3CF=CH_2$
Molecular Weight (g/mol)	200	102	114
Freeze Point (°C)	-122.5	-103.3	-150
Boiling Point @ 1 atmosphere (°C)	34	-26	-29
Critical Temperature (°C)	165	101	95
Liquid Density (kg/m^3)	1400	1206	1094
Critical Pressure (MPa)	2.48	4.06	3.38
Flash Point (°C)	None	250	Not applicable
Appearance	Clear, colourless	Colourless gas	Colourless gas
Flammability	Non-flammable	Non-flammable	Mildly-Flammable
Ozone Depletion Potential (ODP)	Zero	Zero	Zero
Global Warming Potential (GWP)	530*	1430*	4*

*GWP 100-year integrated time horizon (ITH). IPCC 2013 [72].

HFE-7000 is not considered a direct replacement of HFC-134a and has wide range of applications areas where it can be used besides being used in compressors. It has already been investigated and used in solar organic Rankine cycle [73], in renewable energy systems [60, 61], in Electrohydrodynamics applications [74] as jet impinging dielectric coolant [75], etc. This study is focusing on how the refrigerant will perform at low loads and low temperatures. Some of the studies have shown [8, 11] that refrigerants that do not form protective surface films under normal compressor operating conditions have the possibility to decompose and form surface films under severe and extremely harsh operating conditions. A refrigerant usually exists in heated vapour state in a refrigeration cycle and also undergoes a phase change; transitioning from a liquid to vapour state and when saturation temperature-pressure conditions are changed, a reversal of phase change occurs. Most of the studies involving the tribological investigation of refrigerants are concerned with the refrigerant/lubricant mixture with the refrigerant in vapour state applied in high load conditions. This study however looks into the tribological performance of one of the future generation refrigerants by experimentally assessing its performance under relatively low loads and low temperatures in liquid state without the influence of any conventional lubricant. If HFE-7000 chemically reacts with the interacting surfaces and forms protective tribo-films, it can be deduced that it demonstrates good tribological performance within the context of various operating loads and temperatures.

2. Experimental setup

Experimental configuration for conducting this research is based on an existing reciprocating micro-friction machine, Phoenix Tribology TE-57 Pressurized Lubricity Tester. The machine was modified to enable the tribological testing of the future generation of refrigerants. A modified bespoke test rig design is schematically shown in figure 1. The testing chamber houses the components under

investigation. The design of the chamber allows it to be fully sealed and maintain pressures in the range of -1 to $+3$ bar. O-rings and steel bellows seal the interacting components within the test chamber to form an integral part of the test chamber. All O-ring seals are static and all the relative movement is accommodated by the bellows. The setup can be used to test various contact configurations which include line contact, point contact and area contact. A ball-on-flat i.e. point contact geometry has been used for experimentation in this investigation.

The bench testing setup comprises of a variable speed PID (Proportional-Integral-Derivative) controlled DC motor. A scotch yoke mechanism is used to transmit the power from the motor to slide a lower flat plate against a fixed upper specimen in a reciprocating motion. The stroke length can be varied continuously between $1-5$ mm, the frequency of oscillation can be adjusted between $2.5-50$ Hz. Normal load can be applied in the range of $5-50$ N. With the material samples used in this study the load range of $5-50$ N with a ball-on-flat contact configuration translates into a Hertzian Contact Stress range of $781-1682$ MPa. A heater block comprising of electric heating elements is located at the bottom of the chamber which is used to heat up the refrigerant. Two K-type thermocouples are used to monitor and control the temperature of the refrigerant inside the test chamber. One of the thermocouples is directly embedded in the heater block and gives its temperature. The heater block can be heated up to 200°C. The second thermocouple is a wire type thermocouple which is secured in the specimen holding cup and is used to measure the temperature of the refrigerant under investigation. Temperature readings from the wire type thermocouple are used as feedback in a PID control algorithm to maintain the temperature of the refrigerant during the course of a test. The chamber pressure is controlled in the test chamber to keep the refrigerant in liquid state at all times during the course of a test. The test chamber is fitted with a pressure transducer and a manual pressure gauge to record, monitor and control the chamber pressure. A friction force transducer is installed to a yoke, the yoke is connected to a force feedback rod upon which a housing is mounted that holds the fixed sample. The values of the friction force and the applied normal load are used to calculate the coefficient of friction. All the parameters being controlled, monitored and recorded are displayed in real-time in the software GUI (Graphical User Interface).

All the inputs and outputs are fed through a purpose built data acquisition system which serially transmits the data to a microprocessor. The computer has a specialised software that is used to monitor, control and record the operating parameters.
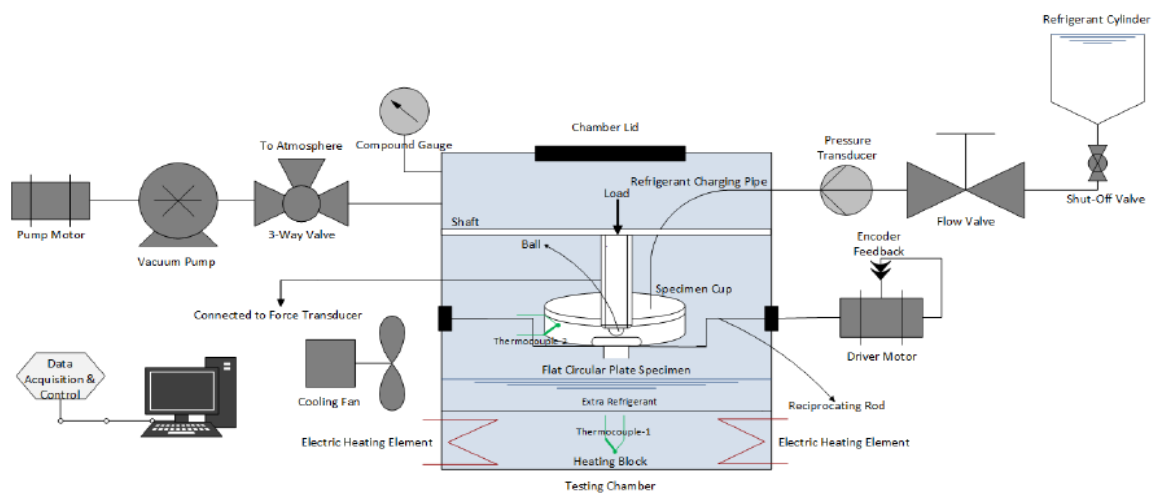

Figure 1: Test rig schematic.

5

3. Testing Procedure

The steel flat circular specimen is placed in the cup which is then secured on the oscillating rod with the help of screws. Then the wire type thermocouple is fastened into position. Steel ball is fixed on the ball-holder with the help of grub screws and ball holder is connected to the ball holder shaft. The shaft provides a means to secure the ball-holder in position and also functions as a means to apply the vertical normal load. After this the chamber is closed and sealed. The chamber is then vacuumed so as to minimise the effects of oxygen and ambient air during testing.

After the chamber has been vacuumed, HFE-7000 is introduced in the system by using the shut-off and flow valves. Sufficient amount of refrigerant is charged so that the cup overflows and the bottom flat specimen is fully immersed in the fluid which ensures fully lubricated conditions at all times. The extra overflown refrigerant gets collected at the bottom of the chamber where the heating block is located. This overflown refrigerant assists heat transfer from the heater block and helps maintain the refrigerant temperature in the specimen cup. The vacuum inside the test chamber and gravitational force helps the refrigerant to flow from the cylinder into the cup. The chamber lid has a transparent glass top which allows the operator to physically observe chamber conditions at all times. Next the desired load is manually applied. After this the control algorithm is run and the refrigerant inside the cup in the testing chamber is heated to the required temperature. The refrigerant temperature is controlled by using values from the wire type thermocouple and feedback PID control. Once the temperature reaches its specific value, the temperature of the refrigerant is stabilised and maintained for one hour before starting a test. After the temperature has been stabilised and has been maintained to the desired value for one hour, a test is run for two hours.

The oscillating frequency is controlled by using feedback controlled driver motor. The motor, the heater and all the transducers are connected to a microprocessor based central data acquisition and control system. The values of the friction force, the chamber pressure values, the temperature readings from the heater block, temperature of the refrigerant and the motor speed are continuously recorded in a spreadsheet.

Flat circular plate specimens of three different values of average surface roughness, $0.05\ \mu m, 0.1\ \mu m$ and $1\ um$ made of EN1A steel were used. The balls were made of AISI 52100 steel having an average surface value of $0.010\ \mu m$. The flat specimens are circular in shape having thickness of 2.75 mm and 30 mm diameter. The steel balls are 10 mm in diameter. Three different loads $10\ N, 20\ N$ and $30\ N$ were applied. Three different temperatures $20°C, 30°C$ and $40°C$ were used in this study. All tests were performed at a constant reciprocating frequency of $5\ Hz$ having a stroke length of $5\ mm$. Each flat disc sample was mechanically grinded and then polished to the desired surface roughness after which each sample was ultrasonically treated with acetone for five minutes and then dried with warm air using a specimen drier before each experiment. The grinding and polishing process followed by the ultrasonic treatment with acetone of the specimens assured the removal of any unwanted/oxide surface films pre-experimentation. Each experiment lasted two hours and repeatability was ensured by conducting each experiment at least twice.

4. Results and discussion

4.1. Friction

Results of friction have been discussed in terms of real-time coefficient of friction values, average coefficient of friction and average frictional force. Kinematic viscosity of HFE-7000 at 20°C is 0.32 cSt, at 30°C is 0.29 cSt and at 40°C is 0.27 cSt [58]. A detailed discussion on results of friction obtained in this study is provided in sections 4.1.1, 4.1.2 and 4.1.3 respectively.
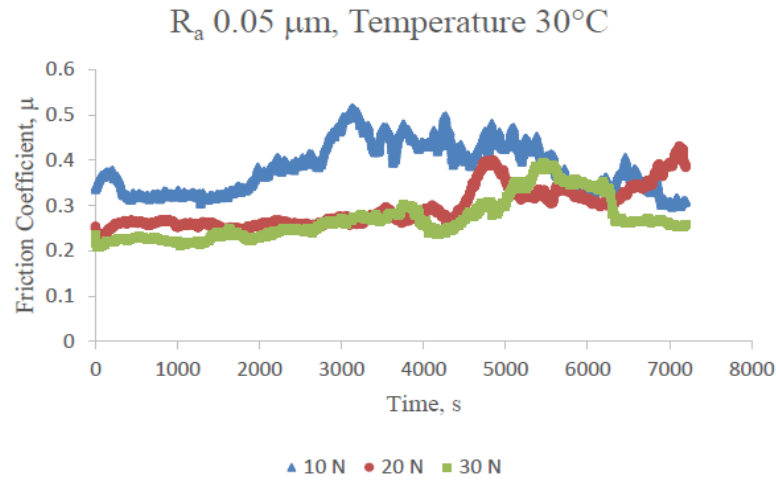
4.1.1. Coefficient of Friction

Fully lubricated conditions were established at the start of an experiment and were maintained throughout the test. The results of the variation of the coefficient of friction with changing normal load, refrigerant temperature and average surface roughness are presented in figures 2, 3 and 4 respectively.

For R_a of 0.05 μm the values of the friction coefficient decreased with an increase in load at HEF-7000 temperature of 20°C. An increase in normal load from 10 N to 30 N resulted in fewer overall variations in the coefficient of friction and more stable values. For normal load of 10 N and fluid temperature of 20°C the coefficient of friction increased almost linearly to a maximum value after which it started to decrease. With some fluctuations, the coefficient of friction decreased after increasing initially and reached a stable value at the end of the experiment.

(a)

7

R_a 0.05 μm, Temperature 30°C

(b)

R_a 0.05 μm, Temperature 40°C
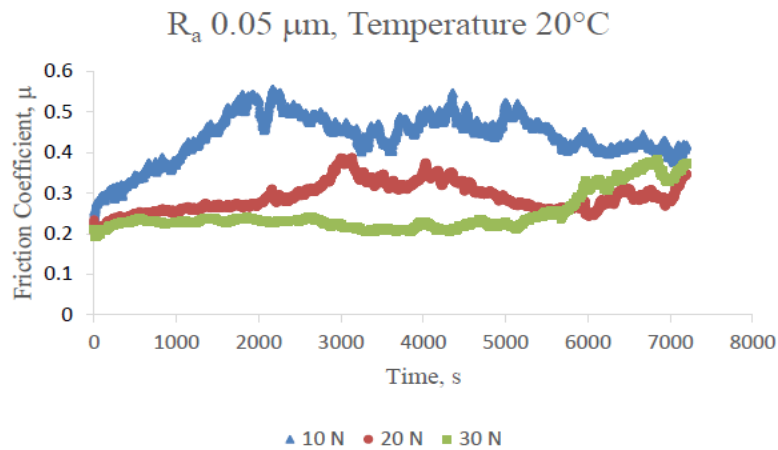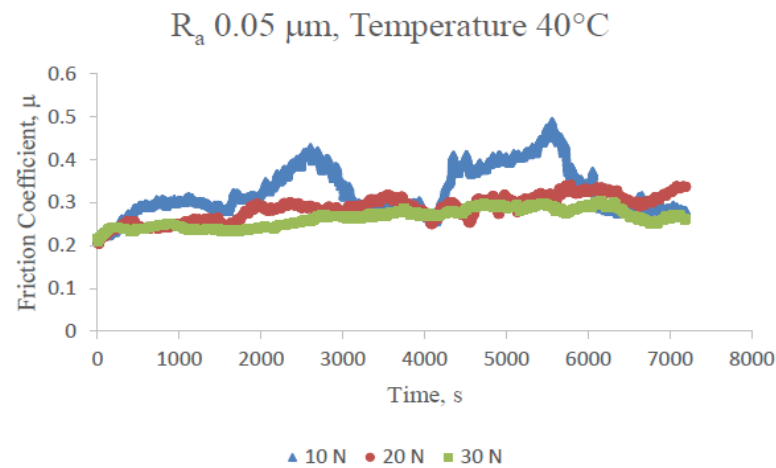
(c)

Figure 2: Coefficient of friction graphs for R_a 0.05 μm, refrigerant temperature: (a) 20°C (b) 30°C (c) 40°C.

For 20 N load and 20°C fluid temperature, the overall coefficient of friction and the rate of increase of the coefficient of friction was lower as compared to 10 N, 20°C.

For 30 N, 20°C the friction coefficient was very stable and demonstrated much lower values for over one hour of experimentation. The coefficient of friction however increased towards the end of the experiment.

In comparison to 20°C, 10 N the values of 30°C, 10 N were lower. There was also no steep gradient at the start of the experiment. The friction coefficient showed similar fluctuations as 20°C, 10 N. Friction coefficient values for 30°C, 10 N decreased at the end of the experiment reaching to values which were similar to those that were at the start of the experiment.

8

The values for the friction coefficient for 30°C, 20 *N* were similar to the values of 20°C, 20 *N*. The values for the coefficient of friction remained fairly stable for the first hour of testing after which an increase in these values was observed.

The results of the coefficient of friction for 30°C, 30 *N* as compared to 20°C, 30 *N* were also similar. The results of 30°C, 30 *N* followed the same pattern and had similar values as 20°C, 30 *N* for the first hour of testing. For the second half of the testing, a rise and fall in the friction coefficient can be observed. The friction coefficient is seen to reach a low, stable and steady value at the end of the experiment.

In comparison to 20°C, 10 *N* and 30°C, 10 *N* the values of the coefficient of friction for 40°C, 10 *N* were lower. The values fluctuated with the passage of time but the results did not show a sharp increase in the values in the first 30 mins of testing. The values stabilised for some time after the very initial increase in the coefficient of friction. The values however increased and decreased twice in the testing period resulting in the formation of two peaks. The second peek was higher than the first peak.

The overall coefficient of friction of 40°C, 20 *N* was similar to 20°C, 20 *N* and 30°C, 20 *N*. The values of friction coefficient showed some fluctuations but there were no major peaks and sharp gradients.

The overall coefficient of friction of 40°C, 30 *N* was also similar to 20°C, 30 *N* and 30°C, 30 *N* as well. The values of friction coefficient showed very minor fluctuations and presented the most stable friction coefficient from all the tests which were performed at R_a 0.05 *μm*.
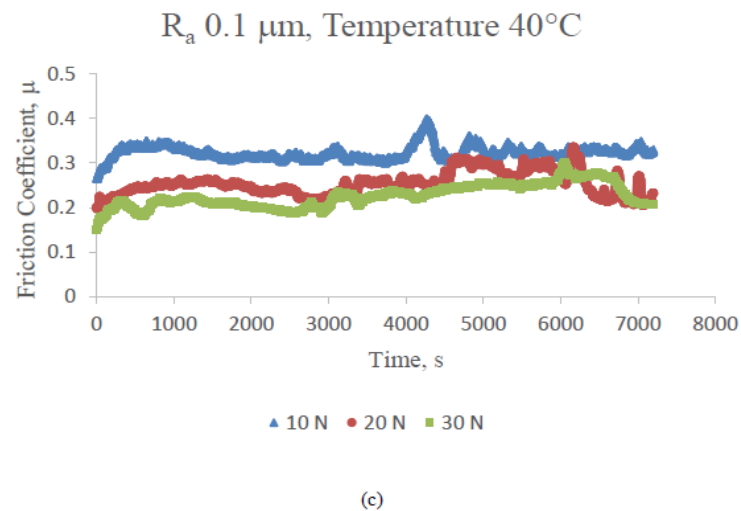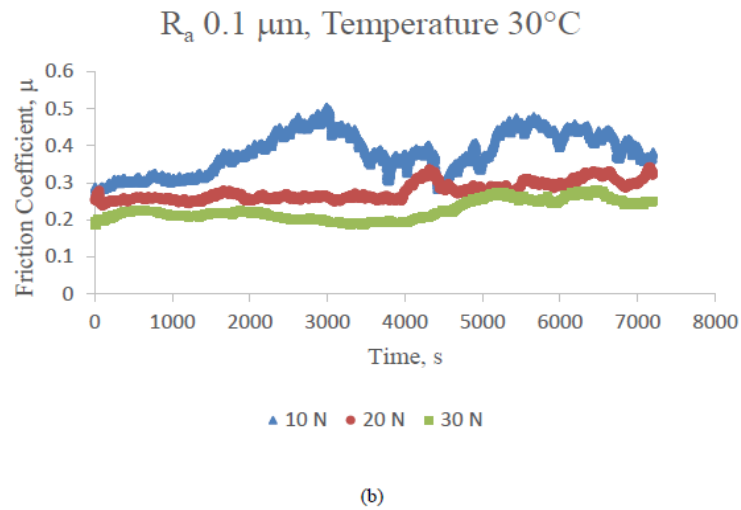

(a)

R_a 0.1 µm, Temperature 30°C

(b)

R_a 0.1 µm, Temperature 40°C

(c)
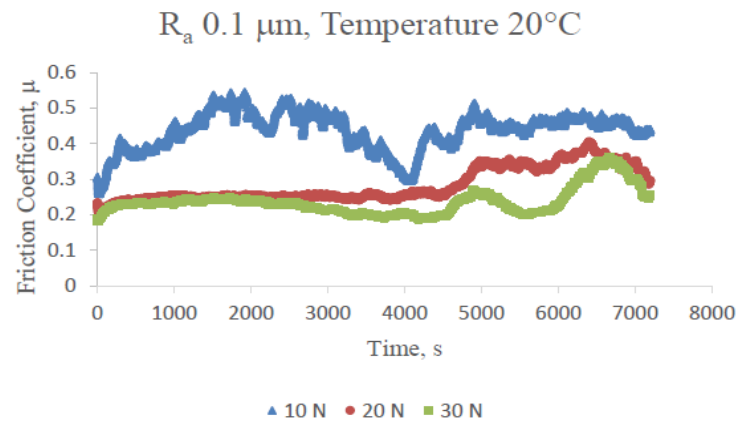
Figure 3: Coefficient of friction graphs for R_a 0.1 µm, refrigerant temperature: (a) 20°C (b) 30°C (c) 40°C.

For R_a of 0.1 µm the coefficient of friction displayed similar results to those obtained by using samples having R_a of 0.05 µm. For a normal load of 10 N, HFE-7000 temperature of 20°C and R_a of 0.1 µm the variations in the coefficient of friction and the overall values of the friction coefficient were very similar to those obtained by using R_a 0.05 µm, normal load 10 N and fluid temperature 20°C. The friction coefficient showed a similar initial rise, fluctuations and then stabilisation.

For R_a of 0.1 µm, load 20 N and temperature 20°C the initial results of the coefficient of friction are very similar to those obtained at R_a of 0.05 µm, load 20 N and temperature 20°C. The results obtained at R_a of 0.1 µm presented a stable friction coefficient for a longer time period. The friction coefficient increased after more than one hour of testing.

For R_a of 0.1 µm, load 30 N and temperature 20°C the range of values of the coefficient of friction are very similar to those obtained at R_a of 0.05 µm, load 30 N and temperature 20°C.

10

R_a of $0.1\,\mu m$, HFE-7000 temperature 30°C and normal loads of $10\,N$ and $20\,N$ showed similar results to R_a of $0.05\,\mu m$, HFE-7000 temperature 30°C and normal loads $10\,N$ and $20\,N$ respectively. At R_a $0.1\,\mu m$, normal load $30\,N$ and HFE-7000 temperature 30°C the overall coefficient of friction was lower as compared to R_a of $0.05\,\mu m$ with the same load and refrigerant temperature.

With an increase in temperature to 40°C, R_a $0.1\,\mu m$, and normal load of $10\,N$, the friction coefficient reduced and became more stable as compared to R_a $0.1\,\mu m$, normal load $10\,N$ and refrigerant temperatures of 20°C *and* 30°C. In comparison to R_a $0.05\,\mu m$, load $10\,N$ and HFE-7000 temperature 40°C the friction coefficient, in this case, was also more stable and had a lower overall value.

For R_a $0.1\,\mu m$, refrigerant temperature of 40°C and normal load of $20\,N$ the friction coefficient was lower than R_a $0.1\,\mu m$, normal load $20\,N$ and temperatures 20°C *and* 30°C. The values in this case were also lower than R_a $0.05\,\mu m$, load $20\,N$ and temperature 40°C. This indicates that increasing the temperature from 20°C *to* 40°C for the same applied load has a positive effect on the friction coefficient.

The values for the friction coefficient at R_a $0.1\,\mu m$, load $30\,N$ and temperature 40°C were lower than R_a of $0.05\,\mu m$, load $30\,N$ and temperature 40°C. However in comparison to 20°C *and* 30°C the values at 40°C, R_a of $0.1\,\mu m$ and normal load of $30\,N$ were mostly similar.
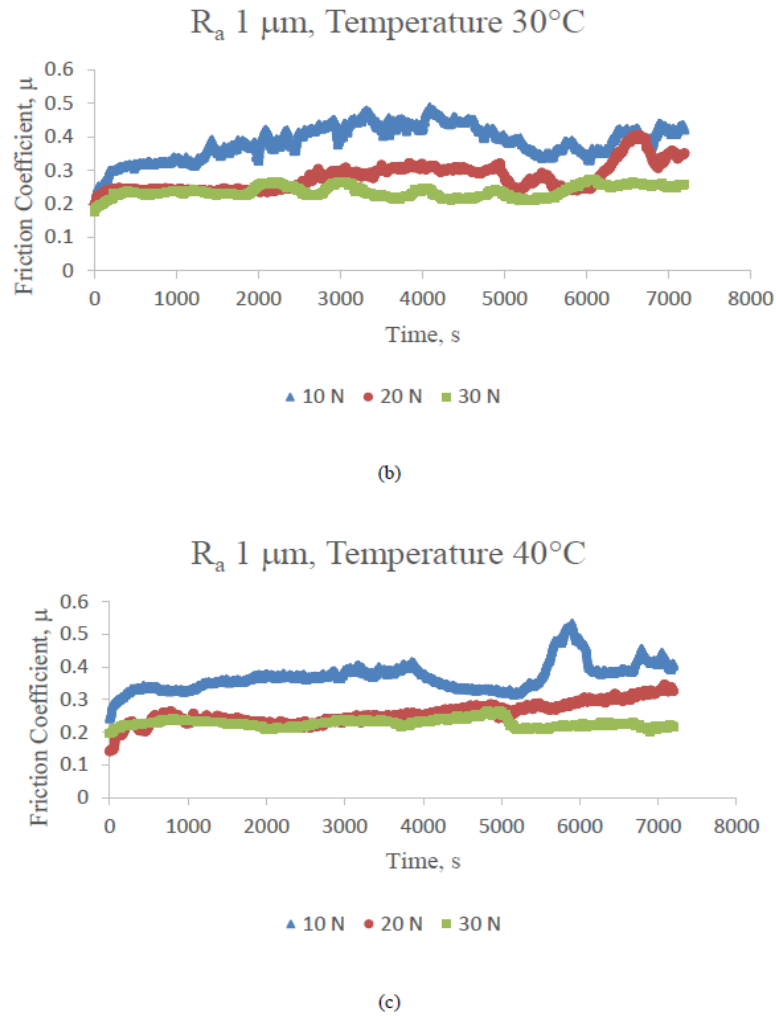

(a)

(b)

(c)
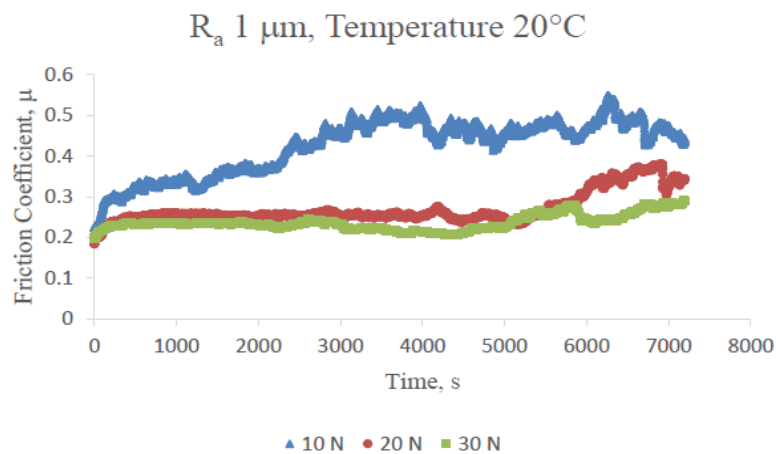
Figure 4: Coefficient of friction graphs for R_a 1.0 μm, refrigerant temperature: (a) 20°C (b) 30°C (c) 40°C.

A 10 times increase in average surface roughness from 0.1 μm to 1.0 μm resulted in very similar behaviour and overall values of friction coefficient for all testing conditions. The increase in the values of the friction coefficient during the course of a test is associated with the change in the apparent contact area. The steel ball wears during experimentation resulting in an increase in the contact area. The wear scar generated on a steel ball in a ball-on-flat contact geometry with a stationary steel ball loaded against a disc has been reported to change shape and result in an increase in the apparent area of contact leading to a reduction in average contact pressure [76]. Hertzian diameter of 52100 steel balls has also been reported to increase with wear in a reciprocating ball-on-flat test configuration [77]. The friction coefficient decreases due to the development of protective surface films on the freshly exposed metallic surfaces. As the contact geometry becomes more favourable and once the tribo-films have been formed on the entire wear track the friction coefficient reaches a stable value. Some of the testing conditions generated multiple peaks. The first peak is an indication of the initiation of the flattening of the ball and the second peak shows a further change in the ball contact area. The shape of the wear scar also changes depending on the loading and testing conditions. The shape of the wear scar has been known to shift from a circular shape at lower loads to

12

an elliptical shape at higher loads [76]. An increase in surface roughness for the same testing conditions leads to more asperity interactions resulting in an accelerated change in contact area of the ball, at the same time however these hasher operating conditions help in the formation of protective surface tribo-films.

The fluctuations in the friction coefficient are believed to have been caused by the generated wear debris and three body abrasive wear phenomenon. The initial fluctuations after the start of an experiment especially at lower surface roughness can also be caused by the uneven formation of the surface films, these films are believed to have been uniformly adhered after a certain amount of time which is also evident from the coefficient of friction graphs which tend to stabilise with time. The fluctuating friction coefficient is also associated with adhesive wear. The soft EN1A steel is adhered to the surface of the hard 52100 steel ball and the continuation of the reciprocating motion with adhered particles on the ball also gives rise to variations and fluctuations in the coefficient of friction.
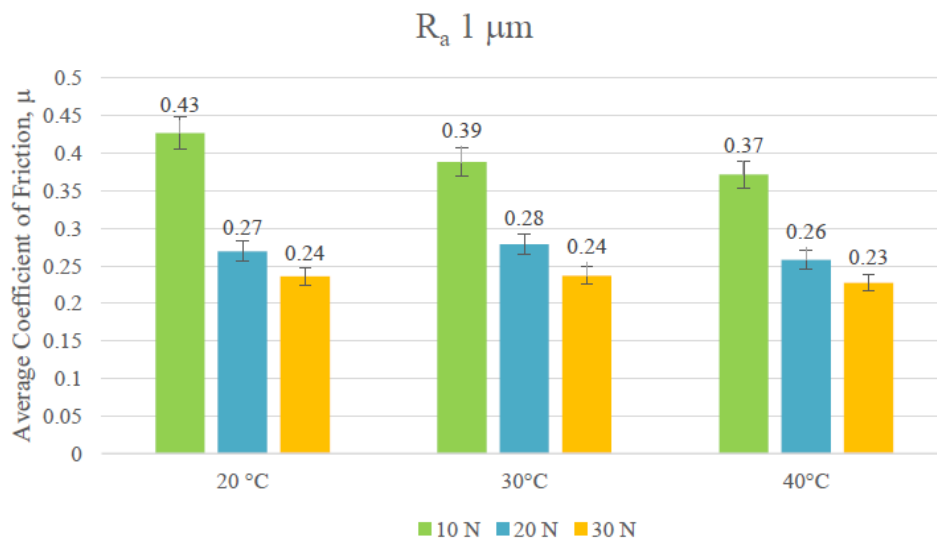
4.1.2. Average Coefficient of Friction

The results of the average coefficient of friction for all testing conditions are presented in figure 5. The data revealed a similar pattern for all investigated surface roughness values. With an increase in load at a constant temperature the friction coefficient was reduced. Increase in load results in harsher operating environment which facilitates chemical reactions between HFE-7000 and the interacting metals. Unlike HFCs that have carbon-carbon bonds, HFEs have a carbon-oxygen bond as well which has been reported to be weaker than carbo-carbon bond [63]. The breakage of the carbon-oxygen bond and the chemical reaction between the refrigerant and freshly exposed metal produces protective tribological films on the top surfaces which reduces the friction coefficient. With an increase in temperature at $10\ N$ load the coefficient of friction also reduced. At higher loads an increase in temperature at the same applied load did not produce a significant change in the coefficient of friction. Increase in temperature at any given load reduces the viscosity of the refrigerant resulting in the reduction of separation between the rubbing components which should increase the friction coefficient due to higher asperity interactions. However the friction coefficient reduced at lower loads and remained almost constant at higher loads with increase in temperature. This indicates that at higher temperatures the reactivity of HFE-7000 is increased which accelerates the formation of protective surface films.

13

$$R_a\ 0.1\ \mu m$$

(b)

$$R_a\ 1\ \mu m$$
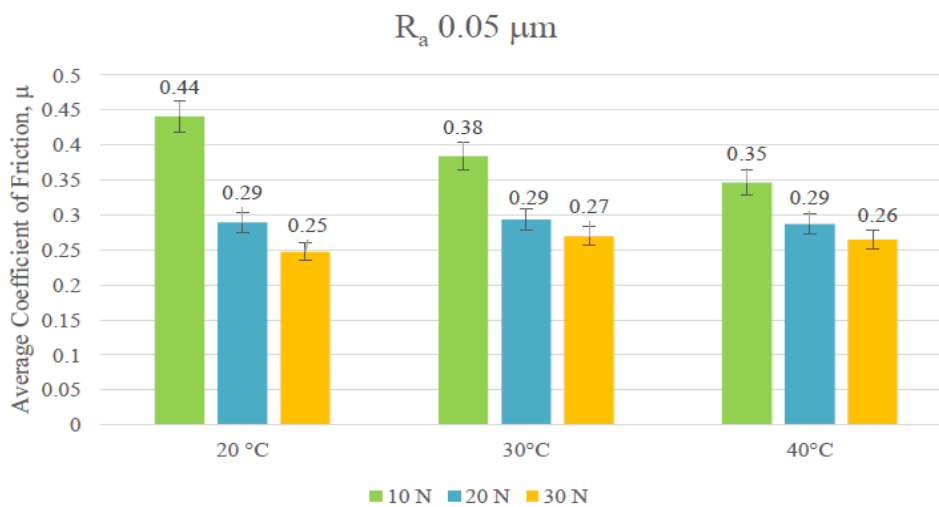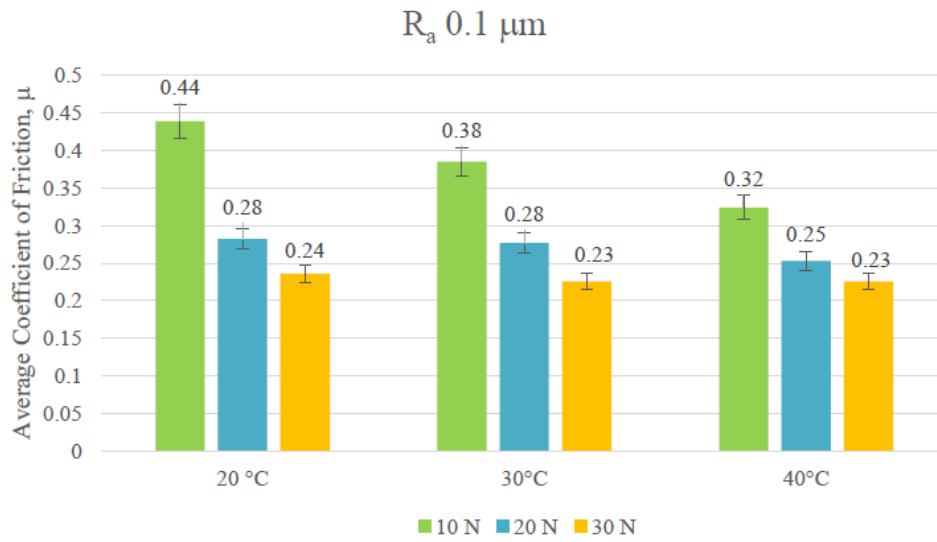
(c)

Figure 5: Average coefficient of friction plots: (a) R_a 0.05 μm (b) R_a 0.1 μm (c) R_a 1.0 μm.
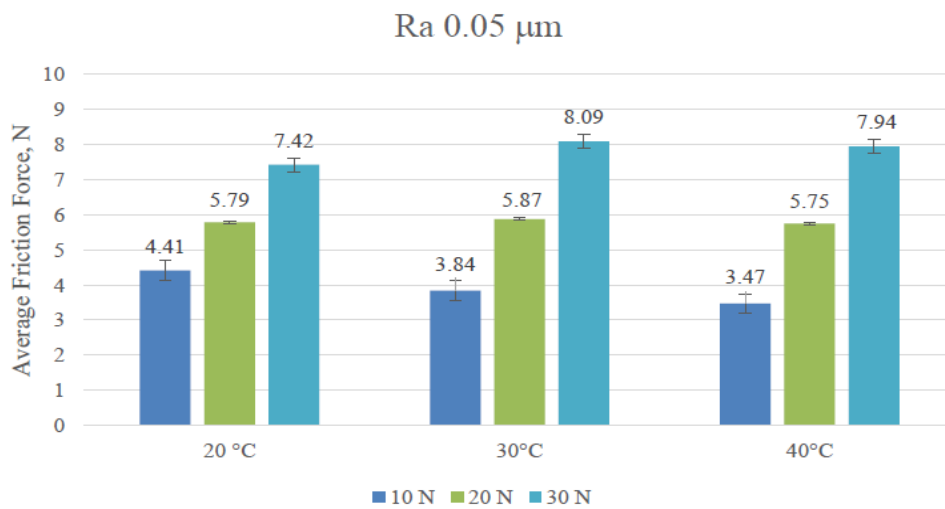
4.1.3. Average Friction Force

The results of the average friction force for all the testing conditions are presented in figure 6. The frictional force increased with an increase in load at a constant temperature for all the surface roughness values tested. A reduction in frictional force was observed with increasing temperatures for all surface roughness values at low normal load of 10 N. Normal loads of 20 N and 30 N at R_a 0.05 μm and R_a 1.0 μm caused a slight increase in friction force as the refrigerant temperature was

14

increased from 20°C to 30°C, friction force however reduced for both these loads with a further increase in temperature from 30°C to 40°C.

For R_a 0.1 μm the frictional force values reduced with an increase in temperature at 20 N load. With 30 N load at R_a 0.1 μm the values of friction force decreased with an increase in temperature from 20°C to 30°C. The values of friction force remained almost constant with a further increase in refrigerant temperature from 30°C to 40°C.

The minimum values of friction force were observed at 40°C and R_a of 0.1 μm for all the applied loads in comparison to R_a 0.05 μm and R_a 1.0 μm. This shows that there exists an optimum value of surface roughness at which the best frictional force values are obtained when operating at higher temperatures.
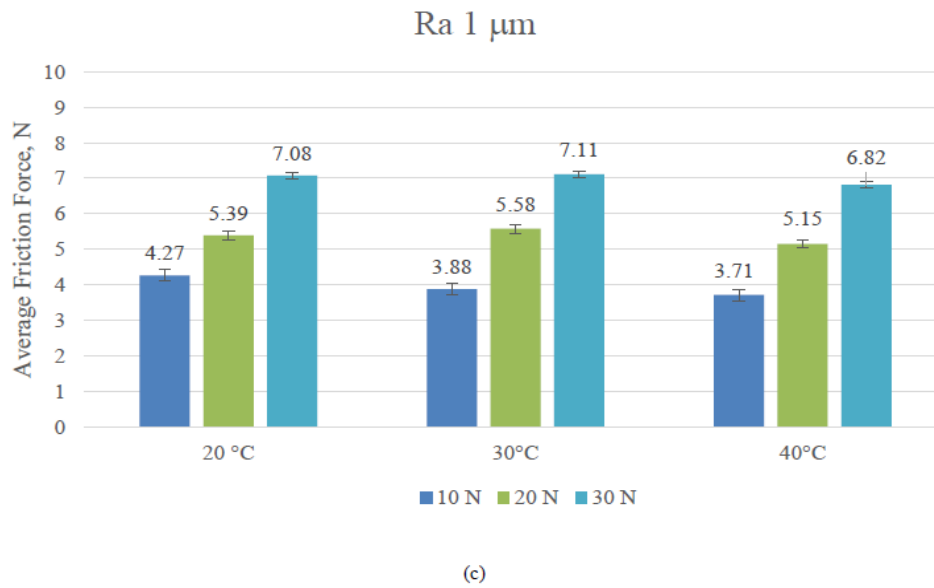

(a)

(b)

Ra 1 μm

(c)
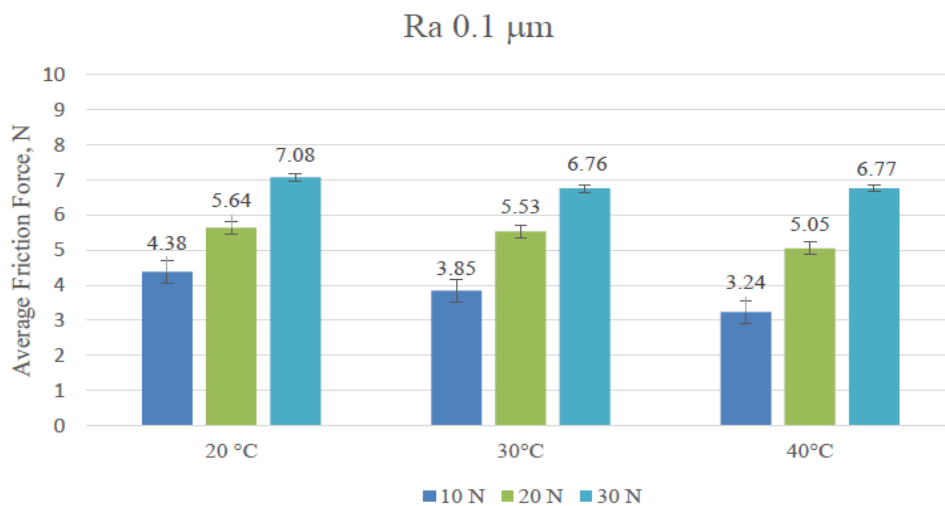
Figure 6: Average friction force plots: (a) R_a 0.05 μm (b) R_a 0.1 μm (c) R_a 1.0 μm.

5. Wear

A combination of abrasive and adhesive wear was witnessed on the flat and ball specimens. Adhesive wear mostly occurred at the ends of the wear track. Abrasive wear was more prominent in the middle section of the wear track. The soft EN1A steel was ploughed by the hard 52100 steel. Material pileup was witnessed at the edges of the wear scar. SEM (Scanning Electron Microscope) micrographs of the flat circular specimens of average surface roughness 0.05 μm are shown in figure 7. Interestingly it was also noted that for 20 N loads for all the temperatures of the refrigerant there was less adhesive wear and more abrasive wear. Magnified images of the steel ball tested against EN1A steel having average surface roughness 0.05 μm at refrigerant temperature of 20°C and normal applied load of 10 N are presented in figure 8. The high magnification SEM images show adhered EN1A steel on the surface of the hard 52100 steel ball. Adhesive wear is believed to have been more dominant during the start of a test when the entire contact load is carried only by very small area of asperity contacts producing very high real contact pressure values, which results in detachment of fragments from EN1A steel surface and attachment to the hard steel ball under relative motion. With the flat EN1A steel sliding against the stationary hard steel ball under the influence of normal load, the adhesive junction breaks. As sliding continues fresh junctions form and rupture. When the contact geometries became more favourable after running-in of the components is achieved and after the initiation of the formation of tribo-films the wear mechanism shifts towards abrasive wear. Generated wear debris result in three body abrasive wear phenomenon as they are trapped inside the flat specimen and refrigerant holding cup. The reciprocating motion causes material pileup on the sides and ploughing of EN1A steel by the hard steel ball. Similar results were seen by observing the other surface roughness values tested under Scanning Electron Microscope as well.
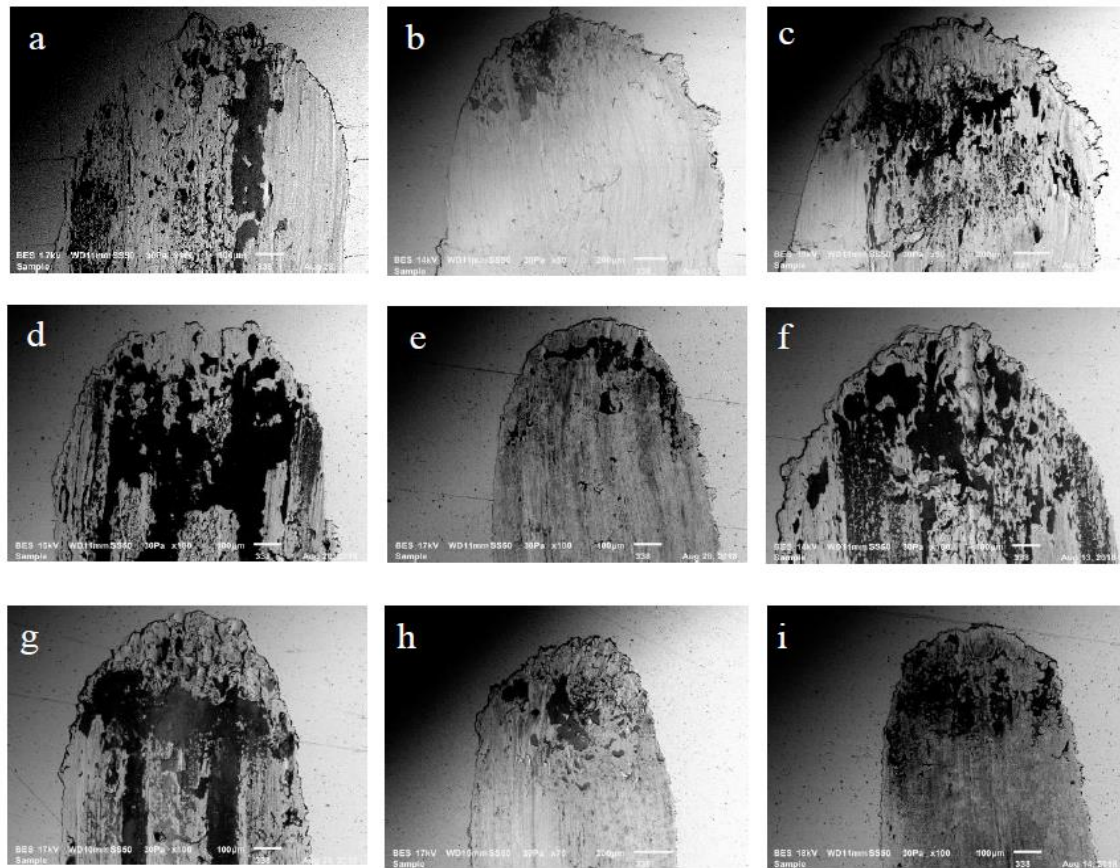
Figure 7: Micrographs of wear track on disc samples with R_a 0.05 μm: (a) 10 N, 20°C (b) 20 N, 20°C (c) 30 N, 20°C (d) 10 N, 30°C (e) 20 N, 30°C (f) 30 N, 30°C (g) 10 N, 40°C (h) 20 N, 40°C (i) 30 N, 40°C


Figure 8: Magnified images of the ball sample tested at 10 N, 20°C.

5.1. Wear Volume

Flat disc samples were also analysed under a white light interferometer to generate 3D plots. 3D plots obtained by using the interferometer were used to compute the wear volume for each sample tested. 3D oblique plots of all the tests that were conducted during this research on flat disc samples of average surface roughness of 0.05 μm are shown in figure in 9.

For HEF-7000 temperature 20°C, an increase in load generates a deeper and wider wear track resulting in increased wear volume. This pattern is also observed at 30°C fluid temperature, increasing load produces more wear. It can also be observed from the plots that increasing temperature from

17

20°C *to* 30°C at any given load reduces the depth and width of the wear track thus lowering wear. HFE-7000 temperature 40°C and 20 *N* load generated the shallowest wear tracks. Compared to 20°C *and* 30°C, wear tracks are less deep at 40°C at any given load.
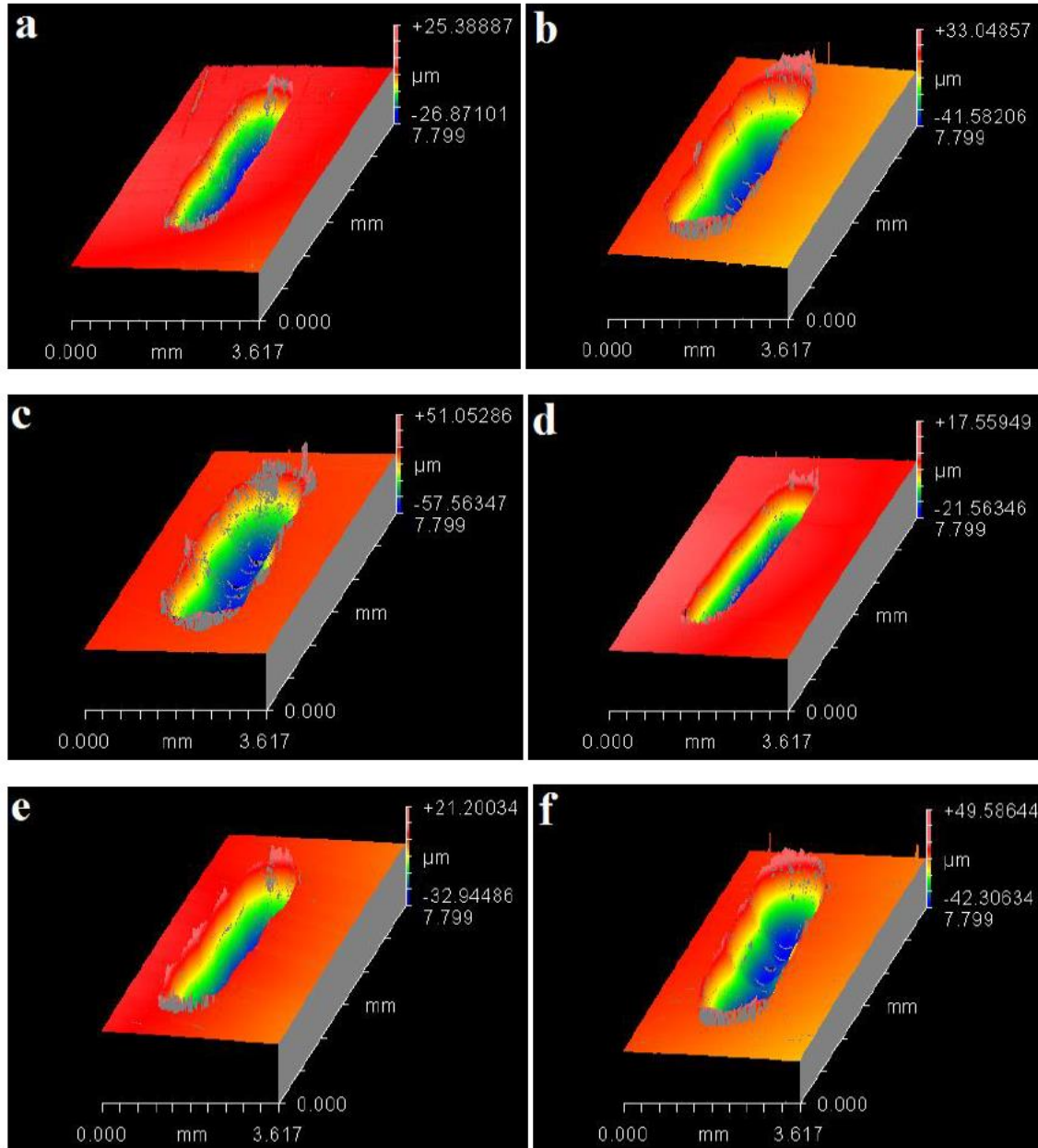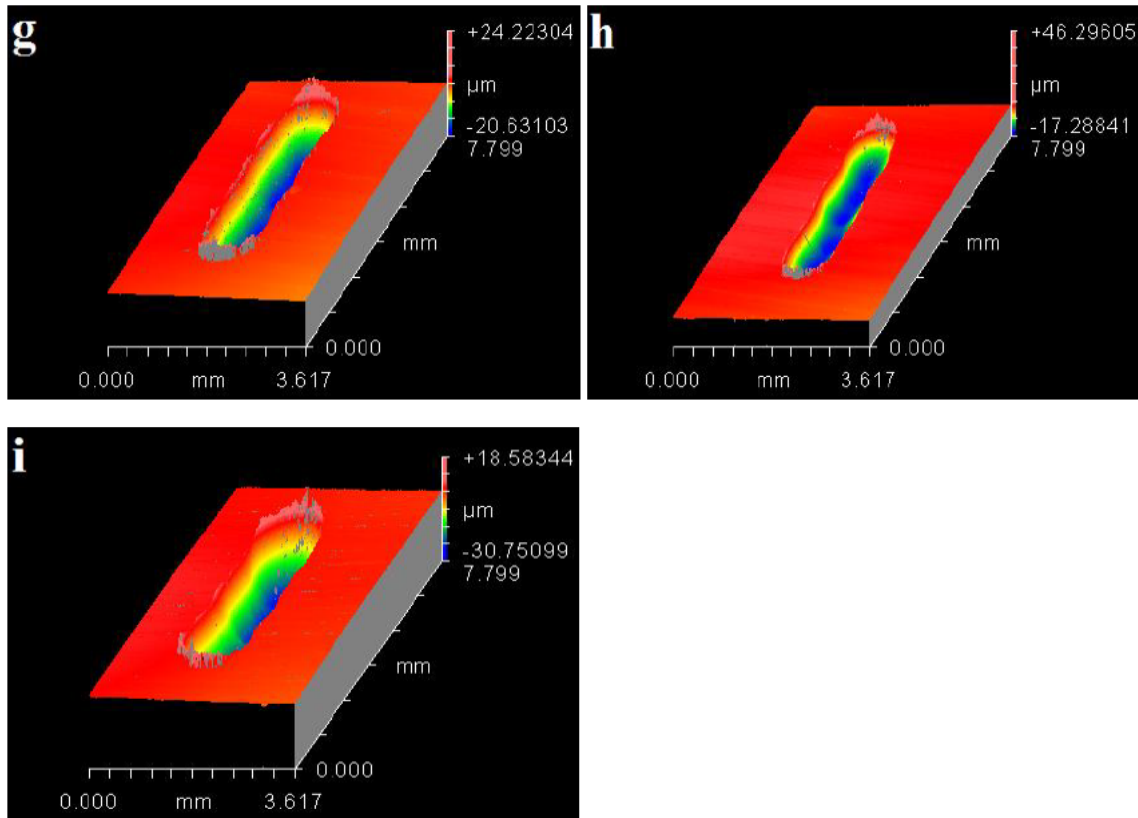
Figure 9: 3D oblique plots of wear track on disc samples with $R_a 0.05 \, \mu m$: (a) $10 \, N, 20°C$ (b) $20 \, N, 20°C$ (c) $30 \, N, 20°C$ (d) $10 \, N, 30°C$ (e) $20 \, N, 30°C$ (f) $30 \, N, 30°C$ (g) $10 \, N, 40°C$ (h) $20 \, N, 40°C$ (i) $30 \, N, 40°C$

Wear volume for all the flat samples tested was measured and the corresponding results are presented in figure 10. For a given surface roughness, a rise in temperature has a positive effect on decreasing the wear volume for the same applied load. This indicates that an increase in temperature increases the reactivity of the refrigerant HFE-7000 with the interacting metallic surfaces which leads to a faster development of protective surface films on the rubbing top surfaces resulting in a drop in wear volume. For all the surface roughness values tested the amount of wear increases with an increase in load for refrigerant temperatures of 20°C and 30°C. However at 40°C the wear volume at $20 \, N$ is less than the wear volume at $10 \, N$. At any given temperature the wear volume has the highest value at $30 \, N$ for all surface roughness values examined. This shows that there exists an optimum combination of load and temperature which produces minimal wear.
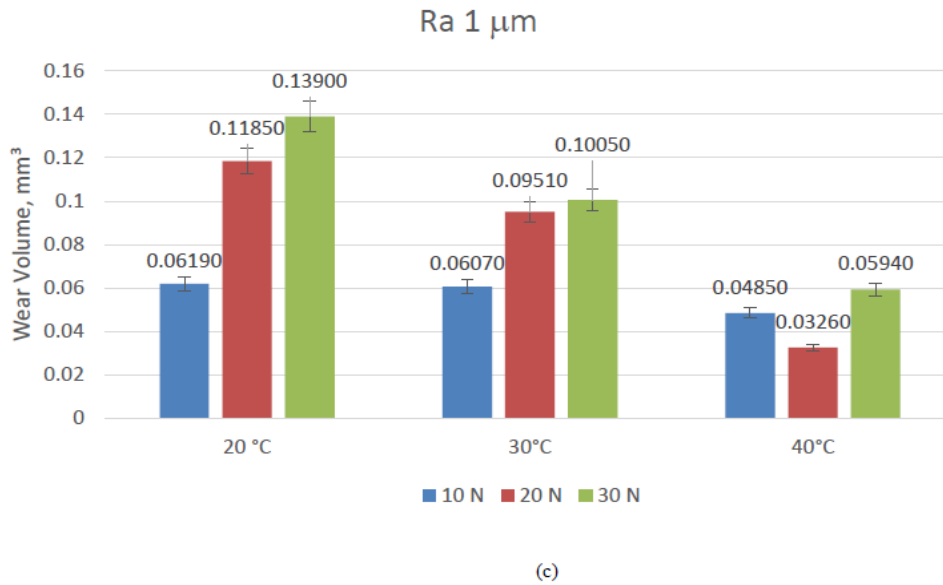
Ra 0.05 µm

(a)

Ra 0.1 µm

(b)

(c)
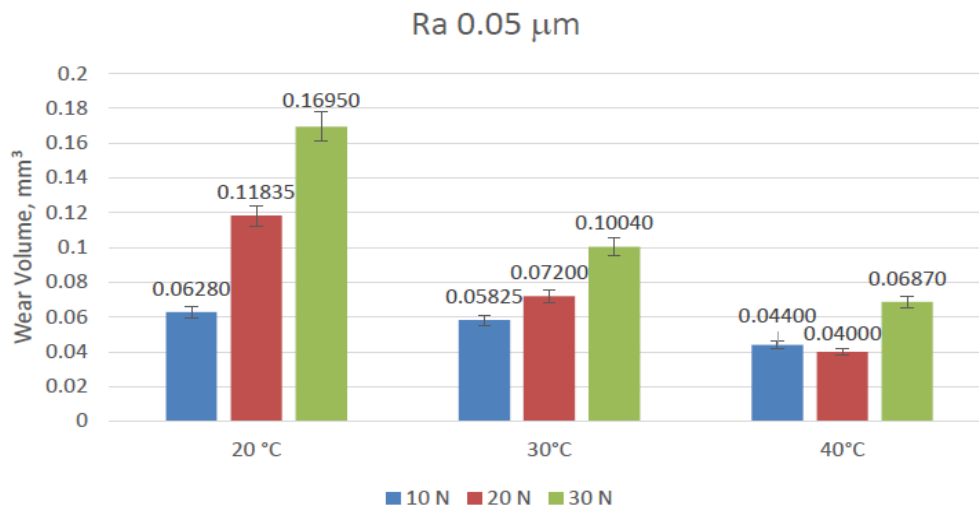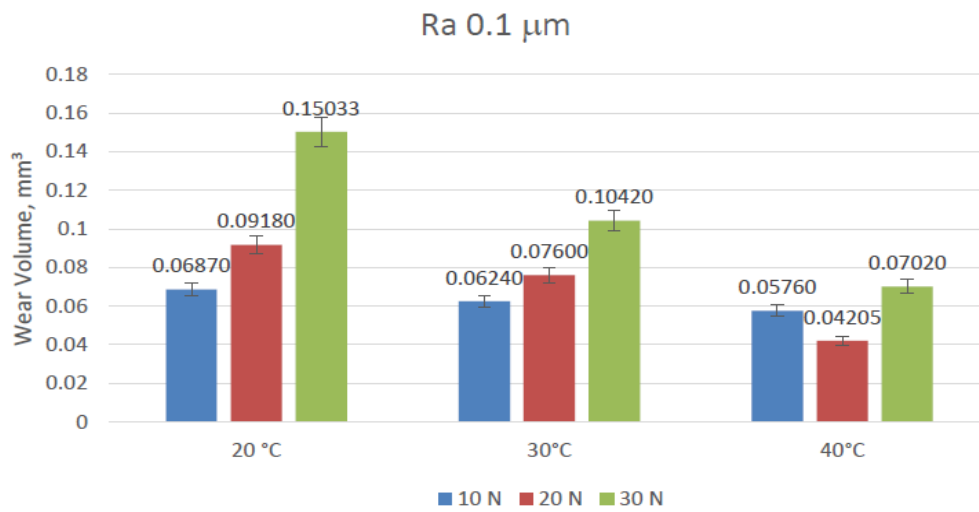
Figure 10: Wear volume plots: (a) $R_a 0.05 \, \mu m$ (b) $R_a 0.1 \, \mu m$ (c) $R_a 1.0 \, \mu m$.

At $10 \, N$ load for all the tested temperatures an increase in average surface roughness from $0.05 \, \mu m$ to $0.1 \, \mu m$ generated more wear. Further increasing the surface roughness from $0.1 \, \mu m$ to $1.0 \, \mu m$ showed a reduction in wear volume for normal load of $10 \, N$ at each temperature. Minimum wear for $10 \, N$ load was observed at the least rough surface. These results indicate that increasing the surface roughness at lower loads increases wear due to increase in asperity interactions. Further increasing the surface roughness results in harsher operating conditions creating more asperity interactions, these conditions however proved to be more favourable for the chemical breakdown and reaction of HFE-7000 with the metallic surfaces producing protective surface films resulting in wear reduction.

An increase in load from $10 \, N$ to $20 \, N$ at 20°C showed almost the same values of wear volume for $R_a 0.05 \, \mu m$ and $R_a 1.0 \, \mu m$, however at $R_a 0.1 \, \mu m$ wear volume showed the least values for $20°C, 20 \, N$. This shows that for $20 \, N, 20°C$ there exists an optimum value of surface roughness which will result in lower wear. For $20 \, N, 30°C$ conditions the wear volume increases with an increase in surface roughness. At $20 \, N, 40°C$ wear volume increased with an increase in surface roughness from $0.05 \, \mu m$ to $0.1 \, \mu m$, however at $R_a 1.0 \, \mu m$ least values of wear volume were noted. This indicates that although hasher loading conditions promote the production of surface tribo-films, the temperature has to increase as well to accelerate the formation of these surface films. $20 \, N, 40°C$ testing condition for each surface roughness produced the least amount of wear. This indicates that an optimum combination of load and temperature exists which produces least wear irrespective of the surface roughness. Testing conditions of $R_a 1.0 \, \mu m$, HFE-7000 temperature 40°C and normal load of $20 \, N$ produced least overall wear displaying the best operating environment in terms of wear.

For $30N$ load at 20°C an increase in surface roughness resulted in a decrease in wear volume. At $30°C$ and $30 \, N$ load an increase in surface roughness did not have any noticeable effect on the wear volume. At $30 \, N, 40°C$, an increase in surface roughness from $0.05 \, \mu m$ to $0.1 \, \mu m$ increased wear, but increasing surface roughness to $1.0 \, \mu m$ reduced wear and resulted in the least wear volume for these testing conditions.

21

6.   Tribochemistry Discussion

Post experimental Energy-Dispersive X-ray Spectroscopic (EDS) analyses were carried out in a vacuumed chamber on *all* the specimens tested. A strong presence of F and O was detected on *all* of the flat circular specimens as well as on *all* of the steel balls. EDS analysis was also conducted for a selection of the specimens before experimentation. As each sample was grinded, polished and ultrasonically conditioned with acetone pre-experimentation, no oxygen or fluorine was detected on the samples pre-experimentation. X-ray Photoelectron Spectroscopy (XPS) analysis was carried out on a number of sample pairs to study the surface composition post experimentation. EDS results of one of the specimen pairs tested are shown in figure 11 and figure 12 respectively.
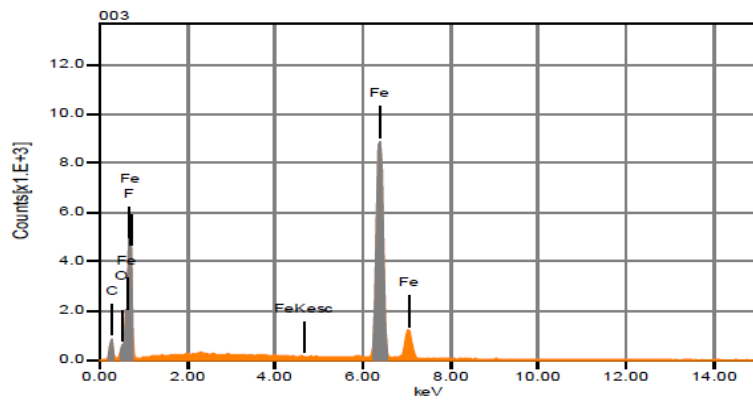
(a)
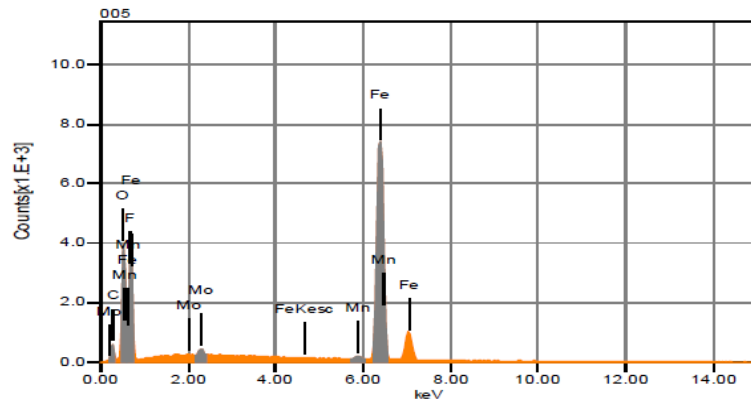
(b)
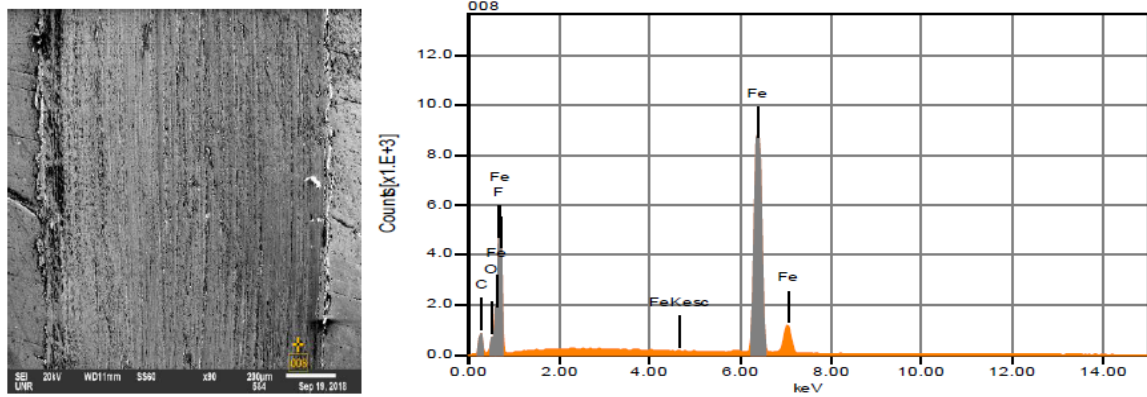
(c)

Figure 11: Magnified images of the wear scar indicating the analysis region along with the EDS results.

Figure 11 shows the magnified image of a wear scar on the EN1A steel flat circular specimen along with the chemical characterization results obtained by analysing different regions on the wear track. Similar results were obtained for the other flat specimens as well. Different regions on the wear track were examined which revealed the presence of both oxygen and fluorine on the wear track indicating the development of tribo-films on the wear scar.

Figure 12 shows the elemental analysis of the 52100 steel ball. The analysis on the ball was also performed at various different regions within the contact zone. The analysis also revealed the presence of both oxygen and fluorine demonstrating that the protective surface tribological films were not only formed on the flat specimen were also formed on the ball specimen as well.
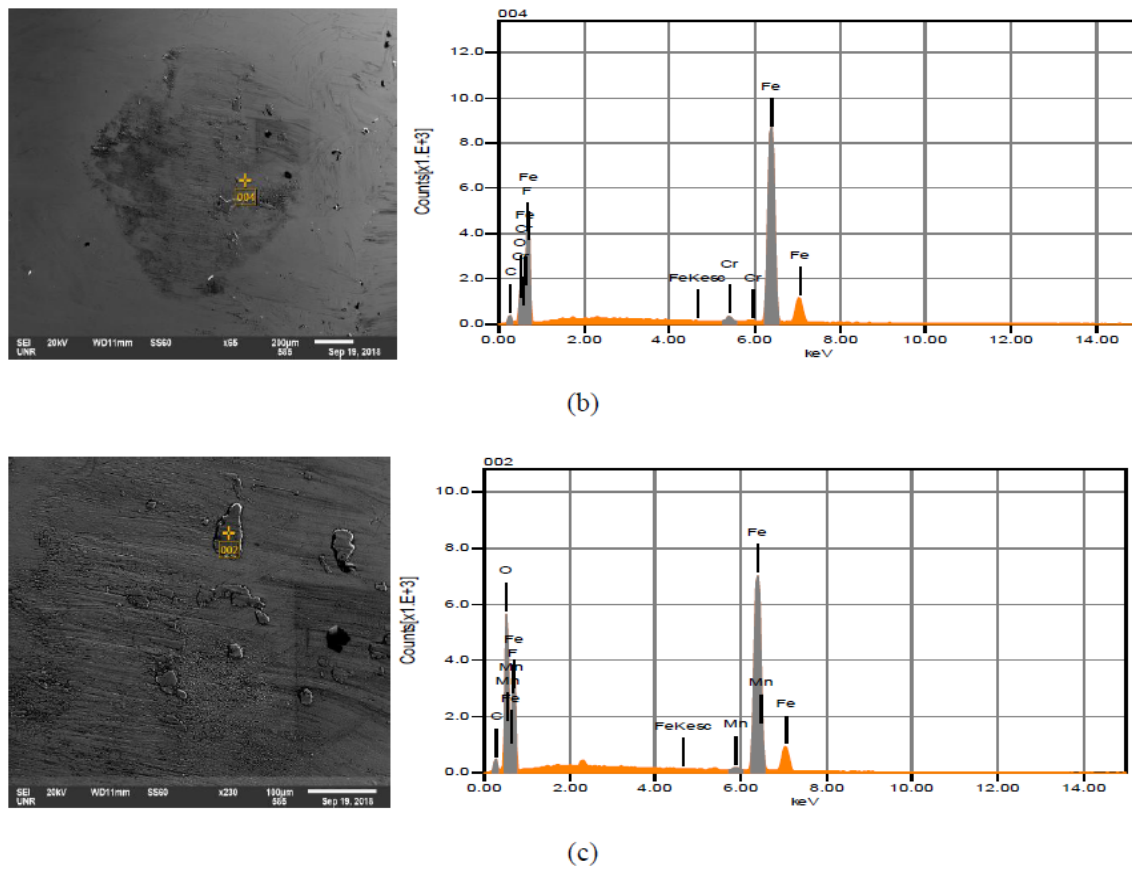

(a)

23

(b)

(c)
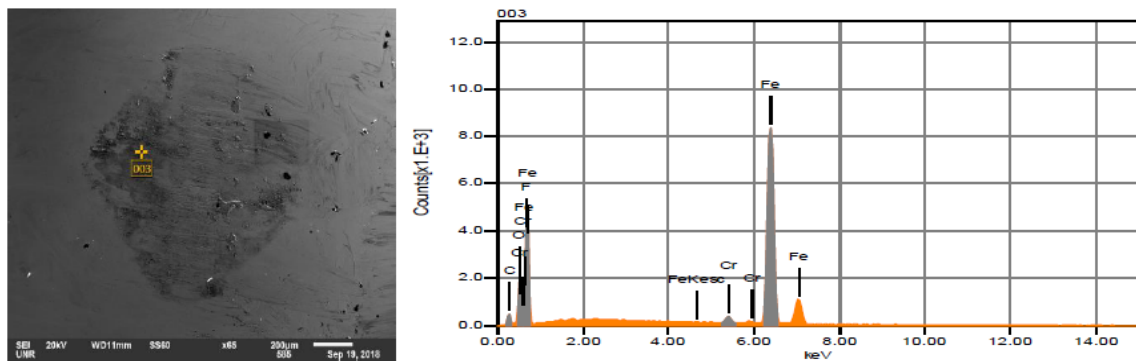
Figure 12: Magnified images of a ball specimen indicating the analysis region along with the EDS results.

The experimentation chamber was vacuumed to minimise the effect of ambient air before introducing the refrigerant in the system and establishing fully lubricated conditions after which the test chamber was sealed, which means that the origin of post experimentation detected oxygen and fluorine is the refrigerant. The samples were stored in a desiccator after experimentation. Even if aerial oxidation is taken into consideration while handling and transporting the sample post-experimentation still will not explain the detection of high percentage of fluorine and oxygen on the surfaces of the tested samples.

X-ray Photoelectron Spectroscopy (XPS) was performed in ultra-high vacuum using Kratos Axis Ultra. A monochromated aluminium X-ray source was operated at 15 KV, 10 mA emission. Each analysis performed had an approximate area of $700 \ \mu m \ X \ 300 \ \mu m$. Analysis conditions used were 160 eV pass energy, 1 eV steps and 0.2 s dwell per step. Survey spectra in the range of 1350 to -10 eV binding energy were taken at 0° emission angle to the surface normal. The XPS survey spectra results of one of the sample pairs tested are shown in figure 13. Besides Iron, Carbon, Silicon, Manganese, Sulphur, Phosphorus and Chromium which are typically present in EN1A steel and 52100 steel, elements such as Sodium, Zinc, Calcium and Nitrogen have also been detected. The source of Sodium, Zinc and Calcium is believed to be the nitrile and latex laboratory rubber gloves which were used for sample handling. Zinc, Sodium and Calcium presence is most probably due to the transfer of components from disposable laboratory gloves onto the surfaces of the ball and disc. Numerous components within a glove material and manufacturing residues left on the surfaces of gloves have been reported to be easily transferred to other materials with Zinc, Sodium and Calcium being a common contamination caused by laboratory gloves [78].

24
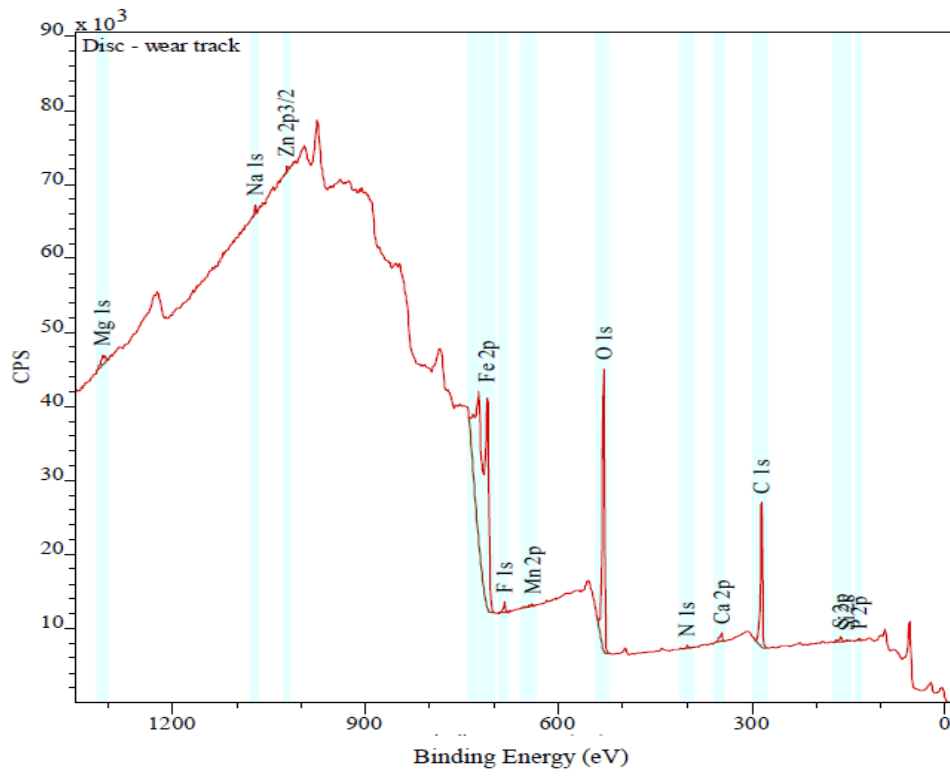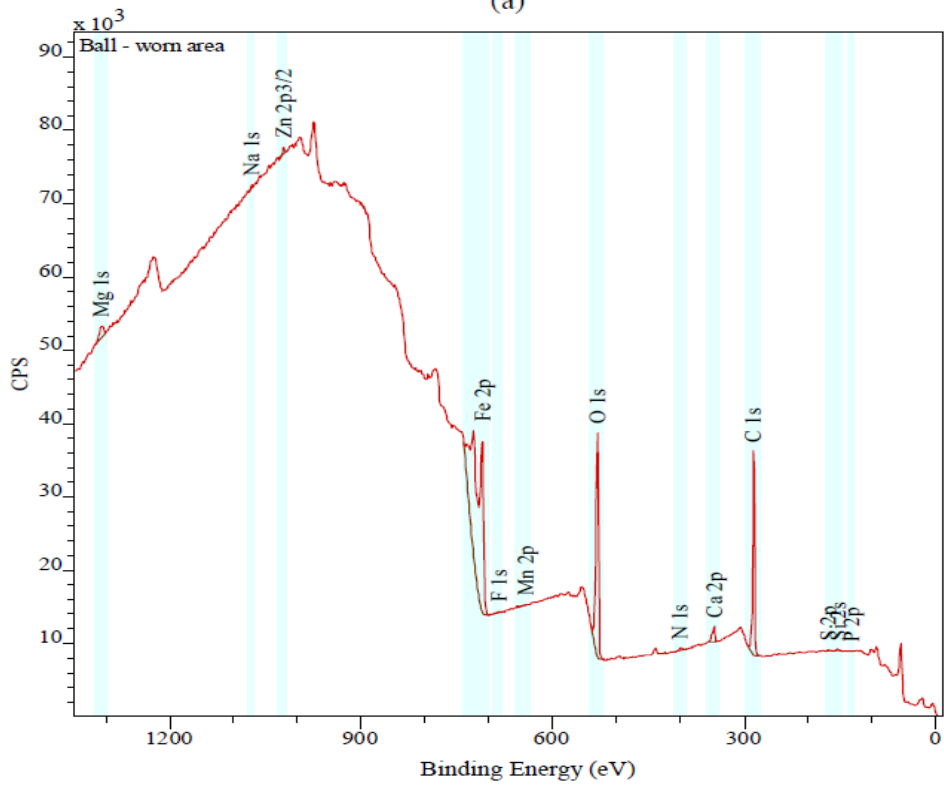
Figure 13: XPS survey spectra: (a) Disc (b) Ball

25

Nitrogen is often associated with carbon contamination from the atmosphere. Elements of interest i.e. the constituents present in the refrigerant and steel samples were further investigated and are presented in figure 14.

Figure 14 shows the XPS high resolution core level spectrum results for Iron, Carbon, Oxygen and Fluorine. Figure 14 (a) shows the Fe2p high resolution core level spectra for the ball and flat circular disc. Binding energy peaks of Fe $2p_{3/2}$ equal to 710.7 eV for the ball as well as the flat sample are present in the results which refer to the formation of Fe_2O_3 [79]. Small $2p_{3/2}$ peak at ~ 706.7 eV is also present in the spectra which indicates Fe metal [79]. Compared to the metal, Iron oxide peaks are significantly shifted to higher binding energy [79].

Figures 14 (b) and 14 (c) illustrate the C1s high resolution core level spectra of the flat circular disc and the ball specimens respectively. The results of the C1s spectra for the flat disc sample can be fitted for four different peaks with respect to the results shown in figure 14 (b). With reference to figure 14 (c), the C1s XPS spectrum obtained for the ball specimen is very similar to the flat sample expect for the fact that the ball spectrum can be fitted for three different peaks instead of four. This implies that similar carbon constituents are present on both the samples, with an additional carbon compound present on the flat disc. The peaks for binding energies between 285.0-285.3 eV are present on both the samples. Of the total percentage of C present on the analysed area on the disc, 80.1% of it is present within these binding energy limits. For the ball sample, 84.5% of the C detected lies within these binding energy limits on the area analysed. For adventitious carbon contamination C-C typically has binding energy of 284.8 eV [79]. The analysis process has an inherited error of at least $\pm$ 0.1 eV to $\pm$ 0.2 eV [80]. It is convenient for organic systems to charge correct to the C-H, C-C signal and set it to 285.0 eV [80]. Further high binding energy components can be analysed above this main peak. +1.6 eV above (285.0-285.3 eV) correspond to C-OH and C-O-C [79, 80]. The third peak that is generated by +2.8 eV above (285.0-285.3 eV) refers to C=O [80], this third peak is only present on the flat sample and not on the ball. The fourth peaks which are in the range of 288.7-288.9 eV denote O-C=O [79, 80]. The binding energies in the range of 288-290 eV for Metal Carbonates also refers to the presence of metal carbonates [80]. Detection of peaks in the C1s spectra on the worn regions within these (288-290 eV) binding energies could possibly also mean the formation of iron carbonates. The results of the C1s spectra for the flat as well as the ball sample indicate the presence of multiple carbon based compounds showing that not only the bonds of the refrigerant have broken but also new bonds have been formed.

The O1s spectrum obtained by analysing the flat disc and ball specimen are shown in figures 14 (d) and 14 (e) respectively. Similar to the C1s spectrum, O1s spectrum for the ball and the flat samples show similar peaks. Multiple peaks are generated at binding energies 529.8 eV to 529.9 eV and 531.5 eV to 531.8 eV for the disc as well as the ball specimens. This indicates that similar oxygen constituents are present on both the tested samples. For the area analysed on the disc, 68% of oxygen is present between 531.5-531.8 eV and 32% of Oxygen is between 529.8-529.9 eV. For the ball sample 64.2% of the oxygen is present between 531.5-531.8 eV and 35.8% is in the range of 529.8-529.9 eV. Besides metal oxides, the O1s binding energy of various species and compounds lies within a very narrow range [79]. Interpretation of the O1s spectra is not straightforward as O1s peaks are broader with multiple overlapping components [79]. Binding energies in the range of 529-530 eV depict the possible formation of metal oxides, most probably Fe_2O_3 [70, 79]. Fe_2O_3 is the mostly likely metal oxide to have formed as Iron (III) Oxide was directly detected in the Fe2p spectra. The binding

energies in the range of 531.5-532 eV imply the presence of C-O [79], C-O was also detected in the C1s spectra. For O1s spectrum, binding energies in the range of 531.5~531.9 also refers to the formation of carbonates and/or bicarbonates [70, 81]. The possible formation of metal carbonates was also detected in the C1s spectrum. Oxygen bonded to organic components can range in the binding energies from as low as 530.9 eV to as high as 533.8 eV and metal hydroxides having a binding energy of 531.3 eV with a standard deviation of 0.3 eV [80]. The most likely metal hydroxides, if present, could be $Fe(OH)_2$ and $Fe(OH)_3$. The results show that a higher percentage, more than 60% of the oxygen detected is bonded to organic components or possibly in the form of metal hydroxides. The rest of the oxygen is bonded to metal with Fe_2O_3 being the mostly probable metal oxide formed on the surface.

F1s spectrum for the disc and ball specimens has been presented in figure 14 (f) and figure 14 (g). Unlike the previous XPS results, the F1s spectra for the ball and the disc are different. 81.7% of the fluorine detected on the disc sample is at 684.4 eV binding energy while 18.3% of fluorine was identified at 688.2 eV binding energy. For the ball specimen, a peak was only detected at ~684.5 eV. For fluorine F1s spectra the binding energies from 684 eV to 685.5 eV indicate the presence of metal fluorides [79] and from 688 eV to 689 eV refers to organic fluorine. A peak was detected in the range of 684 eV to 685.5 eV while no peaks were detected for the ball sample in the range of 688-689 eV, which means that only metal fluorides are present on the ball sample on the area analysed and fluorine is not present in organic state. For the disc sample a very high percentage (81.7%) of fluorine is present as metal fluorides, while a smaller percentage (18.3%) is present as organic fluorine. The presence of metal fluorides and organic fluorine also suggests that the bonds in the refrigerant have been broken and new bonds have been formed on the surfaces of the rubbing metals. These results are in contrast to the results of oxygen. Oxygen is present in a higher percentage in organic form while a smaller percentage of oxygen is present as metal oxides as discussed in the O1s spectrum results. In addition metal fluorides are present on both the samples while organic fluorine is present only on the disc sample. This indicates that fluorine in HFE-7000 has a higher tendency to form metal fluorides in comparison to oxygen in HFE-7000 to from metal oxides. The metal fluorides are most probably FeF_2 and/or FeF_3 [53, 54, 63].

The detection of inorganic compounds such as iron (III) oxide and metal fluorides originate from the tribochemical reaction between the steel ball/disc and the fragmented species coming from the HFE-7000 refrigerant breakdown. The organic species have been reported to act as the third body ensuring sustainability of the interface in terms of wear and friction, whereas the metallic components (fragmented refrigerant reacted with steel) on the other hand provide better adhesion on the surfaces of the rubbing metals [54].
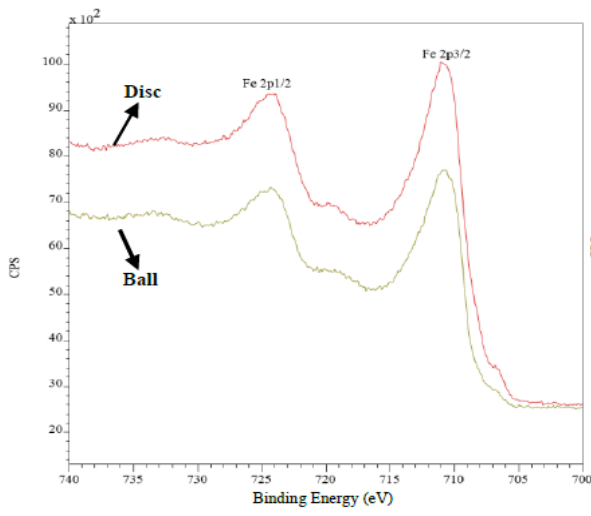
(a)
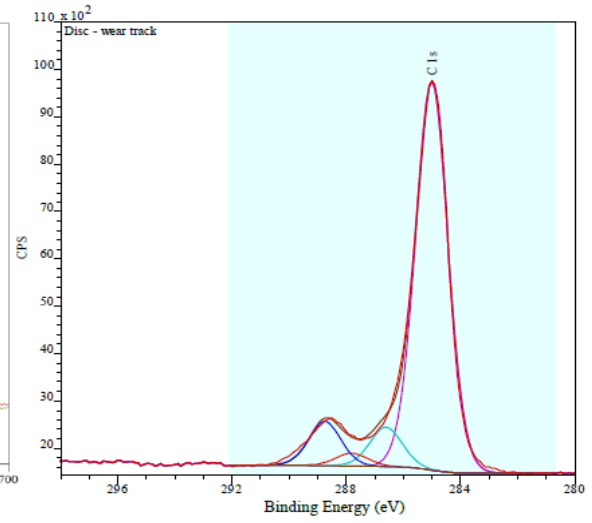
(b)
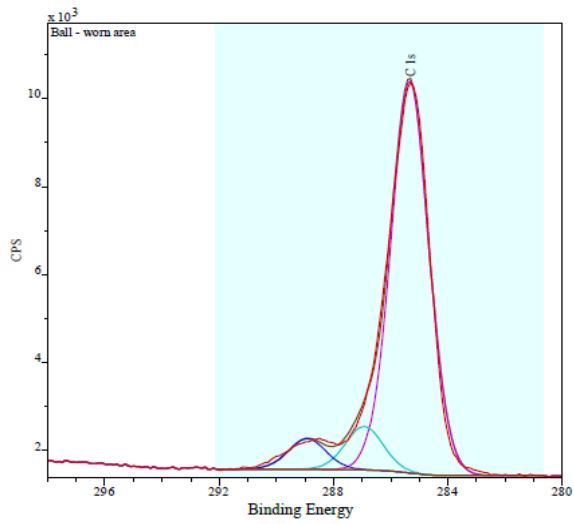
(c)
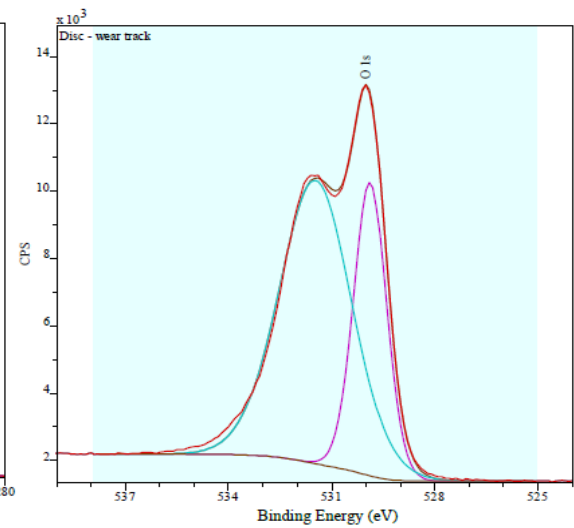
(d)
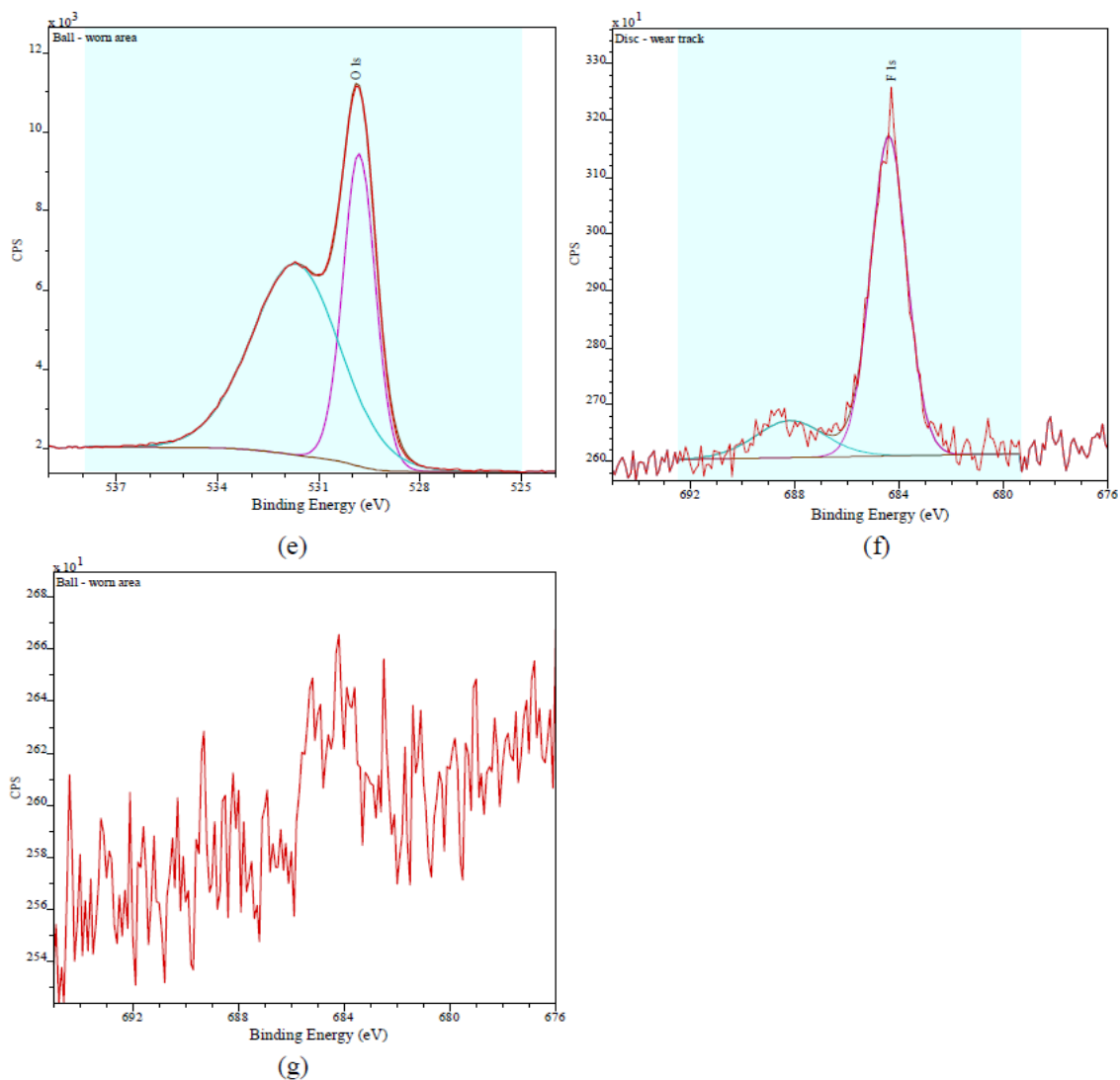
Figure 14: XPS high resolution core level spectrum: (a) Fe2p disc and ball (b) C1s disc (c) C1s ball (d) O1s disc (e) O1s ball (f) F1s disc (g) F1s ball.

The formation of an oxygenated layer in the presence of carbon dioxide [70, 82, 83] and the formation of fluorine-containing tribo-layers by various different refrigerants [8, 11, 51, 53-55, 64] have been reported to be beneficial in improving the tribological performance of rubbing surfaces. The applied normal load, mechanical motion, heat and frictional force facilitate the chemical breakdown of the refrigerant ($C_3F_7OCH_3$). C-F, Carbon-Fluorine single bonds are highly polar bonds ($C^{\delta+} - F^{\delta-}$) and C-F bond is shorter than the C-H bond which makes C-H easier to break in comparison to C-F bond [53, 84]. It has also been reported that the oxygen-carbon bond is weaker than the carbon-carbon bond [63, 85]. It is highly possible that the carbon-oxygen bond in HFE-7000 is the first bond to break which frees OCH$_3$ from the rest of the molecule. During the course of an experiment; material removal from the surface of EN1A steel by hard 52100 steel ball leads to the exposure of fresh surface which contains immobilised free radicals or dangling bonds. Unlike free radicals, immobilised free radicals are kinetically more stable because of their limited mobility in a solid medium. However, similar to free radicals, immobilised free radicals are also extremely reactive. The breakdown of

29

refrigerant and the exposure of fresh highly reactive bonds on the surface of the EN1A steel specimen leads to a chemical reaction between the refrigerant and EN1A steel. This leads to the adsorption of HFE-7000 on to the surfaces therefore forming oxygenated and fluorinated tribo-films which results in reduction in friction and wear. Besides the adhered softer material on the ball, scratch marks are also clearly visible on the surface of the ball in the contact region, which leads to a similar chemical reaction between the ball and the refrigerant as well. These tribo-layers are well adhered to the rubbing surface as the presence of fluorine and oxygen was not only detected throughout the wear scar on the disc specimen but was also detected on different contact regions on the ball specimen.

7. Conclusions

A micro friction machine has been successfully modified and commissioned for bench testing the future generation of refrigerants within tribological context. A series of testes have been conducted to assess the tribological performance of the environmentally friendly refrigerant HFE-7000 by varying the tribo-operating conditions. Variable operating environments have been simulated during this study. Tests have been performed by changing the applied normal load, by using samples of various surface finish and by heating the refrigerant to various temperatures. The tribological performance of the refrigerant HFE-7000 which has wide ranging application areas has been investigated at low loads and low temperatures starting from room temperature. The results have shown that a mechanical system based on HFE-7000 will show good friction and wear performance at higher operating temperatures and loads, in addition HFE 7000 exhibits good tribological performance at lower temperatures and low loads as well. An increase in load even at 20°C results in a significant reduction in the friction coefficient and an increase in temperature at a low load of even $10\ N$ reduces wear.

Overall the results indicate that increasing the operating temperature at a constant load reduces both friction coefficient and wear. Increasing the load at a constant temperature increases wear but results in a reduction in friction coefficient. The reduction in the friction coefficient with increasing load and decrease in wear along with a decrease in coefficient of friction with increasing temperature is believed to be associated with the development of protective tribo-films on the interacting surfaces. The formation of these films is accelerated by an elevation in the refrigerant temperature and increase in the applied load. Increasing the applied load and operating temperature increases the reactivity of the refrigerant HFE-7000 with the rubbing metals. EDS analyses on the samples in the contact region and wear track have shown a significant presence of oxygen, fluorine and carbon on the rubbing surfaces. The detailed high resolution XPS analysis reveal the formation of new bonds/compounds on the surfaces of the interacting metals and indicate breaking up of the bonds of the refrigerant. Analysis on different regions within the contact zone of the rubbing metals post-experimentation has demonstrated that oxygenated and fluorinated layers are well adhered on the disc wear track and ball. It is also observed from the results obtained that the surface roughness does not have a very significant effect on the coefficient of friction and on wear. This shows that metallic parts of a range of surface finish and even parts with rough surface finish can be used in HFE-7000 run interacting systems.

The results of this study show that HFE-7000 which is a promising future generation refrigerant from a thermodynamics point of view has demonstrated good tribological performance. It can be inferred with confidence evidenced by the results presented here, that HFE-7000 based interacting systems will show better friction and wear performance as compared to their predecessors HFCs.

Acknowledgments:

References

[1] McMullan JT. Refrigeration and the environment — issues and strategies for the future. Inter J Refrig. 2002;25:89-99.

[2] Xiang B, Patra PK, Montzka SA, Miller SM, Elkins JW, Moore FL, et al. Global emissions of refrigerants HCFC-22 and HFC-134a: Unforeseen seasonal contributions. Proce Nati Acad Sci. 2014;111:17379-84.

[3] Bhutta MU, Khan ZA, Garland NP, Ghafoor A. A Historical Review on the Tribological Performance of Refrigerants used in Compressors. Tribo Indu. 2018;40:19-51.

[4] Calm JM. The next generation of refrigerants–Historical review, considerations, and outlook. Inter J Refrig. 2008;31:1123-33.

[5] Jollev S. New and Unique Lubricants for Use in Compressors Utilizing R-134a Refrigerant. International Refrigeration and Air Conditioning ConferencePurdue University, Indiana, USA, 17-20 July, 1990, Paper 96.

[6] Davis B, Sheiretov TK, Cusano C. Tribological Evaluation of Contacts Lubricated by Oil-Refrigerant Mixtures. Air Conditioning and Refrigeration Center, College of Engineering, University of Illinois at Urbana-Champaign, USAACRC Technical Report 19, May 1992.

[7] KOMATSUZAKI S, HOMMA Y. Lubricants for HFC Refrigerant Compressors. J Jap Petrole Inst. 1994;37:226-35.

[8] Mizuhara K, Akei M, Matsuzaki T. The friction and wear behavior in controlled alternative refrigerant atmosphere. Tribo Trans. 1994;37:120-8.

[9] Sheiretov T, Glabbeek WV, Cusano C. Tribological evaluation of various surface treatments for M2 tool steel in a refrigerant environment. International Compressor Engineering ConferencePurdue University, Indiana, USA, 19-22 July, 1994, Paper 964.

[10] Akei M, Mizuhara K, Taki T, Yamamoto T. Evaluation of film-forming capability of refrigeration lubricants in pressurized refrigerant atmosphere. Wear. 1996;196:180-7.

[11] Kawahara K, Mishina S, Kamino A, Ochiai K, Okawa T, Fujimoto S. Tribological Evaluation of Rotary Compressor with HFC Refrigerants. International Compressor Engineering ConferencePurdue University, Indiana, USA, 23-26 July, 1996, Paper 1141.

[12] Fujimoto S, Sakitani K, Watada M. Tribology Analysis in Rolling Piston Type Compressor. International Compressor Engineering ConferencePurdue University, Indiana, USA, 1984, Paper 477.

[13] Muraki M, Tagawa K, Dong D. Refrigeration Lubricant Based on Polyolester for Use With HFCs and Prospect of Its Application With R-22 (Part 1) Tribological Characteristics. International Refrigeration and Air Conditioning ConferencePurdue University, Indiana, USA, 23-26 July, 1996, Paper 336.

[14] Tuomas R, Isaksson O. Measurement of lubrication conditions in a rolling element bearing in a refrigerant environment. Indu Lub Tribo. 2009;61:91-9.

[15] Molina MJ, Rowland FS. Stratospheric sink for chlorofluoromethanes: chlorine atom-catalysed destruction of ozone. Nature. 1974;249:810-2.

[16] Nations U. Montreal Protocol on Substances that Deplete the Ozone Layer. United Nations Environment Programme. Montreal, Canada16 September 1987.

[17] Wilson DP, Basu RS. Thermodynamic properties of a new stratospherically safe working fluid-refrigerant 134a. ASHRAE Trans1988. p. Pages 2095-118.

31

[18] Shankland IR, Basu RS, Wilson DP. Thermal conductivity and viscosity of a new stratospherically safe refrigerant-1, 1, 1, 2-tetrafluoroethane (R-134a). International Refrigeration and Air Conditioning ConferencePurdue University, Indiana, USA, 1988, Paper 41.

[19] Spauschus H. HFC 134a as a substitute refrigerant for CFC 12. Inter J Refrig. 1988;11:389-92.

[20] Eckels SJ, Pate MB. An experimental comparison of evaporation and condensation heat transfer coefficients for HFC-134a and CFC-12. Inter J Refrig. 1991;14:70-7.

[21] Khan SH, Zubair SM. Thermodynamic analyses of the CFC-12 and HFC-134a refrigeration cycles. Energy. 1993;18:717-26.

[22] Kitaichi S, Sato S, Ishidoya R, Machida T. Tribological Analysis of Metal Interface Reactions in Lubricant Oils/CFC12 and HFC 134a System. International Refrigeration and Air Conditioning Conference17-20 July, 1990, Purdue University, Indiana, USA, paper 97.

[23] Na BC, Chun KJ, Han D-C. A tribological study of refrigeration oils under HFC-134a environment. Tribo Inter. 1997;30:707-16.

[24] Yamamoto Y, Gondo S. Friction and wear characteristics of lubricants for alternative refrigerant HFC 134a. JSME Inter J C Mech Sys, Machi Eleme Manuf. 1998;41:278-84.

[25] Takesue M, Tominaga S. Wear and Scuffing Characteristics of Polyvinylether (PVE) in an HFC Atmosphere. International Refrigeration and Air Conditioning Conference14-17 July, 1998, Purdue University, Indiana, USA, paper 440.

[26] Yoon H, Sheiretov T, Cusano C. Tribological evaluation of some aluminum-based materials in lubricant/refrigerant mixtures. Wear. 1998;218:54-65.

[27] Sheiretov T, Yoon H, Cusano C. Tribological Evaluation of Various Aluminum Alloys in Lubricant/Refrigerant Mixtures. Air Conditioning and Refrigeration Center, College of Engineering, University of Illinois at Urbana-Champaign. ACRC Technical Report 92, 1996.

[28] Ciantar C, Hadfield M, Smith A, Swallow A. The influence of lubricant viscosity on the wear of hermetic compressor components in HFC-134a environments. Wear. 1999;236:1-8.

[29] Ciantar C, Hadfield M, Swallow A, Smith A. The influence of POE and PVE lubricant blends within hermetic refrigerating compressors operating with HFC-134a refrigerant. Wear. 2000;241:53-64.

[30] Fukui H, Sanechika K-i, Ikeda M. Novel refrigeration lubricants for use with HFC refrigerants. Tribo Inter. 2000;33:707-13.

[31] Yamamoto Y, Gondo S, Kim J. Solubility of HFC134a in Lubricants and Its Influence on Tribological Performance. Tribo Trans. 2001;44:209-14.

[32] Ciantar C, Hadfield M. A study of tribological durability with associated environmental impacts of a domestic refrigerator. Materi Desig. 2004;25:331-41.

[33] Lee Y-Z, Oh S-D. Friction and wear of the rotary compressor vane–roller surfaces for several sliding conditions. Wear. 2003;255:1168-73.

[34] Wardle F, Jacobson B, Dolfsma H, Hoglund E, Jonsson U. The effect of refrigerants on the lubrication of rolling element bearings used in screw compressors. International Compressor Engineering ConferencePurdue University, Indiana, USA, 14-17 July, 1992, Paper 843.

[35] Jacobson B. Lubrication of Screw Compressor Bearings in the Presence of Refrigerants. International Compressor Engineering ConferencePurdue University, Indiana, USA, 19-22 July, 1994, Paper 966.

[36] Hamada T, Nishiura N. Refrigeration lubricant based on polyolester for use with HFCs and prospect of its application with R-22 (Part 2) Hydrolytic stability and compressor endurance test results. International Refrigeration and Air Conditioning ConferencePurdue University, Indiana, USA, 23-26 July, 1996, Paper 337.

[37] Jacobson B. Ball Bearing Lubrication in Refrigetation Compressors. International Compressor Engineering ConferencePurdue University, Indiana, USA, 23-26 July, 1996, Paper 1090.

[38] Akei M, Mizuhara K. The Elastohydrodynamic Properties of Lubricants in Refrigerant Environments©. Tribo Trans. 1997;40:1-10.

[39] Jacobson BO, Espejel GEM. High pressure investigation of refrigerants HFC245fa, R134a and R123. International Compressor Engineering Conference Purdue University, Indiana, USA, 17-20 July, 2006, Paper 1789.

[40] Tuomas R, Isaksson O. Compressibility of Oil/Refrigerant Lubricants in Elasto-Hydrodynamic Contacts. J Tribo. 2005;128:218-20.

[41] Breidenich C, Magraw D, Rowley A, Rubin JW. The Kyoto protocol to the United Nations framework convention on climate change. Ame J Inter Law. 1998;92:315-31.

[42] Garland N, Hadfield M. Environmental implications of hydrocarbon refrigerants applied to the hermetic compressor. Materi Desig. 2005;26:578-86.

[43] Khan ZA, Hadfield M, Wang Y. Pressurised chamber design for conducting rolling contact experiments with liquid refrigerant lubrication. Materi Desig. 2005;26:680-9.

[44] Khan ZA, Hadfield M, Tobe S, Wang Y. Ceramic rolling elements with ring crack defects—A residual stress approach. Mater Sci Eng: A. 2005;404:221-6.

[45] Khan ZA, Hadfield M, Tobe S, Wang Y. Residual stress variations during rolling contact fatigue of refrigerant lubricated silicon nitride bearing elements. Ceram Inter. 2006;32:751-4.

[46] Khan ZA, Hadfield M. Manufacturing induced residual stress influence on the rolling contact fatigue life performance of lubricated silicon nitride bearing materials. Materi Desig. 2007;28:2688-93.

[47] Sariibrahimoglu K, Kizil H, Aksit MF, Efeoglu I, Kerpicci H. Effect of R600a on tribological behavior of sintered steel under starved lubrication. Tribo Inter. 2010;43:1054-8.

[48] De Mello J, Binder R, Demas N, Polycarpou A. Effect of the actual environment present in hermetic compressors on the tribological behaviour of a Si-rich multifunctional DLC coating. Wear. 2009;267:907-15.

[49] Solzak TA, Polycarpou AA. Tribology of hard protective coatings under realistic operating conditions for use in oilless piston-type and swash-plate compressors. Tribo Trans. 2010;53:319-28.

[50] Spatz M, Minor B, DuPont H. HFO-1234yf A low GWP refrigerant for MAC. Honeywell/DuPont joint collaboration. SAE World Congress 14-17 April, 2008, Detroit, Michigan, USA.

[51] Tatsuya Sasaki HN, Hideaki Maeyama, Kota Mizuno. Tribology Characteristics of HFO and HC Refrigerants with Immiscible Oils - Effect of Refrigerant with Unsaturated Bond. International Compressor Engineering ConferencePurdue University, Indiana, USA, 12-15 July, 2010, Paper 1946.

[52] Mishra SP, Polycarpou AA. Tribological studies of unpolished laser surface textures under starved lubrication conditions for use in air-conditioning and refrigeration compressors. Tribo Inter. 2011;44:1890-901.

[53] Akram MW, Polychronopoulou K, Polycarpou AA. Lubricity of environmentally friendly HFO-1234yf refrigerant. Tribo Inter. 2013;57:92-100.

[54] Akram MW, Polychronopoulou K, Seeton C, Polycarpou AA. Tribological performance of environmentally friendly refrigerant HFO-1234yf under starved lubricated conditions. Wear. 2013;304:191-201.

[55] Akram MW, Polychronopoulou K, Polycarpou AA. Tribological performance comparing different refrigerant–lubricant systems: The case of environmentally friendly HFO-1234yf refrigerant. Tribo Inter. 2014;78:176-86.

[56] Akram MW, Meyer JL, Polycarpou AA. Tribological interactions of advanced polymeric coatings with polyalkylene glycol lubricant and r1234yf refrigerant. Tribo Inter. 2016;97:200-11.

[57] Hulse RJ, Basu RS, Singh RR, Thomas RH. Physical properties of HCFO-1233zd (E). J Chemi Eng Data. 2012;57:3581-6.

[58] Data sheet. https://multimedia.3m.com/mws/media/121372O/3m-novec-7000-engineered-fluid-tds.pdf3M™ Novec™ 7000 Engineered Fluid.

[59] Akasaka R, Kayukawa Y. A fundamental equation of state for trifluoromethyl methyl ether (HFE-143m) and its application to refrigeration cycle analysis. Inter J Refrig. 2012;35:1003-13.

[60] Helvaci H, Khan ZA. Experimental study of thermodynamic assessment of a small scale solar thermal system. Ener Conv Manage. 2016;117:567-76.

33

[61] Helvaci HU, Khan ZA. Heat transfer and entropy generation analysis of HFE 7000 based nanorefrigerants. Inter J Heat Mass Trans. 2017;104:318-27.

[62] Sekiya A, Misaki S. The potential of hydrofluoroethers to replace CFCs, HCFCs and PFCs. J Fluori Chemi. 2000;101:215-21.

[63] Muraki M, Sano T, Dong D. Elastohydrodynamic properties and boundary lubrication performance of polyolester in a hydrofluoroether refrigerant environment. Proc Instit Mech Engs Prt J: J Eng Tribo. 2002;216:19-26.

[64] Bhutta M, Khan Z, Garland N. Wear Performance Analysis of Ni–Al_2O_3 Nanocomposite Coatings under Nonconventional Lubrication. Materials. 2018;12:36.

[65] Vergne P, Fillot N, Bouscharain N, Devaux N, Morales-Espejel GE. An experimental and modeling assessment of the HCFC-R123 refrigerant capabilities for lubricating rolling EHD circular contacts. Proc Instit Mech Engs Prt J: J Eng Tribo. 2015;229:950-61.

[66] Cannaday ML, Polycarpou AA. Tribology of unfilled and filled polymeric surfaces in refrigerant environment for compressor applications. Tribo Lett. 2005;19:249-62.

[67] Yeo SM, Polycarpou AA. Fretting experiments of advanced polymeric coatings and the effect of transfer films on their tribological behavior. Tribo Inter. 2014;79:16-25.

[68] Solzak TA, Polycarpou AA. Tribology of protective hard coatings for use in oil-less, piston-type compressors. International Compressor Engineering ConferencePurdue University, Indiana, USA, 17-20 July, 2006, Paper 1790.

[69] Demas NG, Polycarpou AA. Tribological investigation of cast iron air-conditioning compressor surfaces in CO_2 refrigerant. Tribo Lett. 2006;22:271-8.

[70] Nunez EE, Polychronopoulou K, Polycarpou AA. Lubricity effect of carbon dioxide used as an environmentally friendly refrigerant in air-conditioning and refrigeration compressors. Wear. 2010;270:46-56.

[71] Minor BH, Herrmann D, Gravell R. Flammability characteristics of HFO-1234yf. Process Safety Progress. 2009;29:150-4.

[72] Global Warming Potential Values, https://www.ghgprotocol.org/sites/default/files/ghgp/Global-Warming-Potential-Values%20%28Feb%2016%202016%29_1.pdf.

[73] Helvaci H, Khan Z. Thermodynamic modelling and analysis of a solar organic Rankine cycle employing thermofluids. Ener Conv Manage. 2017;138:493-510.

[74] Blaineau B, Dutour S, Callegari T, Lavieille P, Miscevic M, Blanco S, et al. Experimental investigation of a dielectric liquid-vapor interface between two vertical planar electrodes: Influence of the DC electric field and temperature. Experimental Thermal and Fluid Science. 2019;105:144-52.

[75] Shin J-H, Rozenfeld T, Shockner T, Kumar Vutha A, Wang Y, Ziskind G, et al. Local heat transfer under an array of micro jet impingement using HFE-7000. Applied Thermal Engineering. 2019:113716.

[76] Jean-Fulcrand A, Masen MA, Bremner T, Wong JSS. High temperature tribological properties of polybenzimidazole (PBI). Polymer. 2017;128:159-68.

[77] Deshpande P, Minfray C, Dassenoy F, Thiebaut B, Le Mogne T, Vacher B, et al. Tribological behaviour of TiO2 Atmospheric Plasma Spray (APS) coating under mixed and boundary lubrication conditions in presence of oil containing MoDTC. Tribo Inter. 2018;118:273-86.

[78] Spectroscopy: http://www.spectroscopyonline.com/xps-surface-characterization-disposable-laboratory-gloves-and-transfer-glove-components-other-surfac.

[79] Thermo Scientific XPS , https://xpssimplified.com/periodictable.php. Thermo Scientific.

[80] X-ray Photoelectron Spectroscopy (XPS) Reference Pages, http://www.xpsfitting.com/.

[81] Wu X, Cong P, Nanao H, Minami I, Mori S. Tribological behaviors of 52100 steel in carbon dioxide atmosphere. Tribo Lett. 2004;17:925-30.

[82] Jeon H-G, Oh S-D, Lee Y-Z. Friction and wear of the lubricated vane and roller materials in a carbon dioxide refrigerant. Wear. 2009;267:1252-6.

34

[83] Cannaday M, Polycarpou A. Advantages of CO_2 compared to R410a refrigerant of tribologically tested Aluminum 390-T6 surfaces. Tribo Lett. 2006;21:185-92.

[84] Gu G, Wu Z, Zhang Z, Qing F. Tribological properties of fluorine-containing additives of silicone oil. Tribo Inter. 2009;42:397-402.

[85] Lide DR. CRC handbook of chemistry and physics, : CRC Press, Boca Raton, Florida; 73rd edition, 1992-1993, pp. 9-145.

35

Paper V

Wear and friction performance evaluation of nickel based nanocomposite coatings under refrigerant lubrication

Muhammad Usman Bhutta* [a,b], Zulfiqar Ahmad Khan [a]

[a] NanoCorr, Energy & Modelling (NCEM) Research Group, Department of Design & Engineering, Bournemouth University, Talbot Campus, Fern Barrow, Poole, BH12 5BB
[b] School of Mechanical & Manufacturing Engineering (SMME), National University of Sciences & Technology (NUST), Campus H-12, Islamabad, Pakistan
*Corresponding author: zkhan@bournemouth.ac.uk

Abstract

Environmental concerns related to global warming has enforced the introduction of newly artificially formulated refrigerants. HFE-7000 is a replacement solution for the existing harmful refrigerants and thermo-fluids having a broad range of application areas including usage in green energy, low carbon technologies, in aerospace and automotive industries. In this study five different types of coatings namely, Ni-ZrO$_2$, Ni-Al$_2$O$_3$, Ni-SiC, Ni-Graphene and Nickel-only have been used to study the wear and friction performance of these coatings in systems based on HFE-7000 refrigerant. Extensive experimentation has been performed on these coated contacts using a modified pressurised lubricity tester by changing the refrigerant temperature and the applied normal load in an attempt to enhance the tribological performance of interacting machine parts employing HFE-7000. EDS analysis performed on all the sample pairs within the contact region revealed the presence of fluorine and oxygen based tribo-films. These oxygenated and fluorinated tribo-films help prevent metal-to-metal contact leading to a drop in friction and wear. All coatings presented an improvement in the micro-hardness and in hardness to elastic modulus ratio compared to uncoated steel. The results of friction and wear of coated samples were compared to uncoated steel as well. The results show an improvement in wear and friction at most of the operating conditions by applying nickel based coatings on a steel substrate in the presence of HFE-7000. Friction and wear performance of nickel based coatings does drop for some of the coatings at particular testing conditions which leads to conclude that a careful selection of the coatings has to be made depending on the operating refrigerant temperature and load. The results of this study provide a guideline and will be extremely useful in selecting the type of coating based on the application area.

Keywords: Nanocomposite coatings, Friction, Wear, Environment-friendly refrigerants, Reciprocating Motion

1. Introduction

Over the past century refrigerants have slowly progressed from the first generation to their fourth generation [1]. The gradual progression and development of refrigerants is linked to their flammability, toxicity and environmental impact. Toxicity and flammability of the first generation of refrigerants which were naturally occurring led to the search for replacement refrigerants in the 1920s [2]. Research for non-flammable and non-toxic refrigerants brought forward the first family of artificially formulated refrigerants; CFCs (Chlorofluorocarbons) and HCFCs (Hydrochlorofluorocarbons). The destruction of the ozone layer by these refrigerants enforced a ban on CFCs and HCFCs through the Montreal Protocol on Substances that Deplete the Ozone layers in 1987 [3]. HFCs (Hydrofluorocarbons) were introduced as response to the ban on CFCs and HCFCs.

1

In contrast to CFCs and HCFCs, HFCs displayed poorer friction, wear and overall tribological performance [2]. The inferior friction, wear and tribological performance of HFCs is due to their inability to chemically react with the rubbing surfaces to produce protective surface tribo-films at typical compressor operating conditions [2]. In contrast CFCs and HCFCs reacted with the mating metal surfaces forming protective surface tribo-films which gave CFCs and HCFCs excellent tribological properties [2]. HFCs were later identified amongst the primary contributors to global warming and as per the 1997 Kyoto Protocol to the United Nations Framework Convention of Climate Change [4] these refrigerants are in the process of being phased out. Naturally occurring compounds with zero Ozone Depletion Potential (ODP) and very low Global Warming Potential (GWP) have become of particular interest as well since the Kyoto Protocol in search for suitable replacement refrigerants.

Non-toxic, non-flammable Carbon dioxide which has a Global Warming Potential value of one and an Ozone Depletion Potential value of zero has been studied for its tribological performance [5-10] as a possible replacement refrigerant. Operating pressures when using CO_2 however are extremely high compared to the traditional refrigerants which requires special equipment design for its viable commercialization [2]. Another family of environmental family refrigerants are Hydrocarbons (HCs) which have zero ODP and low GWP values have also been studied for their friction, wear, fatigue and overall power consumption [11-16]. HCs are used in domestic and commercial applications but are inheritably highly flammable which restricts their application areas.

As a result to the legislations on environmental impact and the toxicity/flammability issues of naturally occurring compounds the fourth generation of artificially formulated refrigerants which not only have zero ODP but also have lower GWP have been introduced [1, 2].

Hydrofluoroethers (HFEs) are amongst the family of the fourth generation of future refrigerants having high commercialization potential and applications. HFE-7000 is a non-flammable, non-corrosive refrigerant having zero ODP, low GWP, good materials compatibility, excellent dielectric properties and good thermal stability [17]. Its applications include usage in fuel cells, in electronic cooling units, in medical laboratories, in chemical reactors, in freeze dryers, in dry etchers, in high voltage transformers, in auto-cascaded refrigeration systems, etc. [17]. HFE-7000 has a boiling point much higher than HFC-134a and is not considered a direct 'drop-in' solution and replacement of HFC-134a in compressors [2]. HFE-7000 has a broader range of fields where it can be utilized. It has been successfully used in renewable energy systems and low carbon technologies [18, 19], in solar organic Rankine cycle [20], in Electrohydrodynamics applications [21], as a jet impinging dialectic coolant [22], etc. Different physical and chemical properties of Hydrofluoroether-7000 have been listed in table 1. Various different properties of HFC-134a, which was a highly used Hydrofluorocarbon have also been listed in table 1. Both HFE-7000 and HFC-134a have an ODP value of zero but the GWP value of HFE-7000 is about one third to that of HFC-134a. HFE-7000 has kinematic viscosity of 0.32 cSt at 20°C, 0.29 cSt at 30°C and 0.27 cSt at 40°C [17].

2

Table 1. Different properties of HFE-7000 and HFC-134a [17, 23, 24].

Refrigerant	HFE-7000	HFC-134a
Structure	$C_3F_7OCH_3$	Ch_2FCF_3
Molecular Weight (g/mol)	200	102
Freezing Point (°C)	-122.5	-103.3
Boiling Point @ 1 atmosphere (°C)	34	-26
Critical Temperature (°C)	165	101
Liquid Density (kg/m³)	1400	1206
Critical Pressure (MPa)	2.48	4.06
Flash Point (°C)	None	250
Appearance	Clear, colourless	Colourless gas
Flammability	Non-flammable	Non-flammable
Ozone Depletion Potential (ODP)	Zero	Zero
Global Warming Potential (GWP)	530*	1430*

*GWP 100-year integrated time horizon (ITH). IPCC 2013 [25].

This research has been conducted to assess the wear and friction behaviour of interacting parts at relatively low loads subject to nanocomposite coatings under HFE-7000 lubrication. This study is a continuation of our previous pilot study [24] which evaluated the possibility to enhance wear performance of rubbing parts by using Ni-Al$_2$O$_3$ nanocomposite coatings subject to HFE-7000 lubrication. The study showed a very significant enhancement in wear at low as well as high loads, but not at intermediate loads. In the current study five different types of coatings namely, Ni-ZrO$_2$, Ni-Al$_2$O$_3$, Ni-SiC, Ni-Graphene (Ni-GPL) and Nickel-only have been used with increased testing conditions. Nanostructured layout and design achieved through the electrodeposition of nano sized particles into the Nickel matrix has been proved to enhance friction, wear, corrosion and overall mechanical performance of interacting parts under a range of testing conditions [26-35].

A ball-on-flat disc contact geometry has been employed in this research by using a modified tribo-meter with HFE-7000 under saturated liquid state with fully lubricated conditions. All coatings were developed on a steel substrate through the pulse coating technique.

2. Materials and Methods

A modified Phoenix Tribology TE-57/77 reciprocating tribo-meter as described in [24, 36, 37] was used in this study. The equipment is fully capable of testing the future generation of environmentally friendly refrigerates [24, 36]. The apparatus provides the flexibility to vary the testing conditions by varying the operating temperature, by changing the applied normal load, by altering the reciprocating frequency and by controlling the chamber pressure. Details with description of the modified test rig are provided in [36].

AISI 52100 steel balls were used as the ball sample against normally loaded reciprocating nano coated flat samples. Each flat sample was coated on EN1A (230M07) steel. The flat sample is housed in the specimen cup which is then fastened on the reciprocating rod. The ball sample is fixed in the ball holder by grub screws which is then screwed to the horizontal shat. After the samples have been installed the test chamber is sealed after which it is vacuumed in order to reduce the effects of atmospheric air and ambient oxygen. Refrigerant is then introduced in to the vacuumed test chamber and fully lubricated conditions are established. The reciprocating frequency and refrigerant temperature are controlled through PID control. Chamber pressure is monitored and recorded through a pressure gauge and pressure transducer. The heater block is positioned at the very bottom of the chamber. A wire-type thermocouple is located directly inside the specimen and refrigerant cup which

is used to monitor the refrigerant temperature. Data from all the transducers is continuously recorded, monitored and controlled using a purpose built software COMPEND.

2.1. Sample preparation

Flat circular samples having a diameter of 30 mm were machined into 2.75 mm thickness. Each flat specimen was then mechanically grinded followed by surface polishing to obtain an average surface roughness (R_a) of 0.05 μm. After the grinding and polishing process an ultrasonic bath was used to ultrasonically condition each test sample for five minutes with acetone, after which a specimen drier was used to dry each sample with warm air. The mechanical grinding and polishing process followed by the ultrasonic surface conditioning of each flat sample with acetone ensured the removal of any oxides or undesired surface films that might be present.

Coatings of ~ 10 μm thickness were deposited on the flat circular steel specimens through pulse electrodeposition. Five different electrolytic base solutions were prepared by using H_3BO_3, $NiSO_4.6H_2O$ and $NiCl_2.6H_2O$. Each base solution contained 31 g/L of H_3BO_3, 265 g/L of $NiSO_4.6H_2O$ and 48 g/L of $NiCl_2.6H_2O$. To develop Ni-Al_2O_3 nanocomposite coatings the first base solution was added with 20 g/L Al_2O_3 nanoparticles with average particle size of less than 50 nm. The second base solution was added with 20 g/L ZrO_2 nanoparticles having particle size between 20-30 nm for the development of Ni-ZrO_2 nanocomposite coatings. To deposit Ni-SiC nano coatings the third base solution was added with 20 g/L SiC nanoparticles having particle size between 50-60 nm. For the deposition of Ni-Graphene (Ni-GPL) nanocomposite coatings the fourth base solution was added with 0.1 g/L Graphene nanoparticles having particle size of 6-8 nm. Nano particles were not added in the fifth base solution as this solution was used in the preparation of pure Nickel coatings. Each solution was stirred magnetically for 24 hours after which the nanoparticles containing solutions were ultrasonically agitated for 4 additional hours. This process confirmed proper dispersion and suspension of particles inside the solution. To start the coating process each solution was heated to 40°C after which a solution is ready for the deposition process. Grinded, polished and ultrasonically treated flat steel circular specimen was suspended in the prepared solution along with a pure nickel sheet. The steel sample acted as the cathode and Nickel sheet was used as anode. For the deposition of nanocomposite coatings the solutions were ultrasonically agitated, magnetically stirred constantly and maintained at 40°C during the entire deposition process. Pure nickel coatings were prepared through the same process expect that Nickel-only solutions were not ultrasonically agitated. The duty cycle for pulse coating was fixed at 20% with pulse OFF-ON time of (80 ms-20 ms) with the current density being maintained at (3 A/dm²). All the pulse parameters were maintained at a constant level throughout the coating process and deposition procedure was stopped after 1 hour.

Microstructures of the developed coatings were studied using a Scanning Electron Microscope (SEM). Energy Dispersive X-ray Spectroscopic (EDS) Analysis were performed on each coating at several different regions on the surface. High magnification images and EDS results of all the coatings are shown in figure 1. EDS results clearly show the presence of Nickel on the top surface of each of the prepared coatings along with the presence of respective Nano particles embedded in the Nickel matrix. The microstructure and EDS results of these coatings is in accordance with the results reported by various researchers [32-34, 38, 39]. These results show that coatings have been successfully prepared. The high magnification micrographs reveal pores on the top surface of all the coatings. These pores are randomly distributed on the surface of all the coatings and are better highlighted by applying false colour to the grayscale micrographs. These false coloured images of each coatings are also shown in figure 1. These pores are an inherent property of Nickel based nanocomposite coatings [24, 32-34].
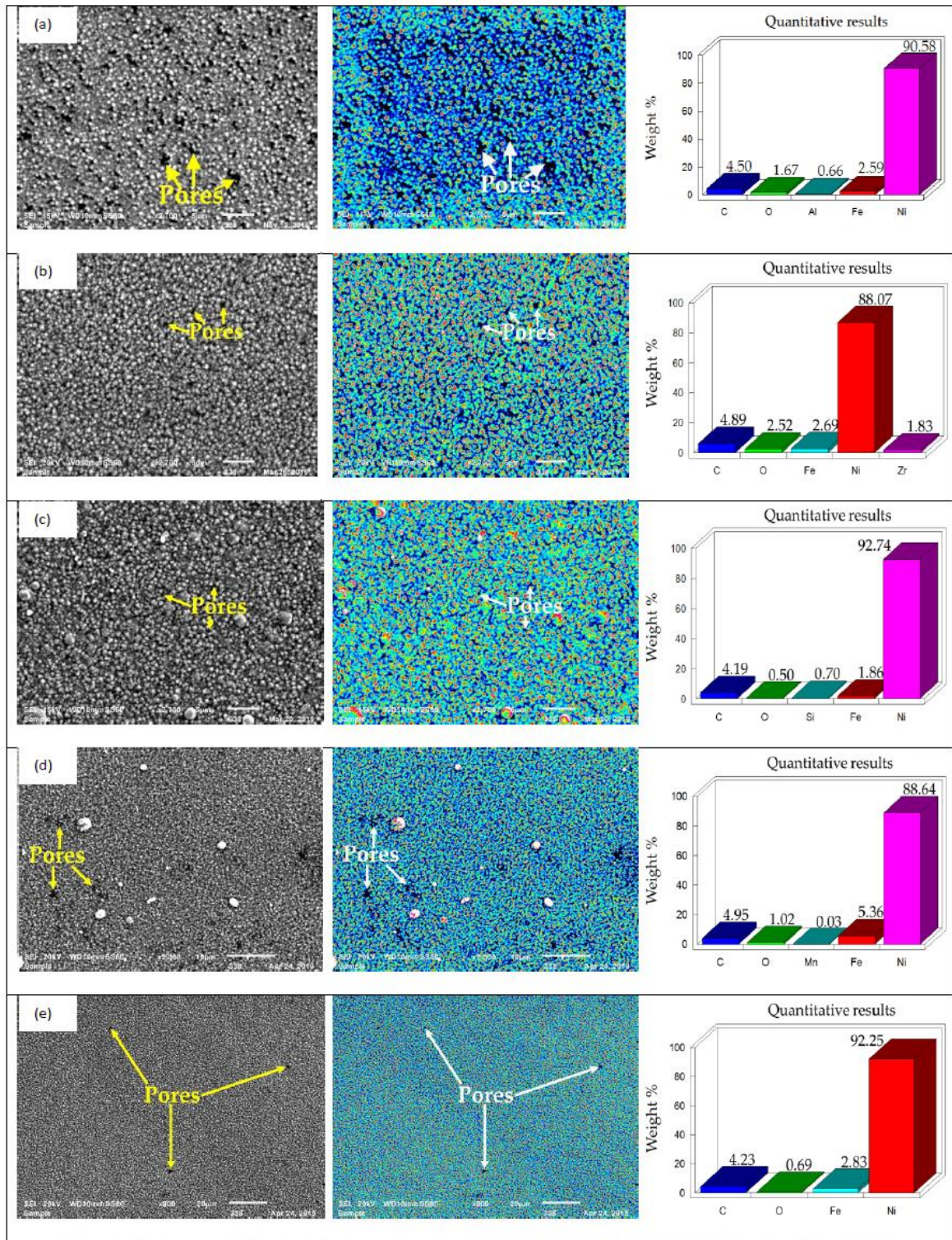
4

Figure 1: SEM images and EDS analysis of coated samples; (a) Ni-Al₂O₃ (b) Ni-ZrO₂ (c) Ni-SiC (d) Ni-GPL (e) Pure Nickel.

5

Grain size measurement was performed on all the prepared coatings pre-experiment using optical microscopy. The results of the grain size measurement have been presented in figure 2. The grain size measurement results show Ni-SiC and Ni-ZrO$_2$ to have the highest results of maximum average grain size values flowed by Ni-Al$_2$O$_3$ and Ni-Only coatings, Ni-Graphene displayed the lowest results of the maximum average grain size values.
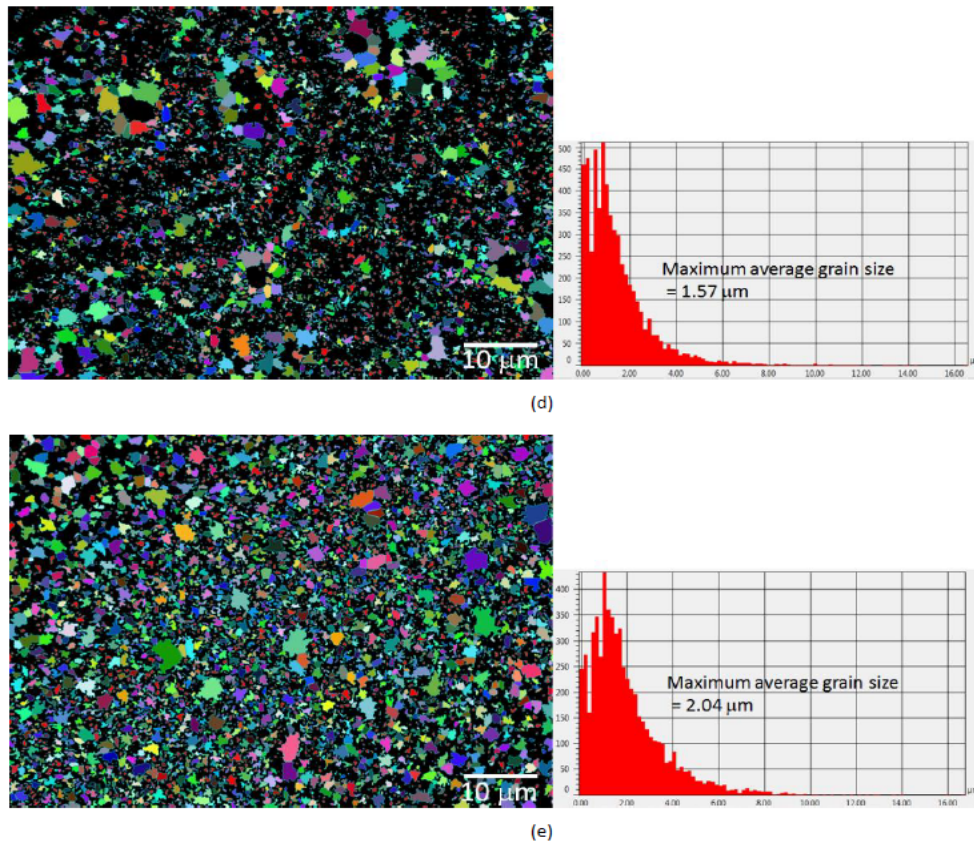

(a)

(b)

(c)

6
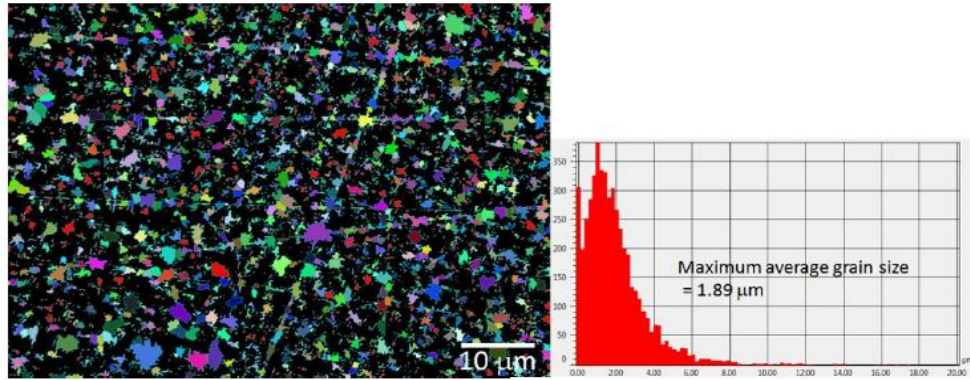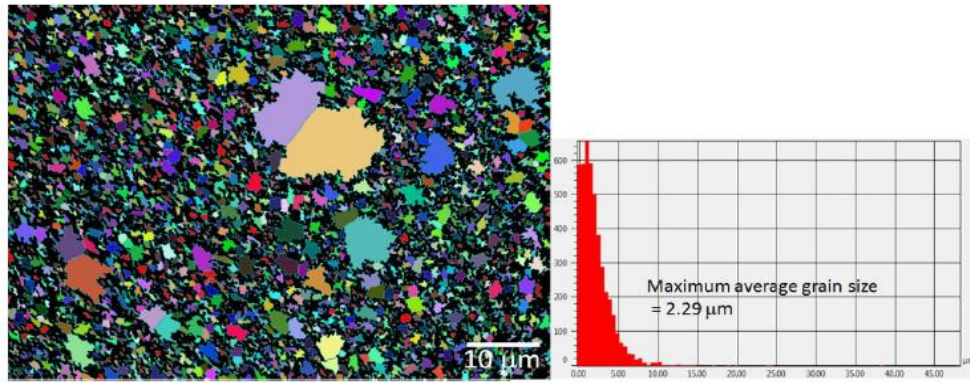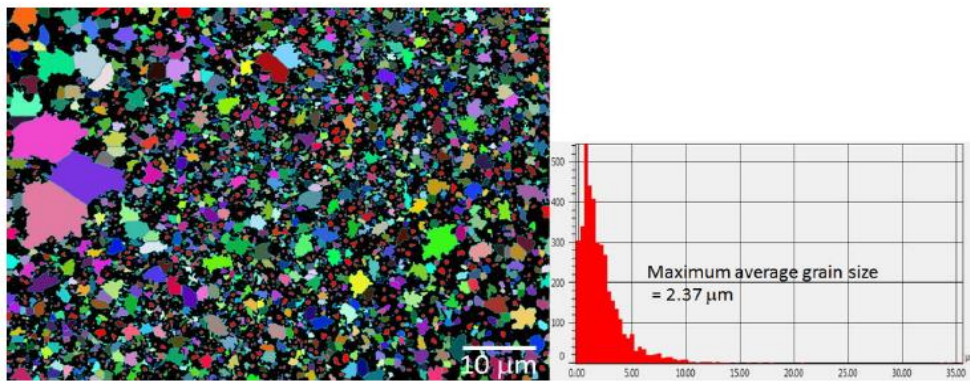
Figure. 2. Pre-test grain size maps: (a) Ni-Al₂O₃ (b) Ni-ZrO₂ (c) Ni-SiC (d) Ni-GPL (e) Nickel-only.

Ni-GPL coatings have been known to have refined grains, Ni-SiC and Ni-ZrO₂ have been reported to have large grains while Ni-Al₂O₃ have been observed to have larger grain size than Ni-GPL but smaller than Ni-SiC and Ni-ZrO₂ [34]. A cause of higher grain size of Ni-ZrO₂ and Ni-SiC is due to particle agglomeration [32], agglomerated particles are also present on Ni-GPL which gives rise to higher surface roughness values. Ni-GPL coatings deposited through electrodeposition on a steel substrate have been reported to develop bulges morphology and agglomeration effect which depends on the Watts bath temperature [40]. Increasing the temperature of the bath increases the surface roughness of the prepared coatings while a Watts bath temperature of 45°C has been reported to produce minimum grain size and best hardness results [40]. The pulse electrodeposition of Ni-GPL produced coatings having maximum surface roughness values compared to all the other coatings.
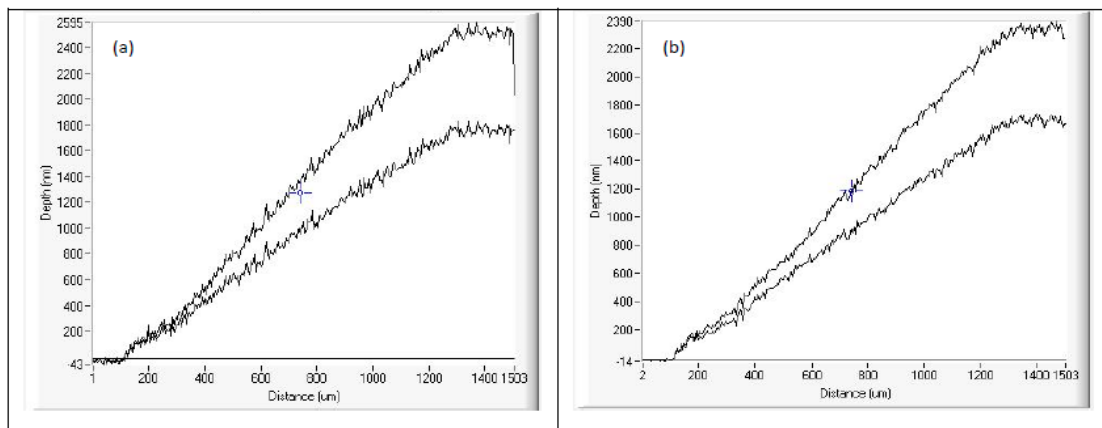
A Nano indentation setup was used to measure the micro-hardness, the elastic modulus and to perform scratch tests on each of the prepared coatings. Depth controlled indentations were performed by keeping the depth of penetration of the indenter to 1/10 of the thickness of the coatings to mitigate the effects on the substrate on the measured data. The average surface roughness of all the coatings was measured through ZYGO (a white light interferometer). The results of the measured micro hardness, elastic modulus and average surface roughness have been presented in table 2. Ni-GPL, Ni-Al₂O₃ and Ni-SiC nanocomposite coatings demonstrated the maximum nano-hardness values followed by Ni-ZO₂. Compared to the uncoated steel sample, an improvement in surface hardness was also shown by Nickel-only coatings. Micro-hardness improved for all the coated samples. Finer surface morphology of Ni-Al₂O₃ resulted in Ni-Al₂O₃ having the least values for average surface roughness followed by pure Nickel, higher grain size and particle agglomeration cause higher surface

7

roughness values for Ni-ZrO$_2$ and Ni-SiC [32, 34]. The Pulse deposited Ni-GPL showed the maximum surface roughness values in contrast to all the prepared samples. The high average surface values of Ni-GPL is because of the presence of embedded graphene nanoparticles on the very top of the coated surface which gives Ni-GPL a rough surface finish and a blackish grey appearance. Ni-GPL are known to have coarser surface and higher surface roughness values at higher deposition temperatures [40].

Table 2. Measured mechanical properties of the disc samples.

Specimen	Ni-Al$_2$O$_3$	Ni-ZrO$_2$	Ni-SiC	Ni-GPL	Nickel	Uncoated
Ra (μm)	0.045	0.20	0.18	1.17	0.12	0.10
Hardness (GPa)	3.85±0.28	3.54±0.36	3.84±0.24	3.87±0.38	3.22±0.22	3.00±0.09
Elastic Modulus (GPa)	203.48±11.67	207.17±12.88	247.76±27.24	212.86±15.73	215.94±14.87	212.28±9.32
Mean (H/E) Ratio	0.0189	0.0171	0.0154	0.0182	0.0149	0.0141

Scratch tests were performed on all the coatings. The results of the scratch test have been shown in figure 3. The loading conditions were kept constant for all the scratch tests. Multi-pass Wear Tests were conducted with a scanning velocity of 20 μm/s with 4 passes and 2 scratches per topography. Scratch load of 150 mN was applied as following the loading shown in figure 3 (f) using spherical indenter of 5 μm. The multi-pass wear test results of the scratch test indicate Ni-GPL to have very good wear resistance, the spikes in the data are due to the high surface roughness value of Ni-GPL coating and due to the removal of the loosely embedded graphene nano particles from the top surface of the coating by applying the load during scratch test. Nickel only, Ni-Al$_2$O$_3$ and Ni-ZO$_2$ exhibited an increase in wear scratch depth on the second pass; maximum wear depth was noted for Nickel-only coatings. Ni-SiC coatings also showed good resistance to wear. The thickness of all the coatings was in the range of 8-10 μm and none of the scratches was able to penetrate the entire depth of a coating. In fact the penetration depth was less the 50% of the thickness of any given coating.
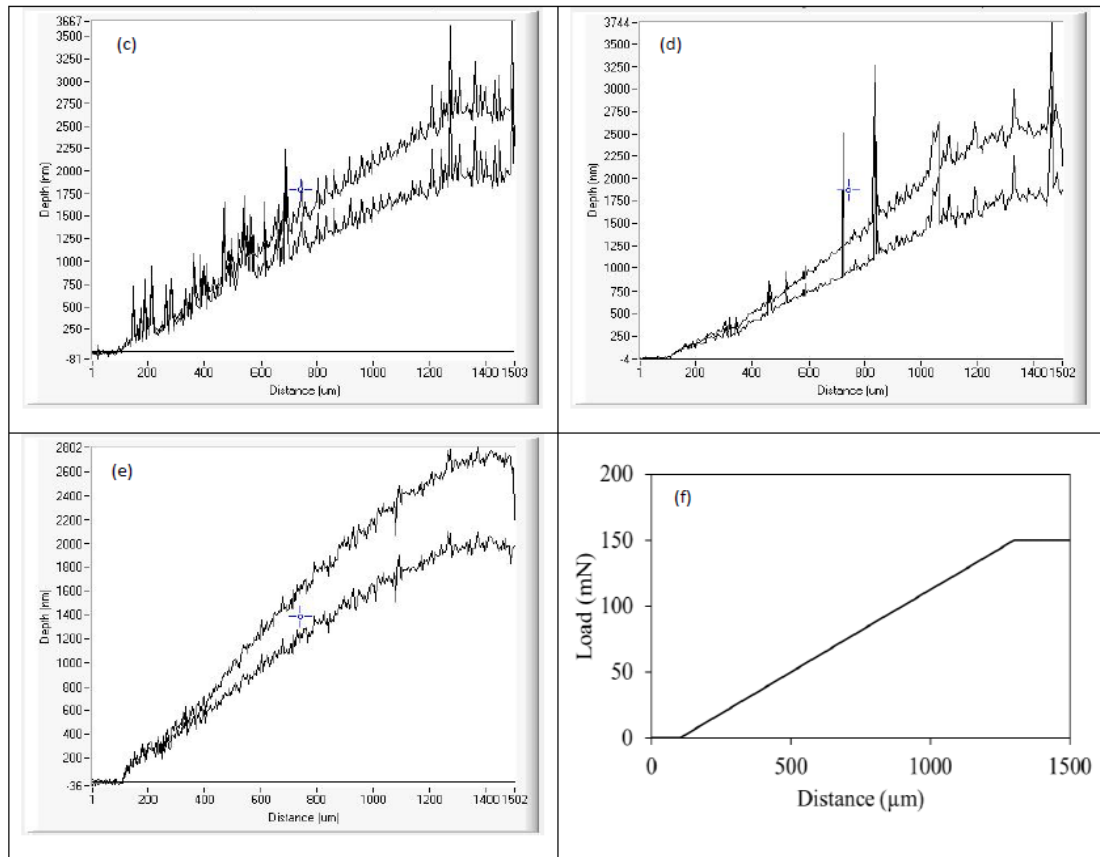

8

Figure. 3. Scratch Test Results: (a) Ni-Al$_2$O$_3$ (b) Ni-ZrO$_2$ (c) Ni-SiC (d) Ni-GPL (e) Nickel-only (f) Loading profile.

3. Testing Procedure

The same testing procedure as described in [24, 36] was followed to conduct all the experiments to ensure identical operating conditions. Once the samples are in position the chamber is sealed and then vacuumed. HFE-7000 is then introduced into the vacuumed chamber. Abundant amount of refrigerant is introduced in the system so that the sample and refrigerant holding cup overflows, this ensures fully lubricated conditions throughout a test. After this the normal load is applied and the experimental control algorithm is initiated. The initial step of the algorithm is the heating of the refrigerant inside the specimen cup. Once the desired refrigerant temperature has been reached, the temperature is maintained and stabilised for 1 hour before starting an experiment. After stabilising and maintaining the refrigerant temperature for 1 hour a test is run for the duration of 2 hours.

The reciprocating frequency is continuously controlled through a driver motor with feedback control. All the transducers, the electric heating elements and the motor are all connected and controlled through a microprocessor based DAQ (data acquisition) and control system. Values obtained by the pressure transducer of the chamber pressure, readings from the two thermocouples, frictional force values from the friction force transducer and the motor speed are constantly logged by using a specialized software COMPEND.

9

There are in total five different coating that were investigated under identical testing conditions. Three different loads i.e. 10 N, 20 N and 30 N were applied in conjunction with three different refrigerant temperatures of 20°C, 30°C and 40°C. All tests were carried out with a stroke length of 5 mm and a reciprocating frequency of 5 Hz. Repeatability of the results was ensured by performing each test at least two times.

4. Results and discussion

Results of wear and friction have been presented in this study. Each sample pair was studied using SEM to observe the extent and type of wear. EDS analysis was also performed within the contact regions of each flat and ball specimen to investigate the development of tribological films on the top mating surfaces and to gauge the extent of wear on the flat disc samples. After this ZYGO was used to measure the wear volume of the wear scars on the disc samples. The results of wear volume of all the coatings were compared to one another and also to an uncoated flat disc sample which was tested under identical operating conditions in our previous study [36]. After this the results of friction are presented as real-time coefficient of friction and average coefficient of friction plots. The coefficient of friction results of each coating were also compared with one another and also to the uncoated steel. This uncoated steel is the steel substrate that was used to apply these coatings. The results highlight and indicate whether or not these coatings are useful for improving the tribological properties of rubbing parts using HFE-7000 refrigerant.

5. Wear

EDS elemental analysis results and SEM micrographs of $Ni-ZrO_2$ are presented in figure 4, figure 5 and figure 6.

(a)
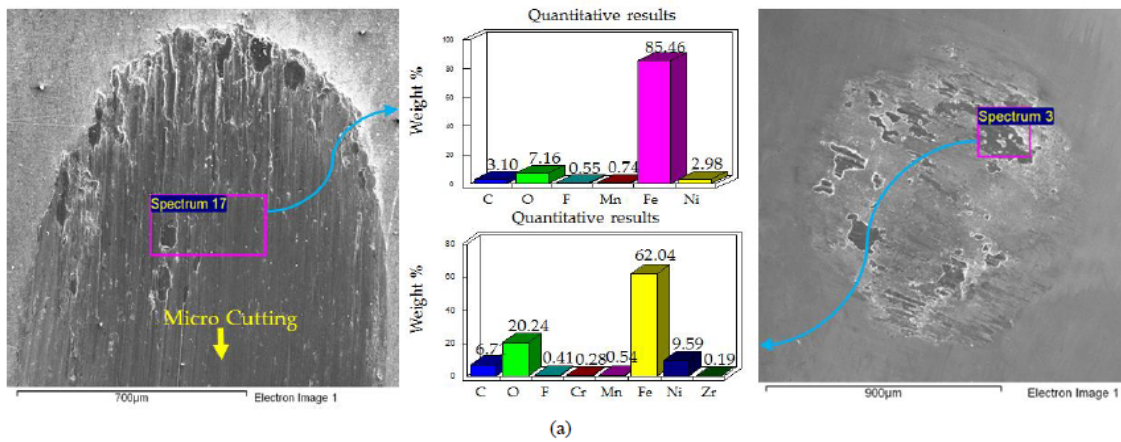
Figure 4: EDS elemental results and SEM Micrographs of Ni-ZrO₂ coated flat samples and counter steel ball: (a) 20°C, 10 N (b) 20°C, 20 N (c) 20°C, 30 N.

Adhesive and abrasive wear mechanism was noted by studying the ball and disc samples under high magnification. A combination of micro-cutting, micro-ploughing and micro-delamination was observed on the worn tracks. For all coatings plastic deformation was apparent due to the higher hardness value of the counter steel ball in comparison to the coatings.
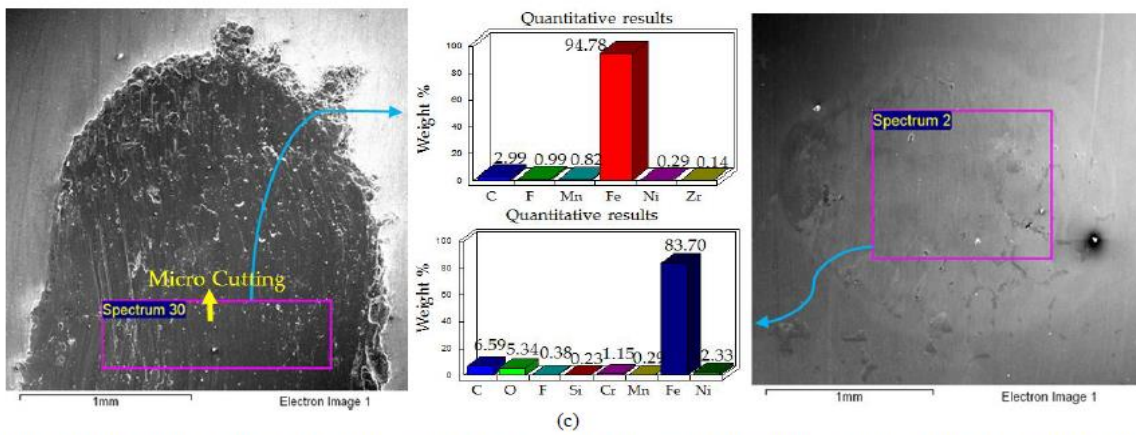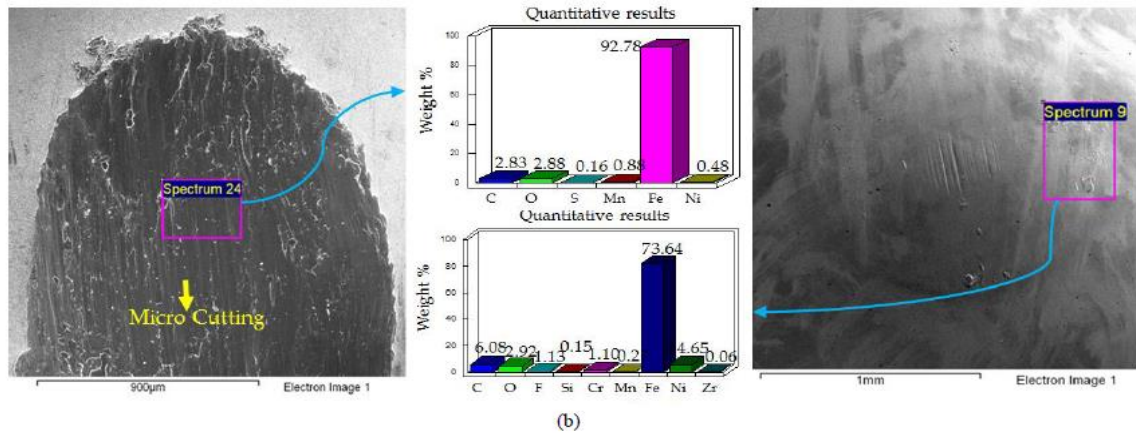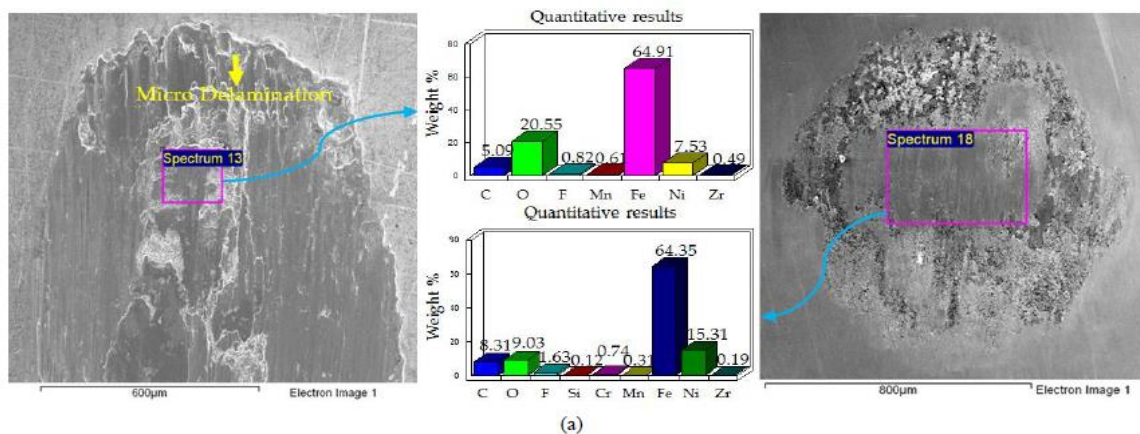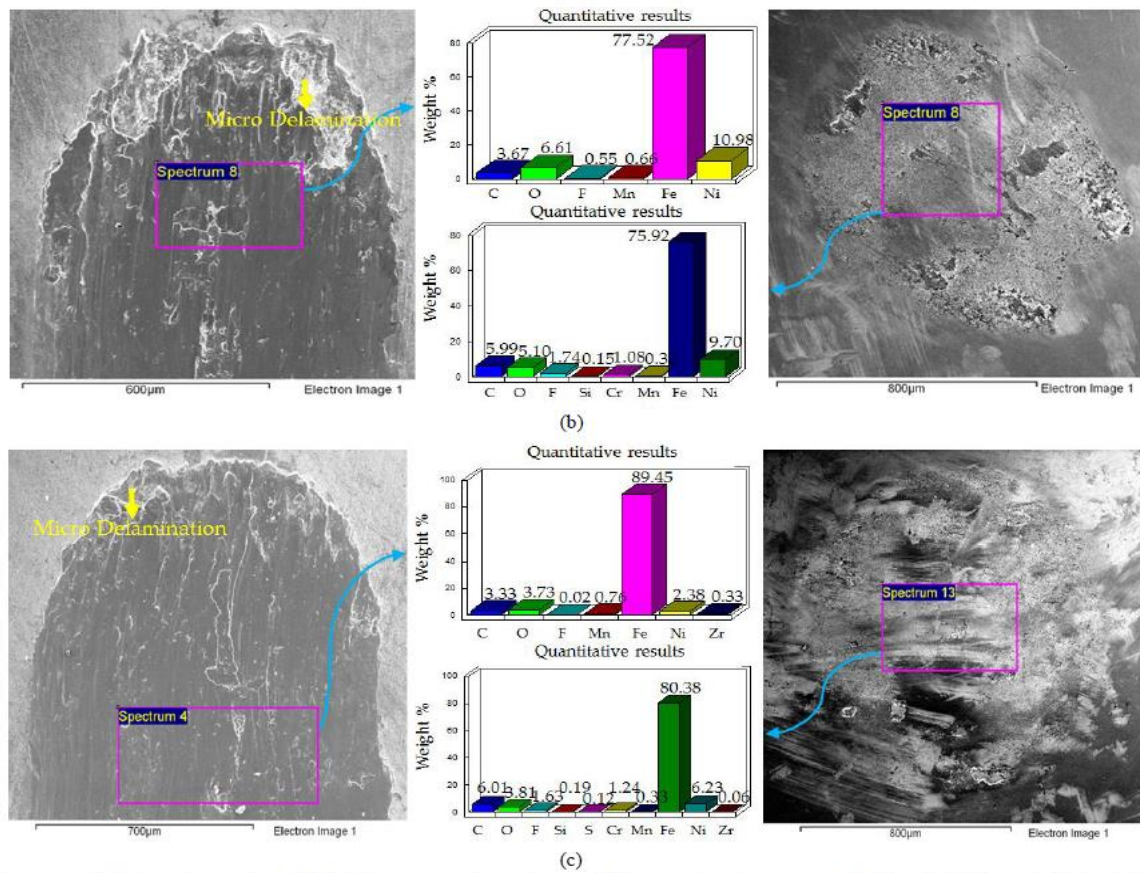
Figure 5: EDS elemental results and SEM Micrographs of Ni-ZrO$_2$ coated flat samples and counter steel ball: (a) 30°C, 10 N (b) 30°C, 20 N (c) 30°C, 30 N.

Maximum wear is apparent at lower refrigerant temperature as shown in figure 4. With a rise in temperature of the refrigerant to 40°C from 20°C the wear scar becomes narrower. EDS elemental analysis of the wear scar at 20°C reveal only a slight presence of nickel and a high presence of iron indicating that the coatings have completely worn out. EDS analysis performed on the wear scar also reveal a presence of oxygen and/or fluorine. SEM images of the 52100 steel ball display adhesion of the counter surface on the surface of the steel ball. EDS elemental results of the steel ball in the contact region also confirm adhesion of the delaminated coatings on the hard 52100 steel surface with more adhesion present at 10 N in comparison to higher loads. EDS of the ball samples also demonstrates the presence of oxygen (O) and fluorine (F). Detection of O and F on the steel surfaces indicates formation of surface tribo-films on the mating surfaces. An increase in load at 20°C refrigerant temperature increases wear; the EDS results of the wear track also reveal a reduced percentage of oxygen and fluorine with increase in load as shown in figure 4.

Figure 6: EDS elemental results and SEM Micrographs of Ni-ZrO$_2$ coated flat samples and counter steel ball: (a) 40°C, 10 N (b) 40°C, 20 N (c) 40°C, 30 N.

Increasing the refrigerant temperature to 30°C from 20°C results in a higher percentage of O and F on the wear scar as shown in figure 5. EDS results of the disc samples also show a higher percentage of nickel and zirconium presence on the wear scar indicating a decrease in wear. Micrographs of the wear track reveal micro-cutting and micro-delamination of the coated surfaces. SEM images and EDS analysis of the counter steel ball show more adhesion of the coatings on the ball surface in contrast to tests conducted at 20°C.
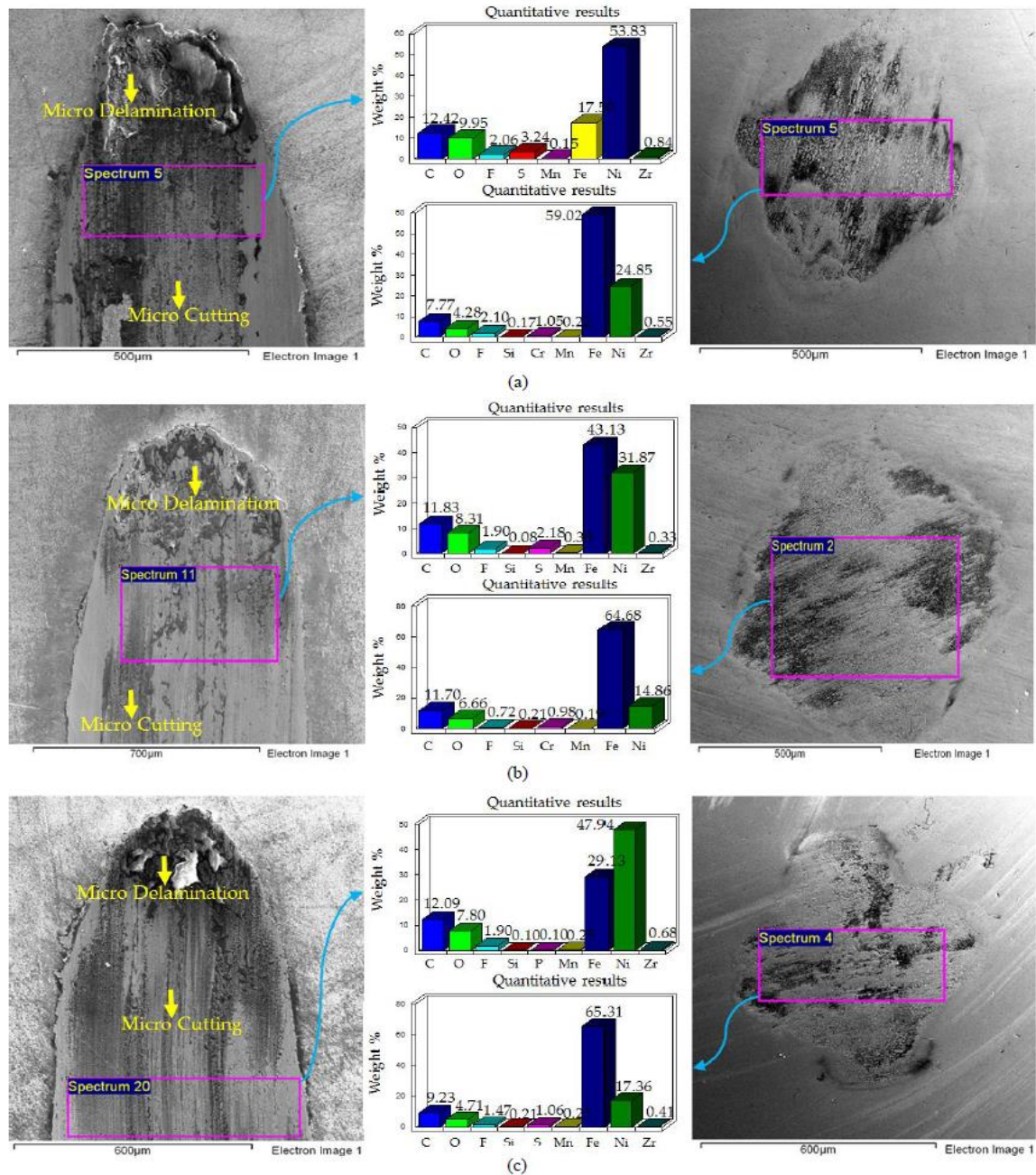
Figure 7: EDS elemental results and SEM Micrographs of Ni-SiC coated flat samples and counter steel ball: (a) 20°C, 10 N (b) 20°C, 20 N (c) 20°C, 30 N.

Micrographs of the wear track generated by a further rise in the refrigerant temperature to 40°C from 30°C show a decrease in wear track width and overall wear as shown in figure 6. This is also visible from the EDS results; which reveal a significant presence of nickel and zirconium in comparison to the tests conducted at 20°C and 30°C. EDS analysis also reveal a higher percentage of F and O on the disc as well as the ball surfaces in comparison to the tests conducted at a lower temperatures.

14

The micrographs of the ball and flat specimens indicate that wear occurred primarily due to micro cutting at 20°C refrigerant temperature, micro-delamination was the dominant wear phenomenon at 30°C and a mix of micro-cutting and micro-delamination occurred at 40°C.

The SEM images and the EDS results of the tests conducted on Ni-SiC nanocomposite coatings are presented in figures 7, 8 and 9. Figure 7 shows the results of all the tests conducted at 20°C refrigerant temperature. The micrographs show micro-cutting and micro-delamination of Ni-SiC coatings. At refrigerant temperature 20°C, wear has occurred due to micro-cutting and micro-delamination at 10 N and 20 N, increase in load to 30 N at 20°C shifts the mechanism more towards micro-cutting as shown in figure 7. An increase in the temperature of the refrigerant from 20°C to 30°C shows a decrease in wear and a shift in wear mechanism towards micro-cutting as shown in figure 8. An increase in refrigerant temperature also results in more adhesion of the worn coatings onto the steel ball. EDS results also show a higher presence of nickel on the top surfaces at 30°C refrigerant temperature in comparison to tests conducted at 20°C.
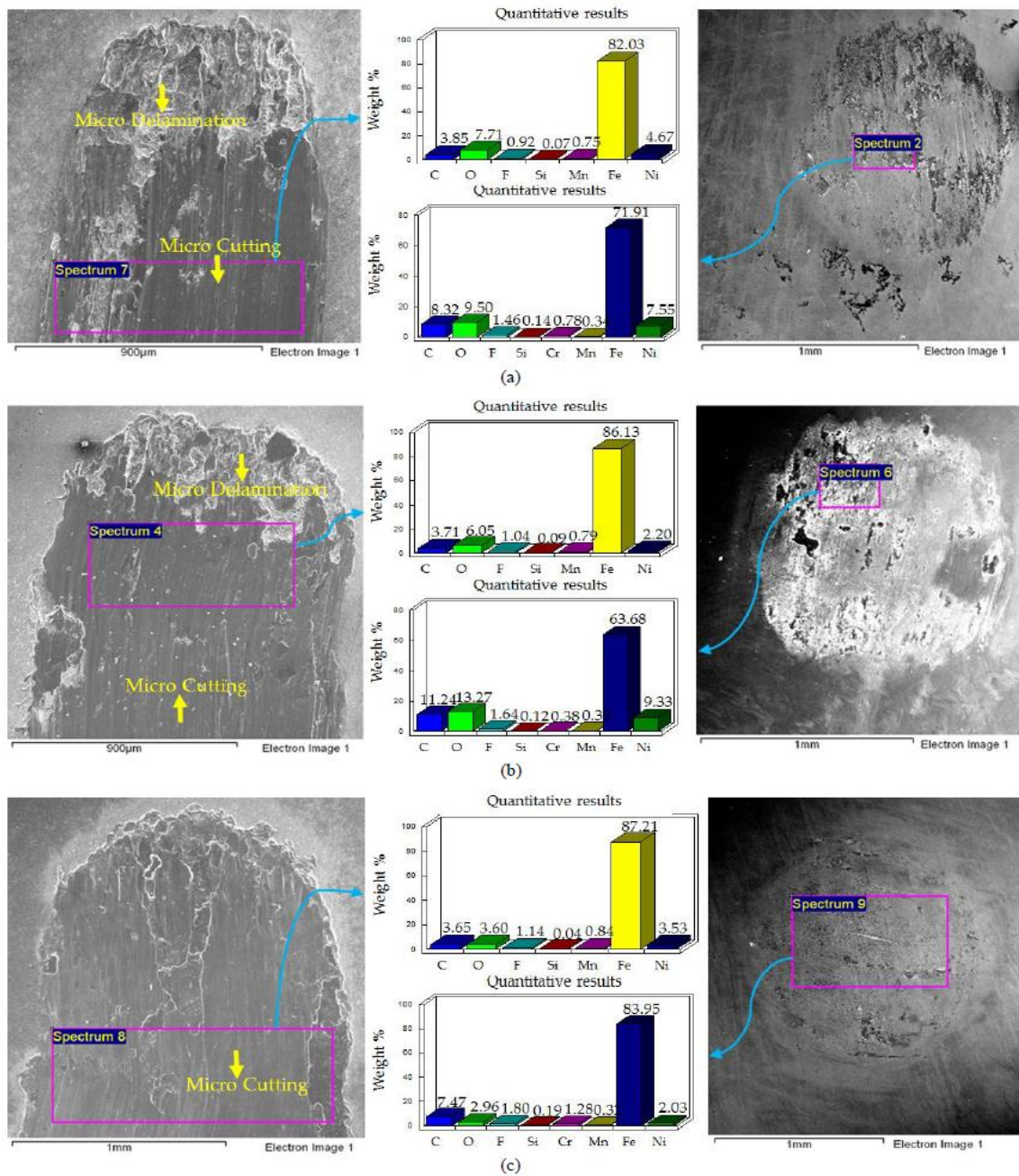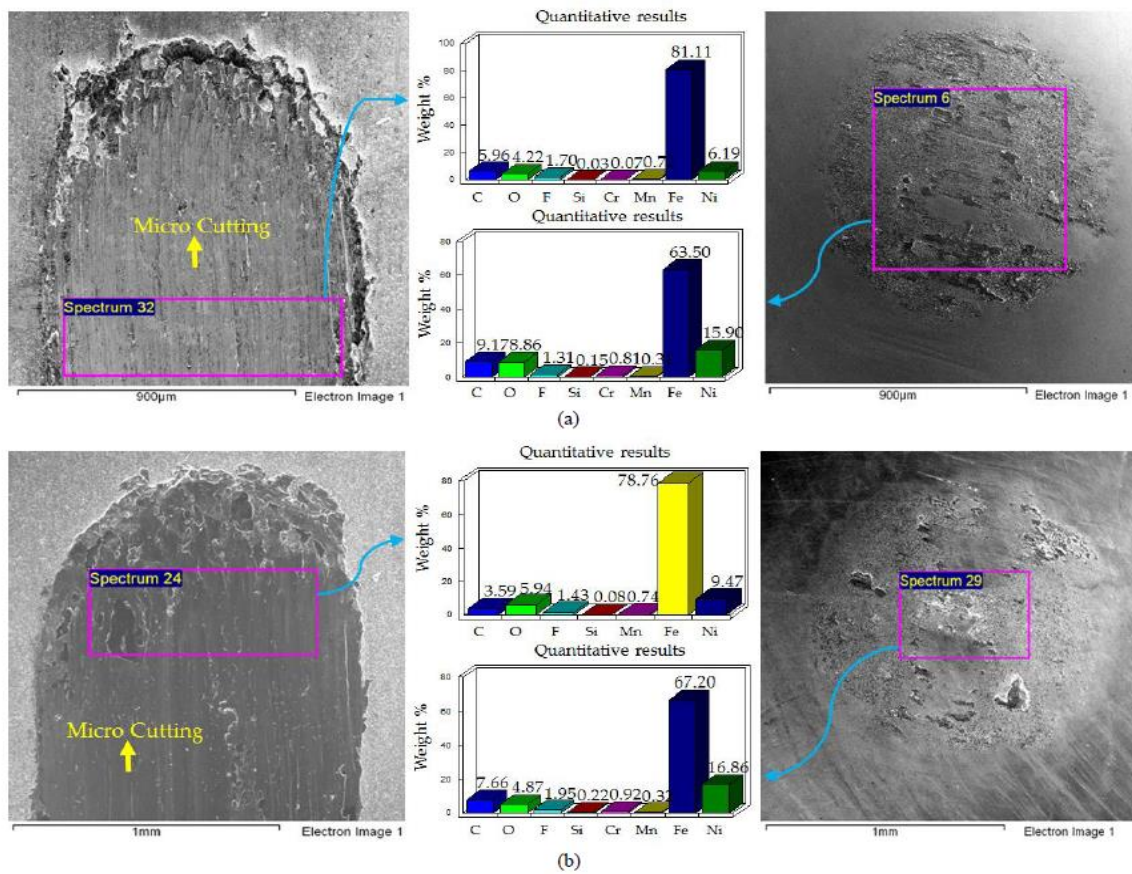
Figure 8: EDS elemental results and SEM Micrographs of Ni-SiC coated flat samples and counter steel ball: (a) 30°C, 10 N (b) 30°C, 20 N (c) 30°C, 30 N.

An additional increase in the temperature of the refrigerant from 30°C to 40°C reduces the severity of wear. As shown in figure 9 micro-delamination and micro-cutting is observed on the wear track at 40°C/10 N; while micro-ploughing and micro-delamination is apparent at 40°C/20 N and 40°C/30 N. Adhesion of the coatings is also visible on the counter steel ball at the tests conducted at 40°C.
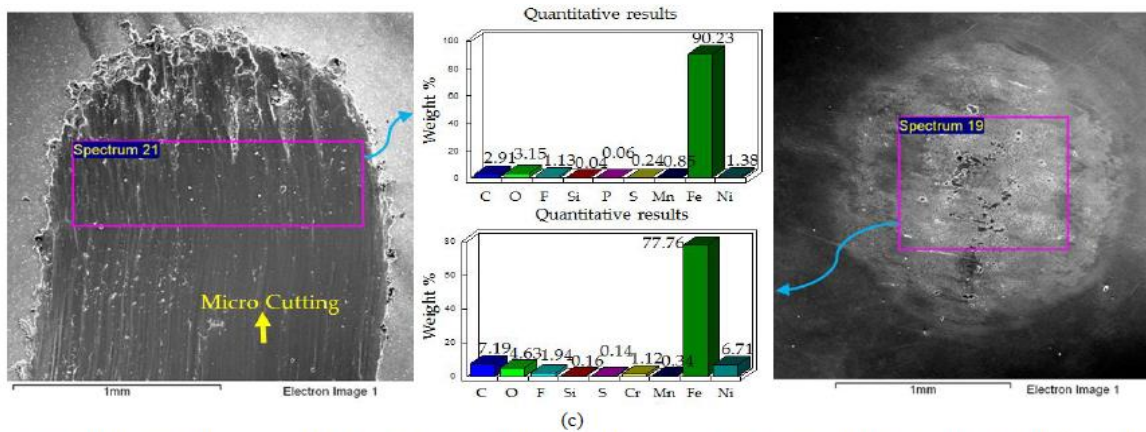

16

Figure 9: EDS elemental results and SEM Micrographs of Ni-SiC coated flat samples and counter steel ball: (a) 40°C, 10 N (b) 40°C, 20 N (c) 40°C, 30 N.

EDS analysis on the wear scar show a higher percentage of nickel and silicon on the flat disc implying the presence of the nanocomposite coatings and a reduction in wear.

High magnification images and EDS results of Ni-Al$_2$O$_3$ are presented in figures 10, 11 and 12. At 20°C, increase in load increased wear. Delamination of the coatings occurred at 20°C/20 N and 20°C/30 N which is evident from the micrographs and EDS results shown in figure 10. At 20°C/10 N and 20°C/30 N testing conditions micro-delamination and micro cutting resulted in the wear of the disc sample. SEM images at 20°C/20 N testing conditions present micro-cutting to be the main cause of wear.

Figure 10: EDS elemental results and SEM Micrographs of Ni-Al$_2$O$_3$ coated flat samples and counter steel ball: (a) 20°C, 10 N (b) 20°C, 20 N (c) 20°C, 30 N [24].

Increasing the temperature of the refrigerant to 30°C had a significant positive impact on reducing wear at 20 N as shown in figure 11. Complete coating delamination was not observed at 30°C/20 N. Results at 30°C/30 N were analogous to the results obtained at 20°C/30 N. The coating delaminated completely at 30°C/30 N as well. Results at 30°C/10 N were different in terms of wear phenomenon; micro-delamination is the more governing wear mechanism at 20°C/10 N whereas wear primarily due to micro-cutting can be observed at 30°C/10 N.

Results of increasing the refrigerant temperature to 40°C from 30°C have been displayed in figure 12. At 40°C/10 N a combination of micro-delamination and micro-cutting can be observed. EDS analysis of all the tests carried out at normal load of 10 N show a significance presence of nickel along with aluminium indicating that Ni-Al$_2$O$_3$ coatings did not totally wear out at low loads. Micro-cutting can be observed on the wear scar with an increase in load at 40°C to 20 N. An additional increase load to 30 N at 40°C resulted in micro-cutting and micro-delamination. EDS examination of the wear scars at 40°C on all the disc samples showed a significance presence of nickel which shows that at higher refrigerant temperatures wear has been reduced.
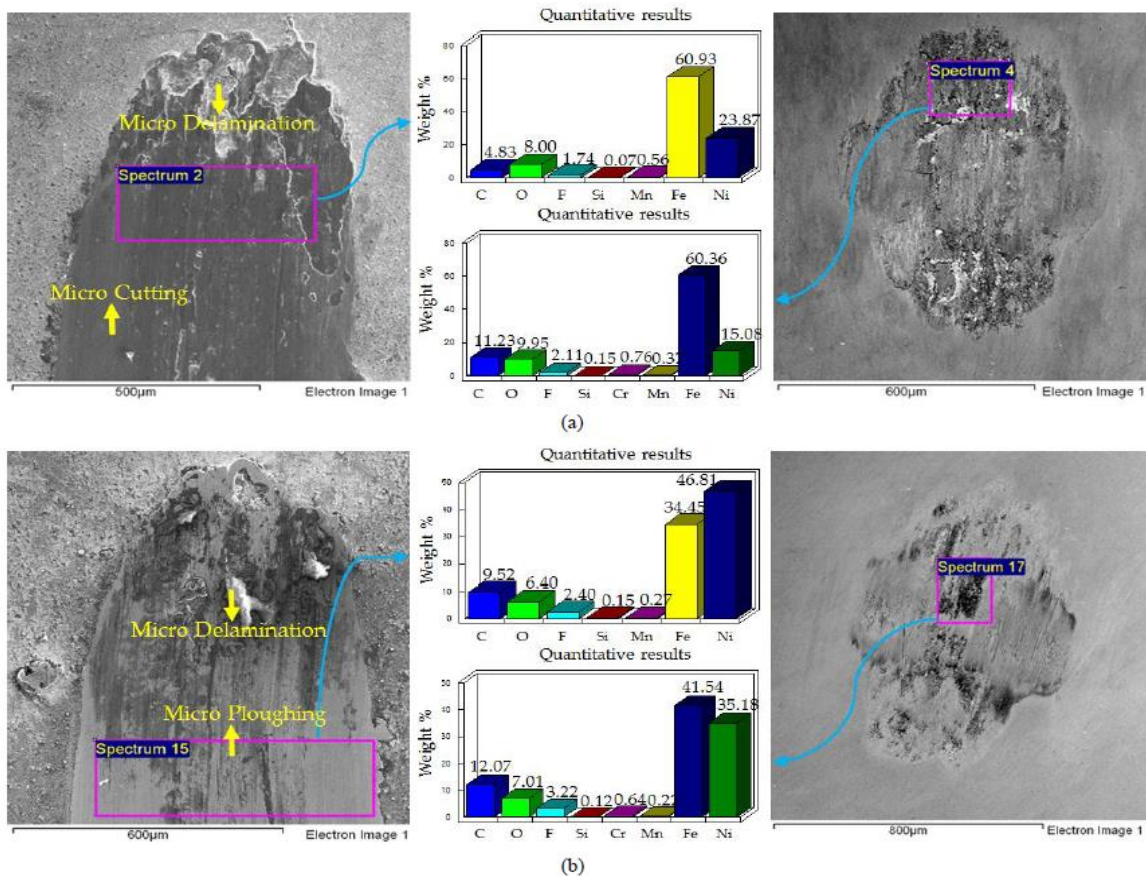
18

Figure 11: EDS elemental results and SEM Micrographs of Ni-Al₂O₃ coated flat samples and counter steel ball: (a) 30°C, 10 N (b) 30°C, 20 N (c) 30°C, 30 N.
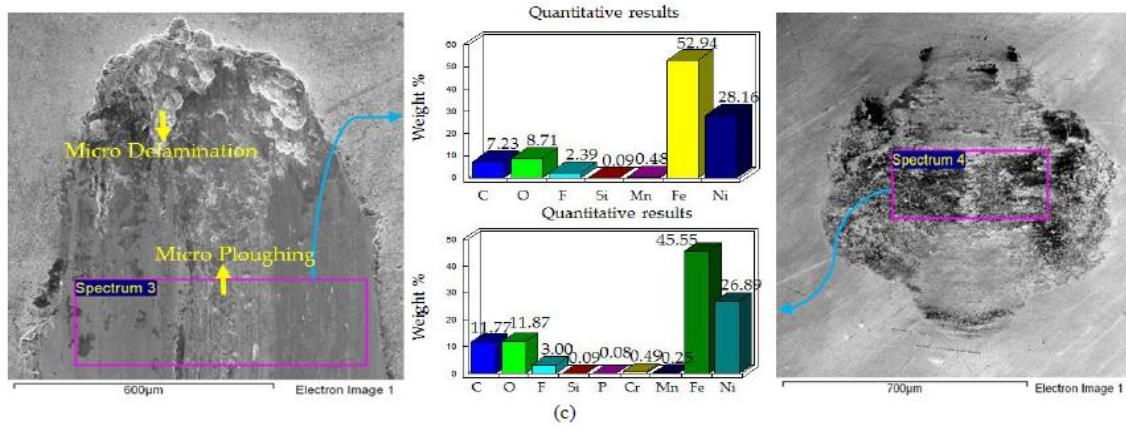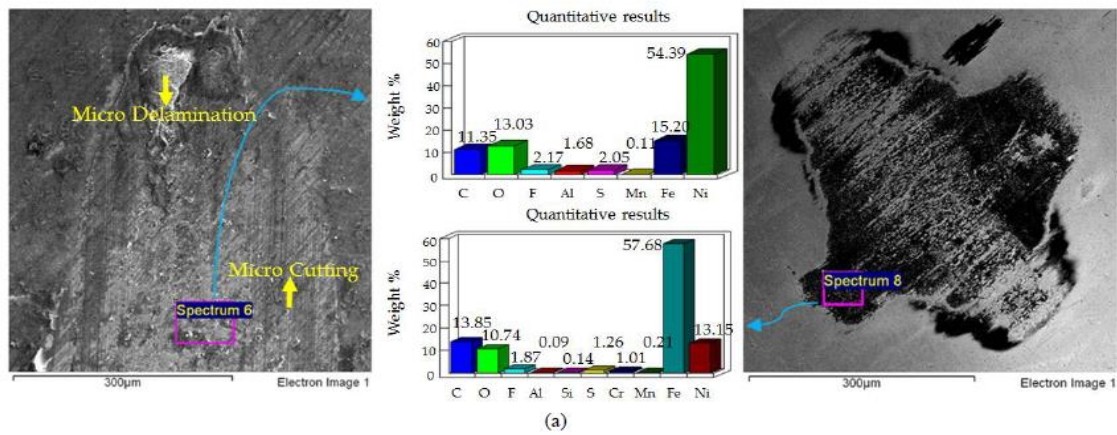
Figure 12: EDS elemental results and SEM Micrographs of Ni-Al₂O₃ coated flat samples and counter steel ball: (a) 40°C, 10 N (b) 40°C, 20 N (c) 40°C, 30 N [24].

EDS elemental analysis results and SEM Micrographs of the tests conducted on Nickel-Graphene (Ni-GPL) coatings have been presented in figures 13, 14 and 15. SEM images at refrigerant temperature 20°C at any given applied load show high wear and the results reveal Ni-GPL coatings to be completely worn out mainly due to micro-cutting as presented in figure 13.
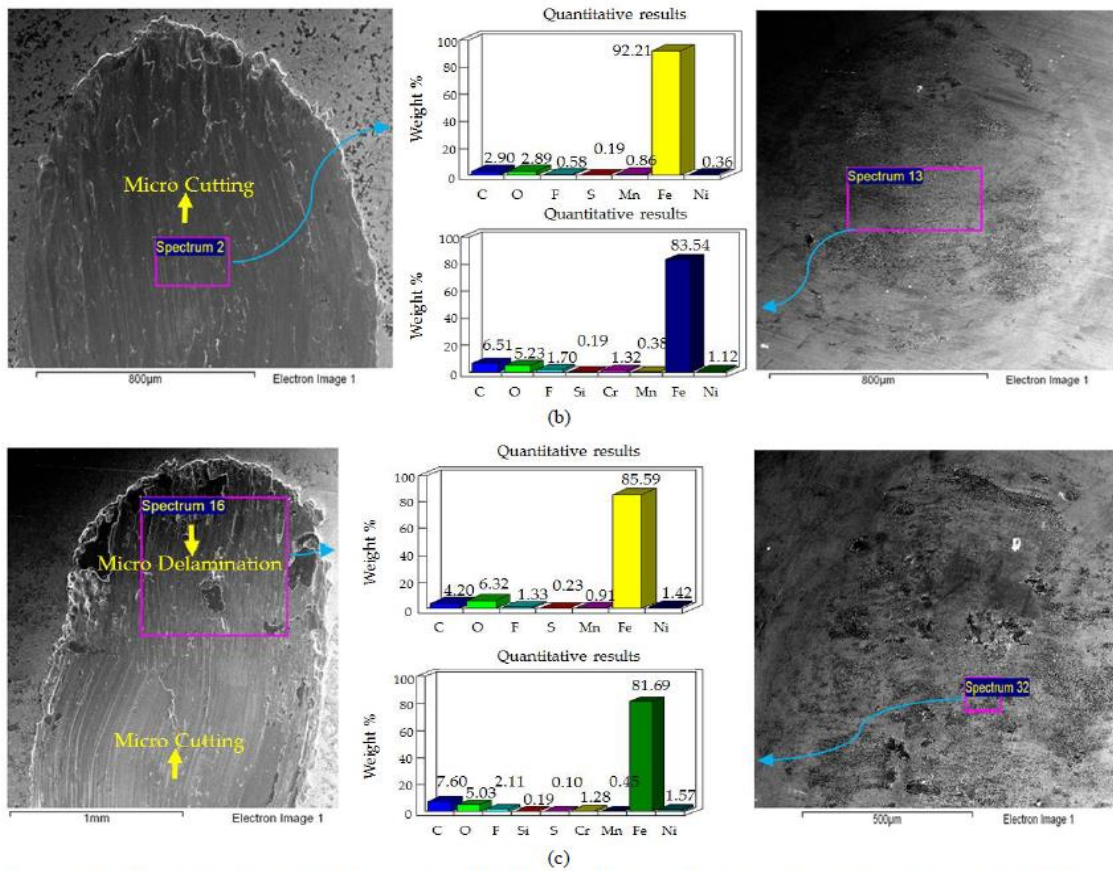
Figure 13: EDS elemental results and SEM Micrographs of Ni-GPL coated flat samples and counter steel ball: (a) 20°C, 10 N (b) 20°C, 20 N (c) 20°C, 30 N.

Increasing the refrigerant temperature to 30°C from 20°C at 10 N load results in lesser damage and micro-ploughing can be observed on the wear track at 30°C/10 N as shown in figure 14. At 30°/20 N and 30°/30 N a mix of micro-ploughing and micro-delamination can be observed. EDS results at 30° for all the loads show a higher presence of nickel in comparison to the tests conducted at 20°C, this indicates a reduction in wear by an increase in refrigerant temperature.

21

Figure 14: EDS elemental results and SEM Micrographs of Ni-GPL coated flat samples and counter steel ball: (a) 30°C, 10 N (b) 30°C, 20 N (c) 30°C, 30 N.

Micro-cutting and micro-delamination can be observed at 40°C/10 N and 40°C/30 N while wear primarily due to micro-ploughing and micro-delamination took place at 40°C/20 N as shown in figure 15. EDS results at 40°C/10 N present the highest percentage of nickel amongst all the tests that were conducted on Ni-GPL. EDS on the wear track of all the disc samples at 40°C show a higher percentage of nickel at any given load in contrast to tests conducted at lower refrigerant temperatures. This shows a decrease in wear when using Ni-GPL coatings by increasing the temperature to 40°C

22

from 20°C. Increase in the temperature of the refrigerant to 40°C from 20°C also results in an increase in adhesion of the coatings on the steel ball.
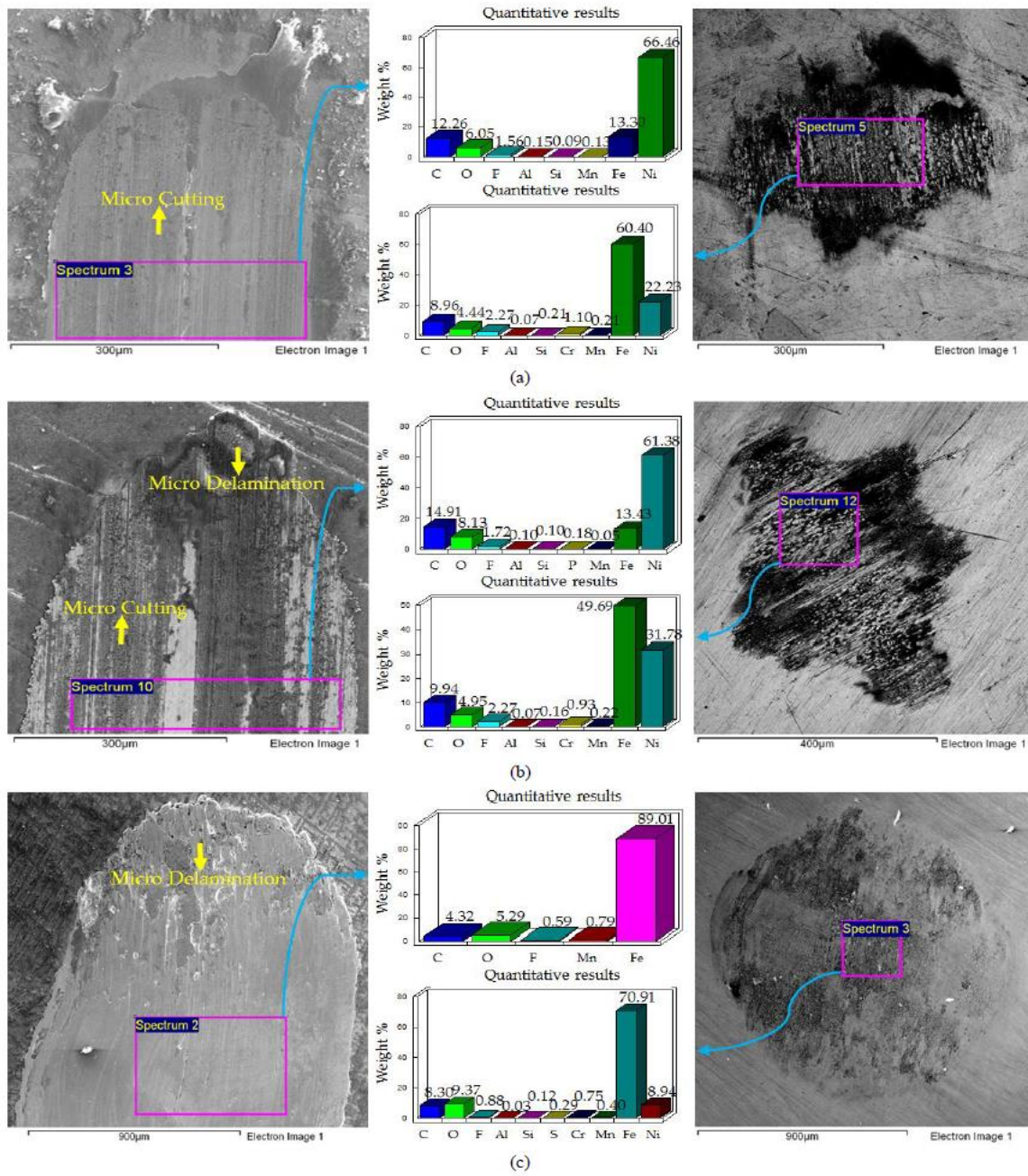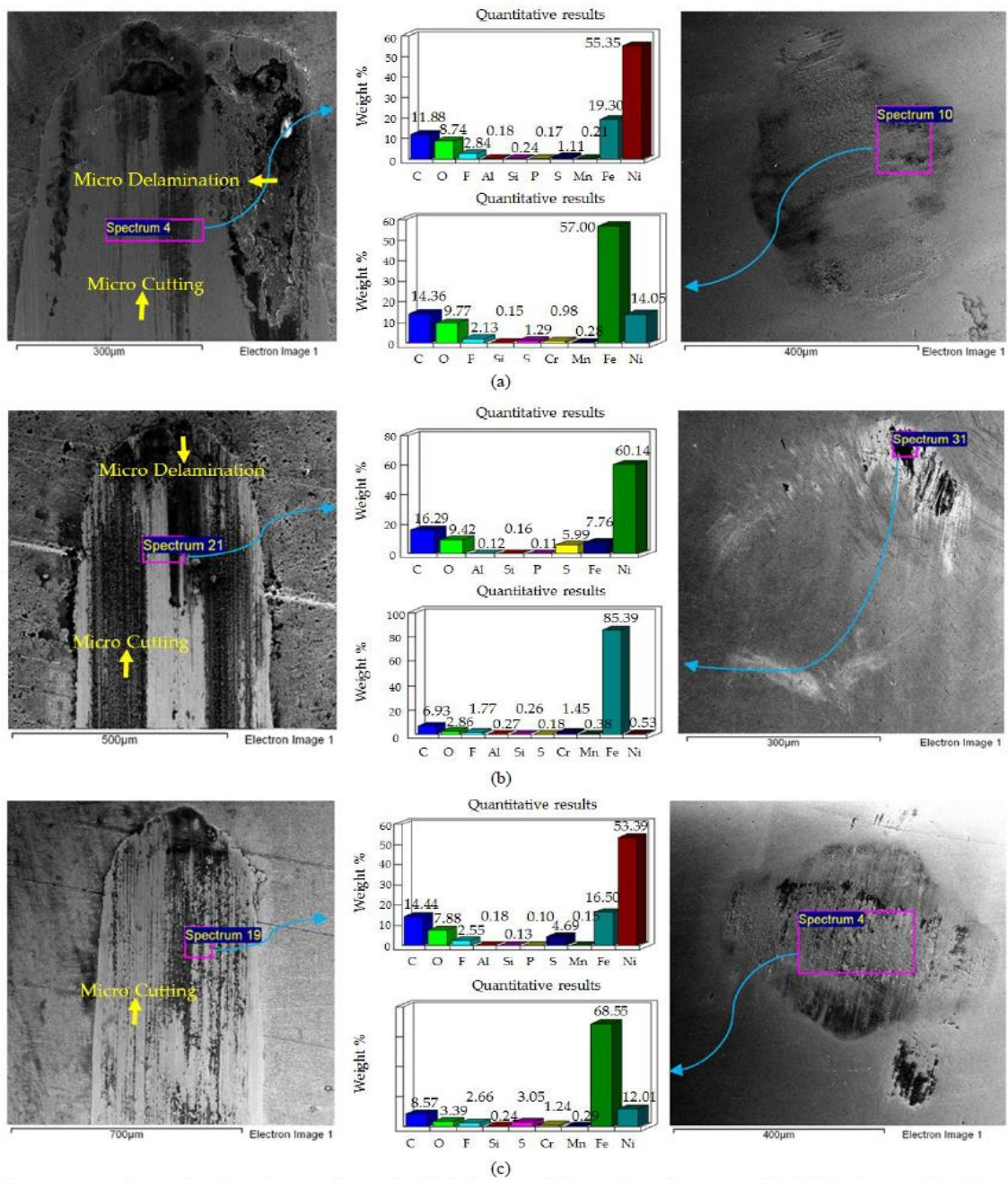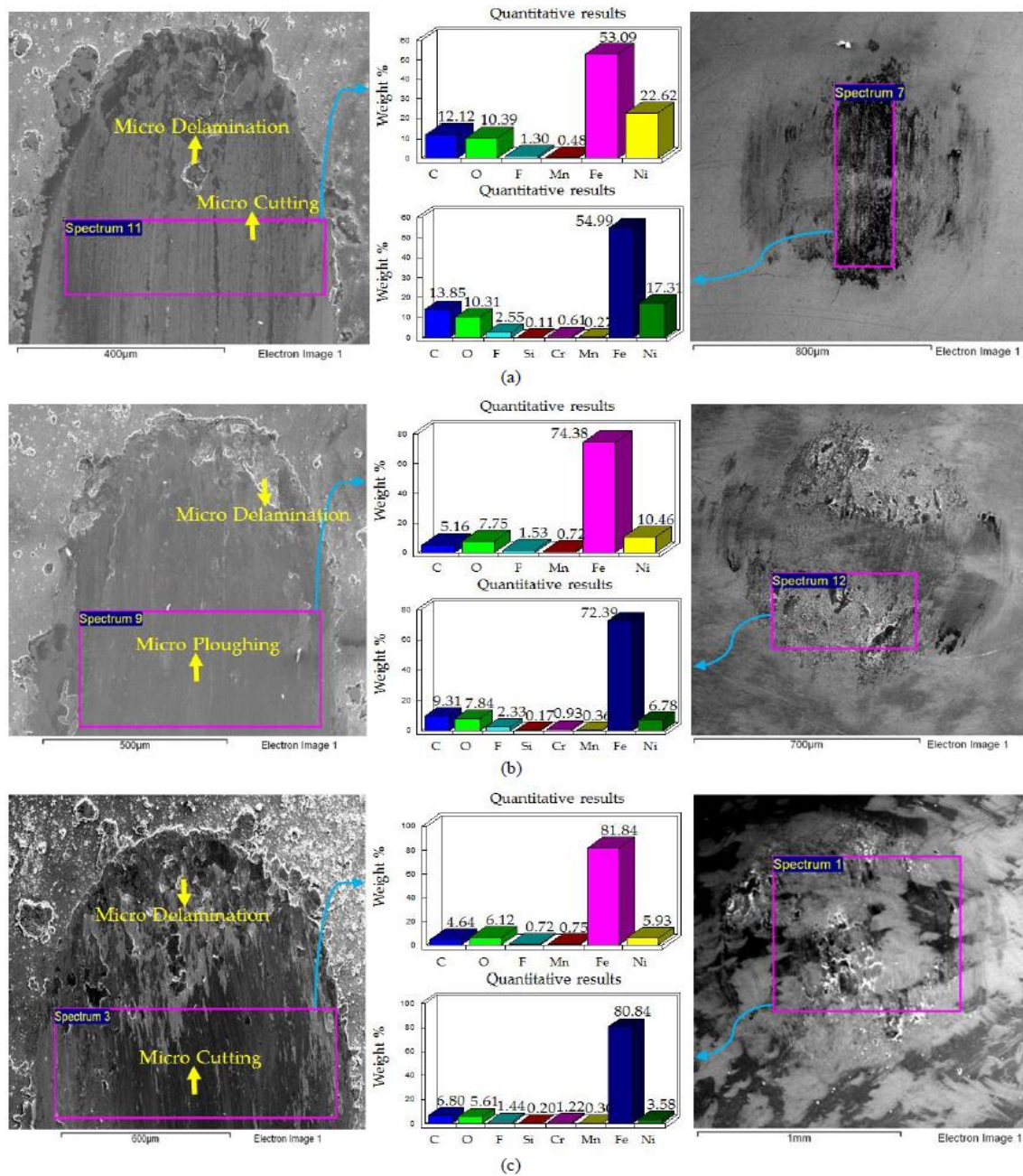

Figure 15: EDS elemental results and SEM Micrographs of Ni-GPL coated flat samples and counter steel ball: (a) 40°C, 10 N (b) 40°C, 20 N (c) 40°C, 30 N.

High magnification images and EDS examination of Nickel-only coated samples are displayed in figure 16, 17 and 18. Tests conducted at 20°C refrigerant temperature show wear primarily due to micro-cutting and micro-delamination as shown in figure 16. EDS analysis show only a small percentage of nickel on the wear track indicating high wear at low refrigerant temperature. Micro-

delamination is more prominent at 20°C/10 N and micro-cutting is more dominating wear mechanism at 20°C/30 N.
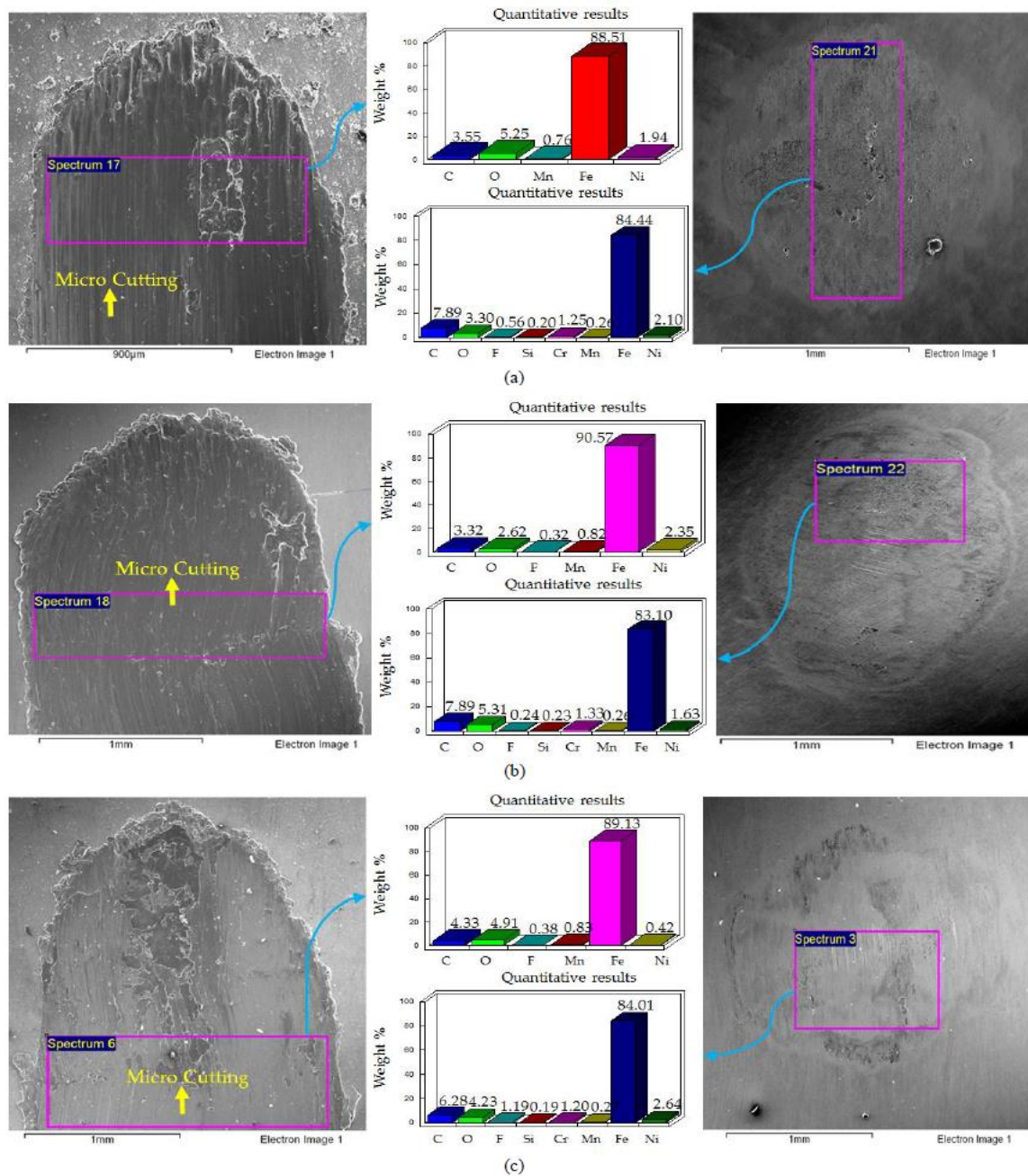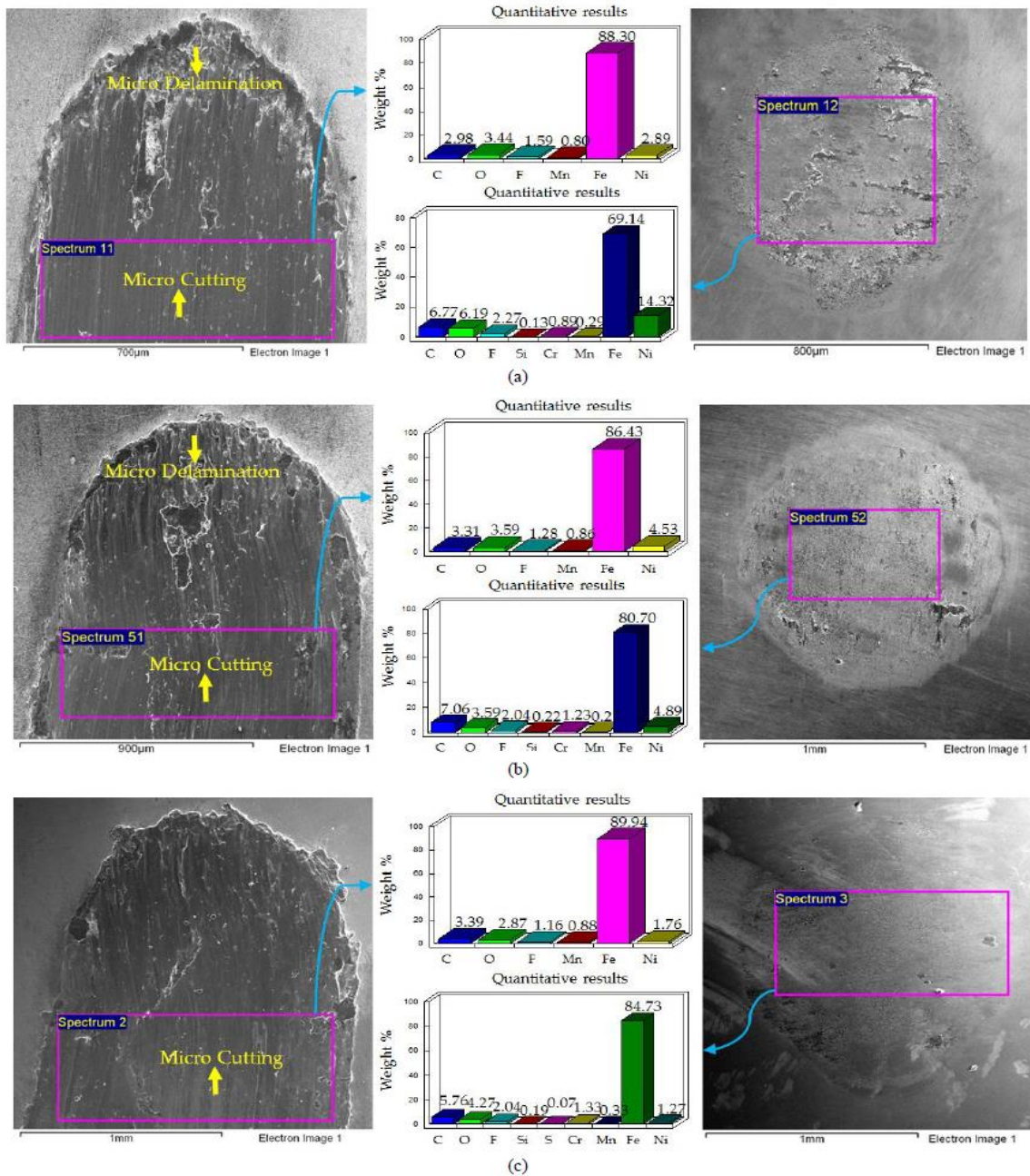

Figure 16: EDS elemental results and SEM Micrographs of Nickel-only coated flat samples and counter steel ball: (a) 20°C, 10 N (b) 20°C, 20 N (c) 20°C, 30 N.

EDS results of increasing the temperature of the refrigerant to 30°C presented in figure 17 show a higher presence of nickel in comparison to the tests conducted at 20°C which shows a decrease in wear by increase in temperature. Wear at 30°C is also mainly due to micro-cutting and micro-

delamination. Wear at 30°C/20 N is mainly due to micro-cutting whereas wear occurs due to a mix of micro-delamination and micro-cutting at 30°C/10 N and 30°C/30 N.
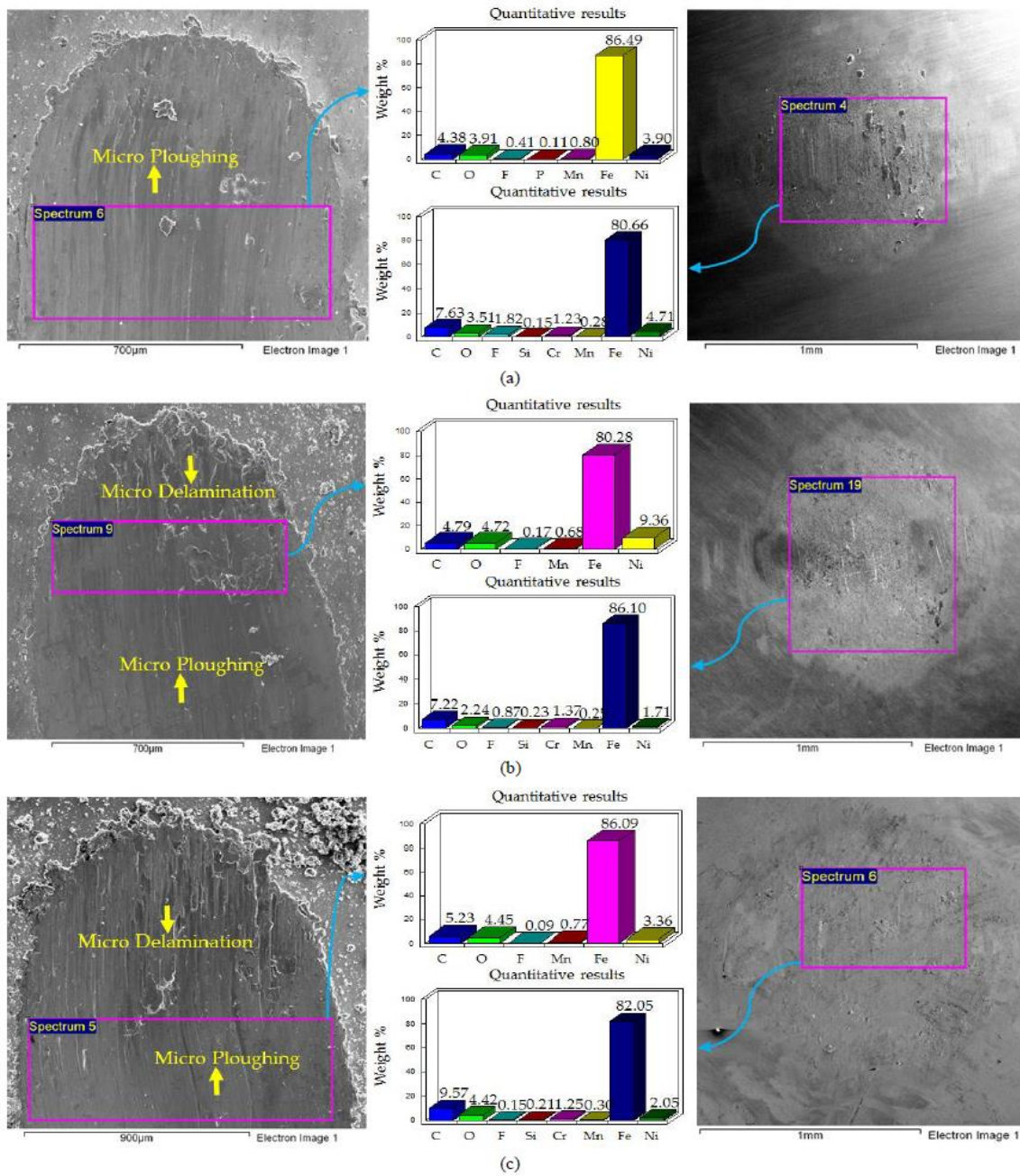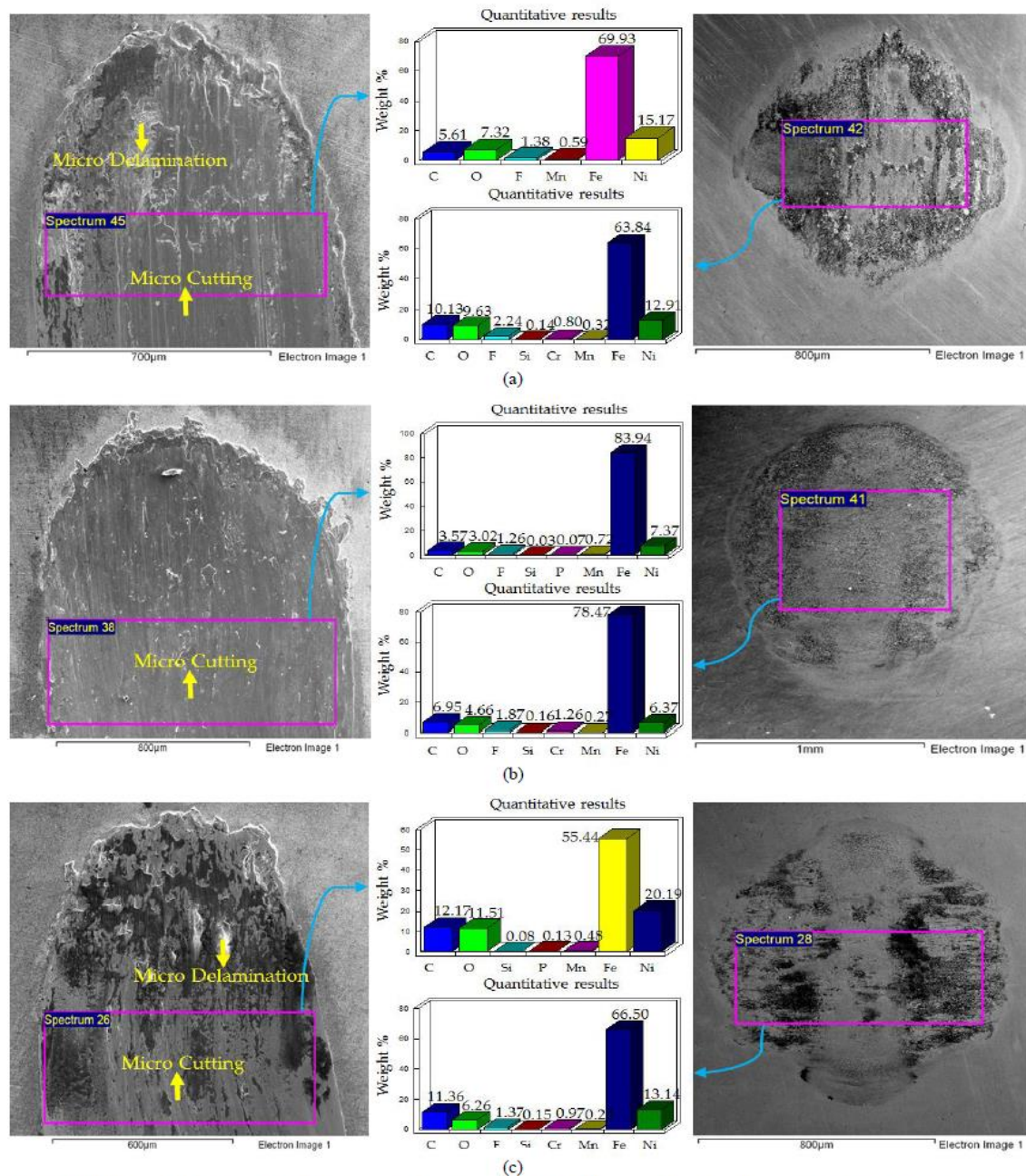

Figure 17: EDS elemental results and SEM Micrographs of Nickel-only coated flat samples and counter steel ball: (a) 30°C, 10 N (b) 30°C, 20 N (c) 30°C, 30 N.

EDS results at 40°C presented in figure 18 reveal an even higher percentage of nickel at any given load on the wear track implying a further reduction in wear by increasing the temperature of the refrigerant. 40°C/10 N and 40°C/20 N operating conditions show wear due to micro-delamination and micro-cutting; whereas wear at 40°C/30 N occurred due to micro-ploughing.

25
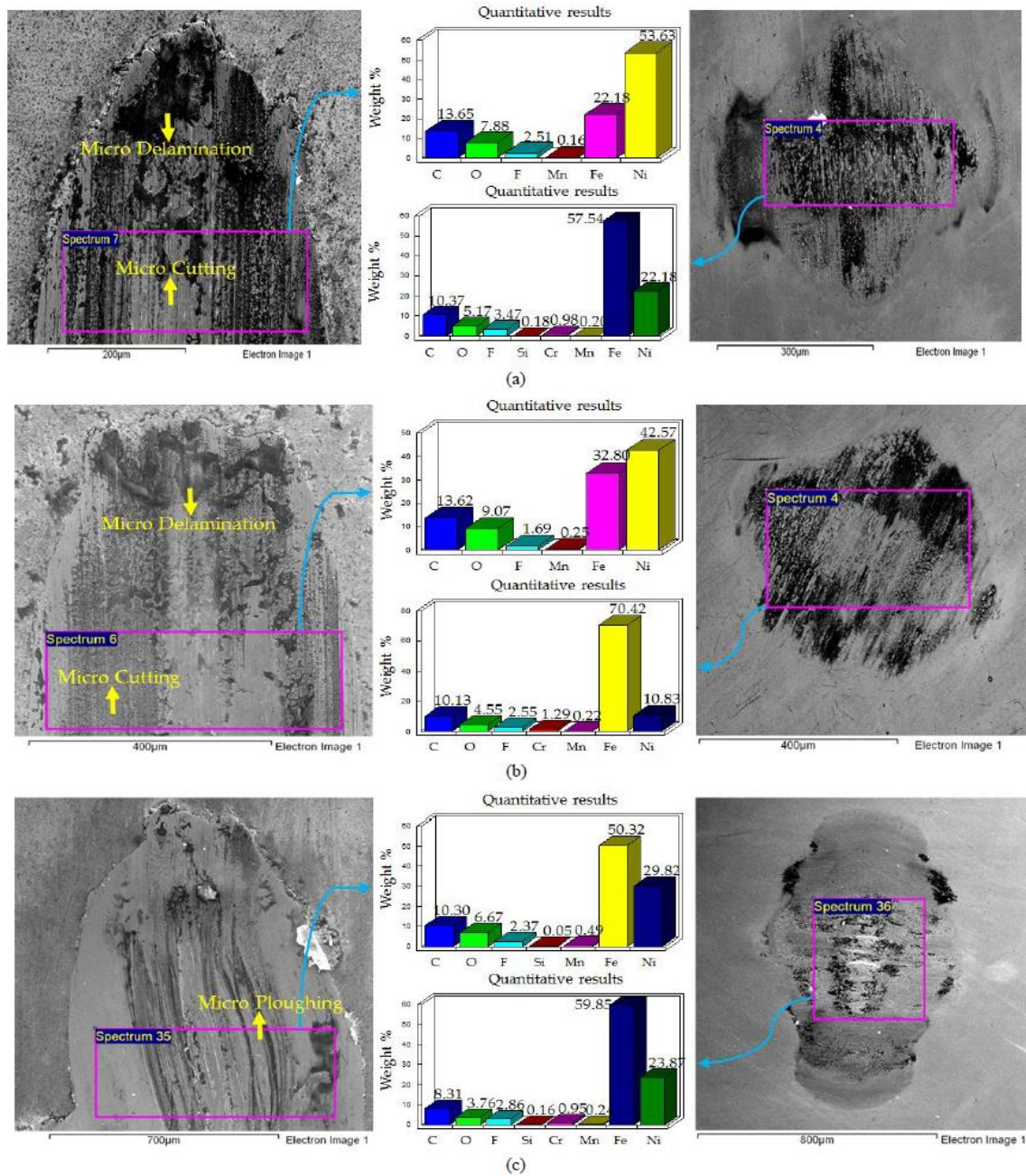
Figure 18: EDS elemental results and SEM Micrographs of Nickel-only coated flat samples and counter steel ball: (a) 40°C, 10 N (b) 40°C, 20 N (c) 40°C, 30 N.

5.1. Wear Volume

The wear scar produced on each disc sample was studied under ZYGO to measure the wear volume of the wear track. Each wear scar was stitched to generate a 3D plot of the complete wear track. Results of Ni-ZrO$_2$ obtained from the interferometer have been presented in figure 19. Similar wear profiles were obtained for the other coatings as well. Wear volume was measured using the 3D plots and the interferometer.

26
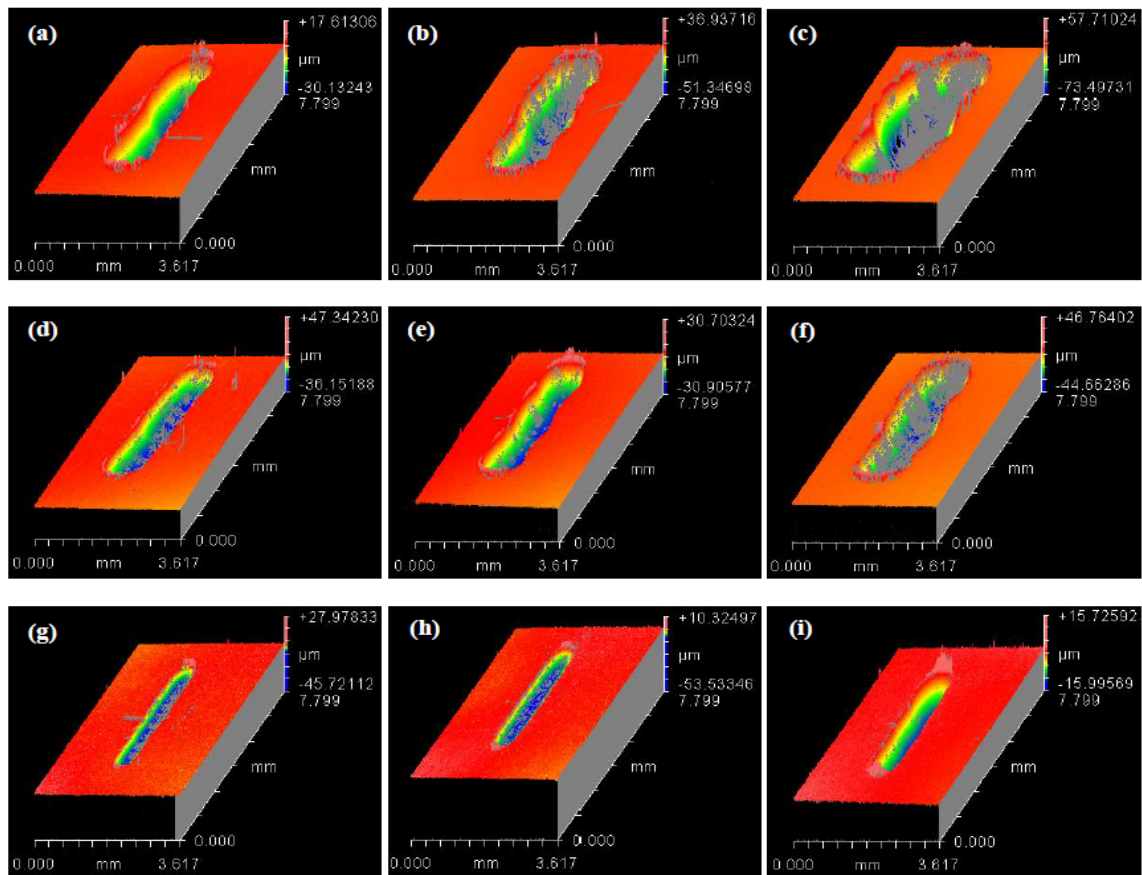
Figure 19: 3D plots of the wear tracks of Ni-ZrO₂ coated specimens. (a) 20°C, 10 N (b) 20°C, 20 N (c) 20°C, 30 N (d) 30°C, 10 N (e) 30°C, 20 N (f) 30°C, 30 N (g) 40°C, 10 N (h) 40°C, 20 N (i) 40°C, 30 N

Results of wear of the uncoated flat samples having R_a of 0.1 μm from our previous study [36] have been presented in figure 20 for reference. Wear volume produced on each coated sample was compared to the uncoated samples to study the effect of using nickel based nanocomposite coatings in comparison to non-coated specimens. Figure 21 shows the wear volume plot of Ni-ZrO₂ nanocomposite coatings and the percentage effect in wear volume by the application of Ni-ZrO₂ on a steel substrate in comparison to uncoated steel. At a lower refrigerant temperature of 20°C, an increase in load increases the wear volume. Increasing the refrigerant temperature to 30°C generates almost the same amount of wear as 20°C at 10 N load, however at higher loads i.e. 20 N and 30 N; there is a very significant drop in wear volume in comparison to wear at 20°C. Interestingly for 30°C refrigerant temperature, least amount of wear was generated at 20 N load and 10 N load resulted in maximum wear. An additional increase in temperature by 10°C dropped wear even further and it can be seen from the results that least amount of wear occurred at 40°C at any given load for Ni-ZrO₂ coatings. This drop in wear with rise in temperature is due to the formation oxygenated and fluorinated anti-wear tribo-films on the top surfaces of the mating parts. EDS analysis show a clear presence of O and F on the wear scar as well as the counter steel ball. EDS results also show an increase in the percentage of oxygen and fluorine on the wear scar with rise in refrigerant temperature to 40°C from 20°C. Overall least amount of wear was observed at 40°C/20 N.

27
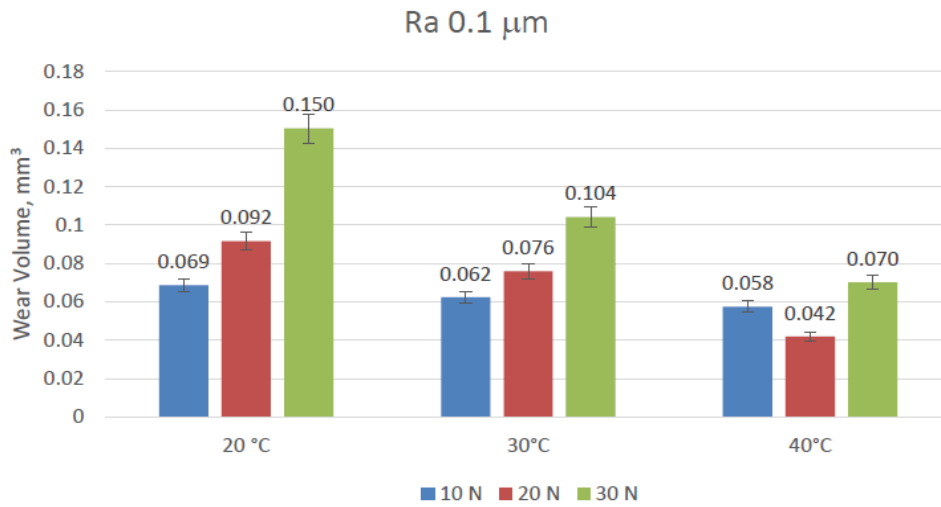
Ra 0.1 μm

Figure 20: Wear volume plot of uncoated disc sample with R_a 0.1 μm [36].

Wear volume generated by using Ni-ZrO$_2$ nanocomposite coatings at each testing condition was also compared to the uncoated steel sample. Percentage wear volume change by using Ni-ZrO$_2$ show a clear decrease in wear volume at all the testing conditions. Improvement in wear reduction is less at lower refrigerant temperature of 20°C and maximum wear reduction occurs at higher refrigerant temperature of 40°C. Minimum wear improvement was observed at 20°C/20 N testing conditions, SEM images and EDS results at these conditions show high wear due to micro-cutting and almost complete wear out of the coatings. A combination of micro-cutting and micro-delamination of the coatings at 30°C/10 N also produce high wear which results in the least improvement in wear at 30°C. At 40°C refrigerant temperature wear decreases by over 70% for 10 N and 30 N loads; at 40°C/20 N the improvement was just below 65%. Both the uncoated steel and Ni-ZrO$_2$ coated samples showed best wear results at 40°C/20 N, this indicates that exists an optimal temperature and load combination that generates best wear performance when using HFE-7000.

Wear produced by using Ni-ZrO$_2$

(a)

28

% change in wear by application of Ni-ZrO$_2$
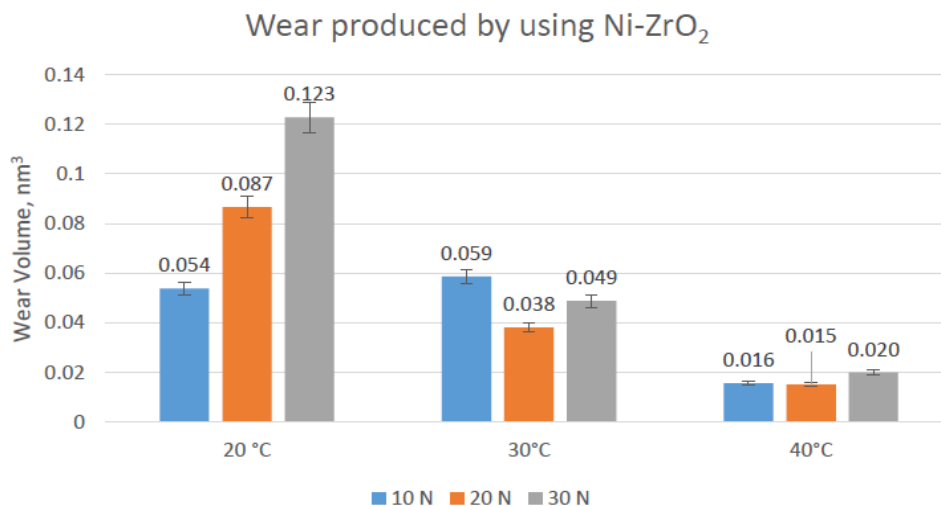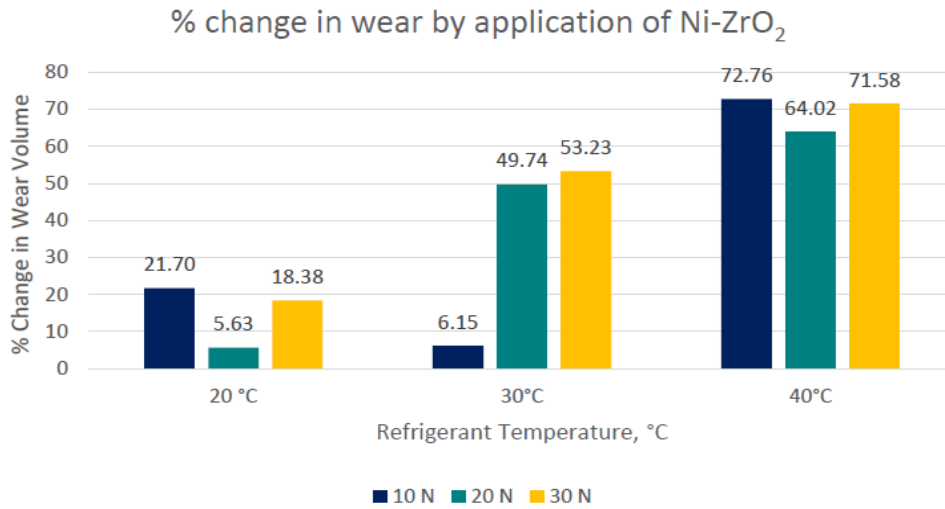
(b)

Figure 21: (a) Wear volume plot of Ni-ZrO$_2$ (b) Change in wear volume by application of Ni-ZrO$_2$

Compared to the uncoated steel, there is an improvement in the micro-hardness and H/E ratio by applying Ni-ZrO$_2$ coatings which improved the wear performance of interacting parts under reciprocating motion.

Results of wear volume produced by applying Ni-SiC nanocomposite coatings on the steel substrate have been presented in figure 22. At temperatures of 20°C and 30°C, increase in load generates higher wear. A reduction in wear is witnessed by increasing the temperature of the refrigerant from 20°C to 30°C. Wear reduces further by an increase in the temperature of the refrigerant to 40°C. This drop in wear volume with increase in refrigerant temperature is linked with the formation of oxygen and fluorine containing tribo-films on the top surfaces.

Wear Produced by using Ni-SiC

(a)
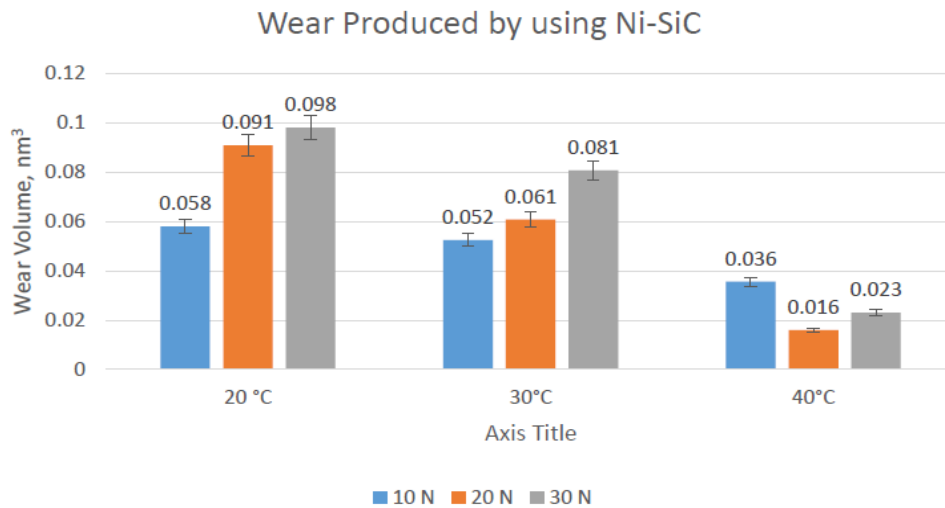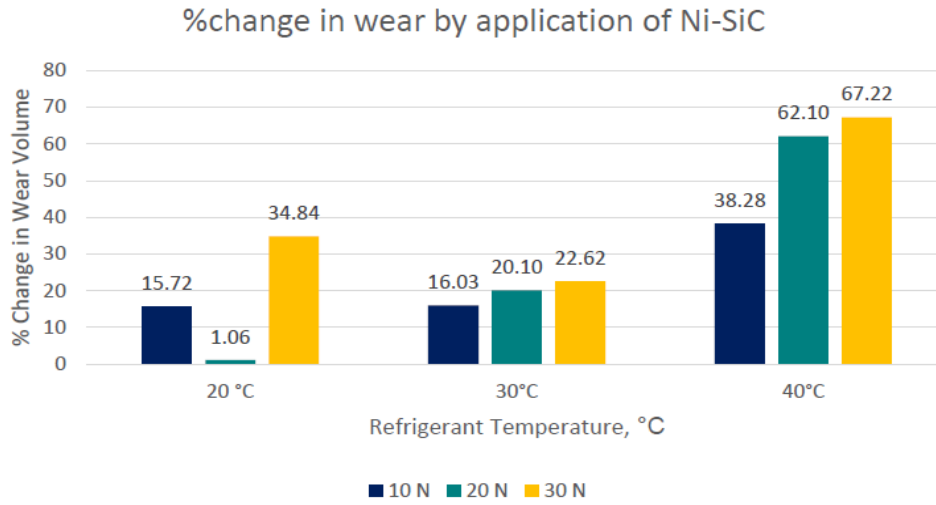
Figure 22: (a) Wear volume plot of Ni-SiC (b) Change in wear volume by application of Ni-SiC

Similar to uncoated steel and Ni-ZrO$_2$ coated steel samples, minimum wear occurs at 40°C/ 20 N for Ni-SiC coated samples as well. EDS results show an increase in the content of fluorine and oxygen on the wear scar indicating an accelerated formation of protective surface films. Comparing wear produced by using Ni-SiC nanocomposite coatings to the uncoated steel show a clear reduction in wear volume. Similar to Ni-ZrO$_2$, Ni-SiC coatings also produced the least positive effect at 20°C/ 20 N. High wear occurred at 20°C/ 20 N due to micro-delamination and micro-cutting at these testing conditions. In contrast to Ni-ZrO$_2$ coatings at which 10 N load resulted in the highest wear drop, 30 N load proved to be more beneficial for Ni-SiC at 20°C refrigerant temperature. At refrigerant temperatures of 30°C and 40°C, increase in load produced a higher percentage drop in wear volume by applying Ni-SiC coatings when compared to uncoated steel. Ni-SiC coatings improved the micro-hardness of the surface and had the third best hardness amongst the coatings produced. (H/E) ratio also improved by applying Ni-SiC coatings in comparison to the steel substrate. An enhancement in the mechanical properties improved the wear resistance of the coatings and resulted in a decrease in wear.

Wear volume results of Ni-Al$_2$O$_3$ nanocomposite coatings have been presented in figure 23. The very first testing condition of 20°C/10 N show a very significant drop in wear volume as compared to uncoated steel and also in comparison to Ni-ZrO$_2$ and Ni-SiC. Percentage wear volume change by applying Ni-Al$_2$O$_3$ coatings when compared to uncoated steel show remarkable improvement in wear loss and a drop in wear by over 92%. Ni-Al$_2$O$_3$ nanocomposite coatings showed the second best hardness and the best (H/E) ratio as compared to all the other samples. This improvement in mechanical properties provides better wear resistance which reduces wear significantly. Increasing the applied normal load to 20 N at 20°C generates significant wear. Percentage wear volume change graph also shows an increase in wear at 20°C/20 N by applying Ni-Al$_2$O$_3$ coatings. This shift in wear is due to the delamination of these coatings from the steel substrate by increasing load. Constant oscillating/reciprocating motion has been known to delaminate Ni-Al$_2$O$_3$ coatings [24, 34]. Delamination of Ni-Al$_2$O$_3$ coatings from the steel substrate is also evident from the micrographs presented in figure 10. As observed with the other coatings, increasing the applied normal load to 30 N at 20°C further increases wear. Comparing the results of wear of Ni-Al$_2$O$_3$ coatings with uncoated

30

steel show an improvement in wear loss. Although a complete delamination of the coatings is also observed at 20°C/30 N similar to 20°C/20 N, however more O and F were present on the wear scar at 30°C/30 N in contrast to 20°C/20 N; which indicates a higher presence of tribo-films which play a key role in reducing wear.
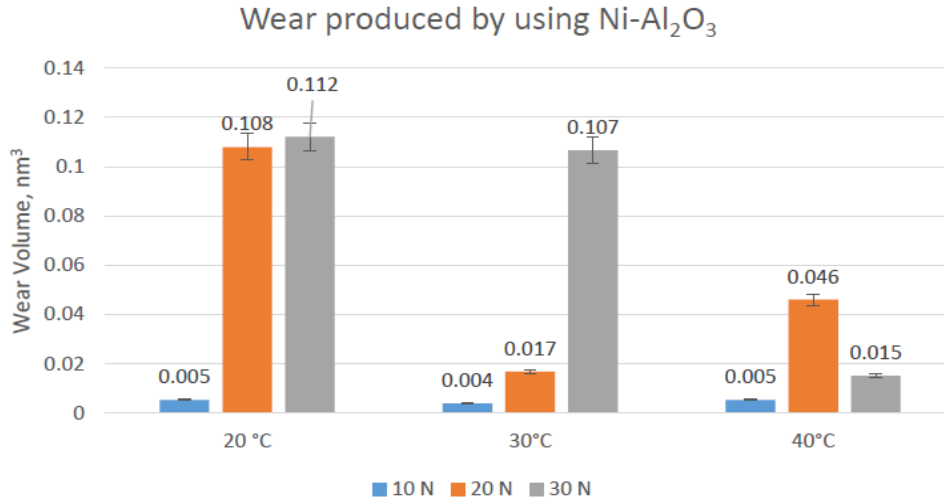
(a)
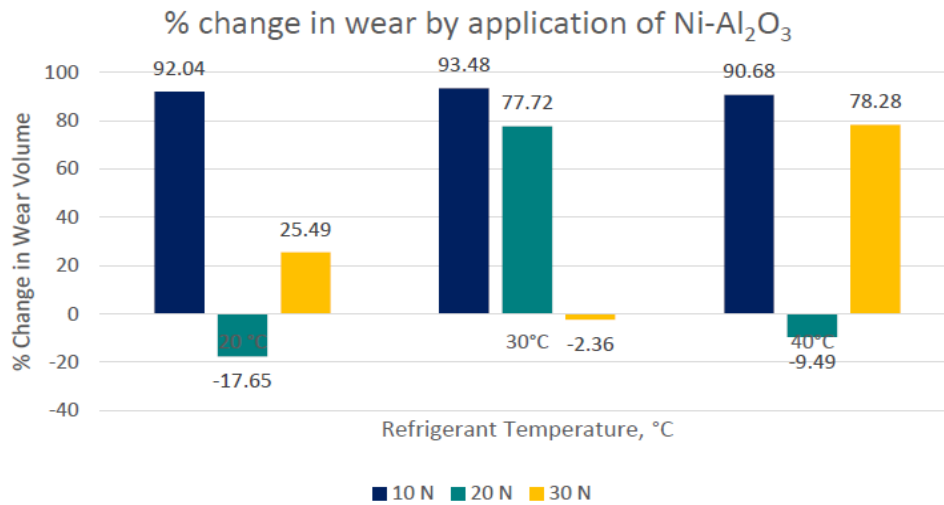
(b)

Figure 23: (a) Wear volume plot of Ni-Al$_2$O$_3$ (b) Change in wear volume by application of Ni-Al$_2$O$_3$

Wear volume decreases by increasing the temperature of the refrigerant to 30°C from 20°C at any given load by applying Ni-Al$_2$O$_3$ nanocomposite coatings. 30°C/10 N testing conditions also result in a very significant decline in wear, in comparison to uncoated steel wear decreases by over 93% by using Ni-Al$_2$O$_3$ coatings at these operating conditions. Unlike 20°C/20 N testing conditions, the tests conducted at 30°C/20 N reduced wear and when comparing to uncoated steel wear volume decreased by over 77% at 30°C/20 N. 30°C/30 N test also produced a different result in contrast to 20°C/30 N,

31

wear volume decreased at 20°C/30 N whereas wear increased at 30°C/30 N in comparison to uncoated steel. SEM images presented in figure 11 show complete delamination of these coatings at 30°C/30 N which results in higher wear. Results at 40°C refrigerant temperature were similar to the results obtained at 20°C, wear reduction was observed at 10 N and 30 N whereas increase in wear occurred at 20 N. Compared to uncoated steel wear volume decreased by more than 90% at 40°C/10 N and more than 78% at 40°C/30 N. The micrographs and EDS analysis results as presented in figure 12 show a significant presence of nickel at 40°C/20 N showing that the coating has not worn out but still compared to the uncoated test conducted at 40°C/20 N the amount of wear produced is more by employing Ni-Al$_2$O$_3$ coatings in comparison to uncoated steel. The reason for higher wear production at 40°C/20 N by applying Ni-Al$_2$O$_3$ coating is because 40°C/20 N condition was the most optimum testing condition which produced least amount of wear with uncoated steel. A higher percentage of oxygen and fluorine was also present on uncoated steel samples in contrast to Ni-Al$_2$O$_3$ coated samples at 40°C/20 N [24] which highlights the significance of oxygenated and fluorinated films in reducing wear. Compared to the other coatings and the uncoated sample, Ni-Al$_2$O$_3$ coated samples at 40°C/20 N did not result in minimum wear. Minimum wear for Ni-Al$_2$O$_3$ coated samples was observed at 30°C/10 N.

Wear volume results by using Ni-GPL have been presented in figure 24. Ni-GPL coatings had the best hardness values and the second best (H/E) ratio amongst all the coatings produced in this study. The results however show a totally different pattern by using Ni-GPL at 20°C refrigerant temperature compared to the rest of the coatings. Maximum wear at 20°C is observed at 20 N instead of 30 N. Wear volume produced at 20°C/10 N and 20°C/20 N is considerably high, both of these testing conditions when using Ni-GPL coatings have an adverse effect on wear and wear volume has increased drastically. Ni-GPL coatings at these conditions have completely worn out and EDS results on the wear track at 20°C/10 N show no fluorine and at 20°C/20 N only a very small percentage of oxygen and fluorine was detected as shown in figure 13. This shows extreme wear and a very minor presence of anti-wear tribo-films under these conditions. Comparing uncoated steel with Ni-GPL shows an increase in wear by over 67% at these conditions. This high wear when using Ni-Graphene is believed to be because of two reasons.

(a)

% change in wear by application of Ni-GPL
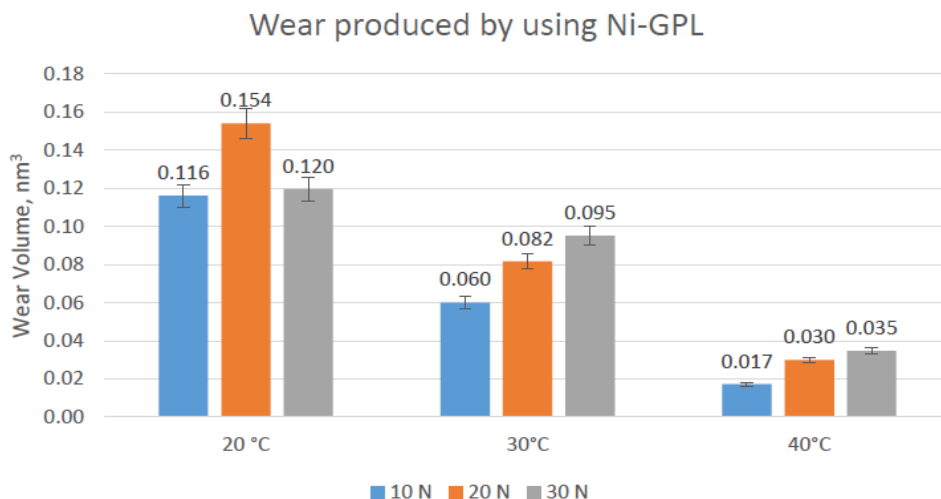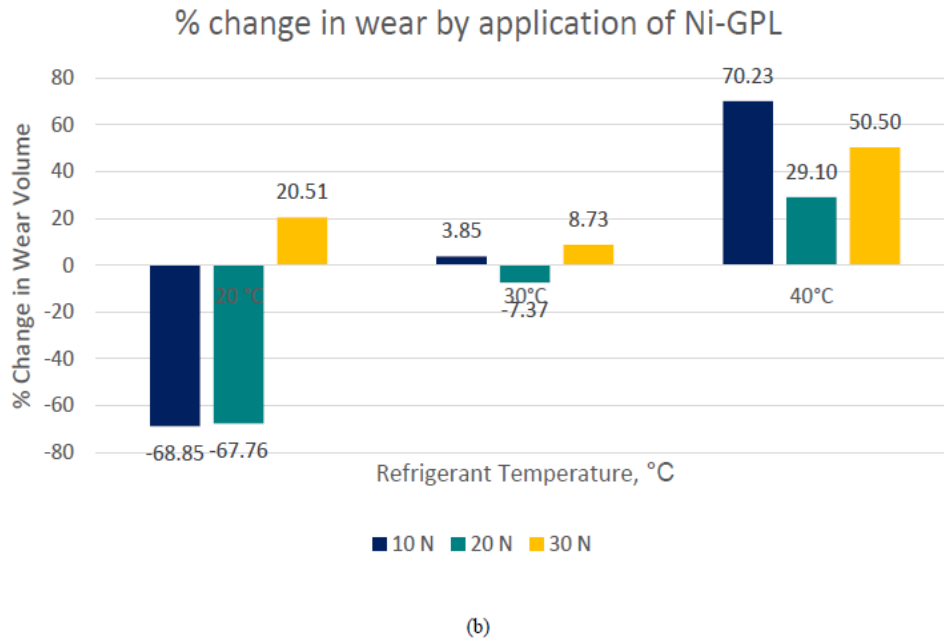
Figure 24: (a) Wear volume plot of Ni-GPL (b) Change in wear volume by application of Ni-GPL

The first reason is most probably the incompatibility of HFE-7000 with Graphene based Nano coatings. HFE-7000 has a chemical formula $C_3F_7OCH_3$, Carbon-Fluorine (C-F) single bonds are highly polar bonds and HFE-7000 has been reported to break and from new bonds which results in the development of tribo-films [36]. In addition, C-H bond is weaker than C-F [23, 36, 41] bonds and C-O bond is weaker than the C-C bond [36, 42, 43]. Breaking of the molecular structure of the refrigerant means it could result in the generation of carbonyl products e.g. esters which are also polar in nature [44]. On the other hand electron mobility in Graphene is extremely high [45] and graphene crystallites demonstrate graphene to have the fastest electron motilies in comparison to all other materials [45]. Graphene also shows exceptional electrocatalytic behaviour that is accredited to its unique chemical and physical properties, such as subtle electronic characteristics ($\pi - \pi$ interactions and its strong absorptive capability) [45, 46]. Graphene has large surface area, ballistic electron motilies and excellent conductivity [47]. In addition the presence of the extended C=C conjugation in graphene is also likely to shuttle electrons [47]. These properties show that Graphene is not only rich in electrons but also has the fastest electron mobility and possesses electrocatalytic behaviour which results in pulling out of graphene nanoparticles from the nanocoatings due to the polar nature of the refrigerant. Nano particles with larger particle size (≥ 20 nm) were used in all the other coatings prepared in this study except for Graphene for which nanoparticles of 6-8 nm were used. The small size of the electron rich Graphene nanoparticles in the presence of polar molecules at fully lubricated refrigerant conditions at constant reciprocating motion ejects the nanoparticles from the coatings. In addition, very low oxygen and fluorine was detected on the wear tracks of these tests post experimentation showing that Graphene is not favourable for the generation of tribo-films at low operation temperatures and low applied loads. Increase in load to 30 N at 20°C facilitates the chemical breakdown of the refrigerant and establishment of tribological films on the wear scar which reduces

33

wear at 20°C/30 N. Increase in load also helps retain Graphene in the Nickel matrix which helps in wear reduction.

Increasing the refrigerant temperature to 30°C had a slight positive effect on wear at 10 N load and 30 N load. Higher percentage of nickel is also observed on the wear track as shown in figure 14 confirming a decrease in wear. EDS results also show a greater presence of oxygen and fluorine signifying a higher presence of surface tribo-films as compared to the tests conducted at 20°C. Increasing the temperature of the refrigerant to 30°C at 20 N load however did not have a positive impact on wear and wear volume in fact increased at these conditions, this is probably due to the accelerated development of tribo-films on the uncoated surface as compared to Ni-GPL coated surface under these testing conditions. Increasing the refrigerant temperature further to 40°C resulted in a drop in wear at all loads, highest drop in wear was observed at 10 N load and the least positive effect on wear was seen at 20 N load. EDS results presented in figure 15 reveal the highest percentage of nickel presence at 40°C/10 N for Ni-GPL amongst all the tests and a good percentage of oxygen/fluorine presence which help reduce wear. Unlike Ni-SiC, Ni-ZrO$_2$ and the uncoated steel, minimum wear for Ni-GPL coatings was also observed at 40°C/10 N.
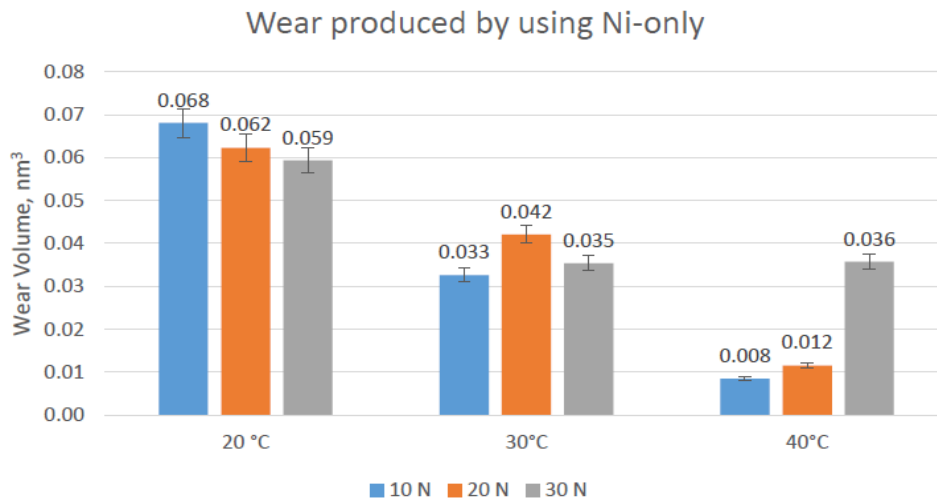
(a)
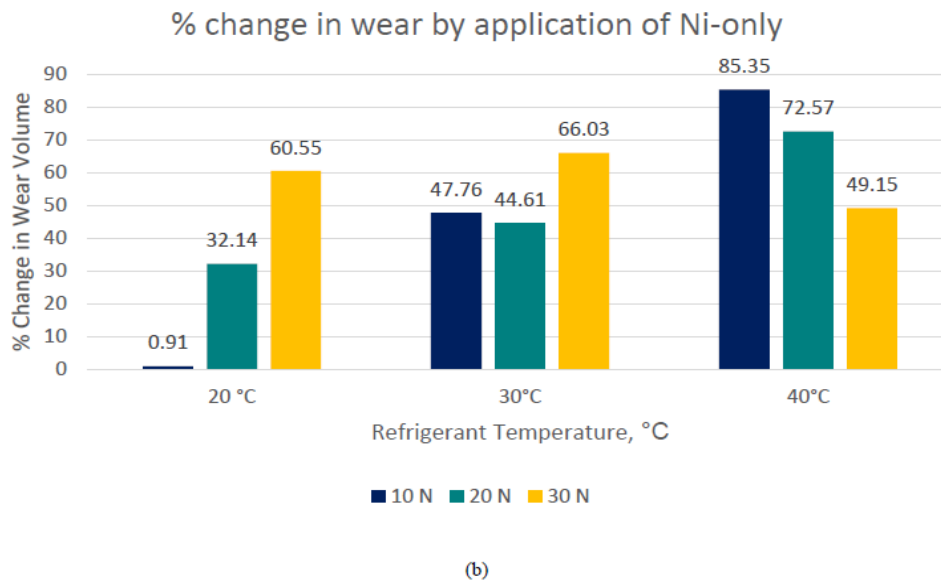
Figure 25: (a) Wear volume plot of Nickel (b) Change in wear volume by application of Nickel

Results of wear for Nickel-only coatings have been presented in figure 25. The results of wear volume show a different trend at 20°C refrigerant temperature as compared to uncoated, Ni-ZrO$_2$, Ni-SiC and Ni-Al$_2$O$_3$ coated contacts; at 20°C all these samples showed an increase in wear whereas Nickel-only coatings show a decrease in wear by increasing the load at 20°C refrigerant temperature. For Nickel-only coatings a combination of micro-delamination and micro-cutting is observed at 20°C/ 10 N; the wear mechanism however shifts mainly towards micro-cutting and less micro-delamination occurs with increase in applied load as shown in figure 16, this shift in wear mechanism helps reduce wear with increase in load for Nickel-only coatings at 20°C refrigerant temperature. Comparison of the wear volume between uncoated and Nickel coated samples show a decline in wear volume by the application of Nickel-only coatings. Increasing the load at 20°C produces a greater percentage reduction in wear, this is due to fact that wear reduces with increase in load for Nickel-only coatings at 20°C. By increasing the refrigerant temperature to 30°C a reduction in wear is observed. Maximum wear at 30°C refrigerant temperature is observed at 20 N load which is due to the accelerated micro-cutting of the coating at 30°C/20 N in comparison to 30°C/10 N and 30°C/30 N as shown in figure 17. EDS results also confirm a lesser presence of Nickel at 30°C/20 N in contrast to 30°C/10 N and 30°C/30 N. Percentage effect on wear volume by applying Nickel-only coatings shows a decrease in wear at all applied loads in comparison to uncoated steel sample. A further rise in the temperature of the refrigerant to 40°C decreases wear. Similar to Ni-GPL; wear increase with increase in load at 40°C and also the least amount of wear is produced at 40°C/10 N. Comparing to the uncoated steel, wear has reduced by applying Nickel-only coatings. Maximum positive effect on wear occurs at 40°C/10 N. Due to an increase in wear volume with increase in load at 40°C, the positive effect on wear drops from about 85% to about 49%.

To summarize, similar to the behaviour noted by using uncoated steel wear volume also decreased with increase in refrigerant temperature for *all* of the coatings used in this study. Wear primarily occurred due to micro-delamination, micro-cutting and micro-ploughing. Wear mechanism depends on the type of coating [32, 34], wear phenomenon also shifted from one form to another for the same coatings at different testing conditions. The amount of wear volume produced is also dependent on the production of protective surface tribological films on the mating metals, increasing the temperature of

35

the refrigerant increases the reactivity of the refrigerant HFE-7000 with the rubbing surfaces which accelerates the formation of these tribological films on the mating surfaces which help reduce wear [24, 36]. Irrespective of the coatings tested in this study when the amount of fluorine and/or oxygen detected on the rubbing surfaces increased with an increase in refrigerant temperature indicates a higher presence of tribological films on the top surfaces of the interacting parts which play a vital role in wear reduction. Micro-hardness and hardness to elastic modulus ratio (H/E) improved by applying Nickel based coatings on the steel substrate. Ni-GPL showed the highest hardness values followed by Ni-Al$_2$O$_3$. Ni-Al$_2$O$_3$ displayed the highest hardness to elastic modulus (H/E) ratio, the second best (H/E) ratio was shown by Ni-GPL. Ni-ZrO$_2$ showed an improvement in wear at all operating conditions in comparison to the uncoated steel and the highest drop in wear was observed at higher refrigerant temperature of 40°C at which wear dropped by more than 72% at 40°C/10 N. Ni-SiC coatings also had a positive effect on wear reduction, similar to Ni-ZrO$_2$, Ni-SiC coatings also showed good wear performance for all testing conditions and maximum positive effect on wear was also observed at 40°C refrigerant temperature. However the maximum effect on wear loss occurred at 40°C/30 N by using Ni-SiC coatings whereas the maximum effect on wear loss for Ni-ZrO$_2$ was at 40°C/10 N. Ni-Al$_2$O$_3$ coatings gave some interesting results in terms of wear volume. In comparison to the uncoated steel samples, three of the testing conditions (20°C/20 N, 30°C/30 N and 40°C/20 N) resulted in an increase in wear volume by employing Ni-Al$_2$O$_3$ coatings. Ni-Al$_2$O$_3$ coatings are prone to delaminate under the influence of reciprocating motion [24, 34] which increases wear. Ni-Al$_2$O$_3$ coatings however presented the second best hardness and the best (H/E) ratio amongst all the coatings produced which results in a significant drop in wear loss especially at low loads; all the test conducted at low loads (20°C/10 N, 30°C/10 N and 40°C/10 N) show a drop in wear by more than 90%. None of the other coatings tested in this study show such a significant drop in wear at low loads; 20°C/30 N, 30°C/20 N and 40°C/30 N also proved to be beneficial in wear reduction. Ni-GPL displayed the best micro-hardness value but resulted in a drastic increase in wear volume at low testing temperature of 20°C and at low loads. This is believed to be due to the incompatibility of HFE-7000 with Graphene nanoparticles and the slower formation of tribo-films. Increasing the load and the temperature of the refrigerant however proves to be beneficial in reducing wear for Ni-GPL, wear drops at higher temperature and at higher loads due to the acceleration in the production of tribo-films which help decrease wear. All the tests conducted at 40°C for Ni-GPL show a reduction in wear volume. Nickel-only coatings also provided good results in terms of wear reduction. Higher wear reduction was noted at higher refrigerant temperatures. Nickel-only coatings also produced the maximum drop in wear at 40°C/10 N. When comparing to uncoated steel, Nickel-only coatings proved to be beneficial in reducing wear at all the testing conditions. Good performance of Nickel-only coatings in comparison to other coatings is believed to be associated with three body abrasive wear. The wear debris produced during testing have been reported to be entrapped in the disc and refrigerant holding cup [36]; all of the nanocomposite coatings contain hard nanoparticles, the worn out coating and hard nanoparticles trapped in the cup cause three body wear and result in increase in wear. Wear debris produced by Nickel-only coatings do not contain hard nanoparticles and three body abrasive wear phenomenon which is also believed to take place when using Nickel-only coatings does not produce the same amount of damage. Nickel-only coatings are also believed to be more beneficial in the development of surface films in comparison to coatings different nano-particles in the Nickel matrix.

6. Friction

The influence on the friction coefficient by the application of coatings was also analysed in this study. Results of the coefficient of friction have been presented as real-time friction coefficient graphs and also as average coefficient of friction plots. Results obtained from each of the coatings were also

compared to the uncoated samples with R_a of 0.1 µm. Results of the average friction coefficient of the uncoated samples have been provided in figure 26 for reference.

Results of Ni-ZrO$_2$ coated steel have presented in figure 27. Figures 27 (a), 27 (b) and 27 (c) show the real-time coefficient of friction plots. All these plots show a decrease in the friction coefficient values with increase in applied load. An increase in the temperature of the refrigerant from 20°C to 30°C does not a have noticeable change on the friction coefficient values. Increasing the temperature of the refrigerant to 40°C however has a positive influence on the friction coefficient values. The friction coefficient drops at each of the applied normal loads by increasing the refrigerant temperature from 20°C to 40°C, this is also evident from the average coefficient of friction plots shown in figure 27 (d). There are more fluctuations in the friction coefficient at lower loads, increase in load at any given temperature reduces not only the coefficient of friction but also the fluctuations in the friction coefficient.
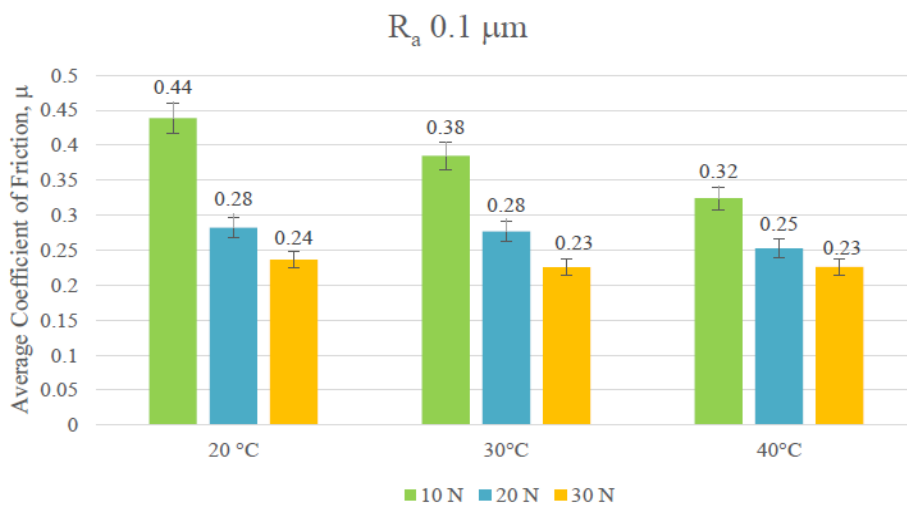
Figure 26: Average coefficient of friction plot for uncoated steel sample with R_a 0.1 µm [36].
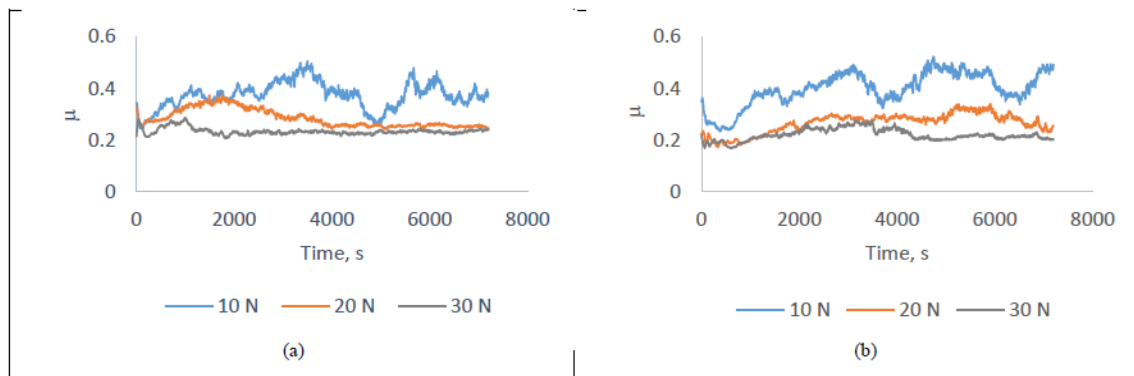
Figure 27: Coefficient of friction graphs for Ni-ZrO₂: Real-time coefficient of friction at refrigerant temperature (a) 20°C (b) 30°C (c) 40°C (d) Average coefficient of friction plot (e) Percentage in average friction coefficient by applying Ni-ZrO₂

This decline in friction coefficient with increase in refrigerant temperatures and the decrease in average friction coefficient values with increase in normal load at any given temperature is linked with the development of protective tribological films on the surfaces of the interacting parts. A comparison of the average coefficient of friction of Ni-ZrO₂ to uncoated steel is shown in figure 27 (e). The plot shows that all operating conditions are not beneficial in reducing friction, a slight increase in the average coefficient of friction is observed at 20°C/20 N and 30°C/10 N. These two testing conditions also proved to be least beneficial in improving wear. Maximum improvement in friction coefficient was observed at 20°C/10 N. 40°C refrigerant temperature improved friction at all loads when compared to the uncoated steel samples.

Figure 28 shows the results of the coefficient of friction obtained by applying Ni-SiC coatings. Similar to Ni-ZrO₂ nanocomposite coatings, Ni-SiC coatings also show a drop in the friction coefficient with increase in applied normal load at any given temperature. In addition a constant decline in the coefficient of friction is observed with an increase in refrigerant temperature. The average coefficient of friction decreases by increasing the load at all testing temperatures and a decline in the average coefficient of friction by increasing the refrigerant temperature to 40°C from 20°C can be observed in figure 28 (d). Similar to the real time coefficient of friction results, higher fluctuations in the friction coefficient are visible at lower loads and increase in load reduces the fluctuations in the friction coefficient.

Figure 28: Coefficient of friction graphs for Ni-SiC: Real-time coefficient of friction at refrigerant temperature (a) 20°C (b) 30°C (c) 40°C (d) Average coefficient of friction plot (e) Percentage in average friction coefficient by applying Ni-SiC

Comparing the results of the average friction coefficient of Ni-SiC to the uncoated steel shows an improvement in the friction coefficient at almost all of the testing conditions, only 20°C/30 N and 40°C/10 N showed a slight increase (less than 1%) in the average friction coefficient by applying Ni-SIC coatings. Other than these two conditions an improvement in the average coefficient can be clearly seen in the plot presented in figure 28 (e). Testing conditions of 30°C/20 N showed the maximum improvement in the coefficient of friction by applying Ni-SiC coatings.

Results of the coefficient of friction for Ni-Al$_2$O$_3$ have been presented in figure 29. These results show a different behaviour in comparison to Ni-ZrO$_2$ and Ni-SiC.

39

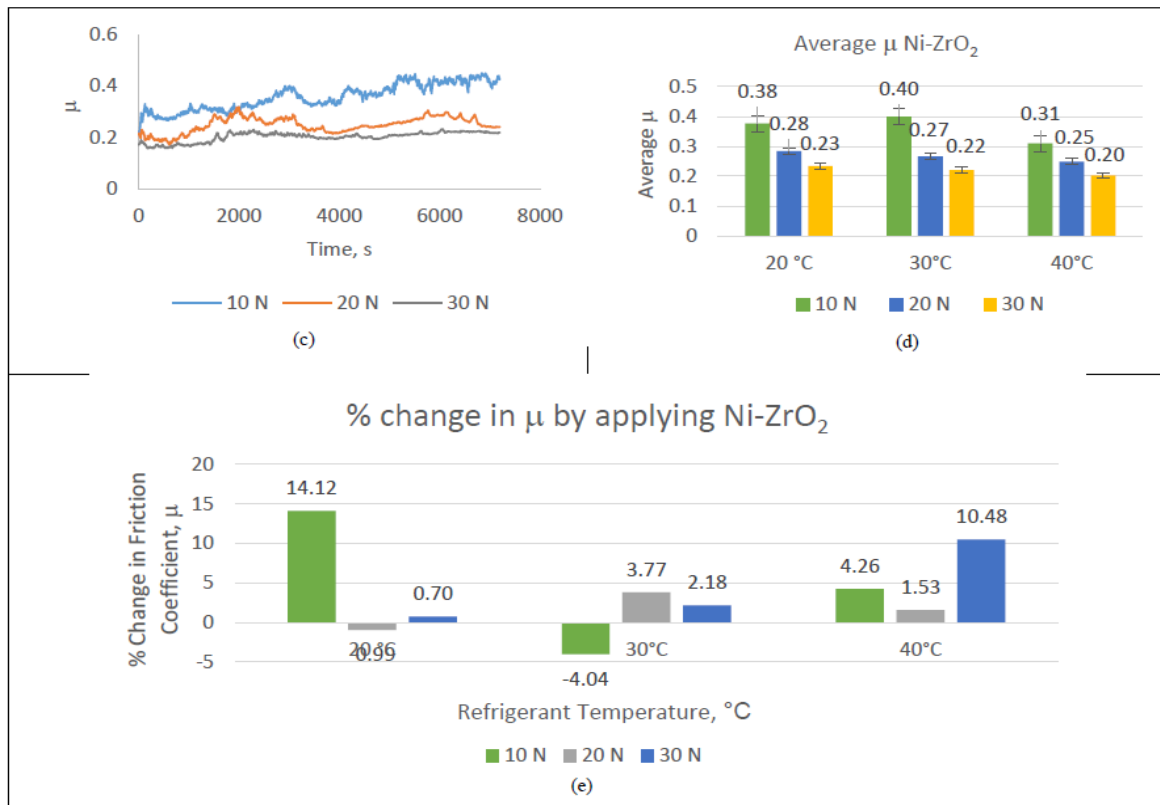Figure 29: Coefficient of friction graphs for Ni-Al₂O₃: Real-time coefficient of friction at refrigerant temperature (a) 20°C (b) 30°C (c) 40°C (d) Average coefficient of friction plot (e) Percentage in average friction coefficient by applying Ni-Al₂O₃

Fluctuations and spikes in the real-time coefficient of friction graphs at 10 N load as observed for the previous two coatings were not observed in the case of Ni-Al₂O₃. At low loads Ni-Al₂O₃ also presented the best wear results compared to all the other coatings tested in this study. A reduction in wear at low loads leads to less wear debris and a significant reduction in three-body abrasive wear which reduces the variations/fluctuations in the coefficient of friction. Ni-Al₂O₃ nanocomposite coatings had the best surface finish amongst all the coatings prepared in this study and had R_a of only 0.045 μm. A smoother surface means less asperity interactions which reduces friction as well as wear. Average friction coefficient plots for Ni-Al₂O₃ are also different from the Ni-SiC, Ni-ZrO₂ and the uncoated steel samples. Increasing the load to 20 N from 10 N at 20°C reduces friction coefficient, but

a further increase in load to 30 N does not affect the average coefficient of friction. Increasing the temperature to 30°C does result in a drop in the friction coefficient compared the 20°C, however increasing load at 30°C does not have any influence on the coefficient of friction. Increasing the temperature to 40°C increases the friction coefficient slightly at 40°C/10 N in comparison to 30°C/10 N. 40°C/20 N and 40°C/30 N show a drop in the average friction coefficient compared to 30°C/20 N and 30°C/30 N. Comparing the average coefficient of friction results of Ni-Al$_2$O$_3$ to uncoated steel show an improvement in the coefficient of friction values at all the testing conditions. The highest improvement was noted at 30°C/10 N at which the coefficient of friction improved by over 40%, 30°C/10 N also showed the best improvement in wear for Ni-Al$_2$O$_3$. Ni-Al$_2$O$_3$ also did not show an increase in the average friction coefficient values in comparison to uncoated steel at any of the testing conditions.

Similar to the results of wear, Ni-GPL also showed poor coefficient of friction results at lower refrigerant temperature. At 20°C an increase in applied load to 20 N from 10 N dropped the coefficient of friction but an additional increase in load to 30 N from 20 N at 20°C did not affect the average coefficient of friction as shown in figure 30. Ni-GPL coatings had the highest average surface roughness value (1.17 μm) compared to all the other coatings and also when compared to the uncoated steel disc samples. This high surface value was due the presence of nano graphene particles at the very top of the surface and also due to particle agglomeration. 20°C/10 N showed an improvement in the coefficient of friction when compared to the uncoated steel, however increase in load at 20°C produced larger coefficient of friction values in comparison to uncoated steel and the friction coefficient increased by approximately 45% at 20°C/30 N. Increase in refrigerant temperature to 30°C from 20°C however proved to be extremely beneficial in reducing the coefficient of friction and when compared to the uncoated steel, the coefficient of friction dropped by more than 33% at 30°C/10 N. Although the refrigerants viscosity decreases with an increase in temperature which leads to more asperity interaction that should increase friction, but the friction coefficient reduces which is because of the increase in refrigerants reactivity with the rubbing surfaces and formation of tribo-films. Wear however did not show a very significant improvement for 30°C tests and in fact wear volume increased at 30°C/20 N. Increasing the temperature of the refrigerant to 40°C drops the coefficient of friction at 40°C/20 N and 40°C/30 N in comparison to the tests conducted at lower temperatures, however in contrast to 30°C/10 N the average friction coefficient is seen to increase slightly at 40°C/10 N. Comparing the results of Ni-GPL to uncoated steel also show that these coatings improve friction at 40°C at all the loads. Wear was seen to improve as well at 40°C for Ni-GPL.

Results obtained by the application of Nickel-only coatings have been presented in figure 31. The results of the real-time friction coefficient show variations in the coefficient of friction as well especially at low loads. Increasing the load at any particular temperature also reduces the real-time coefficient of friction as well as the average friction coefficient. Increase in temperature of the refrigerant from 20°C to 30°C did not have any influence on the average friction coefficient. An additional rise in the temperature of the refrigerant to 40°C however produces a drop in the coefficient of friction values. 40°C/30 N presented the least average friction coefficient not only for the Nickel coatings but also in comparison to all the other coatings. Nickel-only coatings also had the second best surface finish amongst all the coatings. When comparing the data of the average friction coefficient to the uncoated steel a very slight increase in the friction coefficient was observed at 20°C/30 N and an increase in friction was also observed at 30°C/30 N. Other than these two conditions the friction coefficient improved by applying Nickel-only coatings.
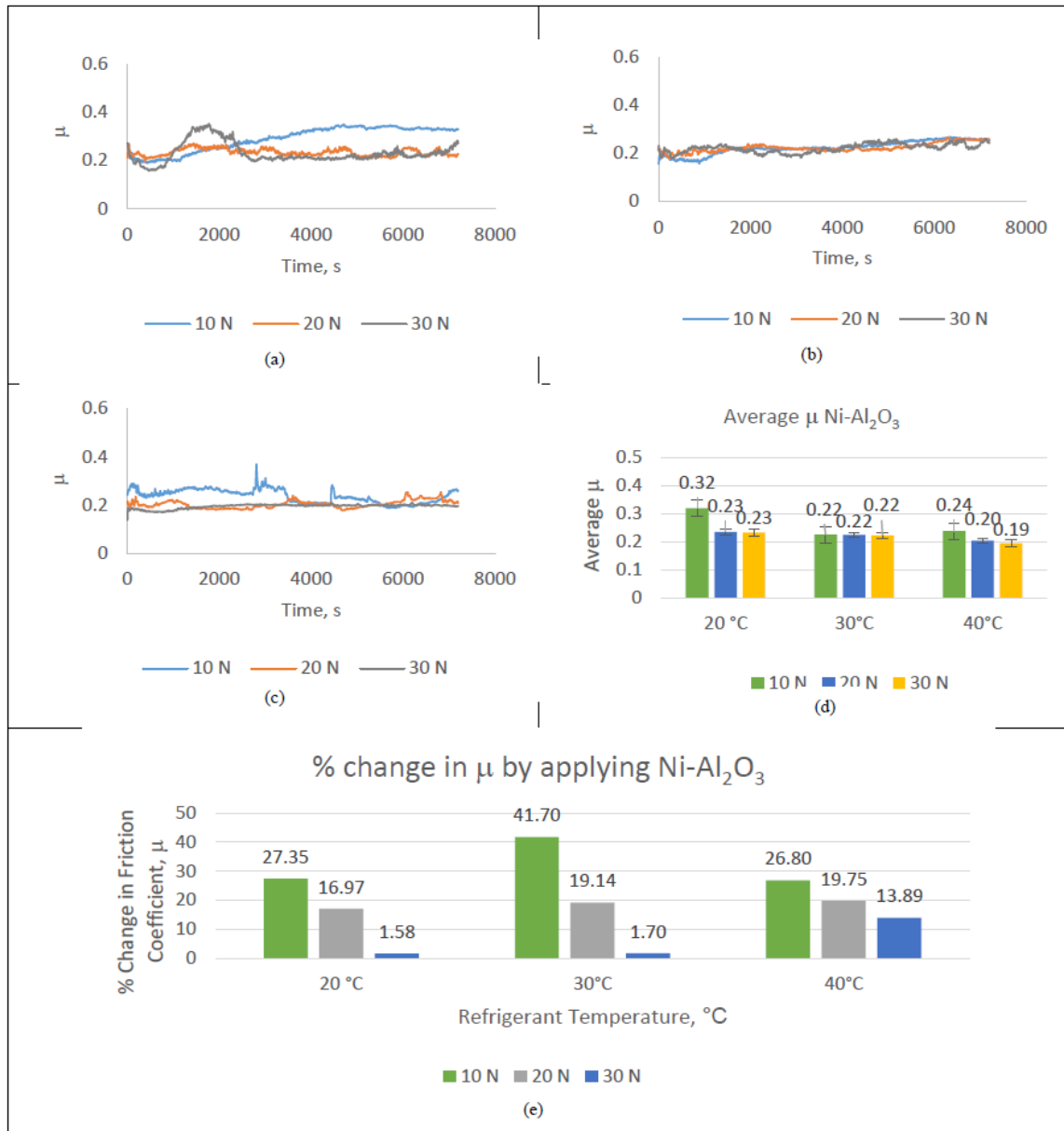
41
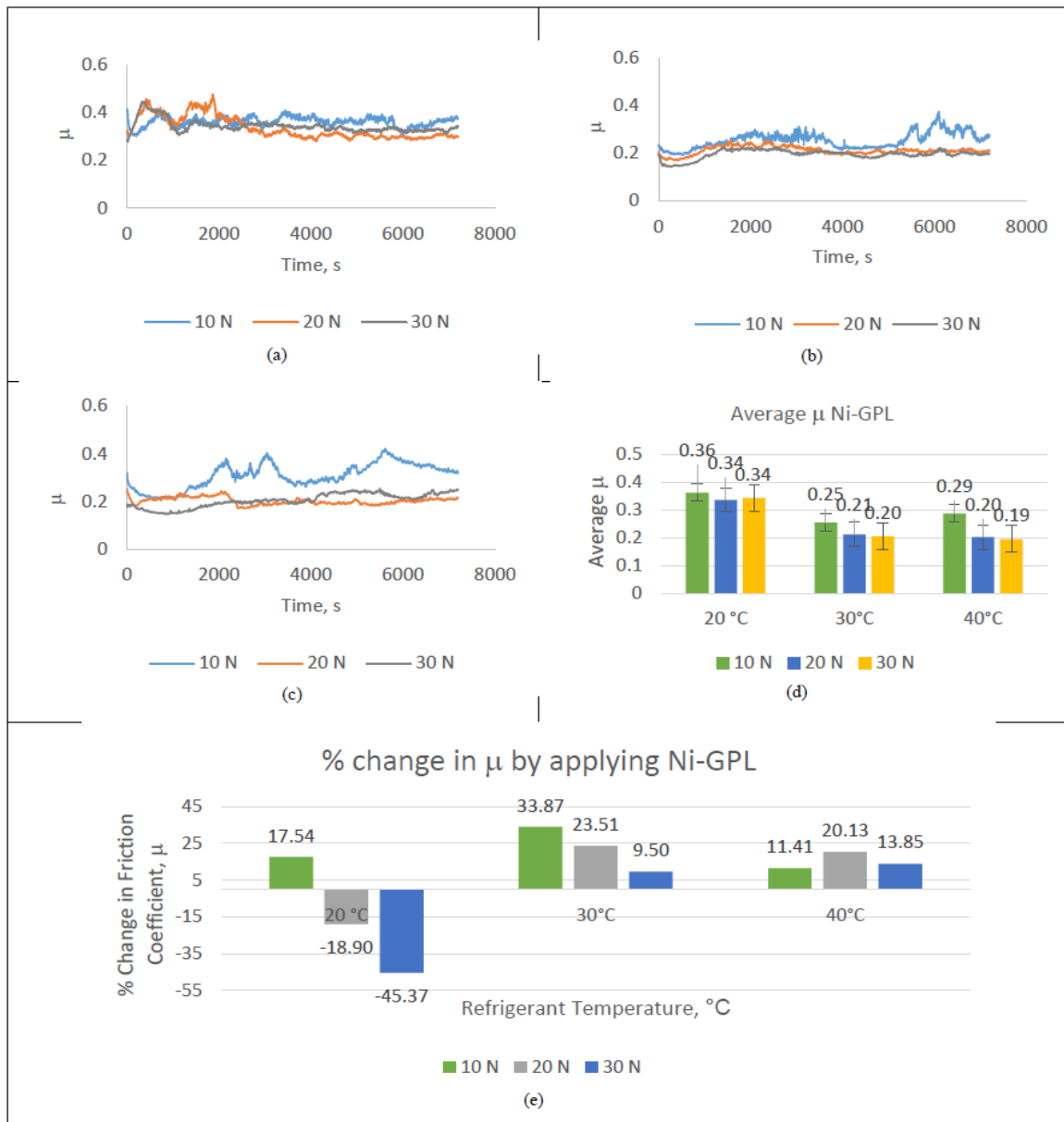
Figure 30: Coefficient of friction graphs for Ni-GPL: Real-time coefficient of friction at refrigerant temperature (a) 20°C (b) 30°C (c) 40°C (d) Average coefficient of friction plot (e) Percentage in average friction coefficient by applying Ni-GPL

Wear and friction coefficient for Nickel-only coatings did not follow the same trend. At 20°C and 40°C wear increases by increasing the load whereas friction coefficient decreases by increasing the applied load at 20°C and 40°C for Nickel-only coatings. For 20°C, parentage change in coefficient of friction drops by increasing the load whereas for 20°C, percentage change in wear increases by increasing the load. At 40°C, percentage change in wear volume decreases with increase in load while percentage change in the friction coefficient increases by increasing the load. Wear volume results improved at all the testing conditions by applying Nickel-only coatings whereas two of the testing conditions increased friction coefficient for Nickel-only coatings.

42

Figure 31: Coefficient of friction graphs for Nickel-only: Real-time coefficient of friction at refrigerant temperature (a) 20°C (b) 30°C (c) 40°C (d) Average coefficient of friction plot (e) Percentage in average friction coefficient by applying Nickel-only

An improvement in the coefficient of friction was observed by the deposition of nanocomposite coatings for most of the conditions. Cavities and micro-dimpled groves have been known to enhance the tribological behaviour and performance of rubbing parts [48, 49] and pores in Ni-Al$_2$O$_3$ coatings have been reported to retain liquid refrigerant and to improve the lubricity of interacting parts which helps improve wear [24]. All the prepared coatings have micro-pores as shown in figure 1, these micro-pores also help in lubricant retention which reduces friction. The peaks in the real-time coefficient of friction appear due to the variation in the contact area of the counter steel ball. Wear occurs on the steel ball which increases the apparent contact area during the course of a test. The increase in contact area increases the coefficient of friction. The Hertzian diameter of 52100 steel ball

43

is known to increase with increase in wear for a reciprocating/oscillating ball-on-flat contact geometry [50]. The wear scar produced on a 52100 steel ball with a fixed steel ball against a reciprocating disc in a ball-on-flat contact geometry has also been reported to change shape which increases the apparent area of contact and reduces contact pressure [51]. High magnification SEM images of the wear scar generated on the steel ball show that the shape and size of the wear scar changes with a change in loading conditions and by changing the type of coating. Wear scar on a stationary 52100 steel ball loaded against a reciprocating flat sample shifts from circular contact at lower loads to an elliptical contact at higher applied loads [36, 51]. Multiple peaks and sharp gradients were generated at a few of the testing conditions as seen in some of the real-time coefficient of friction graphs. The first peak is due to the initiation of the change in the apparent contact area of the steel ball and the additional peaks indicates a further alteration in the contact area of the ball [36]. Fluctuations and variations in the friction coefficient are believed to be due to the alteration in the area of contact of the steel ball, due to three body abrasive wear caused by the wear debris trapped inside the refrigerant holding cup, due to the uneven formation of surface tribo-films especially at lower loads and due to the adhesion of the worn coatings on the surface of the steel ball; continuous reciprocating motion of the steel ball with adhered particles leads to rise in fluctuations in the friction coefficient.

Formation of oxygen and fluorine containing tribo-films on the mating surfaces by different refrigerants has been known to enhance the tribological i.e. wear, lubricity and friction performance of mating machine parts [7, 23, 24, 52-58]. EDS analysis was performed within the contact region on each and every sample pair tested in this study. EDS results show a clear presence of oxygen and fluorine post experimentation. Pre-test EDS elemental analysis was also done on each of the prepared coatings and also on the steel balls, the results did not show any fluorine. The test chamber was vacuumed before starting any test which leads to the conclusion that the source of fluorine on the surfaces is the refrigerant. Our previous study on uncoated steel contacts showed that the refrigerant HFE-7000 breaks down by the application of reciprocating motion, load, frictional force and heat [36]. The refrigerant then chemically reacts with the dangling bonds on the freshly exposed metallic surfaces of the steel samples leading to the production of tribo-films [36]. Similar to the uncoated steel discs, HFE-7000 reacted with the coated specimens as F and O were detected at different regions on the wear scar and also on the ball samples. The results also show a decline in friction coefficient and wear for the same applied load at higher refrigerant temperatures. This decrease in wear and friction is because of the increase in reactivity of HFE-7000 with increase in temperature as more oxygen and fluorine was detected at elevated refrigerant temperatures.

Conclusions

A modified and commissioned micro-fiction that is fully capable of testing the future generation of environmentally friendly refrigerants was used to assess the performance of nickel based nanocomposite coatings under HFE-7000 refrigerant by using fully lubricated conditions. Normal load was applied through a stationary steel ball to coated samples under reciprocating motion. The results of friction and wear by using nanocomposite coatings were compared to uncoated contacts in an attempt to enhance the tribological performance of rubbing parts utilizing HFE-7000. Following conclusions can be drawn from this study.

1. Friction and wear of nickel based coatings applied on a steel substrate under HFE-7000 lubrication is not straightforward. A mix of micro-delamination, micro-cutting and micro-ploughing was observed on the worn surfaces. Wear mechanism was seen to change with a change in coating and also with a change in testing conditions.

44

2. Deposition of Nickel based coatings on a steel substrate through the pulse coating technique resulted in an improvement in the surface mechanical properties of *all* the prepared coatings. The hardness and the hardness to elastic modulus ratio is improved for all coatings. Ni-GPL nanocomposite coatings showed the highest hardness which was followed by Ni-Al$_2$O$_3$, Ni-SiC, Ni-ZrO$_2$ and Nickel. Nickel-only coatings showed the least values of micro-hardness as it did not contain the hard nanoparticles imbedded in its matrix. Ni-Al$_2$O$_3$ nanocomposite coatings showed the best (H/E) ratio along with the best surface roughness values while Ni-GPL coatings presented the worst values of surface roughness.

3. Different coatings behaved differently under the same testing conditions.

   a) Ni-Al$_2$O$_3$ nanocomposite coatings showed the best performance in terms of coefficient of friction in comparison to all the other coatings. Testing conditions of 30°C/10 N showed an improvement of over 40% in the coefficient of friction in comparison to uncoated steel. Wear results showed an improvement of over 90% in wear at low loads by applying Ni-Al$_2$O$_3$ coatings, none of the other coatings showed such an improvement at any of the testing condition. Some of the conditions did result in an increase in wear which is because of the delamination of these coatings. However it can be stated with confidence that Ni-Al$_2$O$_3$ nanocomposite coatings are most suitable for improving both friction and wear at low loads at a range of operating temperatures.

   b) Ni-SiC coatings proved to be beneficial in improving wear in comparison to uncoated steel at all testing conditions. Only a slight improvement of 1% was observed at 20°C/20 N, other than that all other testing conditions improved wear by at least 15%. Highest improvement was observed at 40°C/30 N, 40°C in general proved to be beneficial in improving wear. Friction coefficient also reduced by using Ni-SiC in comparison to uncoated steel at all the testing conditions except for 20°C/30 N and 40°C/10 N, these two conditions increased the friction coefficient but only by less than 1%. Maximum reduction in friction coefficient was observed at 30°C/20 N. This leads to the conclusion that Ni-SiC nanocomposite coatings are beneficial in enhancing the tribological performance of rubbing parts in comparison to uncoated steel.

   c) Ni-ZrO$_2$ coatings displayed the best results of wear at 40°C refrigerant temperature. None of the other coatings showed such an improvement i.e. an improvement of over 64% at all loads at 40°C. Maximum improvement in wear was observed at 40°C/10 N and the results also show an improvement in wear at all testing conditions. The results of friction coefficient however show an increase in friction coefficient by almost 1% at 20°C/20 N and by about 4% at 30°C/10 N. All other testing conditions show an improvement in friction coefficient by using Ni-ZrO$_2$ coatings and maximum improvement in friction coefficient was observed at 20°C/10 N. It can be inferred from these results that Ni-ZrO$_2$ coatings are extremely beneficial in reducing wear in comparison to uncoated steel. These coatings can be used with assurance at higher operating temperatures at which not only a substantial reduction in wear was observed but also higher refrigerant temperature resulted in a drop in friction coefficient.

   d) Ni-GPL nanocomposite coatings showed the worst results in terms of friction and wear at lower refrigerant temperature of 20°. The poor performance of Nickel-Graphene coatings is believed to be due the incompatibility of these coatings with HEF-7000. Graphene has large surface area which is rich in fast moving mobile electrons and HEF-7000 is polar in nature. Higher wear at low loads is believed to

45

be due to the ejection of graphene from the surface by the polar refrigerant. Increase in load helps retain Graphene in the Nickel matrix. An increase in refrigerant temperature proves to be extremely helpful in reducing the coefficient of friction. A decrease in the coefficient of friction almost by 34% can be seen at 30°C/10 N. 30°C refrigerant temperature however does not show a substantial improvement in wear and 30°C/20 N conditions resulted in an increase in wear in comparison to the uncoated steel. Refrigerant temperature of 40°C however proved to be extremely helpful in not only reducing friction but also in reducing wear. Wear volume dropped by about 70% at 40°C/10 N and by almost 50% at 40°C/30 N. From these results it can be seen that one has to be extremely careful in using Ni-GPL nanocomposite coatings in systems utilizing HFE-7000. At higher operating temperatures these coatings can be used but if a system is operating at varying load and changing refrigerant temperatures then Ni-GPL coatings would not be recommended.

e) Nickel-only coatings resulted in an improvement in the micro-hardness, (H/E) ratio and average surface roughness in comparison to uncoated steel. This helped improve wear at all the operating conditions. Minimum improvement in wear was noticed at 20°C/10 N and maximum improvement in wear occurred at 40°C/10 N. Nickel-only coatings did not contain the hard nanoparticles in the nickel matrix, these hard nanoparticles are believed to increase wear by three body abrasive wear phenomenon when using nanocomposites. Friction coefficient results show a decrease in the coefficient of friction values at 40°C for all loads. A slight increase in friction coefficient was however observed at 20°C/30 N and 30°C/30 N in comparison to uncoated steel. Nickel-only coatings also show very good results especially for wear improvement and these coatings can be recommended for use in HFE-7000 based systems.

4. Friction and wear of Nickel based coatings under HFE-7000 lubrication is a complex mix of different mechanisms which is not only determined by the type of coating but is also highly dependent on the reaction of the refrigerant with the metallic surfaces. Application of load, heat, friction and mechanical motion results in the breakdown of HFE-7000. HFE-7000 breaks and forms new bonds with the freshly exposed worn surfaces. This results in the formation of oxygenated and fluorinated surface films on the top surfaces. These tribo-films results in a drop in friction and wear.

5. It is believed that the nano-particles embedded in the Nickel matrix hinder the development of anti-wear tribo-films and pure metal surfaces are more favourable in the tribo-chemical reaction between the refrigerant and the mating surfaces

6. A general trend in the reduction in wear with increase in refrigerant temperature and a decrease in friction coefficient with increase in applied normal load and temperature can be observed from the results presented in this study. This is due to the increase in reactivity of HFE-7000 with the interacting metals with increase in temperature and load.

7. Nanocomposite coatings show a clear improvement in friction and wear at most of the testing conditions. Selection of a particular coating depends on load and operating temperature.

Acknowledgments:

References

[1] Calm JM. The next generation of refrigerants – Historical review, considerations, and outlook. La prochaine génération de frigorigènes – historique, analyse et perspectives. 2008;31:1123-33.

[2] Bhutta MU, Khan ZA, Garland NP, Ghafoor A. A Historical Review on the Tribological Performance of Refrigerants used in Compressors. Tribo Indu. 2018;40:19-51.

[3] Nations U. Montreal Protocol on Substances that Deplete the Ozone Layer. United Nations Environment Programme. Montreal, Canada16 September 1987.

[4] Breidenich C, Magraw D, Rowley A, Rubin JW. The Kyoto protocol to the United Nations framework convention on climate change. Ame J Inter Law. 1998;92:315-31.

[5] Wu X, Cong P, Nanao H, Minami I, Mori S. Tribological behaviors of 52100 steel in carbon dioxide atmosphere. Tribo Lett. 2004;17:925-30.

[6] Demas NG, Polycarpou AA. Ultra high pressure tribometer for testing CO_2 refrigerant at chamber pressures up to 2000 psi to simulate compressor conditions. Tribo Trans. 2006;49:291-6.

[7] Jeon H-G, Oh S-D, Lee Y-Z. Friction and wear of the lubricated vane and roller materials in a carbon dioxide refrigerant. Wear. 2009;267:1252-6.

[8] Nunez EE, Polycarpou AA. Wear study of metallic interfaces for air-conditioning compressors under submerged lubrication in the presence of carbon dioxide. Wear. 2015;326-327:28-35.

[9] Nunez EE, Demas NG, Polychronopoulou K, Polycarpou AA. Comparative scuffing performance and chemical analysis of metallic surfaces for air-conditioning compressors in the presence of environmentally friendly CO_2 refrigerant. Wear. 2010;268:668-76.

[10] Demas NG, Polycarpou AA. Tribological investigation of cast iron air-conditioning compressor surfaces in CO_2 refrigerant. Tribo Lett. 2006;22:271-8.

[11] Garland N, Hadfield M. Environmental implications of hydrocarbon refrigerants applied to the hermetic compressor. Materi Desig. 2005;26:578-86.

[12] Khan ZA, Hadfield M, Tobe S, Wang Y. Ceramic rolling elements with ring crack defects—A residual stress approach. Mater Sci Eng: A. 2005;404:221-6.

[13] Khan ZA, Hadfield M, Tobe S, Wang Y. Residual stress variations during rolling contact fatigue of refrigerant lubricated silicon nitride bearing elements. Ceram Inter. 2006;32:751-4.

[14] Khan ZA, Hadfield M. Manufacturing induced residual stress influence on the rolling contact fatigue life performance of lubricated silicon nitride bearing materials. Materi Desig. 2007;28:2688-93.

[15] Sariibrahimoglu K, Kizil H, Aksit MF, Efeoglu I, Kerpicci H. Effect of R600a on tribological behavior of sintered steel under starved lubrication. Tribo Inter. 2010;43:1054-8.

[16] Górny K, Stachowiak A, Tyczewski P, Zwierzycki W. Lubricity evaluation of oil–refrigerant mixtures with R134a and R290. Inter J Refrig. 2016;69:261-71.

[17] 3M. ™ Novec™ 7000 Engineered Fluid Data sheet, https://multimedia.3m.com/mws/media/121372O/3m-novec-7000-engineered-fluid-tds.pdf3M (accessed on 17 February 2019).

[18] Helvaci H, Khan ZA. Experimental study of thermodynamic assessment of a small scale solar thermal system. Ener Conv Manage. 2016;117:567-76.

[19] Helvaci HU, Khan ZA. Heat transfer and entropy generation analysis of HFE 7000 based nanorefrigerants. Inter J Heat Mass Trans. 2017;104:318-27.

[20] Helvaci H, Khan Z. Thermodynamic modelling and analysis of a solar organic Rankine cycle employing thermofluids. Ener Conv Manage. 2017;138:493-510.

[21] Blaineau B, Dutour S, Callegari T, Lavieille P, Miscevic M, Blanco S, et al. Experimental investigation of a dielectric liquid-vapor interface between two vertical planar electrodes: Influence of the DC electric field and temperature. Experimental Thermal and Fluid Science. 2019;105:144-52.

[22] Shin J-H, Rozenfeld T, Shockner T, Kumar Vutha A, Wang Y, Ziskind G, et al. Local heat transfer under an array of micro jet impingement using HFE-7000. Applied Thermal Engineering. 2019:113716.

47

[23] Akram MW, Polychronopoulou K, Polycarpou AA. Lubricity of environmentally friendly HFO-1234yf refrigerant. Tribo Inter. 2013;57:92-100.

[24] Bhutta M, Khan Z, Garland N. Wear Performance Analysis of Ni–Al_2O_3 Nanocomposite Coatings under Nonconventional Lubrication. Materials. 2018;12:36.

[25] ipcc. The Intergovernmental Panel on Climate Change, Global Warming Potential Values, https://www.ghgprotocol.org/sites/default/files/ghgp/Global-Warming-Potential-Values%20%28Feb%2016%202016%29_1.pdf (accessed on 17 February 2019).

[26] Chen L, Wang L, Zeng Z, Xu T. Influence of pulse frequency on the microstructure and wear resistance of electrodeposited Ni–Al_2O_3 composite coatings. Surf Coati Tech. 2006;201:599-605.

[27] Chen L, Wang L, Zeng Z, Zhang J. Effect of surfactant on the electrodeposition and wear resistance of Ni–Al_2O_3 composite coatings. Mater Sci Eng: A. 2006;434:319-25.

[28] Zhou Q, He CL, Cai QK. Effect of Al_2O_3 Powders on Properties of Electrodeposited Ni Matrix. Adv Mat Res. 2009;79-82:631-4.

[29] Saha RK, Khan TI. Effect of applied current on the electrodeposited Ni–Al_2O_3 composite coatings. Surf Coati Tech. 2010;205:890-5.

[30] Borkar T, Harimkar SP. Effect of electrodeposition conditions and reinforcement content on microstructure and tribological properties of nickel composite coatings. Surf Coati Tech. 2011;205:4124-34.

[31] Bajwa R, Khan Z, Nazir H, Chacko V, Saeed A. Wear and Friction Properties of Electrodeposited Ni-Based Coatings Subject to Nano-enhanced Lubricant and Composite Coating. Acta Metal Sin (Eng Lett). 2016;29:902-10.

[32] Bajwa RS, Khan Z, Bakolas V, Braun W. Water-lubricated Ni-based composite (Ni–Al_2O_3, Ni–SiC and Ni–ZrO_2) thin film coatings for industrial applications. Acta Metal Sin (Eng Lett). 2016;29:8–16.

[33] Nazir MH, Khan ZA, Saeed A, Bakolas V, Braun W, Bajwa R, et al. Analyzing and Modelling the Corrosion Behavior of Ni/Al_2O_3, Ni/SiC, Ni/ZrO_2 and Ni/Graphene Nanocomposite Coatings. Materials. 2017;10:1225.

[34] Nazir MH, Khan ZA, Saeed A, Bakolas V, Braun W, Bajwa R. Experimental analysis and modelling for reciprocating wear behaviour of nanocomposite coatings. Wear. 2018;416-417:89-102.

[35] Kasar AK, Bhutta MU, Khan ZA, Menezes PL. Corrosion performance of nanocomposite coatings in moist SO_2 environment. The International Journal of Advanced Manufacturing Technology. 2020.

[36] Bhutta MU, Khan ZA. Friction and wear performance analysis of hydrofluoroether-7000 refrigerant. Tribo Inter. 2019;139:36-54.

[37] Bhutta MU, Khan ZA, Garland N. Novel experimental setup to assess surfaces in tribo-contact lubricated by the next generation of environmentally friendly thermofluids. International Journal of Computational Methods and Experimental Measurements. 2019;7:226-35.

[38] Bajwa RS, Khan Z, Bakolas V, Braun W. Effect of bath ionic strength on adhesion and tribological properties of pure nickel and Ni-based nanocomposite coatings. J Adhes Sci Tech. 2016;30:653-65.

[39] Algul H, Tokur M, Ozcan S, Uysal M, Cetinkaya T, Akbulut H, et al. The effect of graphene content and sliding speed on the wear mechanism of nickel–graphene nanocomposites. App Surf Sci. 2015;359:340-8.

[40] Jabbar A, Yasin G, Khan WQ, Anwar MY, Korai RM, Nizam MN, et al. Electrochemical deposition of nickel graphene composite coatings: effect of deposition temperature on its surface morphology and corrosion resistance. 2017;7:31100-9.

[41] Gu G, Wu Z, Zhang Z, Qing F. Tribological properties of fluorine-containing additives of silicone oil. Tribo Inter. 2009;42:397-402.

[42] Muraki M, Sano T, Dong D. Elastohydrodynamic properties and boundary lubrication performance of polyolester in a hydrofluoroether refrigerant environment. Proc Instit Mech Engs Prt J: J Eng Tribo. 2002;216:19-26.

[43] Lide DR. CRC handbook of chemistry and physics, : CRC Press, Boca Raton, Florida; 73rd edition, 1992-1993, pp. 9-145.

48

[44] Tsai W-T. Environmental risk assessment of hydrofluoroethers (HFEs). Journal of Hazardous Materials. 2005;119:69-78.

[45] Brownson DAC, Banks CE. Graphene electrochemistry: an overview of potential applications. Analyst. 2010;135:2768-78.

[46] Kang X, Wang J, Wu H, Liu J, Aksay IA, Lin Y. A graphene-based electrochemical sensor for sensitive detection of paracetamol. Talanta. 2010;81:754-9.

[47] Liu C, Alwarappan S, Chen Z, Kong X, Li C-Z. Membraneless enzymatic biofuel cells based on graphene nanosheets. Biosensors and Bioelectronics. 2010;25:1829-33.

[48] Abdullah MU, Shah SR, Bhutta MU, Mufti RA, Khurram M, Najeeb MH, et al. Benefits of wonder process craft on engine valve train performance. Proc Instit Mech Engs Prt D: J Auto Eng. 2018.

[49] Bai L, Meng Y, Khan ZA, Zhang V. The Synergetic Effects of Surface Texturing and MoDDP Additive Applied to Ball-on-Disk Friction Subject to Both Flooded and Starved Lubrication Conditions. Tribo Lett. 2017;65:163.

[50] Deshpande P, Minfray C, Dassenoy F, Thiebaut B, Le Mogne T, Vacher B, et al. Tribological behaviour of TiO2 Atmospheric Plasma Spray (APS) coating under mixed and boundary lubrication conditions in presence of oil containing MoDTC. Tribo Inter. 2018;118:273-86.

[51] Jean-Fulcrand A, Masen MA, Bremner T, Wong JSS. High temperature tribological properties of polybenzimidazole (PBI). Polymer. 2017;128:159-68.

[52] Mizuhara K, Akei M, Matsuzaki T. The friction and wear behavior in controlled alternative refrigerant atmosphere. Tribo Trans. 1994;37:120-8.

[53] Kawahara K, Mishina S, Kamino A, Ochiai K, Okawa T, Fujimoto S. Tribological Evaluation of Rotary Compressor with HFC Refrigerants. International Compressor Engineering ConferencePurdue University, Indiana, USA, 23-26 July, 1996, Paper 1141.

[54] Tatsuya Sasaki HN, Hideaki Maeyama, Kota Mizuno. Tribology Characteristics of HFO and HC Refrigerants with Immiscible Oils - Effect of Refrigerant with Unsaturated Bond. International Compressor Engineering ConferencePurdue University, Indiana, USA, 12-15 July, 2010, Paper 1946.

[55] Akram MW, Polychronopoulou K, Seeton C, Polycarpou AA. Tribological performance of environmentally friendly refrigerant HFO-1234yf under starved lubricated conditions. Wear. 2013;304:191-201.

[56] Akram MW, Polychronopoulou K, Polycarpou AA. Tribological performance comparing different refrigerant–lubricant systems: The case of environmentally friendly HFO-1234yf refrigerant. Tribo Inter. 2014;78:176-86.

[57] Nunez EE, Polychronopoulou K, Polycarpou AA. Lubricity effect of carbon dioxide used as an environmentally friendly refrigerant in air-conditioning and refrigeration compressors. Wear. 2010;270:46-56.

[58] Cannaday M, Polycarpou A. Advantages of CO_2 compared to R410a refrigerant of tribologically tested Aluminum 390-T6 surfaces. Tribo Lett. 2006;21:185-92.

49

Paper VI

ORIGINAL ARTICLE

Corrosion performance of nanocomposite coatings in moist SO$_2$ environment

Ashish K. Kasar [1] · Muhammad U. Bhutta [2] · Zulfiqar A. Khan [2] · Pradeep L. Menezes [1]

Abstract

This paper presents a study of corrosion behavior of electrodeposited Ni, Ni-Al$_2$O$_3$, Ni-ZrO$_2$, and Ni-graphene (Gr) coatings in moist SO$_2$ environment. Nanocomposite coatings were deposited on steel substrate by pulse electrodeposition technique with an average thickness of 9 ± 1 μm. Coatings were characterized by using nanoindentation and scratch tests to measure their mechanical properties prior to conducting corrosion tests. The corrosion resistance of coatings was evaluated according to G87–02 Method B, employing SO$_2$ cyclic spray in the presence of moisture followed by drying. The results indicated that the addition of nanoparticles is beneficial both for enhancing mechanical properties and improving the corrosion resistance of these coatings. Higher surface corrosion resistance was observed for Ni-Gr coating. Corrosion behavior of coating was also quantified by open circuit potential measurement in 0.5 M H$_2$SO$_4$ environment. The results suggest that the nanocomposite Ni coatings have improved corrosion resistance compared to pure Ni coating. This work will bring significant impacts in terms of industrial applications such as architectural, automotive, and marine industries in the presence of S-pollutants because it can cause corrosion either due to acid rain or by the reaction of moisture with dry deposition of sulfur.

Keywords Electrodeposition · Ni coating · Nanocomposite coating · Moist SO$_2$ environment

1 Introduction

Ni coatings are mainly applied for protection against corrosion, erosion, and abrasion. Ni coating by electrodeposition method is one of the most technologically and economically suitable techniques. Electrodeposition can be performed in three ways: (i) direct current (DC), (ii) pulse current (PC), and (iii) pulse reverse current (PRC) electrodeposition. The coating developed by DC electrodeposition suffers from poor adhesion, porosity, and undesirable microstructure defects, whereas PC and PRC provide better physical, mechanical, and corrosion properties [1–3]. Additionally, pulse electrodeposition technique can also

✉ Pradeep L. Menezes
  pmenezes@unr.edu

  Zulfiqar A. Khan
  zkhan@bournemouth.ac.uk

[1] Department of Mechanical Engineering, University of Nevada, Reno, NV 89557, USA

[2] NanoCorr, Energy and Modelling (NCEM) Research Group, Department of Design and Engineering, Bournemouth University Talbot Campus, Poole, Dorset BH12 5BB, UK

be used for deposition of composite coatings. Electrodeposition of composite involves co-deposition of various micro- or nanometallic, nonmetallic, or polymer particles within the electrolytic bath with suitable electroplating conditions. Quality of nanocoating is mainly governed by pulse physical parameters, nanoconstituents, substrate roughness, and coating thickness.

Corrosion failure of coatings combined with wear has been studied recently to develop synergistic wear-corrosion models for prediction of coating failures. Recently reported models [4] attempt to predict wear-corrosion in bulk materials or metals only; therefore, these models lack the capacity to predict the performance of nanocomposite coatings subject to wear and corrosion during their applications. It has been always remained the key issue to predict the precise role of Eigen-stresses, grain size, porosity, and thermal mismatch of nanocomposites, as intrinsic nanomechanics parameters in synergistic wear-corrosion phenomenon [4]. Following from the above rationale and its significance, a unified Khan-Nazir II numerical model has been developed and reported [4]. Interfacial characteristics have been studied recently and have suggested that interfacial strength between Ni coating and the substrate can be obtained by controlling interface roughness and coating thickness [5]. The influence of Ni ion

Table 1 Properties of electrodeposited Ni-nanocomposite coatings

Coating	Particle size	Mechanical properties	Electrochemical properties	Reference
Ni-SiC	SiC: 1.2 μm	Knoop hardness = 900 (4.5 times higher than the steel substrate)	–	[7]
Ni-SiC	SiC: 20 nm	Friction coefficient (μ) of composite coating = 0.25, μ of Ni = 0.35	Corrosion potential (E_{corr}) of composite coating = −212.5, (E_{corr} of pure Ni = −281.6) in 0.5 M Na_2SO_4	[8]
Ni-SiC	SiC: 50 nm	Microhardness (HV) of composite coating = 720, HV of pure Ni = 540	E_{corr} of composite coating = ~0.35 V, E_{corr} of pure Ni = 0.45 V in 0.5 M NaCl solution	[9]
Ni-Al_2O_3	Al_2O_3: 0.6 μm	HV of composite coating ~525, HV of pure Ni ~375	–	[10]
Ni-carbon nanotube (CNT)	–	HV of composite coating = 600, HV of pure Ni = 300	–	[11]
Ni-CNT	–	–	E_{corr} of composite coating = −0.55 V, E_{corr} of Ni ~0.48 V in 3.5 wt.% NaCl	[12]
Ni-ZrO_2	ZrO_2: 10 μm	HV of composite coating 1100, HV of pure Ni ~210.	E_{corr} of composite coating = −0.34 V in 0.5 M K_2SO_4	[13]
Ni-graphene (Gr)	–	HV of composite coating ~375, HV of Ni ~275	E_{corr} of composite coating = −0.398 V, E_{corr} of pure Ni = −0.492 V in 3.5 wt.% NaCl	[14]
Ni- Al_2O_3, Ni-SiC, and Ni-ZrO_2	–	HV for composites: Ni-Al_2O_3 = 380, Ni-SiC = 500, ZrO_2 = 400, and for pure Ni = 450	–	[15]

concentration has also been observed to evaluate its effects on the tribological and corrosion properties of pure Ni and Ni-Al_2O_3 composite coating due to surface roughness and wettability [6]. Some of the Ni composite coatings and their properties are listed in Table 1.

From Table 1, it can be seen that micro-nano particles improve both mechanical properties and enhance corrosion properties. Extensive work on nanocoating failure, prediction, and prognosis have been conducted at NanoCorr, Energy and Modeling Research Group, UK [16]. A comprehensive study of thin coating-substrate system deterioration enhanced by a combination of fracture and corrosion has been reported and modeled as Khan-Nazir I model [16, 17]. This study provides an understanding of bi-material characteristics of coatings, mixed mode interfacial cracks, and combination of mechanics and diffusion concepts within the context of corrosive degradation. Wear-corrosion synergistic model Khan-Nazir II has been reported, which provides more accurate prediction

compared to the conventional model, which were reported earlier [4]. Modeling of metal coating failure due to environmental factors has been published in [18]. Corrosion behavior of several Ni-based nanocomposite coating to include Ni-Al_2O_3, Ni-SiC, Ni-ZrO_2, and Ni-graphene has been reported [19]. Recently, mathematical models have been developed for the prediction of uniform corrosion rate of structural steel subjected to acid rain and low pH conditions; the study investigated corrosion performance of steel in moist sulfur dioxide environment [20]. Lopez et al. [21] tested the electrodeposited Ni-Samarium (Sm) coating in NaCl environment as per ASTM B117 and ISO 10289 standards. Authors reported 6000 h of salt spray exposure time without any corrosion in the presence of 34.6 mM of Sm^{3+}.

Table 2 Chemical and nanoparticle composition of bath for electrodeposition of Ni and Ni-nanocomposite coatings

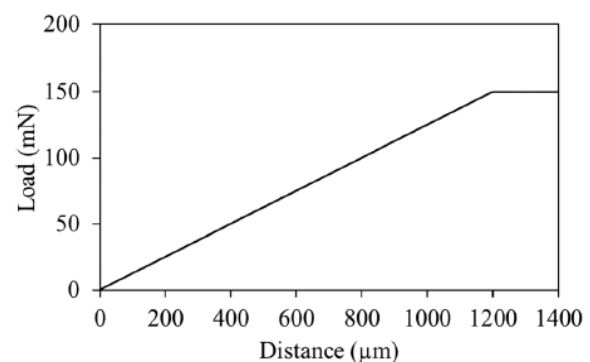| Coating	Chemical composition (g/L)			
	Nickel sulfate	Nickel chloride	Boric acid	Nanoparticles
Ni	265	48	31	–
Ni-Al_2O_3	265	48	31	20
Ni-ZrO_2	265	48	31	20
Ni-Gr	265	48	31	0.1

Fig. 1 Loading profile during scratch tests on coatings using spherical indenter

Fig. 2 Ni and Ni-nanocomposite-coated steel samples during moist SO$_2$ exposure tests

However, these coatings have not been tested in moist air containing SO$_2$, which is a major air pollutant and causes aggressive corrosion due to catalytic effect of iron oxide and hydroxide on the formation of H$_2$SO$_4$ from SO$_2$, H$_2$O, and O$_2$. Limited accelerated corrosion studies have been conducted to assess nanocoating in moist SO$_2$ environment. Therefore, it is important to study the corrosion behavior of Ni-nanocomposite coatings in moist SO$_2$ environment for real-world applications such as automotive, architecture, and marine applications where S-pollutants can cause corrosion due to formation of sulfuric/sulfurous acids either by acid rain or by reaction between moisture and dry deposition of sulfur.

The present work is aimed to evaluate the corrosion behavior of electrodeposited Ni-nanocomposite coatings in moist SO$_2$ environment. This paper presents a detailed experimental study of four various types of nanocomposite coatings: Ni, Ni/Al$_2$O$_3$, Ni/ZrO$_2$, and Ni/Graphene (Gr). ASTM Standard G87–02 Method B has been applied during the investigation of the nanocoatings mentioned above. Corrosion behavior of these coatings was also monitored by using open circuit potential (OCP) in H$_2$SO$_4$ environment. These coatings were analyzed by using surface characterization methods, including scanning electron microscopy

(SEM), energy-dispersive X-ray spectroscopy (EDS), and nanohardness testing.

2 Experimental procedure

2.1 Coating preparation

Pure Ni, Ni-Gr, Ni-ZrO$_2$, and Ni–Al$_2$O$_3$ nanocomposite coatings (9 ± 1 μm in thickness) were produced by pulse electrodeposition method. Prior to coating, steel substrates were conditioned with acetone by ultrasonication for 5 min, followed by rinsing with deionized water. For electrodeposition, pulse current condition was controlled by using a pulse interface connected to pulse power supply. Pulse current conditions were kept as current density 3 A/dm^2, pulse on/off time (20–80 ms), and a duty cycle of 20%. An optimized Watt's bath chemical composition was used for the deposition process as listed in Table 2 [6]. For the development of nanoenhanced composite coating, Gr platelets (6–8 nm), ZrO$_2$ (30–40 nm), and Al$_2$O$_3$ (50–60 nm) nanoparticles were added into an electroplating bath that was under continuous magnetic stirring process. Moreover, to ensure better suspension of particles, the chemical solution was ultrasonically stirred

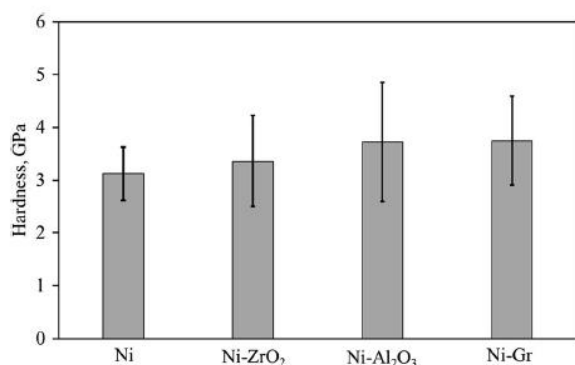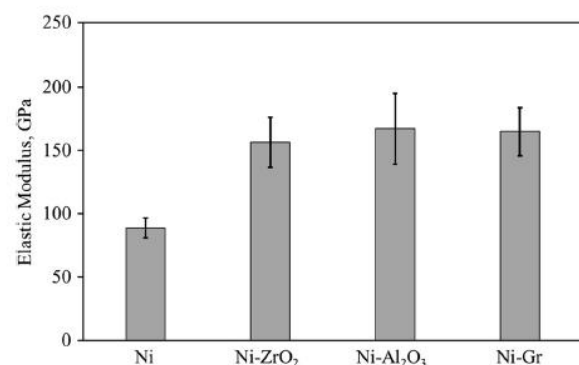**Fig. 3** The hardness of the electrodeposited Ni and Ni-nanocomposite film by nanoindentation using Berkovich indenter

Fig. 4 Elastic modulus of the electrodeposited Ni and Ni-nanocomposite film by nanoindentation using Berkovich indenter
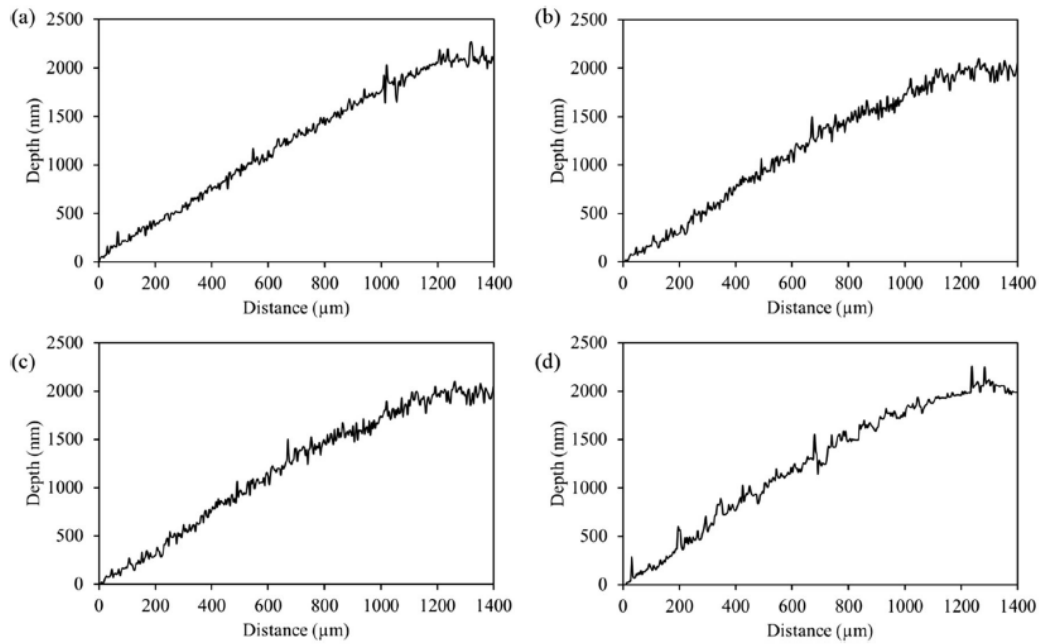
Fig. 5 Scratch test profile on (**a**) Ni, (**b**) Ni-ZrO$_2$, (**c**) Ni-Al$_2$O$_3$, and (**d**) Ni-Gr using a spherical indenter with a gradual increase in load up to 150 mN

during the deposition process. A nickel sheet of 99.99% purity (Wieland Edelmetalle GmbH, Germany) was used as an anode, and a section of steel circular plate was coated while using it as a cathode. Standard surface conditioning was deployed before the coating development process. Flat plate samples with a surface area of 0.09 dm^2 was mechanically polished to an average roughness of 0.05 μm and ultrasonically conditioned with ethanol followed by acetone and then coating was conducted. Surface morphology of electrodeposited samples was studied by using a SEM. Elemental analysis was conducted by using an EDS.

2.2 Nanoindentation and scratch test

To determine the hardness of Ni and Ni-nanocomposite thin coating, indentation hardness measurements were conducted. The tests were conducted using a diamond Berkovich tip in a nanoindentation system under depth-controlled setup with a maximum 1-μm displacement. The choice of indentation depth was to utilize 10% of the thickness of the coating to avoid the coating to substrate transitioning hardness measurement. The indentations were made with a dwell period of 10 s at maximum load.

Nanoscratch tests were performed on the coating by using spherical indenter with a gradual increase in load from 0 to 150 mN, and total distance was 1500 μm as shown in Fig. 1.

2.3 Corrosion tests

According to ASTM Standard G87–02 Method B alternating exposure [22], synthetic industrial atmosphere tests in moisture containing SO$_2$ were conducted to quantify the protection provided by the coating. This test is more correctly a porosity test because it finds (and sometimes creates) holes through the coating to the substrate. Testing was conducted in an alternating atmosphere by using a dosing volume of 2000 cm^3 of SO$_2$. The test duration was two cycles, each cycle consisting of 8 h of SO$_2$ exposure at 40 °C ± 3 °C followed by 16 h under ambient conditions. Only the coated sections of the circular steel disc were exposed to a moist SO$_2$
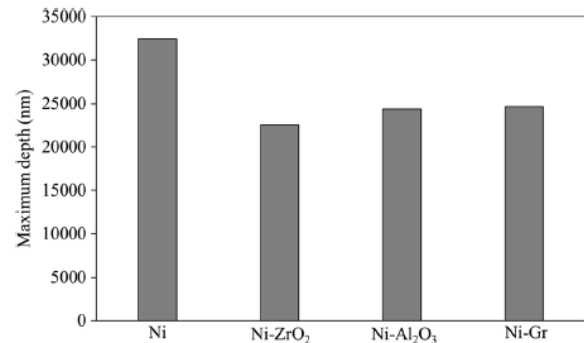

Fig. 6 Maximum scratch depth on Ni-based coatings after two cycles of corrosion tests in moist SO$_2$ environment

environment, and the rest of the steel surface was covered with wax, as shown in Fig. 2.

Corrosion behavior of Ni-nanocomposite coatings was quantitatively measured by open circuit potential (OCP) in 0.5 M H_2SO_4 solution. The OCP was measured by using a three-electrode setup. A graphite electrode was employed as a counter electrode, and a saturated calomel reference electrode (SCE) was used as a reference electrode.

3 Results and discussion

3.1 Nanoscale characterization

Hardness and elastic modulus measured by nanoindentation using a Berkovich indenter are plotted in Figs. 3 and 4, respectively. Due to the addition of the nanoparticles, the mean hardness and elastic modulus have increased significantly compared to pure Ni coating. Ni-Gr was observed to have 3.74 GPa mean hardness, which is the highest among all of the coatings, and it is 19.9% higher than Ni coating. Similarly, mean elastic modulus was ~86% higher for Ni-Gr and Ni-Al_2O_3 as compared to Ni coating.

Scratch resistance of the coating was analyzed using a spherical indenter with a gradual increase in load up to 150 mN. All the four coatings showed a similar trend with ~2000 nm depth after 1500 μm scratch as presented in Fig. 5. However, after two cycles of corrosion tests in moist SO_2 environment, the maximum scratch depth increased by one order of magnitude compared to non-corroded samples. This increase in scratch depth is due to the formation of corrosion products on the surface of the coatings. The maximum scratch depth on the

corroded samples is shown in Fig. 6. The maximum scratch depth of 32 μm was observed for pure Ni coating, whereas nanocomposite Ni coatings yielded a maximum scratch depth of 24–25 μm.

3.2 Surface corrosion

Figure 7 shows the corrosion status of bare steel, Ni, and Ni-nanocomposite coatings before and after two cycles of moist SO_2 exposure. The images of pre- and post-corrosion surface clearly show that the highest surface corrosion on the bare steel surface (Fig. 7(a)), where Ni-ZrO_2 and Ni-Al_2O_3 were observed to have some brown spots that suggest ferrous corrosion. In the case of pure Ni and Ni-Gr coatings, no ferrous corrosion was observed. This behavior is also in good agreement with the accelerated corrosion on these coatings during salt spray testing of 450 h [19], where lowest surface corrosion was observed on Ni-Gr coating.

Pre-corrosion SEM micrographs for all the coating surfaces are shown in Fig. 8 along with their chemical compositions observed by EDS. The EDS spectrum confirms the presence of nanoparticles in the matrix. It also indicates that large particle size in Ni-Al_2O_3 (Fig. 8 (e)) and Ni-ZrO_2 (Fig. 8 (c)) coatings accounted for the large porous structure that can make the surface prone to ferrous corrosion. However, the Ni-Gr coating has the smallest particle size and formed a very smooth coating, which has also been observed in the previous study [19].

Post-corrosion SEM micrographs for the coatings are shown in Fig. 9. It can be observed that all the top surfaces of the coating start breaking into small fragments due to corrosion. Ni-ZrO_2 (Fig. 9 (b)) and Ni-Al_2O_3 (Fig. 9 (c)) coatings were observed to have smaller fragments compared to Ni and Ni-Gr coating. Smaller fragments have larger surface fraction
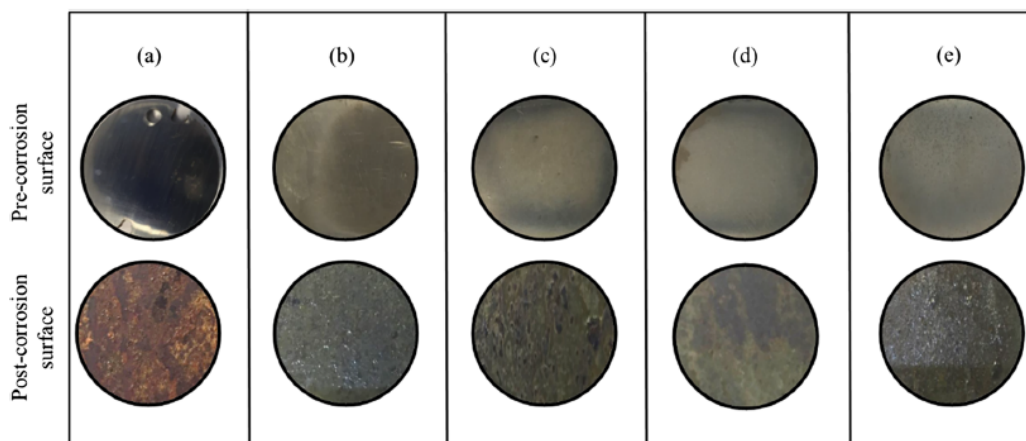
Fig. 7 Pre- and post-corrosion status of (**a**) bare steel, (**b**) Ni, (**c**) Ni-ZrO_2, (**d**) Ni-Al_2O_3, and (**e**) Ni-Gr electrodeposited coatings
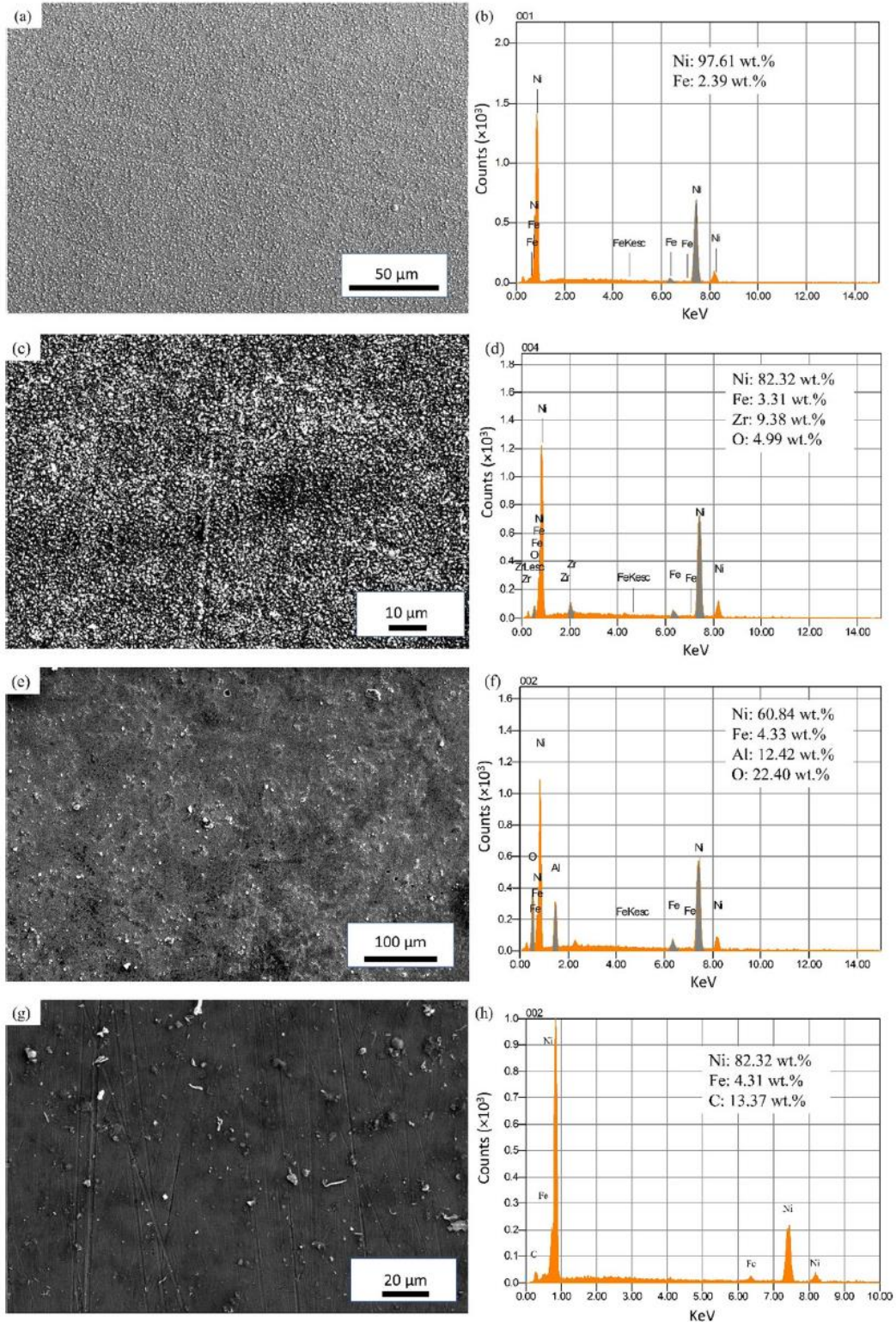
Fig. 8 Pre-corrosion surface morphology of (**a**) Ni, (**c**) Ni-ZrO$_2$, (**e**) Ni-Al$_2$O$_3$ and (**g**) Ni-Gr with chemical composition observed by EDS

Table 3 Amount and cost of nanoparticles for 10 μm thick coating over 1 × 1 m²

Material	Density (g/cm³)	Cost (USD/kg)	Amount of material required (g)	Cost for required weight (USD)
Al₂O₃	3.95	150 [28]	3.95–11.85	1.77
ZrO₂	5.68	200 [28]	5.68–17.04	3.04
Gr	2.26	220 [29]	2.26–6.80	1.49

lower surface corrosion was observed for Ni-Gr followed by Ni-ZrO₂, Ni-Al₂O₃, and pure Ni. The OCP of Ni-Gr and Ni-Al₂O₃ is more positive than that of pure Ni; it suggests improved corrosion resistance.

References

1. Qu N, Zhu D, Chan K, Lei W (2003) Pulse electrodeposition of nanocrystalline nickel using ultra narrow pulse width and high peak current density. Surf Coat Technol 168(2–3):123–128
2. Aperador Chaparro WA, Lopez EV (2007) Electrodeposition of nickel plates on copper substrates using PC y PRC. Matéria (Rio de Janeiro) 12(4):583–588
3. Balasubramanian A, Srikumar D, Raja G, Saravanan G, Mohan S (2009) Effect of pulse parameter on pulsed electrodeposition of copper on stainless steel. Surf Eng 25(5):389–392
4. Nazir MH, Khan ZA, Saeed A, Siddaiah A, Menezes PL (2018) Synergistic wear-corrosion analysis and modelling of nanocomposite coatings. Tribol Int 121:30–44. https://doi.org/10.1016/j.triboint.2018.01.027
5. Nazir MH, Khan Z (2015) Maximising the interfacial toughness of thin coatings and substrate through optimisation of defined parameters. Int J Comput Methods Exp Meas 3(4):316–328
6. Bajwa RS, Khan Z, Bakolas V, Braun W (2016) Effect of bath ionic strength on adhesion and tribological properties of pure nickel and Ni-based nanocomposite coatings. J Adhes Sci Technol 30(6):653–665
7. Kim SK, Yoo HJ (1998) Formation of bilayer Ni–SiC composite coatings by electrodeposition. Surf Coat Technol 108:564–569
8. Benea L, Bonora PL, Borello A, Martelli S (2001) Wear corrosion properties of nano-structured SiC–nickel composite coatings obtained by electroplating. Wear 249(10–11):995–1003
9. Vaezi M, Sadrnezhaad S, Nikzad L (2008) Electrodeposition of Ni–SiC nano-composite coatings and evaluation of wear and corrosion resistance and electroplating characteristics. Colloids Surf A Physicochem Eng Asp 315(1–3):176–182
10. Chen L, Wang L, Zeng Z, Xu T (2006) Influence of pulse frequency on the microstructure and wear resistance of electrodeposited Ni–Al2O3 composite coatings. Surf Coat Technol 201(3–4):599–605
11. Borkar T, Harimkar S (2011) Microstructure and wear behaviour of pulse electrodeposited Ni–CNT composite coatings. Surf Eng 27(7):524–530
12. Chen X, Chen C, Xiao H, Cheng F, Zhang G, Yi G (2005) Corrosion behavior of carbon nanotubes–Ni composite coating. Surf Coat Technol 191(2–3):351–356
13. Benea L (2009) Electrodeposition and tribocorrosion behaviour of ZrO 2–Ni composite coatings. J Appl Electrochem 39(10):1671
14. Kumar CP, Venkatesha T, Shabadi R (2013) Preparation and corrosion behavior of Ni and Ni–graphene composite coatings. Mater Res Bull 48(4):1477–1483
15. Bajwa RS, Khan Z, Bakolas V, Braun W (2016) Water-lubricated Ni-based composite (Ni–Al 2 O 3, Ni–SiC and Ni–ZrO 2) thin film coatings for industrial applications. Acta Metall Sin (Engl Lett) 29(1):8–16
16. Nazir M, Khan ZA, Saeed A, Stokes K (2015) Modeling the effect of residual and diffusion-induced stresses on corrosion at the interface of coating and substrate. Corrosion 72(4):500–517
17. Nazir M, Khan ZA (2017) A review of theoretical analysis techniques for cracking and corrosive degradation of film-substrate systems. Eng Fail Anal 72:80–113
18. Nazir M, Khan Z, Stokes K (2015) Modelling of metal-coating delamination incorporating variable environmental parameters. J Adhes Sci Technol 29(5):392–423
19. Nazir MH, Khan ZA, Saeed A, Bakolas V, Braun W, Bajwa R, Rafique S (2017) Analyzing and modelling the corrosion behavior of Ni/Al2O3, Ni/SiC, Ni/ZrO2 and Ni/Graphene nanocomposite coatings. Materials 10(11):1225
20. Nazir MH, Saeed A, Khan Z (2017) A comprehensive predictive corrosion model incorporating varying environmental gas pollutants applied to wider steel applications. Mater Chem Phys 193:19–34
21. Lopez J, Stremsdoerfer G, Trejo G, Ortega R, Perez J, Meas Y (2012) Corrosion resistance of nickel coatings obtained by electrodeposition in a sulfamate bath in the presence of samarium (III). Int J Electrochem Sci 7:12244–12253
22. ASTM G87–02 Standard Practice for Conducting Moist SO2 Tests (2002) ASTM International, West Conshohocken. https://doi.org/10.1520/G0087-02
23. Aruna S, Bindu C, Selvi VE, Grips VW, Rajam K (2006) Synthesis and properties of electrodeposited Ni/ceria nanocomposite coatings. Surf Coat Technol 200(24):6871–6880
24. Donohue B (2020) How it works-the ins and outs of electroplating. Today's Machining World. https://todaysmachiningworld.com/magazine/how-it-works-the-ins-and-outs-of-electroplating/. Accessed 03 January 2020
25. Kuo S-L, Chen Y-C, Ger M-D, Hwu W-H (2004) Nano-particles dispersion effect on Ni/Al2O3 composite coatings. Mater Chem Phys 86(1):5–10. https://doi.org/10.1016/j.matchemphys.2003.11.040
26. Ciubotariu AC, Benea L, Lakatos-Varsanyi M, Dragan V (2008) Electrochemical impedance spectroscopy and corrosion behaviour of Al2O3–Ni nano composite coatings. Electrochim Acta 53(13):4557–4563. https://doi.org/10.1016/j.electacta.2008.01.020
27. Electroless Nickel Plating Services (2020) Surface treatment experts. https://www.sharrettsplating.com/coatings/electroless-nickel. Accessed 03 January 2020
28. US Research Nanomaterials, Inc. (2019). https://www.us-nano.com/. Accessed 25 December 2019
29. GRAPHENE PRICE (2020) Graphene Lab. http://www.i-graphenelab.com/price/. Accessed 03 January 2020

⚛ Springer

Appendix B:
Research Ethics Checklist

Research Ethics Checklist

Reference Id	13375
Status	Approved
Date Approved	27/10/2016

Researcher Details

Name	Muhammad Bhutta
Faculty	Faculty of Science & Technology
Status	Postgraduate Research (MRes, MPhil, PhD, DProf, DEng)
Course	Postgraduate Research - FST
Have you received external funding to support this research project?	No
Please list any persons or institutions that you will be conducting joint research with, both internal to BU as well as external collaborators.	Dr. Zulfiqar Kha (Faculty of Science & Technology (BU)), Dr. Abdul Ghafoor (Principal & Dean (SMME-NUST))

Project Details

Title	Development and modelling of self-lubricated thin-film coatings incorporating corrosion
Proposed Start Date of Data Collection	24/10/2016
Proposed End Date of Project	24/10/2019
Supervisor	Zulfiqar Khan
Approver	Zulfiqar Khan

Summary - no more than 500 words (including detail on background methodology, sample, outcomes, etc.)
NanoCorr, Energy & Modelling (NCEM) Research Theme within the Faculty of Science & Technology is led by Dr Zulfiqar Khan (Associate Professor) as a theme leader. This was previously known as Sustainable Design Research Centre was led by Dr Zulfiqar Khan as Director. Centre received its REF14 Panel Feedback as, "Sustainable Design Research Group had the highest proportion of outputs judged to be internationally excellent" Studies of surface wear mechanisms and integration of sustainable development issues within advanced engineering components and systems is the underlying principle of this research centre. Issues of tribology (friction, wear and lubrication), corrosion, thin nano-films and thermal behaviour are studied to help understand their influence on product durability and energy consumption. NCEM has significant industrial funding and partnerships in research in structural integrity in terms of corrosion, corrosion condition monitoring and prediction, nano coatings and renewable technology which includes subjects as heat transfer and thermofluids. NCEM within the Department of Design & Engineering at BU has been conducting research in surface engineering to enhance reliability and durability of complex interacting systems. These systems operate in harsh environmental and operational conditions e.g. high temperatures, high humidity, extreme pressures, corrosive environment and starved lubrication. Surface Engineering has been key activity at NCEM to optimise coating solutions to enable components to withstand these operating conditions. The proposed research will focus on the optimisation of properties for ceramic-based polymeric nano composites followed by advanced characterisation techniques. Tribological properties of the newly developed coatings and enhancement in their performance subject to conventional lubrication conditions in sliding contact will also be investigated.

External Ethics Review

Does your research require external review through the NHS National Research Ethics Service (NRES) or through another external Ethics Committee?	No

Research Literature

Is your research solely literature based?	No

Human Participants

Will your research project involve interaction with human participants as primary sources of data (e.g. interview, observation, original survey)?	No

Final Review

Will you have access to personal data that allows you to identify individuals OR access to confidential corporate or company data (that is not covered by confidentiality terms within an agreement or by a separate confidentiality agreement)?	No
Will your research involve experimentation on any of the following: animals, animal tissue, genetically modified organisms?	No

Will your research take place outside the UK (including any and all stages of research: collection, storage, analysis, etc.)?	No

Please use the below text box to highlight any other ethical concerns or risks that may arise during your research that have not been covered in this form.
My research project is in collaboration with the School of Mechanical and Manufacturing Engineering, National University of Sciences and Technology , Pakistan.

Researcher Statement

JOURNALISM / BROADCAST RESEARCHERS: I confirm that I have consulted and understand the Research Ethics Supplementary Guide: For Reference by Researchers Undertaking Journalism and Media Production Projects (available on the Research Ethics page)	Yes

Appendix C:

TE-57/77 Calibration and Maintenance Report

Official Purchase Order (ESC02636)

Phoenix Tribology
 	
Transmitted By email to info@phoenix-tribology.com
	Order No **ESC02636**
	Order Date 02/01/2018 3:50PM
	Requested By Malcolm Green
	                   SciTech
	                   GreenM@bournemouth.ac.uk

Order From Basket 02/01/2018 2:56PM

Please supply the following goods or services

No	Item Code / Job	Product / Service Description	Unit Price	Qty	VAT	Total
1		To undertake fault finding and calibration of TE57Tribometer. All as per quote 2342R1, dated 02/01/18	£850.00 / Each	1	£170.00	**£850.00**

	Total (excl.VAT)	£850.00
	VAT	£170.00
	Total (incl.VAT)	£1020.00

Delivery Address: Poole House / ROB GARDINER

Ship to:

Poole House
Fern Barrow
Poole BH12 5BB
Dorset
UK

Mark For:

Name	Rob Gardiner
Room	PG 89
Building	POOLE HOUSE
Service Dates	02/01/2018 -
Tel No	01202 965729

Payment Method: To Be Invoiced - Bournemouth University

Accounts Payable
2nd Floor Melbury House
1-3 Oxford Road
Bournemouth
BH8 8ES

Payment Type	To Be Invoiced
Name on Invoice	Bournemouth University
Cheque with Order	No

Important Instructions to Suppliers/Vendors:

Please ensure you have a valid Purchase Order number on your invoice otherwise we reserve the right to refuse payment.

We require one Purchase Order per invoice for us to be able to process a payment.

You can submit your own invoices through your parabilis log in. This is free of charge and when the invoice is received the person whom raised the order is notified of the invoices arrival to automatically prompt them to receive the goods/service and activate payment.

You can also keep your address information up to date by logging into your area of Parabilis and amending as necesary - change of address or phone number so we can ensure we send orders to the correct place.

Terms and Conditions:

BOURNEMOUTH UNIVERSITY HIGHER EDUCATION CORPORATION
TERMS AND CONDITIONS OF PURCHASE

Please note: save where the goods and/or services listed on this purchase order are subject to a separate written agreement between

Report- TE57/ 100/ 2002

Initial Findings

After receiving the control cabinet it was thoroughly inspected and powered on.

The following items were checked:

Operation of digital output relays (motor enable, heater enable, temperature out).

The operation of the analogue outputs for speed (0-10v) and temperature (PWM).

4-20mA input on Anin 8.

Friction input.

The following points were noted:

The cabinet cooling fan is not working- this should not be an issue and the main function is to cool the amplifier board (not fitted to this machine).

The Contact potential connector on the SLIM board is loose but still working OK.

The following adjustments were made:

The contact potential range was adjusted to 0-50mV, and COMPEND calibrated to match.

The Machine Reset/ Enable box (SLIM digital output 4) was re-added to the software to enable the machine to be reset when not running a test sequence.

On Site Findings

Reported problems was the speed and heating not working, and that the motor frequently loses speed control and accelerates out of control.

Before powering the machine on, the power module was checked for problems and found to be OK.

Checked machine operation one item at a time, all found to be operating OK.

Several tests were run with no issues seen.

Finally, the speed control issue was traced to the speed feedback cable, which when moved used the speed feedback to be list, leading to the motor running out of control. The cable will be changed, however, if this does not solve the problem then the connector on the SLIM board should be changed also.

Calibration

AUXILLARY TEMPERATURE

Connection:	SLIM ANIN 1							
Input Type:	4-20mA self powered							
Temperature Range:	0 - 600 C	Simulator Temperature	0	20	50	100	200	300	400
		Compend Reading	0	20	50	100	200	300	400
Unit Low:	0	Simultator Temperature	500	600					
Unit High:	600	Compend Reading	500	600					
Bit Low:									
Bit High:									
Fail Safe Temperature:									

SPECIMEN TEMPERATURE

Connection:	SLIM ANIN 2							
Input Type:	4-20mA self powered							
Temperature Range:	0 - 600 C	Simulator Temperature	0	20	50	100	200	300	400
		Compend Reading	0	20	50	100	200	300	400
Unit Low:	0	Simultator Temperature	500	600					
Unit High:	600	Compend Reading	500	600					
Bit Low:	829								
Bit High:	3203								
Fail Safe Temperature:	741								

Contact Potential:

Connection:	SLIM ANIN 3	Head Position	In Contact	Removed
Input Type:	0-2V	Voltage (mV)	0.0	50.0
Range:	50mV			
Unit Low:	0			
Unit High:	50			
Bit Low:	44			
Bit High:	2765			

Friction Force- Standard Setup:

Connection:	SLIM ANIN 7 (Friction Input)
Input Type:	0-10V
Load Range:	10V
Transducer Sensitivity:	-48.58
Unit Low:	0
Unit High:	9.42
Bit Low:	8
Bit High:	3921

Follow Up

Send replacement cable.

Confirm the correct assembly of the friction force transducer.